# Microwave-assisted multicomponent reaction for the synthesis of 2-amino-4H-chromene derivatives by $Ni_{0.5}Co_{0.5}Fe_2O_4$ nanoparticles as a magnetic catalyst under solvent-free conditions

**Sajjad Moradi[1], Saeid Taghavi Fardood[1,*], Ali Ramazani[1,2], Nadia Fattahi[1]**
[1]Department of Chemistry, University of Zanjan, Zanjan, Iran
[2]Research Institute of modern biological techniques, University of Zanjan, P O Box 45195-313, Zanjan, Iran
*E-mail: saeidt64@gmail.com*

Multi-component metal oxides in comparison with simple metal oxides have the crystal structures and merits of tuning chemical compositions. This specification also enables multi-component metal oxides to show various unique properties such as giant dielectric or catalytic activities and superconductivity [1,2]. $Ni_{0.5}Co_{0.5}Fe_2O_4$ has potential applications in high temperature integrated circuits, spintronic, chemical catalysts, high power electronic devices and photocatalysts [3,4].
2-Aminochromenes are the main components of many naturally occurring products and have been considered in recent years due to useful biological and pharmacological aspects, such as spasmolytic, anticoagulants, diuretic, anticancer, insecticide and antianaphylactin activity [5].
In this study, synthesis of $Ni_{0.5}Co_{0.5}Fe_2O_4$ nanoparticles (NPs) was performed by the sol–gel method. The sample was characterized by Fourier transform infrared spectrophotometer (FTIR), X-ray powder diffraction (XRD) and scanning electron microscopy (SEM). The catalytic activity of $Ni_{0.5}Co_{0.5}Fe_2O_4$ NPs has been evaluated for the synthesis of 2-Amino-4H-Chromenes derivatives through three-component under conditions Microwave irradiation and solvent free. The final product was investigated by $^1$HNMR and $^{13}$CNMR spectroscopy. Advantageous features of this study, including green, easy and inexpensive synthesis of nanoparticles, use of microwave irradiation in conditions solvent free, short reaction times, Simple work-up, mild reaction conditions.

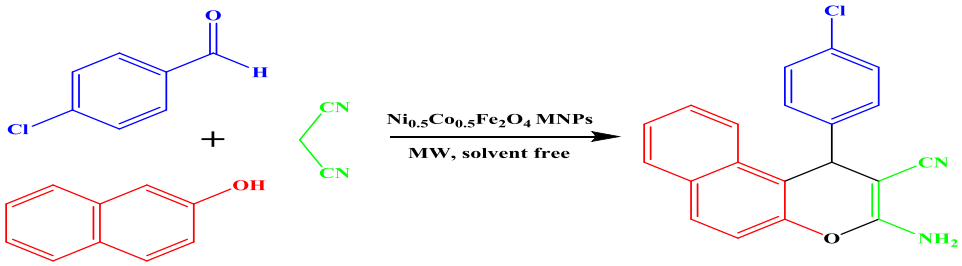


***Scheme 1.*** *Synthesis of 2-Amino-4H-Chromenes derivatives*

***Keywords:*** *Multi-component metal oxides, 2-Aminochromenes, Sol–gel method, Microwave irradiation.*

## References

[1] T. Wu, H. Mayaffre, S. Krämer, M. Horvatić, C. Berthier, W. Hardy, R. Liang, D. Bonn and M.-H. Julien, *Nature*, **2011**, *477*, 191.
[2] X. Guan, L. Li, J. Zheng and G. Li, *RSC Adv.*, **2011**, *1*, 1808-1814.
[3] A. Azizi, H. Yoozbashizadeh, A. Yourdkhani and M. Mohammadi, *J. Magn. Magn. Mater.*, **2010**, *322*, 56-59.
[4] S. Farooq, A. Saeed, M. Sharif, J. Hussain, F. Mabood and M. Iftekhar, *J. Water Process Eng.*, **2017**, *16*, 132-141.
[5] L. Bonsignore, G. Loy, D. Secci and A. Calignano, *Eur. J. Med. Chem.*, **1993**, *28*, 517-520.

# Green synthesis of magnesium oxide nanoparticles using henna powder extract and its use as an efficient catalyst for the synthesis of pyrimidine derivatives

**Reza Forootan[1], Saeid Taghavi Fardood[1,*], Ali Ramazani[1,2]**
[1]Department of Chemistry, University of Zanjan, Zanjan, Iran
[2]Research Institute of Modern Biological Techniques (RIMBT), University of Zanjan, Zanjan, Iran
*E-mail: saeidt64@gmail.com*

In the recent years, green chemistry methods for synthesis of metal oxide nanoparticles has become a major focus in current society. Its more eco-friendly, low toxicity and exhibit long term stability. Generally green synthesis nanoparticles extract from fungi, bacteria, algae and green plants. Plant leaf extracts have been extensively used for green synthesis. A wide range of bioactive phytochemicals as plants are widely available, safe to handle and possess a variety of metabolites that function as reducing agents in nanoparticle synthesis [1,2].

Magnesium oxide (MgO) is an attractive and basic metal oxide material. It's generally used as a catalyst, electrochemical biosensor, and pharmaceutical industry and paints. The highly crystalline MgO nanoparticles exhibit low electrical conductivity and higher thermal stability [3,4].

In this work, the precursor materials was $Mg(NO_3)_2$ and Henna powder extract. The Henna powder extract acting as a reducing agent in the reaction. The sample was characterized by powder X-ray diffraction (XRD), fourier transform infrared spectroscopy (FTIR), and scanning electron microscopy (SEM). Thereupon, MgO NPs as an efficient catalyst was used for the synthesis of pyrimidine derivatives via multi-component reactions in ethanol under reflux conditions (scheme 1). This method has many advantages such as high yields, relatively short reaction times, mild reaction condition, easy work up, and using a highly recyclable catalyst.

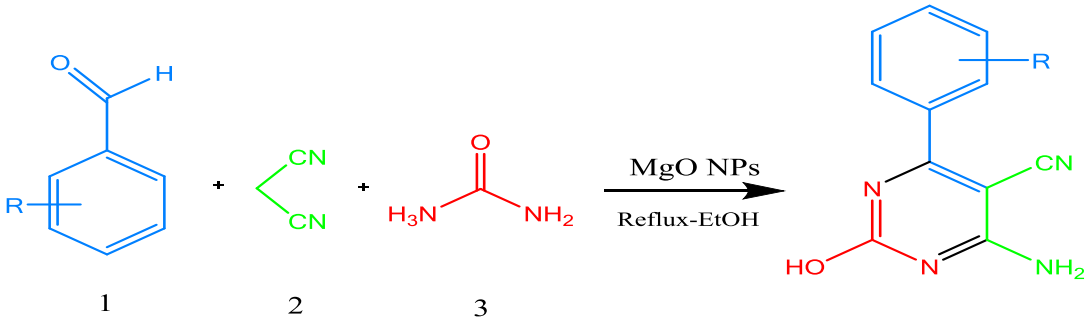


***Scheme 1.*** *Synthesis of 6-Amino-5-Cyano-4-Phenyl-2-Mercapto Pyrimidine*

***Keywords:*** *Magnetic catalyst; Zinc Ferrite Nanoparticles; 3,4-dihydropyrimidin-2-(1H)-ones*

## References

[1] Q. Sun, X. Cai, J. Li, M. Zheng, Z. Chen and C.-P. Yu, *Colloids Surf., A*, **2014**, *444*, 226-231.
[2] S. Iravani, *Green Chem.*, **2011**, *13*, 2638-2650.
[3] S.K. Moorthy, C.H. Ashok, K.V. Rao and C. Viswanathan, *Mater. Today:. Proc.*, **2015**, *2*, 4360-4368.
[4] L. Umaralikhan and M. Jamal Mohamed Jaffar, *Iran. J. Sci. Technol. A*, **2018**, *42*, 477-485.

# Microwave-assisted multicomponent reaction for the synthesis of phthalhydrazide derivatives using $FeCl_3$ as a catalyst

**Saeid Taghavi Fardood[1,*], Fateme Yekke Zare[1], Ali Ramazani[1,2]**
[1]Department of Chemistry, University of Zanjan, Zanjan, Iran
[2]Research Institute of Modern Biological Techniques (RIMBT), University of Zanjan, Zanjan, Iran
*E-mail: saeidt64@gmail.com*

Nitrogen-containing heterocycles have wide range of biologically activities such as antibiotics, fungicides, antibiotics agents, anti-cancer, anti-inflammatory, anti-allergic, analgesic, glucagon receptor antagonism, herbicides, and insecticides. Phthalazine derivatives have attracted much attention owing to their biological activities such as anticonvulsant, cardiotonic, vasorelaxant, pharmacological properties, and many other applications are well documented. Due to their importance, some methods have been reported for synthesis of phthalazine derivatives [1,2].
$FeCl_3$ is a 'green' and efficient Lewis acid catalyst is potentially attractive in current organic synthesis by forming carbonecarbon and carboneheteroatom bonds. In recent years there have been many reports unraveling the utility of $FeCl_3$ in a wide variety of organic transformations. Moreover, $FeCl_3$ is inexpensive, easy to handle, and are environmentally friendly [3-5].
An efficient, inexpensive, environmentally friendly one-pot route to phthalhydrazide derivatives has been developed, involving three-component reaction of phthalhydrazide, aldehydes, and barbituric acid catalyzed by $FeCl_3$ in solvent free condition under microwave irradiation (scheme 1). This method should provide high yields, shorter reaction time, easy work-up and cleaner reaction. It is a new strategy for N-fused heterocycles synthesis, which has wider application in organic and medicinal chemistry.

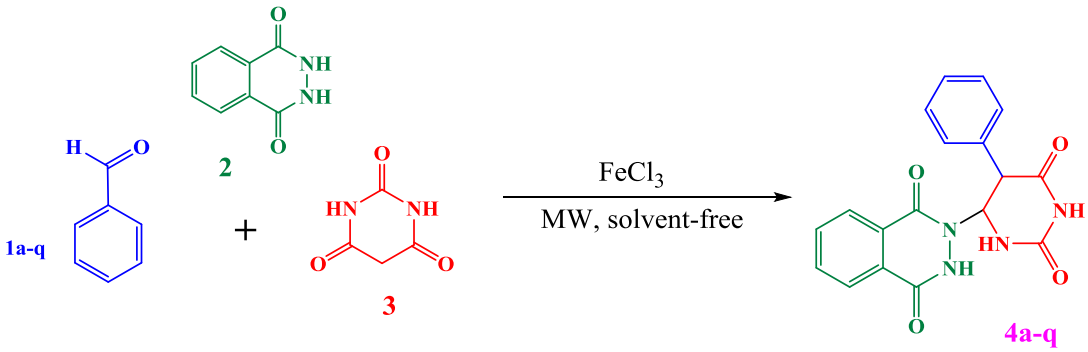


***Scheme 1.*** *Three-component reaction of barbituric acid, phthalhydrazide and aromatic aldehydes*

***Keywords:*** *Microwave irradiation, Solvent-free, phthalhydrazide derivatives*

## References

[1] J.S. Kim, H.-K. Rhee, H.J. Park, S.K. Lee, C.-O. Lee and H.-Y.P. Choo, *Biorg. Med. Chem.*, **2008**, *16*, 4545-4550.
[2] L.-P. Liu, J.-M. Lu and M. Shi, *Org. Lett.*, **2007**, *9*, 1303-1306.
[3] X. He, Y. Shang, Y. Zhou, Z. Yu, G. Han, W. Jin and J. Chen, *Tetrahedron*, **2015**, *71*, 863-868.
[4] M. Tajbakhsh, M. Heidary, R. Hosseinzadeh and M.A. Amiri, *Tetrahedron Lett.*, **2016**, *57*, 141-145.
[5] A. Mondal and C. Mukhopadhyay, *ACS Combinatorial Science*, **2015**, *17*, 404-408.

# Synthesis of amorphous $Al_2O_3$ nanoparticles using arabic gum as the photocatalyst in degradation of direct red 128 from aqueous solution

**Kobra Atrak[1], Saeid Taghavi Fardood[1,*], Ali Ramazani [1,2]**
[1]Department of Chemistry, University of Zanjan, Zanjan, Iran
[2]Research Institute of Modern Biological Techniques (RIMBT), University of Zanjan, Zanjan, Iran

**E-mail: saeidt64@gmail.com*

Dyes are widely used in the variety of industries such as textile, plastic, paper, leather, printing, and cosmetic industries. Most dyes are toxic and it is essential to treat the dyeing wastewater prior to their discharge into the environment. The emission of organic pollutants is a potential danger to the receiving water [1]. Various chemical, biological, and physical methods have been used for degrading dyes. Among all the techniques presented, photocatalytic degradation is one of the most efficient methods for wastewater treatment [2,3].
We have synthesized amorphous $Al_2O_3$ nanoparticles using arabic gum via sol-gel procedure, which is simple and eco-friendly. This study has evaluated the efficiency of obtained NPs in the photocatalytic degradation of direct red 128 from an aqueous solution under visible light irradiation. The prepared nanoparticles were then characterized by Fourier transform infrared spectroscopy (FTIR), X-ray powder diffraction (XRD), and field emission scanning electron microscopy (FESEM).
The photocatalytic studies were carried out at different initial dye concentration, photocatalyst dosage, and irradiation time. Based on the results, amorphous $Al_2O_3$ NPs can degrade of DR128.

***Keywords:*** *amorphous $Al_2O_3$ nanoparticles, degradation of dye, photocatalyst.*

## References

[1] Y. Zhang, F. Gao, B. Wanjala, Z. Li, G. Cernigliaro and Z. Gu, *Appl. Catal., B*, **2016**, *199*, 504-513.
[2] D. Ding, K. Liu, S. He, C. Gao and Y. Yin, *Nano Lett.*, **2014**, *14*, 6731-6736.
[3] N. Daneshvar, S. Aber, M.S. Dorraji, A. Khataee and M. Rasoulifard, *Sep. Purif. Technol.*, **2007**, *58*, 91-98.

# Immobilized polyoxometalate on PANi and ZnO as an efficient and reusable photocatalyst for dye degradation

**Parvin Rahmani, Mohammad Ali Rezvani *, and Fatemeh Parchegani***

Department of Chemistry, Faculty of Science, University of Zanjan, 451561319, Zanjan, Iran
**E-mail: marezvani@znu.ac.ir, f-parchegani94@phd.araku.ac.ir*

A literature review showed that dye removal using the immobilized POM onto the ZnO and polyaniline (PANi) nanoparticle as a photocatalyst. The immobilized mono substituted tungstophosphoric acid onto the ZnO and PANi nanoparticle as an environmentally friendly catalyst was used for photocatalytic dye degradation. The synthesized nanocomposite $PW_{11}Mn$@ZnO@PANi was characterized using FTIR. Basic red was used as model dyes.

Photocatalytic degradation method as an advanced oxidation process is an efficient procedure to degrade dyes and it includes irradiation of semiconductors as photocatalysts [1]. Herein, a new mono substituted phosphotungstate supported polyaniline and ZnO was investigated and demonstrated to be effective for dye degradation. Mono substituted phosphotungstate $H_3[PW_{11}Mn]$ and ZnO nanoparticles and $PW_{11}Mn$@ZnO@PANi catalyst were synthesized according to a reported procedure [2]. The identification of specific chemical bands and functional groups of the synthesized samples was characterized using FT-IR spectroscopy to confirm their successful incorporation (Fig 1).

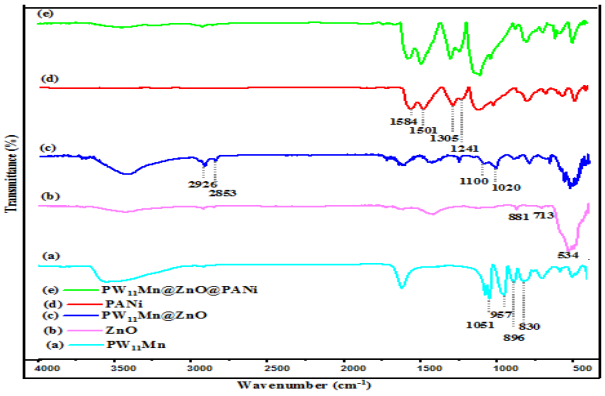


***Fig. 1.*** *FT-IR spectrum of the synthesized nanomaterials (a) $PW_{11}Mn$, (b) ZnO, (c) $PW_{11}Mn$@ZnO (d) PANi (e) $PW_{11}Mn$@ZnO@PANi*

The photocatalytic activity of as-obtained samples was estimated through the photodegradation of basic red. The as prepared solution was illuminated under UV light irradiation, and absorption was measured at the maximum absorption wavelength of 531 nm.

***Keywords:*** *Keggin-type polyoxometalate, Nanocomposite, Dye degradation, Photocatalysts*

## References

[1] M. A. Rezvani, S. Khandan, N. Sabahi, Energy Fuels, **2017**, 31, 5472−5481.
[2] M. A. Rezvani, A. Fallah Shojaie, M. H. Loghmani, Catal. Commun, **2012**, 25, 36–40.

# Synthesis of $Cu_{0.5}Zn_{0.5}FeAlO_4$ nanoparticles using the sol-gel method and study of its photocatalytic activity

**Kobra Atrak[1], Saeid Taghavi Fardood[1]*, Ali Ramazani [1,2], Reza Forootan[1]**
[1]Department of Chemistry, University of Zanjan, Zanjan, Iran
[2]Research Institute of Modern Biological Techniques (RIMBT), University of Zanjan, Zanjan, Iran

**E-mail: saeidt64@gmail.com*

Spinel compounds have been extremely interesting subjects for many scientists owing to their unique characteristics and broad practical applications in various fields including magnetic drug delivery, ferrofluids, and degradation of organic pollutants [1,2]. Among them, spinel ferrite nanoparticles have been gained interest in their synthesis. The textile industry produces a huge amount of dye wastewater and it is essential that the dye effluents be treated prior to release into the water sources [3].

The first goal of this work is to synthesis $Cu_{0.5}Zn_{0.5}FeAlO_4$ nanospinel using tragacanth gel by the means of sol-gel method which is less time consuming, simple, and eco-friendly. The obtained nanoparticles were then identified using different analytical techniques such as Fourier transform infrared spectroscopy (FTIR), X-ray powder diffraction (XRD), and field emission scanning electron microscopy (FESEM). XRD results confirmed the spinel ferrite phase formation.

Evaluation of photocatalytic activity of synthesized nanoparticles as a photocatalyst in dye degradation, direct blue 129 (DB129) under visible light irradiation is the second aim. In the next step, the effect of different factors including initial dye concentration, photocatalyst dosage, and irradiation time was examined. Based on the results, $Cu_{0.5}Zn_{0.5}FeAlO_4$ nanoparticles possess degradation efficiency.

***Keywords:*** *Tragacanth gel, Spinel compounds, Nanoparticles.*

## References

[1] L.K. De Souza, J.R. Zamian, G.N. da Rocha Filho, L.E. Soledade, I.M. dos Santos, A.G. Souza, T. Scheller, R.S. Angélica and C.E. da Costa, *Dyes Pigm.*, **2009**, *81*, 187-192.
[2] K. Wang, D. Lee, L. Horng and G. Chern, *J. Magn. Magn. Mater.*, **2004**, *282*, 73-77.
[3] X. Wang, N. Zhu and B. Yin, *J. Hazard. Mater.*, **2008**, *153*, 22-27.

# An expedient one-pot process for synthesis of 3,4-dihydropyrimidin-2-ones *via* synthesized $ZnMn_2O_4$ nanoparticles as catalyst

**Farzaneh Moradnia[1,]*, Saeid Taghavi Fardood[1], Ali Ramazani[1,2]**
[1]Department of Chemistry, University of Zanjan, Zanjan, Iran
[2]Research Institute of Modern Biological Techniques (RIMBT), University of Zanjan, Zanjan, Iran
**E-mail: farzaneh2856@gmail.com*

Dihydropyrimidinones (DHPMs) are important substructures present in a wide variety of biologically active natural products [1]. On the other hand, One-pot multicomponent condensation reactions represent an efficient tool to perform efficient synthesis, because they allow the assembly of complex molecules with maximum simplicity and brevity [2]. The use of natural gel is generating interest of researchers toward cost-effective, nontoxic, economic viability and eco-friendly green synthesis of nanoparticles [3]. In this work, $ZnMn_2O_4$ NPs were synthesized using tragacanth gum as biotemplate and Metals nitrate as the metal source by the sol-gel method without using any organic chemicals. Henceforth, $ZnMn_2O_4$ nanoparticles as an efficient catalyst were used for the synthesis of 3,4-dihydropyrimidin-2-ones derivatives via solvent free multi-component reactions (Scheme 1). Simple work-up, mild reaction conditions, short reaction times, use of an economically convenient catalyst, and excellent product yields are the advantageous features of this method. The molecular structure of products has been determined by IR, $^1$HNMR, and $^{13}$CNMR techniques.

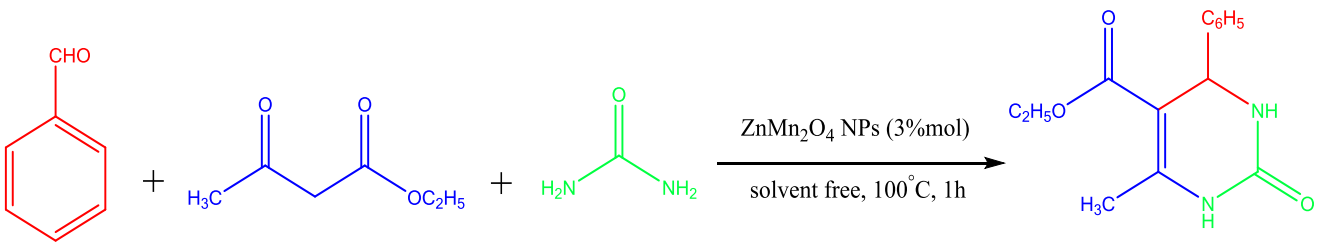


***Scheme 1.*** *Synthesis of dihydropyrimidin derivatives*

***Keywords:*** *Dihydropyrimidin, Spinel nanoparticle, Sol-gel method.*

## References

[1] S. Gore, S. Baskaran and B. Koenig, *Green Chem.*, **2011**, *13*, 1009-1013.
[2] T. Hudlicky, *Chem. Rev.*, **1996**, *96*, 3-30.
[3] S.T. Fardood, A. Ramazani and S. Moradi, *J. Sol-Gel Sci. Technol.*, **2017**, *82*, 432-439.

# One-pot synthesis of tetrahydrobenzo[b]pyran derivatives through three-component condensation using $Ni_{0.5}Zn_{0.5}Fe_2O_4$ magnetic nanoparticles as reusable catalyst

**Sajjad Moradi[1], Saeid Taghavi Fardood[1,*], Ali Ramazani[1,2], Zahra Hosseinzadeh[1]**
[1]Department of Chemistry, University of Zanjan, Zanjan, Iran
[2]Research Institute of modern biological techniques, University of Zanjan, P O Box 45195-313, Zanjan, Iran
*E-mail: saeidt64@gmail.com

Nowadays, magnetic nanoparticles (MNPs) as catalysts are interested of reserchers because of their advantages such as green, efficient, low-cost, magnetic properties and reusable catalysts [1]. One series of natural products that has structural unit are 4H-Pyrans. In the last decades, 4H-Benzo[*b*]pyrans have received considerable attention, that because of this attention due to their wide range activities such as anticoagulant, anticancer, anti-anaphylactic activities and diuretic [2-5]. Also this component can be employed as photoactive materials, pigments and utilized as potential biodegradable agrochemicals [6].

In the present study, we have reported green synthesis of $Ni_{0.5}Zn_{0.5}Fe_2O_4$ MNPs using that was carried out by the sol–gel method in arabic gum as a biopolymeric template. The catalyst was characterized by Fourier transform infrared spectrophotometer (FTIR), vibrating sample magnetometer (VSM), X-ray powder diffraction (XRD), scanning electron microscopy (SEM). The X-ray powder diffraction analysis revealed the formation of cubic phase ferrite MNPs with average particle size of 31 nm. The catalytic activity of $Ni_{0.5}Zn_{0.5}Fe_2O_4$ MNPs has been evaluated for the synthesis of tetrahydrobenzo[b]pyran derivatives through three-component under conditions Microwave irradiation and solvent free. Products were elucidated by $^{1}$HNMR and $^{13}$CNMR spectroscopy. Simple work-up, short reaction times, mild reaction conditions and excellent product yields (83–97%) are the advantageous features of this method.

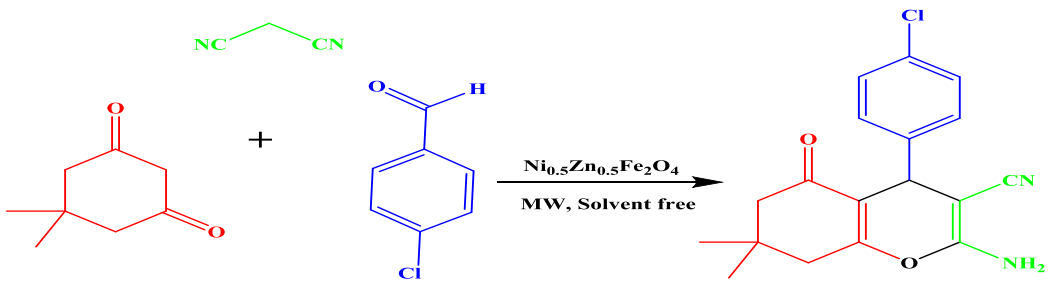


***Scheme 1.*** *Synthesis of tetrahydrobenzo[b]pyran derivatives*

***Keywords:*** *Sol–gel method, Arabic gum, Tetrahydrobenzo[b]pyran, Microwave irradiation.*

## References

[1] X. Cai, H. Wang, Q. Zhang and et al., *J. Sol-Gel Sci. Technol.* **69**, 33 (2014).
[2] L. Bonsignore, G. Loy, D. Secci and et al., *Eur. J. Med. Chem.* **28**, 517 (1993).
[3] A.L. LAZZERI, and E. Lapi, *Bollettino chimico farmaceutico* **99**, 583 (1960).
[4] X.-S. Wang, D.-Q. Shi, S.-J. Tu and et al., *Synth. Commun.* **33**, 119 (2003).
[5] D. Fang, H.B. Zhang, and Z.L. Liu, *J. Heterocycl. Chem.* **47**, 63 (2010).
[6] G. Sabitha, K. Arundhathi, K. Sudhakar and et al., *Synth. Commun.* **39**, 433 (2009).

# Hydrogel as an efficient catalyst for the synthesis of polyhydroquinoline derivatives under eco-friendly conditions

**Zahra Hosseinzadeh[1,*], Saied Taghavi-Fardood[1], Ali Ramazani[1], Nima Razzaghi-Asl[2]**
[1]Department of Chemistry, University of Zanjan, Zanjan, Iran
[2]Department of Medicinal Chemistry, School of Pharmacy, Ardabil University of Medical Sciences, Ardabil, Iran
*E-mail: zahra.hosseinzadeh@znu.ac.ir

Polyhydroquinolines are one of the most important classes of heterocyclic scaffolds providing major ligands for biological receptors. Polyhydroquinolines the source of some valuable drugs which are very important in pharmacy. For instance, they demonstrate activity for the treatment of angina pectoris and hypertension [1,2]. The aim of the present work was to search simple and green method for the preparation of polyhydroquinoline derivatives. Poly (2-acrylamido-2-methyl-1-propansulfonic acid) (p(AMPS)) hydrogel [3,4] is used as an efficient heterogeneous catalyst for the synthesis of polyhydroquinoline analogues in high yields via eco-friendly simple reaction method. The catalyst is reusable and can be applied several times without any excessive reduction in of its activity. This new protocol for has significant advantages such as green synthesis, high yields of the products, easy isolation and reusability of the catalyst and free of formation of any hazardous by products.

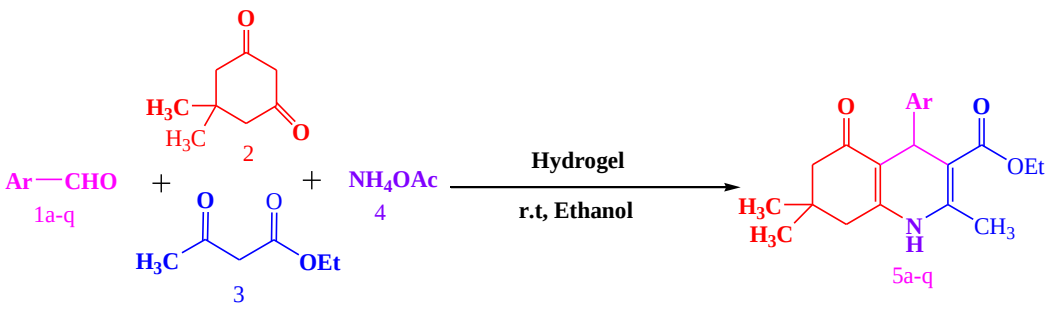


***Scheme 1.*** *Synthesis of polyhydroquinoline derivatives*

***Keywords:*** *Hydrogel, polyhydroquinoline, Reusable catalyst*

## References

[1] M.G. Dekamin, N. Kheirabi and Z. Karimi,
[2] M.G. Dekamin, S. Ilkhanizadeh, Z. Latifidoost, H. Daemi, Z. Karimi and M. Barikani, *RSC Adv.*, **2014**, *4*, 56658-56664.
[3] N. Sahiner, H. Ozay, O. Ozay and N. Aktas, *Appl. Catal., B*, **2010**, *101*, 137-143.
[4] E.M. Ahmed, *J. Adv. Res.*, **2015**, *6*, 105-121.

# Green one-pot solvent-free synthesis of pyrano[2,3-c]-pyrazoles Catalyzed by cerium oxide nanoparticles under microwave irradiation

**Fateme Yekke Zare**[1], **Saeid Taghavi Fardood**[1,*], **Ali Ramazani**[1]
[1]Department of Chemistry, University of Zanjan, Zanjan, Iran
[2]Research Institute of Modern Biological Techniques (RIMBT), University of Zanjan, Zanjan, Iran
*E-mail: saeidt64@gmail.com

Green chemistry is an increasingly important aspect of chemical research devoted to minimizing the use and generation of hazardous substances, organic solvents, and toxic catalysts on the environment. Pyrano[2,3-c]pyrazoles are an important class of heterocyclic compounds that play an essential role as biologically active compounds and represent an interesting template in medicinal chemistry. Many types of bioactive molecules with broad medicinal and agrochemical applications contain both pyran and pyrazole rings such as pyrano[2,3-c]pyrazoles. The pyrano[2,3-c]pyrazole heterocyclic scaffold is an important substructure showing anticancer, anti-inflammatory, anti-microbial, hypoglycaemic, analgesic, and Chk1 kinase inhibitory properties; it is also used in biodegradable agrochemicals. Multicomponent reactions (MCRs) are the most efficient one-pot route to achieving structural diversity. MCRs provide a rapid and powerful method for synthesizing versatile heterocycles. They are also useful for drug discovery, from the initial recognition of a lead structure to the production of large libraries of analogs. The use of MCRs in green synthesis has been reviewed recently [1-4].
In this work, a facile one-pot, multicomponent protocol for the synthesis of pyrano[2,3-c]-pyrazoles derivatives in the presence of cerium oxide nanoparticles as a highly effective heterogeneous base catalyst in solvent free conditions is reported. This transformation proceeds via a four component reaction of ethyl acetoacetate, hydrazine hydrate, malononitrile and various aldehydes. This synthetic method has several advantages, including good yield, simple work-up, harmless by-products, and simple purification.

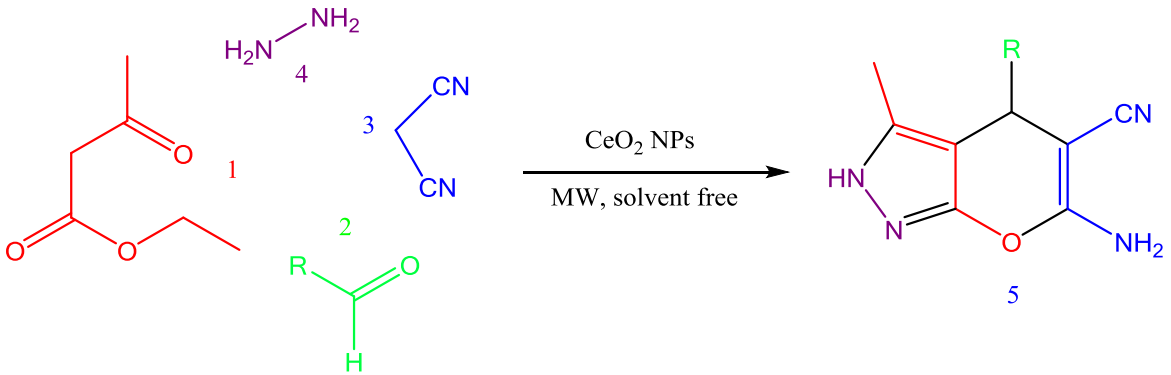


***Scheme 1.*** *The preparation of Pyrano[2,3-c]Pyrazoles derivatives using $CeO_2$ NPs as catalyst*

***Keywords:*** *Cerium oxide nanoparticles, Green method, Pyrano[2,3-c]Pyrazoles derivatives*

## References

[1] M. Zakeri, M.M. Nasef, T. Kargaran, A. Ahmad, E. Abouzari-Lotf and J. Asadi, Res. Chem. Intermed., **2017**, 43, 717-728.
[2] W. Li, R. Ruzi, K. Ablajan and Z. Ghalipt, Tetrahedron, **2017**, 73, 164-171.
[3] M. Babaie and H. Sheibani, Arabian J. Chem., **2011**, 4, 159-162.
[4] H.M. Al-Matar, K.D. Khalil, A.Y. Adam and M.H. Elnagdi, Molecules, **2010**, 15, 6619-6629.

# Green synthesis of zinc ferrite magnetic nanoparticles using Arabic gum and its catalytic activity in the synthesis of polyhydroquinoline derivatives

**Saeid Taghavi Fardood[1,*], Reza Forootan[1], Ali Ramazani[1,2]**
[1]Department of Chemistry, University of Zanjan, Zanjan, Iran
[2]Research Institute of Modern Biological Techniques (RIMBT), University of Zanjan, Zanjan, Iran
*E-mail: saeidt64@gmail.com

Arabic gum-assisted sol-gel method was employed for the preparation of magnetic zinc ferrite nanoparticles (MNPs) using zinc nitrate and iron nitrate as the metal source by the novel sol–gel method without adding external surfactant. The sample calcined at 600 °C. The green synthesized $ZnFe_2O_4$ MNPs are characterized by powder X-ray diffraction (XRD), Fourier Transform Infrared Spectroscopy (FTIR), vibrating sample magnetometer (VSM) and scanning electron microscopy (SEM). XRD analysis revealed the formation of cubic phase ferrite MNPs with average crystallite size of 38 nm. The $ZnFe_2O_4$ nanoparticles have high catalytic activity and gave the desired products in good to high yields. The catalyst can be easily recovered by filtration and was used at least three times with only a slight reduction in its catalytic activity [1,2].

A four-component reaction of aldehydes, dimedone, ammonium acetate and ethyl acetoacetate was achieved in the presence of $ZnFe_2O_4$ MNPs as a heterogeneous catalyst to produce polyhydroquinoline derivatives (scheme 1). Synthesis of polyhydroquinoline has been reported using $ZnFe_2O_4$ nanoparticles at 100 °C under reflux condition in ethanol. However, some of the reported methods have disadvantages including long reaction times, harsh reaction conditions, and use of toxic and non-reusable catalysts. Therefore, to avoid these limitations, the exploration of an efficient and reusable catalyst with high catalytic activity for the preparation of polyhydroquinoline is still favored. Atom economy, excellent yields in short times, high catalytic activity, recycling of catalyst, and environmental benignity are some of the important features of this protocol [3].

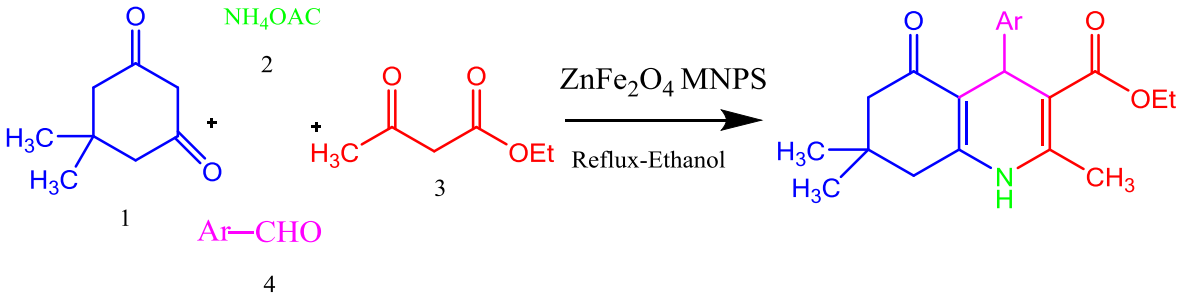


***Scheme 1.*** *Synthesis of polyhydroquinoline derivatives*

***Keywords:*** *Arabic gum; Sol-gel method; Magnetic zinc ferrite nanoparticles; Polyhydroquinoline derivatives*

## References

[1] H. Mirzaei and A. Davoodnia, *Chin. J. Catal.*, **2012**, *33*, 1502-1507.
[2] A. Ramazani, S. Taghavi Fardood, Z. Hosseinzadeh, F. Sadri and S.W. Joo, *Iran. J. Catal.*, **2017**, *7*, 181-185.
[3] J. Shapoori, J. Safaei-Ghomi and M.A. Ghasemzadeh, *Iran. J. Catal.*, **2017**, *7*, 47-52.

# Highly efficient, one-pot, solvent-free synthesis of 1,8-dioxo-octahydroxanthene derivatives by $ZnMn_2O_4$ nanoparticles as efficient heterogeneous catalyst

**Farzaneh Moradnia[1,*], Saeid Taghavi Fardood[1], Ali Ramazani[1,2], Ilnaz Abdolmaleki[3]**
[1]Department of Chemistry, University of Zanjan, Zanjan, Iran
[2]Research Institute of Modern Biological Techniques (RIMBT), University of Zanjan, Zanjan, Iran
[3]Department of Science, Payame Noor University (PNU), PO Box 19395-4697, Tehran, Iran
*E-mail: farzaneh2856@gmail.com

Xanthene derivatives have attracted considerable interest in both pharmaceutical and medicinal chemistry because of their numerous pharmacological properties such as antibacterial, antiviral, anti-inflammatory, or anticancer activities [1]. Furthermore, in addition to their use as valuable synthetic precursors for many organic compounds and dyes xanthene derivatives have also found use in laser technologies and fluorescent materials for visualization of biomolecules [2]. In recent years, spinel nanostructures have attracted attention for their use as catalyst. A large class of mixed valence metal oxides crystallizes in spinel structure with a general formula of $AB_2O_4$, where, for the most spinels, A and B are di- and trivalent cations (2–3 spinels), respectively. Zinc manganite ($ZnMn_2O_4$) is known as the most attractive spinel due to its low potential of oxidation and low material cost. $ZnMn_2O_4$ is often used in lithium ion batteries because of environmental friendliness, low cost and much lower operating voltage [3,4]. In this work, $ZnMn_2O_4$ tetragonal-spinel nanoparticles was used as efficient heterogeneous catalyst. Henceforth, 1,8-dioxo-octahydroxanthene derivatives were synthesized *via* solvent free multi-component reactions. 2 mmol dimedone and 1mmol benzaldehyde were used as starting materials (Scheme 1). This method provides several advantages such as environment friendliness, high yields and simple work-up procedure. The molecular structure of products has been determined by IR, $^1$HNMR, and $^{13}$CNMR techniques.

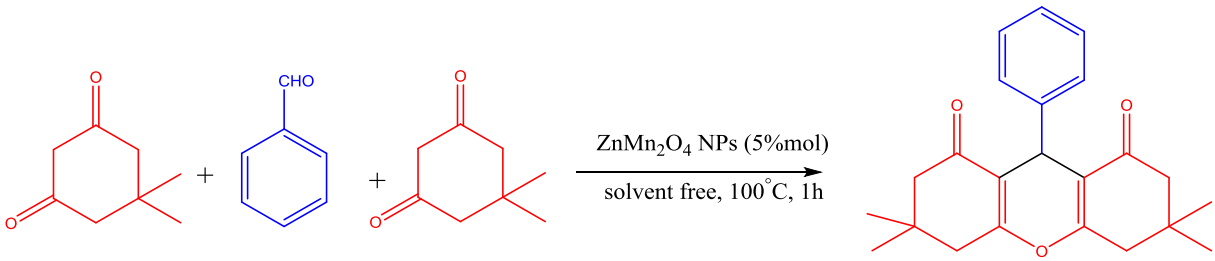


***Scheme 1.*** *Synthesis of 1,8-dioxo-octahydroxanthene derivatives*

***Keywords:*** *Sol-gel method, Spinel nanoparticle, 1,8-dioxo-octahydroxanthene.*

## References

[1] N. Mulakayala, P.V.N.S. Murthy, D. Rambabu, M. Aeluri, R. Adepu, G.R. Krishna, C.M. Reddy, K.R.S. Prasad, M. Chaitanya, C.S. Kumar, M.V. Basaveswara Rao and M. Pal, *Bioorg. Med. Chem. Lett.*, **2012**, *22*, 2186-2191.
[2] N. Mulakayala, G. Pavan Kumar, D. Rambabu, M. Aeluri, M.V. Basaveswara Rao and M. Pal, *Tetrahedron Lett.*, **2012**, *53*, 6923-6926.
[3] H. Li, B. Song, W. Wang and X. Chen, *Mater. Chem. Phys.*, **2011**, *130*, 39-44.
[4] F.M. Courtel, H. Duncan, Y. Abu-Lebdeh and I.J. Davidson, *J. Mater. Chem.*, **2011**, *21*, 10206-10218.

# Preparationand identification polysiloxane by the sol-gel process and modification by silver particles

**Mitra Dini[1], Mehdi Mirzaei[2]***
[1]Department of Chemistry, Sharood University of Thechnology, Semnan, Iran
[2]Department of Chemistry, Sharood University of Thechnology, Semnan, Iran
**E-mail: mmirzaee@sharooddut.ac.ir*

Polysiloxane (PMSQ) microsphere is a type of organosilicone materials with the molecular structure of $RSiO_{3/2}$, where R represents the organic groups such as methyl, phenyl, mercapto, amine, epoxy acrylic and isocyanate. With the specific organic-inorganic hybrid structure and regular morphology (mono-dispersed sphere with size ranging from nano - to micro-meter), PAMSQ microsphere has been widely applied in chemistry and physic fields. Poly (aminopropyl/methyl) silsesquioxane (PAMSQ) particles were obtained by hydrolytic co-condensation of 3- aminopropyltriethoxysilane (APTES) with methyltrimethoxysilane (MTMS) in aqueous medium. Synthesis of polysilsesquioxane (PAMSQ) particles is reported here. Synthesis of PAMSQ particles with controllable amount of aminopropyl functional groups using APTES and MTMS as precursors by hydrolytic co-condensation process were conducted. Generally, hydrolytic condensation of the organotrimethoxysilanes in water or ethanolwater was quite rapid under basic conditions. Initial hydrolysis of the APTES and MTMS resulted in silanol oligomers. Silanol (Si–OH) was very reactive and then condensed to form polysilsesquioxanes in the presence of base catalyst.For PAMSQ preparation, 3-aminopropyl triethoxy silane (3ml) was dissolved in MTMS (3ml) and after 10 minutes 60 ml of water to this solution, whit continuous stirring. So that the molar concentration of APTES / MTMS in the mixture is 4:6. A white colored precipitate gradually formed within 10 min and was stirred at ambient temperature for 24 h for the reaction to reach completion. The material formed was dried at 50 °C for 14 h. Yield 2 g. The final products were thoroughly characterized by Fourier Transform Infrared spectroscopy (FT-IR), X-ray powder diffraction (XRD), Field Emission Scanning Electron Microscopy (FE-SEM) along with Energy Dispersive X-ray (EDX) Spectroscopy, thermo gravimetric and differential thermal analysis (TG/DTA) and X-ray photoelectron spectroscopy (XPS) [1].

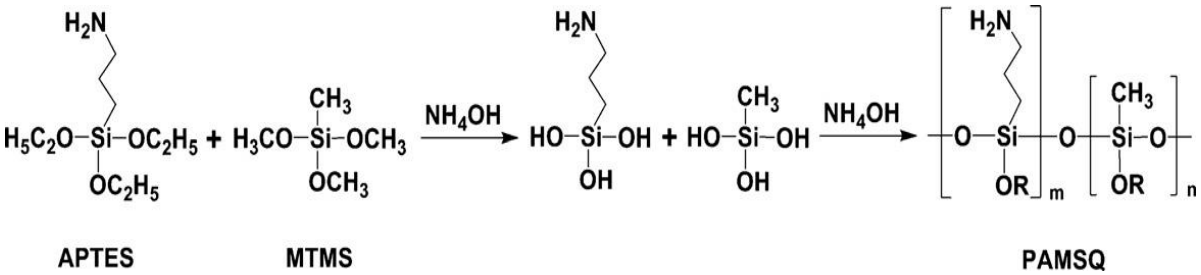


***Scheme 1.*** *Schematic illustration of the synthetic strategy for PAMSQ particles. Note that "OR" can present either silanol (OH) or other silane units* [1].

Synthesis of micron-$SiO_2$ nano Ag particles: In this paper Micron-$SiO_2$ nano Ag particle shave been synthesized using a certain amount $AgNO_3$ aqueous solution and PAMSQ. Then $NaBH_4$ (10ml) dropped into Relevant solution and stirred at room temperature for 5 h. The reaction After 5 h of stirring, the solution changed to dark color which illustrated that the reduction of Ag+ was completed. Finally, the as synthesized particles were dried at 60$^{\circ C}$ in the oven [2].

***Keywords:*** *polysiloxan, polymer, Micron-$SiO_2$ nano Ag particles*

## References

[1] X. Lu, Q. Yin, Z. Xin, Y. Li and T. Han, *J. Hazard. Mater.*, **2011**, *196*, 234-241.
[2] M. Wang, D. Tian, P. Tian and L. Yuan, *Appl. Surf. Sci.*, **2013**, *283*, 389-395.

# Magnetically Nanoparticles of Antimony-Modified Nickel Ferrite: An Efficient Catalyst for Synthesis of Biscoumarins from 4-Hydroxycoumarin and Aromatic Aldehydes

**Behzad Zeynizadeh and Maedeh Rabiei***

Faculty of Chemistry, Urmia University, Urmia 5756151818, Iran,
*E-mail: rabiei.maedeh72@gmail.com*

4-Hydroxycoumarin and its derivatives are known for their anticoagulant [1], spasmolytic [2], antibacterial, and antifungal activities [3]. In addition, certain derivatives have also been reported as antitumor and anti-HIV agents. Besides, coumarins find diverse applications as agrochemicals. Bis (4-hydroxycoumarin-3-yl) methanes are obtained by the condensation of two molecules of 4-hydroxycoumarin with one reusable catalyst. This subject prompted us to prepare $NiFe_2O_4$/Sb as an efficient nanocatalyst toward synthesis of bis-coumarins with 4-hydroxycoumarin and aromatic aldehydes in ethylene glycol (Scheme 1). High activity and easy separation makes $NiFe_2O_4$/Sb as an ideal catalyst for this transformation. The procedure has the advantages of mild reaction conditions, high yields of products, short reaction time, and simple experimental technique, making it a useful and attractive process.

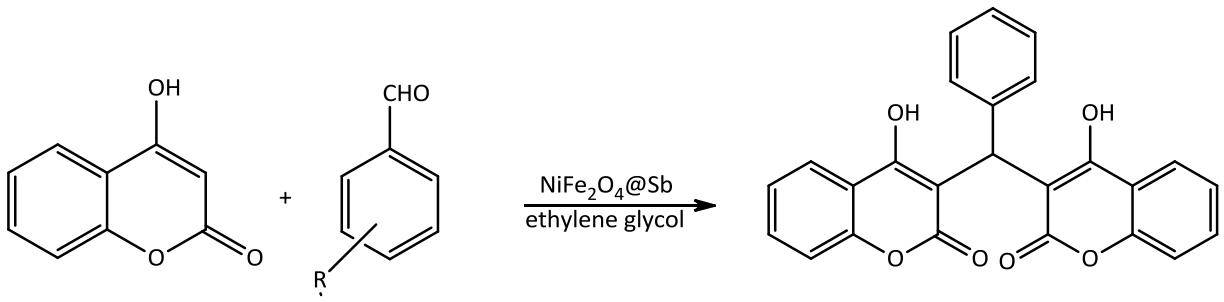


***Scheme 1.*** *Synthesis of biscoumarins with $NiFe_2O_4$/Sb*

***Keywords:*** *Biscoumarin, 4-hydroxycoumarin , $NiFe_2O_4$*

## References

[1] R.S. Overman, M.A. Stahmann, C.F. Huebner, W.R. Sullivan, L. Spero, D.G. Doherty, M. Ikawa, L. Graf, S. Roseman and K.P. Link, *J. Biol. Chem.*, **1944**, *153*, 5-24.
[2] I. Kostova, I. Manolov, I. Nicolova, S. Konstantinov and M. Karaivanova, *Eur. J. Med. Chem.*, **2001**, *36*, 339-347.
[3] Z.H. Chohan, A.U. Shaikh, A. Rauf and C.T. Supuran, *J. Enzyme Inhib. Med. Chem.*, **2006**, *21*, 741-748.

# Efficient One-Pot synthesis of hantzsch 1,4- dihydropyridine derivatives using magnetic nickel ferrite nanoparticles as a heterogeneous and reusable catalyst

**Saeid Taghavi Fardood [1,*], Shahin Abdpour[1], Morteza Ayubi[1], Ali Ramazani[1]**
[1]Department of Chemistry, University of Zanjan, Zanjan, Iran
[2]Research Institute of Modern Biological Techniques (RIMBT), University of Zanjan, Zanjan, Iran
*E-mail: saeidt64@gmail.com*

In recent years, magnetic nanoparticles (MNPs) have emerged as an attracting class of catalysts, because of the increasing need to develop low-cost, green, efficient, and reusable catalysts. Their nano-size property maximizes the contact between reactants and the catalyst, thus mimicking a heterogeneous catalyst. Use of magnetically separable catalysts is one of the most promising strategies. These systems combine the advantages of nanosized catalysts and magnetic properties, thus, providing the opportunity for quantitative recovery of the catalyst by the use of an external magnet, making it cost-effective and potentially applicable for industrial application [1,2].
Quinoline derivatives with 1,4-dihydropyridine scaffolding have pharmacological properties. Some compounds of this family are antimalarial, anti-asthmatic, anti-inflammatory, antibacterial, and tyrosine kinase inhibiting agents. Other researches indicate that 1,4-DHPs express different medical functions as neuroprotectants, having platelet anti-aggregatory activity, cerebral anti-ischemic agents, and chemosensitizers. Also, numerous synthetic methods by MCRs have been reported for the preparation of 1,4-dihydropyridine derivatives under different conditions [3].
In this work, a green, convenient, and environment-friendly approach for the synthesis of biologically active Hantzsch 1,4-dihydropyridine derivatives in the presence of magnetic nickel ferrite nanoparticles, as a heterogeneous and reusable catalyst, has been developed via a one-pot multicomponent reaction of various aldehydes, ethyl acetoacetate and ammonium acetate in solvent-free conditions under microwave irradiation. The proposed methodology is capable of providing the desired products in good to excellent yields and short reaction time with straightforward work-up and a low-cost procedure (Scheme 1).

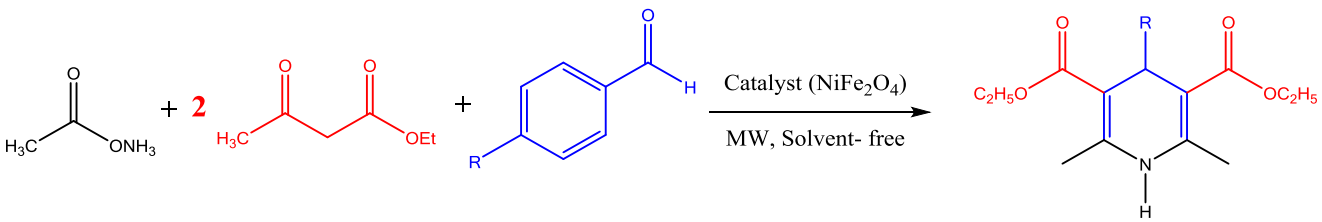


**Scheme 1.** Synthesis of 1,4- dihydropyridine derivatives

***Keywords:*** *Nickel ferrite, Hantzsch 1,4-dihydropyridine derivatives, Magnetic catalyst.*

## References

[1] P. Sivakumar, R. Ramesh, A. Ramanand, S. Ponnusamy and C. Muthamizhchelvan, *Mater. Res. Bull.*, **2011**, *46*, 2208-2211.
[2] M.R. Poor Heravi and N. Morsalie, *Iran. Chem. Commun.*, **2017**, *6*, 1-6.
[3] M. Yarhosseini, S. Javanshir, M.G. Dekamin and M. Farhadnia, *Monatsh. Chem.*, **2016**, *147*, 1779-1787.

# Ciric acid as a green catalyst for the synthesis of substituted pyrroles under eco-friendly conditions

**Zahra Hosseinzadeh[1,*], Ali Ramazani[1], Saeid Taghavi-Fardood[1], Nadia Fattahi[1], Nima Razzaghi-Asl[2]**
[1]Department of Chemistry, University of Zanjan, Zanjan, Iran
[2]Department of Medicinal Chemistry, School of Pharmacy, Ardabil University of Medical Sciences, Ardabil, Iran
*E-mail: zahra.hosseinzadeh@znu.ac.ir

Pyrroles are very important compounds as they exist in a large number of natural product and show a variety of biological and pharmacological effects. A diverse range of pharmacological properties,

Including antibacterial, antitumor, anti-infammatory, antioxidant, antianginal and antifungal activities of this important class of heterocycles has been reported in the literature [1-3]. Citric acid (2-hydroxy-1,2,3-propanetricarboxylic acid) is a weak organic acid of huge industrial importance. It was known as harmless to the environment and commercially available with stability toward humidity. The aim of the present work was to search simple and green method for the preparation of substituted pyrroles. Green synthesis, high yields of the products and reusability of the catalyst and free of formation of any hazardous by products are some of important advantages of this procedure.

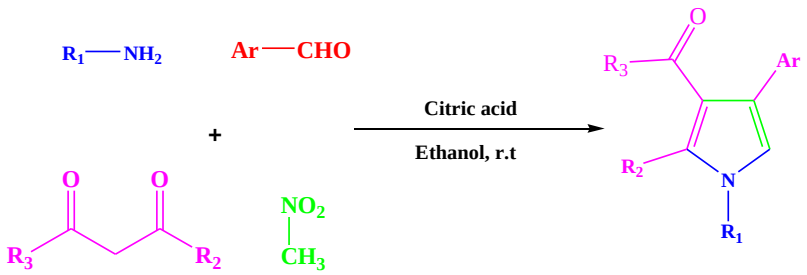


***Scheme 1.*** *Synthesis of substituted pyrroles*

***Keywords:*** *Citric acid, Substituted Pyrroles, Green Chemistry*

## References

[1] H. Fan, J. Peng, M.T. Hamann and J.-F. Hu, *Chem. Rev.*, **2008**, *108*, 264-287.
[2] M. Reisser and G. Maas, *J. Org. Chem.*, **2004**, *69*, 4913-4924.
[3] J. Lehuédé, B. Fauconneau, L. Barrier, M. Ourakow, A. Piriou and J.-M. Vierfond, *Eur. J. Med. Chem.*, **1999**, *34*, 991-996.

# $SnCl_2.2H_2O$ as a green and readily available catalyst for the preparation of 2H-indazolo [1,2-b]-phthalazine-triones under solvent free and microwave irradiation Conditions

**Fateme Yekke Zare[1], Saeid Taghavi Fardood[1,*], Ali Ramazani[1]**
[1]Department of Chemistry, University of Zanjan, Zanjan, Iran
[2]Research Institute of Modern Biological Techniques (RIMBT), University of Zanjan, Zanjan, Iran
*E-mail: saeidt64@gmail.com

Generally, nitrogen containing heterocyclic compounds have a wide range of pharmacological and clinical applications. Among them, phthalazine derivatives have been given considerable attention in recent years because of their wide range of pharmaceutical and biological activities such as antimicrobial, anticonvulsant, antifungal, anticancer, and anti-inflammatory. Moreover, these compounds display good agreement as new luminescent materials or fluorescence probes. In recent years, the development of new methods for the synthesis of heterocyclic rings containing phthalazine is an interesting challenge and therefore a number of procedures have been reported for the synthesis of phthalazine derivatives [1-3]. The first synthesis of indazolo[1,2-b]-phthalazinetriones was reported by Bazgir et al. [4] using p-toluene sulfonic acid (p-TSA) as a catalyst.

In this work, an efficient and eco-friendly procedure has been developed for the synthesis of biologically active heterocyclic compounds including 2H-indazolo[1,2-b]-phthalazinetriones in the presence of $SnCl_2.2H_2O$ as a catalyst through a one-pot three-component condensation reaction of aromatic aldehydes, dimedone, and phthalhydrazide without solvent under microwave irradiation (scheme 1). The present approach provides several advantages such as excellent yields, mild reaction conditions, short reaction times, easy workup compared to the conventional method of syntheses.

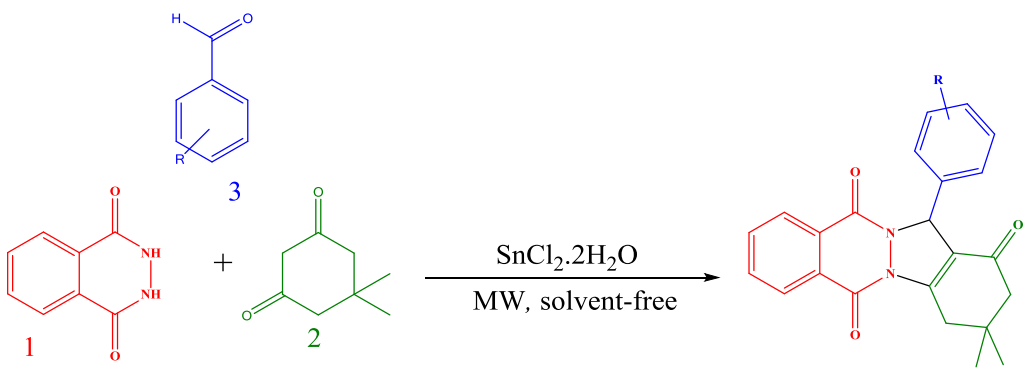


***Scheme 1.*** *Three-component reaction of dimedone, phthalhydrazide and aromatic aldehydes*

***Keywords:*** *$SnCl_2.2H_2O$, 2H-Indazolo [1,2-b]-phthalazine-trione, Multicomponent reaction*

## References

[1] W. Xiao, M. Wei-Wei, W. Li-Qiang and Y. Fu-Lin, *J. Chin. Chem. Soc.*, **2010**, *57*, 1341-1345.
[2] H. Wu, X.-M. Chen, Y. Wan, H.-Q. Xin, H.-H. Xu, R. Ma, C.-H. Yue and L.-L. Pang, *Lett. Org. Chem.*, **2009**, *6*, 219-223.
[3] F. Khajoee Nejad, M. Khosravan, S.Y. Ebrahimipour and F. Bisceglie, *Appl. Organomet. Chem.*, **2018**, *32*, e3907.
[4] M. Sayyafi, M. Seyyedhamzeh, H.R. Khavasi and A. Bazgir, *Tetrahedron*, **2008**, *64*, 2375-2378.

# Shape Control of Zn(II) Metal–Organic Frameworks by Modulation Synthesis and Their Morphology-Dependent Catalytic Performance

**Fatemeh Rafizadeh Masuleh[a], Mohammad Yaser Masoomi[a], Ali Morsali[a,*]**

[a] Department of Chemistry, Faculty of Sciences, Tarbiat Modares University, P.O. Box 14117-13116, Tehran, Islamic Republic of Iran

*E-mail: morsali_a@modares.ac.ir

Micro- and nanorods and plates of three porous Zn(II)-based metal−organic frameworks, $[Zn_2(oba)_2(4\text{-bpdb})]_n\cdot 2(DMF)$ (TMU-4), $[Zn(oba)(4\text{-bpdh})_{0.5}]_n\cdot 1.5(DMF)$ (TMU-5), and $[Zn(oba)(4\text{-bpmb})_{0.5}]_n$ 1.5(DMF) (TMU-6) were synthesized by the coordination modulation method. The effects of concentration of modulator, temperature, and time of reaction on size and morphology have been investigated. Also, catalytic performance of TMU-5 nanosized metal−organic framework in Knoevenagel condensation reaction was evaluated.

*Keywords: Metal-Organic Frameworks, MOF, Catalysis*


## References

[1] Masoomi, M. Y.; Morsali, A. *RSC Adv.* **2013**, *3*, 19191−19218.
[2] Yaghi, O. M.; Li, H.; Davis, C.; Richardson, D.; Groy, T. L. *Acc. Chem. Res.* **1998**, *31*, 474−484.

# Efficient one pot synthesis of 1,8-dioxo-octahydroxanthene derivatives using $ZnAl_2O_4$ nanoparticles as a catalyst

**Sara Ganjkhanlu[1], Saeid Taghavi Fardood[1,*], Ali Ramazani[1,2]**
[1]Department of Chemistry, University of Zanjan, Zanjan, Iran
[2]Research Institute of Modern Biological Techniques (RIMBT), University of Zanjan, Zanjan, Iran
*E-mail: saeidt64@gmail.com

1,8-dioxo-octahydroxanthenes are important class of oxygen heterocycles in which a phenyl substituted pyran ring is fused on either side with two cyclohexanone rings. Presence of conjugated bis-dienone functionality makes these compounds sensitive to be attacked by nucleophiles and light energy. In the past decade, synthesis of xanthenes derivatives has been of considerable interest to organic chemists because they possess various biological and pharmaceuticals activities such as antiviral, antibacterial and anti-inflammatory properties. These are being utilized as antagonists for paralyzing action of zoxazolamine and in photodynamic therapy [1,2]. Xanthenes and benzoxanthenes derivatives are the parent frame works found in a large number of naturally occurring as well as synthetic products possessing prominent position in medicinal chemistry. Xanthenediones are likewise special structural units constituting various natural products and being used as versatile synthons, because of inherent reactivity of their inbuilt pyran ring [3,4].
In this work, 1,8-Dioxo-octahydroxanthenes have efficiently been synthesized from dimedone and aromatic aldehydes using $ZnAl_2O_4$ spinel nanoparticles as a heterogeneous catalyst in ethanol media (scheme 1). The experimental procedure is very simple and the products are formed in high yields.

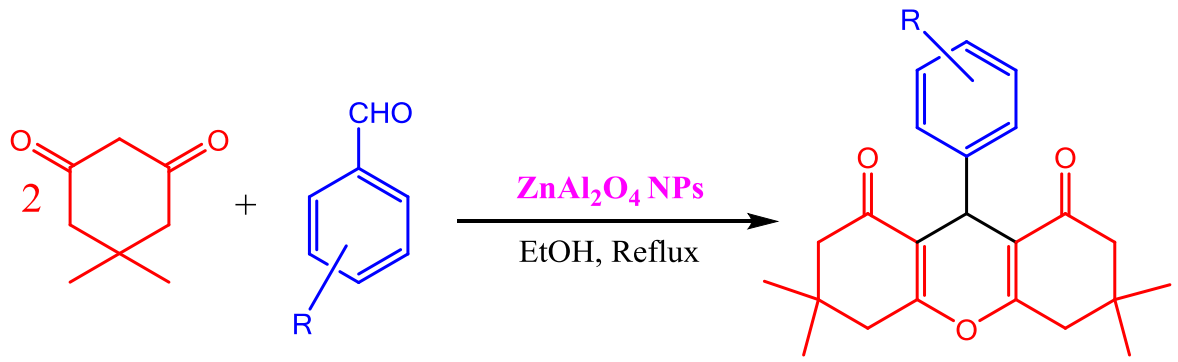


***Scheme 1.*** *One pot synthesis of 1,8-dioxo-octahydroxanthene derivatives using $ZnAl_2O_4$ as a catalyst.*

***Keywords:*** *$ZnAl_2O_4$ nanoparticles, 1,8-dioxo-octahydroxanthene derivatives, heterogeneous catalyst*

## References

[1] N. Mulakayala, G.P. Kumar, D. Rambabu, M. Aeluri, M.B. Rao and M. Pal, *Tetrahedron Lett.*, **2012**, *53*, 6923-6926.
[2] B. Das, P. Thirupathi, K.R. Reddy, B. Ravikanth and L. Nagarapu, *Catal. Commun.*, **2007**, *8*, 535-538.
[3] K. Gong, H. Wang, S. Wang, Y. Wang and J. Chen, *Chin. J. Catal.*, **2015**, *36*, 1249-1255.
[4] H.N. Karade, M. Sathe and M. Kaushik, *Arkivoc*, **2007**, *13*, 252-258.

# Photocatalytic degradation of reactive blue 21 dye *via* $Zn_{0.5}Cu_{0.5}Mn_2O_4$ spinel nanoparticles

**Farzaneh Moradnia[1,]*, Saeid Taghavi Fardood[1], Ali Ramazani[1,2], Ilnaz Abdolmaleki[3]**
[1]Department of Chemistry, University of Zanjan, Zanjan, Iran
[2]Research Institute of Modern Biological Techniques (RIMBT), University of Zanjan, Zanjan, Iran
[3]Department of Science, Payame Noor University (PNU), PO Box 19395-4697, Tehran, Iran
*E-mail: farzaneh2856@gmail.com

Nanotechnology can be described as the capability to operate, measure, make and manufacture the particles at the size of 1–100 nm [1]. Materials and it Nanotechnology is an interdisciplinary knowledge, it is the interdisciplinary, including toxicology, medical, physics, chemistry, biology, mechanics, engineering, and recently environment [2]. Water pollution is categorized as part of the main types of environmental pollution. Water pollution has harmful effects on the environment and also on the living, so providing a solution to reduce water pollution is particularly important [3]. Among the pollutant agent, we can point to organic dyes from industrial processes and textile as one of the main polluting water sources and create an important environmental crisis. Photocatalysis is considered as one of the important and efficient approaches to dismiss the dyes in wastewater [4,5]. The photocatalytic activity of $Zn_{0.5}Cu_{0.5}Mn_2O_4$ photo-catalyst was evaluated in the degradation of reactive blue 21 dye at room temperature in aqueous solution so that 95% of reactive blue 21 dye was degraded in 60 min. $Zn_{0.5}Cu_{0.5}Mn_2O_4$ spinel nanoparticles characterized by energy dispersive X-ray analysis (EDX), powder X-ray diffraction (XRD), field emission scanning electron microscopy (FESEM), Fourier transforms infrared spectroscopy (FTIR), and percent of RB21 degradation which was followed by UV–Visible spectroscopy.

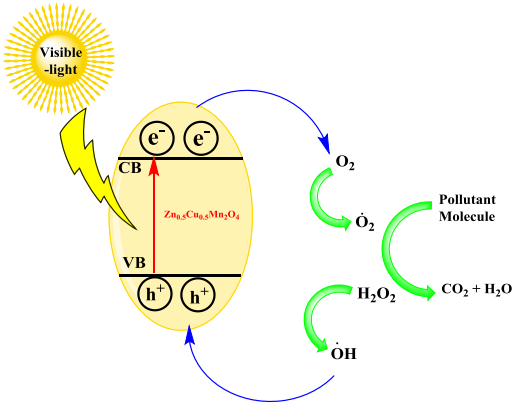


***Fig 1.*** *Proposed mechanism for the photodegradation of dye*

***Keywords:*** *Photocatalytic activity, $Zn_{0.5}Cu_{0.5}Mn_2O_4$ Spinel nanoparticles, Reactive blue 21.*

## References

[1] K.L. Kelly, E. Coronado, L.L. Zhao and G.C. Schatz, *J. Phys. Chem. B*, **2003**, *107*, 668-677.
[2] X. Zhang, M. Yang, X. Zhao, Y. Wang, M. Wang and L. Ma, *J. Mater. Sci. Mater. Electron.*, **2015**, *26*, 6366-6372.
[3] K.P. Singh, S. Gupta, A.K. Singh and S. Sinha, *J. Hazard. Mater.*, **2011**, *186*, 1462-1473.
[4] L. Zhao, X. Li and J. Zhao, *Appl. Surf. Sci.*, **2013**, *268*, 274-277.
[5] M. Ramezani, S.M. Hosseinpour-Mashkani, A. Sobhani-Nasab and H. Ghasemi Estarki, *J. Mater. Sci. Mater. Electron.*, **2015**, *26*, 7588-7594.

# Mechanosynthesis of new azine-functionalized Zn(II) metal–organic frameworks for improved catalytic performance

**Mahsa Abbasi Azad, Mohammad Yaser Masoomi, Saeideh Beheshti, Ali Morsali***
[1]Department of Chemistry, Faculty of Sciences, Tarbiat Modares University, Tehran, Iran
**E-mail: morsali_a@modares.ac.ir*

Knoevenagel condensation of aldehydes with active methylene compounds is a usefultransformation that has been widely employed for carbon–carbon bond formation in the synthesis of several fine chemicals. The condensation is usually catalyzed by solid bases like alkali or alkaline-earth metal oxides. Over the last few years, a wide range of catalysts have been investigated for this reaction such as Lewis acids, amine-functionalized solid supports, cation-exchanged zeolites, ionic liquids and organometallic catalysts. However, most of these methods have significant drawbacks, such as using hazardous and carcinogenic solvents, high catalyst loading or non-recoverable catalysts that sometimes contain toxic metals. Therefore, there is a great need for new catalytic methods that do not have these problems. MOFs have shown a high catalytic activity to promote condensation reactions. Three 3D, porous Zn(II)-based metal–organic frameworks, TMU-4, TMU-5 and TMU-6, containing azine-functionalized pores, were readily and quickly prepared via mechanosynthesis. Catalytic performance of these MOFs and the effect of N-donor ligands with diverse basicity in the Knoevenagel condensation reaction are investigated. Increasing the basicity of N-donor ligands leads to improvement in catalytic activity. Results show that among the three compounds, TMU-5 has the highest catalytic activity upon increasing its basicity of azine function in the N-donor ligand. These catalysts maintain their crystalline framework after the reaction and are easily recycled [1,2].

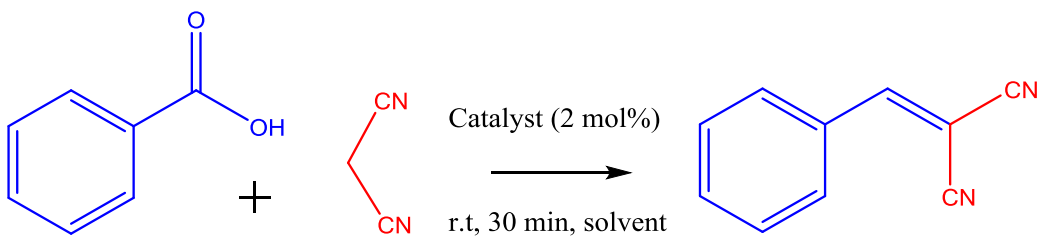


***Scheme 1.*** *Synthesis of Benzylidenemalononitrile*

***Keywords:*** *metal–organic framework, Knoevenagel condensation reaction, catalyst.*

## References

[1] M.Y. Masoomi, K.C. Stylianou, A. Morsali, P. Retailleau and D. Maspoch, *Cryst. Growth Des.*, **2014**, *14*, 2092-2096.
[2] S.-N. Kim, S.-T. Yang, J. Kim, J.-E. Park and W.-S. Ahn, *CrystEngComm*, **2012**, *14*, 4142-4147.

# Microwave-assisted multicomponent reaction for the synthesis of 2-amino-4,6-diphenylpyridine-3-carbonitrile derivatives using ZnO nanoparticles as a catalyst

**Saeid Taghavi Fardood[1,*], Vahid Faramarzi[1], Ali Ramazani[1,2]**
[1]Department of Chemistry, University of Zanjan, Zanjan, Iran
[2]Research Institute of Modern Biological Techniques (RIMBT), University of Zanjan, Zanjan, Iran
*E-mail: saeidt64@gmail.com*

Functionalized nitrogen-heterocycles play a predominant role in medicinal chemistry. The pyridine nucleus is prevalent in numerous natural products and is extremely important in the chemistry of biological systems. It plays a key role catalyzing both biological and chemical systems. Many pyridine derivatives are of commercial interest and find application in areas where bioactivity is important, as in medicinal drugs [1]. Some of them have been used as herbicides, fungicides, pesticides, medicines, and dyes. Several cyanopyridine moiety compounds show interesting pharmacological and chemotherapeutic activities, such as anticancer, antitubercular, antimicrobial, etc. [2,3].

In the current project, a green and convenient approach to the synthesis of 2-amino-4,6-diphenylpyridine-3-carbonitrile *via* four-component reaction of malononitrile, aromatic aldehydes, acetophenone and ammonium acetate in the presence of ZnO nanoparticles as a highly effective heterogeneous catalyst under solvent free and microwave irradiation conditions is described (scheme 1). This method has the advantage of short routine, high yields and being environmentally-friendly. The catalyst could be quantitatively recovered from the reaction mixture by simple filtration and reused at least eight times with almost consistent activity.

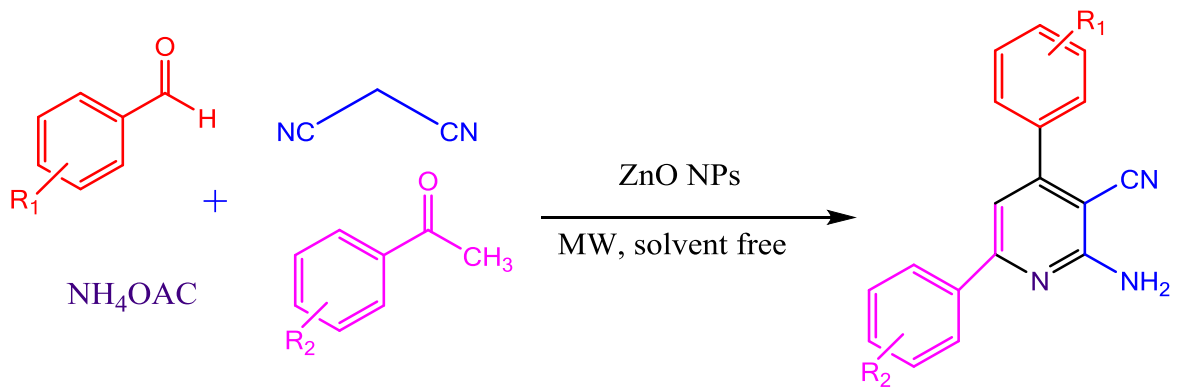


***Scheme 1.*** *One-pot synthesis of 2-amino-4,6-diphenylpyridine-3-carbonitrile*

***Keywords:*** *Microwave irradiation, ZnO nanoparticles, 2-amino-4,6-diphenylpyridine-3-carbonitrile*

## References

[1] N.R. Challa, B. Mamidisetty, M.R. Ghanta and P.R. Padi, *J. Saudi. Chem. Soc.*, **2014**, *18*, 513-519.
[2] H. Sheibani, K. Saidi, M. Abbasnejad, A. Derakhshani and I. Mohammadzadeh, *Arabian J. Chem.*, **2016**, *9*, S901-S906.
[3] S.S. Mansoor, K. Aswin, K. Logaiya and S. Sudhan, *J. Saudi. Chem. Soc.*, **2016**, *20*, 517-522.

# Application of $CoCrMnO_4$ spinel Nanoparticles as a photocatalyst for degradation of organic dyes under visible light

**Farzaneh Moradnia[1], Saeid Taghavi Fardood[1,*], Ali Ramazani[1,2]**
[1]Department of Chemistry, University of Zanjan, Zanjan, Iran
[2]Research Institute of Modern Biological Techniques (RIMBT), University of Zanjan, Zanjan, Iran
*E-mail: saeidt64@gmail.com*

Spinel is a cubic structure with the public formula $AB_2O_4$, that A and B are cations settled in the tetrahedral and octahedral positions, respectively. therefore, a spinel has 56 atoms in any one cell. The dispensation of ions in A and B sites are subject to the ion equilibrium [1]. Materials and it Nanotechnology is an interdisciplinary knowledge, it is the interdisciplinary, including toxicology, medical, physics, chemistry, biology, mechanics, engineering, and recently environment [2]. in the last decade, environmental pollution has enhancement more and more public worry. for example, wastewater including dyes arriving from paper, textiles, plastic and leather industries is usually high in organic compounds and color [3]. This pollutant agent create important environmental problems. So, providing effective and efficient method for their removal from wastewater is necessary. Photocatalysis is one of this efficient approach to remove the dyes from wastewater [4]. Among the pollutant agent, we can point to organic dyes from industrial processes and textile as one of the main polluting water sources and create an important environmental crisis. Photocatalysis is considered as one of the important and efficient approaches to dismiss the dyes in wastewater [5]. In this paper a novel and inexpensive route for the preparation of spinel $CoCrMnO_4$ nanoparticles is proposed and Congo red was used as model dye. The obtained nanoparticles were then identified using different analytical techniques such as Fourier transform infrared spectroscopy (FTIR), X-ray powder diffraction (XRD), and field emission scanning electron microscopy (FESEM). The X-ray powder diffraction (XRD) confirmed the formation of cubic spinel phase $CoCrMnO_4$. The photocatalytic activity of $CoCrMnO_4$ nanoparticles were studied by performing the decomposition of Congo red dye under visible light irradiation. The effects of process parameters like, catalyst dosage, initial dye concentration, and visible light irradiation on dye degradation have been investigated.

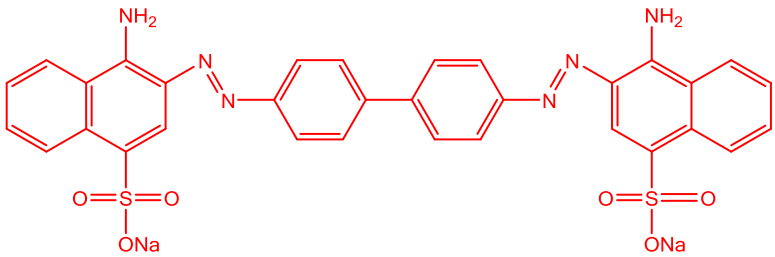


***Fig 1.*** *Structure of Congo red*

***Keywords:*** *$CoCrMnO_4$ Spinel nanoparticles, Photocatalytic activity, Congo red.*

## References

[1] X. Huang, J. Zhang, S. Xiao, T. Sang and G. Chen, *Mater. Lett.*, **2014**, *124*, 126-128.
[2] X. Zhang, M. Yang, X. Zhao, Y. Wang, M. Wang and L. Ma, *J. Mater. Sci. Mater. Electron.*, **2015**, *26*, 6366-6372.
[3] R. Talebi, *J. Mater. Sci. Mater. Electron.*, **2016**, *27*, 6974-6978.
[4] P. Rajaei and M. Ranjbar, *J. Mater. Sci. Mater. Electron.*, **2016**, *27*, 1708-1712.
[5] L. Zhao, X. Li and J. Zhao, *Appl. Surf. Sci.*, **2013**, *268*, 274-277.

# Synthesis and characterization of a new nano molybdenum complex derived from (E)-2-hydroxy-5-(4-nitrophenyl)diazenyl benzaldehyde and $Fe_3O_4$@$SiO_2$ and investigation of its catalyst and photophysical properties

**Ehsan Mohseni[1], Saeed Menati[1*] ,**
[1]Department of Chemistry, Khorramabad Branch, Islamic Azad University, Khorramabad, Iran
*E-mail:Saiedmenati@gmail.com

In this work, a heterogeneous nanocatalyst was prepared via branch coated of dioxomolybdenum(VI) schiff base complex on the core shell structure $Fe_3O_4$@$SiO_2$.The properties and the nature of the surface-fixed complex identified by a set of characterization techniques such as, fourier transform infrared spectroscopy (FT-IR), scanning electron microscopy (SEM) and energy dispersive x-ray analysis (EDX) and vibrating sample magnetometry (VSM). The synthesized hybrid material an efficient nanocatalyst for the selective epoxidation of alkenes using tert-butyl hydroperoxide as an oxidant in 1,2-dichloroethane in high yield and selectivity.Epoxidation of alkens in the presence of nanocatalyst was performed more efficiently. We were able the supermagnetic nanocatalyst to separate by using and external magnetic field. And to use the nanocatalyst at least five successive times without significant decrease in conversion. The supermagnetic nanocatalyst has advantages in catalytic activity, selectivity, catalytic reaction and reusability by easy separation.

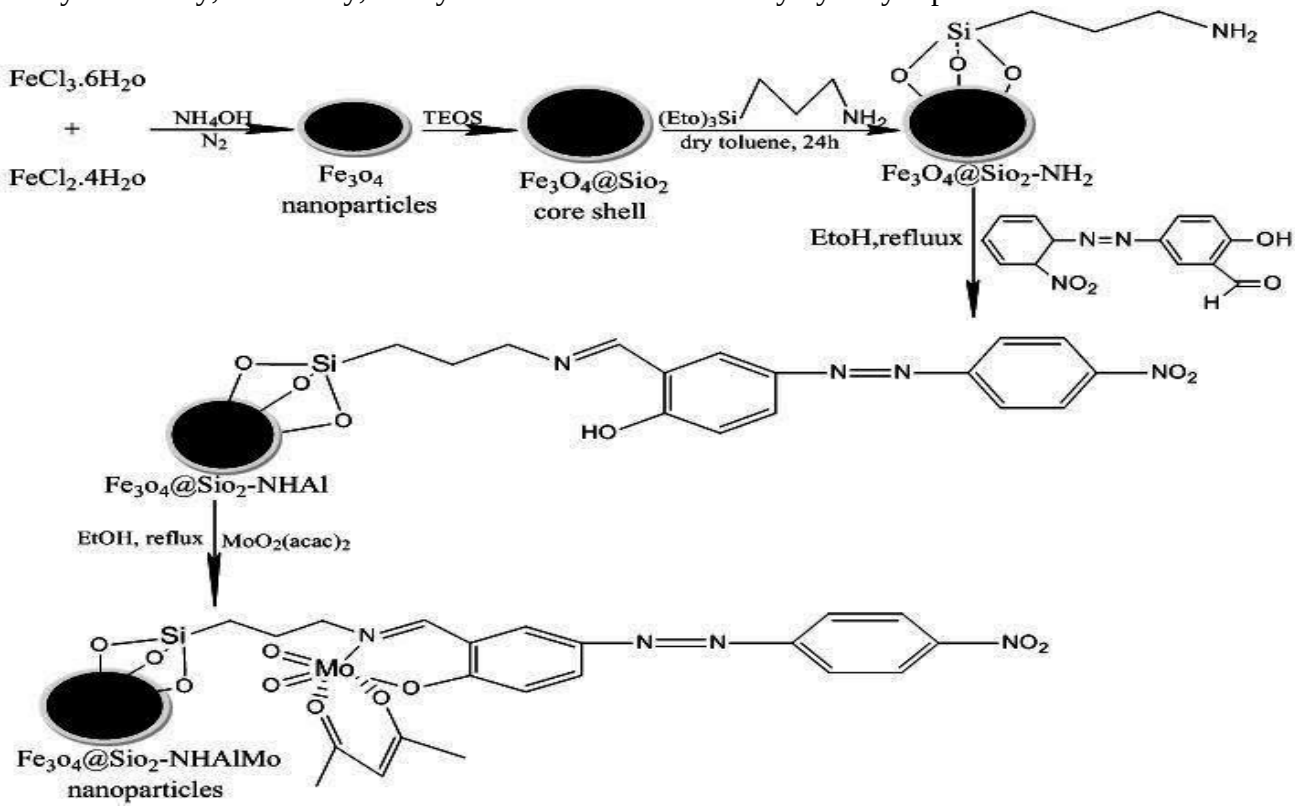


***Scheme 1.*** *Synthesis of nanocatalyst molybdenum (VI)*

***Keywords:*** *Nanoparticles, Nanocatalyst, Core-shell, Epoxidation*

## References

[1] P. j. Robinson, P. Dunni, and M.D. lilli, Biotechnol, (**1973**)15-603-606.
[2] P. Bhattacharya, S. Frisbie, E. Smith, R. Naidu, G. Jacks and B. Sarkar, *Handbook of heavy metals in the environment. Marcell Dekker Inc., New York*, **2002**, 147-215.

# The Study of the Catalytic Activity in the Mn(II) Coordination Polymer

**Ahmad Morsali***, **Hassan Hosseini-Monfared**
Department of Chemistry, University of Zanjan, Zanjan, Iran
**E-mail: morsaliahmad@yahoo.com*

The favorable design and syntheses of novel coordination polymers have attracted a great attention not only due to the fascinating structural motifs of them but also because of their promising applications such as catalysis, magnetism, nonlinear optics and luminescence [1,2]. In industry, synthesis of chemical compounds is often accompanied by environmental pollution and hazardous substances are released into the environment. The use of heterogeneous catalysts is a useful way to reduce such contamination [3]. In this work, a Mn(II) coordination polymer of formulation $[Mn(L1)_2(N_3)_2]_n$ (1), L1 =3,4-bis(4-pyridyl)-5-(2-pyridyl)-1,2,4-triazole, synthesized and it was characterized by X-ray crystallography, thermal studies, elemental analysis, IR, $^1$H NMR and $^{13}$C NMR spectroscopy. Nanostructures of **1** was prepareded by sonochemical process at ambient temperature. The catalytic operation of this compound was investigated.

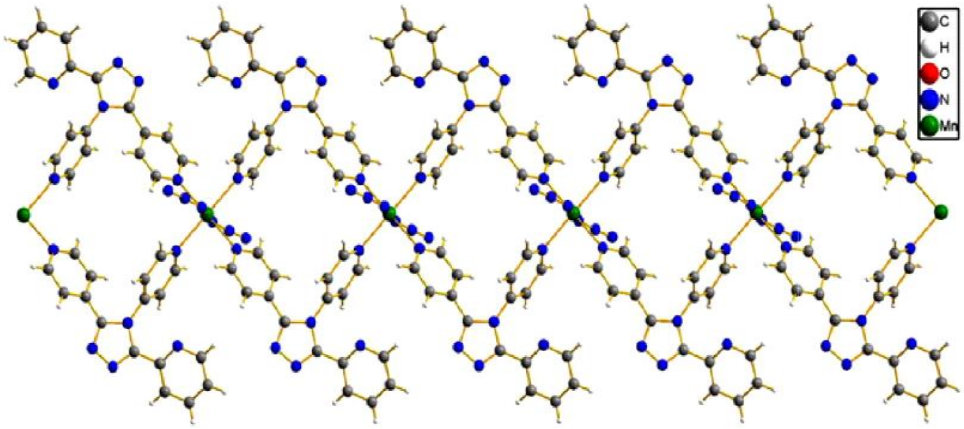


***Scheme 1.*** *Depiction of the layers of 1-D coordination polymer $[Mn(L_1)_2(N_3)_2]_n$ (**1**) constructed by L1 bridges.*

***Keywords:*** *Mn(II) coordination polymer, nanostructure, catalysis.*

## References

[1] F. Bigdeli, A. Morsali and P. Retailleau, *Polyhedron*, **2010**, *29*, 801-806.
[2] A. Bhunia, M.A. Gotthardt, M. Yadav, M.T. Gamer, A. Eichhöfer, W. Kleist and P.W. Roesky, *Chemistry–A European Journal*, **2013**, *19*, 1986-1995.
[3] F. Bigdeli, S. Abedi, H. Hosseini-Monfared and A. Morsali, *Inorg. Chem. Commun.*, **2016**, *72*, 122-127.

# Nickel oxide nanoparticles as an efficient catalyst for one-pot synthesis of 1-amidoalkyl-2-naphthol derivatives

**Saeid Taghavi Fardood [1,*], Morteza Ayubi[1], Shahin Abdpour[1], Ali Ramazani[1,2]**
[1]Department of Chemistry, University of Zanjan, Zanjan, Iran
[2]Research Institute of Modern Biological Techniques (RIMBT), University of Zanjan, Zanjan, Iran
*E-mail: saeidt64@gmail.com*

1-amidoalkyl-2-naphthols and their derivatives bearing 1,3-amino oxygenated functional groups are the key intermediate in number of natural products and synthetic pharmaceuticals and act as potential drugs in number of nucleoside antibiotics and HIV protease inhibitors. In addition, they also shows potential biological activities, such as antibiotic, anticonvulsant, antimalarial, antihypertensive, antitumor, antirheumatic, analgesic, antipsychotic, antianginal. Owing to their unique biological profile, synthesis of 1-Amidoalkyl-2-naphthols and their derivatives is of prime task for the organic chemist. The synthesis of 1-amidoalkyl-2-naphthols has been carried out by multi-component condensation reaction of 2-naphthol, aromatic aldehydes, and acetonitrile or various amides in the presence of different catalysts [1,2].

In modern science, one of the growing and important fields is nanotechnology. Because of different physical and chemical properties of nano-sized catalysts in comparison with bulk material, they attract interest from different researcher areas. Since the particles are in small size, the surface area exposed to the reactant is maximized, thus allowing more reactions to occur at the same time; hence, the process is speeded up. Among various metal nanostructures, nickel oxide nanoparticles have been employed as heterogeneous catalysts for various organic transformations. An increasing number of examples are available in the literature where Nickel-based nanoparticles have been used as catalysts during organic transformations [3,4]. Since these nanoparticles are often recovered easily by simple workup, which prevent contamination of products, they may be considered as promising, safe, and reusable catalysts compared to traditional catalysts. In this work, an efficient catalytic protocol for the synthesis of 1-amidoalkyl-2-naphthol derivatives is developed in a one-pot three-component approach involving β-naphthol, aromatic aldehydes and urea under microwave irradiation in solvent free condition (scheme 1). The advantageous features of this methodology are operational simplicity, high yield processing, and easy handling.

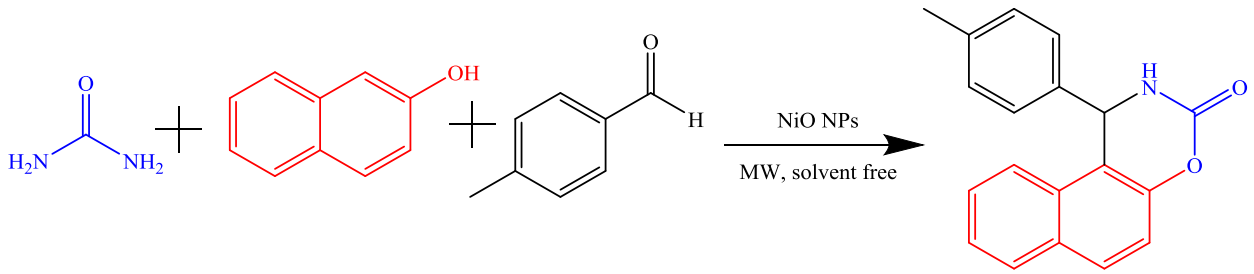


**Scheme 1.** NiO NPs catalyzed synthesis of 1-amidoalkyl-2-naphthol derivatives

***Keywords:*** *Nickel Oxide nanoparticles, 1-Amidoalkyl-2-naphthol, Microwave irradiation.*

## References

[1] H. Ren, S. Grady, D. Gamenara, H. Heinzen, P. Moyna, S.L. Croft, H. Kendrick, V. Yardley and G. Moyna, *Bioorg. Med. Chem. Lett.*, **2001**, *11*, 1851-1854.
[2] H. Taghrir, M. Ghashang and M.N. Biregan, *Chin. Chem. Lett.*, **2016**, *27*, 119-126.
[3] V. Polshettiwar, B. Baruwati and R.S. Varma, *Green Chem.*, **2009**, *11*, 127-131.
[4] F. Alonso, P. Riente and M. Yus, *Acc. Chem. Res.*, **2011**, *44*, 379-391.

# Solvent free synthesis of 3,4-dihydropyrimidine-2-(1*H*)-ones/thiones catalyzed by zinc aluminate spinel nanoparticles

**Saeid Taghavi Fardood[1,*], Sara Ganjkhanlu[1], Ali Ramazani[1,2]**
[1]Department of Chemistry, University of Zanjan, Zanjan, Iran
[2]Research Institute of Modern Biological Techniques (RIMBT), University of Zanjan, Zanjan, Iran
*E-mail: saeidt64@gmail.com

The Biginelli reaction is an acid-catalyzed, three component, reaction between an aldehyde, *β*-ketoester or *β*-diketone and urea or thiourea. Dihydropyrimidinones (DHPMs) and their derivatives have attracted considerable interest due to their wide spectra of biological activities such as antiviral, antitumor, antibacterial, anti-inflammatory and antihypertensive. The multi-component DHPM-yielding Biginelli reaction was first established in 1893 and was ignored for many years until recently [1,2].

Particular enantiomers are progressively more important for drug applications. Chiral detection allows one enantiomer to treat a disease, while another one may be harmful. An asymmetric carbon exists at the 4-position of the dihydropyrimidone ring and they are generally formulated as racemic mixtures. The absolute configuration in the center of the molecule can have important biological and pharmacological effects. In many cases chiral dihydropyrimidones have exhibited higher activities or, in the case of enantiomers, a contrary pharmacological activity [3,4].

We report herein, the usage of zinc aluminate nanoparticles as a new catalyst for three component condensation of an aldehyde, ethyl acetoacetate and urea/thiourea under solvent free conditions (scheme 1) at 100 °C to afford the corresponding 3,4-dihydropyrimidine-2-(1*H*)-ones/thiones (DHPMs) in good to excellent yields.

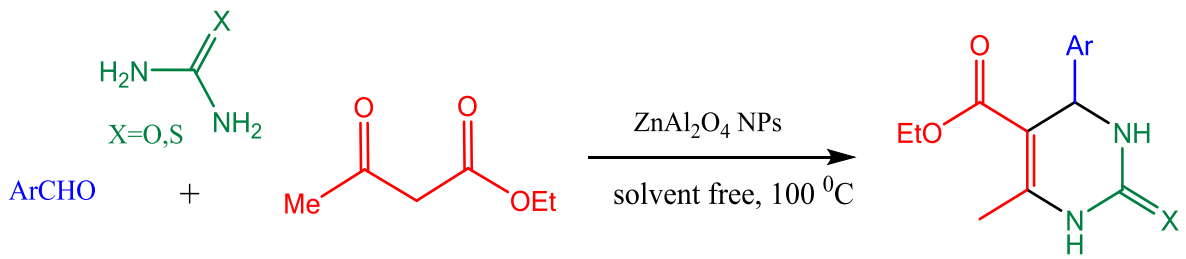


***Scheme 1.*** *Synthesis of 3,4-dihydropyrimidinones/thiones under solvent free conditions*

***Keywords:*** *Solvent free, 3,4-Dihydropyrimidinones, 3,4-Dihydropyrimidithiones*

## References

[1] C.O. Kappe, *Eur. J. Med. Chem.*, **2000**, *35*, 1043-1052.
[2] Y.L.N. Murthy, A. Rajack and K. Yuvaraj, *Arabian J. Chem.*, **2016**, *9*, S1740-S1746.
[3] N. M Thorat and S. R Thopate, *Lett. Org. Chem.*, **2015**, *12*, 210-216.
[4] M.M. Heravi, K. Bakhtiari and F.F. Bamoharram, *Catal. Commun.*, **2006**, *7*, 373-376.

# Photocatalytic degradation of acid red 14 dye by $ZnGa_2O_4$ spinel nanoparticles under visible light irradiation

**Alireza Yaghoubi[1], Saeid Taghavi Fardood[1,*]. Ali Ramazani[1,2]**
[1]Department of Chemistry, University of Zanjan, Zanjan, Iran
[2]Research Institute of Modern Biological Techniques (RIMBT), University of Zanjan, Zanjan, Iran
*E-mail: saeidt64@gmail.com

The photocatalysts consisting of p-block metal ions with $d^{10}$ configuration have different electronic structures from the conventional photocatalysts containing transition metal ions with $d^0$ configuration by the DFT (Density Functional Thoery) calculation [1]. Photocatalysts with the p-block metal ions like $Ga^{3+}$, $In^{3+}$, $Ge^{4+}$, $Sn^{4+}$ and $Sb^{5+}$ have shown high photocatalytic activities [2]. $ZnGa_2O_4$, a binary compound oxide consisting of ZnO and $Ga_2O_3$ with an optical bandgap of 4.4 eV, is widely studied as fluorescent material and photocatalyst [3].
In this paper a novel and inexpensive route for the preparation of spinel $ZnGa_2O_4$ nanoparticles is proposed. $ZnGa_2O_4$ nanoparticles photocatalyst was synthesized *via* sol–gel method using natural gel and calcination at 600 °C. This method has many advantages such as nontoxic, economic viability, ease to scale up, less time consuming and environmental friendly approach for the synthesis of $ZnGa_2O_4$ nanoparticles without using any harmful chemicals. Acid red 14 was used as model dye. The obtained nanoparticles were then identified using different analytical techniques such as Fourier transform infrared spectroscopy (FTIR), X-ray powder diffraction (XRD), and field emission scanning electron microscopy (FESEM). The X-ray powder diffraction (XRD) confirmed the formation of cubic spinel phase $ZnGa_2O_4$. The photocatalytic activity of $ZnGa_2O_4$ nanoparticles were studied by performing the decomposition of Acid red 14 dye under visible light irradiation. The effects of process parameters like, catalyst dosage, initial dye concentration, and visible light irradiation on dye degradation have been investigated.

***Keywords:*** *$ZnGa_2O_4$ Spinel nanoparticles, Photocatalytic activity, Sol-gel method.*

## References

[1] K. Ikarashi, J. Sato, H. Kobayashi, N. Saito, H. Nishiyama and Y. Inoue, *J. Phys. Chem. B*, **2002**, *106*, 9048-9053.
[2] A. Kudo and Y. Miseki, *Chem. Soc. Rev.*, **2009**, *38*, 253-278.
[3] L.-C. Tien, C.-C. Tseng, Y.-L. Chen and C.-H. Ho, *J. Alloys Compd.*, **2013**, *555*, 325-329.

# Green synthesis of $ZnZrO_3$ nanoparticles using tragacanth gel and its photocatalytic activity study in the degradation of malachite green dye under visible light irradiation

**Alireza Yaghoubi[1,*], Saeid Taghavi Fardood[1], Ali Ramazani[1,2]**
[1]Department of Chemistry, University of Zanjan, Zanjan, Iran
[2]Research Institute of Modern Biological Techniques (RIMBT), University of Zanjan, Zanjan, Iran
**E-mail:* alirezayaghoubi62@yahoo.com

The removal of organic pollutants in wastewater is a huge task in environmental protection, because they have led to serious contamination in many countries worldwide. Photosensitized degradation on an applicable catalyst has been proven to be the most widely used method. Therefore, searching for a catalyst with high efficiency has caught much attention for good piezoelectric properties, catalytic properties and damping properties [1,2].

Perovskite oxides are one of the most widely investigated classes of materials due to their important physical properties in ferroelectricity, piezoelectricity, dielectricity, ferromagnetism, magnetoresistance, and multiferroics, which find a widely variety of applications in ferroelectric random access memories, multilayer ceramic capacitors, sensors and actuators, magnetic random access memories, and the potential new types of multiple-state memories and spintronic devices controlled by electric and magnetic fields [3,4].

In this work, perovskite $ZnZrO_3$ nanoparticles have been synthesized from the reaction of zinc nitrate (($Zn(NO_3)_2$ .$6H_2O$), zirconium(IV) chloride ($ZrCl_4$) as precursors and water as the solvent, in the presence of tragacanth gel as a novel biotemplate and chelating agent by the sol-gel method.

The product was characterized by X-ray diffraction (XRD), Fourier transform infrared spectroscopy (FT-IR), scanning electron microscopy (SEM), energy dispersive analysis of X-ray (EDAX) and UV-vis spectroscopy (UV-vis). XRD data confirmed the formation of nanostructure perovskite zinc zirconate ($ZnZrO_3$) nanoparticles. Effects of some parameters such as amount of catalyst, irradiation time and initial dye concentration were studied and obtained results demonstrated that the degradation efficiency was affected by initial concentration of the dye.

***Keywords:*** *Perovskite $ZnZrO_3$ nanoparticles, Green synthesis, Photocatalytic activity.*

## References

[1] Z. Li, P. Zhang, J. Li, T. Shao, J. Wang and L. Jin, *Catal. Commun.*, **2014**, *43*, 42-46.
[2] X. Liu, L. Pan, T. Lv, Z. Sun and C.Q. Sun, *J. Colloid Interface Sci.*, **2013**, *408*, 145-150.
[3] K. Ivaniuk, V. Cherpak, P. Stakhira, G. Baryshnikov, B. Minaev, Z. Hotra, P. Turyk, Y. Zhydachevskii, D. Volyniuk, O. Aksimentyeva, B. Penyukh, A. Lazauskas, S. Tamulevičius, J.V. Grazulevicius and H. Ågren, *Dyes Pigm.*, **2017**, *145*, 399-403.
[4] X. Zhu, J. Zhou, J. Zhu, Z. Liu, Y. Li and T. Al‐Kassab, *J. Am. Ceram. Soc.*, **2014**, *97*, 1987-1992.

# Design and preparation of N-doped ordered mesoporous carbon with *Ia3d* symmetry as bifunctional enzyme-like catalyst for conversion of carbohydrates

**Hamzeh Hassanaki Veisi**[1], **Babak Karimi**[1]*
[1]Department of Chemistry, Institute for Advanced Studies in Basic Science, Zanjan, Iran
*E-mail: karimi@iasbs.ac.ir

Inspired by synergistically cooperation of two or more active sites in enzymes, we have prepared a novel bifunctional acid-base ordered mesoporous carbon denoted as **I**onic liquid derived **B**imodal cubic **O**rdered **M**esoporous **C**arbon (IBOMC) via nanocasting protocol using KIT-6 as a hard template. High basicity, significant surface acidity, high surface area, well-defined pore size, high thermal stability and high nitrogen content are the noticeable properties of this carbon that has never been collectively observed in other carbon materials. By attention to these fascinating properties, especially the balance between the basic and acidic sites, we considered the performance of this material in preparation of 5-hydroxymethylfurfural (5-HMF) as a versatile intermediate between biomass-based carbohydrate chemistry and petroleum-based industrial organic chemistry. The efficiency of this material as an acid carbocatalyst was proven in formation of 5-HMF from fructose with 98% yield. Moreover, the one-pot conversion of complex carbohydrates such as glucose, sucrose and cellulose was performed with taking advantage of the double-acting acid-base character of this carbocatalyst. It was shown that the presence of base active site is crucial for isomerization of glucose into fructose. The catalyst could be recycled up to 5 cycles. In addition, this unique catalyst displayed the excellent performance in selective aerobic oxidation of 5-HMF into Diformylfuran (DFF) in the absence of any metal (Scheme 1).
For the first time, this study has revealed the importance of morphology and balanced acid-base properties of carbon catalysts for the conversion of biomass.

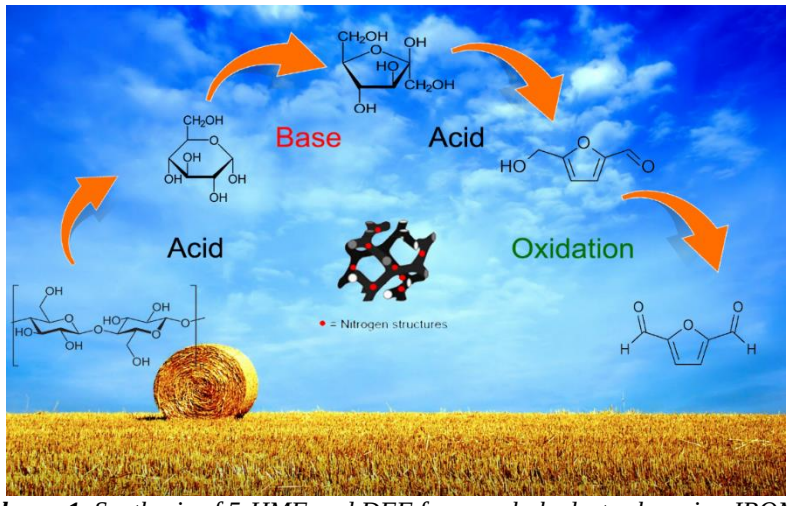


***Scheme 1.*** *Synthesis of 5-HMF and DFF from carbohydrates by using IBOMC*

***Keywords:*** *5-hydroxymethylfurfural (5-HMF), Ordered mesoporous carbon, Bifunctional acid-base Catalyst, Carbohydrate, Oxidation.*

## References

[1] B. Karimi, H. M. Mirzaei, H. Behzadnia, and H. Vali, *ACS Appl. Mater. Interfaces*, **2015**, *7* (34), 19050–19059.
[2] X. Cao, S. P. Teong, D. Wu, G. Yi, H. Su and Y. Zhang, *Green Chem.*, **2015**, *17*, 2348-2352.
[3] H. M. Mirzaei, B. Karimi, *Green Chem.*, **2016**, *18*, 2282-2286.

# Synthesis of Nitrogen-rich Ordered Mesoporous Carbon and Its Application as a Support for Immobilization of Ruthenium Nanoparticles and Using of That in Aerobic Oxidation of Alcohols

**Mohsen Heydari Rouchi**, **Babak Karimi**[1,*]

[1]Department of Chemistry, Institute for Advanced Studies in Basic Sciences (IASBS) Zanjan, Iran
[*]*E-mail: karimi@iasbs.ac.ir*

The principal aim of this project was design, synthesis, and characterization of nitrogen-rich mesoporous carbon with three-dimensional cubic structure and application of that in aerobic oxidation of alcohols.
The nitrogen-rich mesoporous carbon was synthesized via Nano-casting method using KIT-6 as a template and an ionic liquid as a precursor. Characterization of this material using different analysis proved the fascinating properties of this carbon such as High basicity, significant surface acidity, high surface area, well-defined pore size, high thermal stability and high nitrogen content [1].
Afterward, this novel mesoporous carbon was used as an effective and unique support for immobilizing Ruthenium nanoparticles without using a reducing agent.
The catalytic performance of the as-prepared catalyst was investigated in the Aerobic Oxidation of benzylic, aliphatic, cyclic and heteroatom-containing alcohols to aldehydes (Scheme1) without additives under an atmosphere of oxygen [2].
It has also been demonstrated that this catalyst is an effective and recoverable catalyst for consecutive runs without noticeable deactivation.

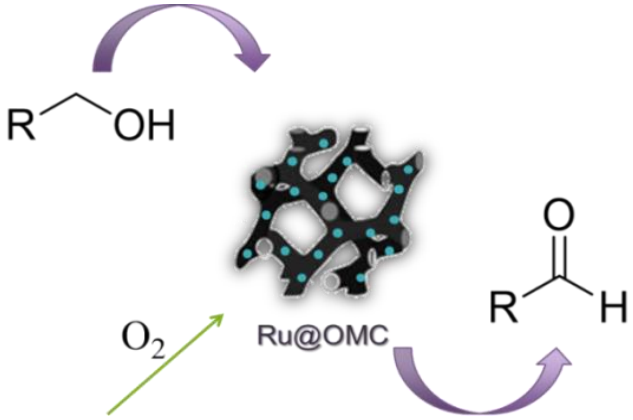


***Scheme**1. Aerobic oxidation of alcohols with Ru@OMC*

***Keywords**: Mesoporous carbon, Aerobic oxidation of alcohols, Ionic liquid, Ruthenium nanoparticle.*

## References

[1] A. Karimi, B.; B. Barzegar, H.; and C. Vali, H, *Chem. Commun.*, **2018**, *54*, 7155.
[2] A. Karimi, B.; B. Elhamifar, D.; C. Yari, O.; D. Khorasani, M.; E. Vali, H.; F. Clark, J. H.; and G. Hunt, A. *Chem. Eur. J.*, **2012**, *18*, 13520 – 13530.

# Preparation of Ordered Mesoporous Polypyrrole/Carbon Composite via Nanocasting Method and Its Application as a New Catalyst Support for Aerobic Oxidation of Alcohols

**Nasim Ganji[1], Babak Karimi[1]***
[1]Department of Chemistry, Institute for Advanced Studies in Basic Sciences (IASBS), Zanjan, Iran
*E-mail: karimi@iasbs.ac.ir

Recently, preparation of composite materials, because of combining the properties of the individual components and using the advantage of their synergistic effects, have attracted the attention of researchers in both academy and industry. Among diverse materials, carbon materials, due to the unique structure and remarkable mechanical, electrical, thermal, optical and catalytic properties, have widely been studied as a second phase to create high performance composites. In spite of performing numerous studies in these field, preparation of carbon/polymer composites with controlled meso-structure in an easy and cost-effective way and use of them in organic transformation are still the live challenges. In this regard, we have presented a novel example of preparation of ordered mesoporous carbon/polypyrrole composite by nanocasting process, combining the impregnation–carbonization of carbon precursor and in situ polymerization process. Characterization of structure and morphology of the composite, indicated a material with the ordered mesoporous structure, high specific surface areas, uniform pore size distributions and high stability.

To take advantage of this mesoporous structure possessing the precious properties in organic transformations, the performance of this material was evaluated as an extraordinary support for immobilization and stabilization of metal nanoparticles and investigation of that in aerobic oxidation of alcohols to the corresponding carbonyl compounds with $O_2$ as the green oxidant in the aqueous medium. High catalytic performance of the catalyst in oxidation of different primary and secondary alcohols, using of water as a green solvent, easy recovery and considerable reusability without significant loss of performance are some advantages of this article.

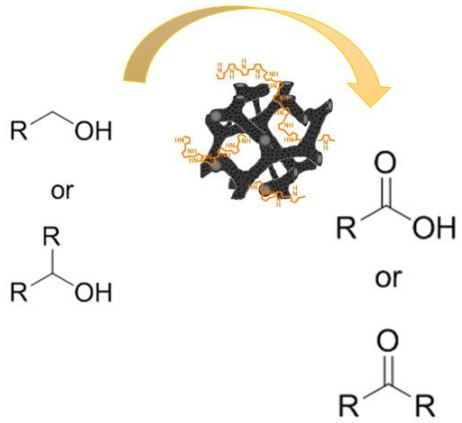


***Scheme 1.*** *Oxidation of Alcohols using Metal@PPY/Carbon composite*

***Keywords:*** Nanocasting, Mesoporous Composite, Oxidation.

## References

[1] S. Y. Huang, P. Ganesan, and B. N. Popov, *Applied Catalysis B: Environmental*, **2009**, *93*, 75.
[2] M. S. Ahmed, D. S. Mannel, T. W. Root, and S. S. Stahl, *Org. Process Res. Dev.* **2017**, *21*, 1388.

# Synthesis and Characterization of Novel Cross-linked Magnetic Ionic Liquid Nanoporous Network and Their Application for immobilization of metal Nanoparticle in the Aerobic Oxidation of Alcohols reactions

**Sepideh Asgari**, **Babak Karimi***
Department of Chemistry, Institute for Advanced Studies in Basic Sciences (IASBS) Zanjan, Iran
*E-mail: karimi@iasbs.ac.ir

In this work, we have concentrated on design and synthesis of a novel catalytic system which is consisted of a Cross-linked Magnetic Ionic Liquid Nanoporous Network. The magnetic $Fe_3O_4$@$SiO_2$ with a core-shell structure and a narrow pore size distribution was synthesized by employing the microemulsion method. Magnetic material grafted with polyionic liquids was successfully prepared by oligomerization of ionic liquid units on the surface of mercaptopropyl-modified silica-coated Fe3O4, and well characterized by several model technologies [1]. This magnetic material was applied as support to prepare immobilized perruthenate ions (RuO4-). The catalytic performance of the as-prepared magnetic catalyst has been investigated in the aerobic oxidation of different alcohols such as benzylic, aliphatic, cyclic and heteroatom-containing alcohols with molecular oxygen as the sole oxidant and toluene as the solvent [2].
The investigation has shown that these obtained materials acted as an efficient, stable and recyclable heterogeneous catalyst for the oxidation of alcohols to aldehydes (scheme1).

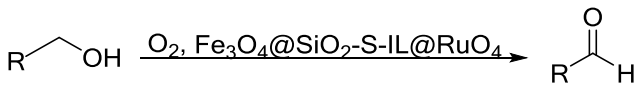


***Scheme 1.*** *Aerobic oxidation of alcohols with $Fe_3O_4$@$SiO_4$-S-IL@$RuO_4$*

***Keywords****: Magnetic, Core-shell, Aerobic oxidation of alcohols, Ionic liquid, Perruthenate ions.*

## References

[1] Karimi, B.; Mansouri, F.; Vali, H. *Green Chem.* **2014**, *16*, 2587.
[2] Karimi, B.; Elhamifar, D.; Yari, O.; Khorasani, M.; Vali, H.; Clark, J. H.; Hunt, A. J. *Chem. Eur. J.***2012,** 18, 13520.

# Biosynthesis of zinc aluminate nanoparticles for effective photocatalytic degradation of direct blue 129 dye

**Sara Ganjkhanlu[1], Saeid Taghavi Fardood[1,*], Ali Ramazani[1,2]**
[1]Department of Chemistry, University of Zanjan, Zanjan, Iran
[2]Research Institute of Modern Biological Techniques (RIMBT), University of Zanjan, Zanjan, Iran
*E-mail: saeidt64@gmail.com

$ZnAl_2O_4$ spinel belongs to $Fd\bar{3}m$ space group and has a close-packed face-centered cubic structure. In $ZnAl_2O_4$, the valence band is formed by the hybridization of 2p orbitals of $O^{2-}$ and 3d orbitals of $Zn^{2+}$ while the conduction band is made up of 2p and s orbitals of $Al^{3+}$ atom [1]. It is transparent for light of the wavelengths > 320 nm, thus, it finds applications in ultraviolet (UV) photoelectronic devices. If the surface area of $ZnAl_2O_4$ spinel is high, it is a useful catalyst and catalyst support as well as photocatalyst for the degradation of dyes. The surface charge of the photocatalyst also plays important role in dye adsorption and degradation process, anionic dyes adsorb well on the surface of a material with the positive value of zeta potential or vice versa, due to the attraction of opposite charge particles [2].
The photocatalytic degradation of organic pollutants in the water and air, such as dyes [1], phenols, pesticides, and acetone, using different semiconductor materials has attracted much attention recently [3,4]. In this work, $ZnAl_2O_4$ nanocrystals were successfully synthesized by using sol-gel method. The structural properties of the photo-catalyst were investigated by energy dispersive X-ray analysis (EDX), powder X-ray diffraction (XRD), field emission scanning electron microscopy (FESEM), Fourier transforms infrared spectroscopy (FTIR), and percent of DB129 degradation which was followed by UV–Visible spectroscopy. The photocatalytic activity of $ZnAl_2O_4$ nanoparticles was evaluated in the degradation of direct blue 129 dye at room temperature in aqueous solution so that 90% of direct blue 129 dye was degraded in 60 min. Therefore, the $ZnAl_2O_4$ nanocrystals were able to be employed for the removal of dyes from wastewater under visible light irradiation.

***Keywords:*** *$ZnAl_2O_4$ nanoparticles, Photocatalyst, Visible light irradiation.*

## References

[1] F. Zerarga, A. Bouhemadou, R. Khenata and S. Bin-Omran, *Solid State Sci.*, **2011**, *13*, 1638-1648.
[2] M. Miyauchi, A. Ikezawa, H. Tobimatsu, H. Irie and K. Hashimoto, *PCCP*, **2004**, *6*, 865-870.
[3] E.L. Foletto, S. Battiston, J.M. Simões, M.M. Bassaco, L.S.F. Pereira, É.M. de Moraes Flores and E.I. Müller, *Microporous Mesoporous Mater.*, **2012**, *163*, 29-33.
[4] A. Chaudhary, A. Mohammad and S.M. Mobin, *Mater. Sci. Eng., B*, **2018**, *227*, 136-144.

# Solvent free synthesis of 2, 4, 5-triarylimidazole derivatives catalyzed by $CoCl_2.6H_2O$ as a cheap, and effective catalyst under microwave irradiation

**Zolfa Afshari[1], Saeid Taghavi Fardood[1,*], Ali Ramazani[1,2]**
[1]Department of Chemistry, University of Zanjan, Zanjan, Iran
[2]Research Institute of Modern Biological Techniques (RIMBT), University of Zanjan, Zanjan, Iran
*E-mail: saeidt64@gmail.com*

Imidazole derivatives are very interesting class of Nitrogen containing 5-membered heterocyclic compounds. Because of their wide range of pharmacological importance and significant role in biochemical processes, the Biological importance of the poly substituted imidazole ring system has made it a common structure in numerous synthetic compounds, such as fungicides, herbicides, therapeutic agents and plant-growth regulators. This core also has been utilized in diverse pharmaceutical applications such as anti-inflammatory, anti-thrombotic and antitumor agents. Due to their great biological importance of poly substituted imidazole framework, the synthesis of Poly substituted imidazoles has attracted much attention in organic synthesis [1-3].

Cobalt salts and complexes are well known to have catalytic abilities in coordinating with the carbon-carbon multi bond for π- complex and to produce many valuable products through enynecoupling (Pauson-Khand reaction), Alder-Ene and many other reactions [4,5].

In the present work, an efficient, inexpensive, environmentally friendly one-pot route to 2,4,5-triarylimidazole derivatives has been developed, involving three-component reaction of benzyl, aldehydes, and ammonium acetate catalyzed by $CoCl_2.6H_2O$ in solvent free condition under microwave irradiation (scheme 1). The present methodology offers several advantages such as high yields, relatively short reaction times, mild reaction condition, easy work up, and cleaner reaction.

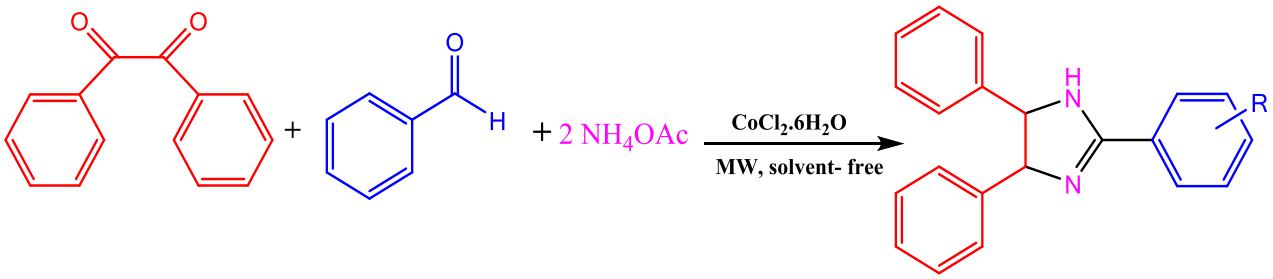


***Scheme 1.*** *Synthesis of 2, 4, 5-triarylimidazole derivatives*

***Keywords:*** *$CoCl_2.6H_2O$; 2, 4, 5-triarylimidazole derivatives; microwave irradiation*

## References

[1] J.G. Lombardino and E.H. Wiseman, *J. Med. Chem.*, **1974**, *17*, 1182-1188.
[2] G. Sharma, Y. Jyothi and P.S. Lakshmi, *Synth. Commun.*, **2006**, *36*, 2991-3000.
[3] K. Shelke, S. Sapkal and M. Shingare, *Chin. Chem. Lett.*, **2009**, *20*, 283-287.
[4] S.E. Gibson and N. Mainolfi, *Angew. Chem. Int. Ed.*, **2005**, *44*, 3022-3037.
[5] G.K. Rastogi, S.K. Ginotra, A. Agarwal and V. Tandon, *Org. Biomol. Chem.*, **2015**, *13*, 1000-1007.

# Synthesis of $MgSnO_3$ nanoparticles by co-precipitation method and investigation of their photocatalytic activity for degradation of malachite green dye

**Samaneh Tavousi[1], Maryam Shaterian[1,*], Saeid Taghavi Fardood[1], Zahra Faramarzloo[1]**
[1]Department of Chemistry, University of Zanjan, Zanjan, Iran
*E-mail:* shaterian@znu.ac.ir

Metal metastannates, with structures closely related to the perovskite one, are of particular interest due to their unusual dielectric and semiconducting properties, leading to various applications such as thermally stable capacitors, ceramic dielectric bodies, gas and humidity sensors and battery electrode materials. Cubic perovskite type of metal stannates ($MSnO_3$) have attracted considerable attention for potential applications [1,2].

With the development of urbanization and industrialization, environmental problems have become increasingly serious. Photocatalysis based on semiconductors has been investigated due to the demand for organic dyes degradation. Organic dyes, like malachite green (MG) and methyl orange (MO), are toxic and hardly decompose quickly. Photocatalytic degradation of MG is of high performance and cost-effective, it seldom discharges any perilous chemicals [3,4].

In this work, $MgSnO_3$ nanoparticles have been synthesized using co-precipitation method. The X-ray diffraction (XRD) pattern was used to determine the structure of $MgSnO_3$ nanoparticles. The presence of $MgSnO_3$ nanoparticles was confirmed by the FT-IR spectrum. The details of the surface morphology and particle size of $MgSnO_3$ nanoparticles were obtained by Scanning Electron Microscopic analysis (SEM). The photocatalytic activity of $MgSnO_3$ nanoparticles was investigated for malachite green (MG) degradation under visible light irradiation. The $MgSnO_3$ nanoparticles photocatalyst exhibited superior photocatalytic activity, and about 98% of MG was removed within 50 minutes of irradiation. The enhanced photocatalytic activity could be attributed to the effective visible light absorption and separation of electrons and holes. Therefore, it is reasonable to believe that the $MgSnO_3$ NPs photocatalyst has great potential in environmental remediation.

***Keywords:*** *$MgSnO_3$ nanoparticles, Photocatalytic activity, Co-precipitation method.*

## References

[1] M. Rashad and H. El-Shall, *Powder Technol.*, **2008**, *183*, 161-168.
[2] Z. Lu, L. Chen, Y. Tang and Y. Li, *J. Alloys Compd.*, **2005**, *387*, L1-L4.
[3] H. Wang, X. Yuan, G. Zeng, Y. Wu, Y. Liu, Q. Jiang and S. Gu, *Adv. Colloid Interface Sci.*, **2015**, *221*, 41-59.
[4] J. Reddy, S. Kurra, R. Guje, S. Palla, N.K. Veldurthi, G. Ravi and M. Vithal, *Ceram. Int.*, **2015**, *41*, 2869-2875.

# $FeTiO_3$ Catalyzed one-pot synthesis of tetrahydrobenzo[b]pyran derivatives

**Sajjad Moradi[1], Saeid Taghavi Fardood[1,*], Ali Ramazani[1,2]**
[1]Department of Chemistry, University of Zanjan, Zanjan, Iran
[2]Research Institute of modern biological techniques, University of Zanjan, P O Box 45195-313, Zanjan, Iran
*E-mail: saeidt64@gmail.com

Multi-component metal oxides in comparison with simple metal oxides have the crystal structures and merits of tuning chemical compositions [1]. One of these multi-component metal oxides is $FeTiO_3$ that show behavior antiferromagnetic and has a wide band gap (2.54 eV) [2]. $FeTiO_3$ has potential applications in high temperature integrated circuits, spintronics, chemical catalysts, high power electronic devices and photocatalysts [2-4].
Benzopyrans and their derivatives have wide range of biologicaland and pharmacological properties such as diuretic, antisterility, spasmolytic, antianaphylactin and anticancer agents [5,6]. Also, this component can be used as cognitive enhancers for the therapy of neurodegenerative disease including Huntington's disease, amyoprophic lateral sclerosis, alzheimer's disease, Parkinson's disease, Down's syndrome and AIDS associated dementia [7].
In this work, a simple and efficient one-pot synthesis of tetrahydrobenzo[b]pyrans from the three-component reaction between dimedone, aldehydes, and malononitrile in the presence of $FeTiO_3$ as a magnetic heterogeneous catalyst under microwave irradiation and solvent free conditions is described (scheme 1). The catalyst exhibits remarkable reactivity and is reusable. The final product was investigated by $^1$HNMR and $^{13}$CNMR spectroscopy. Advantageous features of this work including green, short reaction times, Simple work-up, easy, inexpensive and mild reaction conditions.

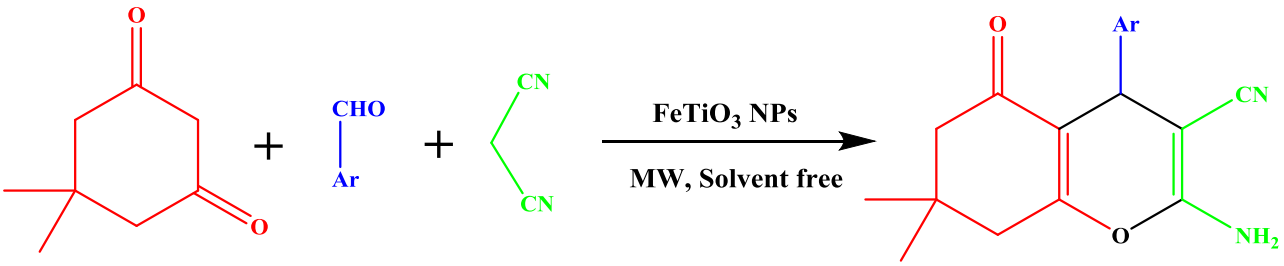


***Scheme 1.*** *Synthesis of tetrahydrobenzo[b]pyran derivatives*

***Keywords:*** *Sol–gel method, Arabic gum, Tetrahydrobenzo[b]pyran, Microwave irradiation.*

## References

[1] T. Wu, H. Mayaffre, S. Krämer, M. Horvatić, C. Berthier, W. Hardy, R. Liang, D. Bonn and M.-H. Julien, *Nature*, **2011**, *477*, 191.
[2] T. Fujii, M. Kayano, Y. Takada, M. Nakanishi and J. Takada, *Solid State Ionics*, **2004**, *172*, 289-292.
[3] F. Zhou, S. Kotru and R.K. Pandey, *Mater. Lett.*, **2003**, *57*, 2104-2109.
[4] T. Fujii, M. Kayano, Y. Takada, M. Nakanishi and J. Takada, *J. Magn. Magn. Mater.*, **2004**, *272*, 2010-2011.
[5] G.M. Ziarani, A. Abbasi, A. Badiei and Z. Aslani, *J. Chem.*, **2011**, *8*, 293-299.
[6] J. Montandon, F. Zijlstra, J. Wilson, E. Grandjean and L. Cicurel, *Int. J. Tiss. React.*, **1989**, *11*, 107-112.
[7] S. Balalaie, M. Sheikh-Ahmadi and M. Bararjanian, *Catal. Commun.*, **2007**, *8*, 1724-1728.

# Immobilization of horseradish peroxidase (HRP) enzyme on Silica nanoparticles

**Bahram Amini[1*], Vahab Jafarian[1*], Hamid Reza Taheri[2], Jamshid Mehrvand[1]**

[1] Department of Biology, Faculty of Science, University of Zanjan, Zanjan, Iran

[2] Department of Biology, Faculty of Sciences, Zanjan Branch, Islamic Azad University, Zanjan, Iran.

Corresponding authors: *bamini50@yahoo.com, v.jafarian@znu.ac.ir*

Immobilized enzymes have several advantages over soluble enzymes such as retention and repeating of their catalytic activities. The stabilization of enzyme activity was the most important character for its immobilizing. The immobilized enzymes are useful in diagnostics, bio-affinity chromatography, and biosensor applications. In the present study, horseradish peroxidase (HRP) was immobilized on silica nanoparticles. For achieving this purpose, firstly, silica nanoparticles were synthesized. Then, the nanoparticles were conjugated with HRP (1 µL, 1000 µg $mL^{-1}$) using 1-(3-Dimethylaminopropyl)-3-ethylcarbodiimide hydrochloride (EDC, 0.5 mg $mL^{-1}$ ) and N-hydroxysuccinimide (NHS, 0.5 mg $mL^{-1}$) at 25 °C for 12h. The silica-HRP complex was rinsed three times with $H_2O$. Afterwards, the silica-HRP complex structure was screened by SEM and DLS. The activity of silica-HRP complex was measured by adding tetramethylbenzidine (TME) to mixture reaction. The reaction was stopped with adding 50 µL HCl (10 mM) and the result was evaluated by UV-Vis spectrophotometry. The result revealed that the structure and size of silica nanoparticles were spherical and 121-172 nm, respectively. Also, the stability and activity of enzyme were increased up to 1.7 and 1.2 times, respectively. Overall, silicon nanoparticles could be used as immobilizing agents in order to enhance the stability and activity of the enzyme.

***Keywords:*** *Enzyme immobilization, Horseradish peroxidase, Silica nanoparticles.*

## References

[1] T. Zhang, X. Xu, Y.N. Jin, *Journal of Molecular Catalysis B: Enzymatic*, **2014**, 106, 56–62.
[2] P.P. Waifalkar, A.D. Chougale, P. Kollu, *Colloids and Surfaces B: Biointerfaces*, **2018**, 167, 425–431.
[3] C. Gong, Y. Gong, *Biosensors and Bioelectronics*, **2017**, 96, 351–357.

# Effects of immobilization on activity of catechol 2, 3 dioxygenase enzymes on Magnetic nanoparticles

**Souraia Mohammadzadeh[1], Vahab Jafarian[1*], Bahram Amini[1*], Nasrin Ahmadpour[1], Jamshid Mehrvand[1]**

[1] Department of Biology, Faculty of Science, University of Zanjan, Zanjan, Iran

Corresponding authors: *v.jafarian@znu.ac.ir*, *bamini50@yahoo.com*

Catechol 2,3-dioxygenase (C2, 3O) are a key enzyme in the meta-cleavage pathway of catechol metabolism. In the present study, the C2, 3O enzyme was immobilized on magnetic nanoparticles (MNPs). Firstly, the C2, 3O enzyme was purified of E. coli. Then magnetic nanoparticles were synthesized by sol-gel method. C2, 3O enzyme was conjugated with MNPs using1-(3-Dimethylaminopropyl)-3-ethylcarbodiimide hydrochloride (EDC, 0.5 mg $mL^{-1}$) and N-hydroxysuccinimide (NHS, 0.5 mg $mL^{-1}$) at 25 ˚C for 12h. Subsequently, MNP-C2, 3O complex was washed three times with tris-base. The size, structure pure magnetic nanoparticles and MNP-C2, 3O complex were evaluated by SEM and DLS. The activity of MNP-C2, 3O complex was measured by adding catechol as substrate to mixture reaction using UV-Vis spectrophotometry. The result revealed that the structure and size of MNPs and MNP-C2, 3O complex were spherical and 21-43 nm, respectively. Also, Immobilization of C2, 3O enzyme on MNPs improved the stability toward the denaturation induced by pH, heat, and metal ions.

***Keywords:*** *Enzyme immobilization, Catechol 2,3-dioxygenase, magnetic nanoparticles (MNPs).*

## References

[1] T. Zhang, X. Xu, Y.N. Jin, *Journal of Molecular Catalysis B: Enzymatic*, **2014**, 106, 56–62.
[2] P.P. Waifalkar, A.D. Chougale, P. Kollu, *Colloids and Surfaces B: Biointerfaces*, **2018**, 167, 425–431.
[3] C. Gong, Y. Gong, *Biosensors and Bioelectronics*, **2017**, 96, 351–357.
[4] M. Takeo, M. Nishimura, *Biosci. Biotechnol. Biochem*, **2007**, 71, 1668–1675.

# Photocatalytic degradation of reactive blue 21 dye in aqueous solution by using $CoSnO_3$ nanoparticles

**Zahra Faramarzloo[1], Maryam Shaterian[1,*], Saeid Taghavi Fardood[1], Samaneh Tavousi[1]**
[1]Department of Chemistry, University of Zanjan, Zanjan, Iran
*E-mail: shaterian@znu.ac.ir*

With an increase of the industrialization, environmental pollution problem are getting worse. Many contaminants are often discharged from industrial and wastewater treatment plants and contaminate groundwater and surface water. Therefore, it is urgent for the scientist to find solutions to mitigate the damage that is caused by these pollutants. Several studies using catalysts have been employed to decompose harmful organic and inorganic pollutant into harmless chemicals. The remarkable progress of photocatalytic has been limited to ultraviolet light although visible light range is far more useful in the solar spectrum. Hence, the development of catalyst that can be activated in the visible region has become important topic research today [1,2]. Perovskite-type materials with the general formula of $ABO_3$ have attracted considerable attention in the field of catalysis. It is reported that perovskite oxide exhibits high photocatalytic activity towards degradation of organic contaminant under visible light irradiation and stable in various environment. Therefore, perovskite oxide with appropriate crystal structure, morphology and optical properties for improvement of photocatalytic efficiency is paid much attention by researchers [3-5].
$CoSnO_3$ nanoparticles were prepared using co-precipitation method with tin (II) chloride dehydrate ($SnCl_2.2H_2O$) and cobalt (II) chloride hexahydrate ($CoCl_2.6H_2O$) as raw material. The synthesized nanoparticles were characterized by means of X-ray diffraction (XRD), Infrared absorption spectroscopy (IR) and scanning electron microscopic analysis (SEM). Reactive blue 21 was used as dye model. Photocatalytic dye degradation by $CoSnO_3$ NPs was studied by UV–Vis spectrophotometer. The photocatalytic ability of the $CoSnO_3$ nanoparticles was demonstrated by the degradation of reactive blue 21 dye under visible light irradiation. The effects of operational parameters on decolorization such as catalyst dosage, dye concentration, and contact time were studied. The experimental results indicated that the photocatalytic property of the $CoSnO_3$ nanoparticles was excellent. Thus, these nanoparticles could play a vital role in the environmental catalytic remediation of polluted water.

***Keywords:*** *$CoSnO_3$ nanoparticles, Reactive blue 21 dye, Photocatalytic degradation.*

## References

[1] K. Pirkanniemi and M. Sillanpää, *Chemosphere*, **2002**, *48*, 1047-1060.
[2] A. Srinivasan and T. Viraraghavan, *J. Environ. Manage.*, **2010**, *91*, 1915-1929.
[3] J. Shi and L. Guo, *Progress in Natural Science: Materials International*, **2012**, *22*, 592-615.
[4] M. Yang, A. Xu, H. Du, C. Sun and C. Li, *J. Hazard. Mater.*, **2007**, *139*, 86-92.
[5] Y. Cao, L. Zhang, D. Tao, D. Huo and K. Su, *Electrochim. Acta*, **2014**, *132*, 483-489.

# Preparation of $NiSnO_3$ nanoparticles and their photocatalytic activity for degradation of Congo red dye under visible light irradiation

**Masoume Sohrabi[1], Maryam Shaterian[1,*], Saeid Taghavi Fardood[1], Zeinab Imani[1]**
[1]Department of Chemistry, University of Zanjan, Zanjan, Iran
*E-mail: shaterian@znu.ac.ir

Photocatalysis has long been studied for clean energy and environmental applications. Over the past two decades, the number of applications based on photocatalysis has increased sharply, while a wide range of materials systems have been developed. Photocatalysis has been of particular interest in the production of hydrogen from water using solar energy. Further, conversion of $CO_2$ to hydrocarbons (fuels) is also of significant interest, as it is a solution to reduce $CO_2$ emissions across the globe. Apart from the clean energy generation, photocatalysis has several promising applications in the environmental field. Some of the applications include degradation of volatile organic compounds (VOC) for water treatment, germicide and antimicrobial action, de-coloration of industrial dyes, nitrogen fixation in agriculture, and removal of $NO_x/SO_x$ air pollutants [1-3].
Perovskites are the class of compounds presenting the general formula $ABO_3$. Generally, in this crystal structure, the A site is occupied by the larger cation, while the B site is occupied by the smaller cation. Perovskites are one of the most important families of materials exhibiting properties suitable for numerous technological applications. Perovskite compounds such as $PbZrO_3$, $BaTiO_3$, and $PbTiO_3$ are most commonly used piezoelectric compounds. $BiFeO_3$ thin films show multiferroic behavior, while compounds such as $SrTiO_3$ have shown excellent photocatalytic properties. The origin of such properties lies in the crystal structure of perovskites [4,5].
In this work, $NiSnO_3$ nanoparticles have been prepared by co-precipitation method. The sample was characterized by powder X-ray diffraction (XRD), Fourier transform infrared spectroscopy (FTIR), and scanning electron microscopy (SEM). The photocatalytic efficiency of $NiSnO_3$ NPs has been evaluated for Congo red dye degradation as an environment polluting model under visible light irradiation. The photocatalytic activity of $NiSnO_3$ nanoparticles was investigated with changing factors including photocatalyst dosage, initial dye concentration, and contact time. The results presented that $NiSnO_3$ NPs could degrade 90% of the Congo red dye.

***Keywords:*** *$NiSnO_3$ nanoparticles, Co-precipitation method, degradation of dye*

## References

[1] W. Hou and S.B. Cronin, *Adv. Funct. Mater.*, **2013**, *23*, 1612-1619.
[2] R.J. Tayade, P.K. Surolia, R.G. Kulkarni and R.V. Jasra, *Sci. Technol. Adv. Mater.*, **2007**, *8*, 455-462.
[3] P. Kanhere and Z. Chen, *Molecules*, **2014**, *19*, 19995-20022.
[4] A. Bhalla, R. Guo and R. Roy, *Mater. Res. Innovations*, **2000**, *4*, 3-26.
[5] Q. Jia, A. Iwase and A. Kudo, *Chemical Science*, **2014**, *5*, 1513-1519.

# Sol-gel synthesis of $Al_2O_3$@$ZrO_2$ nanocomposite as a photocatalyst for degradation of reactive blue 222 dye under visible light irradiation

**Alireza Yaghoubi**[1,*], **Saeid Taghavi Fardood**[1], **Ali Ramazani**[1, 2]
[1]Department of Chemistry, University of Zanjan, Zanjan, Iran
[2]Research Institute of Modern Biological Techniques (RIMBT), University of Zanjan, Zanjan, Iran
*E-mail: alirezayaghoubi62@yahoo.com

Zirconia ($ZrO_2$), as an inorganic coating material, is an important n-type semiconductor material that with a great numbers of catalysis in oxidation and reduction can be operated. $ZrO_2$ has attractive properties, showing mild acid catalytic behavior and good mechanical, chemical, and thermal stabilities. In addition, the hydroxyl groups onto the surface of $ZrO_2$ are able to react with different reagents and materials. Therefore, the addition of metal oxide nanoparticles into a layer of $ZrO_2$, providing a core-shell structure (i.e. M (metal oxide)@$ZrO_2$) that may have properties different from each of the components considered separately [1,2].

$Al_2O_3$–$ZrO_2$ composite ceramics is a promising material since it possesses the crack resistance and hardness higher than pure aluminum oxide and zirconium oxide, respectively. The combination of mechanical properties and a proper biocompatibility makes the use of the $Al_2O_3$–$ZrO_2$ composite ceramics rather promising in dentistry and orthopedic surgery (tooth and joint implants). The $Al_2O_3$–$ZrO_2$ composite ceramics can be produced via mixing the aluminum and zirconium oxide powders. However, the nanoscale composite powders are more preferable to apply for the production of composite ceramics. Aluminum and zirconium oxides are not mutually-soluble, however, in the nanoscale state they form mixed oxides [3,4].

In the present work, $Al_2O_3$@$ZrO_2$ nanocomposite was prepared using the new sol-gel method. The structure and morphology of samples were characterized by X-ray diffraction (XRD), scanning electron microscopy (SEM), Fourier transform infrared spectroscopy (FT-IR) and energy dispersive analysis of X-ray (EDAX) and UV-vis spectroscopy (UV-vis). Obtained results of XRD data confirmed the formation of $Al_2O_3$@$ZrO_2$ nanocomposite. The photocatalytic activity of the nanocomposite was evaluated by studying the degradation of reactive blue 222 as a model dye under visible light irradiation. Obtained results showed that some parameters such as amount of catalyst, irradiation time and initial dye concentration effect on the degradation efficiency of reactive blue 222 dye. The experimental results indicated that the photocatalytic property of the $Al_2O_3$@$ZrO_2$ nanocomposite was excellent.

***Keywords:*** *Sol-gel synthesis, $Al_2O3$@$ZrO_2$ nanocomposite, photocatalytic activity, visible light.*

## References

[1] J. Kašpar, P. Fornasiero and N. Hickey, *Catal. Today*, **2003**, *77*, 419-449.
[2] G. Sunita, B.M. Devassy, A. Vinu, D.P. Sawant, V. Balasubramanian and S. Halligudi, *Catal. Commun.*, **2008**, *9*, 696-702.
[3] K.R. Nemade, R.V. Barde and S.A. Waghuley, *Ceram. Int.*, **2015**, *41*, 4836-4840.
[4] W.-J. Liu, F.-X. Zeng, H. Jiang, X.-S. Zhang and W.-W. Li, *Chem. Eng. J.*, **2012**, *180*, 9-18.

# $Be_{12}S_{12}$ nano-cage: A Promising Hydrogen Storage Medium From a theoretical point of view

**Mozhgan Sabzehzari**[1*]
[1]Department of Chemistry,college of science,Jundi Shapur University of Technology-Dezful, Iran
*E-mail: msabzehzari@jsu.ac.ir

## Abstract

In recent years, much effort has been dedicated to fabricate nanostructures, which can absorb hydrogen molecules with high storage capacity. Different nanostructured materials have been studied in detail to enhance hydrogen storage capacity. Hydrogen storage materials must represent appropriate thermodynamic properties and have sufficiently prompt kinetics of $H_2$ charging and discharging. Therefore, seeking novel hydrogen storage materials has remained an important issue. Recently, the adsorption of some gases such as $H_2O$, $CH_4$, $NH_3$, $H_2$ and CO on BeO nanomaterial has been studied [1,2]. Nonetheless, several materials, like as aluminum nitride (AlN) nanostructures [3], boron nitride (BN) systems [4] and fullerene clusters [5], boron buckyballs and sheets, B80 [6] have been tested experimentally and theoretically as potential storage materials for hydrogen.

First-principles calculations based on density functional theory were performed to study the hydrogen adsorption and $H_2$ storage on the beryllium sulfide nano-cage ($Be_{12}S_{12}$ nanocage). The adsorption of $H_2$ molecules on the nano-cage depends on the polarization and charge of the atom surface. The transfer of charge from the Be atom to its neighboring S atoms in the surface of the cluster indicates the ionic character of the Be–S bond, so that Be–S bonds are polarized. The results show that the $H_2$ molecule is significantly adsorbed on the $Be_{12}S_{12}$ nano-cage surface, so that the $H_2$ prefers to be adsorbed atop a Be atom as compared to solfur atoms of the cluster surface. Our calculations also reveal that the gravimetric uptake can overpass the value of 7.6 wt % with an average adsorbed energy (Eads) of -0.89 eV. These findings have important implications on designing of hydrogen storage materials and significantly broadening the spectrum of strategies for fabricating of new nanostructures to enhance hydrogen storage capacity.

**Keywords:** *DFT calculation, hydrogen storage, beryllium sulfide, nanocage.*

## References:

[1] R. Shinde, M. Tayade, *J. Phys. Chem. C* ,(2014) **118** 17200-17204.

[2] M. Samadizadeh, S.F. Rastegar, A.A. Peyghan, *Struct. Chem.* , (2015) **26** 809-814.

[3] Q. Wang, Q. Sun, P. Jena, Y. Kawazoe, *ACS nano* ,(2009) **3** 621-626.

[4] A.A. Peyghan, S.A. Aslanzadeh, A. Samiei, *Monatshefte für Chemie-Chem. Month.* (2014) **145** 1083-1087.

[5] Y.-H. Kim, Y. Zhao, A. Williamson, M.J. Heben, S. Zhang, *Phys. Rev. lett.* ,(2006) **96** 016102.

[6] S. Er, G.A. de Wijs, G. Brocks, *J. Phys. Chem. C*, (2009) **113** 18962-18967.

# Theoretical Study of Hydrogen Storage in lower diamondoids: adamantane and diamantane

**Mozhgan Sabzehzari**[1*]
[1]Department of Chemistry, Faculty of science, Jundi Shapur University of Technology-Dezful,, Iran
*E-mail: msabzehzari@jsu.ac.ir

In recent years, much effort has been dedicated to fabricate carbon based nanostructures, which can absorb hydrogen molecules with high storage capacity. Different nanostructured materials have been studied in detail to enhance hydrogen storage capacity such as powdered graphite, carbon nanotubes and graphene. Several studies on graphene have highlighted the potential application of this unique material for hydrogen storage as a promising media for the efficient solid-state hydrogen storage systems [1, 2]. But according to our knowledge, there is no work and research of the ability to absorb the hydrogen gas by adamantane and diamantane (lower diamondoids), which are found major applications as templates and as molecular building blocks in nanotechnology and host-guest [3,4]. In this paper, we have investigated the ability to absorb hydrogen by adsorption on the outer and inner sites of adamantane and diamantane with applying ab initio-DFT calculations. The results show that hydrogen molecule is well absorbed by both ways, and adamantan shows a high potential for absorption of hydrogen molecules. Although the free energy of the Gibbs of adsorption, when the hydrogen molecule is encapsulated inside adamantane cage, is more negative, indicating that adsorption is better than inner sites.

**Keywords:** *Diamondoids, Adamantane, Diamantane, DFT calculations, adsorption, hydrogen storage.*

## References

[1] R.E. Morris, and P.S. Wheatley, Angewandte Chemie International 2008 474966.
[2] S. Gadipelli, and Z.X. Guo, Progress in Materials Science, 2015 69 1.
[3] Y. Xue; G.A.Mansoori Int. J. Mol .Sci .2010 11 288.
[4] G.A. Mansoori, Advances in Chemical Physics, 2007 136 207.

# Synthesis, characterization of MOF-derived carbon Nano structures and their catalytic and conductivity studies

**Mina Naghiloo[1], Somayeh Tarasi[2], Reza Rasuli[1], Ali Morsali[2]**
[1]Department of Physic, University of Zanjan, Zanjan, Iran
E-mail: r_rasuli@znu.ac.ir
[2]Department of Chemistry, Faculty of Sciences, Tarbiat Modares University, P.O. Box: 14115-175, Tehran, Iran. E-mail: Morsali_a@modares.ac.ir

In the past decade, metal−organic frameworks (MOFs) have attracted considerable interest because of their potential applications in different fields such as catalysis, gas storage, and sensing [1]. This interest is largely based on the ability to tailor the topology, pore size, and functionality by judicious selection of the molecular building blocks. A porous Zn(II)-based metal–organic frameworks, PG/TMU-21(RL2), containing Amin-functionalized pores, were readily and quickly prepared via mechanosynthesis. The structure of this framework has been determined further characterized by Fourier transform infrared spectroscopy and Thermogravimetric analysis. A catalytic performance and conductivity study of these MOF is investigated. Results show that among the similar compounds, PG/TMU-21(RL2) with BET 3,375.21 m²/g has the highest catalytic activity. These catalysts maintain their crystalline framework after the reaction and are easily recycled.

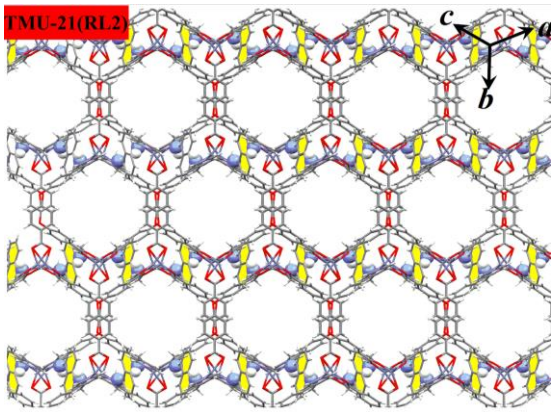


***Scheme 1.*** *showing the honeycomb channels along the [1 0 1̄] direction for TMU-21(RL2).*

**Keywords***: metal–organic frameworks, catalytic, conductivity.*

## References

[1] A. Azhdari Tehrani, H. Ghasempour, A. Morsali, G. Makhloufi and C. Janiak, *Cryst. Growth Des.*, **2015**, *15*, 5543-5547.

# Photocatalytic degradation of Congo red dye in the presence of nanostructured zinc stannate

**Zeinab Imani[1], Maryam Shaterian[1,*], Saeid Taghavi Fardood[1], Masoume Sohrabi[1]**
[1]Department of Chemistry, University of Zanjan, Zanjan, Iran
*E-mail: shaterian@znu.ac.ir

With growing industrialization and population, environmental contamination caused by organic pollutants is being one of the overwhelming problems all over the world. However, its horrible adverse effects have appeared in the shape of environmental collapse. The domestic use and industrial activity both produce a large amount of wastewater, which then disposed into natural channels leading to a high pollution risk. A small quantity of polluted water is sufficient to contaminate much greater capacity of clean water. Synthetic dyes are toxic refractory chemicals, which generate murky color to the water and are hazardous to the environment. The dyes were detected in a dissolved state in wastewater. Most of these dyes are toxic and carcinogenic in nature. One must note down that, a wide spectrum of compound can transform themselves into potentially dangerous substances during the water treatment process. A non-biodegradable pollutant present in wastewater is a point of major serious pain to the researchers in the world [1,2].

Recently, zinc stannate ($ZnSnO_3$) has attracted considerable attention due to its potential applications in the fields of photo-electrochemical device, photocatalyst, gas sensor, and electrical nanodevice. Nowadays, $ZnSnO_3$ micro- and nanostructures with various morphologies have been synthesized by various synthesis routes, including thermal evaporation, co-precipitation method, and hydrothermal synthesis [3-5].

Oxidation by Fenton reactions a proven and economically feasible process for destruction of a variety of hazardous pollutants in wastewater. In this paper, we report a simple co-precipitation synthesis method for a light-induced heterogeneous oxide photocatalyst, $ZnSnO_3$. The catalyst was characterized by various investigative techniques, like Infrared Fourier Transform Spectroscopy (FTIR), X-ray Diffraction (XRD), and Scanning Electron Microscopy (SEM) analysis to carry out structural and spectroscopic properties of the photocatalyst. The visible light mediated degradation of Congo red dye was achieved by using $ZnSnO_3$. Effects of various experimental parameters of the oxidation reaction of the dye were investigated. The studied parameters were the contact time, the catalyst mass, and the dye concentration. The optimum conditions had been determined, and it was found that efficiency of degradation obtained was about 90%. The main advantage of photocatalytic is that, the process takes place at ambient temperature without overpressure. The oxygen used for oxidation can be directly obtained from atmosphere.

***Keywords:*** *$ZnSnO_3$ nanoparticles, photocatlysis, Congo red dye.*

## References

[1] F. Esther, C. Tibor and O. Gyula, *Env. Inter*, **2004**, *30*, 953-971.
[2] N. Barka, S. Qourzal, A. Assabbane, A. Nounah and Y. Ait-Ichou, *Arabian J. Chem.*, **2010**, *3*, 279-283.
[3] A.V. Borhade and Y.R. Baste, *Arabian J. Chem.*, **2017**, *10*, S404-S411.
[4] M. Miyauchi, Z. Liu, Z.-G. Zhao, S. Anandan and K. Hara, *Chem. Commun.*, **2010**, *46*, 1529-1531.
[5] C. Fang, B. Geng, J. Liu and F. Zhan, *Chem. Commun.*, **2009**, 2350-2352.

# Enhanced photocatalytic efficiencies over A-sites substituted $LaFeO_3$/ZnO nanocomposites

**Masoumeh Doulabi, Ali Reza Mahjoub*, Masoumeh Chamack**
Department of chemistry, Faculty of sciences, Tarbiat Modares University, P.O.Box 14115-4838, Tehran, Islamic Republic of Iran
*mahjouba@modares.ac.ir

Perovskite oxide $LaFeO_3$ (LF) is extensively used in the advanced technology such as electrode materials of solid oxide fuel cells [1], catalyst, high-temperature oxygen-permeable membranes, gas sensors, magnetic materials, super conductors, and so on. Nanocrystal perovskite oxide lanthanum orthoferrite is a P-type semiconductor with excellent properties such as high thermal stability, non-toxic and high-efficiency. LF has an orthorhombic perovskite structure.

It is still challenging to obtain novel desired A- or B-sites substituted compounds structured of LF with a lot of applications that may changes the composition and symmetry of the perovskite and create cation or oxygen vacancies, which have a major effect on the band structures and photocatalytic activity of these materials. Moreover, many other properties, such as adsorption properties can also be designed by substitution on both A and B sites. In addition, doping of the X site could also affect the structure and BG of perovskites. The substitutions at A and/or B site of LF carried out by many ions such as Ag, Zn, Pb, Cr, Co are observed to have a great influence on the particle size, magnetic properties and photocatalytic activity of LF. In the past ten years, much attention has been paid to investigate how can be possible to improve photocatalytic activity of LF powders by doping elements. Muhammad Humayun et al. [2] Synthesis of ZnO/Bi-doped porous LF nanocomposites as highly efficient nano-photocatalysts and the prepared materials showed significantly improved visible-light activities.

Among several perovskites it has been found that LF is visible-light photocatalytic active due to its excellent optoelectronic properties and narrow band gap in visible light region. Which makes it a candidate for photocatalytic reaction. However, single LF perovskite catalyst also exhibit high recombination of photogenerated electron/hole pairs which weakens the function of the photocatalytic performance and doesn't show the complete degradation of organic pollutant, which is attributed to the low utilization of visible-light excited high level energy electrons and limited visible-light absorption.

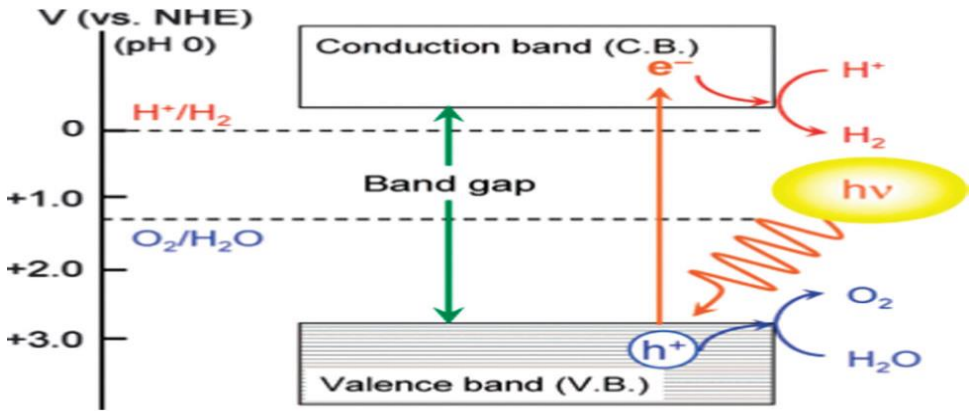


***Scheme 1.*** *Basic principle of the overall water splitting on a heterogeneous photocatalyst. Reproduced with permission from ref. 31. Copyright 2007, American Chemical Society.*

***Keywords:*** *perovskite, photocatalyst, sol-gel*

## References

[1] F. Bidrawn, G. Kim, N. Aramrueang, J. Vohs and R. Gorte, *J. Power Sources*, **2010**, *195*, 720-728.
[2] I. Troyanchuk, D. Karpinsky, R. Szymczak and H. Szymczak, *J. Magn. Magn. Mater.*, **2006**, *298*, 19-24.

# Fabrication of Amine and imine-functionalized Isoreticular Metal-Organic Frameworks for improved catalytic performance

**Somayeh Tarasi [1], Ali Morsali [1,*]**

[†]Department of Chemistry, Faculty of Sciences, Tarbiat Modares University, P.O. Box: 14115-175, Tehran, Iran. E-mail: Morsali_a@modares.ac.ir

Metal−organic frameworks (MOFs) are a class of porous materials with great potentials in catalysis , gas storage, and sensing [1]. An important feature of MOFs over other porous materials is the ability to tune their pore size, topology, and functionality by the deliberate design and selection of organic and inorganic molecular building blocks from which the network is constructed [2]. Taking advantage of this feature, chemists have tried to design and synthesize novel MOFs having particularly desired and predetermined functions and properties. In the present work, we could successfully indicate that subtle substrate selectivity can be induced in the catalytic system by designing a series of isoreticular MOFs with slight structural modifications. Four MOF catalysts possess imine and/or amine basic N-donor pillars bearing phenyl or naphtyl cores owing different hydrophobic character around the basic reaction center were prepared via simple mechano-chemical synthesis. They were characterized thoroughly using TG, IR and PXRD analysis. For the first time, aldol-type condensation reaction of malononitrile with ketone functionalized carbonyl substrates developed in the presence of the basic MOF organocatalysts.

***Keywords:*** *Metal-Organic Frameworks, catalytic.*

## References

[1] A. Azhdari Tehrani, L. Esrafili, S. Abedi, A. Morsali, L. Carlucci, D.M. Proserpio, J. Wang, P.C. Junk and T. Liu, *Inorg. Chem.*, **2017**, *56*, 1446-1454.
[2] T.R. Cook, Y.-R. Zheng and P.J. Stang, *Chem. Rev.*, **2013**, *113*, 734-777.

# Magnetic Mesoporous SBA-15 Functionalized with a NHC Pd(II) Complex: An Efficient and Recoverable Nanocatalyst for Hiyama Reaction

Ayat Nuri, Yagoub Mansoori*, Abolfazl Bezaatpour, Fatemeh Ghahramani
Department of Applied Chemistry, Faculty of Science, University of Mohaghegh Ardabili, Ardabil, Iran, 56199-11367.
*E-mail: ya_mansoori@yahoo.com; ya_mansoori@uma.ac.ir

In this study, magnetic nanoparticles (MNPs) were prepared by co-precipitation method under ultrasound and then successively covered by a silica shell and a mesoporous silica (SBA-15) with a high surface area. Magnetic mesoporous nanoparticles of $Fe_3O_4$@$SiO_2$@SBA-15 were then reacted with 3-chloropropyltriethoxysilane (CPTS), sodium salt of imidazole and 2-bromopyridine to give $Fe_3O_4$@$SiO_2$@SBA-15 functionalized with 3-(pyridin-2-yl)-1H-imidazol-3-ium-propyl (PIP) [1] as a supported pincer ligand for Pd(II). The functionalized mesoporous MNPs were then treated with *t*-BuOK at -80°C in THF and then reacted with $[PdCl_2(SMe_2)_2]$ to give supported Pd(II)-carbene complex containing C,N-bidentate ligand. The chloride ions were then exchanged by bromide ions using a NaBr solution of diethylether/acetone mixture, Scheme 1. The prepared magnetic nanoparticles were effectively used in the coupling reaction of triethoxyphenylsilane with aryl halides (Hiyama reaction) in the presence of a base [2]. The reaction parameters such as solvents, amount of catalyst, base and temperature were optimized. The catalyst was then magnetically decanted, washed, and reused several times.

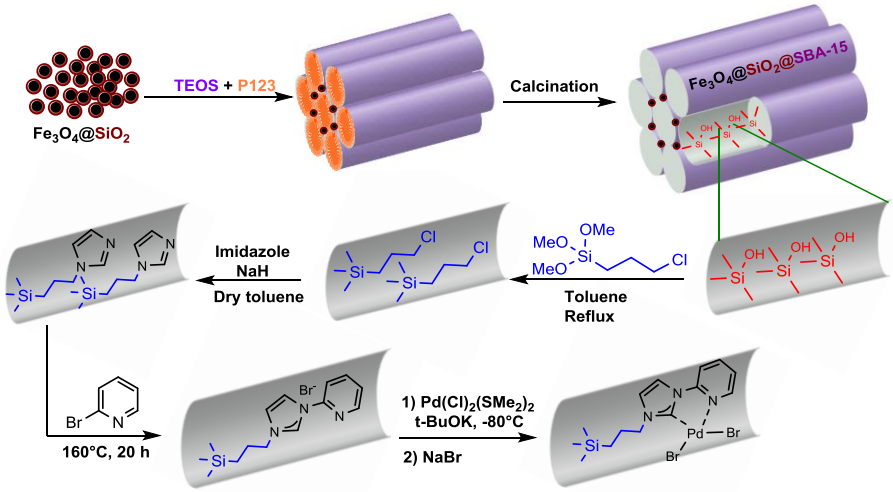


***Scheme 1.*** Synthesis of supported PIP-Pd(II) complex.

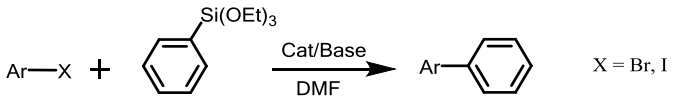


***Scheme 2.*** *Hiyama reaction*

***Keywords:*** *Carbene-pyridine Pd(II) complex, Hiyama reaction, Heterogeneous catalyst, magnetic mesoporous nanoparticles.*

## References

[1] Loch J.A., Albrecht M., Peris E., Mata J.,. Faller J.W, Crabtree R.H., *Organometallics*, **2002,** *21*, 700-6.
[2] Santosh K. Gurung, Surendra Thapa, Adarsh S. Vangala, and Ramesh Giri, *Organic Letters*, **2013**, *15*, 5378-5381.

# Oxo-vanadium Schiff base supported on $Fe_3O_4$ nanoparticles as a magnetically separable nanocatalyst for epoxidation of olefins

**Mojtaba Bagherzadeh[1], Mohammad Bahjati[1]***
[1]Department of Chemistry, Sharif University of Technology, Tehran, Iran
**E-mail: mohammad.bahjati@ch.sharif.edu*

Oxidative catalysis is an important part of research for the preparation of chemical products in industry and chemistry. Oxidation in the presence of metal that has the ability to activate the oxidant for oxidation reaction is one of the most important chemical reactions [1]. In the last decade, due to the rapid development of nanoscience, nanocatalysts developed for different reactions such as C-C coupling and oxidation reactions. The separation of nanocatalysts using magnetic nanoparticles enables us to easily recover nanocatalysts after reaction. Also, due to the size of nanoparticles, magnetic nanocatalysts exhibit high activity [2].

A new magnetically recoverable nanocatalyst has been developed via covalent grafting of the vanadyl acetylacetonate complex ($VO[acac]_2$) onto modified magnetic nanoparticles (MNPs). The nanocatalyst was characterized by elemental analysis (CHN), FT-IR, X-ray powder diffraction (XRD), field emission scanning electron microscopy (FE-SEM), inductively coupled plasma optical emission spectrometry (ICP-OES) and thermogravimetric analysis (TGA). The resulting nanoparticles were used as a recyclable catalyst for the epoxidation of olefins (Scheme 1). To find suitable conditions for epoxidation reaction, different parameter such as solvent, temperature, reaction time, amount of the nanocatalyst and oxidant/substrate molar ratio has been investigated. Eventually, conversion of various substrates was measured by gas chromatography (GC). To examine the stability and reusability of the nanocatalyst, at the end of each reaction, the nanocatalyst was separated from the reaction mixture with a magnet, washed with $C_2H_4Cl_2$ and dried to prepare for the next run.

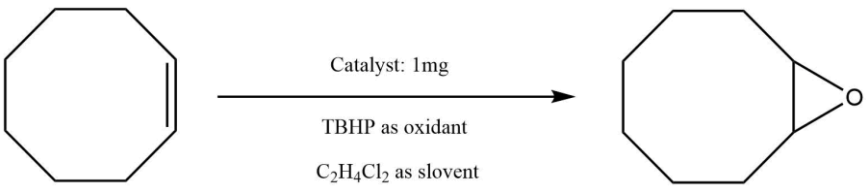


***Scheme 1.*** *Epoxidation of cis-cyclooctene*

***Keywords:*** *Magnetically nanocatalyst, Epoxidation, Olefin.*

## References

[1] R.K. Sharma, M. Yadav, Y. Monga, R. Gaur, A. Adholeya, R. Zboril, R.S. Varma and M.B. Gawande, *ACS Sustainable Chemistry & Engineering*, **2016**, *4*, 1123-1130.
[2] V. Polshettiwar, R. Luque, A. Fihri, H. Zhu, M. Bouhrara and J.-M. Basset, *Chem. Rev.*, **2011**, *111*, 3036-3075.

# Ultrasound-assisted synthesis of tetrahydrobenzo[b]pyran derivatives catalyzed by cobalt ferrite magnetic nanoparticles

**Miad Mostafaei**[1], **Saeid Taghavi Fardood**[1,*], **Fariba Saadati**, **Ali Ramazani**[1,2]
[1]Department of Chemistry, University of Zanjan, Zanjan, Iran
[2]Research Institute of modern biological techniques, University of Zanjan, P O Box 45195-313, Zanjan, Iran
*E-mail: saeidt64@gmail.com

The synthesis of tetrahydrobenzo[b]pyran derivatives is important because of their wide range of applications. These molecules are commonly employed in many felds such as anticoagulant, anticancer, spasmolytic, antibacterial, anti-anaphylactic activity, and diuretic [1,2].
Sonochemical synthesis is a facile, rapid, powerful and environmentally friendly technique, which has recently been applied to the synthesis of organic compounds. Ultrasonic irradiation formed bubbles, and their collapse generated localized hot spots with very short life-times and extremely high temperatures and pressures (up to 5000 °C and 2000 atm). An ultrasound approach is an important technique with prominent features including increased reaction rates, high yields, easier manipulation, mild reaction conditions, and waste minimization compared with traditional methods. Ultrasound is a more convenient method for green and sustainable synthetic processes [3,4].
In the present study, we have reported an efficient and convenient approach to the green synthesis of tetrahydrobenzo[b]pyrans using cobalt ferrite magnetic nanoparticles as the catalyst under ultrasound irradiation. This reaction was carried out through a three-component condensation reaction of malononitrile, dimedone and aldehyde in the presence of cobalt ferrite magnetic nanoparticles as a catalyst in water under ultrasound irradiation. This method provides several advantages such as environment friendliness, high yields and simple work-up procedure. Also, this catalyst can be easily separated from the reaction and recycled six times without activity loss.

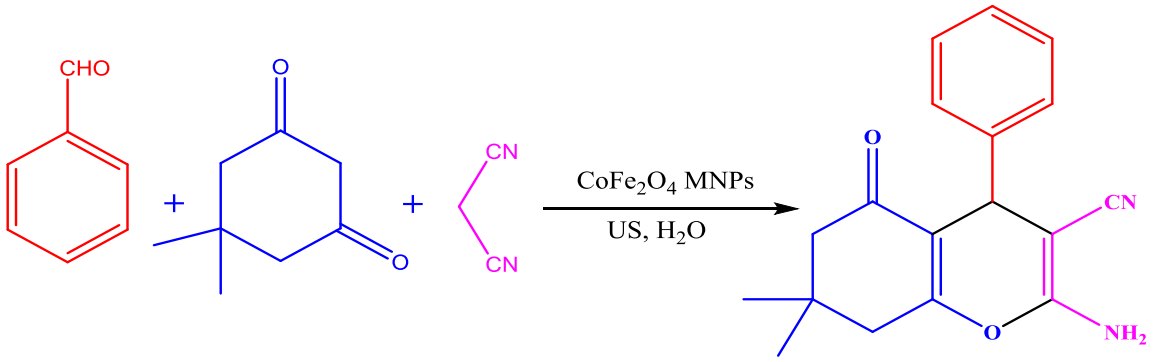


***Scheme 1.*** *Synthesis of tetrahydrobenzo[b]pyran derivatives*

***Keywords:*** *Tetrahydrobenzo[b]pyran, Ultrasound irradiation, Magnetic catalyst*

## References

[1] H. Naeimi and M.F. Zarabi, *Res. Chem. Intermed.*, **2018**, *44*, 3227-3247.
[2] A. Saini, S. Kumar and J.S. Sandhu, *Synlett*, **2006**, *2006*, 1928-1932.
[3] T.-S. Jin, J.-S. Zhang, A.-Q. Wang and T.-S. Li, *Ultrason. Sonochem.*, **2006**, *13*, 220-224.
[4] A.V. Chate, U.B. Rathod, J.S. Kshirsagar, P.A. Gaikwad, K.D. Mane, P.S. Mahajan, M.D. Nikam and C.H. Gill, *Chin. J. Catal.*, **2016**, *37*, 146-152.

# Copper ferrite as a magnetic heterogeneous catalyst for the synthesis of 2-Amino-4H-Chromenes

**Behrooz Ebadzadeh[1,*], Saeid Taghavi Fardood[1], Ali Ramazani[1,2]**
[1]Department of Chemistry, University of Zanjan, Zanjan, Iran
[2]Research Institute of Modern Biological Techniques (RIMBT), University of Zanjan, Zanjan, Iran
*E-mail: ebadzade33@yahoo.com

The development and improvement of eco-friendly technologies is the most challenging task in the contemporary chemistry and chemical industry. With this objective, the reduction of wastes together with the use of renewable feedstocks, environmentally benign solvents and reagents, effectively recoverable catalysts are important parameters to achieve more sustainable approaches according to the green chemistry principles. Due to high atom economy, great efficiency and procedural convenience in the construction of complex structures from three or more reactants, multicomponent reactions (MCRs) have been an efficient and powerful tool in the modern synthetic chemistry. And the discovery of novel MCRs and development of known MCRs are highly compatible with the aims of sustainable and green chemistry [1-4].

In this work, an efficient and eco-friendly procedure for the synthesis of 2-Amino-4H-Chromenes has been developed through a one-pot three-component condensation of aldehydes with 2-naphthol and malononitrile in the presence of magnetic Copper ferrite nanoparticle as a heterogeneous catalyst under solvent-free conditions (Scheme 1). This new procedure offers several advantages such as short reaction time, excellent yields, operational simplicity and without any tedious work-up for catalyst recovery or product purification. Moreover, the catalyst could be simply separated by an external magnet and reused four times without significant loss of catalytic activity.

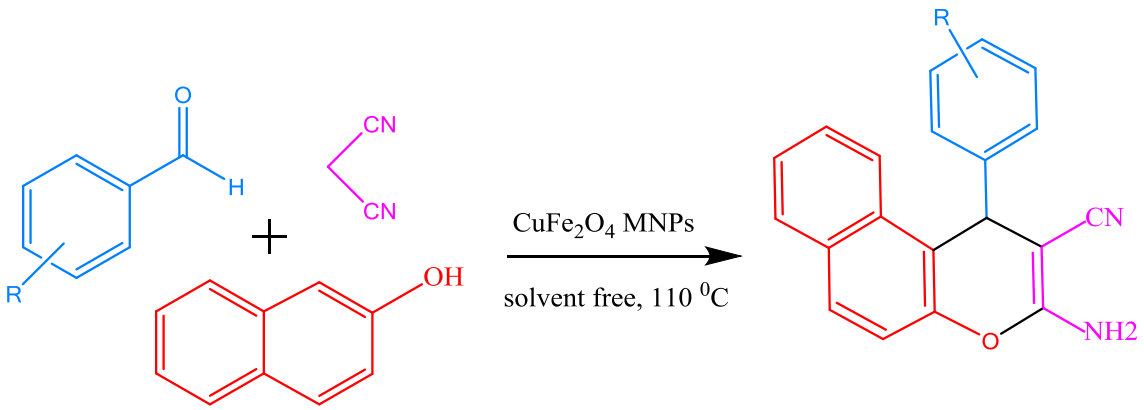


***Scheme 1.*** *The synthesis of 2-amino benzo[h]chromenes catalyzed by $CuFe_2O_4$ MNPs as catalyst*

***Keywords:*** *Copper ferrite nanoparticle; Benzochromene derivatives; Solvent free*

## References

[1] C.H. Christensen and J.K. Nørskov, *Science*, **2010**, *327*, 278-279.
[2] A.R. Moosavi-Zare, M.A. Zolfigol, O. Khaledian, V. Khakyzadeh, M.D. farahani, M.H. Beyzavi and H.G. Kruger, *Chem. Eng. J.*, **2014**, *248*, 122-127.
[3] H. Sheibani, K. Saidi, M. Abbasnejad, A. Derakhshani and I. Mohammadzadeh, *Arabian J. Chem.*, **2016**, *9*, S901-S906.
[4] R. Ballini, G. Bosica, M.L. Conforti, R. Maggi, A. Mazzacani, P. Righi and G. Sartori, *Tetrahedron*, **2001**, *57*, 1395-1398.

# A Review on Catalytic Applications of Metal-Organic Frameworks

**Roghayyeh Hosseininia and Farough Nasiri***
Department of Applied Chemistry, Faculty of Science, University of Mohaghegh Ardabili, Ardabil, Iran, 56199-11367.
**E-mail: nasiri@uma.ac.ir*

Metal organic frameworks (MOFs) are porous crystalline materials that they constructed by the building units include metal ion/cluster and organic bridging ligands using strong chemical bonds to create open crystalline network with fixed porosity [1, 2]. These porous materials with high surface area and large structural variety lead to a wide range of applications including separations, gas capture and storage, ion-exchange, drug delivery, sensing and catalysis. In recent years the application of MOFs as catalyst in organic reactions such as tandem reactions has attracted more attention due to their adjustable open metal center, functional organic linker, and active guest species in their pores (Fig. 1). In this review paper, the catalytic applications of MOFs with multiple active sites in organic catalysis, photocatalysis and tandem reactions are discussed.

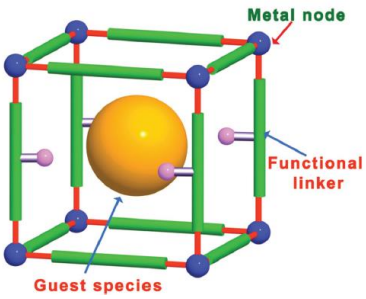


**Fig. 1** Different types of MOF active sites, including metal nodes, functional organic linkers, and guest species in the pores.

***Keywords:*** *Metal-organic frameworks, Porous materials, Organic bridging ligands, Catalysis, Tandem reactions*

## References

[1] H. Furukawa, K. E. Cordova, M. O'Keeffe, O. M. Yaghi, *Science* **2013**, 341, 1-12.
[2] YB. Huang, J. Liang, XS. Wang, R. Cao, *Chem. Soc. Rev.*, **2017**, 46, 126-157.

# Trietheylamine Catalyzed One- Pot Solvent-Free Synthesis Of 3-Alkyl-5-((5-(Chloromethyl)Furan-2-yl)methylene)-2-Thioxothiazolidine-4-One

**Leila Sabahi-Agabager and Farough Nasiri*,**
Department of Applied Chemistry, University of Mohaghegh Ardabili, Ardabil, Iran, 56199-11367,
**Email: nasiri@uma.ac.ir*

Rhodanines, thiazolidinediones, and related heterocycles have been discussed extensively and controversially as key structures in medicinal chemistry [1]. Rhodanines are known to have biological activities, such as anti-diabetic, anti-inflammatory, anti-oxidant, anti-tubercular, anti-microbial, anti-convulsant and cytotoxic activities [2]. Rhodanine derivatives with the exocylic double bond at position five are the most commonly synthesized rhodanine derivatives. 5-Arylmethylidenerhodanines usually synthesized by base-catalyzed Knoevenagel condensation between rhodanines or *N*-substituted rhodanines and aromatic aldehydes, using either conventional or microwave heating [3]. 5-(Chloromethyl)furfural (CMF) is newable platform molecule which can be derived in a single step from sugars, cellulose, or raw biomass [4].
In this paper we wish to report a simple one-pot solvent-free procedure to prepare 3-alkyl-5-((5-(chloromethyl)furan-2-yl)methylene)-2- thioxothiazolidine-4-ones via the reaction of primary amines, carbon disulfide, and bromoethylacetate and CMF in the presence of a catalytic amount of triethylamine (Scheme 1). The structure of the synthesized compounds were fully confirmed by spectroscopic (IR, $^{1}$HNMR, $^{13}$C NMR, and Mass) analysis.

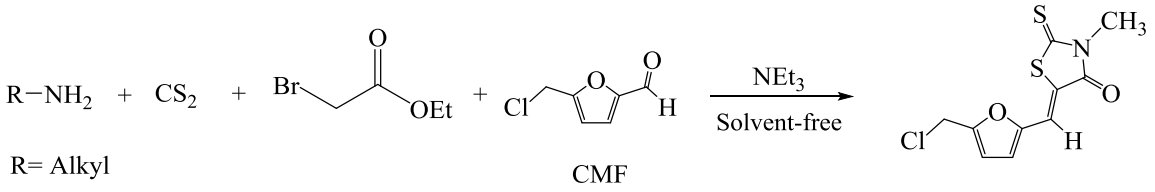


***Scheme 1.*** *One-pot solvent-free synthesis of 3-alkyl-5-((5- (chloromethyl)furan-2-yl)methylene)2- thioxothiazolidine-4-one*

***Keywords:*** *5-Arylmethylidenerhodanines, one-pot, 5- Chloromethylfurfural.*

## References

[1] A C. Nitsche, V.N. Schreier, M. A. M. Behnam, A. Kumar, R.Bartenschlager and C. D. Klein, *J. Med. Chem*. **2013**, *56*, 8389-8403.
[2] S. Mandal, M. Mithuna, A. Garg, S. sahetya, N. Ramesh, S. Vashitha, M. Mendon Manjunath, S. Sitaram, M. Soni, N. Baig, V. Kumar and P. Kumar, *RSC Adv.*, **2016**, *6*, 58641-58653.
[3] S.S. Alneyadi, *Heterocycles*, **2018**, *96*, 803 - 838.
[4] F.Chang, W.-H. Hsu, M. Mascal, *Sustainable Chemistry and Pharmacy*, **2015**, *1*, 14-18.

# Multicomponent, solvent-free synthesis of 12-aryl-8,9,10,12-tetrahydrobenzo[*a*]-xanthen-11-one derivatives catalyzed by copper ferrite magnetic nanoparticles

**Behrooz Ebadzadeh[1,*], Saeid Taghavi Fardood[1], Ali Ramazani[1,2]**
[1]Department of Chemistry, University of Zanjan, Zanjan, Iran
[2]Research Institute of Modern Biological Techniques (RIMBT), University of Zanjan, Zanjan, Iran
**E-mail:* ebadzade33@yahoo.com

Xanthenes and its derivatives are known as an important class of heterocyclic compounds widely used as leco-dye, in laser technology and pH sensitive fluorescent materials. Although not widely found in nature, xanthenes and compounds based on these core templates exhibit a broad spectrum of pharmaceutical activities. These compounds are also utilized as antagonists for paralyzing action of zoxazolamine and in photodynamic therapy. Thus a broad utility range has made xanthenes prime synthetic candidates thereby accentuating the need to develop newer synthetic routes for scaffold manipulation of xanthene derivatives. A few methods have been developed for the synthesis of 12-aryl-8,9,10,12-tetrahydrobenzo[a]xanthen-11-one derivatives. One-pot three-component condensation of aldehydes, 2-naphthol and cyclic 1,3-dicarbonyl compound is the most convenient method for the preparation of these compounds. In this context some methods and catalysts have been reported. However, these methodologies show varying degrees of success as well as limitations due to use of toxic organic solvents, expensive catalyst, prolonged reaction times, the requirement of special apparatus, or harsh reaction conditions. Thus, there is a certain need for the development of an alternative route for the production of these derivatives, which surpasses those limitations [1-4].
In this work, an efficient and direct protocol for the preparation of 12-aryl-8,9,10,12-tetrahydro-benzo[a] xanthen-11-one derivatives employing a three-component one-pot reaction of aryl aldehydes, 2-naphthol and dimedone in the presence of a catalytic amount of copper ferrite nanoparticles under solvent-free conditions is described (Scheme 1). High yields, ease of recovery, and reusable catalyst with consistent activity makes this protocol efficient and environmentally benign.

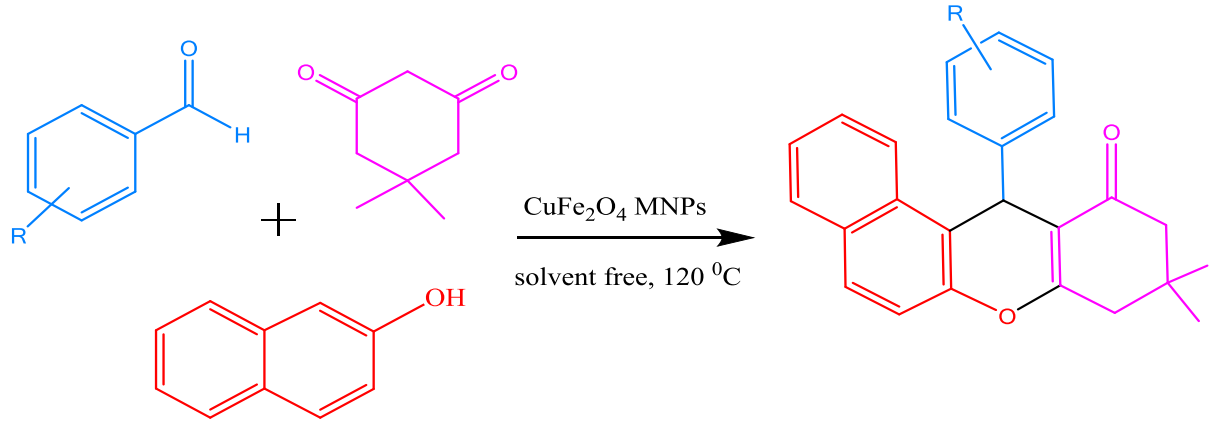


***Scheme 1.*** *Synthesis of 12-aryl-8,9,10,12-tetrahydrobenzo[a]xanthen-11-one derivatives*

***Keywords:*** *Copper ferrite nanoparticle; Xanthenes; Multicomponent reactions*

## References

[1] Z. Karimi-Jaberi and M.M. Hashemi, *Monatsh. Chem.*, **2008**, *139*, 605-608.
[2] M.A. Pasha and V.P. Jayashankara, *Bioorg. Med. Chem. Lett.*, **2007**, *17*, 621-623.
[3] B. Bi Fatemeh Mirjalili, A. Bamoniri and L. Zamani, *Lett. Org. Chem.*, **2012**, *9*, 338-343.
[4] G.C. Nandi, S. Samai, R. Kumar and M. Singh, *Tetrahedron*, **2009**, *65*, 7129-7134.

# Mo(VI)-Supported Complex on Birhodanine Anchored Magnetite Nanoparticles for Epoxidation Reaction

**Arman Rahmaninia [1], Yagoub Mansoori [1*], Farough Nasiri [1], Abolfazl Bezaatpour [1], Behnam Babaei [1]**

[1] Department of Applied Chemistry, Faculty of Science, University of Mohaghegh Ardabili, Ardabil, Iran, 56199-11367.

*E-mail: ya_mansoori@yahoo.com; ya_mansoori@uma.ac.ir

Herein, we have examined magnetite support birhodanine (TMOS-BIRD) in the synthesis of a new Mo(VI) heterogeneous catalyst, (Scheme 1). The new nanocatalyst ($Fe_3O_4$@TMOS-BIRD/$MoO_2$) was characterized using Fourier Transform infrared (FT-IR) spectroscopy, scanning electron microscopy (SEM), transmission electron microscopy (TEM), diffuse reflectance spectroscopy (DRS), vibrating sample magnetometry (VSM), energy-dispersive X-ray spectroscopy (EDX), Brunauer-Emmett-Teller surface area analysis (BET) and powder X-ray diffraction (XRD).

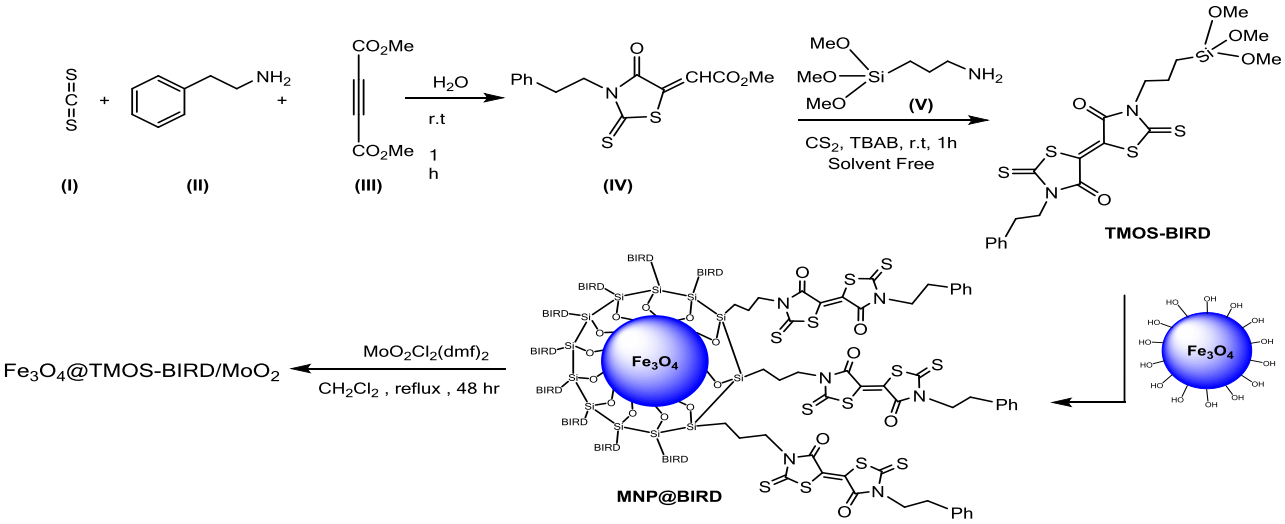


*Scheme 1. Synthesis of MNP@BIRD-Mo nanoparticles.*

We have tested the applicability of the obtained magnetic catalyst in the epoxidation reaction of olefins with tert-butyl hydroperoxide (TBHP) as oxidant. The final results has confirmed our vision as anticipated. The supported Mo complex exhibited 100 % selectivity for epoxidation of cyclooctene with 97 % conversion, (Scheme 2). The catalytic activity and selectivity of heterogeneous catalyst have not changed after three times of reusing [1-3].

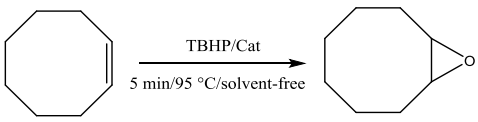


*Scheme 2. Catalytic epoxidation reaction of olefins*

***Keywords***: Mo(VI) complex, Birhodanine, Magnetic Nanoparticles, Catalysis, Epoxidation

## References

[1] A. Bezaatpour, E. Askarizadeh, S. Akbarpour, M. Amiria and B. Babaei, *Molecular Catalysis*, **2017**, *436*, 199-209.
[2] A. Bezaatpour, S. Khatami and M. Amiri, *RSC Adv.*, **2016**, *6*, 27452-27459.
[3] J. Zhang, P. Jiang, Y. Shen, W. Zhang and G. Bian, *J. Porous Mater.*, **2016**, *23*, 431-440.

# Photocatalytic reduction of environmental pollutant Cr (VI) in a pillared metal–organic framework by Solvent-Assisted Ligand exchange.

**Nasrin Shokouhfar, Mohammad Yaser Masoomi, Ali Morsali***
Department of chemistry, Tarbiat Modares University, Tehran, Iran
*Morsali_a@modares.ac.ir

Metal–organic frameworks (MOFs) are an attractive class of hybrid materials that incorporate the rigidity of inorganic compounds with the flexibility and the tunability of organic materials.[1] Solvent-assisted linker exchange (SALE) is a postsynthesis route that has been approved as a practical strategy to alter the structures and properties of MOFs.[2] Organic ligand substitutions which take place at metal ions are essentially attributed to the reversible nature of the coordination bonds between metal ions and organic ligands in MOFs. SALE can provide pore engineering mechanisms including the control of the pore volume and environment while creating missing linker "defects" at metal centers.[3] Moreover, SALE enhances MOF performance in gas uptake, catalysis, proton conductivity, etc.[4] Herein, SALE was performed on a pillared metal–organic framework (MOF), $[Zn_2(oba)_2(4\text{-bpdb})]_n\cdot(DMF)_2$ (TMU-4), to tune their photocatalytic properties. The pillar ligands were successfully incorporated into this MOFs to generate daughter MOFs TMU-4′ and TMU-6′, which possess higher BET surface areas. Moreover, a study was performed to examine the photocatalytic performance of these parent and daughter MOF in photoreduction of Cr(VI) under visible light irradiation. Finally, the reduction mechanism was investigated by using various scavengers including $AgNO_3$, t-butyl alcohol, BQ and ammonium oxalate.

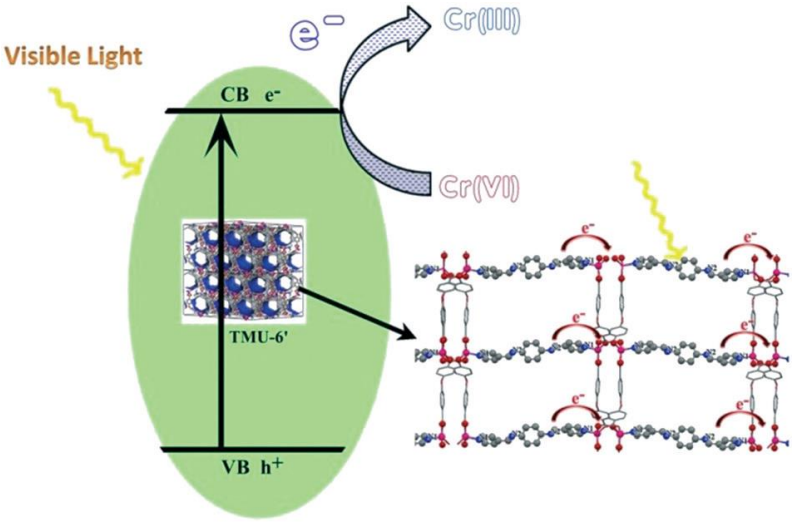


***Scheme 1.*** *A schematic illustration of Cr(VI) reduction over the TMU-6′ photocatalyst under visible light irradiation.*

***Keywords:*** *Metal–organic frameworks (MOFs), Solvent-assisted linker exchange (SALE), photoreduction of Cr(VI).*

## References

[1] P. Falcaro, R. Ricco, C. M. Doherty and K. Liang, *Chem. Soc. Rev.*, **2014**, *43*, 5513–5560.
[2] C. J. Stephenson, J. T. Hupp and O. K. Farha, *Inorg. Chem.*, **2016**, *55*, 1361–1363.
[3] J. Canivet, M. Vandichel and D. Farrusseng, *Dalton Trans.* , **2016**, *45*, 4090–4099.
[4] S. Kim, K. W. Dawson, B. S. Gelfand, J. M. Taylor and G. K. Shimizu, *J. Am. Chem. Soc.*, **2013**, *135*, 963–966.

# Nano-$CeO_2$ Catalyzed Efficient Synthesis of Benzoxazole and Benzimidazole by the Reaction Between 2-Amino phenol and 1, 2-Phenyldiamine with Trimethyl orthoformate

**Reyhaneh Samae[1], Bita Baghernejad[2] and Farough Nasiri[1]**
[1]Department of Applied Chemistry, Faculty of Science, University of Mohaghegh Ardabili, Ardabil, Iran, 56199-11367.
*E-mail: nasiri@uma.ac.ir
[2]Department of Chemistry, School of Science, Payame Noor University, Iran,
E-mail: bitabaghernejad@yahoo.com

Benzoxazoles are the most important heterocyclic compounds that have wide range of pharmacological activities, synthetic and industrial applications [1]. Benzoxazoles have also attracted considerable research attention due to their unique properties and wide applications.
Benzimidazoles are very useful intermediates for the development of molecules of pharmaceutical or biological interest [2]. In this work we wish to report efficient synthesis of benzoxazole from the reaction of 2-aminophenol and trimethylortho formate in the presence of nano cerium oxide (IV) as a catalyst in DMF under reflux condition for specified time at a certain temperature (Scheme 1).
Benzimidazole also was synthesized from the reaction of 1,2-phenyldiamine with trimethylortho formate in the presence of nano cerium oxide (IV) as a catalyst (Scheme 2).
Nano cerium oxide (IV) is not soluble in the solvent and can separate very simple from the reaction. Another benefit of this method can be referred to high yield and easy work-up.

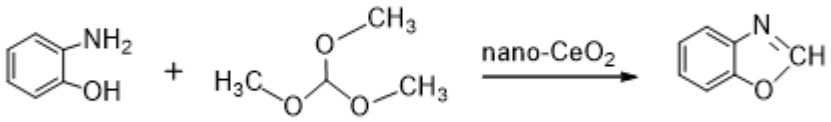


***Scheme 1***: Synthesis of benzoxazole

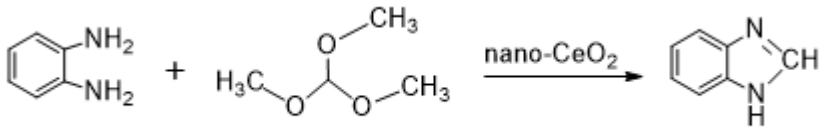


***Scheme 2***: Synthesis of benzimidazole

***Keywords:*** *2-Amino phenol, 1 ,2-phenyldiamine, trimethylortho formate, nano catalyst, cerium oxide (IV)*

## References

[1] Y. Sato, M. Yamada, Yoshida, S. Soneda, T. Ishikawa, M. Nizato, T. Suzuki, K. Konno, *J. Med. Chem.* **1998**, *41*, 3015-3021.
[2] Z. S. Zaho, D. O. Arnaiz, B. Griedel, S. Sakata, J. L. Dallas, M. Whitlow, L. Trinh, A. Liang, M. M. Morrissey, K. J. Shaw, *Bioorg. Med. Chem. Lett.* **2000**, *10*, 963-966.

# Magnetic nanocomposite based on nickel-bismuth ferrite for photocatalytic degradation of organic dyes

**Alireza Yaghoubi[1,*], Saeid Taghavi Fardood[1], Ali Ramazani[1, 2]**
[1]Department of Chemistry, University of Zanjan, Zanjan, Iran
[2]Research Institute of Modern Biological Techniques (RIMBT), University of Zanjan, Zanjan, Iran
**E-mail:* alirezayaghoubi62@yahoo.com

Multiferroics are class of materials that have ferroelectric, ferromagnetic or antiferromagnetic properties [1].The one of the most largely studied multiferroic materials over the last decade is about bismuth-ferrite ($BiFeO_3$) because it is the only single phase material that can act both as antiferromagnetic and ferroelectric at room temperature [2].The addition of Ni, Zn, Mn, Ti, Zr etc. to $BiFeO_3$ improves the ferroelectric properties [3, 4]. Among the many atoms, Ni is the best candidate in improving the ferromagnetic properties. In addition, the Ni substitution is also found to be effective for enhancing the ferroelectricity in $BiFeO_3$ [3-5]. It has been indicated that $BiFeO_3$ nanoparticles have a band gap in the range of 2.5–3.0 eV. [5, 6].

In the present study, Ni-Bi-Fe magnetic photocatalysts were successfully synthesized by the sol–gel technique using nickel, bismuth and iron nitrate powders as precursor. Synthesized photocatalyst exhibited excellent catalytic activity for the degradation of Congo red and reactive blue 222 as model dyes in water under visible irradiation. The results showed that degradation efficiency depend on amount of catalyst, initial dye concentration, and irradiation time. The structural and properties of The as-synthesized photocatalyst was characterized by different techniques including X-ray diffraction (XRD), Scanning electron microscopy (SEM), Fourier transform infrared (FT-IR) spectroscopy, energy dispersive analysis of X-ray (EDAX) and UV-vis spectroscopy (UV-vis).

The photocatalyst could easily be separated from the reaction mixture due to the it's magnetic properties and remain active.

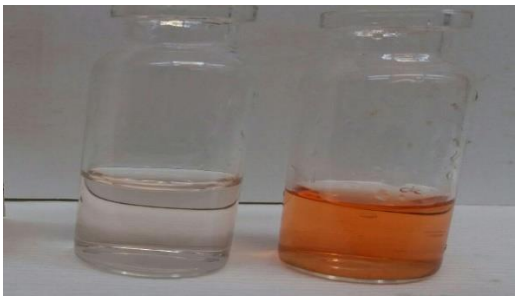

***Scheme 1.*** *Degradation of Congo red dye (20 ppm) using synthesized photocatalyst (0.02 g) in 70 minute under visible irradiation.*

***Keywords:*** *Nickel–bismuth ferrite, Magnetic nanocomposite, photocatalytic degradation.*

## References

[1] P. Borisov, A. Hochstrat, X. Chen, W. Kleemann, C. Binek, *Phys. Rev. Lett.* **2005**, 94, 117203-4.
[2] P. Fischer, M. Polomska, I. Sosnowska, M. Szymanski, *J. Phys. C. Solid State*, **1980**, 13 1931–1940.
[3] S.K. Singh, H. Maruyama Kand Ishiwara, *Appl. Phys. Lett.*, **2007**, 91,112913.
[4] S.K. Singh, R. Palai, H. Maruyama Kand Ishiwara, *Electrochem. Solid-State Lett.*, **2008,** 11, G30–2.
[5] X. Xu, W. Liu, H. Zhang, M. Guo, P. Wu, S. Wang , J. Gao and G. Rao, *J. Appl. Phys.*, **2015**, 117 174106
[6] J. Zhao , X. Zhang ,S. Liu , W. Zhang and Z. Liu, *J. Alloys Compd.*, **2013**, 557, 120–3.

# Green synthesis of $AlFeO_3$ nanoparticles using tragacanth gum as a photocatalyst in degradation of Congo red dye from aqueous solution

**Saeid Taghavi Fardood[1,*], Miad Mostafaei[1], Fariba Saadati[1], Ali Ramazani[1,2]**
[1]Department of Chemistry, University of Zanjan, Zanjan, Iran
[2]Research Institute of modern biological techniques, University of Zanjan, P O Box 45195-313, Zanjan, Iran
*E-mail: saeidt64@gmail.com

$ABO_3$ type perovskites are of abiding interest to both experimentalists and theoreticians due to their practical applications in catalysis, sensing, magnetoresistance devices and spintronics. In addition to their engineering relevance, recent studies have revealed rich underlying physics. $ABO_3$ type perovskite oxides with B-site doping have been extensively studied to optimize relevant physical properties such as ferroelectricity, superconductivity, and ferromagnetism in the product phases. It may be noted that typically, in this system, the A sites are occupied by divalent or trivalent metals and the B sites are occupied by tetravalent or trivalent ions. B cations are known to be substantial determinants of the physical properties of the $ABO_3$ system. This is due to the localized and/or collective behavior of the d-electrons associated with the B ion. Iron-based semiconductors ($AFeO_3$), such as $BiFeO_3$, $LaFeO_3$, $YFeO_3$ etc., have also drawn attention in recent years; primarily owing to the possibility of developing narrow band gap semiconductors, and hence opening new possibilities for harnessing sun light (eg. through visible light photocatalysis) [1-3].
AFeO3 has also found a unique place in research of ferroic systems. In fact one of the recent developments in this family of perovskite oxides is the discovery of ferroelectricity and magnetic ordering in $AlFeO_3$ material. An important report comes from the experimental work of Bouree et al. [4], wherein they reported the synthesis and detailed study of the crystal structure of $AlFeO_3$. They also studied the magnetic structure of piezoelectric, ferrimagnetic and magnetoelectric properties of $AlFeO_3$ from neutron powder diffraction.

$AlFeO_3$ nanoparticles have been produced via a simple green method from zinc nitrate, iron nitrate and tragacanth gel as biotemplate. Prepared $AlFeO_3$ nanoparticles (NPs) were investigated by employing through X-ray diffraction (XRD), Fourier transform infrared (FTIR), field emission-scanning electron microscope (FE-SEM), and energy dispersive X-ray analysis (EDX), respectively. XRD, FTIR, EDX show that the highly pure $AlFeO_3$ nanostructures. Moreover, the photocatalytic activity of synthesized $AlFeO_3$ in the reduction of Congo red dye under visible light irradiation was studied by UV–Vis spectroscopy. The effects of initial dye concentration, photocatalyst dose, and visible light irradiation on dye degradation were assessed. The results exhibition that the catalyst could remove *ca.* 93% of the Congo red dye.

***Keywords:*** *Congo red dye, Green synthesis, Photocatalyst, $AlFeO_3$ nanoparticles*

## References

[1] H. Lee, S. Cheong and B.G. Kim, *J. Solid State Chem.*, **2015**, *228*, 214-220.
[2] Q. Li, S. Wang, Y. Yuan, H. Gao and X. Xiang, *J. Sol-Gel Sci. Technol.*, **2017**, *82*, 500-508.
[3] Y. Kozuka, M. Kim, C. Bell, B.G. Kim, Y. Hikita and H. Hwang, *Nature*, **2009**, *462*, 487.
[4] F. Bourée, J.-L. Baudour, E. Elbadraoui, J. Musso, C. Laurent and A. Rousset, *Acta Crystallographica Section B*, **1996**, *52*, 217-222.

# Sol-gel synthesis of $NiAL_2O_4$ nanoparticles and study of their photocatalytic activity for the degradation of direct blue 129 dye

**Saeid Taghavi Fardood[1], Behzad Eskandari Azar[1,*], Ali Ramazani [1,2]**
[1]Department of Chemistry, University of Zanjan, Zanjan, Iran
[2]Research Institute of Modern Biological Techniques (RIMBT), University of Zanjan, Zanjan, Iran

**E-mail: Eskandari.azar1980@gmail.com*

Materials at the nanometer scale have been studied for decades because of their unique properties arising from the large fraction of atoms residing on the surface, and also from the finite number of atoms in each crystalline core. Especially, because of the increasing need for high are a density storage, the synthesis and characterization of semiconductor nanocrystals have been extensively investigated [1,2]. The search for low cost and efficient photocatalysts is still continuing. Some spinel-type oxides such as $NiAl_2O_4$, $ZnAl_2O_4$ and $CuAl_2O_4$ used as photocatalysts are semiconductor materials with narrow band high and these materials have been proven to be an efficient in the degradation of pollutants and/or the production of photo-catalytic hydrogen [3-6]. Among the many types of oxide spinel materials، $NiAL_2O_4$ show a high catalytic property. In addition، nickel aluminate has a high thermal stability، high mechanical resistance، hydrophobicity and low surface acidity [7].
In this work, we have reported the synthesis of $NiAL_2O_4$ aluminate spinel nanoparticles (NPs) using sol-gel method and its photocatalytic dye degradation ability from aqueous solution were investigated. This method has various advantage such as nontoxic, economic viability, ease of scaling up, less time consuming and environmental friendly approach for the synthesis of $NiAL_2O_4$ NPs without using any organic chemicals. The synthesized nanoparticles were characterized by energy dispersive X-ray analysis (EDX), powder X-ray diffraction (XRD), field emission scanning electron microscopy (FESEM), Fourier transforms infrared spectroscopy (FTIR) and percent of dye degradation which was followed by UV–Visible spectroscopy. The effects of process parameters like, catalyst dosage, initial dye concentration, and visible light irradiation on dye degradation have been studied. The current photocatalyst exhibited notable catalytic activity for the degradation of direct blue 129 in water under visible light irradiation. This result suggests that as-obtained nanocrystalline nickel aluminate as favorable material has high potential to be used for photocatalytic applications under visible light.

***Keywords:*** *Sol-gel method, $NiAL_2O_4$ nanoparticles, Degradation of dye.*

## References

[1] S. Khademolhoseini, M. Zakeri, S. Rahnamaeiyan, M. Nasiri and R. Talebi, *J. Mater. Sci. Mater. Electron.*, **2015**, *26*, 7303-7308.
[2] F. Beshkar and M. Salavati-Niasari, *J. Nanostruct.*, **2015**, *5*, 17-23.
[3] L.K. De Souza, J.R. Zamian, G.N. da Rocha Filho, L.E. Soledade, I.M. dos Santos, A.G. Souza, T. Scheller, R.S. Angélica and C.E. da Costa, *Dyes Pigm.*, **2009**, *81*, 187-192.
[4] S. Khademolhoseini and R. Talebi, *J. Mater. Sci. Mater. Electron.*, **2016**, *27*, 2938-2943.
[5] M. Maddahfar, M. Ramezani, M. Sadeghi and A. Sobhani-Nasab, *J. Mater. Sci. Mater. Electron.*, **2015**, *26*, 7745-7750.
[6] R. Talebi, *J. Mater. Sci. Mater. Electron.*, **2016**, *27*, 5665-5669.
[7] X. Wang, N. Zhu and B. Yin, *J. Hazard. Mater.*, **2008**, *153*, 22-27.

# Photocatalytic degradation of acid orange 7 dye in the presence of $CuO/Al_2O_3$ nanocomposite

**Behzad Eskandari Azar[1], Saeid Taghavi Fardood[1]*, Ali Ramazani [1,2]**

[1]Department of Chemistry, University of Zanjan, Zanjan, Iran
[2]Research Institute of Modern Biological Techniques (RIMBT), University of Zanjan, Zanjan, Iran

**E-mail: saeidt64@gmail.com*

Waste water containing dyes originating from textile industrials is strongly toxic and carcinogenic. Therefore reducing dyes pollution, it is desirable to degrade the dye into nontoxic form before it is entered into nature, a wide range of remediation techniques as: biological, physical, and chemical methods have been applied for water decontamination [1,2]. Photocatalytic degradation is one of the most excellent green chemistry technology to convert the dyes due to its nontoxicity, inexpensive and harm- less by products. $Al_2O_3$ was used as a catalyst for the photo degradation organic dyes [3]. Introduction of some transition metals, such as Cr, V, Fe, Cu, Mn, Co, Ni, Mo etc. may lead to higher catalytic activity [4]. Concluded that the presence of a semiconductor like ($TiO_2$, ZnO, CuO and other) with $Al_2O_3$ lead to synergism between them, which improved their photocatalytic performance. In the present study, we synthesized a novel, simple and green method for the synthesis of synergism $CuO/AL_2O_3$ nanocomposite using natural gel as a biotemplate source by the means of sol-gel method and its photocatalytic dye degradation ability from aqueous solution were investigated. The synthesized nanocomposite was characterized by XRD, EDX, FT-IR, UV-visible spectroscopy. The effects of process parameters like, catalyst dosage, initial dye concentration, and visible light irradiation on dye degradation have been studied. The results displayed that catalytic activity of $CuO/AL_2O_3$ being more effective than CuO for degradation Acid orange 7.

***Keywords:*** *$CuO/Al_2O_3$ nanocomposite, Photocatalysis, Visible light irradiation*

## References

[1] A. Rubio-Clemente, R.A. Torres-Palma and G.A. Peñuela, *Sci. Total Environ.*, **2014**, *478*, 201-225.
[2] J. Trujillo-Reyes, J. Peralta-Videa and J. Gardea-Torresdey, *J. Hazard. Mater.*, **2014**, *280*, 487-503.
[3] F. Tzompantzi, Y. Pina, A. Mantilla, O. Aguilar-Martínez, F. Galindo-Hernandez, X. Bokhimi and A. Barrera, *Catal. Today*, **2014**, *220*, 49-55.
[4] I. Fechete, Y. Wang and J.C. Védrine, *Catal. Today*, **2012**, *189*, 2-27.

# Metal-Organic Frameworks for Catalytic Applications

**Najmeh varnaseri *, Ali ramazani**
Department of Chemistry, University of Zanjan, Zanjan, Iran
**E-mail: varnaserinajme@yahoo.com*

Metal-organic frameworks (MOFs) are formed by reticular synthesis, which creates strong bonds between inorganic and organic units The flexibility with which the constituents, geometry, size, and functionality can be varied has led to more than 20,000 different MOFs being reported and studied within the past decade. The surface area values of such MOFs typically range from 1000 to 10,000 m2/g, thus exceeding those of traditional porous materials such as zeolites and carbons. The extraordinary skeleton structure of MOFs provides many possibilities for incorporation of diverse basic functionalities, which is unachievable for conventional solid base. These aspects have made MOFs ideal candidates for storage of fuels (hydrogen and methane), capture of carbon dioxide, and catalysis applications.These solid bases have potential to catalyze some well-known "base-catalyzed reactions" like Knoevenagel condensation, aldol condensation, and Michael addition. Meanwhile, in contrast to conventional solid bases, MOFs show some different catalytic properties due to their special structural and surface properties. In this paper we provide a comprehensive review of MOFs derived solid bases, summarizing recent advances from various research groups.

***Keywords:*** *heterogeneous catalysis , metal–organic frameworks ,porosity*

## References

[1] M. Zhao, K. Yuan, Y.Wang,G.Li, J.Guo, H. Zhao, L.Gu, W.Hu and Z. Tang, *Nature* **2016**, 539, 76-80
[2] S. Lee, E. Kapustin and O.M Yaghi, *Science*, **2016**, 353, 808-811

# $Fe_3O_4$@RGO@Au@C Composite with Magnetic Core and Au Enwrapped in Double-Shelled Carbon: An Excellent Catalyst in the Reduction of Nitroarenes and Suzuki–Miyaura Cross-Coupling

**Noushin Farajinia Lehi**[1], **Minoo Dabiri**[1,*]
[1]Faculty of Chemistry and Petroleum Sciences, Shahid Beheshti University, Tehran 1983969411, Islamic Republic of Iran
*E-mail: m-dabiri@sbu.ac.ir

Magnetic core double-shelled carbon with Fe3O4 nanoparticles as the core, reduced graphene oxide (RGO) as the inner shell and carbon (C) layer as the outer shell, have been successfully designed and prepared. This tailor-making structure acts as an excellent capsule for encapsulating Au nanoparticles (Au NPs), which could effectively prevent Au NPs from aggregation and leaching. Because of its structural features, magnetic coredouble-shell Fe3O4@RGO@Au@C architecture exhibits extremely high catalytic performance on two different kinds of organic reactions (1) reduction of nitroarenes, and (2) Suzuki–Miyaura cross coupling of phenyl boronic acid with aryl halides. Moreover, the synthesized catalyst can be easily recovered and reused for at least ten cycles due to its magnetically separable feature and good stability.

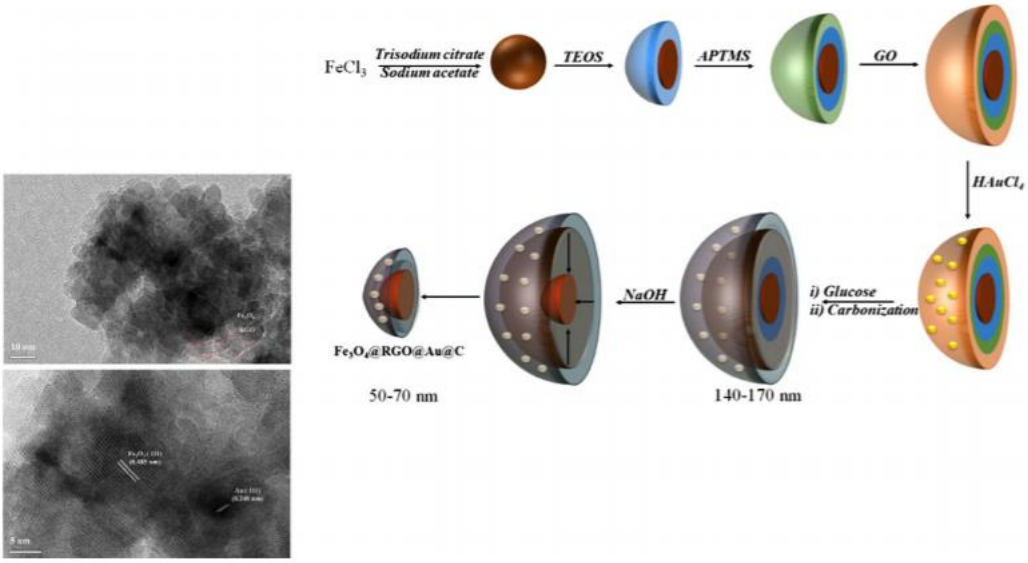


***Scheme 1.*** *Schematic diagram illustrating the synthesis of a RGO@Pd@C hollow sphere b magnetic core/double-shell $Fe_3O_4$@RGO@Au@C CDSNs architectures*

***Keywords:*** *Heterogeneous catalysis Suzuki reaction Nanostructure Reduction*

## References

[1] L. H. Reddy, J. Nicolas, J. L. Arias, P. Couvreur, *Chem Rev*. **2011**, *112*, 5818.

# DFT study of the effect of L-Proline as organocatalyst on nitoaldol condensation reaction

**Yasaman Nobakht*** **and Nematollah Arshadi**
Department of Chemistry, University of Zanjan, Zanjan, Iran

**E-mail: yasaman.nobakht@znu.ac.ir*

The nitroaldol condensation reaction is one of the most synthetically useful organic reaction [1-2]. Organic catalysts such as L-proline have the ability to increase the rate of the reaction via covalent or non-covalent interactions. Theoretical studies is a powerful tool to find more details about the effect of organocatalyst on the rate and stereoselectivity of an organic reaction [4-5]. Our proposed mechanism for the nitroaldol reaction between acetone and nitromethane in the presence of L-proline as catalyst was studied by DFT methods at the B3LYP/6-31G**/PCM and M06-2X/6-31+G*/PCM levels of theory in DMSO as solvent at room temperature. The results show that the covalent interactions between the reactant and the catalyst makes the reaction path more energetic that the non-covalent one. Also, a reasonable explanation is found for the weakness of the covalent pathway to form both products of the reaction as observed in the experiments.

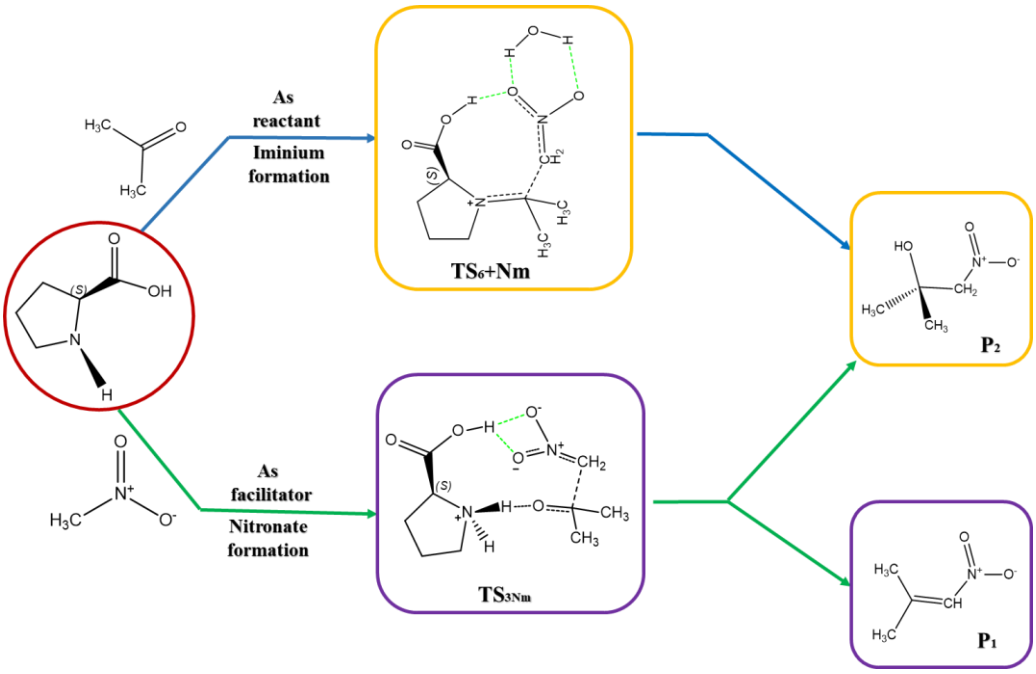


*The proposed covalent and non-covalent mechanisms of the L-proline-catalyzed nitroaldol reaction*

***Keywords:*** *Nitroaldol reaction, L-proline, Organocatalysis, reaction mechanism, computational method*

## References

[1] J. G. Hernandez, E. Juaristi, *Tetrahedron*. **2011**, 67, 6953.
[2] K. N. Rankin, J. W. Gauld, R. J. Boyd, *J. Phys. Chem. A.* **2002**, 106, 5155.
[3] B. Escuder, J. F. Miravet, *J. Am. Chem. Soc.* **2009**, 131, 11478.
[4] B. Escuder, J. F. Miravet, *New J. Chem.* **2010**, 34, 1044.
[5] R-CH. Tang, Z. Guan, Y-H. He, W. Zhu, *J. Mol. Catal. B: Enzym*, **2010**, 63, 62.

# Theoretical study of the catalytic effect of a new L-proline derived organocatalyst designed for asymmetric nitoaldol reaction

**Yasaman Nobakht* and Nematollah Arshadi**
Department of Chemistry, University of Zanjan, Zanjan, Iran
**E-mail: yasaman.nobakht@znu.ac.ir*

L-Proline as an efficient chiral organocatalyst has two functional groups that act both as acid and base and can also facilitate some chemical reaction such as aldol and nitroaldol reactions [1-2]. A proline amide containing two hydrogen bond donor groups show more organocatalytic effect in nitroaldol reaction. Our main aim is designing a new hydrogen bond-donating bifunctional aminocatalyst that is derived from L-proline to increasing the rate and steroselectivity of asymmetric nitroaldol reaction [3-5]. We proposed a completely different mechanism for nitroaldol reaction based on non-covalent interactions by **1** as the organocatalyst. Then the stereoselectivity of the reaction was evaluated by comparison of the activation energies of the two concurrent reaction paths. The pathways was computationally investigated in DMSO as solvent at room temperature by DFT method at the B3LYP/6-31G**/PCM level of theory. The work introduces a more suitable and reasonable pathway to explain the distribution and stereoselectivity of the reaction product.

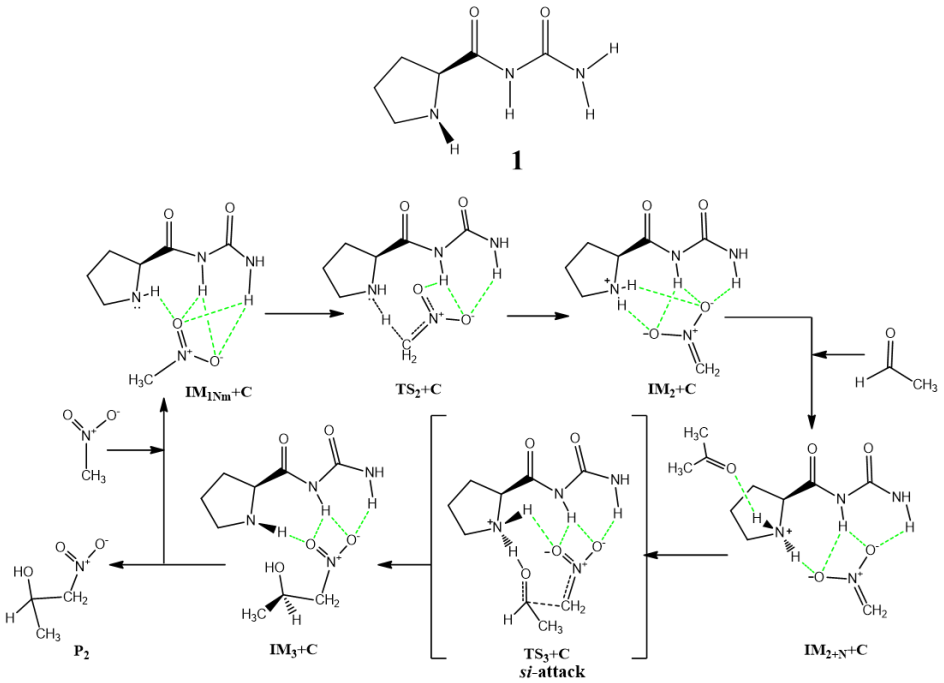


*The proposed non-covalent mechanism of the catalyzed nitroaldol reaction*

***Keywords:*** *nitroaldo reaction, organocatalysis, non-covalent interactions, reaction mechanism, computational method*

## References

[1] G. Yang, L. Zhou, *Catal. Sci. Technol*. **2016**, 6, 3378.
[2] B. List, *Tetrahedron* **2002**, 58, 5573.
[3] K. A. Jorgensen, Ł. Albrecht, H. Jiang, *Chem. Eur. J.* **2014**, 20, 358.
[4] C-L. Cao, M-C. Ye, X-L. Sun, Y. Tang, *Org. Lett.* **2006**, 8, 2901.
[5] S. S. Ganesan, A. Ganesan, J. Kothandapani, *Synlett*, **2014**, 25, 1847.

# Synthesis a carbon base cathode with using of metal organic Frameworks

**Fatemeh Arshadi [1], Hussein Gharibi [1,*], Ali morsali**

[†]Department of Chemistry, Faculty of Sciences, Tarbiat Modares University, P.O. Box: 14115-175, Tehran, Iran.

E-mail: gharibi@modares.ac.ir

The bottleneck of the commercialization for fuel cell technologies lies in the high expense of platinum group metal (PGM) electrocatalysts for catalyzing the oxygen reduction reaction (ORR) at the cathode.[1–2] To address this issue, the exploration of high-performance and cost-effective non-PGM electrocatalysts is of vital importance. Transition-metal and nitrogen codoped nanocarbons (TM−N−C, TM: Fe, Co, Ni, Cu, etc.) are regarded as one kind of promising non-PGM ORR electrocatalysts because of their outstanding electrocatalytic activity, superior electrochemical stability, and methanol tolerance. There are increasing demands toward the efficient catalysts in cathode of fuel cells. Fuel cells are the suitable items to be a promising vehicle of energy generation. Nodaway, one of the most promising candidates to replace communications catalyst (Pt/C) in cathode is using metal organic Frameworks, where metal and nitrogen embedded in carbon matrix are regarded active site for Oxygen Reduction Reaction.

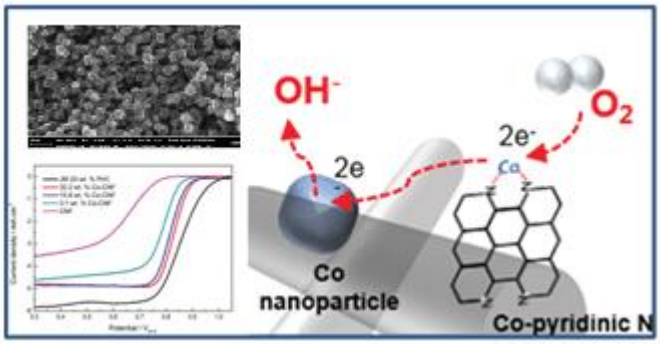


***Keywords:*** *Metal organic Frameworks, Catalysts, Fuel cells.*

## *REFERENCES*

*(1) Debe, M. K. Electrocatalyst Approaches and Challenges for Automotive Fuel Cells. Nature 2012, 486, 43−51.*

*(2) Zhong, C.-J.; Luo, J.; Njoki, P. N.; Mott, D.; Wanjala, B.; Loukrakpam, R.; Lim, S.; Wang, L.; Fang, B.; Xu, Z. Fuel Cell Technology: Nano-Engineered Multimetallic Catalysts. Energy Environ. Sci. 2008, 1, 454−466.*

# A Simple and Efficient Synthesis of 12-Aryl-8,9,10,12-tetrahydrobenzo[a]xanthen-11-ones by $Mg_{0.5}Co_{0.5}Fe_2O_4$ magnetic nanoparticles

**Roghayeh Mohammadi[1], Maryam Shaterian[1,*], Saeid Taghavi Fardood[1]**
[1]Department of Chemistry, University of Zanjan, Zanjan, Iran
*E-mail:*shaterian@znu.ac.ir

Multi-component reactions (MCRs) have emerged as an important tool for building of diverse and complex organic molecules through carbon–carbon and carbon–heteroatom bond formations taking place in tandem manner. Particularly, in the last three decades a number of three and four-component reactions have been developed [1]. Xanthene derivatives are very important heterocyclic compounds and have been widely used as dyes fluorescent materials for visualization of bio-molecules and laser technologies due to their useful spectroscopic properties. They have also been reported for their agricultural bactericide activity, photodynamic therapy, anti-flammatory effect and antiviral activity [2,3]. Due to their wide range of applications, these compounds have received a great deal of attention in connection with their synthesis. A number of methods have been developed for the preparation of the xanthenes.

A three-component reaction of aldehydes, dimedone, and 2-naphtol was achieved in the presence of $Mg_{0.5}Co_{0.5}Fe_2O_4$ MNPs as a heterogeneous catalyst to produce 2-aryl-8,9,10,12-tetrahydro-benzo[a] xanthen-11-one derivatives (scheme 1). Synthesis of 2-aryl-8,9,10,12-tetrahydro-benzo[a] xanthen-11-one derivatives has been reported using $Mg_{0.5}Co_{0.5}Fe_2O_4$ MNPs at 100 °C under solvent free conditions. Atom economy, excellent yields in short times, high catalytic activity, recycling of catalyst, and environmental benignity are some of the important features of this method.

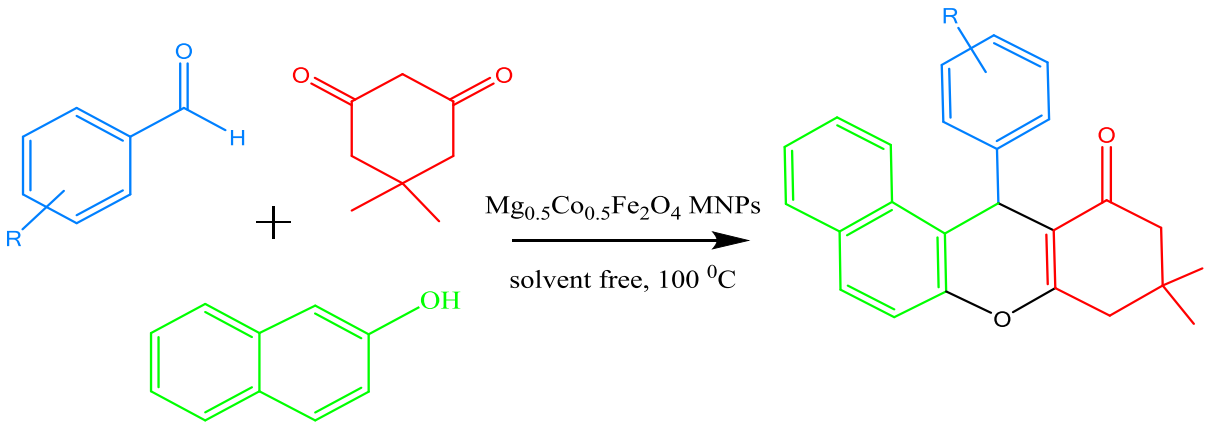


***Scheme 1.*** *Synthesis of 12-aryl-8,9,10,12-tetrahydrobenzo[a]xanthen-11-one derivatives*

***Keywords:*** *Magnetic nanoparticle; Xanthenes; Solvent free*

## References

[1] G.C. Nandi, S. Samai, R. Kumar and M. Singh, *Tetrahedron*, **2009**, *65*, 7129-7134.
[2] A. Saini, S. Kumar and J.S. Sandhu, *Synlett*, **2006**, *2006*, 1928-1932.
[3] N. Mulakayala, G. Pavan Kumar, D. Rambabu, M. Aeluri, M.V. Basaveswara Rao and M. Pal, *Tetrahedron Lett.*, **2012**, *53*, 6923-6926.

# Effect of nanomaterials on activity of immobilized lipases

**Hoda Nassira[1,*]**
[1]Department of Chemistry, University of Zanjan, Zanjan, Iran
**E-mail: nassira@znu.ac.ir*

In last few decades lipases have gained lots of interest in biotechnological and industrial processes due to its capability to catalyze a wide range of reactions [1]. But its aqueous solubility and instability, have been limited the practical applications of lipases. To take advantage of this potential enzyme, it is suggested to immobilized it on nanomaterials (NMs) through varieties of methodologies such as adsorption, entrapment, covalent coupling or cross-linking [2]. The immobilized lipase has shown superiority to the free lipase in term of reusability, pH and thermal stability, and the capacity of being stored. However, high production cost, non-uniformity and aggregation potential of NMs as well as lack of knowledge on mechanisms of immobilization severely limit the applicability of them [3]. Therefore, reviewing the influence of characteristic features of NMs on their performance including type, size, surface charge and type of modifying agents constitutes a topic of great importance. Considering the unique functions of lipases and NMs as novel and promising supports, this review discusses on conformational changes, kinetic behavior, feasible mechanisms and challenges for commercialization of nanobiocatalysts.

***Keywords:*** *Lipase, Immobilization, Nanomaterials.*

## References

[1] A. K. Singh, M.Mukhopadhyay, *Appl. Biochem. Biotechnol*, **2012**, *166*, 486-520.
[2] I.V.Pavlidis, M.Patila, U.T.Bornscheuer, D.Gournis, H.Stamatis, *Trends Biotechnol*, **2014**, *32*, 312-320.
[3] N.Hindryawati, G.Maniam, C.Feng, M.Karim, **2018**, *Journal of Bio-Science*, *23*, 1-17.

# Enhancement of lipase reusability upon immobilization on graphene derivatives

**Hoda Nassira[1,*]**
[1]Department of Chemistry, University of Zanjan, Zanjan, Iran
*E-mail: nassira@znu.ac.ir

Recent advances in bio-nanotechnology have increased the demand for lipases as a kind of biocatalyst with high-performance under mild conditions [1]. However the major challenge associated with the enzyme-catalyzed bioprocesses is their short catalytic lifespan that hinder their utility and increases the operational costs. Thus, numerous attempts have aimed to improve enzymes reuse capacity by immobilization technique. So far, a variety of materials in micro and nano scale have been explored as carriers or supports to immobilize the lipases [2]. Among nanostructured materials, graphene, a carbon-based nanomaterial, having a unique combination of structural and physiochemical properties, have attracted considerable attention as a promising carrier for lipase immobilization [3-5]. This paper aims to review recent developments and applications of the graphene derivatives for retaining lipase as nanocarrier. The essential properties of graphene for enzyme immobilization was highlighted. The advancements of up-to-date strategies for immobilizing lipase onto graphene structure by physical adsorption, covalent binding, cross-linking or specific ligand spacers are discussed. It is also noted that considerable increase in catalytic activity and reusability of immobilized lipase to free lipase, probably influenced by high surface area, two-dimensional structures, availability of surface functionalization, high loading of biomacromolecules and suspending ability of graphene as supports. Nonetheless, several challenges associated with designing and development of bioprocess applications still remains. These challenges was suggested to be addressed through interdisciplinary collaboration of chemists, engineers and material scientists.

***Keywords:*** *Lipase, reusability, graphene.*

## References

[1] G.Sandoval, *Lipases and Phospholipases*, Springer, New York (2012).
[2] M.N.Gupta , M.Kaloti , M.Kapoor and K.Solanki, *Artifi cial Cells, Blood Substitutes, and Biotechnology*, **2015**, *39*, 98–109.
[3] G.Zhang, J.Ma, J.Wang, Y.Li, G.Zhang, F.Zhang, and X.Fan, *Ind. Eng. Chem. Res.*, **2014**, *53*, 19878-19883.
[4] W.Xie, M.Huang, *Energy Conversion and Management*, **2018**, *159*, 42-53.
[5] N.Dutta and M.K.Saha, *Methods in Enzymology*, Elsevier, New York (2018).

# چکیده مقالات فارسی

# ارایه شده

# به صورت پوستر

# تاثیر روش سنتز بر فعالیت فوتوکاتالیستی فریت بیسموت خالص و ترکیب $Bi_{0.8}La_{0.2}FeO_3$

**حامد مالکی[1*]**

[1]دانشکده فیزیک، دانشگاه شهید باهنر کرمان، کرمان، ایران

ایمیل نویسنده مسئول: hamed.maleki@uk.ac.ir

## چکیده

در این پژوهش تاثیر روش سنتز بر فعالیت فوتوکاتالیستی و خواص ساختاری، نوری و مولتی فروئیکی (فروالکتریکی و مغناطیسی) نانوذرات و نانو میله های $BiFeO_3$ (BFO) و $Bi_{0.8}La_{0.2}FeO_3$ (BLFO) تهیه شده به روش های سل-ژل خوداحتراقی و هیدروترمال مورد مطالعه قرار گرفته است. محصولات به دست آمده توسط الگوی پراش اشعه ایکس (XRD)، طیف سنجی تبدیل فوریه مادون قرمز(FT-IR) و (UV-Vis) و میکروسکوپ الکترونی عبوری (TEM) و مغناطیس سنج نمونه ارتعاشی (VSM) مورد شناسایی قرار گرفتند [۱]. برای فعالیت فوتوکاتالیستی نیز آهنگ حذف مولکول های متیلن بلو (MO) تحت تابش نور مرئی مورد ارزیابی قرار گرفت. اضافه کردن لانتانیوم در ساختار فریت بیسموت، منجر به کاهش گاف انرژی فریت بیسموت می شود و میزان خاصیت فوتوکاتالیستی را بطور چشمگیری افزایش می دهد. نتایج همچنین نشان می دهد که نانوذرات ساخته شده به روش سل-ژل نسبت به نانومیله های سنتزشده به روش هیدروترمال فعالیت فوتوکاتالیستی بهتری از خود نشان می دهد.

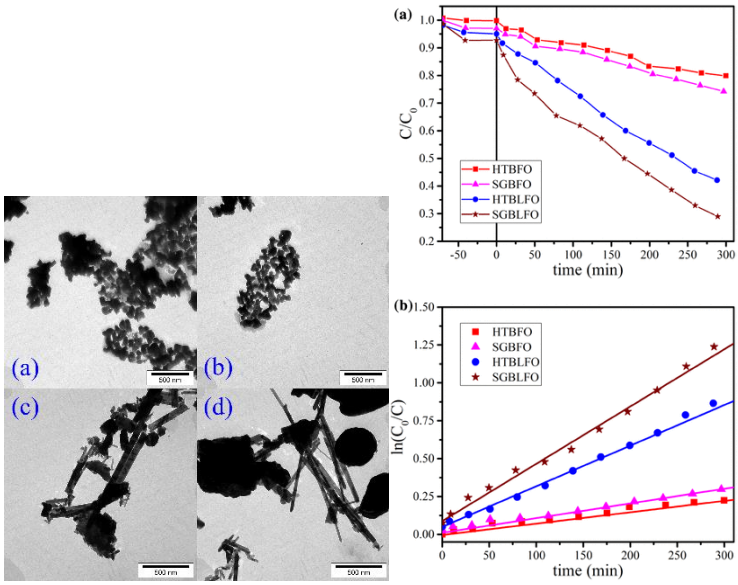


شمای ۱. سمت راست: تخریب محلول متیلن بلو در حضور نانو ذرات مغناطیسی BFO و BLFO تهیه شده به روش های سل-ژل خوداحتراقی و هیدروترمال. سمت راست: (a) و (b) تصاویر TEM از فریت بیسموت خالص و آلاییده به لانتانیوم و تهیه شده به روش سل-ژل خوداحتراقی را نشان می دهد؛ و (c) و (d) تصاویر TEM از BFO و BLFO سنتز شده به روش هیدروترمال است.

**کلمات کلیدی:** فوتوکاتالیست مغناطیسی؛ مولتی فروئیک؛ بیرنگ کردن متیلن بلو؛ خواص فروالکتریکی؛ خواص مغناطیسی.

## منابع

[1] H. Maleki, *Journal of Magnetism and Magnetic Materials*, **2018**, *458*, 277.

# سنتز و شناسایی نانوکامپوزیت اکسید مولیبدن قرار گرفته روی کربن نانوتیوب اصلاح شده با پلی اتیلن گلیکول و بررسی فعالیت فوتوکاتالیستی آن در تخریب رنگ متیلن بلو

نگار اختر[۱]، حسین صلواتی[۱]، عباس تیموری[۱]

[۱]دانشکده شیمی، دانشگاه پیام نور تهران، تهران، ایران

ایمیل نویسنده مسئول: Negarakhtar@yahoo.com

## چکیده

امروزه تصفیه‌ی پساب‌ها، مسئله‌ای بسیار حیاتی برای صنایع شیمیایی به شمار می‌رود. در این میان پساب کارخانه‌های رنگرزی به دلیل حضور رنگ‌ها مشکل‌ترین پساب‌ها از نظر تصفیه محسوب می‌شوند [۱]. رنگ‌های آزو بزرگترین گروه رنگ‌های مورد استفاده در صنعت نساجی و دیگر رنگ‌های صنعتی به عنوان یکی از بزرگترین گروه ترکیبات آلی هستند که باعث آلودگی در محیط زیست می‌شوند [۲]. در ساختمان بعضی رنگ‌ها فلزات سنگین سمی وجود دارد حضور آنها در آب خسارات جبران ناپذیر برای محیط زیست بهمراه دارد [۳]. روش‌های معمولی برای حذف رنگ‌ها از پساب‌ها به طور اختصاصی مؤثر نیستند. استفاده از فوتوکاتالیست‌ها به عنوان یکی از فرآیندهای اکسیداسیون پیشرفته یک تکنیک مؤثر در تخلیص آب و هوا است. فوتوکاتالیست‌ها با تخریب آلاینده و تبدیل آن به موادی با خطر، در حضور نور فرابنفش و یا نوری نزدیک به طیف فرابنفش آلاینده را از بین می‌برد. به علاوه این فرآیند می‌تواند در فشار اتمسفری و در دمای اتاق یا نزدیک به آن مورد استفاده قرار بگیرد [۴]. با ظهور نانوفناوری و وجود ویژگی مهم نسبت بالای سطح به حجم در مقیاس نانو، کارایی کاتالیست‌های شیمیایی به نحو مؤثری بهبود یافت. مزیت نانوکاتالیست‌ها نسبت به سایر کاتالیست‌ها در زمینه‌ی حذف رنگ‌ها، سطح تماس بالا و سرعت بالای واکنش‌ها می‌باشد. از معایب این نوع نانوکاتالیست جداسازی دشوار آن از محیط واکنش می‌باشد که با استفاده از بسترهای جامد می‌توان این مشکل را حل نمود [۵].

در این پژوهش، یک بستر کارآمد با استفاده از کربن نانوتیوب اصلاح شده با قابلیت جداسازی آسان تهیه و فعالیت فوتوکاتالیستی آن جهت تخریب رنگ متیلن بلو در شرایط مختلف مورد بررسی قرار گرفت. ابتدا نانولوله های کربنی پس از اعمال حرارت ۳۰۰ درجه‌سانتیگراد در کوره‌ی الکتریکی، با استفاده از اسید نیتریک و اسید سولفوریک فعال‌سازی شد. سپس پلی‌اتیلن‌گلیکول بر روی آن بعنوان بستری برای اتصال اکسید مولیبدن قرار داده شد. نمونه‌های سنتز شده توسط تکنیک‌های دستگاهی مختلف از جمله طیف‌سنجی پراش اشعه‌ی ایکس، میکروسکوپ الکترونی روبشی، طیف‌سنجی مادون قرمز تبدیل فوریه و طیف‌سنجی مرئی- ماوراء بنفش شناسایی و ساختار کاتالیست سنتز شده تایید گردید. پارامترهای موثر بر فعالیت فوتوکاتالیستی مانند زمان، دما، pH، غلظت رنگ و مقدار کاتالیست بهینه سازی شد. حداکثر میزان تخریب در شرایط بهینه ۹۹٪/۵ به دست آمد.

**کلمات کلیدی:** فوتوکاتالیست، متیلن‌بلو، اکسیدمولیبدن،کربن‌نانوتیوب، پلی‌اتیلن‌گلیکول

## منابع

[1] RP. Schwarzenbach, BI. Escher, K. Fenner, TB. Hofstetter, CA. Johnson, U. Von Gunten, and B. Wehrli, *Science*, **2006**, 313(5790), 1072.
[2] AK. Verma, RR. Dash, and P. Bhunia, *Journal of environmental management*, **2012**, 93(1), 155.
[3] SH. Lin, and CF. Peng, *Water research*. **1990**, 30(3), 587.
[4] MA. Shannon, PW. Bohn, M. Elimelech, JG. Georgiadis, BJ. Marinas, and AM. Mayes, *Nature*, **2008**, 452(7185), 301.
[5] S. Chaturvedi, PN. Dave, and NK. Shah, *Journal of Saudi Chemical Society*, **2012**, 16(3), 308.

# سنتز و شناسایی کاتالیست فتالوسیانین مس قرار گرفته روی پلی وینیل کلراید به عنوان بستر جامد و بررسی فعالیت فتوکاتالیستی آن در تخریب رنگ کنگورد

نهال صابری[۱]، حسین صلواتی[۱]، مریم موحدی[۱]

[۱]دانشکده شیمی، دانشگاه پیام نور تهران، تهران، ایران
ایمیل نویسنده مسئول: nahalsaberi@yahoo.com

## چکیده

رنگ‌ها بعنوان یکی از مهم‌ترین آلاینده‌های موجود در فاضلاب صنایع مختلف مانند نساجی و رنگرزی، غالبا سمی، سرطان‌زا، جهش‌زا و غیرقابل‌تجزیه از نظر بیولوژیکی می‌باشند. همچنین رنگ‌ها یکی از بزرگترین گروه از ترکیبات آلی بوده که باعث آلودگی محیطزیست می‌شوند. ازاین رو حذف و یا تخریب آنها امری بسیار ضروری و مهم است. [۱]. در سال‌های اخیر، از روش‌های مختلفی برای حذف و تخریب آلاینده‌های آب استفاده شده است. برخی از این روش ها شامل استفاده از نانوکامپوزیت‌ها و نانوجاذب‌ها به عنوان یک فوتوکاتالیست، به منظور حذف و تخریب رنگ‌ها می‌باشد. امروزه کاتالیست‌ها بعنوان یکی از قدرتمندترین ابزارها در تصفیه فاضلاب‌ها مطرح بوده و با سرعت در حال پیشرفت می‌باشند[۲]. دراین میان کاتالیست‌های ناهمگن به دلیل جداسازی آسان و ارزان بسیار مورد توجه هستند. نانوکامپوزیت‌ها موادی مرکب با ویژگی‌های منحصر بفرد می‌باشند که در گروه کاتالیست‌های ناهمگن قرار می‌گیرند[۳]. امروزه پلی‌وینیل‌کلراید به دلیل دارابودن خواصی مانند پایداری حرارتی و مکانیکی، هزینه تولید پایین، استحکام و مقاومت بالا توانسته است به عنوان بستر جامد برای نانوکامپوزیت‌ها مورد توجه محققان قرار گیرد [۴]. فتالوسیانین‌مس رنگدانه‌ای با ساختار بلوری و آبی رنگ، به عنوان رنگ در پلاستیک‌ها، پوشش‌ها و رنگ‌های نساجی و چاپ استفاده می‌شود. همچنین اخیرا بعلت داشتن خاصیت حساس کنندگی رنگ و فعالیت کاتالیستی بالا برای بهبود فعالیت کاتالیستی فوتوکاتالیست‌ها نیز بکار گرفته شده است[۵].

در این پژوهش، کاتالیست فتالوسیانین مس قرار گرفته بر پلی‌وینیل‌کلرید بعنوان بستر جامد سنتز شد و فعالیت فوتوکاتالیستی آن در تخریب رنگ کنگورد و در شرایط مختلف مانند نور مرئی، نور فرابنفش و امواج فراصوت بررسی شد. کاتالیست سنتزشده با استفاده از روش‌های دستگاهی مانند طیف سنجی مادون قرمز تبدیل فوریه، پراش اشعه ایکس، میکروسکوپ الکترونی روبشی و طیف سنجی مرئی- ماورابنفش شناسایی شد و نتایج بدست آمده، ساختار کاتالیست را تایید نمود. اثر عوامل تاثیرگذار بر فعالیت فوتوکاتالیستی در تخریب رنگ کنگورد مانند مقدار کاتالیست سنتزشده، غلظت رنگ کنگورد، زمان تابش نور مرئی، دما و pH محلول اولیه نیز مورد بررسی قرار گرفت. بر اساس نتایج بهینه‌سازی پارامترها، حداکثر کارایی تخریب رنگ کنگورد توسط کاتالیست سنتز شده در شرایط مطلوب ۹۹٪ به دست آمد.

**کلمات کلیدی:** کاتالیست، بستر جامد، پلی وینیل کلراید، فتالوسیانین مس

## منابع

[1] A. Fraiwan, L. Kwan, and S. Choi, *Biosensors and Bioelectronics*, **2016**, 15;85,190-7.
[2] X. Wang, K. Maeda, A. Thomas, K. Takanabe, G. Xin, JM. Carlsson, K. Domen, and M. Antonietti, *Nature materials*, **2009**, 8(1), 76-79.
[3] A. Kudo, and Y. Miseki, *Chemical Society Reviews*, **2009**, 38(1), 253-78.
[4] H. Bockhorn, A. Hornung, U. Hornung, and P. Jakobstroer, *Combustion science and technology*, **1998**, 134(1-6), 12.
[5] MA. Zanjanchi, A. Ebrahimian, and M, Arvand, *Journal of hazardous materials*, **2010**, 175, 992.

# تأثیر فلزات روی، منیزیم، کبالت و باریم مورد استفاده در سنتز نانو کاتالیست های پروسکیتی جهت حذف ترکیبات BTX با کمک فناوری پلاسما

نوشین پرویزی[۱و۲]، نادر راحمی[۱و۲]، سمیه اللهیاری[۱و۲]، شایان حسینی[۱و۲]

[۱]دانشکده مهندسی شیمی، دانشگاه صنعتی سهند، شهر جدید سهند، تبریز، ایران
[۲]مرکز تحقیقات مهندسی محیط زیست، دانشگاه صنعتی سهند، شهر جدید سهند، تبریز، ایران

ایمیل نویسنده مسئول: no_parvizi@sut.ac.ir

## چکیده

ترکیبات آلی فرار از جمله بنزن، تولوئن و زایلن (BTX)، آلاینده های مهم در محیط هستند که اثرات مخرب قابل توجهی بر سلامتی انسان ها و تخریب محیط زیست دارند. در این مطالعه به منظور افزایش راندمان و کارایی بیشتر مصرف انرژی در تجزیه آلاینده ها، تلفیقی از تکنولوژی پلاسمای غیر حرارتی و نانوکاتالیست های پروسکیتی با ساختار $La_{0.8}A_{0.2}MnO_3$ (A: روی، منیزیم، کبالت و باریم) برای حذف BTX ها مورد استفاده قرار گرفته است. پلاسمای غیرحرارتی یک فناوری نو ظهور در زمینه کنترل آلودگی های هوا و به خصوص ترکیبات آلی فرار است [۱]. پروسکایت ها نیز با فرمول عمومی $ABO_3$ به عنوان کاتالیست های فعال در حذف ترکیبات آلی فرار عملکرد قابل قبولی از خود نشان داده اند [۲].

نانوکاتالیست های پروسکیتی ذکر شده با استفاده از روش سل-ژل احتراقی تهیه و در دمای ۷۰۰ $^{\circ}C$ کلسینه شدند. جهت تولید پلاسمای غیر حرارتی از مکانیسم تخلیه دی الکتریک (DBD) استفاده گردید. با ورود همزمان بنزن، تولوئن و زایلن، پلاسما با ولتاژ ۱۰ ولت روشن شده و در زمان های ۱۰، ۳۰ و ۵۰ دقیقه عملیات حذف مورد بررسی قرار گرفته است. نتایج حاصل نشان می دهد که در میان پروسکیت سنتزی ذکر شده، نانو کاتالیست پروسکیتی همراه با فلز روی ($La_{0.8}Zn_{0.2}MnO_3$) در زمان ۱۰ دقیقه بهترین عملکرد را با میزان حذف بنزن ۹۹٪، تولوئن ۹۳٪ و زایلن ۷۳٪ از خود نشان داد.

**کلمات کلیدی:** ترکیبات آلی فرار، پروسکیت، نانوساختار، پلاسمای غیرحرارتی.

## منابع

[1] O. Karatum, M. A. Deshusses, *Chemical Engineering Journal*, **2016**, *Volume294*, Page1.

[2] M. Misono, *studies in surface science and catalysis*, **2013**, *volume176*, pages67-95.

# سنتز اسپینل های بر پایه تیتانیم و بررسی فعالیت فوتوکاتالیستی آنها در حذف آلاینده قرمز بازی

**پروانه نخستین پناهی*، فرشاد ناجی**

*گروه شیمی، دانشکده علوم، دانشگاه زنجان، زنجان، ایران*

*ایمیل نویسنده مسئول: panahi@znu.ac.ir*

## چکیده

در سالهای اخیر، مشکلات زیست محیطی ناشی از آلودگی منابع آب توسط مواد رنگزا توجه زیادی را به خود جلب کرده است. فرآیندهای نوری، یکی از روشهای مؤثر در حذف آلاینده ها از فاضلاب ها می با شند [۱]. اکسیدهای فلزی مختلط کارایی بالایی را در حذف مواد رنگزا از خود نشان می دهند [۲]. در کار پژوهشی حاضر ابتدا اکسیدهای فلزی مختلط با ساختار اسپینل($TiM_2O_4$ (M= Mn, Cu, Ni, Fe به روش سل-ژل با استفاده از اسید سیتریک به عنوان عامل کمپلکس ساز سنتز شده و سپس فعالیت فوتوکاتالیستی این اسپینل ها در فرایند حذف آلاینده قرمز بازی تحت تشعشع نور uv و مرئی مورد بررسی قرار گرفت. نتایج نشان داد که $TiNi_2O_4$ و $TiMn_2O_4$ فعالیت بیشتری را در نور uv و مرئی نسبت به اسپینل های دیگر از خودشان نشان می دهند. در مرحله بعد ویژگی های فیزیکی و شیمیایی $TiNi_2O_4$ و $TiMn_2O_4$ با استفاده از پراش اشعه ایکس (XRD)، میکروسکوپ الکترونی روبشی (SEM) و طیف سنجی بازتابشی انتشاری (DRS)بررسی شد. طیف های XRD تشکیل ساختار اسپینل و تصاویر SEM تشکیل ذرات اسپینل با اندازه نانومتری را تایید کردند. همچنین طیف های بازتابشی انتشاری این اسپینل ها، جذب قوی را در ناحیه uv و مرئی نشان دادند. بنابراین این اسپینل ها امکان انجام واکنش های فوتوشیمیایی تحت برانگیختگی نور مرئی را دارند. فلز منگنز بخاطر دارا بودن حالت های اکسایشی متفاوت ($Mn^{2+}$, $Mn^{3+}$, $Mn^{4+}$) باعث به دام انداختن فوتوالکترون ها و حفره های تولید شده در اثر فرایند فوتو شده و در نتیجه باعث تفکیک بهتر فوتوالکترون ها و حفره ها می شود و فعالیت فوتوکاتالیستی افزایش می یابد [۳].

**کلمات کلیدی:** اسپینل، فوتوکاتالیست، آلاینده قرمز بازی

## منابع

[1] Han, F., Kambala, V. S. R., Srinivasan, D., Rajarathnam, R. Appl. Catal. A., **2009**, 39, 25-40.

[2] Jung, W. Y., and Hong, S. S. J Ind Eng Chem., **2013**, 19, 157–160.

[3] Wei, Z.X., Xiao, C.M., Zeng, W.W., Liu. J.P. J. Mol. Catal. A: Chem., **2013**, 370, 35-43.

# حذف فوتوکاتالیستی آلاینده قرمز بازی توسط $TiNi_2O_4$ و $TiMn_2O_4$ بارگذاری شده با گرافن تحت تشعشع نور مرئی

**پروانه نخستین پناهی*، فرشاد ناجی**

*گروه شیمی، دانشکده علوم، دانشگاه زنجان، زنجان، ایران*

*ایمیل نویسنده مسئول:* panahi@znu.ac.ir

## چکیده

در دسترس بودن آب سالم و پاک یکی از مهم‌ترین مسائل پیش روی بشر می‌باشد. مواد رنگزای سنتزی به طور گسترده در بسیاری از صنایع استفاده می‌شود و بسیاری از رنگ‌ها به دلیل داشتن ساختمان آروماتیکی، در برابر تجزیه بیولوژیکی مقاوم هستند، بنابراین تصفیه پساب‌های رنگی قبل از تخلیه آن‌ها به محیط‌زیست ضروری است. یکی از روشهای مؤثر در حذف آلاینده ها از فاضلاب ها، روش اکسایش فوتوکاتالیزوری است. طی فرآیند اکسایش فوتوکاتالیزوری مواد آلاینده موجود در آب در اثر تابش نور و در حضور کاتالیزورهای نیمه‌رسانا به دی اکسیدکربن و آب و یا سایر مواد بی‌ضرر تجزیه می‌شوند[۱]. اکسیدهای فلزی مختلط کارایی بالایی را در فرآیند اکسایش فوتوکاتالیزوری از خود نشان داده اند [۲]. در کار پژوهشی حاضر ابتدا اسپینل های $TiNi_2O_4$ و $TiMn_2O_4$ به روش سل-ژل با استفاده از اسید سیتریک به عنوان عامل کمپلکس ساز سنتز شده و سپس بر روی گرافن (G) با روش تلقیح بارگذاری شدند. فعالیت فوتوکاتالیستی این اسپینل ها و اسپینل های بارگذاری شده با گرافن ($TiNi_2O_4/G$ و $TiMn_2O_4$ /G) در فرایند حذف آلاینده قرمز بازی تحت تشعشع نور مرئی مورد بررسی قرار گرفت. نتایج نشان داد که فعالیت فوتوکاتالیستی اسپینل ها در اثر بارگذاری گرافن به مقدار زیادی افزایش می یابد و در نهایت ۶۰ درصد رنگ قرمز بازی تحت تشعشع نور مرئی حذف شد. گرافن به عنوان پذیرنده و انتقال دهنده الکترون عمل کرده و موجب تفکیک بهتر حامل های بار می شود و در نتیجه عملکرد فوتوکاتالیستی افزایش می یابد [۳]. ویژگی های فیزیکی و شیمیایی اسپینل ها و اسپینل های بارگذاری شده با گرافن با استفاده از پراش اشعه ایکس (XRD)، میکروسکوپ الکترونی روبشی (SEM) و طیف سنجی بازتابشی انتشاری(DRS) بررسی شد. طیف های XRD نشان داد که در اثر بارگذاری گرافن ساختار اسپینل تغییر نمی کند و تصاویر SEM نیز نشان دادند که ذرات اسپینل روی گرافن به خوبی پخش شده و در نتیجه سطح ویژه افزایش می یابد. طیف های بازتابشی انتشاری $TiNi_2O_4/G$ و $TiMn_2O_4/G$ جذب قوی را در ناحیه مرئی نشان دادند. در واقع در اثر بارگذاری گرافن شدت جذب در ناحیه مرئی به طور قابل ملاحظه ای افزایش می یابد و این باعث افزایش فعالیت فوتوکاتالیست می شود.

**کلمات کلیدی:** اسپینل، فوتوکاتالیست، آلاینده قرمز بازی، گرافن

## منابع

[1] Matilainen, M., and Sillanpa, H. Journal of Chemosphere, **2010**, 80, 351-365.

[2] Jung, W. Y., and Hong, S. S. J Ind Eng Chem., **2013**, 19, 157–160.

[3] Hu, J., Ma, a. J., Wang, L., Huang, H., J. Alloys Compd., **2014**, 583, 539–545.

# سنتز نانو ذره جاذب آئروویلیوس و حذف آنیلین توسط آن و بررسی سینتیک، ترمودینامیک و ایزوترم های مربوطه

**عاطفه بدری** [۱]

[۱] آموزش و پرورش ناحیه ۳ استان اصفهان
ایمیل نویسنده مسئول: atefe_badri@yahoo.com

## چکیده

جاذب $SrBi_4Ti_4O_{15}$ توسط یک روش اصلاح شده رسوبی ساده تهیه شد و در ادامه در ۵۵۰ درجه سانتی گراد و ۶۵۰ درجه سانتیگراد منجر به تولید ساختار اورتورومبیک تک فاز شد که با استفاده از آنالیز XRD تایید شد. بر اساس تجزیه و تحلیل SEM، ذرات همگن و میله ای شکل بوده و اندازه ذرهٔ ۱۳-۴۷ نانومتر می باشد که مشخص شد روش تهیه و درجه حرارت کلسینه می تواند مورفولوژی و خلوص محصول نهایی را تعیین می کند. نانوذرات به عنوان جاذب برای بررسی رفتار جذب آنیلین از محلول های آبی استفاده شد. نتایج نشان می دهد که رفتار جذب این مواد مطلوب بوده و با افزایش ظرفیت جذب برای انیلین در محلول آبی تایید شد. مقدار جذب آنیلین بر روی سطح نانوذرات SBT با زمان تماس، مقدار جاذب، pH و دما تحت تاثیر قرار بود. جذب انیلین از آب سریع بود و تقریبا ظرفیت جذب تعادلی پس از اولین ۶۰ دقیقه به ۹۰٪ رسیده است. علاوه بر این، فرآیندهای جذب آنیلین بر نانوذرات SBT از سینتیک شبه مرتبه دوم تبعیت می کند و ایزوترم جذب را می توان به خوبی توسط مدل فروندلیچ شبیه سازی کرد. تجزیه و تحلیل ترمودینامیکی به دست آمده از ایزوترم جذب وابستگی به دما را نشان می دهد که واکنش های جذب آنیلین گرمازا بوده و در دماهای کم به بالاترین حد جذب آنیلین می رسد.

**کلمات کلیدی:** اکسیدهای آئروویلیوس۱، سینتیک جذب ۲، ایزوترم حذف ۳، آنیلین ۴، ترمودینامیک ۵

## منابع

[1] "Aurivillius phases". Moscow State University *website*. Retrieved 14 November 2013.

[2] Rui Hu, Xiangke Wang, Songyuan Dai, Dadong Shao, Tasawar Hayat, Ahmed Alsaedi. Application of graphitic carbon nitride for the removal of Pb(II) and aniline from aqueous solutions. *Chemical Engineering Journal*, **(2015) 260**, 469–477.

[3] S. K. Rout, E. Sinha, A. Hussian, J. S. Lee, C. W. Ahn, I. W. Kim, and S. I. Woo. Phase transition in ABi4Ti4O15 (A=Ca,Sr,Ba) Aurivillius oxides prepared through a soft chemical route. *Journal Of Applied Physics105*, **(2009)** 024105.

# سنتز مشتقات وینیل فسفونات با استفاده از فنیل پروپیولات ها و دی آلکیل فسفیت ها در حضور کاتالیست NaCN

مریم عدلو[۱]، عیسی یاوری[۱و۲*]

[۱] گروه شیمی، دانشکده علوم پایه، واحد علوم و تحقیقات، دانشگاه آزاد اسلامی، تهران، ایران
Maryam_adlu@yahoo.com
[۲] استاد گروه شیمی، دانشگاه تربیت مدرس، تهران، ایران
*نویسنده مسئول: yavarisa@modares.ac.ir

## چکیده

ترکیبات ارگانوفسفر ترکیبات آلی شامل پیوند کربن-فسفر، به عنوان بخش جدایی ناپذیر مولکول هستند. از میان این ترکیبات وینیل فسفونات های عامل دار بطور گسترده برای سنتزهای شیمی آلی در دو دهه اخیر مورد بررسی قرار گرفته اند. از مهمترین کاربردهای ترکیبات وینیل فسفونات ها می توان به تهیه حشره کش ها، علف کش ها و تنظیم کننده های رشد گیاه در صنعت کشاورزی، تهیه کاتالیزورها، معرف های پایدار کننده در صنایع پلاستیک، تهیه داروهای ضد سرطان و ضد ویروس و پوکی استخوان در صنعت داروسازی اشاره کرد. همچنین ترکیبات وینیل فسفونات به عنوان حدواسط در سنتز تعداد زیادی کربوکسیلیک های غیرحلقوی و سنتز ترکیبات هتروسیکل استفاده می شوند[۴-۱].

در این تحقیق واکنش بین فنیل پروپیولات ها و دی آلکیل فسفیت ها در مجاورت کاتالیزور سدیم سیانید در محیط آبی انجام شد و مشتقات وینیل فسفونات تحت شرایط ملایم و تک مرحله ای، در مدت زمان کوتاه با بازده بالا تهیه شدند.

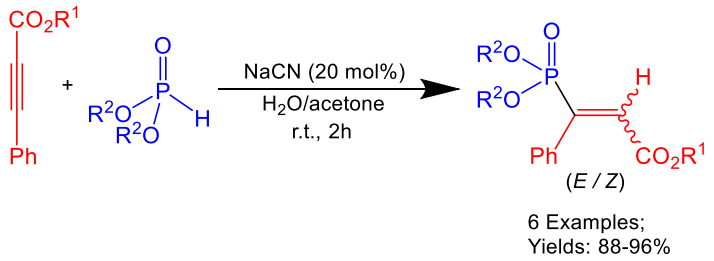


شمای ۱. سنتز مشتقات وینیل فسفونات

**کلمات کلیدی:** وینیل فسفونات، فنیل پروپیولات، دی آلکیل فسفیت، کاتالیست NaCN

## منابع

[1] X-G. Liu, Y. Wei, M. Shi, *Tetrahedron*, **2010**, *66*, 304.

[2] P. Karanam, G. M. Reddy, S. R. Koppolu, W. Lin, *Tetrahedron Letters*, **2018**, *59*, 59-76.

[3] I. Yavari, M. Nematpour, Z. Hossaini, *Mol. Divers*, **2009**, *10*, 479.

[4] M. Adlu, R. Aliveisi, I. Yavari, *Phosphorus Sulfur Silicon Relat. Elem*, **2017**, *192*, 1, 19-22.

# تهیه نانوکامپوزیت پلي تیوفن/گرافن اکساید کاهش یافته اصلاح شده (FRGO/PTH) با نانوذرات فلزي با روش پلیمریزاسیون درجا و مشخصه یابي خواص آن

علیرضا کرمانی جمکرانی [۱]، زهرا رفیعی [۲*]

[۱]دانشکده شیمی، دانشگاه یاسوج، یاسوج، ایران

[۲]دانشکده شیمی، دانشگاه یاسوج، یاسوج، ایران

kermanialireza332@yahoo.com

## چکیده

دراین تحقیق نانوکامپوزیت پلی تیوفن/گرافن اکساید کاهش یافته اصلاح شده (RGO) با نانوذرات پلادیم و طلا با روش پلیمریزاسیون درجا توسط امواج فراصوت سنتز شد. برای اصلاح شیمیایی گرافن اکساید کاهش یافته از L-سیستین و پارا فنیلن دی آمین و نشاندن نانوذرات طلا و پلادیم استفاده شد. نانوذرات فلزی به دلیل داشتن نسبت سطح به حجم بسیار بالا، فعالیت الکتروکاتالیستی بسیار مناسبی از خود نشان می دهند[۱]. روش مشخصه یابی گوناگونی جهت بررسی ساختار و خواص نانوکامپوزیت پلیمری وگرافن اکساید کاهش یافته (RGO) انجام گرفته شده است. از جمله این آزمون ها طیف سنجی مادون قرمز تبدیل فوریه (FTIR) و مورفولوژی آنها با استفاده از آزمون پراش اشعه ایکس (XRD) و میکروسکوپ الکترونی روبشی (SEM) بررسی شد. نتایج بدست آمده حاکی از آن دارد که گرافن اکساید (GO) با موفقیت به گرافن اکساید کاهش یافته (RGO) تبدیل شده و در نتیجه نانوکامپوزیت پلیمری (FRGO/PTH) تولید شده به خوبی قابل اثبات می‌باشد.

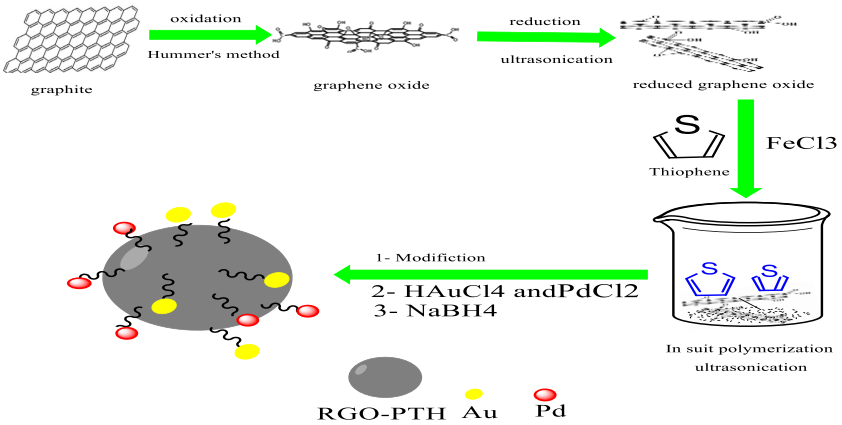


شمای ۱. سنتز نانوکامپوزیت پلی تیوفن/گرافن اکساید کاهش یافته اصلاح شده(FRGO/PTH) با نانوذرات طلا و پلادیم

**کلمات کلیدی:** نانوکامپوزیت، پلی تیوفن، گرافن، گرافن اکساید کاهش یافته

## منابع

[1] Vivek Polshettiwar, Rajender S. Varma, Green chemistry by nano-catalysis, *Green Chem*, **2010**, *12*, 743–754.

# تثبیت کمپلکس منگنز-پورفیرین بر روی نانوذرات مغناطیسی و کاربردآن به عنوان کاتالیزور دراکسایش سولفیدها و اپوکسایش آلکن ها

سید مرتضی حسینی[۱]، مجتبی باقرزاده[۱*]

[۱]دانشکده شیمی، دانشگاه صنعتی شریف، تهران، ایران

ایمیل نویسنده مسئول: bagherzadeh@sharif.edu

## چکیده

امروزه گسترش سیستم های کاتالیزوری که از یک طرف موجب افزایش سرعت واکنش ها شده و از طرف دیگر به صورت گزینش پذیر عمل کنند، حائز اهمیت است. در این پژوهش نانوذرات مغناطیسی$Fe_3O_4$ با پوشش سیلیکا عامل دار شده به منظور تثبیت کمپلکس منگنز-پورفیرین [۱] نامتقارن مورد استفاده قرار گرفته است. که هدف سنتز و مطالعه خواص کاتالیزوری این کمپلکس در واکنش اکسایش سولفید ها و اپوکسایش آلکن ها است. در سنتز چند مرحله ای این کاتالیزور ابتدا نانوذرات مغناطیسی آهن تهیه شده سپس با سیلان دار کردن این نانو ذرات با استفاده از معرف تترا اتوکسی ارتوسیلیکات (TEOS ) آن را سیلیکا عامل دار نموده و در ادامه با استفاده از واکنشگر ۳-کلرو تری متوکسی سیلان این معرف را برروی بستر تثبیت نموده و بلافاصله با استفاده از نمک سدیم آزید آن را آزید دار می کنیم [۳,۲] در ادامه این سنتز با تهیه ۴-هیدروکسی فنیل پورفیرین (THPP ) و پروپارژیله کردن یکی از موقعیت های پورفیرین با استفاده از واکنشگر پروپارژیل برمید ، ان را تبدیل به یک پورفیرین نامتقارن نموده و سپس آن را با فلز منگنز وارد واکنش نموده و در انتها این کمپلکس را با استفاده از نمک CuI بر روی بستر مورد نظر تثبیت می کنیم. و شناسایی کاتالیزور حاصل بوسیله روش های طیف سنجی فرابنفش (UV)، زیر قرمز(IR)، پراش اشعه ایکس(XRD)، میکروسکوپ الکترونی روبشی (SEM)، مغناطیس سنج نمونه مرتعش(VSM)، و آنالیز توزین حرارتی(TGA) انجام گرفت. به منظور یافتن شرایط مناسب و بهینه برای انجام واکنش ،اثر پارامترهای مختلف نظیر دما ،حلال ، اکسنده و زمان بر روی واکنش اکسایش سولفید ها و اپوکسایش آلکن ها مورد استفاده قرار گرفت. نانو کاتالیزور سنتز شده با داشتن قابلیت بازیابی مغناطیسی از طریق آهنربا می تواند چندین بار بدون از دست دادن فعالیت کاتالیزوری مورد استفاده قرار گیرد.

**کلمات کلیدی:** ۱-نانو ذرات مغناطیسی۲-نانو کاتالیزور۳- منگنز-پورفیرین۴- اکسایش سولفیدها۵- اپوکسایش آلکن ها

[1] Bagherzadeh, M, & Mortazavi-Manesh, A. *RSC Advances*, 2016, **6**, 41551-41560
[2] Raphael Turgis, Guilhem Arrachart, Carole Delchet, Chem. Mater. 2013, **25**, 4447-4453
[3] Yuling Zhu, Weiya Zhang, Lixia Li, Caiying Wu, Anal. Methods, 2014, **6**, 2102–2111
[4]Paola Riente, Carolina Mendoza, Miquel A. Peric , J. Mater. Chem., 2011, **21**, 7350–7355

# بهبود خواص کاتالیستی زئولیت ZSM-5 در فرایند تبدیل متانول به بنزین از طریق توسعه مزوپوروسیتی تحت شرایط بهینه با استفاده از باز آلی

مینا صدرآرا[۱]، محمدرضا خانمحمدی خرمی[۲*]، امیر باقری گرمارودی[۳]

[۱،۲،۳] دانشکده علوم، دانشگاه بین المللی امام خمینی (ره) قزوین، قزوین، ایران

ایمیل نویسنده مسئول: Minasadrara@gmail.com

## چکیده

تبدیل کاتالیستی متانول به بنزین (MTG) ، یک جایگزین جذاب برای تهیه سوخت از منابع کم‌ارزش و تجدیدپذیر است. متانول از گازهای سنتزی و گازهای سنتزی از ذغال‌سنگ، گاز طبیعی، زیست توده و حتی پسماندهای صنعتی به دست می‌آیند. واکنش تبدیل متانول به هیدروکربن‌ها (MTH) توسط زئولیت‌های اسید برونشتد و مواد زئولیت‌مانند کاتالیز می شود. فعالیت، گزینش‌پذیری و سرعت غیرفعال‌شدن کاتالیست‌های زئولیتی در فرایند MTG به متغیرهایی مانند مساحت سطح ویژه، تعداد و قدرت سایت‌های اسیدی و سایز کریستال و حفره بستگی دارد [۱]. با وجود نقش موثر میکروحفرات در فراهم کردن گزینش‌پذیری، این میکروحفرات سبب محدودیت‌های نفوذی، تشکیل زودهنگام کک و کاهش طول عمر کاتالیست می‌شوند [۲]، در نتیجه تهیه زئولیتی با شبکه میکروحفره کریستالین به صورت ترکیبی با ساختار مزوحفره، سبب افزایش چشمگیر کارایی کاتالیستی در واکنش MTG می‌شود.

در تحقیق پیش رو، سنتز نانوزئولیت ZSM-5 و اصلاح آن از طریق فرایند سیلیس‌زدایی جهت بهبود کارایی کاتالیستی در فرایند تبدیل متانول به بنزین ارائه می‌شود. ابتدا زئولیت میکروحفره ZSM-5 سنتز شد و پس از فرایند کلسینه شدن، جهت تشکیل مزوحفره تحت فراوری قلیایی با باز آلی تترامتیل آمونیوم هیدروکسید TMAOH قرار گرفت. خصوصیات کاتالیست اولیه و تاثیر فراوری قلیایی با باز آلی بر روی مشخصات حفره، کریستالیتی، مورفولوژی و اسیدیته‌ی کاتالیست با استفاده از نتایج حاصل از روش‌های آنالیز جذب و واجذب نیتروژن، XRD ، SEM و $NH_3$-TPD بررسی شدند. نتایج نشان داد در فراوری قلیایی تحت شرایط بهینه (۰/۱۵ M از TMAOH)، مساحت سطح از $m^2g^{-1}$ ۳۴۰ در زئولیت اولیه به $m^2g^{-1}$ ۳۶۰ و اندازه حفره از nm ۲/۱ در زئولیت اولیه به nm ۳/۵ در زئولیت فراوری شده افزایش یافت. کاتالیست فراوری شده پس از تعویض یونی برای فرایند تبدیل متانول به هیدروکربن در راکتور بستر ثابت در دمای ۳۹۰°C و $WHSV=4\ h^{-1}$ مورد استفاده قرار گرفت. افزایش مساحت سطح در دسترس کاتالیست سبب افزایش میزان تبدیل متانول (اکتیویته) از ۸۵٪ به بیش از ۹۵٪ به مدت ۲۰ ساعت شد. همچنین افزایش نسبت مزوحفره به میکروحفره و کاهش غلظت کل سایت های اسیدی در کاتالیست فراوری شده، سبب افزایش طول عمر کاتالیست به میزان ۱۵٪ و افزایش تولید هیدروکربن‌های آروماتیکی به میزان ۱۰٪ نسبت به نانوزئولیت ZSM-5 اولیه شد.

**کلمات کلیدی**: زئولیت ZSM-5، مزوحفره، فرایند MTG

## منابع

[1] Teketel S, Skistad W, Benard S, Olsbye U, Lillerud K P, Beato P, Svelle S. *ACS Catal*. **2011**, 2, 26–37

[2] J. Kim, M. Choi, R. Ryoo, *J. Catal*. 269, **2010**, 219

# اکسایش مشتقات الکلی به آلدئیدها و کتونها توسط

# نانو کاتالیزور قابل بازیافت مس تثبیت شده بر پایه ارگانو سیلیکای منظم

فاطمه رجبی[1]، سید احمد محسنی تکیه[1]

[1]دانشکده شیمی، دانشگاه پیام نور،تهران، ایران

ایمیل نویسنده مسئول: f_rajabi@pnu.ac.ir

## چکیده

در سالهای اخیر به منظور کاهش مسایل زیست محیطی و اقتصادی که همواره از مشکلات عمده صنایع محسوب می شود، توجه به کاتالیزورهای جدید ناهمگن قابل بازیافت که باعث افزایش راندمان، زیست تخریب پذیری، مسیر کوتاه واکنشها، خالص سازی آسانتر، انجام واکنش در شرایط خفیف عاری از حلال، کاهش تولید ضایعات و زمان کوتاهتر می شود، رو به رشد است. از این رو نگرش جدیدی به مواد ارگانوسیلیکای مزومتخلخل به عنوان بستر برای ناهمگن سازی کاتالیزورهای همگن شده است [۱]. در همین راستا در تحقیق حاضر، نانوکاتالیزور مس تثبیت شده (Cu-L@ PMO) با استفاده از شیف باز حاوی پیریدین و نمک مس سنتز شد. سپس فعالیت کاتالیزوری آن به عنوان یک کاتالیزور کارآمد و قابل بازیافت در اکسایش الکلهای نوع اول و دوم به آلدئیدها و کتونها [۲ ] با استفاده از هیدروژن پراکسید به عنوان اکسنده دوستدار محیط زیست بررسی شد (شمای ۱) و فعالیت قابل ملاحظه ای از نانوکاتالیزور(Cu-L@ PMO) در این واکنش مشاهده شد.

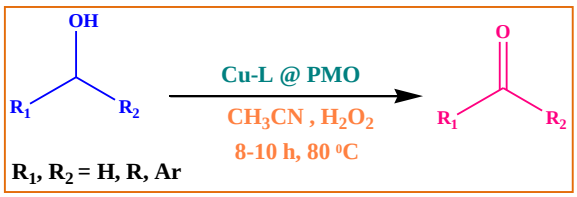


شمای ۱. اکسایش الکلها در حضور نانوکاتالیزور (Cu-L @ PMO)

**کلمات کلیدی:** نانو کاتالیزور، اکسایش، ارگانو سیلیکا

## منابع

[1] F. cardona, C. Parmeggiani, and C. Matassini, *Green chem*, **2017**.

[2] G. Tojo and M. Fernández, *Oxidation Alcohols*, Springer, New York (2010).

# سنتز نانو کاتالیزور قابل بازیافت آهن تثبیت شده بر پایه ارگانو سیلیکای منظم و کاربرد آن در اکسایش الکلها به ترکیبات کربونیل

فاطمه رجبی[۱]، سید احمد محسنی تکیه[۱]

[۱]دانشکده شیمی، دانشگاه پیام نور ، تهران، ایران

ایمیل نویسنده مسئول: f_rajabi@pnu.ac.ir

## چکیده

در میان مولکولهای فعال بیولوژیکی، ترکیبات آلی از اهمیت ویژه‌ای برخوردارند. توسعه روش‌های کارآمد در تشکیل این ترکیبات جهت کاربردهای گسترده آنها در صنایع دارویی و هم چنین به عنوان سموم گیاهی و ... امری مهم و ضروری است. یکی از مشکلات موجود در سنتز این ترکیبات، جداسازی سخت کاتالیزور از محصول واکنش و هم چنین سمیت این کاتالیزورهاست، که این مشکل در کاتالیزورهای زیست تخریب پذیر ناهمگن [۱-۳] رفع شده و این کاتالیزورهای ناهمگن به راحتی توسط فیلتراسیون از مخلوط واکنش جدا شده و هم چنین قابل بازیافت می باشند. از این رو نگرش جدیدی به مواد ارگانوسیلیکای مزومتخلخل به عنوان بستر برای ناهمگن سازی کاتالیزورهای همگن شده است. در همین راستا در تحقیق حاضر، نانوکاتالیزور آهن تثبیت شده (Fe-L@ PMO) بر پایه مواد مزومتخلخل ارگانوسیلیکا سنتز شد. سپس فعالیت کاتالیزوری آن به عنوان یک کاتالیزور کارآمد و قابل بازیافت در اکسایش الکلهای نوع اول و دوم به آلدئیدها و کتونها با استفاده از هیدروژن پراکسید به عنوان اکسنده دوستدار محیط زیست بررسی شد (شمای ۱) و فعالیت قابل ملاحظه ای از نانوکاتالیزور(Fe-L@ PMO) در این واکنش مشاهده شد.

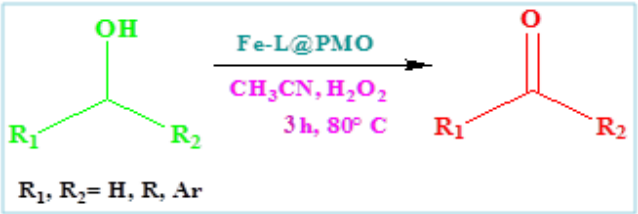


شمای ۱. اکسایش الکلها در حضور نانوکاتالیزور (Fe-L @ PMO)

**کلمات کلیدی:** نانوکاتالیزور، ارگانوسیلیکا، اکسایش

## منابع

[1] C. Bodhak, A. Kundu, and A. Pramanik, *Tetrahedron Letters*, **2015**, 419-424.

[2] M. J. Climent, A. Corma and S. Iborra, *RSC Advances*, **2011**.

[3] H. G. O. Alvim, T. B. Lima, A. L. de Oliveira, H. C. B. de Oliveira, F. M. Silva, F. C. Gozzo, R. Y. Souza, W. A. de Silva and B. A. D. Neto, *J. Org. Chem*, **2014**, 79, 3383-3397.

# بررسی عملکرد راکتور فیبر نوری پوشیده شده با تیتانیوم دی‌اکسید و متصل شده به LED به عنوان منبع نور در تخریب نوری برخی آلاینده‌های رنگی از آب

سید رضا نبوی [۱]. سید سعید ابراهیم رادیان [۲]، امین قادی [۳]

[۱] عضو هیئت علمی دانشکده شیمی، دانشگاه مازندران، بابلسر ، ایران
[۲] دانشجو کارشناسی ارشد دانشکده شیمی، دانشگاه مازندران، بابلسر ، ایران
[۳] عضو هیئت علمی دانشکده فیزیک، دانشگاه مازندران، بابلسر، ایران
ایمیل نویسنده مسئول: srnabavi@umz.ac.ir

## چکیده

نور رسانی به فوتوکاتالیست یک مانع کلیدی در روش‌های تصفیه فوتوکاتالیستی آب محصوب می‌شود که آلاینده‌ها خود باعث جلوگیری از نور رسانی به فوتوکاتالیست می‌شوند و همچنین فوتوکاتالیست بعد از تصفیه نیاز به جداسازی دارد. برای رفع این مشکل فوتوکاتالیست را به صورت یک فیلم روی بستر تثبیت می‌کنند و نور را به سطح آن می‌تابانند. [۱]
در این پژوهش از فیبرهای نوری پوشیده شده با تیتانیوم دی‌اکسید و LED برای بهبود نور رسانی استفاده شده است. همچنین روی فاکتورها و مکانیسم‌های مختلفی همچون تاثیر تعداد LED ، تعداد فیبر نوری بکار برده شده، تعداد دفعات پوشش‌دهی شده و نحوه اتصال فیبر نوری به LED به طور کامل مورد بررسی قرارگرفته است.
برای بررسی تاثیر متغییرها آزمایش‌های مختلف انجام شد ونتایج نشان داد با قرار دادن راکتور در معرض نور مرئی بعد از زمان ۲ ساعت حدود ۷۰ درصد از آلاینده رودامین بی از آب حذف می شود. همچنین آلاینده‌های دیگر رنگی هم مورد بررسی قرار گرفت.

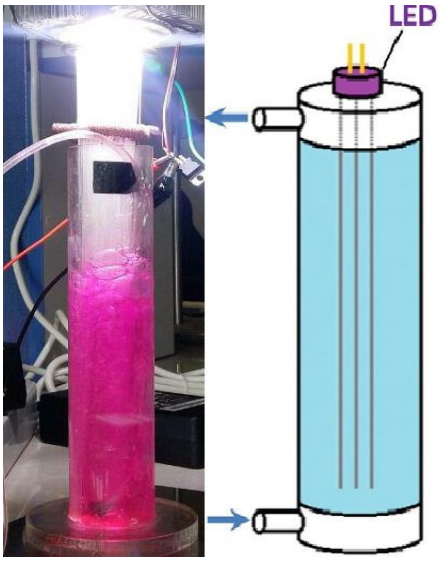


شمای ۱. تصویر راکتور فیبر نوری متصل به LED

**کلمات کلیدی:** فوتوکاتالیست، فیبر نوری، تیتانیوم دی‌اکسید، LED

## منابع

[1] Tugaoen, H. O. N., Garcia-Segura, S., Hristovski, K., & Westerhoff, P, *Journal*, **2018**, Science of the Total Environment, 613, 1331-1338.

# بررسی کارایی کاتالیزور کامپوزیتی ZSM-5/11 اصلاح شده با فلز در تبدیل متانول به بنزین

مریم جوی بار *[1]، محمد رضا خان محمدی[1]، امیر باقری گرمارودی[1]

[1]گروه شیمی، دانشکده علوم پایه، دانشگاه بین المللی امام خمینی (ره) قزوین، ایران

نویسنده مسئول: Maryamjuybar.gu@gmail.com

## چکیده

تبدیل کاتالیتیکی متانول به بنزین (MTG) با استفاده از کاتالیزورهای زئولیتی یکی از فرایندهای نوید بخش برای تولید سوخت های بکار رفته در حمل و نقل و سایر صنایع با استفاده از منابعی به غیر از منابع پتروشیمی معمولی می باشد[1]. برای اولین بار در سال ۱۹۷۷ این فرایند توسط شرکت Exxon Mobil با استفاده از کاتالیزور زئولیتی ZSM-5 برای تولید هیدروکربن های گستره بنزینی با عدد اکتان(RON) ۹۶-۹۰ بکار گرفته شد[2]. زئولیت ZSM-5 دارای یک ساختار آلومینا سیلیکاتی کریستالی با اسیدیته بالا می باشد که قادر به تبدیل متانول بوده و همچنین با ساختار میکروپور یکنواخت(۰/۵۵ nm) تولید محصولات گستره بنزینی را کنترل می کند. اما به دلیل همین سیستم حفره ای میکروپور انتقال محصولات هیدروکربنی ایجاد شده در کانال های زئولیت محدود شده و منجر به تشکیل کک و غیر فعال شدن سریع کاتالیزور طی واکنش MTG می شود. بنابراین در طول سالهای گذشته روش های مختلفی برای افزایش کارایی و طول عمر این کاتالیزورها بکار رفته است. یکی از موثرترین روش ها برای اصلاح ساختار کاتالیزور بکارگیری فلزات و اکسید آنها به دلیل تغییر در اسیدیته و ایجاد ساختار مزوپور می باشد[3].

در این پروژه نیز ابتدا یک ساختار نانوکامپوزیتی از زئولیت های ZSM-5 و ZSM-11 با یک ساختار Intergrowth بین دو زئولیت با ساختار مشابه، سنتز شد و سپس با فلز گالیوم به روش سنتز مستقیم برای بهبود خواص ساختاری و عملکرد آن در فرایند MTG اصلاح شد. خصوصیات و مورفولوژی کاتالیزور تولید شده توسط روش های مختلف طیف بینی مانند XRD، BET، SEM، TEM، $NH_3$-TPD و FTIR بررسی شد. نتایج نشان می دهد که ساختار کریستالی پس از اصلاح حفظ شده و مساحت سطح وحجم حفره افزایش می یابد. همچنین نتایج $NH_3$-TPD نشان امی دهد که شدت و قدرت اسیدیته لوئیس و برونستد تغییر و سایت های اسیدی جدید برای افزایش عملکرد کاتالیتیکی کاتالیزور سنتز شده ایجاد می شود. همچنین فعالیت کاتالیتیکی این زئولیت اصلاح شده با گالیوم در فرایند MTG بررسی و مشاهده می شود که طول عمر کاتالیزور از ۳۰ ساعت به ۴۸ ساعت و گزینش پذیری نسبت به ترکیبات آروماتیکی نیز افزایش می یابد.

**کلمات کلیدی:** نانو کامپوزیت زئولیتی، اصلاح کاتالیزور، متانول به بنزین

## منابع

[1] A.Zhijian Wan, B. Wei Wu, C. Gang (Kevin) Li, Applied Catalysis A: General, **2016**, *523*, 312–320.

[2] A. Fanjun Meng, B.Yaquan Wang, C. Shougui Wang, Comptes Rendus Chimie, **2017**, *20*, 385-394.

[3] A. Kristof Van der Borght, B. Vladimir V. Galvita, Applied Catalysis A: General, **2015**, *504*, 621-630.

# بررسی خواص نوری و الکتریکی نانوکاتالیست های تهیه شده از پلی آنیلین و اکسیدهای کروم و منگنز دارای پتانسیل حذف سرب از آبهای آلوده

احمد ستاری[۱*]، محمدرضا محمد شفیعی[۲]، محبوبه کارگر[۳]

[۱]دانشکده شیمی، دانشگاه زنجان، زنجان، ایران
[۲]دانشکده شیمی، دانشگاه آزاد واحد نجف آباد، نجف آباد ، ایران
[۳]دانشکده فیزیک، دانشگاه اصفهان، اصفهان، ایران
ایمیل نویسنده مسئول: a.sattari@znu.ac.ir

## چکیده

اخیرا موضوع نانوکاتالیست ها (کاربرد نانوذرات برای کاتالیست کردن واکنش ها) رشد سریعی در زمینه کاتالیزورهای همگن و ناهمگن داشته است[۱]. نسبت سطح به حجم بالای این مواد در مقایسه با مواد توده جذابیت آنها را برای تسریع واکنش ها در عرصه های مختلف از جمله تصفیه آب، سلول های سوختی، ذخیره انرژی و ... بالا برده است[۲-۴]. در تحقیق حاضر نانوکاتالیست های پلیمری بر پایه پلی آنیلین و اکسیدهای فلزی کروم و منگنز به روش اکسیداسیون- احیا تهیه گردید[۵و۶]. از اختلاط محلول آنیلین با نمک های فلزی کروم و منگنز در حضور عامل اکسید کننده، مونومرهای آنیلین به صورت پوسته در سطح اکسیدهای فلزی تولید شده در ظرف واکنش پلیمریزه شده و کامپوزیت $MnO_2@Cr_2O_3@Pani$ را تولید کردند. تصاویر میکروسکوپ الکترونی پویشی (FESEM) اندازه و مورفولوژی نانوذرات تهیه شده را نشان داد. طیف های مادون قرمز (FT-IR) نشانگر حضور پلی آنیلین در فرم امرآلدین (Emeraldine) در ساختار نانوکامپوزیت ها بود. آنالیز فرابنفش-مریی (Uv-Visible) علاوه بر تایید فرم ساختاری پلیمر در نانوکامپوزیت، خواص نوری آن را نیز آشکار کرد. اثر هیپسوکرومی ناشی از انتقالات n به π* و قطبی نانوکاتالیست ها نظریه تلفیق مطلوب پلیمر با اکسیدهای فلزی را قوت بخشید. هدایت الکتریکی (σ) اندازه گیری شده با آنالیز چهار پروبه نشان داد که هدایت ذرات پلیمری در حضور اکسیدهای فلزی افزایش یافته است. حذف بالای سرب از آبهای آلوده نشانگر پتانسیل بالای نانوکامپوزیت مذکور در تصفیه آب می باشد.

**کلمات کلیدی:** نانوکاتالیست پلی آنیلین- اکسید فلزی، خواص نوری، هدایت الکتریکی جریان مستقیم، حذف سرب

## منابع

[1] S. Chaturvedi, P. N. Dave, and N.K. Shah, Journal of Saudi Chemical Society, **2012**, 16, 307–325.
[2] L. Lin, and Q. Wu, Polymers & Polymer Composites, **2012**, 20, 4.
[3] A. Shahid Pervez, and M. Faiz, Polymers & Polymer Composites, **2016**, 24, 273-280.
[4] U. Mandi, M. Pramanik, A. Singha Roy, N. Salam, A. Bhaumik and Sk. Manirul Islam, RSC Adv., **2014**, 4, 1543.
[5] Z. Hu, L. Zu, Y. Jiang, H. Lian, Y. Liu, Z. Li, F. Chen, X. Wang, and X. Cui, Polymers, **2015**, 7, 1939–1953.
[6] M. Abdullah Dar, R. K. Kotnala, V. Verma, J. Shah, W. A. Siddiqui, and M. Alam, J. Phys. Chem. C **2012**, 116, 5277−5287.

# گوگردزدایی اکسایشی فتوکاتالیستی سوخت مدل دیزل به کمک نانوذرات $TiO_2$ و هوا تحت تابش نور فرابنفش

**کاوه کلانتری**

*گروه مهندسی شیمی، دانشکده مهندسی، دانشگاه زنجان، زنجان، ایران*

*ایمیل نویسنده مسئول:kalantari_k@yahoo.com*

## چکیده

حذف ترکیبات گوگردی موجود در سوخت‌های مایع بر اساس مقررات زیست محیطی از اهمیت ویژه‌ای برخوردار است. فرآیندهای گوگردزدایی اکسایشی به دلیل عدم نیاز به هیدروژن، هزینه پایین و شرایط عملیاتی ملایم اهمیت فراوانی یافته است. بهره‌گیری از فتوکاتالیست‌ها یکی از روش‌های جدید و موثر برای اکسایش و حذف ترکیبات گوگردی مقاوم مانند دی‌بنزوتیوفن (DBT) است. در مقاله حاضر از نانوذرات $TiO_2$ به عنوان فتوکاتالیست برای گوگردزدایی اکسایشی فتوکاتالیستی در فاز آلی و در دمای محیط بهره گرفته شد. گوگردزدایی اکسایشی فتوکاتالیستی DBT در سوخت مدل دیزل تحت تابش نور فرابنفش (UV) و هوا به عنوان اکسید کننده انجام شد. نتایج آنالیز گازکروماتوگرافی جرمی (GC-MS) حضور سولفون و سولفوکسید دی‌بنزوتیوفن را تأیید کرد. اثر شرایط عملیاتی مختلف مانند میزان اکسید کننده، میزان بارگذاری کاتالیست بر میزان تبدیل DBT مورد بررسی قرار گرفت. مطالعات سینتیکی نشان داد که اکسایش فتوکاتالیستی DBT از مدل شبه درجه یک پیروی می‌کند.

**واژگان کلیدی :** نانوذرات $TiO_2$، گوگردزدایی اکسایشی فتوکاتالیستی، نور فرابنفش

# جذب فلز سرب از آب های آلوده با استفاده از نانوکاتالیست SrBi4Ti4O15 با ساختار آئریوویلیوس

**عاطفه بدری [۱]، محمود ابراهیمی [۲]**

*[۱]آموزش و پرورش ناحیه ۳ استان اصفهان*
*[۲]دانشکده شیمی، دانشگاه آزاد مشهد، مشهد، ایران*

*ایمیل نویسنده مسئول:* atefe_badri@yahoo.com

## چکیده

در این تحقیق سنتز نانو کاتالیست SrBi4Ti4O15 با مورفولوژی دو لایه ای آئریوویلیوس از جایگزینی استرانسیوم در بیسموت و تیتانیوم اکسید با استفاده از یک روش اصلاحی سل- ژل انجام شد و عملکرد آن در جذب کاتیون سرب به عنوان یک فلز سنگین و سمی که بر سلامت انسان و محیط زیست تاثیر دارد از آب های آلوده بررسی شد. الگوهای XRD و خطوط پراش تیز و با شدت بالای ترکیب حاصل انطباق آن را با فاز بلوری ارتورومبیک نشان داد. تصاویر FESEM جهت بررسی شکل شناسی و اندازه نانو ذرات، حاکی از ذرات همگن، یکنواخت و به صورت میله ای شکل و با اندازه ۴۵ نانو متر بود. آزمایش های طراحی شده ظرفیت جذب و سینتیک جذب را به روی جاذب تعیین کرد. بهینه سازی بعضی از پارامترهای جذب مانند اثر زمان تماس، pH، غلظت اولیه یون هدف و مقدار جاذب در تعیین عملکرد جاذب نشان می دهد که اکسیدهای آئریوویلیوس (Aurivillius) ظرفیت جذب مطلوب برای یونهای سرب را دارا می باشند. با استفاده از مدل های سینتیکی به وسیله داده های تجربی، مشخص شد که جذب سرب (II) بر جاذب بسیار سریع و کارآمد بوده و از معادله سرعت سینتیک جذب شبه مرتبه دوم تبعیت می کند. علاوه بر این، مدل سیپس بهتر از مدل های لانگمیر و فروندلیچ در فرآیند جذب سرب و توصیف داده های تجربی موفق بوده است. مطالعات جذب بر اساس دما بررسی شد و با استفاده از آن پارامترهای ترمودینامیکی انرژی آزاد $\Delta G^0$ و آنتالپی جذب $\Delta H^0$ و بی نظمی $\Delta S^0$ ارزیابی شد که تعیین کرد که فرآیند گرماگیر بوده و دارای افزایش روند جذب اتفاقی می باشد. بنابراین جاذب سنتز شده به دلایل کم هزینه بودن و مقرون به صرفه بودن، راندمان بالای جذب، گزینش پذیری یا انتخاب یونی و سینتیک سریع می توانید به عنوان یک جاذب مناسب در فرایند حذف یون های سرب از محلولهای آبی عمل کند.

**کلمات کلیدی:** اکسیدهای آئروویلیوس۱، سینتیک جذب ۲، ایزوترم حذف ۳، سرب ۴، ترمودینامیک ۵، *نانو ۶*

## منابع

[1] M. A. K. Moharram, K. Tohami, W. M. El Hotaby, A. M. Bakr, *Reactive and functional polymers*, **2016**, *101*,9-19.

[2] ] E.M. Mager, K.V. Brix, R.M. Gerdes, A.C. Ryan, M. Grosell, *Ecotoxicology and Environmental Safety*, **2011**, *74*, 238-243.

[3] R. Hu, X. Wang, S. Dai, D. Shao, T. Hayat, A. Alsaedi, *Chemical Engineering Journal*, **2015,** *260*, 469–477.

# سنتز سبز مشتقات تترازول با استفاده از چارچوب فلز-آلی نانوحفره MOF-199

سامی سجادی‌فر[1*]، زینب ارزه‌گر[1]

[1]دانشگاه پیام نور، گروه شیمی، 4657 15359 ، تهران، ایران

ایمیل نویسنده مسئول: ss_sajjadifar@yahoo.com

## چکیده

تاکنون تلاش‌های زیادی برای کشف روش‌هایی جدید برای سنتز تترازول‌ها صورت گرفته است. فعالیت فیزیولوژی بالای باعث می‌شود که تترازول‌ها ترکیباتی کارآمد و مفید برای مقاصد دارویی باشند. از مشتقات تترازول در تهیه داروهای ضد فشار خون، ضدآلرژی و نیز در تهیه آنتی‌بیوتیک‌ها، داروی ضدغش و ضدگرفتگی عضلات استفاده می‌شود [۱-۲]. این ترکیبات به دلیل سمیت کمتر، تولید دوده کمتر و قدرت بیشتر جایگزین مناسبی برای موادی از قبیل TNT می‌باشند [۳]. در این مقاله با روشی ساده و ملایم ترکیبات تترازول با استفاده از مشتقات مختلف نیتریل سدیم آزید در مجاورت مقادیر کاتالیزوری از چارچوب فلز-آلی نانوحفره MOF-199 در حلال پلی‌اتیلن گلیکول ۴۰۰ و دمای ۱۲۰ درجه سانتی‌گراد سنتز شدند. تمام محصولات با بازده‌های بالابه‌دست آمدند. چارچوب فلز-آلی نانوحفره MOF-199 به‌کار برده شده، دارای مزایایی از جمله غیرسمی بودن، پایدار بودن در حلال‌ها و شرایط سخت، سنتز آسان، فعالیت بالا و جداسازی آسان توسط صاف شدن از مخلوط واکنش می‌باشد.در این کار قابلیت استفاده مجدد چارچوب فلز-آلی نانوحفره MOF-199 تا ۴ مورد بررسی قرار گرفت و کاهش چشمگیری در بازده واکنش مشاهده نگردید.

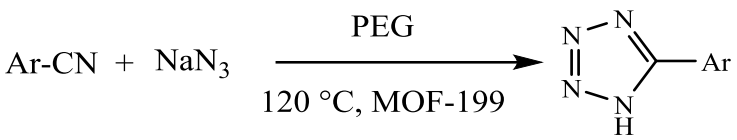


شمای ۱. سنتز مشتقات تترازول

**کلمات کلیدی:** تترازول، چارچوب فاز-آلی، MOF-199، نیتریل، سدیم آزید

## منابع

[1] H. A. Dabbagh, Y. Mansoori, M. Jafary, M. Rostami, *J. Chem. Res.* **2000**, *2000*, 442.

[2]G. F. Holland, and J. N. Pereira, *J. Med. Chem.*, **1967**, *10*, 149.

[۳] م. شهیدزاده، ف. فرزندی، مجله علمی-پژوهشی مواد پر انرژی، **۱۳۹۳**، شماره ۲، ۲۷-۳۴.

# کاربرد بنتونیت جهت کند رها شدن کود اوره

اکبر پایدار[۱]، علی محمدخواه [۱*]، اکبر فرقانی[۲]

[۱]دانشکده علوم پایه، دانشگاه گیلان، رشت، ایران
[۲]دانشکده علوم کشاورزی، دانشگاه گیلان، رشت، ایران

ایمیل نویسنده مسئول: mohammadkhah@guilan.ac.ir

## چکیده

اتلاف کودهای شیمیائی فارغ از نوع ترکیب آنها امری اجتناب ناپذیر بوده و بکارگیری آنها از بازدهی صد درصد برخوردار نمی باشد. این واقعیت گریزناپذیر در مورد کودهای ازته ( یا نیتروژن دار ) مصداق کامل دارد. از سه ماده مغذی اصلی مورد نیاز گیاهان یعنی نیتروژن، فسفر و پتاسیم، نیتروژن سریعتر خاک را ترک می کند. مقدار نیتروژنی که در جریان مصرف کودهای ازته از دست می رود بین ۳۰ تا ۵۰ درصد تخمین زده می شود. از دست دادن این مقدار از کود باعث اتلاف هزینه می شود و بخاطر نیاز گیاه باید کود بیشتری مصرف کرد که این کار مستلزم صرف هزینه‌های کارگری بیشتر و مصرف بیش از اندازه کود می شود. استفاده از مقادیر زیاد کود نه تنها از لحاظ اقتصادی بصرفه نمی‌باشد بلکه به محصول و محیط زیست (آلودگی خاک و منابع زیر زمینی آب) نیز آسیب جدی می رساند [۱]. استفاده کارآمد از کود های معدنی برای فراهم نمود مواد مغذی (نیتروژن، فسفر و پتاسیم) یک راهکار مطلوب در بهره وری کشاورزی است . بکارگیری کودهای آهسته رهش یا کندرها از اتلاف کود جلوگیری نموده و به بهترین شکل هدف ما را تامین می‌کند [۲]. در این پژوهش از سه نوع خاک بنتونیت از معادن ایران برای تهیه کامپوزیت به نسبت های ۱:۱ (۵۰٪ اوره ) و ۱:۲ (۶۶٪ اوره ) و ۱:۴ (۸۰٪ اوره ) وزنی ـ وزنی استفاده شده است که میزان رها شدن کود اوره در آب در مقایسه با کود اوره گرانول مورد بررسی قرار گرفت که بهترین ترکیب ، نسبت یک به یک بنتونیت و کود اوره بدست آمد. سپس این کامپوزیت در نمونه های خاک شالیزار با بافت رسی و رسی-لومی مورد آزمایش قرار گرفت که در مقایسه با کود اوره بازده ای بالایی دارد.

**کلمات کلیدی:** بنتونیت ، اوره ، کند رها

## منابع

[1] B. Azeem, K. KuShaari, Z. B. Man, A. Basit, T. H. Trinh, *Journal of Controlled Release*, **2014**, *181*, 11.

[2] E. I. Pereira, F. B. Minussi, C. C. T. da Cruz, A. C. C. Bernardi, C. Ribeiro, *Journal of agricultural and food chemistry*, **2012**, *60*, 5267.

# سنتز چهار جزئی مشتقات ۱،٤- دی هیدروپیریدین در شرایط بدون حلال

**زهرا فرزین، علیرضا کاظمی زاده**

*آزمایشگاه تحقیقاتی واکنش های چند جزئی، گروه شیمی، دانشگاه آزاد اسلامی واحد زنجان، زنجان، ایران*

*zahrafarzin15@gmail.com*

مشتقات ۱،۴- دی هیدروپیریدین هتروسیکل های مهمی با کاربردهای متنوعی از قبیل خواص ضد سرطان [1]، ضد دیابت [2]، ضد التهاب [3]، ضد سل [4] و غیره می باشند. در ادامه علاقه ما برای سنتز هتروسیکل ها [5]، مشتقات ۱،۴- دی هیدروپیریدین **(۵)** از واکنش چهار جزئی بین آلدئیدهای آروماتیک **(۱)**، مالونونیتریل یا اتیل سیانواستات **(۲)**، دی آلکیل استیلن دی کربوکسیلات ها **(۳)** و آمین ها **(۴)** در شرایط بدون حلال سنتز گردید (**شمای ۱**). روش ارائه شده روشی آسان، راحت و دوستدار محیط زیست برای سنتز مشتقات ۱،۴- دی هیدروپیریدین می باشد.

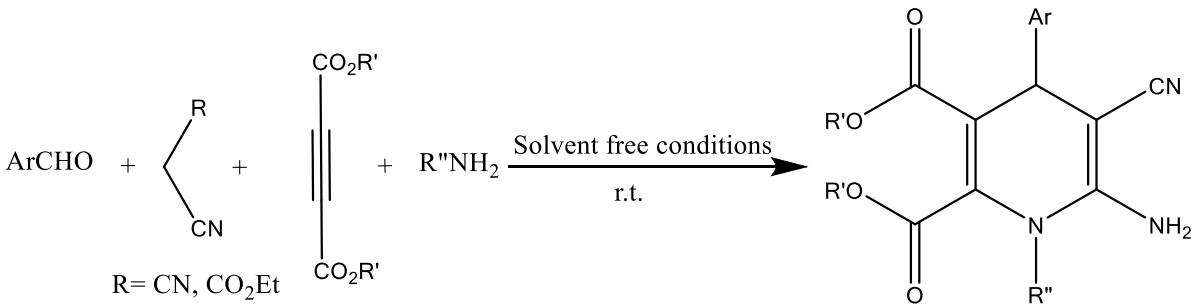


**(1)** **(2)** **(3)** **(4)** **(5)**

**Scheme 1.** Four component synthesis of 1,4-dihydropyridine.

## References

[1] T. Tsuruo, H. Iida, M. Nojiri, S. Tsukagoshi, and Y. Sakurai, *Cancer Research*, **1983**, *43*, 2905.

[2] W. J. Malaise, and P. C. F. Mathias, *Diabetologia*, **1985**, *28*, 153.

[3] B. Sushilkumar, and S. Devanand, *Acta Pharmaceutica*, **2002**, *52*, 281.

[4] G. A. Wachter, and M. C. Davis, *J. Med. Chem.*, 1998. *41*, 2436.

[5] a) A. R. Kazemizadeh, N. Shajari, R. Shapouri, N. Adibpour, R. Teimuri-Mofradd, and P. Dinmohammadi, *Appl. Organometall. Chem.*, **2016**, *30*, 148; b) A. R. Kazemizadeh, N. Shajari, R. Shapouri, N. Adibpour, and R. Teimuri-Mofradd, *J. Iran Chem. Soc.* **2016**, *13*, 1349.

# سنتز دوستدار محیط زیست و سه جزئی مشتقات ایزوکسازول-۵ (*H*٤)- اون در محیط آبی

**سپیده کاظمی، علیرضا کاظمی زاده**

*آزمایشگاه تحقیقاتی واکنش های چند جزئی، گروه شیمی، دانشگاه آزاد اسلامی واحد زنجان، زنجان، ایران*

*sepidehkazemi1370@gmail.com*

## چکیده

ایزوکسازول ها دارای خواص بیولوژیکی متنوعی از قبیل ضد باکتری [1]، ضد سرطان [2]، ضد قارچ [3] و غیره می باشند. در ادامه علاقه ما برای سنتز هتروسیکل ها [4, 5]، مشتقات ایزوکسازول-۵ (*H*۴)-اون **(4)** از واکنش ۳ جزئی بین آلدئیدهای آروماتیک **(1)**، هیدروکسیل آمین هیدروکلرید **(2)** و اتیل استواستات **(3)** در حضور سدیم دی هیدروژن فسفات به عنوان کاتالیست در دمای محیط و در حلال آب گزارش می گردد (**شمای ۱**). روش ارائه شده روشی آسان، راحت و دوستدار محیط زیست برای سنتز مشتقات ایزوکسازول-۵ (*H*۴)- اون می باشد.

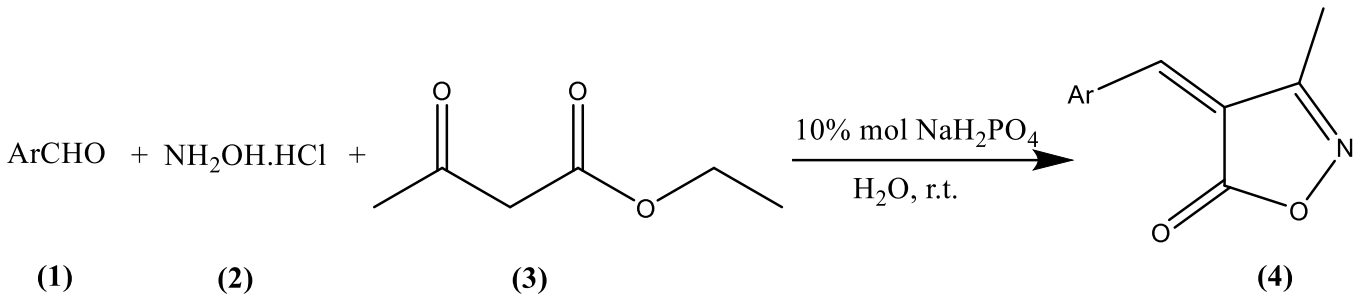


**Scheme 1.** Environmentally friendly synthesis of isooxazole-5(4*H*)-one derivatives.

## References

[1] K. C. Gautam, and D. P. Singh, *Chem. Sci. Trans.*, **2013**, *2*, 992.

[2] S. M. Abu Bakr, S. S. Abd El-Karim, M. M. Said, and M. M. Youns, *Res. Chem. Intermed.* **2016**, *42*, 1387.

[3] F. Chevreuil, A. Landreau, D. Séraphin, G. Larcher, S. Mallet, J. P. Bouchara, and P. Richomme, *J. Enzyme Inhib. Med. Chem.*, **2007**, *22*, 563.

[4] A. R. Kazemizadeh, N. Hajaliakbari, R. Hajian, N. Shajari, and A. Ramazani, *Helv. Chim. Acta*, **2012**, *95*, 594.

[5] A. R. Kazemizadeh, N. Shajari, R. Shapouri, N. Adibpour, R. Teimuri-Mofradd, and P. Dinmohammadi, *Appl. Organometall. Chem.*, **2016**, *30*, 148.

# سنتز و بررسی نانوکامپوزیت‌های پلی آمیدی اصلاح شده با نانوذرات مغناطیسی عامل‌دار شده جدید بر پایه تریس (هیدروکسی) متیل آمینومتان

سمانه بزاز[1]، کاوه خسروی[1*]، خلیل فقیهی[1] . زهرا فلاحی[1]

[1]دانشکده علوم پایه، گروه شیمی، دانشگاه اراک، اراک، ایران، کدپستی۸۳۴۹-۳۸۱۵۶

ایمیل نویسنده مسئول: khosravi.kaveh@gmail.com

## چکیده

ساختارهای پلی آمیدی به دلیل توانایی تشکیل شبکه قوی هیدروژنی بین زنجیره های پلیمری، از خواص ویژه‌ایی مانند پایداری گرمایی و مکانیکی برخوردارند و در صنعت جایگزین مناسبی برای سرامیک‌ها و فلزات به شمار می‌روند [1-2]. امروزه علاوه بر ساختارهای پلی آمیدی، نانوکامپوزیت‌های تقویت شده با نانوذرات اکسید آهن به دلیل ایجاد خواص گرمایی و مغناطیسی بی نظیر و توانایی کاربرد آن‌ها در جداسازی و بازیافت بسیار مورد توجه قرار گرفته‌اند [3]. در این پژوهش، نمونه‌هایی از نانوکامپوزیت پلی آمیدی جدید حاوی حلقه‌های تری آزینی تقویت شده با درصدهای مختلف نانوذرات اکسیدآهن عامل‌دار شده بر پایه تریس هیدروکسی متیل آمینومتان به روش محلول به طور موفقیت آمیزی تهیه شدند (شمای ۱). نمونه‌های تهیه شده با آنالیزهای XRD, H,C-NMR, SEM-EDS, CHNS, DTGA, FT-IR مورد بررسی قرار گرفتند و مشخص شد که اصلاح پلی آمید با نانوذرات اکسید آهن باعث ایجاد خاصیت مغناطیسی و افزایش قابل توجه مقاومت حرارتی شده است.

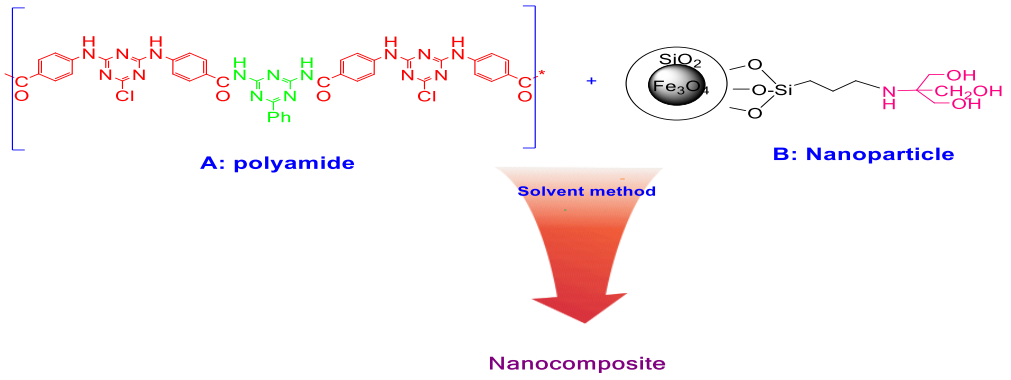


شمای ۱. سنتز نانوکامپوزیت پلی آمیدی

**کلمات کلیدی:** پلی آمید ، نانوکامپوزیت، نانوذره.

## منابع

[1] H. Huang, X. Yang, *Carbohydrate Research*, **2004**, *339*, 2627–2631.

[2] D. J. Liaw, M. Q. Jeng, *Polymer*, **1998**, *39*, 1957.

[3] S. S. Bhattacharya, A. Mandot, *Int. J. Pure Appl. Sci. Technol.*, **2013**, *17(2)*, 36-44.

# سنتز سبز کاتالیست نانوذرات پالادیوم بر روی بستر میوه کاج با استفاده از عصاره گیاه دم اسبی و استفاده از این کاتالیست در تولید هیدروژن از واکنش هیدرولیز سدیم بورو هیدرید

زهرا شیراوژن[۱]، مریم بردبار[۱]
[۱]دانشکده شیمی، دانشگاه قم، قم، ایران

z.shirojan@gmail.com

## چکیده

امروزه طراحی و استفاده از کاتالیست هایی که به محیط زیست صدمه نزنند به یک چالش مهم و اساسی برای دانشمندان تبدیل شده است. کاتالیست سبز یکی از مهمترین زیر شاخه های شیمی سبز است [۱]. با استفاده از روش های سبز می-توان کاتالیست هایی را به منظور کاتالیز واکنش های مختلف از جمله تولید هیدروژن از هیدرولیز سدیم بورو هیدرید تولید کرد. هیدروژن به عنوان یکی از امیدوارکننده‌ترین منابع انرژی پاک محسوب می‌شود. گاز هیدروژن را از دو منبع فسیلی (اکسایش جزئی نفت سنگین، فرایند رفورمینگ گاز طبیعی) و غیر فسیلی تهیه می کنند اما منابع فسیلی محدود و تجدیدناپذیرند و با این وجود درحال حاضر ۹۸ درصد از کل هیدروژن تولید شده در جهان از سوخت‌های فسیلی به دست می‌آید. در این کار نانو ذرات پالادیوم به روش سبز با استفاده از عصاره گیاه دم اسبی بر روی بستر پودر میوه کاج سنتز و با توجه به فعالیت کاتالیزوری خوب آنها در فرآیند هیدرولیز کاتالیزوری سدیم بوروهیدرید به منظور تولید هیدروژن به عنوان کاتالیست استفاده شده است. گیاه دم اسبی منبع غنی از ترکیبات پلی فنولیک مانند فالونوئیدها، تانین ها، استرول ها و اسپانین ها می‌باشد. همچنین در این سنتز، از مواد دورریزی مثل پودر میوه کاج به عنوان بستر استفاده شده است که این بستر به منظور جلوگیری از آگرومره شدن (agglomeration) و پایدار کننده (stabilizer) نانو ذرات به کار برده می‌شود. برای مشخصه یابی این کاتالیست از اسپکتروسکوپی FT-IR، اسپکتروسکوپی UV-Vis، FESEM و XRD استفاده شده است [۲-۴]. کاتالیست نقش مهمی در تولید هیدروژن از محلول سدیم بوروهیدرید دارد. یکی از مشکل های اساسی در هیدرولیز سدیم بوروهیدرید سرعت واکنش است. این واکنش بدون حضور کاتالیست دارای بازده خوب و چشمگیری نیست. کاتالیزور با کاهش انرژی فعال سازی می‌تواند به تولید هیدروژن شتاب دهد [۵].

**کلمات کلیدی**: تولید هیدروژن، سدیم بوروهیدرید، دم اسبی، میوه کاج، نانوذرات پالادیوم.

## منابع

[1] P. Raveendran, J. Fu and S.L. Wallen, *Journal of the American Chemical Society*, **2003**, *125*, 13940-13941.
[2] M. Bordbar and N. Mortazavimanesh, *Environmental Science and Pollution Research*, **2017**, *24*, 4093-4104.
[3] M. Bordbar, Z. Sharifi-Zarchi and B. Khodadadi, *Journal of Sol-Gel Science and Technology*, **2017**, *81*, 724-733.
[4] B. Khodadadi, M. Bordbar, A. Yeganeh-Faal and M. Nasrollahzadeh, *Journal of Alloys and Compounds*, **2017**, *719*, 82-88.
[5] M.D. Ganji, S. Emami, A. Khosravi and M. Abbasi, *Applied Surface Science*, **2015**, *332*, 105-111.

# بررسی و مقایسه دو نوع روش سل-ژل و ژل-احتراقی در سنتز اکسیدهای مخلوط فلزی

سارا مقصودی[1*]، آزاده آبادی[1]، محمد نوذری‌فرد[1]، امین علیپور[1]

[1] گروه مهندسی شیمی، دانشگاه آزاد اسلامی واحد ماهشهر، ماهشهر، ایران.

*E-mail: maghsoodi_mahshahr@yahoo.com

## چکیده

در این تحقیق اکسیدهای فلزی نوع پروسکایت $LaBO_3$ (B=Mn, Cr, Co, Ni) با استفاده از دو روش ژل-احتراقی توسط مایکروویو و سل-ژل سنتز و در دمای ۶۰۰ درجه‌ی سانتیگراد به مدت ۵ ساعت کلسینه شدند. از مزایای بارز روش ژل احتراقی می توان به ساده و سریع بودن، مواد اولیه ارزان، وقت و صرف انرژی کم و سادگی عملیاتی آن اشاره نمود [۱]. روش‌های دما پایین مانند سل ژل نیز در سنتز نانومواد بسیار کاربرد داشته است که روشی قابل دسترس برای تولید در حجم صنعتی می‌باشد و در مواد حاصل ناخالصی کمتر نسبت به سایر روش‌های سنتز گزارش شده است [۲]. تعیین مشخصات نمونه‌های سنتز شده توسط آنالیزهای مختلفی مانند BET، XRD و SEM انجام شد. ساختار اسفنجی و متخلل در تمام پروسکایت‌های سنتز شده با هر دو روش توسط تصاویر SEM مشاهده شد. آنالیز XRD نشان داد که پروسکایت‌ها به صورت تک‌فازی یا فاز غالب تشکیل شده است؛ ولی در نمونه های سنتز شده به روش سل-ژل پیک‌های پروسکایت به صورت شارپ‌تر و خالص‌تر مشاهده شد. مساحت سطح ویژه پروسکایت‌های سنتز شده به روش ژل- احتراقی ($m^2/g$ ۲۶-۳۲) در تمامی حالات بیشتر از پروسکایت‌های سنتز شده به روش سل- ژل ($m^2/g$ ۷-۱۲) می‌باشد. فعالیت اکسیداسیون کاتالیست‌های سنتز شده به منظور اکسیداسیون ppm ۱۰۰۰ تری‌کلرواتیلن که یک ترکیب آلی فرار است، در دماهای مختلف اندازه‌گیری گردید که برای نمونه نتایج آن در شکل ۱ برای پروسکایت‌ای سنتز شده به روش ژل- احتراقی نمایش داده شده است.

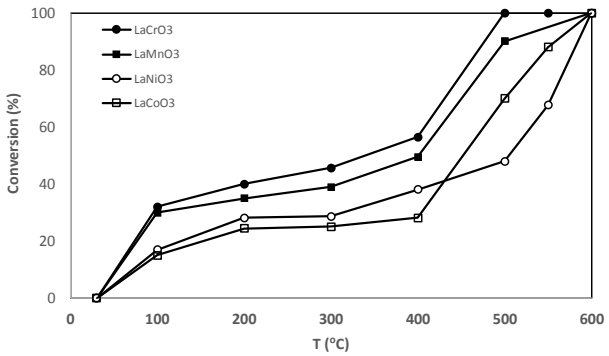


شکل ۱. اکسیداسیون ppm ۱۰۰۰ تری‌کلرو اتیلن در هوا توسط کاتالیست‌های سنتز شده به روش ژل- احتراقی

**کلمات کلیدی:** پروسکایت، کاتالیست، سل- ژل، ژل- احتراقی، ترکیبات آلی فرار

## منابع

[1] M. Misono, *Studies in Surface Science and Catalysis*, **2013**, *176*, 67–95.

[2] S. Maghsoodi, J. Towfighi, A. Khodadadi, Y. Mortazavi, *Chemical Engineering Journal*, ***2013***, 215-216, 827–837.

# بررسی اثر اکسید B مازاد بر ساختار دو نوع پروسکایت $LaBO_3$ (B= Cr, Co)

سارا مقصودی[1*]، فاطمه موسویان[1]، صدف رحیمی[1]

[1] گروه مهندسی شیمی، دانشگاه آزاد اسلامی واحد ماهشهر، ماهشهر، ایران.

*E-mail: maghsoodi_mahshahr@yahoo.com

## چکیده

پروسکایت‌ها در واقع گروهی از ترکیبات هم شکل با فرمول ساختاری $ABO_3$ هستند و علی رغم آنکه در ساختار اغلب پروسکایت‌ها استوکیومتری رعایت گردیده است، اما نشان داده شده است که شمار یکسانی از تهی‌جای‌های A و B در نمونه‌ی پروسکایت $ABO_3$ وجود دارد که می‌تواند به عنوان دریچه‌ای برای سنتز پروسکایت‌های غیراستوکیومتری باشد [۱]. همچنین اثبات شده است که قابلیت آزادسازی اکسیژن در پروسکایت‌های غیراستوکیومتری آسان‌تر می‌باشد [۲]. در این تحقیق پروسکایت‌های $LaCrO_3$ و $LaCoO_3$ به صورت استوکیومتری به روش سل-ژل سنتز می‌شوند و سپس به ترتیب اثر اکسید کروم و اکسید کبالت فرااستوکیومتری (۱۰-۴۰٪) در این ساختارها بررسی می‌شود. نمونه‌های سنتز شده پس از کلسیناسیون در دمای ۸۰۰ درجه سانتی‌گراد تحت جو هوا توسط آنالیزهای مختلفی تعیین مشخصات می‌گردند. ساختار اسفنجی و متخلل در تمام پروسکایت‌های سنتز شده توسط تصاویر SEM مشاهده شد. آنالیز XRD نشان داد که نمونه‌ها به صورت کاملاً تک‌فازی پروسکایت و بدون حضور اکسیدهای فلزی کروم و کبالت حتی در حالت فرااستوکیومتری تشکیل شده است. یک نمونه از این XRDها در شکل ۱الف نمایش داده شده است. فعالیت اکسیداسیون کاتالیست‌های سنتز شده به منظور اکسیداسیون ۱۰۰۰ ppm تری‌کلرواتیلن که یک ترکیب آلی فرار است، در دماهای مختلف اندازه‌گیری گردید که یک نمونه از نتایج آن در شکل ۱ب نمایش داده شده است که بهترین نتیجه با ۳۰٪ کروم اضافی حاصل شده است.

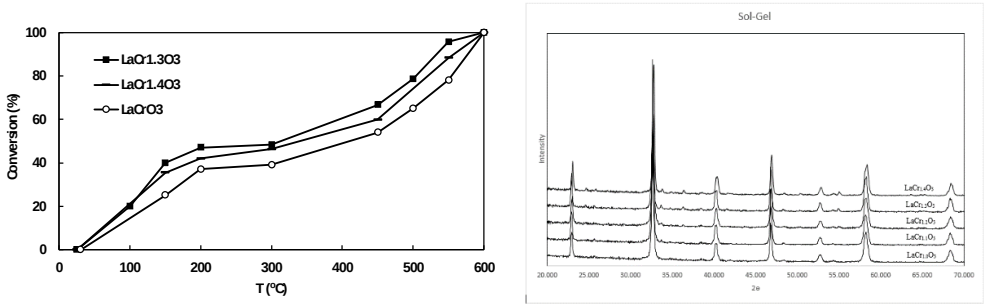


شکل ۱. (الف) نمودار XRD و (ب) فعالیت کاتالیستی در اکسیداسیون ۱۰۰۰ ppm تری‌کلرو اتیلن در هوا توسط پروسکایت $LaCrO_3$ بصورت استوکیومتری و با Cr فرا استوکیومتری (۱۰-۴۰٪)کلسینه شده در دمای ۸۰۰ درجه سانتیگراد

**کلمات کلیدی:** پروسکایت، کاتالیست، سل- ژل، تری‌کلرواتیلن

## منابع

[1] S. Maghsoodi, J. Towfighi, A. Khodadadi, Y. Mortazavi, *Chemical Engineering Journal*, ***2013***, 215-216, 827–837.

[2] D. Fino, N. Russo, G. Saracco, and V. Specchia, Journal of Catalysis, **2003**, 217, 367–375.

# سنتز و بررسی اثر کاتالیستی مزوپورMCM-41 عامل‌دار شده با ۲-آمینو-۲-هیدروکسی متیل-۱،۳-پروپان دی ال در سنتز پیرانوپیرازول‌ها

سمانه بزاز، کاوه خسروی[1*]، مژگان زنده دل[1]. زهرا فلاحی

[1]دانشکده علوم پایه، گروه شیمی، دانشگاه اراک، اراک، ایران۸۳۴۹-۳۸۱۵۶

ایمیل نویسنده مسئول: khosravi.kaveh@gmail.com

## چکیده

امروزه طراحی و سنتز ترکیبات هتروسیکلی بدلیل اهمیت بیولوژیکی آن‌ها بسیار مورد توجه قرارگرفته است. در طراحی مکانیسم‌های سنتز ترکیبات هتروسیکلی انتخاب نوع کاتالیزگر از اهمیت ویژه ای برخوردار است [1-2]. مواد متخلخل به واسطه امتیازات فراوانی از قبیل مساحت سطح و حجم حفره زیاد، پایداری حرارتی و هیدروترمال کاربرد گسترده‌ای در نانوتکنولوژی، صنعت، پزشکی و کاتالیزگری دارند. ساختارهای متخلخل توزیع حفرات متفاوتی دارند. ساختارهایی با قطر ۵۰-۲ نانومتر را ساختارهای مزوپور می‌نامند، ساختار MCM-41 در این گروه قرار می‌گیرد و به عنوان یک کاتالیزگر قابل بازیابی و یا پایه کاتالیزگر مطلوب بسیار مورد توجه قرار گرفته است [3]. در این پژوهش، ساختار مزوپور MCM-41 عامل‌دار شده با ۲،۶-دی آمینو-۴-فنیل-۱،۳،۵-تری آزین به عنوان کاتالیزگر غیرهمگن قابل بازیافت و استفاده مجدد در سنتز ترکیبات هتروسیکلی پیرانو پیرازول با موفقیت استفاده شده است. محصولات با بازده بالا در شرایط ملایم و با خلوص خوب به دست آمده و شناسایی شدند. قابلیت بازیابی کاتالیزگر این روش را در رده روش های دوست‌دار محیط زیست و نسبتاً سبز قرار می‌دهد (شمای ۱).

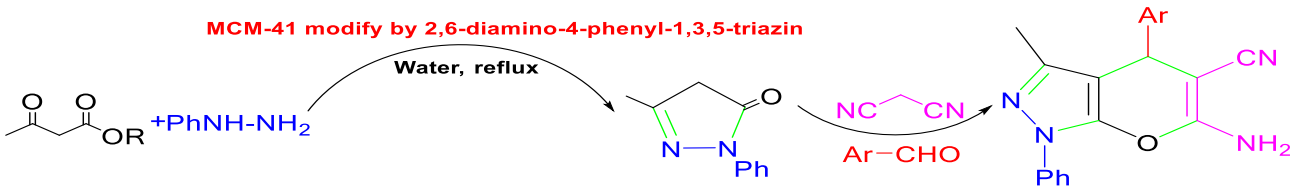


شمای ۱. سنتز ترکیبات پیرانوپیرازول

**کلمات کلیدی:** کاتالیزگر، مزوپور، پیرانو پیرازول، MCM-41

## منابع

[1] G. J. Durant, *Chem. Soc. Rev*, **1985**, *14*, 375.

[2] J. E. Del Ben, *J. Am. Chem.* Soc, **1979**, 101, 6184.

[3]J. T. Richardson, *"principles of catalyst Development"*, University of Houston, Texas (1989).

# بررسی حذف آلاینده‌های مختلف از آب‌های آلوده شده طی فرایندهای فوتوکاتالیستی با استفاده از لامپ‌های UV-LED

مریم گنج خانلو*[۱و۲]، محمدحسین رسولی فرد[۲]، سید علی حسینی[۱]، محمدرضا اسکندریان[۲]

[۱]دانشکده شیمی، دانشگاه ارومیه، آذربایجان غربی، ایران
[۲]دانشکده شیمی، دانشگاه زنجان، زنجان، ایران

*ایمیل نویسنده مسئول: maryamganjkhanloo@yahoo.com

## چکیده

در سراسر جهان استفاده از موادشیمیایی و دارویی (PPCPs) نظیر فنازوپیریدین، استامینوفن، دیکلوفناک، سایپروفلوکساسین، نورفلوکساسین و غیره باعث ایجاد آلودگی در منابع آب شده است. تصفیه آب در منابع آبی کوچک‌تر جهت بدست آوردن آب پاکیزه و جلوگیری از آلودگی در سطوح بالاتر منابع آبی بسیار مهم و حیاتی است[۲و۱]. تاکنون روش‌های مختلفی برای تصفیه آب پیشنهاد شده است که از جمله آن‌ها فرایندهای اکسایش فوتوکاتالیستی مبتنی بر استفاده از یک کاتالیست نیمه هادی می‌باشد[۳]. فوتوکاتالیست‌ها مواد پاک‌کننده محیطی هستند که تحت تابش نور می‌توانند آلاینده‌ها را به کمک مکانیسم‌های مختلف از بین ببرند. عمده هدف این روش‌ها تولید رادیکال‌های فعال هیدروکسیل می‌باشد. طی این فرایند مواد آلاینده به مواد معدنی پایدار مانند آب، دی‌اکسیدکربن، نمک یا پلیمرهای نامحلول تبدیل می‌شود.

لامپ‌های UV دارای منابع بخار جیوه می‌باشند و روی بعضی از اشیا اثر کم‌تری دارد[۴]. توسعه و استفاده از لامپ‌های UV-LED به دلیل انتشار طول موج تک فام، عدم استفاده از جیوه، بازده انرژی بالا، طول عمر زیاد، عدم تولید گرما، اندازه کوچک، وزن کم‌تر و هزینه‌های کم به عنوان جایگزین مناسب برای منابع UV جهت کاربرد آن در فرایندهای فوتوکاتالیستی می‌باشد[۵و۶].

**کلمات کلیدی:** تصفیه آب، فوتوکاتالیست، اکسایش پیشرفته، UV-LED

## منابع

[1] Eskandarian Mohammad Reza, Mostafa Fazli, Mohammad Hossein Rasoulifard, and Hyeok Choi. *Applied Catalysis B: Environmental 183*, **2016,** 407-416.
[2] SoudabehSaeid, Mohammad A. Behnajady, PasiTolvanen, and TapioSalmi. *Russian Journal of Physical Chemistry A* 92, *no. 5*, **2018**, 876-883.
[3] Zhang, Aiyong, Minghua Zhou, Lu Han, and Qixing Zhou. *Journal of hazardous materials* 186, *no. 2-3*, **2011**, 1374-1383.
[4] Ahmad, Shameem, M. A. Raushan, Shalendra Kumar, S. Dalela, M. J. Siddiqui, and P. A. Alvi. *Optik 158*, **2018**, 1334-1341.
[5] KheyrandishAtaollah, MadjidMohseni, and FariborzTaghipour.*Water research 122*, **2017**, 570-579.
[6] Li, Yan, MilošDvořák, Pavel N. Nesterenko, NantanaNuchtavorn, and MirekMacka. *Sensors and Actuators B: Chemical 255*, **2018**, 1238-1243.

# سنتز کاتالیزگرمغناطیسی فریت آهن عامل دارشده با ایمیدازول و استفاده از آن در واکنش‌های استری شدن

نادیا فتاحی*، علی رمضانی، سعید تقوی فردود و زهرا حسین زاده

*دانشکده شیمی، دانشگاه زنجان، زنجان، ایران*

*ایمیل نویسنده مسئول:* n.fatahi92@znu.ac.ir

## چکیده

گروه عاملی استر یکی از مهم ترین و فراوانترین گروه‌های عاملی در شیمی آلی می‌باشد که به وفور در طبیعت یافت می‌شود. با توجه به اهمیت بالای این گروه عاملی، تاکنون روش های زیادی برای سنتز آن گزارش شده است [۱،۲]. در سال‌های اخیر توجه بسیار زیادی به کاتالیزگرهای نانو شده است که در بین آنها کاتالیزگرهای آلی بر پایه‌ی نانوسیلیکاهای مغناطیسی از توجه ویژه ای برخوردار هستند زیرا در این کاتالیزگرها وجود خواص جالب مغناطیسی، بزرگی سطح مخصوص و کنترل آسان اندازه ذرات به هنگام سنتز، باعث برتری این ذرات نسبت به موادی با توده های بزرگتر شده است [۳]. با توجه به اهمیت واکنش های استری شدن در شیمی آلی، در کار تحقیقاتی حاضر، کاتالیزگر مغناطیسی عامل دار شده با ایمیدازول ($Fe_3O_4$@IMI) سنتز و شناسایی گردید. سپس از کاتالیست سنتز شده در واکنش‌های استری شدن کربوکسیلیک اسیدها با ترکیبات الکلی استفاده شد (شمای ۱). این روش سنتز مزایای متعددی مانند زمان واکنش کوتاه، شرایط واکنش ملایم، جداسازی آسان محصولات و بازده بالا را در پی دارد. علاوه بر این، اتصال کاتالیزگرهای آلی بر روی نانوذرات مغناطیسی منجر به بازیافت راحت و استفاده ی مجدد از آن می‌شود.

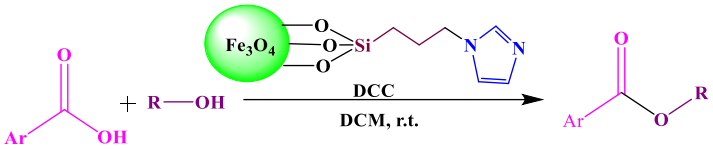


شمای ۱. واکنش های استری شدن در حضور ($Fe_3O_4$@IMI)

**کلمات کلیدی:** ایمیدازول، نانوذرات مغناطیسی، استری شدن

## منابع

[1] E.G. Delany, C.-L. Fagan, S. Gundala, A. Mari, T. Broja, K. Zeitler and S.J. Connon, *Chem. Commun.*, **2013**, *49*, 6510-6512.
[2] N. Nowrouzi and S.Z. Alizadeh, *Tetrahedron Lett.*, **2013**, *54*, 2412-2414.
[3] V. Polshettiwar, R. Luque, A. Fihri, H. Zhu, M. Bouhrara and J.-M. Basset, *Chem. Rev.*, **2011**, *111*, 3036-3075.

# تولید نانوساختار های آلیاژی الکتروکاتالیست بر روی فوم فلزی به روش ولتامتری چرخه ای مورد استفاده در فرآیند تحول هیدروژن

علی کابلی[1*]، محمود علی اف خضرایی[2]، قاسم براتی دربند[1]، علیرضا صبور روح اقدم[1]

[1]دانشکده فنی و مهندسی، دانشگاه تربیت مدرس، تهران، ایران
[2]دانشیار، دانشکده فنی و مهندسی، دانشگاه تربیت مدرس، تهران، ایران
ایمیل نویسنده مسئول: ali.kaboli@modares.ac.ir

## چکیده

واکنش تحول هیدروژن (HER) با وجود سبز بودن، با چالش های زیادی از جمله قیمت بالای الکترود کار و بازده کم فرآیند روبرو است. لذا استفاده از فلزات ارزان و دارای خواص الکتروکاتالیستی مطلوب، پاسخ مناسبی به این نیازها خواهد بود[۱-۳]. در این پژوهش با استفاده از زیرلایه فوم مس سطح موثر به مراتب افزایش داده شد. همچنین برای زبر کردن سطح، نانوساختار های آلیاژی فلزات انتقالی آهن، کبالت و نیکل از یک حمام کلریدی ساده به روش ولتامتری چرخه ای (CV) بر روی سطح آبکاری شد. برای بررسی نانوساختار ها، از میکروسکوپ الکترونی روبشی (SEM)، طیف سنجی پراش انرژی پرتو ایکس (EDS) و پراش اشعه ایکس (XRD) استفاده شد. تصاویر SEM حاکی از تشکیل نانوورق های شش ضلعی پراکنده بر روی سطح بود. آزمون EDS وجود فلزات را تقریبا با همان نسبت های پیش بینی شده، تایید کرد. برای بررسی خواص الکتروکاتالیستی از ولتامتری روبش خطی (LSV) و طیف سنجی امپدانس الکتروشیمیایی پتانسیل پله ای (SP-EIS) در محلول KOH یک مولار استفاده شد. نتایج آزمون LSV نشان داد که استفاده از فوم به جای ورق و نانوساختار کردن سطح تا ۲ برابر سینتیک احیای هیدروژن را بهبود بخشیده است. در آزمون EIS دیده شد که با افزایش اضافه پتانسیل، مقاومت به احیای هیدروژن به مراتب کاهش پیدا کرد. در بررسی پایداری شیمیایی پوشش ها از آزمون کرونوپتانسیومتری (CP)، کرونوپتانسیومتری پله ای (SCP) و CV استفاده شد. در حین آزمون CP تا ۳ ساعت تغییر محسوسی در پتانسیل مشاهده نگردید و در آزمون SCP در هیچ یک از مراحل نوسانات شدید پتانسیل به چشم نخورد. آزمون CV و آزمون LSV پیش و پس از آزمون CV نیز انجام شد و تغییرات اندکی در دانسیته جریان تبادلی و اضافه پتانسیل احیای هیدروژن دیده شد.

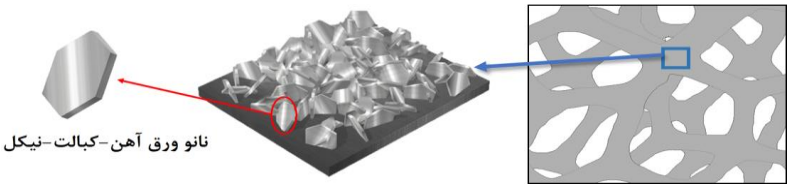


**شمای ۱.** مورفولوژی و ساختار سطح فوم مس پس از سنتز نانوساختار های آلیاژی

**کلمات کلیدی:** الکتروکاتالیست، فلزات انتقالی، واکنش تحول هیدروژن (HER)، نانوساختار، فوم، ولتامتری چرخه ای

## منابع

[1] H. Li, C. Tsai, A.L. Koh, L. Cai, A.W. Contryman, A.H. Fragapane, J. Zhao, H.S. Han, H.C. Manoharan, F. Abild-Pedersen, J.K. Nørskov and X. Zheng, *Nature Materials*, **2016**, *15*, 364.
[2] S. Mandegarzad, J.B. Raoof, S.R. Hosseini and R. Ojani, *Electrochimica Acta*, **2016**, *190*, 729-736.
[3] G. Barati Darband, M. Aliofkhazraei and A. Sabour Rouhaghdam, *Int J Hydrogen Energy*, **2017**, *42*, 14560-14565.

# ساخت، مشخصه‌یابی و بررسی رفتار فتوکاتالیستی نانوذرات اکسید منگنزِ آلاییده‌شده با کلسیم و تقویت‌شده با پورفیرین در کاربرد شکافت آب

زینب دهقان طزره[1*]، سید محمدحسین سیادتی[2]، سعید رعیتی[3]

[1] کارشناسی ارشد، دانشکده مهندسی و علم مواد، دانشگاه صنعتی خواجه نصیرالدین طوسی، تهران، ایران
[2] استادیار، دانشکده مهندسی و علم مواد، دانشگاه صنعتی خواجه نصیرالدین طوسی، تهران، ایران
[3] استاد، دانشکده شیمی، دانشگاه صنعتی خواجه نصیرالدین طوسی، تهران، ایران

zeynabdehghan6@gmail.com

## چکیده

کمبود انرژیِ حاصل از سوخت‌های فسیلی، بشر را به جمع‌آوری و استفاده از انرژی تجدیدپذیر سوق داده است. تولید هیدروژن خورشیدی از طریق فرآیند شکافت آب، یک راه حل کاربردی جهت تأمین نیازهای انرژی آینده است. در نتیجه، تولید یک کاتالیست کارآمد جهت اکسیداسیون آب که نیم‌واکنش چالش‌برانگیزِ فرآیند شکافت آب محسوب می‌شود؛ امری ضروری است که می‌توان با الهام از کاتالیست طبیعیِ موجود در مجموعه‌ی تولیدکننده‌ی اکسیژن (OEC)، سیستم‌های فتوسنتز مصنوعی (APS) را توسعه بخشید [۱-۳]. در این مطالعه، نانوذرات $Mn_3O_4$، $(CaMn)_3O_4$ و نانوکامپوزیت‌های $Mn_3O_4$/TCPP، $(CaMn)_3O_4$/TCPP تولید شد [۴-۷]. مشخصه‌یابی نمونه‌ها جهت شناسایی فاز، تغییر اندازه‌ی ثابت شبکه، از طریق آنالیز پراش اشعه‌ی ایکس (XRD)، جهت شناسایی عناصر موجود در نمونه از طریق طیف‌سنجی پراش انرژی اشعه‌ی ایکس (EDS)، جهت تعیین جذب سطحی پورفیرین و مکانیزم اتصال پورفیرین بر سطح اکسید منگنز از طریق طیف‌سنجی تبدیل فوریه‌ی مادون قرمز (FTIR)، و جهت تعیین اندازه و شکل ظاهری ذرات از طریق میکروسکوپ الکترونی روبشی نشر میدانی (FESEM) انجام شد. رفتار فتوکاتالیستی نمونه‌ها نیز تحت سیستم سه الکترودیِ فتوالکتروشیمیایی مورد بررسی قرار گرفت. نمونه‌هایی که آلایش‌گرِ عنصر کلسیم و تقویت‌کننده‌ی پورفیرین را شامل می‌شدند، فعالیت فتوکاتالیستی بهتری نسبت به نمونه‌های بدون آلایش‌گر و بدون تقویت‌کننده، از خود نشان دادند.

**کلمات کلیدی:** نانوذرات اکسید منگنز، پورفیرین، شکافت آب.

## منابع

[1] M.M. Najafpour, A.N. Moghaddam and S.I. Allakhverdiev, *Biochimica et Biophysica Acta (BBA)-Bioenergetics*, **2012**, *1817*, 1110-1121.
[2] M.M. Najafpour, M.Z. Ghobadi, A.W. Larkum, J.-R. Shen and S.I. Allakhverdiev, *Trends Plant Sci.*, **2015**, *20*, 559-568.
[3] L. Taiz, E. Zeiger, I. Møller and A. Murphy, *MA: Sinauer Associates*, **2015**,
[4] D.M. Robinson, Y.B. Go, M. Mui, G. Gardner, Z. Zhang, D. Mastrogiovanni, E. Garfunkel, J. Li, M. Greenblatt and G.C. Dismukes, *J. Am. Chem. Soc.*, **2013**, *135*, 3494-3501.
[5] K. Maeda, A. Xiong, T. Yoshinaga, T. Ikeda, N. Sakamoto, T. Hisatomi, M. Takashima, D. Lu, M. Kanehara and T. Setoyama, *Angew. Chem.*, **2010**, *122*, 4190-4193.
[6] C.E. Frey, M. Wiechen and P. Kurz, *Dalton Transactions*, **2014**, *43*, 4370-4379.
[7] X. Lü, N. Hu, J. Li, H. Ma, K. Du and R. Zhao, *Res. Chem. Intermed.*, **2014**, *40*, 1911-1922.

# سنتز و خصوصیات نانوکامپوزیت‌های MCSHA و MHACS و مقایسه جذب متیلن آبی با جاذب‌ها

سید عبدالله مویدی [۱*]، عباس تیموری [۲]، حسین صلواتی [۳]

[۱] دانشجو، گروه شیمی آلی، دانشگاه پیام نور، اصفهان، ایران

[۲] پروفسور گروه شیمی آلی، دانشگاه پیام نور، اصفهان، ایران

[۳] پروفسور، گروه شیمی معدنی، دانشگاه پیام نور، اصفهان، ایران

*ایمیل نویسنده مسئول: sayedabdollah.moayedi@yahoo.com

## چکیده

در این تحقیق، نانوکامپوزیت های مغناطیسی آهن اکسید / کیتوسان / هیدروکسی آپاتیت (MCSHA) و مغناطیسی آهن اکسید / هیدروکسی آپاتیت / کیتوسان (MHACS) با دو روش سنتز شدند. در ابتدا نانوذرات مغناطیسی آهن اکسید با استفاده از آهن ۲ و آهن ۳ با روش هم رسوبی تهیه شد [۱]. سپس، در روش اول، پس از ساخت آهن اکسید: آهن، اکسید مغناطیسی با کیتوسان ترکیب شد و در نهایت با هیدروکسی آپاتیت سنتز شد. در روش دوم، پس از تهیه آهن اکسید: مغناطیسی، آن را با هیدروکسی آپاتیت ترکیب کرده و در نهایت سنتز شده با کیتوسان. این جاذب ها توسط طیف سنجی تبدیل فوریه مادون قرمز (FTIR) مشخص شد. با استفاده از هر دو جاذب، رنگ متیلن آبی حذف شده و جدا شده توسط میدان مغناطیسی خارجی جذب شده و با اسپکتروفتومتر قابل مشاهده توسط ماوراء بنفش مقایسه شد. سپس، مورفولوژی سطح و تجزیه و تحلیل عناصر (MCSHA) با میکروسکوپ الکترونی رویشی (SEM) و الگوی پراش اشعه ایکس (XRD) مشخص شد. همچنین میدان مغناطیسی آن با تجزیه و تحلیل مغناطیس نمونه ارتعاشی (VSM) مشخص شد. با توجه به درصد حذف در روش اول، آهن اکسید / کیتوسان / هیدروکسی آپاتیت مغناطیسی (MCSHA) به عنوان یک جاذب برای حذف رنگ کاتدی از متانول آبی از محلول آبی استفاده شد.


**کلمات کلیدی:** نانوکامپوزیت ها، سنتز، مشخصه، مورفولوژی، جاذب ها، تجزیه و تحلیل

## منابع

[1] R. Kant, *Journal of Water Resource and Protection*, **2012**, *4*, 93.

# وانادیوم دی اکسید -فوتوکاتالیستی نوین در حذف آلاینده‌های محیطی

**زهره شهرستانی* و علی رمضانی**

*دانشکده شیمی، دانشگاه زنجان، زنجان، ایران*

*ایمیل نویسنده مسئول:* shahrestanizohre@gmail.com

## چکیده

امروزه تحقیقات به منظور یافتن کاتالیست‌های کارآمد و موثر برای حذف آلاینده‌های محیطی به دلیل وجود بحران‌های شدید زیست محیطی در جهان، بسیار حائز اهمیت هستند. دی اکسید وانادیوم، به عنوان یک ماده نیمه رسانای شناخته شده برای بسیاری از کاربردها مانند ساختارهای ترموکرومیک، خازن‌ها، پوشش‌های هوشمند، مواد الکتروکرومیکی و غیره بسیار مورد توجه است [۱]، براساس ماهیت انتقال فاز فلز به نیمه رسانا در دی اکسید وانادیوم، پوشش‌های هوشمند ساخته شده با این ترکیب می‌توانند در نقش کنترل کننده خودکار نور خورشیدی در پاسخ به حذف آلاینده‌های محیطی ناشی از بکارگیری سیستم‌های تهویه مطبوع رفتار کنند [۲و۳]. جالب است که دی اکسید وانادیوم و کامپوزیت‌های آن هر دو ویژگی صرفه جویی انرژی و حفاظت از محیط زیست را ارائه می‌دهند. اگرچه فعالیت کاتالیستی دی اکسید وانادیوم به منظور تخریب رنگزاهای آلی به تازگی مورد توجه قرار گرفته است اما کاربردهای کاتالیستی بسیاری در مقیاس صنعتی برای پنتا اکسید وانادیوم گزارش شده است [۴و۵]. بررسی رفتار فوتوکاتالیستی دی اکسید وانادیوم در ترکیب با سایر نانو مواد که موجب همترازی مناسب باند انرژی نانومواد برپایه دی اکسید وانادیوم و مولکول‌های آلاینده شود، جالب توجه خواهد بود. بنابراین، این امر می‌تواند نوید دهنده نانومواد‌ی بر پایه دی اکسید وانادیوم برای تخریب فتوکاتالیستی ترکیبات آلی در آینده باشد. کاربرد فرایندهای فوتوکاتالیستی مواد بر پایه دی اکسید وانادیوم را می‌توان با ترکیبات دارای گپ باند انرژی کم مانند $Ba_2CuWO_6$, $WO_3$, $CuWO_4$, $NiWO_4$, $ZnWO_4$ و $Bi_2WO_6$ برای تخریب رنگزاها مورد بررسی قرار داد.

**کلمات کلیدی:** دی اکسید وانادیوم، فوتوکاتالیست، محیط زیست

## منابع

[1] Y. Wang, Z. Zhang, Y. Zhu, Z. Li, R. Vajtai, L. Ci, P.M. Ajayan, *ACS Nano*, **2008**, *2*, 1492-1496
[2] W. Li, S. Ji, G. Sun, Y. Ma, H. Guo, P. Jin, *NJC*, **2016**, *40*,2592-2600.
[3] Y. Li, S. Ji, Y. Gao, H. Luo, M. Kanehira, *Sci. Rep*, **2013**, *3*.
[4] M. Shanmugam, A. Alsalme, A. Alghamdi, R. Jayavel, *ACS Appl. Mater.Interfaces*, **2015**, *7*, 14905-14911.
[5] N. Xiang, R.G. Song, B. Xiang, Y. Xiong, H. Li, Z.X. Wang, *Materials Technology*, **2016**, *31*, 58-63

# سنتز نانو ذرات پلاتین بر روی فوم اکسید مس و بررسی خواص الکتروکاتالیستی آن

ایمان فرح بخش [1*]، محسن وردیان دوغایی[2]، نسترن فرح بخش [3]

۱- گروه مهندسی، دانشگاه جامع علمی کاربردی، مرکز شیروان، خراسان شمالی، ایران

۲- مهندسی مکانیک تبدیل انرژی، واحد قوچان، دانشگاه آزاد اسلامی، قوچان، ایران

۳- گروه نانومواد، دانشگاه تربیت مدرس، تهران، ایران

**Email:** ifarahbakhsh@gmail.com

**چکیده:**

هدف از این تحقیق بهبود خواص الکتروکاتالیستی واکنش آزادسازی هیدروژن (HER) فوم اکسید مس دو ظرفیتی (CuO) به روش رسوب دهی الکتروشیمیایی نانو ذرات پلاتین است. در ابتدا فوم $Cu_2O$ با دیواره های متخلخل دندریتی، به روش رسوب دهی الکتروشیمیایی دو الکترودی سنتز شد، و با عملیات حرارتی و کلسینه کردن آن، فوم CuO با دیواره های متخلخل متشکل از دندریت هایی با دانه بندی نانو متری، ایجاد شد، سپس رسوب دهی الکتروشیمیایی نانو ذرات پلاتین بر روی فوم اکسید مس به روش رسوب دهی الکتروشیمیایی سه الکترودی انجام شد شد، در پروژه ی حاضر تهیه ی لایه های الکتروکاتالیستی با توزیع یکنواخت پلاتین و سایز مناسب ذرات پلاتین مورد مطالعه و تحقیق قرار گرفت. در این تحقیق نانو ذرات پلاتین به عنوان لایه ی الکترکاتالیستی الکترود توسط روش لایه نشانی الکنرشیمیایی در شرایط متفاوت بر روی فوم اکسید مس، پوشش دهی و حالت بهینه بدست آمد. به منظور بررسی ساختاری و ریز ساختاری الکترو کاتالیست های سنتز شده از تکنیک میکروسکوپ الکترونی روبشی (FE-SEM) استفاده شد. تصاویر الکترونی بدست آمده بیانگر پراکندگی یکنواخت نانو ذرات با سایزی متفاوت با توجه به شرایط لایه نشانی بر روی فوم اکسید مس است. از آنالیز EDX و XRD به منظور تایید حضور پلاتین در لایه ی کاتالیست استفاده شد. نتایج بدست آمده از تست های ارزیابی الکتروشیمیایی بیانگر کارایی مناسب سطوح کاتالیستی، به عنوان الکترود کار در واکنش آزاد سازی هیدروژن(HER) در سیستم سه الکترودی می باشد. در مجموع نتایج مطالعات نشان داد که روش پوشش دهی الکتروشیمیایی با ولتامتری چرخه ای به میزان ۲۵ چرخه نسبت به ۵،۱۰و ۲۵ چرخه قابلیت مطلوب لایه نشانی ذرات پلاتین را با بارگذاری مناسب پلاتین و حفظ قدرت الکتروکاتالیستی آن دارد.

**کلمات کلیدی**

خاصیت الکتروکاتالیستی؛ واکنش آزاد سازی هیدروژن(HER)؛ نانو ذرات پلاتین؛ فوم CuO

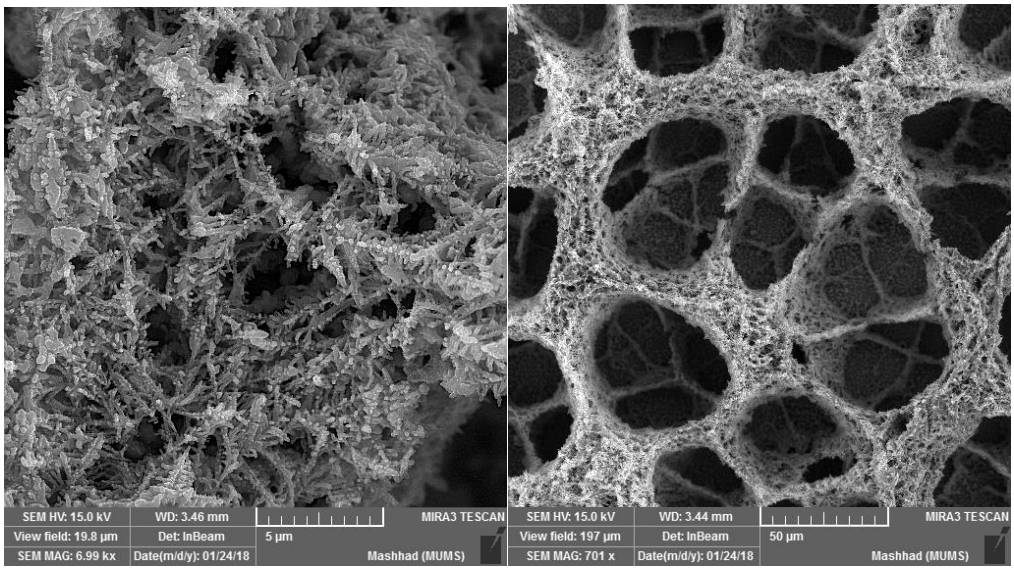


تصاویر FESEM از فوم اکسید مس تولید شده در این تحقیق در بزرگنمایی های مختلف

# بررسی میزان جذب و واجذب هیدروژن نانوکامپوزیت لیتیم آلومینیوم هیدرید و منیزیم به عنوان کاتالیست

ایمان فرح بخش [1*]، بهزاد نایبی [2]، مهدی شاهدی اصل [3]، عباس صباحی نامینی [4]، بابک مزینانی [5]

[1] گروه مهندسی، مرکز شیروان، دانشگاه جامع علمی کاربردی، شیروان، خراسان، ایران
[2] گروه مهندسی معدن و مواد، دانشگاه صنعتی امیرکبیر، تهران، ایران
[3] گروه مهندسی مکانیک، دانشگاه محقق اردبیلی، اردبیل، ایران
[4] گروه مهندسی مواد، دانشگاه صنعتی سهند، تبریز، ایران
[5] دانشکده مهندسی مواد، دانشگاه ملایر، ملایر، ایران
ایمیل نویسنده مسئول: ifarahbakhsh@gmial.com

## چکیده

امروزه هیدروژن به عنوان یکی از بهترین جایگزینها برای سوختهای فسیلی مدنظر می باشد. اما مسئله اصلی استفاده از این انرژی پاک، نحوه ذخیره آن است. هیدروژن را به شیوه های مختلف در دنیا ذخیره می کنند. در بین روش های ذخیره هیدروژن هیدرید های فلزی نسبت به روش های دیگر به دلیل قابلیت ذخیره سازی وزنی، حجمی و ایمنی بالاتر بیشتر مورد توجه قرار گرفته است. از معایب این روش، احتمال کم جذب مولکول های هیدروژن بر روی سطح و علاوه بر این سرعت کند واکنش جذب هیدروژن در دماهای پایین می باشد، که عمدتا به سبب توانایی ضعیف که در تفکیک مولکول های هیدروژن در سطح فلز است. برای غلبه بر این مشکل می توان از کاتالیست های مانند فلزات واسطه، اکسید های فلزی، ترکیبات بین فلزی و کربنی استفاده کرد. استفاده از کاتالیست های مختلفی نظیر آهن، نیکل، پلادیوم، تیتانیوم، وانادیوم گزارش شده است [۱]. در این مقاله، مواد اولیه شامل لیتیم آلومینیوم هیدرید (فاز هیدرید) و منیزیم (به عنوان کاتالیست) ابتدا توسط آسیا ماهواره ای برای مدت زمان ۲۴ ساعت آسیاکاری شدند تا ساختار کاملا یکنواخت و در ابعاد نانویی ایجاد گردد و در نهایت با استفاده از دستگاه سیورت، اندازه گیری میزان جذب و واجذب هیدروژن مورد ارزیابی قرار گرفت. نتایج میزان جذب هیدروژن ۴/۶ درصد و واجذب ۴/۶- هیدروژن گزارش نمود. بهبود حاصل در میزان جذب و واجذب ناشی از حضور کاتالیست در فرآیند می باشد، که این میزان با توجه به هزینه کم ساخت این محصول و سادگی روش تولید، مناسب می باشد.

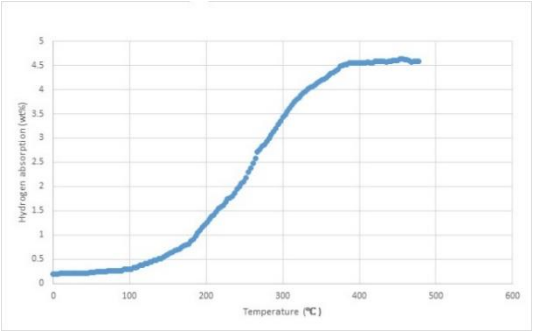


**شکل ۱**: نمودار جذب هیدروژن برای نانو کامپوزیت لیتیم آلومینیوم هیدرید در حضور کاتالیست منیزیم

**کلمات کلیدی:** ذخیره هیدروژن، کاتالیست فلزی، هیدرید فلزی، ظرفیت جذب و واجذب

## منابع

1. Bououdina, M., D. Grant, and G, *G.Walker*, International Journal of Hydrogen Energy, **2006**, 31, 177-182.

# سنتز نانوکاتالیست مغناطیسی $Fe_3O_4@SiO_2@Li$ برای سنتز مشتق‌های پیریمیدین اُن ها در واکنش بیگینلی

**فرشته فخرآذر*، فرشید سلیمی**

*دانشکده علوم پایه، دانشگاه آزاد اسلامی، اردبیل، ایران*

*ایمیل نویسنده مسئول:* fereshteh.fa70@gmail.com

**چکیده**

در این مقاله $Fe_3O_4@SiO_2@Li$ بعنوان کاتالیزوری موثر جهت سنتز مشتقات پیریمیدین اُن ها در دمای ۹۰ درجه سانتیگراد تحت شرایط بدون حلال معرفی شده است. این روش سنتزی جهت تهیه مشتقات پیریمیدین اُن ها نسبت به روش‌های پیشین دارای مزایای زیر است: (۱) واکنش با کاتالیزور ناهمگن دوستدار محیط زیست انجام می‌شود (۲) راندمان بالایی از محصول بدست می‌آید (۳) واکنش در شرایط بدون حلال به سرعت انجام می‌شود (۴) کاتالیزور به سادگی از مخلوط واکنش جدا می شود.

**واژگان کلیدی** : نانوکاتالیست، $Fe_3O_4@SiO_2@Li$، پیریمیدین اُن

**مراجع**

[1] J. A.Schwartz, C. Contescu, A. Contescu, Chem. Rev. **1995**, 95, 477.

[2] G. G. Haltky, Chem. Rev. **2000**, 100, 1347.

**[3]** R. T. Baker, W. Tumas, Science. **1999**, 284, 1477.

**[4]** K. Domen, M. Hara,; S. Hayashi, J. N. Kondo, A. Takagaki,; T. Takata,; T. Yoshida, Angew. Chem., Int. Ed. **2004**, 43, 2955.

**[5]** Y. C. Chen, C. T. Chen, W. Y. Chen, C. Y. Lo, H. Y. Lin, C. C. Liu, National Chiao Tung University, US Patent. **2009**, 252, 6258.

[6] B. Karimi, E. Farhangi, Chem. Eur. J. **2011**, 17, 6056

# سنتز نانوکاتالیست‌های مغناطیسی جدید و کارآمد $Fe_3O_4@SiO_2@Pd$ برای سنتز مشتقات مختلف بیس‌ایندولیل متان‌ها

**فرشته فخرآذر*، فرشید سلیمی**

*دانشکده علوم پایه، دانشگاه آزاد اسلامی، اردبیل، ایران*

*ایمیل نویسنده مسئول: fereshteh.fa70@gmail.com*

**چکیده**

در این مقاله کاتالیزور موثر $Fe_3O_4@SiO_2@Pd$ جهت سنتز مشتقات بیس ایندولیل متان ها در دمای ۸۰ درجه سانتیگراد تحت شرایط بدون حلال معرفی شده است. این روش سنتزی، جهت تهیه مشتقات بیس ایندولیل متان ها نسبت به روش‌های پیشین دارای مزایای زیر است: (۱) راندمان بالایی از محصول بدست می‌آید (۲) واکنش در شرایط بدون حلال به سرعت انجام می‌شود(۳) واکنش با کاتالیزور ناهمگن دوستدار محیط زیست انجام می‌شود (۴) کاتالیزور به سادگی از مخلوط واکنش جدا می شود.

**واژگان کلیدی** : نانوکاتالیست، $Fe_3O_4@SiO_2@Pd$ ، بیس ایندولیل متان

**مراجع**

[1] V. R. Pattabiraman, J. W. Bode, Nature, **2011**, 480, 471.

[2] J. W. Bode, Curr. Opin. Drug Discov. Dev. **2006**, 9, 765.

[3] E. Valeur, M. Bradley, Chem. Soc. Rev. **2009**, 38, 606.

[4] P. Anastas, N. Eghbali, Chem. Soc. Rev. **2010**, 39, 301.

[5] L. U. Nordstrøm, H. Vogt, R. Madsen, J. Am. Chem. Soc. **2008**, 130, 17672.

[6] S. C. Ghosh, S. Muthaiah, Y. Zhang, X. Y. Xu, S. H. Hong, Adv. Synth. Catal. **2009**, 351, 2643.

# سنتز و شناسایی پلیمر مایع یونی تثبیت‌شده روی نانوذرات مغناطیسی $Fe_3O_4$ و کاربرد آن در سیستم رهش دارو

جواد طوماری[1]، ابراهیم احمدی[1*]، محمدرضا معرفت سفیدان[1] و اسماعیل اسمخانی[1]

[1]دانشکده شیمی، دانشگاه زنجان، زنجان، ایران

ایمیل نویسنده مسئول: Ahmadi@znu.ac.ir

## چکیده

در این پژوهش نانوذرات $Fe_3O_4$ سنتز و سپس سطح آن با تترا اتیل‌اورتوسیلیکات (TEOS) اصلاح شد و به دنبال آن با ۳-آمینو پروپیل‌تری اتوکسی سیلان (APTES) آمین‌دار گردید [1]. سپس سطح نانوذرات با استفاده از آلفا برمو ایزو بوتیریل برماید (BIBB) عامل‌دار گردید. دو نوع مونومر مایع یونی ۳-بنزیل-۱-ایمیدازولیوم برماید و ۳-هگزیل-۱-ایمیدازولیوم برماید با استفاده از روش ATRP بر روی سطح نانوذرات مغناطیسی پلیمریزه گردید. سنتز و شناسایی پلیمر مایع یونی تثبیت شده بر روی نانوذرات مغناطیسی توسط آنالیزهای FT-IR، SEM و VSM بررسی شد. در ادامه اولین بار بارگذاری و رهایش داروی بتامتازون دی سدیم فسفات (BSP) روی این نانوذرات مغناطیسی اصلاح شده انجام شد؛ و مقدار بارگذاری در مقادیر بالاتر ۵۶ ٪ صورت گرفت. در ادامه فرایند رهایش در محیط‌های بافری ۱/۲، ۴/۸، ۷/۴ مورد بررسی قرار گرفت که رهایش از حامل ۳-بنزیل-۱-ایمیدازولیوم برماید در سه بافر مختلف در ۷۲ ساعت ادامه داشت در حالی که رهایش از حامل ۳-هگزیل-۱-ایمیدازولیوم برماید در در ساعت‌هایی بالاتر از ۷۲ ساعت ادامه پیدا کرد. میزان رهایش از هر دو حامل در pH=1.2 بالاترین درصد رهایش را نسبت به دو pH دیگر داشت که این میزان بالاتر از ۸۶ درصد بود.

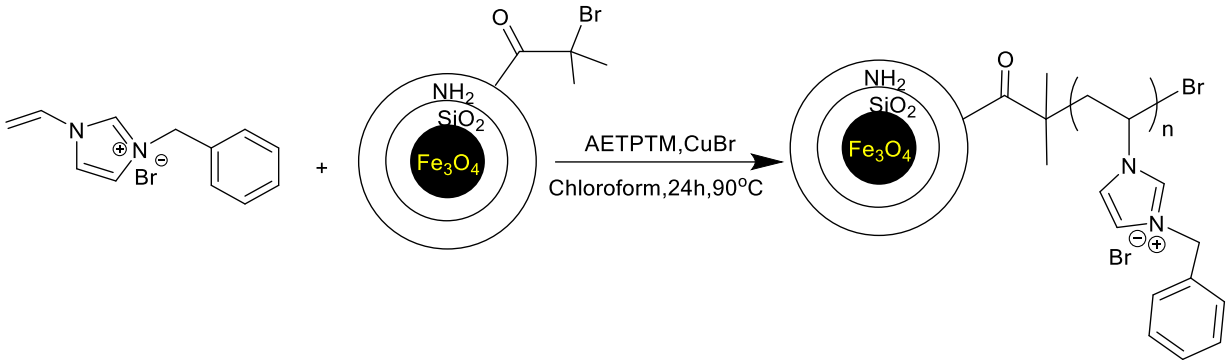


**شمای ۱.** واکنش پلیمریزاسیون رادیکالی انتقال اتم آغاز از سطح مونومر ۳-بنزیل-۱-ایمیدازولیوم برماید

**کلمات کلیدی:** سنتزو شناسایی، نانوذرات مغناطیسی، پلیمر مایع یونی، دارورسانی

## منابع

[1] Wu, C., He, H., Gao, H., Liu, G., Ma, R., An, Y., & Shi, L. *Science China Chemistry*, **2010**, *53*(3), 514-518.

# سنتز مشتقات پروپارژیل آمین با استفاده از نانوکاتالیزگر مغناطیسی بر پایه نانوذرات طلا

حمیده آقاحسینی*، علی رمضانی، سید جمال طباطبایی رضایی، مهسا تدین

*دانشکده شیمی، دانشگاه زنجان، زنجان، ایران*

*ایمیل نویسنده مسئول:* hamideh.aghahosseini@gmail.com

## چکیده

در این پژوهش تهیه‌ی نانوکاتالیزگر مغناطیسی کارآمد بر پایه نانوذرات طلا با استفاده از یک روش بسیار ساده برای نشاندن نانوذرات طلا بر روی پوسته‌ی متخلخل نانوذرات سیلیکای مغناطیسی عامل دار شده به کمک مولکول‌های آلی، از طریق کاهش حرارتی [۱] کمپلکس آلی-فلزی طلای (III) ارائه داده شد. کمپلکس کئوردیناسیونی پلی پیریدیل طلا (III)، می‌تواند به‌عنوان یک هسته دوست با آلکیل هالید موجود در ساختار سیلیکای عامل‌دار شده واکنش داده و نمک آمونیوم نوع چهارم را به‌عنوان بخش مایع یونی در ساختار کاتالیزگر ایجاد نماید [۲] و به دنبال آن لیگاند اکسید شده و نانوذرات طلا در پوسته‌ی متخلخل سیلیکای عامل‌دار شده جای گیرند. نانوکاتالیزگر تهیه شده در سنتز پروپارژیل آمین‌ها در محیط آبی و تحت اتمسفر محیط مورد استفاده قرار گرفت. اثر هم‌افزایی نانوذرات طلا بر روی پوسته سیلیکا آلی متخلخل به‌عنوان بخش فعال کاتالیزگری و پیریدینیوم کلرید به‌عنوان عامل انتقال فاز و هسته‌ی نانوذرات مغناطیسی باعث افزایش راندمان، پایداری، قابلیت بازیافت، قابلیت استفاده مجدد و فرکانس تبدیل مناسب در این نانوکاتالیزگر گردید. همچنین در این پژوهش بهینه سازی روش سنتز، با بررسی اثرات عوامل دانسیته آلدهیدها، مقدار کاتالیزگر و دما، با استفاده از طراحی آزمایش صورت گرفت. روش طراحی آزمایش نشان داد که دانسیته الکترونی آلدهیدها و مقدار کاتالیزگر به‌عنوان عوامل عمده‌ی موثر در سنتر شناخته شدند، در حالی‌که عامل دما در میان سایر عوامل کمترین تاثیر را برروی پیشرفت واکنش از خود نشان داد.

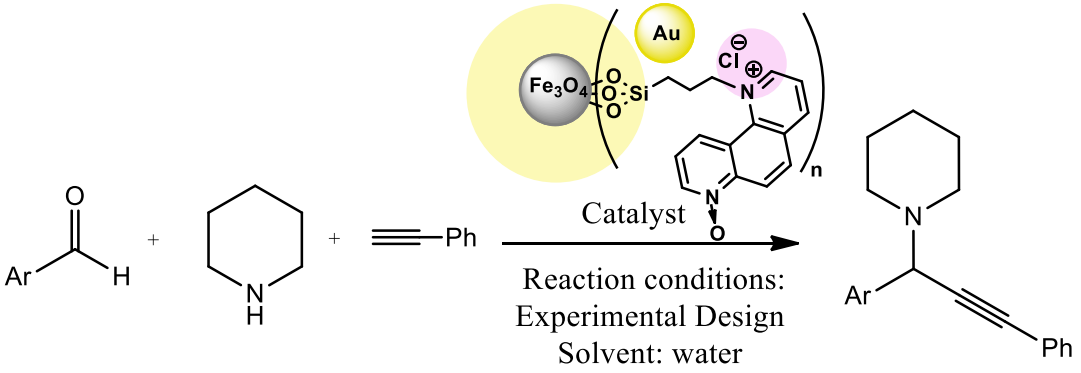


شمای ۱. سنتز مشتقات پروپارژیل آمین با استفاده از نانوکاتالیزگر مغناطیسی بر پایه نانوذرات طلا

**کلمات کلیدی:** نانوکاتالیزگر، نانوذرات مغناطیسی، تتراکلروایورات، پروپارژیل آمین، سنتز

## منابع

[1] Y. Yin, S. Yu, J. Liu and G. Jiang, *Environmental science & technology* **2014**, *48*, 2671-2679.
[2] H. N. Dadhania, D. K. Raval, A. N. Dadhania, *Catalysis Science & Technology* **2015**, *5*, 4806-4812.

# سنتز سبز مشتقات ۱،۴،۲-دی اکسازول با استفاده از کاتالیزگر آلی تری فنیل فسفین و نانوکاتالیزگر *بتا*-سیکلودکسترین در آب

حمیده آقاحسینی*، علی رمضانی، نسترن صفروند جلایر

*دانشکده شیمی، دانشگاه زنجان، زنجان، ایران*

*ایمیل نویسنده مسئول:* hamideh.aghahosseini@gmail.com

## چکیده

در این پژوهش سنتز موثر و سبز مشتقات ۱،۴،۲-دی اکسازول با استفاده از بنزهیدروکسامیک اسیدها و استیلن دی استرها در حلال آب و به کمک کاتالیزگر آلی تری فنیل فسفین و نانوکاتالیزگر *بتا*-سیکلودکسترین ارائه گردید. حفره‌ی آبگریز و سطح خارجی آبدوست نانوواکنشگاه *بتا*-سیکلودکسترین، آن را قادر ساخته که از طریق تشکیل کمپلکس محلول در آب میزبان-مهمان با کاتالیزگر آلی، عملکرد تری فنیل فسفین را در کاتالیز این واکنش به نحو موثری ارتقا بخشد [۱]. در مکانیسم این واکنش حلال پوشی حدواسط واکنش به عنوان مرحله‌ای کلیدی در پیشبرد مسیر واکنش شناخته شده است. علاوه بر اهمیت دارویی مشتقات ۱،۴،۲-دی اکسازول، مانند فعالیت ضد آمیبی [۲] و فعالیت تضعیف متوسط سیستم عصبی مرکزی [۳]، تحقیقات همچنین جنبه های بسیار مهم سنتزی آن‌ها را به عنوان محافظ کننده‌ها [۴]، پیش سازهای نایترن [۵]، عوامل انتقال نایترن [۶] و عوامل آمیداسیون [۷] نشان می‌دهند که بیانگر اهمیت توسعه‌ی روش‌های سبز برای سنتز این رده‌ی مهم از ترکیبات ناجورحلقه است.

ساختار ترکیبات سنتز شده، با استفاده از تکنیک‌های طیف‌سنجی FTIR و NMR و همچنین آنالیز بلورشناسی پرتو ایکس تایید گردید.

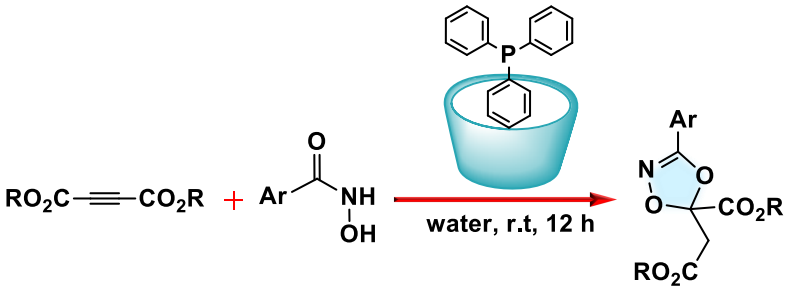


شمای ۱. سنتز مشتقات ۱،۴،۲-دی اکسازول با استفاده از کاتالیزگر آلی تری فنیل فسفین و نانوکاتالیزگر *بتا*-سیکلودکسترین

**کلمات کلیدی:** مشتقات ۱،۴،۲-دی اکسازول، نانوکاتالیزگر، کاتالیزگر آلی، *بتا*-سیکلودکسترین.

## منابع

[1] H. Bricout, F. Hapiot, A. Ponchel, S. Tilloy, E. Monflier, *Sustainability* **2009**, *1*, 924-945.
[2] A. R. Bhat, F. Athar, A. Azam, *European journal of medicinal chemistry* **2009**, *44*, 926-936.
[3] N. D. Heindel, W. P. Fives, R. A. Carrano, *Journal of pharmaceutical sciences* **1977**, *66*, 772-775.
[4] M. Couturier, J. L. Tucker, C. Proulx, G. Boucher, P. Dubé, B. M. Andresen, A. Ghosh, *The Journal of organic chemistry* **2002**, *67*, 4833-4838.
[5] V. Bizet, L. Buglioni, C. Bolm, *Angewandte Chemie International Edition* **2014**, *53*, 5639-5642.
[6] M. Chen, N. Sun, H. Chen, Y. Liu, *Chemical Communications* **2016**, *52*, 6324-6327.
[7] Y. Park, K. T. Park, J. G. Kim, S. Chang, *Journal of the American Chemical Society* **2015**, *137*, 4534-4542.

# بررسی فراسنج مدول یانگ در نانو صفحات گرافنی دوپ شده

مریم کمال*، محمد شادمان [۲]

[۱] دانشگاه زنجان، دانشکده علوم

ایمیل: mkamal@znu.ac.ir

در این مقاله با استفاده از شبیه‌سازی دینامیک مولکولی، مقاومت ساختاری ورقه های گرافنی دوپ شده با نیتروژن و بور برای اهداف مختلف مورد بررسی قرار گرفت. یافته‌های این مقاله پیشنهاد می‌کند که نانو صفحات دوپ شده با بور و نیتروژن کاربرد کاتالیزگری در شیرین‌سازی آب دریا دارد[۱]. فرآیند مورد بررسی با استفاده از بسته نرم افزاری VMD مدل‌سازی و محاسبه‌ها با استفاده از کد دینامیک مولکولی LAMMPS انجام گرفته است. در ورق گرافنی مورد مطالعه به میزان ۱۰ درصد از کل اتم‌ها با بور و نیتروژن جایگزین شده است. این سامانه تحت شرایط مرزی دوره‌ای قرار گرفته و برهم‌کنش‌های درون مولکولی اتم‌های کربن گرافن با پتانسیل ترسوف توصیف شده است. شبیه سازی مدول یانگ در ورق گرافن به فراسنج‌های مختلفی از قبیل ضخامت لایه‌ی گرافن، نوع بارگذاری و برهم‌کنش‌های اتمی وابسته است. از طرفی مدول یانگ گرافن از اتم‌های دوپ شده در ساختار نیز تاثیر می‌پذیرد[۲-۳]. در این مقاله اثر این عامل روی کارایی این نانو کاتالیزگر در فرآیند شیرین سازی آب مورد بررسی قرار گرفته است. نتایج بدست آمده نشان می‌دهد کاتالیزگر گرافنی دوپ شده با بور و نیتروژن همزمان با ارائه‌ی عملکرد بهینه در فرآیند شیرین‌سازی گزینشی آب دریا مقاومت ساختاری قابل قبولی از خود نشان می‌دهد.

| | | |
|---|---|---|
| Pure graphene | 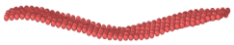 | 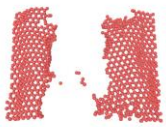 |
| BNdoped graphene | 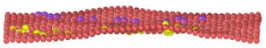 | 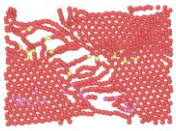 |

شکل ۱- از هم گسیختگی ساختارها بعد از اعمال نیروی مکانیکی نشان داده شده است.

**واژه‌های کلیدی :** مدول یانگ، گرافن دوپ شده، دینامیک مولکولی، کاتالیست شیرین سازی

## منابع

[1] J. N. Coleman, M. Lotya, A. O'Neill, S. D. Bergin, P. J. King, U. Khan, K. Young, A. Gaucher, S. De, R. J. Smith, *Science*. **2011**, 331, 568.
[2] D. Golberg, Y. Bando, Y. Huang, T. Terao, M. Mitome, C. Tang, C. Zhi, *ACS Nano*. **2010**, 4, 2979.
[3] Y. T. Lin, V. Williams, *J. Phys. Chem. Lett.* **2010**, 1, 277.

# تجزیه و تحلیل دوره کامل زمانی سینتیک غیرخطی آنزیم تثبیت شده

هدی نصیرا[1] *

[1]دانشکده شیمی، دانشگاه زنجان، زنجان، ایران

ایمیل نویسنده مسئول: nassira@znu.ac.ir

## چکیده

مهار فعالیت آنزیم تثبیت شده به دلیل پیوند برگشت‌پذیر محصولات واکنش بسیار متداول بوده و علت اصلی مهار منفی عملکرد آنزیم در بسیاری از مسیرهای متابولیک و پیام‌رسانی است[1]. مهار تولید محصول منجر به رفتار غیر خطی در دوره های زمانی پایدار فعالیت آنزیم می‌شود، که کاربرد روش‌های آنزیمی با فرض تولید برگشت ناپذیر محصول را محدود می کند[2]. تلاش‌های متعددی در طی یک قرن برای پیدا کردن یک راه حل ریاضی برای تجزیه و تحلیل دوره‌های سینتیکی با مهار تولید محصول شده است[3]. با این حال، هیچ روش عمومی به طور عملی قادر به استخراج پارامترهای آنزیمی از چنین دوره های غیر خطی نشده است. لذا در کار پژوهشی حاضر یک روش ساده و عملی از تجزیه و تحلیل ارائه می شود که قادر به استخراج کارآمد پارامترهای سینتیکی آنزیم حالت پایدار و ثابت‌های اتصال محصول از دوره‌های زمان سینتیکی غیر خطی با مهار تولید محصول و یا تخلیه پایه جهت تثبیت آنزیم است. به طور کلی این روش مستقل از واکنش‌ها و مسیرها برای تمامی سیستم‌های آنزیمی خالص و تثبیت شده قابل اجرا است.

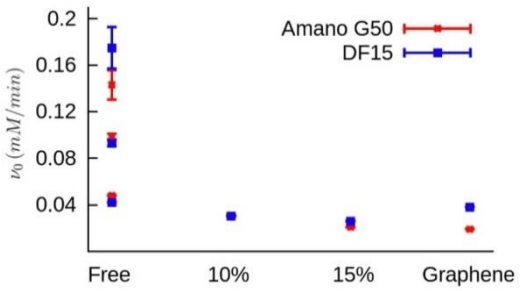


شمای ۱. پارامترهای برازش شده بر آنزیم لیپاز G50وDF15

**کلمات کلیدی:** سینتیک غیرخطی، مهار فعالیت آنزیم، پارامترهای سینتیکی

## منابع

[1] Y. Miao, J. Y. Chen, X. Jiang, Z. Huang, *Appl. Biochem. Biotechnol.* **2012**, *167*, 358.

[2] M. Enrique, E. M. Ostap, *Methods Enzymol.* **2009**, *455*, 157.

[3] K. A. Johnson, R. S. Goody, *Biochemistry* **2011**, *50*, 8264.

# مقالات کامل لاتین

# ارایه شده

# به صورت پوستر

# Mn(II)-Schiff base complex anchored in MCM-41 matrix as a heterogeneous catalyst for epoxidation of alkenes

**Hassan Zakeri[a], Saeed Rayati[b,*], Goldasteh Zarei[a]**

[a]*Department of Chemistry, College of science, Yadegar-e-Imam Khomeini (RAH), Shahre Rey Branch, Islamic Azad University, Tehran, Iran*

[b]*Department of Chemistry, K.N. Toosi University of Technolog, Tehran, P.O. Box 16315-1618, Tehran 15418.*

**Email:rayati@kntu.ac.ir*

**Abstract**

Heterogeneous catalyst containing manganese Schiff base complex is produced by covalent anchoring Schiff base complex in MCM-41. The synthesized catalyst was characterized by X-ray diffraction pattern (XRD), inductivity coupled plasma (ICP) and Fourier transform infrared (FT-IR) spectroscopy and $N_2$ sorbtion-desorbtion isotherm. The results confirmed that the complex was successfully immobilized in MCM-41 matrix. The obtained catalyst was used in the epoxidation of alkenes with hydrogen peroxide ($H_2O_2$) as a green oxidant in the presence of imidazole as co-catalyst in ethanol. Furthermore, the effect of various parameters such as reaction time, amount of catalyst, oxidant and imidazole have been investigated. The catalyst reusability was investigated. Our result reveals that this catalyst shows high catalytic activity in the epoxidation of alkenes.

**Keyword:** MCM-41, Schiff base, Heterogeneous catalyst, Alkene epoxidation

## Introduction

Epoxidation reaction with hydrogen peroxide that is one of the greenest oxidant has attracted lot of attention because of importance of epoxide in the industry. Hydrogen peroxide is preferred oxidant for epoxidation because of its low cost and safety at low concentration. in addition, its by-product is sole water and furthermore has high oxygen content [1].

Manganese Schiff base complexes have high catalytic activity for epoxidation of alkenes in homogeneous phase but this homogeneous catalyst is not facile separated and recycled. Therefore, more attempts have been made for immobilization of homogeneous catalysts on solid support such as MCM-41[2].

Among of the different inorganic supports, MCM-41 materials are very favoruable for researcher because of large surface area, uniform pore size distribytion and high concentration of silanole groups that allow covalently attach metal complex [4].

Several approaches can be utilized to immobilize heterogeneous Schiff base complex onto various supports. Among of these thechniques, the formation of covalent bonds between the support and the Schiff base complex, lead to more resistant catalyst toward leaching during catalytic reaction.

In this work anchoring Mn(II)-Schiff base complex on MCM-41 by forming urethane linkage between the surface hydroxyl groups of MCM-41 and one of the terminal isocyanate groups of 1,4-butanediisocyanate (DIC-4) were described, while the other isocyanate ending was attached the hydroxyl

groups in the salen ligand [5]. The obtained heterogeneous catalyst was evaluated in the epoxidation of olefins with $H_2O_2$ in ethanol as a solvent.

## Experimental

### Materials and Instruments

Chemicals were purchased from Merck or Fluka and used as received without further purification. The solid samples were identified by X-ray powder diffraction (XRD) using asimens D500 diffractometer, Cu-$k_\alpha$ ($\lambda$=4541 ˚A). Infrared spectra were recorded (KBr pellets) on a VECTOR-22 Bruker in the range of 400 to 4000 $cm^{-1}$.The measurement of specific surface area for the prepared samples was performed through measuring $N_2$ adsorption-desorption isotherms at 77 K with a Quanta-chrome NOVA-2200e system**.** Amount of loaded Mn(II) was determined by inductively coupled plasma (ICP-OESJobinYvon). Gas chromatography (GC) analysis were conducted on an Agilent chromatograph (model 7890B) equipped with flame ionization detector (FID) and capillary column HP-5 (phenyl methyl siloxane 30 m × 0.32 mm × 0.25 µm).

### Preparation of manganese Schiff base complex

The complexing agent N,N-bis(4-hydroxysalicylaldehyde)phenylenediimine(4-OHsalophen) was prepared by condensing of the 1,2-phenylenediamine (3.9mmol) and 2,4-dihydroxybenzadehyd (7.8 mmol) in ethanol. A yellow-orange precipitate began to appear however, the reaction required more than 1h for completion. The obtained precipitates were filtrated and dried under vacuum. The Mn(II) Schiff base complex (A) was prepared by refluxing 3 mmol of the prepared ligand and 3.3 mmol of manganese (II) acetate tetra hydrate was refluxed in ethanolic solution for 2h. The crystallization of Mn(II)-complex was performed in a solution of ethanol: acetonitrile(1:1). The obtained product was dried under vacuum, overnight [5] (Scheme1).

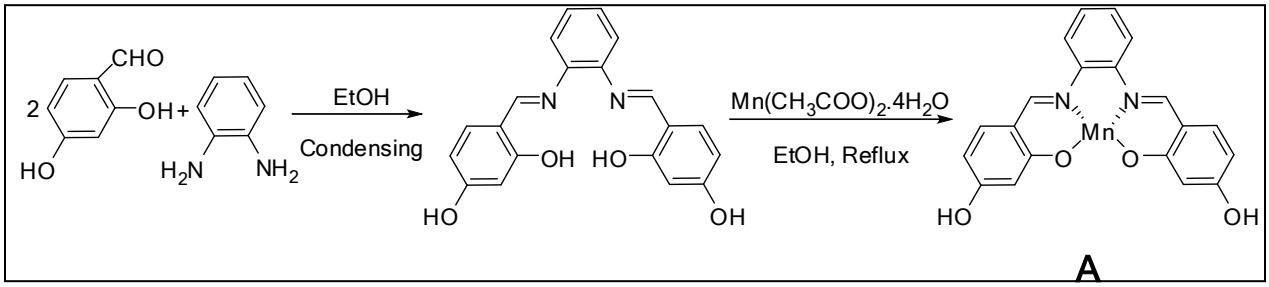


**Scheme 1.**

### Preparation of MCM-41

The MCM-41 was synthesized according to the following procedure previously reported [6].

### Complex anchoring

In order to anchor the prepared catalyst, 1g of the MCM-41 as support was refluxed with 3 mmol of DiC-4 as binder, in dry toluene for 3 h under $N_2$ atmosphere. After cooling down the solution to the room temperature, the Mn(II) complex was added and refluxed for 6 h under $N_2$ atmosphere.

Then the resulting product was extracted through soxhlet mode by ethanol for 24h and dried under vacuum [5]. The resulting material(B) denoted as [Mn(4-OHsalophen)Dic]@MCM-41[3] (Scheme2)

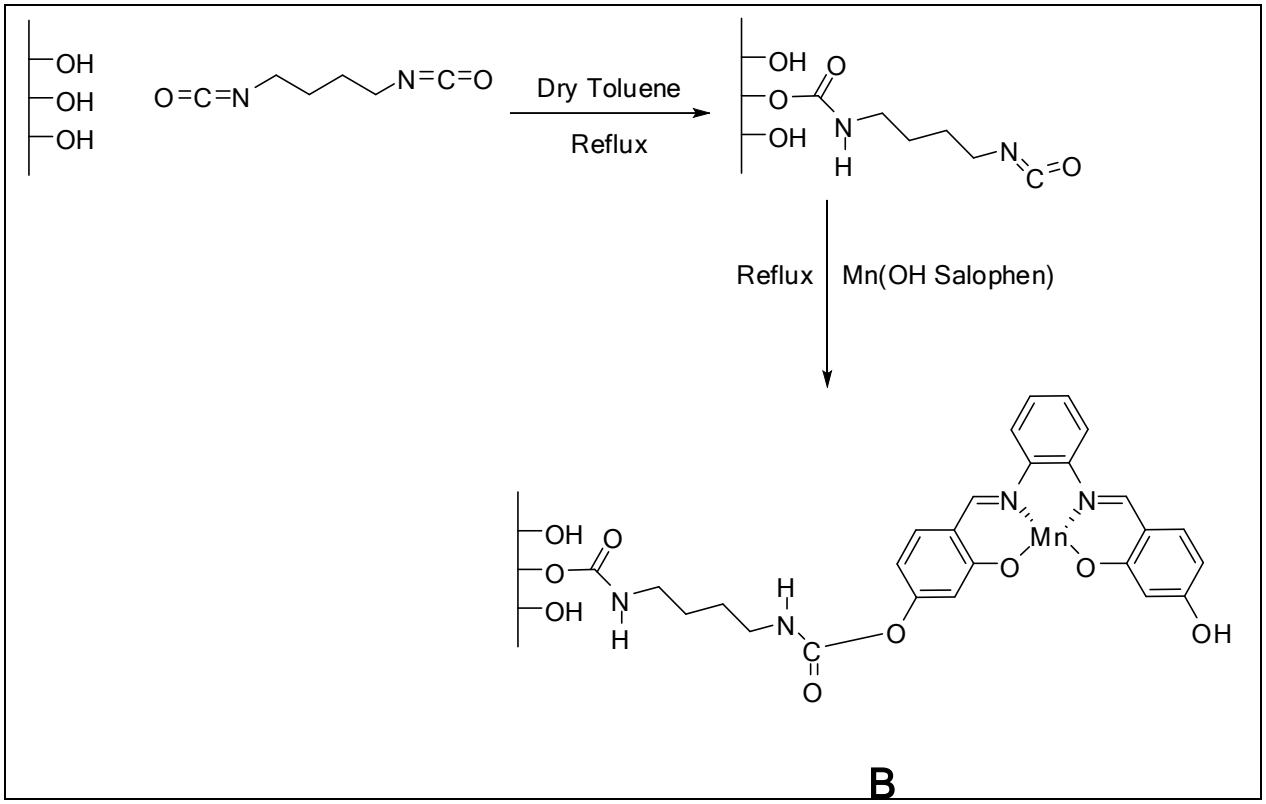


**Scheme 2.**

**Catalytic experiment**

Catalytic expriments were carried out in a 5 ml test tube. In a typical procedure , to a ethanolic solution of cyclooctene, heterogeneius Schiff bsae catalyst, imidazol as a co-catalyst, and hydrogen peroxide as environmental friendly oxidant was added. The mixture was stirred for determined time at room tempreture and the catalyst was removed by centrifugation.

The yields of epoxides were determined at definite time intervals by gas choromatography (GC).

In recycling experiments, the solid catalyst was filtrated, washed with distilled water and ethanol followed by acetone and used for next time.

**Results and discussion**

**Catalyst characterization**

**XRD**

The XRD pattern (Fig. 1) shows a very intense peak due to the (100) reflection that is due to the hexagonal pore structure of MCM-41 and two weaker peak due to (110) and (200) reflections. The mentioned peaks were kept in catalyst loaded MCM-41 sample however, their intensity was decreased which indicates disordering of plane arrangement during catalyst loading in MCM-41 structure [7].

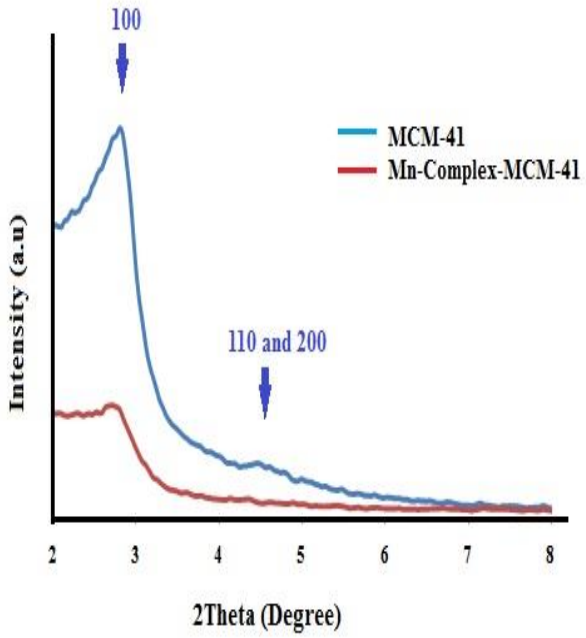


Fig.1. XRD patern of MCM-41 and Catalyst loaded on MCM-41

**FT-IR**

FT-IR spectra of the catalyst (Fig.2) confirms that the MCM-41 framework was not changed during the modification. Bands at ranges of 3300-3770 $cm^{-1}$ are due to the surface hydroxyl groups and to lattice vibration, in the range1300-750 $cm^{-1}$. Bands at about 1215, 1063, 805 and 460 $cm^{-1}$ are assignable to the asymmetric and symmetric stretching (vas(Si-O-Si) andvs(Si-O-Si)) of MCM-41 framework, the band present at about 960 $cm^{-1}$ is attribute to ν(Si-O) vibrations.The observed peak at 1690 $cm^{-1}$ in final product is assigned to carbamate amide group. The spectrum of the modified MCM-41(Figure 2) as well as the spectra of the unmodified MCM-41 is dominated by strong band characteristic of the support matrix, indicating the supperframework remained unchanged.The observed peak in 1580– 1600 $cm^{-1}$ is attributed to thestretching vibrations of the C=N bonds. A new peak was observed at 1440 $cm^{-1}$ can be attributed to the $CH_2$ bending.

Disappearing the-NCO characteristic peak at about 2275 $cm^{-1}$ in (DIC-4) indicates the reaction of both functional groups of 1,4-diisocyanatobutane [8].

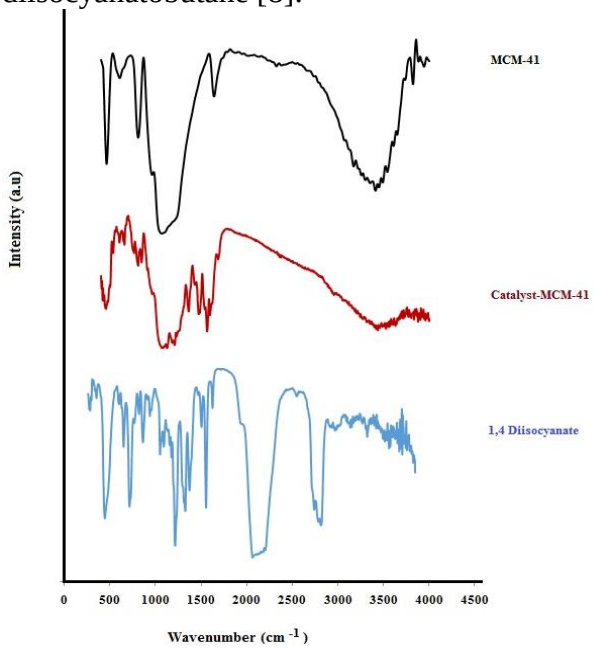


Fig. 2. FT-IR spectra of 1,4dicyanobutan, MCM-41, and Catalyst bonded to MCM-41

**ICP analysis**

The manganese content of heterogeneous catalyst was measured by ICP. Based on this analysis, the Mn content of the catalyst is about 3% (W/W).

**Nitrogen adsorption**

Textural properties of the samples obtained by $N_2$ isotherms are summarized in Table1. The results indicate that surface area, pore volume and diameter of MCM-41 decreased significantly after catalyst modification. The decreased in surface area can be attributed to dispersion and deposition of catalyst particles into MCM-41 pore channels [9].

Table 1. Textural Properties of samples

| Sample Name | BET ($m^2/g$) | Average Pore Diameter (nm) | BJH Pore Volume ($cm^3/g$) |
|---|---|---|---|
| MCM-41 | 1500 | 3.52 | 1.2 |
| Mn(4-OH Sallophen) Dic@MCM-41 | 480 | 2.67 | 0.31 |

**Catalytic Oxidation of Cyclooctene**

The heterogeneous catalyst was used for oxidation of cyclooctene with $H_2O_2$. The effect of various parameters such as time of reaction, amount of catalyst, oxidant and imidazole have been studied. The effect of time on oxidation reaction can be determined by varying the reaction time (Fig. 3). Measuring of conversion value at different reaction time of 2, 8, 24, and 48 h clarified that the highest conversion was obtained after 24 h.

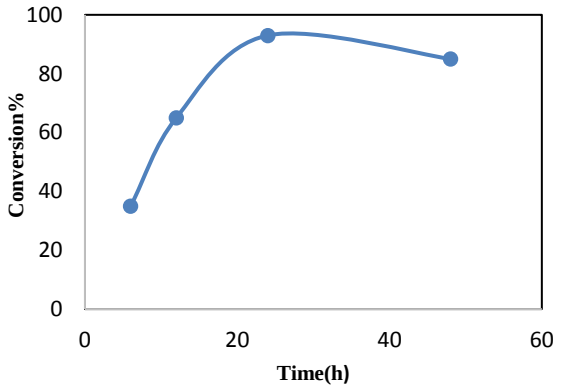


Fig. 3. The effect of reaction time on catalytic efficiency of the heterogeneous catalyst in the oxidation of cyclooctene with hydrogen peroxide

The results of experiments reveals The optimum condition of amount of catalyst, oxidant and imidazole in reaction that presented in Table 2.

Table 2. The optimum reaction condition for oxidation of cyclooctene

| Catalyst to Olefin ratio (mmol) | Catalyst to imidazole ratio (mmol) | $H_2O_2$ |
|---|---|---|
| 1:30 | 1:100 | 1 ml |

**Oxidation of various alkenes with $H_2O_2$ catalyzed by [Mn(4-OHsalophen) Dic] @MCM-41**

The heterogeneous catalyst was used for the oxidation of various olefins with $H_2O_2$ under optimized condition (Table 3).

Table 3. Oxidation of alkenes with hydrogen peroxide

| No. | alkene | Conversion(%) |
|---|---|---|
| **1** | Cyclooctene | 93 |
| **2** | Cyclohexene | 80 |
| **3** | Indene | 93 |
| **4** | Styrene | 45 |
| **5** | Trans Stilbene | 100 |

Catalyst:Imidazole:olefin molar ratio is 1: 100: 30. $H_2O_2$ (30 %) 1ml, 24 h

**Catalyst reuse and stability**

The reusability of a heterogeneous catalyst is of great importance in catalyst design. A suitable heterogeneous catalyst retains its catalytic activity and can be separated from reaction solution. The stability and reusability of catalyst was studied by separation of catalyst and reuse five times again without a detectable catalyst leaching or a significant loss of it activity (Table4).

Table4. The conversion result obtained for five reuse experiment

| No. of cycles | 1 | 2 | 3 | 4 | 5 |
|---|---|---|---|---|---|
| Conversion | 93 % | 93 % | 92 % | 92 % | 92 % |

Reaction condition: Catalyst: Imidazole: Cyclootene ratio was: 1:100:30. $H_2O_2$ (30%)1ml. reaction time 24h.

**Proposed catalytic mechanism**

The proposed mechanism for oxidation of cyclooctene with $H_2O_2$peresented in (Scheme 3.) [10].

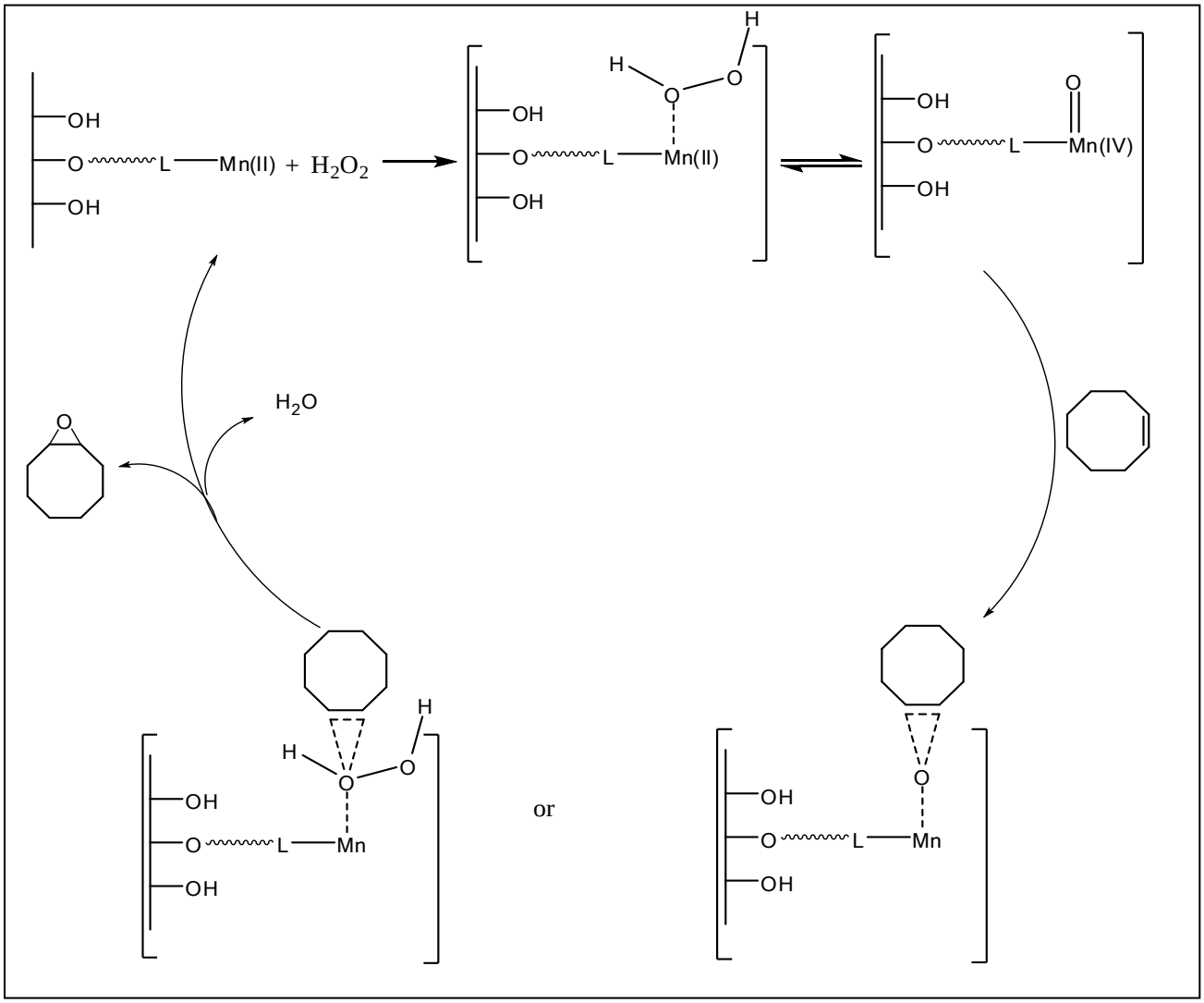


**Scheme 3**

**Conclusion**

[Mn(4-OHsalophen)Dic]@MCM-41was synthesized by covalent grafting of Schiff base complex on MCM-41 by 1,4-diicyanobutane as a binder. The result of XRD, FT-IR, $N_2$adsorbtion and ICP techniques confirm the formation of

heterogeneous catalyst. The result of cyclooctene oxidation shows the maximum conversion (93%) was obtained in optimum condition when Catalyst: Imidazole:olefin molar ratio is 1:100:30. The catalyst reusability confirm that catalyst is stable during oxidation reaction

**References**

[1]A. Mavrogiorgue, M. Baikousi, V. Costas,E.Mouzourakis, Y. Deligiannakiss, M.A. Karakassides, M. Louloudi,*J.Mol. Catal. A: Chem*. **2016**, *413*, 40**.**

[2] S. Rayati, E. Khodaei**,** M. Jafarian, A. Wojtczak*Polyhedron*, **2017,** *17*, 6

[3] K. Krishnan, A, Marria, T. Kallikkakam, S. Sindhu, G. Anilkumar. *Tetrahedron***, 2016**, *72*, 1

[4] M. Hajjami, F. Ghorbani, S. Rahimipanah, S. Roshani, *Chinese journal of Catalysis*, **2015**, *36*, 1852

[5] P. Oliveria,A.Machado,A.M.Ramos, I.Fonseca,F.M.BarazFernandes, A.M.Botelhodo Rego, and J.Vital,*Microporous and Mesoporous Material*, **2009**,*120*,432

[6] G.Zarei and F.Zonouzi, *Journal of Applied Chemical Research*,**2014**, *8*, 37.

7] S. Saladino, E. Kraleva, S. Todorova, A. Spinella, G. Nasillo, E. Caponetti. *Journal of Alloys and Compounds*. **2011**, *509*, 8798

[8]P. Oliveria,A.Machado,A.M.Ramos, I.Fonseca,F.M.BarazFernandes, A.M.Botelhodo Rego, *Catalysis Letters*, **2007**, *114,* 192

[9] R. Ji, K. Yu, L. Lou, S. Liu . *J.Mol. Catal. A: Chem***, 2013**, *378*, 7

[10] R. Egekenze, Y. Gultneh, R. Butcher, *Polyhedron*, **2018**, *144*, 198

# Study of the Operational Conditions on Light Naphtha Isomerization Reaction over Chlorinated $Pt/Al_2O_3$ Catalyst

**Alireza Mohammadrezaei [a,*], Zahra Karegar [a], Reza Golhoseini [b]**

[a] *ExirNovin Farayand Asia Company, 1389714361, Tehran, Iran*

[b] *Department of chemical engineering, University of Kashan, 8731753153, Kashan, Iran*

*Corresponding author Tel.: +98 (912) 2508824; Fax number: +98 (21) 44909070

*E-mail: rezaei.a@exirnovinco.com

## Abstract

Light naphtha isomerization reaction plays an important role in increasing the octane number of gasoline pool. In this research, the operational conditions of light naphtha isomerization reaction at pressure of 34 barg are studied and is used the chlorinated $Pt/Al_2O_3$ catalyst. By increasing of temperature from 140 to 165°C, at apace velocity of 3 $h^{-1}$, $iC_5/\sum C_5$ wt. % and $22DMB/\sum C_6$ wt. % (isomers ratio) increase from 48.9% to 64.5% and 14.8% to 20.3%, respectively. On the other hand, space velocity increasing from 1 to 5 $h^{-1}$ at 150°C, decrease the $iC_5/\sum C_5$ wt. % from 72.5% to 36.8%. Increasing of hydrogen to hydrocarbon molar ratio from 0.13 to 0.25 mol/mol at space velocity of $1h^{-1}$, has not significant effect on isomers ratio.

The maximum $iC_5/\sum C_5$ of 73.5 wt. % and $22DMB/\sum C_6$ of 27.7% wt. % obtain at temperature of 165°C, space velocity of 1 $h^{-1}$ and hydrogen to hydrocarbon of 0.25

**Keywords**: Low temperature isomerization, Light naphtha, Chlorinated alumina catalyst, Operational condition

## Introduction

Isomerization of normal alkanes to iso-alkanes widely use in the refining processes to improve the octane number and it restricts the use of octanizer components such as Methyl Tertiary Butyl Ether (MTBE) and Tetra-ethyl-lead (TEL) in gasoline. These components are harmful for human health and environment [1, 2]. Three types of catalyst supports used in this process, that the use one of them change the operating conditions of process [3]. Industrial isomerization processes categories at four temperature ranges based on catalyst type: high temperature reaction (360-440°C) on alumina catalyst promoted with fluorine, medium temperature (250-300°C) on zeolite catalyst, low temperature (120-180°C) on chlorinated alumina and or sulfated metal oxide (180-210°C) catalysts [3, 4]. The isomerization catalyst consists of noble metal (typically platinum group metals) based on refractory oxide (usually alumina). Pt/alumina (chlorine add to it) due to strong Lewis sites, high activity and high octane number products, is the most common commercial catalyst, industrially [3, 5-7].

Organic chloride compound such as $CCl_4$ and $C_2Cl_4$ promote the catalyst activity [4, 5, 8] and these increase the platinum dispersion and acidity of Lewis on alumina supported [9-11]. Therefore chlorine compound continuously inject into the reactor to maintain the activity of catalyst [2, 9, 10]. These catalysts irreversibly deactivate by oxygen-containing substances such as water and carbon dioxide, therefore feed must be free of these compounds (water content must be lower than 0.1 ppm in feed and hydrogen gas) [1].

Straight-chain alkane isomerization to branched alkane is an equilibrium exothermic reaction. At high temperature exists the thermodynamic limitation and at the low temperature there is kinetic limitation, so optimum temperature should be selected in isomerization reaction, figure 1 [1, 6].

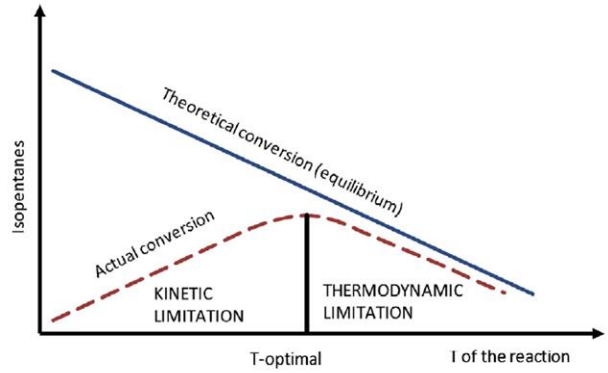


Figure 1. Dependence of n-paraffins conversion on reaction temperature [4]

Figure 2 shows the products of $C_5/C_6$ isomerization reactions and their octane number. Chlorinated $Pt/Al_2O_3$ catalyst formulation contains metallic and acidic function. $C_5$ isomerization reaction occurs in the presence of relatively weak metal function while $C_6$ paraffin isomerization requires the strong metal function for producing of dimethyl butanes with high octane number. It does not need to strong metal function for producing of methyl pentane [1, 3].

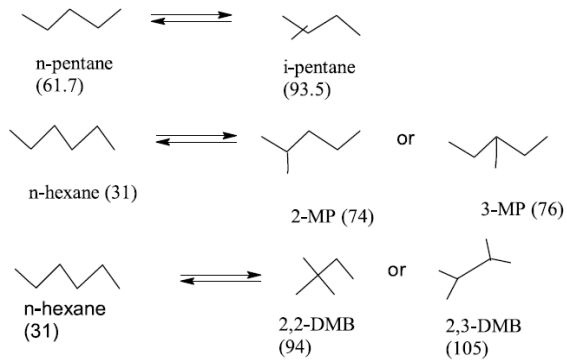


Figure 2. $C_5$ and $C_6$ paraffins isomerization reactions[3]

Side reactions in isomerization process are naphthene ring opening, naphthene isomerization, benzene saturation, hydrocracking and naphthene transalkylation [3, 13].

Mechanism of normal paraffins isomerization reaction include paraffin dehydrogenation on metal sites, formation of olefin, converting of olefin to carbonium ion and isomerization of carbonium ion into iso-paraffinic carbonium ion in the presence of acidic sites, in the end, carbonium ion hydrogenation and formation of iso-paraffin on metal sites [6, 13, 14].

The extent of n-paraffins isomerization reaction depend on the process variables such as reactor temperature, operating pressure, space velocity, and $H_2$/HC molar ratio. Reactor temperature and space velocity are two important process variables during light naphtha isomerization reaction. Reactor operating pressure and hydrogen to hydrocarbon ratio do not have significant effect on the conversion of n-paraffins to isoparaffins under normal operating conditions. Industrial isomerization units are normally operated at hydrogen-to hydrocarbon molar ratio of 0.05 at outlet of the second reactor [3]. Chlorinated $Pt/Al_2O_3$ catalyst is more active at higher pressure. It requirs only a slight excess over stoichiometric hydrogen, since the catalyst does not produce coke [13].

Xiao et al. [15] studied the optimization of $Pt/SO_4^{-2}/ZrO_2$ catalyst for normal hexane hydroisomerization. They indicated that the optimum reaction conditions were temperature from 200-210 ℃, space velocity of 1 $h^{-1}$ and hydrogen to hydrocarbon molar ratio of 5. Adzamic et al. [16] studied the n-hexane isomerization over $Pt/SO_4$-$ZrO_2$ catalyst and found that n-hexane conversion enhance with the increasing of temperature and decreasing of space velocity. Also, they investigated the optimization of n-hexane isomerization process using design of experiment and they indicated that the optimum operational condition were the temperature of 170°C and space velocity of 2 $h^{-1}$. Chekantsev et al. [6] carried out the mathematical modeling of light naphtha isomerization. They offered mathematical model of light alkanes isomerization process for different raw materials composition and catalyst. With using this model, it is possible to compare the efficiency of different isomerization units and choose more suitable of process optimization for given raw materials. Weyda and Kohler [17] reported that the zeolite catalyst has significant activity in isomerization and low selectivity in producing of cracking products.

In previous researches, isomerization reaction are studied on operating condition with experimental feed and often sulfate zirconia and zeolit catalyst that in the refineries are mostly used alumina catalyst for light naphtha isomerization process.

In this study, the chlorinated platinum supported alumina catalyst is used according to industrial operating condition and the effect of them are investigated over isomerization process under constant pressure.

## Experimental

Experiments carried out in the trickle bed reactor with down flow pattern which catalyst bed is fixed and flow pattern is much closer to plug flow. The chlorinated Pt/alumina catalyst is loaded in this reactor. Figure 3 shows the used equipment in this study. Hydrogen gas and liquid feed sent to the reactor and chlorine agent added to liquid feed. The reactor effluent enter into the product vessel then gas product is directly connected to a gas chromatography (Varian-CP 3800, 50 m PONA column, diameter of 0.2 mm and the film thickness of 0.5 μm) equipped with a flame ionization detector. Table 1 presents the weight percentage of the composition of feed.

**Table1**. Spesification of feed composition

| Composition | Wt% |
|---|---|
| **C5** | 33 |
| **C6** | 50 |
| **MCP** | 6.2 |
| **CH** | 2.8 |
| **Bz** | 3 |
| **Other component** | 5 |

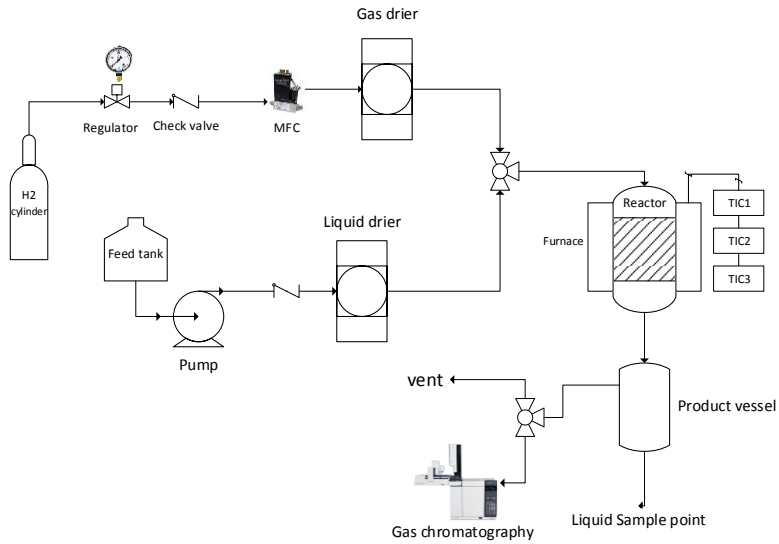


Figure 3. Schematic diagram of the experimental setup for light naphtha isomerization

## Results and discussion

Performance of isomerization reaction represented by an isomers ratio percentage ($iC_5/\sum C_5$ and $22DMB/\sum C_6$). Another $C_6$ isomers include 2MP, 3MP and 23DMB almost appear in equilibrium values and quickly reach to equilibrium [18]. Figure 4 shows the graph of equilibrium iso ratio versus temperature which it indicates isomers ratio decrease by temperature increase.

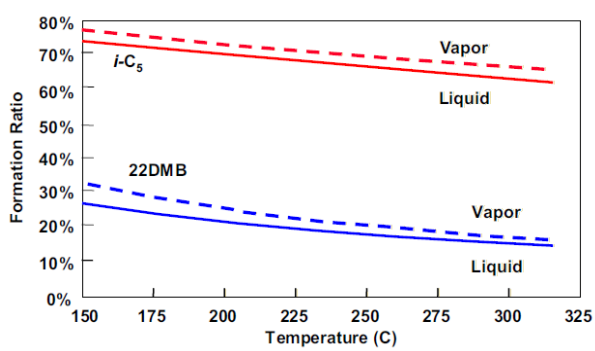


Figure 4. Equilibrium isomer ratio versus temperature[1]

Temperature and space velocity are key process variables in this reaction. Temperature is the most important process variable for making a high octane product. At lower WHSV, residence time is longer and as a result, lower temperature operation is possible, resulting in a higher octane product [13]. Figures 5 and 6 show the effect of temperature and space velocity over $C_5$ and $C_6$ isomers ratio under constant pressure and hydrogen to hydrocarbon molar ratio. At space velocity of 1 $h^{-1}$, catalyst has been more active and the product isomers ratio are higher than another space velocity amounts. In this value, even at lower temperature, catalyst is active and amounts of $iC_5/\sum C_5$ and $22DMB/\sum C_6$ are high but in space velocity of 3 $h^{-1}$ and 5 $h^{-1}$, product isomers ratio are decrease.

Catalyst activity drop due to space velocity increasing is compensated by temperature increase. When temperature increased from 140°C to 165°C, at space velocity of 3 $h^{-1}$ $iC_5/\sum C_5$ % is raised from 49% to 64.5% also, at space velocity of 5 $h^{-1}$, is raised from 32% to 45%, respectively. Figure 6 shows that $22DMB/\sum C_6$ raises from 15% to 20% at space velocity of 3 $h^{-1}$ and it raises from 9% to 12% at WHSV of 5 $h^{-1}$, respectively.

According to endothermic nature of dehydrogenation reaction, increasing temperature leads to increase carbonium ion production and as a result, the iC5 and 22DMB isomers are increased.

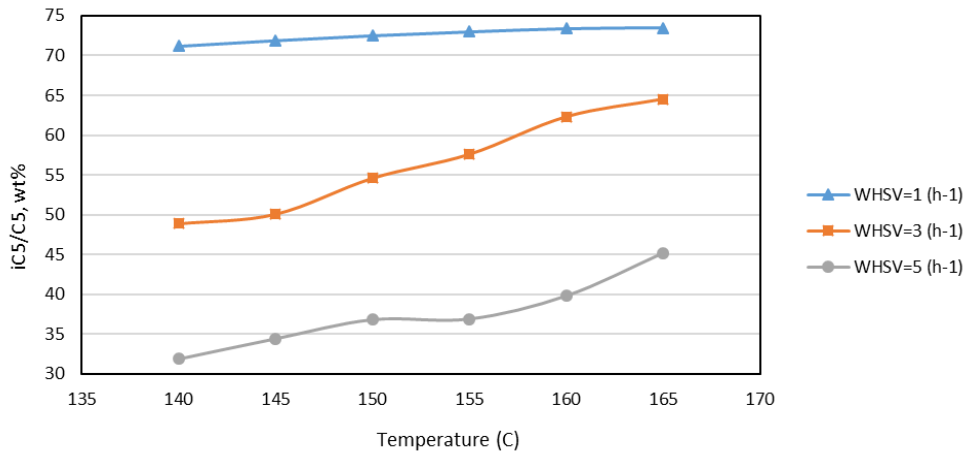


Figure 5. The effect of temperature and WHSV on iC5/∑$C_5$, P=34 barg and $H_2$/HC=0.19

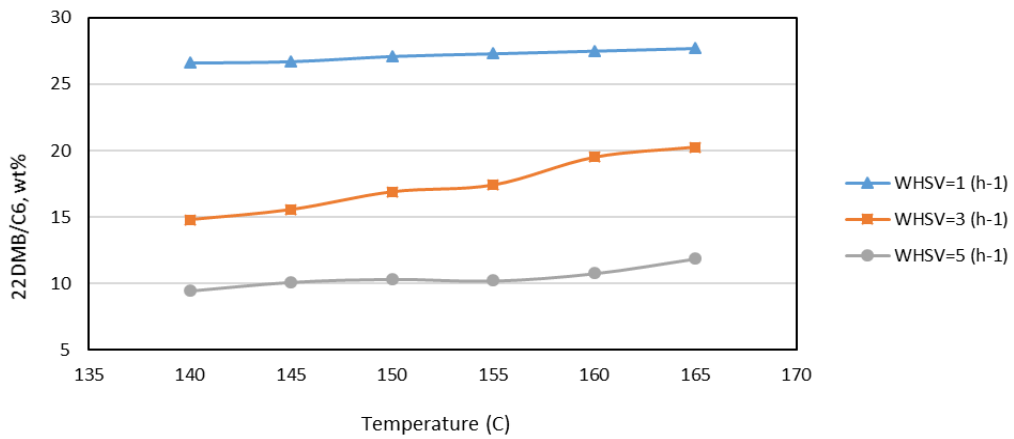


Figure 6. The effect of temperature and WHSV on 22DMB/∑$C_6$, P=34 barg and $H_2$/HC=0.19

Figures 7 and 8 show the effect of hydrogen to hydrocarbon molar ratio on iC5/∑$C_5$ and 22DMB/∑$C_6$, respectively. In space velocity of 1 $h^{-1}$, molar ratio of hydrogen to hydrocarbon is not significant effect on isomers ratio however, in $H_2$/HC of 0.25 the value of i$C_5$/∑$C_5$ and 22DMB/∑$C_6$ are higher than $H_2$/HC of 0.13 and 0.19 (i$C_5$/∑$C_5$ increases from 73.03 wt% to 74.29 wt% by increasing of $H_2$/HC from 0.13 to 0.25).

Nevertheless, in space velocity of 3 $h^{-1}$, the optimum value of isomers ratio obtained at $H_2$/HC of 0.19. For high active catalyst in lower space velocity, amount of $H_2$/HC should be higher to prevent catalytic cracking.

According to the isomerization reaction mechanism, increasing of $H_2$/HC value more than 0.19, reduces dehydrogenation reaction and production of carbonium ions, which leads to reduce the product of isomerization reaction. On the other hand, the increase of hydrogen increases the hydrogenation and hydrogenolysis reactions and thus increases the products of these reactions. Therefore, the optimum value of hydrogen to hydrocarbon molar ratio should use in the isomerization reaction.

Increasing of $H_2$/HC from 0.13 to 0.19 at WHSV of 3 $h^{-1}$, has lower effect on i$C_5$/∑$C_5$ wt. % (1% increase), while this increase has more effect on 22DMB/∑$C_6$ % (2.15% increase).

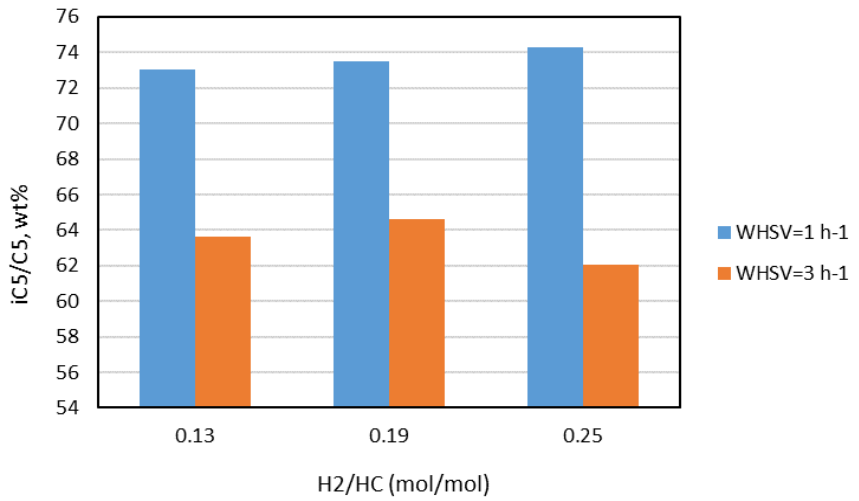


Figure 7. The effect of $H_2$/HC and WHSV on iC5/∑C5 ratio, P=34 barg and temperature=165°C

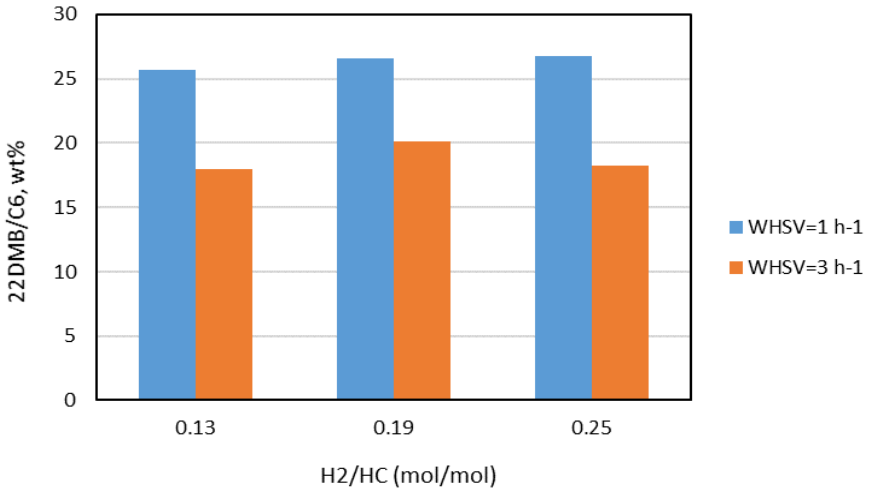


Figure 8. The effect of $H_2$/HC and WHSV on 22DMB/∑C6, P=34 barg and temperature=165°C

## Conclusion

In this paper, the chlorinated $Pt/Al_2O_3$ catalyst is used and the experiments carried out under constant pressure of 34 barg in the fixed bed reactor. The result of experiments at temperature of 140-165°C, $H_2$/HC of 0.13-0.25 mol/mol and space velocity of 1-5 $h^{-1}$, indicated that space velocity and temperature have a significant effect on $iC_5/\sum C_5$ and $22DMB/\sum C_6$. At space velocity of $3h^{-1}$, by increasing of temperature from 140 to 165°C, $iC_5/\sum C_5$ increased from 48.9 wt. % to 64.5 wt%, also, $22DMB/\sum C_6$ increased from 14.8 wt% to 20.26 wt%. Space velocity decreasing from 5 to 3 $h^{-1}$ at 155°C, increased $iC_5/\sum C_5$ and $22DMB/\sum C_6$ from 36.91% to 57.6% and 10.19% to 17.41% respectively.

Analyzing of experiments results show that the optimum value of $H_2$/HC for isomers ratio at WHSV of 3 $h^{-1}$ is 0.19 mol/mol and at WHSV of 1 $h^{-1}$ is 0.25 mol/mol.

The maximum content of $iC_5/\sum C_5$ and $22DMB/\sum C_6$ are 73.5% and 27.7% respectively, which these obtained at 165°C, space velocity of 1 $h^{-1}$ and $H_2$/HC of 0.25 mol/mol.

**Symbol**

| | |
|---|---|
| C5 | Pentane |
| iC5 | Iso-pentane |
| C6 | Hexane |
| $CCl_4$ | Carbon tetrachloride0 |
| $C2Cl_4$ | Tetrachloroethylene |
| 22DMB | 2, 2 dimethyl butane |
| 23DMB | 2, 3 dimethyl butane |
| 2MP | 2-methyl pentane |
| 3MP | 3-methyl pentane |
| MCP | Methyl cyclohexane |
| CH | Cyclohexane |
| Bz | Benzene |
| WHSV | Weight Hourly Space Velocity |
| P | Pressure |
| $H_2$/HC | Hydrogen to hydrocarbon ratio |

**Acknowledgment**

We grade fully acknowledge financial support from ExirNovin Farayand Asia Company.

**References**

[1] V.G. Deak, R.R. Rosin, and D.K. Sullivan, UOP LLC,(2008).

[2] L.I.Ali, G.A.Ali, S.M.Aboul-Fotouh, A.K.Aboul-Gheit, Applied catalyst A: General 205, (2001) 129-146.

[3] G. Valavarasu, B. Sairam, Petroleum Science and Technology, 31, (2013),580–595.

[4] E.A. Yasakova, A.V. Sitdikova, A.F. Achmetov, Oil and Gas Business, UDC 665.656.2 ,(2010).

[5]O.M.Davies,M.F.Olive,T.J.Cook,G.K.Hilde , (1974) Patent NO. 3,791,960.

[6] N.V. Chekantsev, M.S. Gyngazova , E.D. Ivanchina, Chemical Engineering Journal 238, (2014) 120–128.

[7] J. Ross, B. Domergue, L. Watripont, S. Graeme, S. Decker, R. Le Gall, M. van der Laan, National Petrochemical & Refiners Association Annual Meeting San Antonio, TX, (2004).

[8] Hon Yue Chu, Michael P. Rosynek and Jack H. Lunsford, Journal of the Chinese Chemical Society, 45, (1998), 481-489.

[9] H. Knozinger, C.P. Kaerlein, Journal of Catalysis. 25, (1972), 436-438.

[10] R.L. Mieville, Journal of Catalysis. 100, (1986) 482-488.

[11] K.J.Del Rossi, D.J. Dovedytis, D.J. Esteves, M.N. Harandi, United States Patent, Patent NO 5,334,792, (1994).

[12] Zoran Adzamic, Tamara Adzamic, Marko Muzic, Katica Sertic-Bionda, Chemical Engineering Research and Design, 91, (2013), 100–105.

[13] M.Stine, Encyclopaedia of Hydrocarbons, volume II / refining and petrochemicals, isomerization, Istituto della Enciclopedia italiana , (2005), 171-179.

[14] H. A. Elsayed, M. F. Menoufy, S. A. Shaban, H. S. Ahmed, B. H. Heakal, Egyptian Journal of Petroleum, 26 (2017) 885-893.

[15] Y. P. Xiao, Z. Y. Wang, Y. F. Zhang, Y. Q. Song, X. L. Zhou, and C. L. Li, Petroleum Science and Technology, 31, (2013) , 331–340,

[16] Zoran Adzamic, Tamara Adzamic, Marko Muzic, Katica Sertic-Bionda, fuels and lubricants (original scientific paper in Zagreb, Croatia) 50, (2011), 1: 2-21.

[17] Weyda, H., and Kohler, E. Third International Symposium on Fuels & Lubricants, New Delhi, India, October 7–9 (2002).

[18] B. Ducourty , G. Szabo , J.P. Dath , J.P. Gilson , J.M. Goupil , D. Cornet, Applied Catalysis A: General 269, (2004), 203–214.

## Graphical Abstract

# Study of the operational conditions on light naphtha isomerization reaction over chlorinated $Pt/Al_2O_3$ catalyst

**Alireza Mohammadrezaei** [a,*], **Zahra Karegar** [a], **Reza Golhoseini** [b]

[a] *ExirNovin Farayand Asia Company, 1389714361, Tehran, Iran*

[b] *Department of chemical engineering, University of Kashan, 8731753153, Kashan, Iran*

*Corresponding author Tel.: +98 (912) 2508824; Fax number: +98 (21) 44909070

*E-mail: rezaei.a@exirnovinco.com

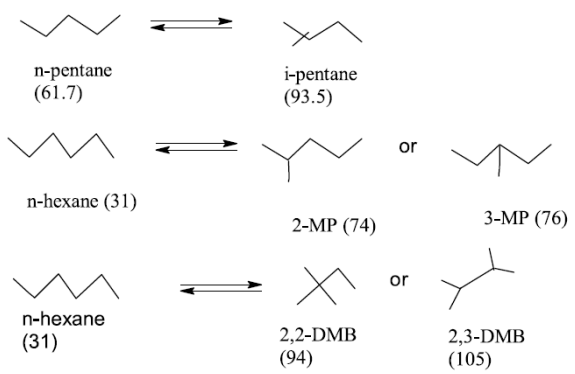


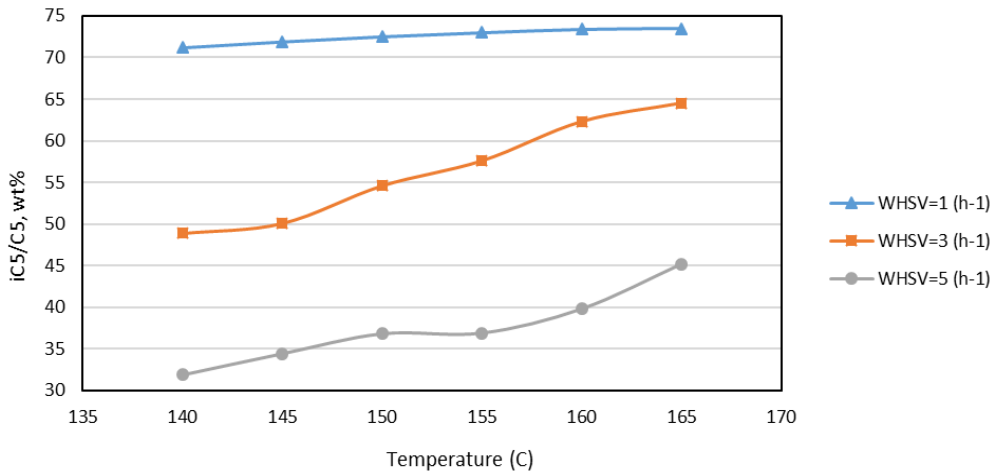

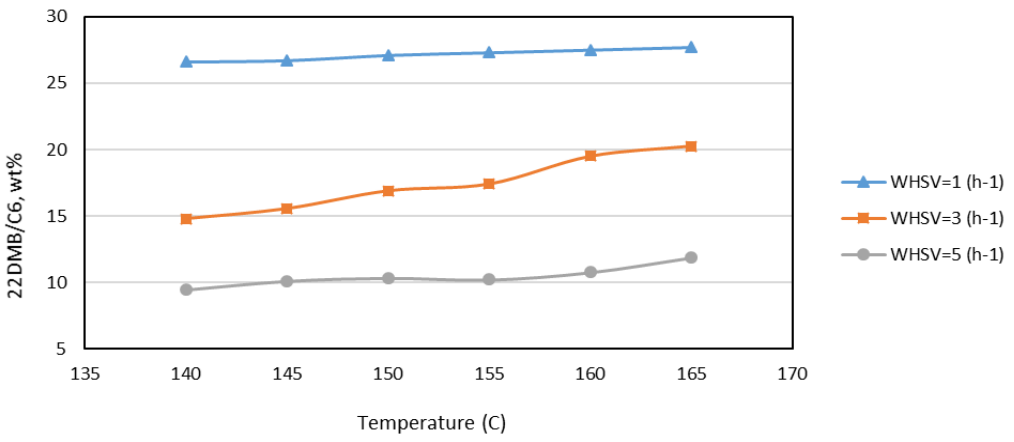
30
25
20
15
10
5
22DMB/C6, wt%
135
140
145
150
155
160
165
170
Temperature (C)
WHSV=1 (h-1)
WHSV=3 (h-1)
WHSV=5 (h-1)

# Preparation and Characterization of CuO Nanostructures through simple precipitation method in the presence of thioglycolic acid

**Parvin Eskandari[a,*], Mohammad Reza Fazlollahi[a]**

[a] *Department of Chemistry, Zanjan Branch, Islamic Azad University, P.O. BOX 49195-467, Zanjan, Iran*

*Corresponding author Tel.: +98 (024) 33420037

*E-mail: eskandari.p14@gmail.com

**Abstract**

The nanosized copper oxides (CuO) were synthesized via a simple chemical precipitation method by using thioglycolic acid (TGA) as a capping agent. By using different concentration of capping agent we could get different sizes of CuO nanostructures. The characterization of the prepared samples was performed by Fourier transform infrared spectroscopy (FT-IR), X-ray diffraction (XRD), scanning electron microscopy (SEM), and UV-vis diffuse reflectance spectroscopy (DRS).

**Keywords**: Copper oxide, Noanostructures, thioglycolic acid, precipitation method.

## Introduction

Significant effort has been developed to design, construct and manipulate nanostructures semiconductor due to their unique quantum confinement effect and size dependent properties [1]. There are many well synthesis routes that developed for the control over the size distribution of semiconductors that is seriously important for defining size-dependent optoelectronic properties [2]. Copper oxide (CuO), a well-known p-type semiconductor with a narrow band gap (Eg = 1.2 eV), is an important industrial material has been extensively investigated for its broad applications such as gas sensors [3], electrode materials [4], magnetic ceramics [5], hydrogen storage materials [6], solar cells [7], and photocatalysis [8]. In recent years, the numbers of methods have been developed for the preparation of CuO nanostructures including wet chemical methods, microwave irradiation, ultrasound-assisted methods, electro deposition, thermal decomposition of different precursors, gas-phase oxidation, electrochemical methods and etc. [9]. Among various process for preparation of the nanoscrystals, the solution based method present considerable advantages, including (i) low reaction temperature, (ii) size selective growth, (iii) morphological control, and (iv) large-scale production [10]. Also the use of chemical precipitation reactions in aqueous media historically was preferred because water is ready available at negligible cost, is safe and suitable to use, and has low environmental impact [11]. Among the several reports on the synthesis of CuO nanostructures in different shapes and sizes, there are a few reports on the simple room temperature synthesis of these nanostructures in the presence of water. In this work, we investigate the synthesis of CuO nanostructures via a single precipitation method by using TGA as a capping agent through a facile and inexpensive synthetic process, in low temperature. By using different concentration of capping agent, various sizes of CuO nanostructures are obtained. Investigations of the photocatalytic activity of prepared samples are currently underway in our laboratory.

## Experimental

### *Materials*

Copper acetate dihydrate $Cu(OAc)_2.2H_2O$ and sodium hydroxide (NaOH) were from Merk Co. and thioglycolic acid (TGA) was from Aldrich Co. All these chemical reagents were used as received and without further purification. Deionized water was used in the preparation of all solutions.

### *Instruments*

The X-ray diffraction (XRD) pattern was recorded on Philips Xpert X-ray diffractometer with Cu Kα radiation (λ=0.15406 nm), employing scanning rate of 1º/min in the 2 range from 20º to 80º. The surface morphology of products was analysed using a scanning electron microscope (SEM), LEO, 1430VP at 14 and 15 Kv accelerating voltage. The Fourier transform infrared spectra were obtained using a Varian-3600 FTIR spectrometer. UV-visible diffusive reflectance spectra (DRS) were obtained using Varian Cary 100 UV-vis spectrophotometer with diffuse reflectance accessory.

### *Preparation of CuO nanostructures*

In a typical synthesis 1g of copper (II) acetate dihydrate ($Cu(OAc)_2.2H_2O$) was dissolved in 20 ml deionized water at room temperature, then appropriate amount of capping agent (TGA: 0, 1, 40, 200 µl) and 20 ml deionized water were added to the copper acetate solution at room temperature and the resulting solution was stirred to 20 min. Then 20 ml of freshly prepared NaOH (5M) solution was added to the above solution dropwise during 20 min with vigorous

stirring. During the reaction, the color of mixture gradually turned from blue to black. Then this mixture kept at room temperature for 20 h without stirring. After that the precipitates were centrifuged and rinsed with deionized water several times until achieving to *p*H=7, then dried in desiccator for 48 hours.

**Results and discussion**

The influence of the amount of the capping agent on the properties of the prepared CuO nanostructures was investigated by carrying out the synthesis of the CuO nanostructures using different amounts of the capping agent (TGA: 0, 1, 40, 200 µl). When the amount of TGA was 0, 1, 40 µl during the reaction, the color of mixture gradually turned from blue to black, but without TGA during the washing the color of precipitate not stabilized and a little blue color was appeared due to the low stability of CuO nanostructures. When the amount of TGA was increased to 200 µl, reddish brown precipitate was observed. This change was well documented as the formation of $Cu_2O$ nanostructures [12]. Also, increasing the amount of the capping agent resulted in decreasing of the nanoparticle size and favored the dissolution of CuO and $Cu_2O$ nanostructures mixtures in aqueous solution. The phase and purity of CuO nanoparticles were determined by XRD and the typical diffraction patterns are shown in Figure 1. As observed, all the peaks correspond to the reflections in the range 20°–80° and can be indexed as C/2c monoclinic phased copper (II) oxide, which are in good agreement with the values on the standard card (JCPDS 45–937) [13]. The crystallite size was calculated from the half-height width of the diffraction peak of XRD pattern using the Debye–Scherrer equation [14]. The crystallite size calculated for samples prepared by 1 and 40 µl of TGA are 99 and 67 nm, respectively. These results clearly indicate the effect of the amount of the capping agent on the crystallite size of CuO nanostructures. The morphology of the products were examined by scanning electron microscope (SEM) at different magnification are shown in Figure 2 for nanostructures prepared with 40 µl of TGA. An overview of images for CuO nanostructures shows that the product consists of nearly nanosheet shape and the thickness of nanosheets about 14-20 nm in diameter.

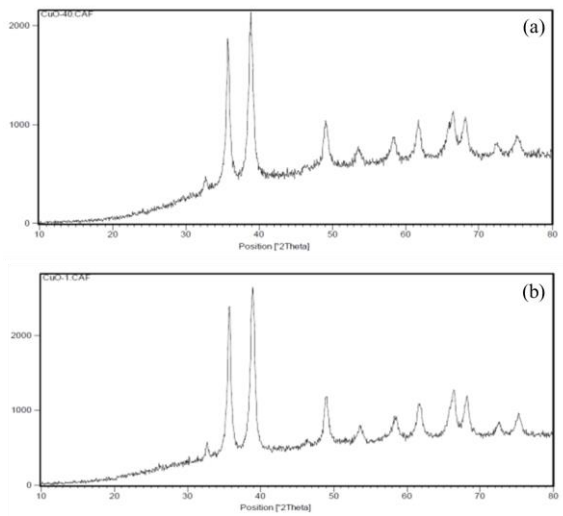


**Figure 1.** X-ray diffraction patterns of samples prepared by a) 1 and b) 40 µl of TGA

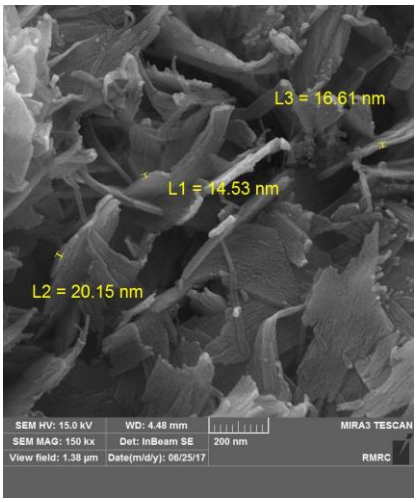


**Figure 2.** SEM image for CuO nanostructure prepared by using 40 µl of TGA

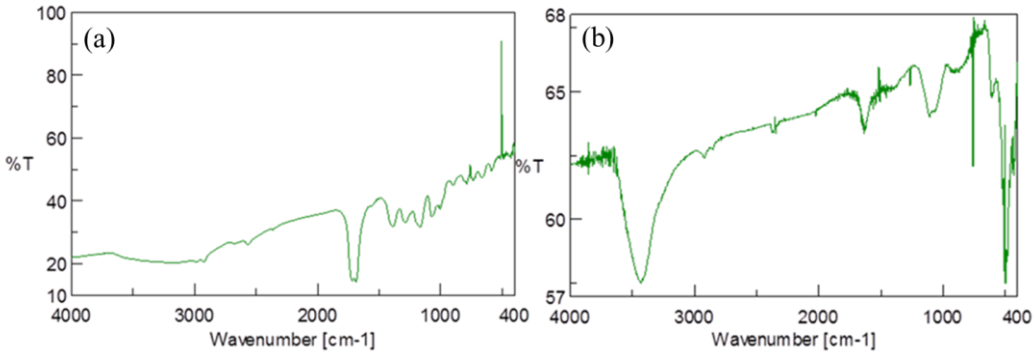


**Figure 3.** FTIR spectra of (a) pure TGA and (b) CuO capped with 40 µl of TGA

The composition and quality of the product was analyzed by the FTIR spectroscopy. Figure 3 shows the FT-IR spectra of obtained samples. In the Figure 3(b), the typical absorbance at 3400, 2300 and 1550 $cm^{-1}$ were revealed, which proved the presence of the thioglycolic acid at the CuO sample [15]. Diffuse reflectance spectra (DRS) of CuO nanostructures are shown in Figure 4. The band gap of the synthesized samples was calculated from UV–vis absorption spectra using the following formula:

$$E = hc/\lambda$$

where h is plank constant, c is velocity of light, and λ is the absorption edge obtained from absorption spectrum [16]. The obtained band gaps were 1.57 and 2.5 eV for samples prepared by 0 and 40 µl of TGA. The band gap energy of the CuO nanostructure prepared in the presence of 40 µl of TGA was higher than band gap of CuO synthesized without the capping agent (1.57 eV) and bulk CuO (1.2 eV).

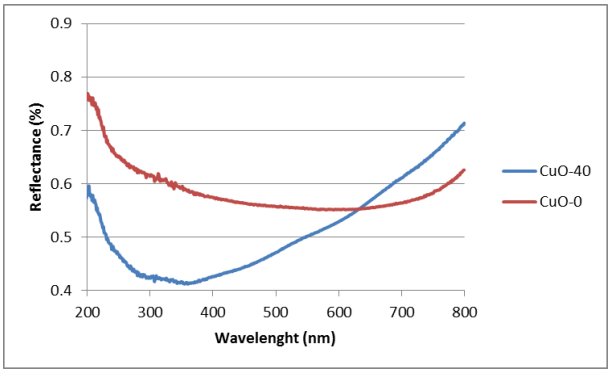


**Figure 4.** Diffuse reflectance spectra (DRS) of CuO nanostructures prepared with 0 and 40 µl of TGA

## Conclusion

In summary, CuO nanostructures were prepared successfully via the simple and easy procedure by using TGA as a capping agent. By controlling the amount of TGA, the variable sizes of CuO nanostructures were obtained.

## Acknowledgments

The authors gratefully acknowledge the support provided by the Zanjan Branch, Islamic Azad University.

**References**

[1] C.B. Murray, C. R. Kagan, and M.G. Bawendi, Annu. *Rev. Mater. Sci.* **2000**, *30*, 545.

[2] J. Rockenberger, L. Troger, A. Kornowski, T. Vossmeyer, A. Eychmuller, J. Feldhaus, and H. Weller, *J. Phys. Chem. B* **1997**, *101*, 2691.

[3] Y. Li, J. Liang, Z. Tao, and J. Chen, Mater. Res. Bull. **2008**, *43*, 2380.

[4] H. Zhang, and M. Zhang, *Mater. Chem. Phys*. **2008**, *108*, 184.

[5] T. I. Arbuzova, B. A. Gizhevskii, S.V. Naumov, A.V. Korolev, V. L. Arbuzov, K. V. Shal'nov, and A. P. Druzhkov, J. Magn. Magn. Mater. **2003**, *258/259*, 342.

[6] P. Gao, Y. Chen, H. Lu, X. Li, Y. Wang, and Q. Zhang, *Int. J. Hydrogen Energy*, **2009**, *34*, 3065.

[7] T. Maruyamat, *Sol. Energy Mater. Sol. Cells*, **1998**, *56*, 85.

[8] D. Barreca, P. Fornasiero, A. Gasparotto, V. Gombac, C. Maccato, T. Montini, and E. Tondello Chem. Sus. Chem., **2009**, *2*, 230.

[9] B. Shaabani, E. Alizadeh-Gheshlaghi, Y. Azizian-Kalandaragh, and A. Khodayari, *Adv. Powder Technol*. **2014**, *25*, 1043.

[10]X. Hu, G. Li, and J.C. Yu, *Langmuir*, **2010**, *26*, 3031.

[11] A. Henglein, Ber. Bunsenges. *Phys. Chem*. **1982**, *86*, 301.

[12] A.S. Ethiraj, and D.J. Kang, *Nanoscale Res. Lett.* **2012**, *7*, 70.

[13] M. Villani, A.B. Alabi, N. Coppede, D. Calestani, L. Lazzarini, and A. Zappettini, *Cryst. Res. Technol.* **2014**, *49*, 594.

[14] B.D. Cullity, *Elements of X-ray Diffraction, 2nd edition*., Addison Wesley Publishing, London (1978).

[15] M. Salavati-Niasari, M.R. Loghman-Estarki, and F. Davar *J. Alloys and Compd*. **2009**, *475*, 782.

[16] P. Eskandari, F. Kazemi, Y. Azizian, *Sep. Pur. Technol*. **2013**, *120*, 180.

# Graphical Abstract

Preparation and Characterization of CuO Nanostructures through simple precipitation method in the presence of thioglycolic acid

Parvin Eskandari,* Mohammad Reza Fazlollahi

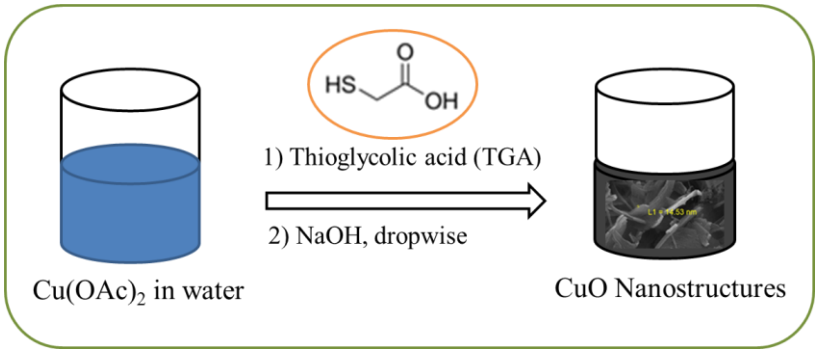

# A hydrophobic heterogeneous acid catalyst for the the one-pot multi-component synthesis of hexahydroquinolines

**Sara Sobhani,* Toktam Yari**

*Department of Chemistry, College of Sciences, University of Birjand, Birjand, Iran*

*Corresponding author Tel.: +98 (56) 32202065; Fax number: +98 (56) 32202065

*E-mail: ssobhani@birjand.ac.ir, sobhanisara@yahoo.com

## Abstract

A hydrophobic heterogeneous acid catalyst is easily synthesized and characterized by different methods. It was used as a magnetically recyclable heterogeneous catalyst for the efficient one-pot multi-component synthesis of hexahydroquinolines. The present catalytic system worked extremely well even up to five subsequent trails without significant loss of its catalytic activity. The strong magnetic properties of the reused catalyst were revealed by complete and easy attraction using an external magnet.

**Keywords**: heterogeneous catalyst, hydrophilic catalyst, multi-component reaction.

## Introduction

The adsorbed water on the surface of the catalyst produces more hydrophilic environment, reducing the mass transfer of hydrophobic starting material towards the active sites of the catalyst and decreases the activity of the catalyst [1-4]. In particular, for one-pot multi-step reactions in which water sensitive intermediates should be subjected to further reaction, the presence of adsorbed water on the catalyst surface retards the progress of the reaction. In fact, the hydrophilic/hydrophobic balance of the catalyst surface could significantly influence the catalytic performance. Therefore, the design of heterogeneous catalysts with suitable surface polarity is an ultimate goal in the development of solid catalysts. Recent investigations have set out to address these issues by immobilizing inert organic groups on the surface to alter the hydrophobicity of the heterogeneous catalysts [5-8].

## Experimental

### General procedure for the synthesis of hexahydroquinolines (HHQs)

A mixture of aryl aldehydes (1 mmol), dimedone (1 mmol), ethyl acetoacetate (1mmol), ammonium acetate (1 mmol) as a nitrogen source and the catalyst (2.0 mol%) was stirred for 30 min at 60 $^{0}$C. EtOAc (10 mL) was added to the reaction mixture and the catalyst was separated by an external magnetic field. Evaporation of the solvent under reduced pressure gave the crude products. The pure products were isolated by chromatography on silica gel eluted with *n*-hexane:EtOAc (4:1).

## Results and discussion

As part of our ongoing research on the development of new heterogeneous catalysts based on magnetic nanoparticles (MNPs) [9-11], herein, we report the synthesis of a hydrophobic Brønsted acid catalyst supported on MNPs (HBA@MNPs).

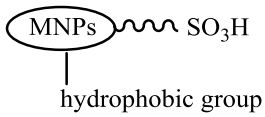


Scheme 1. HBA@MNPs

After the structural characterization of the catalyst, its catalytic activity was investigated for the synthesis of HHQs *via* Hantzsch reaction. At first, one-pot reaction of benzaldehyde, dimedone, ethyl acetoacetate and ammonium acetate was chosen to optimize the reaction conditions such as solvents and molar ratio of the catalyst. It was found that the corresponding HHQ was obtained in the best yield in the presence of 2 mol% of the catalyst under solvent-free conditions, at 60$^{o}$C in 30 min. Then the generality of this method for the reaction of several substituted aryl aldehydes, dimedone, ethyl acetoacetate and ammonium acetate under the optimized conditions was investigated and found that the reactions of different substituted benzaldehydes containing electron-withdrawing or electron-donating groups and halogens on the aromatic ring were successfully proceeded to give the corresponding HHQs in good to high yields (Scheme 2).

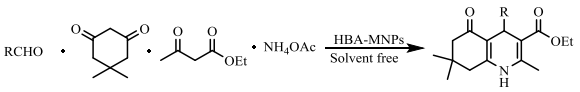


Scheme 2. Synthesis of HHQ

The most important factors concerning a heterogeneous catalyst are its stability and reusability along with the ease of separation. In this regards, the recyclability of hydrophobic HBA@MNPs was investigated in the one-pot four-component reaction of benzaldehyde, dimedone, ethylacetoacetate and $NH_4OAc$ under optimized reaction conditions. After the reaction was completed, EtOAc was added to the reaction mixture. The catalyst was separated by an external magnet, washed several times with EtOAc,

dried and reused for a consecutive run under the same reaction conditions. The catalytic system worked extremely well even up to five subsequent trails without significant loss of its catalytic activity.

## Conclusion

In summary, in this paper, we have successfully synthesized a hydrophobic Brønsted acid catalyst supported on MNPs (HBA@MNPs). After its characterization by different methods, it was used as a magnetically recyclable heterogeneous acid catalyst for the one-pot four-component synthesis of hexahydroquinolines in good to high yields. High efficiency and simple reusability of the catalyst and the use of solvent-free conditions make this method an economical, environmental benign and safety process for the synthesis of hexahydroquinolines. The great catalytic performance is largely attributed to the improvement of the active site accessibility by using hydrophobic groups bounded on the MNPs, which enabled the repulsion of water from the proximity of the active acid sites. Thus, the mass transfer of hydrophobic starting material towards the active sites of the catalyst were not retarded.

## Acknowledgments

We are thankful to University of Birjand Research Council for their support on this work.

## References

[1] F. Liu, X. Meng, Y. Zhang, L. Ren, F. Nawaz, F.-S. Xiao, *J. Catal*. **2010**, *271*, 52.

[2] J. Liu, J. Yang, C. Li, Q. Yang, *J. Porous Mater*. **2009**, *16*, 273.

[3] J. A. Melero, L. F. Bautista, G. Morales, J. Iglesias, D. Briones, *Energy Fuels* **2009**, *23*, 539.

[4] G. Morales, G. Athens, B. F. Chmelka, R. van Grieken, J. A. Melero, *J. Catal*. **2008**, *254*, 539.

[5] F. Liu, W. Kong, C. Qi, L. Zhu, F. - S. Xiao, *ACS Catal*. **2012**, *2*, 565.

[6] Y. Leng, J. Zhao, P. Jiang, D. Lu, *Catal. Sci. Technol*. **2016**, *6*, 875.

[7] K. Inumaru, T. Ishihara, Y. Kamiya, T. Okuhara, S. Yamanaka, *Angew. Chem. Int. Ed*. **2007**, *46*, 7625.

[8] G. Morales, G. Athens, F. B. Chmelka, R. van Grieken, A. J. Melero, *J. Catal*. **2008**, *254*, 205.

[9] S. Sobhani and M. Honarmand, *Appl. Catal*., *A*, **2013**, *467*, 456.

[10] S. Sobhani, Z. Ramezani, *RSC Adv*. **2016**, *6*, 29237.

[11] S. Sobhani, Z. Zeraatkar, F. Zarifi, *New J. Chem*. **2015**, *39*, 7076.

## Graphical Abstract

**A hydrophobic heterogeneous acid catalyst for the the one-pot multi-component synthesis of hexahydroquinolines**

**Sara Sobhani,* Toktam Yari**

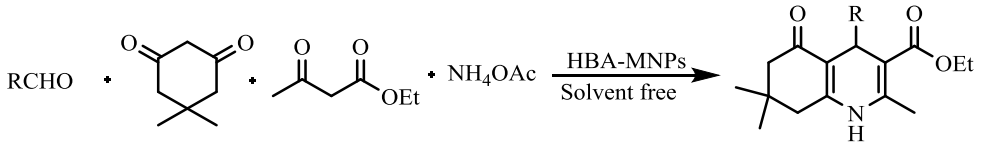

# A novel hydrophilic heterogeneous cobalt catalyst for the Heck, Suzuki and Hiyama coupling reactions in neat water

**Sara Sobhani,*Hadis Hosseini Moghadam**

*Department of Chemistry, College of Sciences, University of Birjand, Birjand, Iran*

*Corresponding author Tel.: +98 (56) 32202065; Fax number: +98 (56) 32202065

*E-mail: ssobhani@birjand.ac.ir, sobhanisara@yahoo.com

**Abstract**

A novel hydrophilic heterogeneous cobalt catalyst was synthesized and characterized by different methods. The hydrophilic character allows dispersion of the catalyst in the aqueous medium which leads to high catalytic performance. It was used as an efficient catalyst for Heck, Suzuki and Hiyama cross coupling reaction in neat water.

**Keywords**: hydrophilic, heterogeneous catalyst, coupling reactions

## Introduction

Transition metal-catalyzed carbon-carbon bond forming reactions [1] have emerged as powerful tools for advanced organic synthesis in both academic [2] and industrial laboratories [3]. Within this area, Heck, Suzuki and Hiyama cross-coupling reactions are important strategies for the formation of carbon-carbon bonds and catalyzed originally by homogeneous Pd catalyst [4]. The use of readily available starting materials, and simplicity and generality of the method make these cross-coupling reactions particularly attractive for the synthesis of a great variety of complex organic molecules such as drugs, fine chemicals, natural products, polymers, agrochemicals and biologically active molecules [5,6]. However, these reactions suffer from problems associated with the separation and recovery of the homogeneous and high cost Pd catalyst, which might result in undesirable metal contamination of the products. Therefore, to have an efficient recovery and recycling of the catalyst, the immobilization of homogeneous catalytic systems on different supporting materials has been the subject of intense research [7,8]. The other challenge facing this field is the design of the heterogeneous catalysts that are efficient in water as green solvent. Along this line, additives such as phase transfer agents,[9] polymers,[10] surfactants,[11] cyclodextrins,[12] organic co-solvents[13] or ionic liquids[14] have been used. A more desirable approach, which avoids using any additives, is designing hydrophilic heterogeneouse catalysts.

## Experimental

*General procedure for the Heck/Suzuki/Hiyama cross-coupling reaction*

A mixture of aryl halide (1 mmol), olefin/phenylboronic acid/phenyl-triethoxysilane (1.1 mmol), base (2 mmol) and catalyst (0.5 mol%) in water (5 mL) was stirred at 90 °C for an appropriate time. The catalyst was separated by filteration. The aqeous layer was washed with EtOAc. Evaporation of the solvent of the organic phase under reduced pressure gave the crude products. The pure products were isolated by chromatography on silica gel eluted with *n*-hexane: EtOAc (50:1).

## Results and discussion

In our continuous interest in developing a greener catalyzed reaction, herein, we have synthesized a novel hydrophilic heterogeneous cobalt catalyst (Scheme 1) and characterized it by different methods.

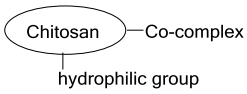


**Scheme 1**.

We have successfuly used this catalyst for the Heck, Suzuki and Hiyama coupling reactions in neat water (Scheme 2).

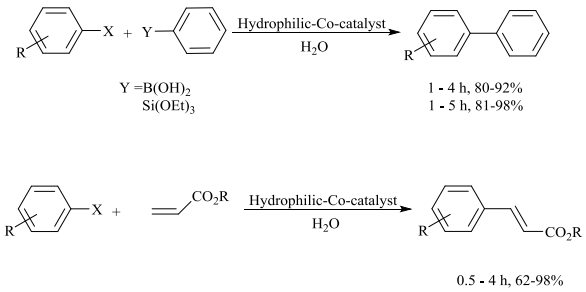


**Scheme 2**

## Conclusion

In summary, a novel hydrophilic heterogeneous cobalt catalyst was synthesized and characterized by different methods. The hydrophilic character allows dispersion of the catalyst in the aqueous medium which leads to high catalytic performance. We have successfully used this catalyst for Heck, Suzuki and Hiyama cross coupling reaction in neat water. Synthesis of this reusable catalyst from commercially available starting materials, good to high yields of the products, use of water as green reaction meida, simple and convenient method for the separation and reuse of the catalyst are the advantages of this catalytic system for C-C bond formation *via* the reaction of aryl halides (iodides, bromides

and chlorides) with olefins, phenylboronic acid and phenylsilane.

**Acknowledgments**

Financial support of this project by University of Birjand Research Council is acknowledged.

**References**

[1] M, Beller, C. Bolm, *Transition Metals for Organic Synthesis*. 2nd Ed. Wiley VCH: Weinheim (2004).

[2] A. Brennfhrer, H. Neumann, M, Beller, *Angew Chem*, **2009**, *121*, 4176.

[3] A H M. de Vries, J H M. Mommers, H J W. Henderickx,J. G. de Vries, *Org Lett*, **2003**, *5*, 3285.

[4] M. Gholinejad, V. Karimkhani, I. Kim. *Appl Organomet Chem*, **2014**, *28*, 221.

[5] H U. Blaser, A. Indolese, F. Naud, U. Nettekoven, A. Schnyder. *Adv Synth Catal*, **2004**, *346*: 1583.

[6] C. Torborg, M. Beller, *Adv Synth Catal*, **2009**, *351*, 3027.

[7] V. Polshettiwar, A. Molnár, *Tetrahedron*, **2007**, *63*, 6949.

[8] A. Zamboulis, N. Moitra, J J E. Moreau, X. Cattoën, M. Wong Chi Man, *J Mater Chem*, **2010**, *20*, 9322.

[9] M. Jin, D. Lee, *Angew. Chemie Int. Ed.*, **2010**, *49*, 1119-1122.

[10] B. R. Vaddula, A. Saha, J. Leazer, R. S. Varma, *Green Chem.*, **2012**, *14*, 2133-2136.

[11] J. Li, Y. Zhang, D. Han, Q. Gao, C. Li, *J. Mol. Catal. A Chem.*, **2009**, *298*, 31-35.

[12] K. Mori, N. Yoshioka, Y. Kondo, T. Takeuchi, H. Yamashita, *Green Chem.*, **2009**, *11*, 1337-1342.

[13] Y. Qiao, H. Li, L. Hua, L. Orzechowski, K. Yan, B. Feng, Z. Pan, N. Theyssen, W. Leitner, Z. Hou, *Chempluschem*, **2012**, *77*, 1128-1138.

[14] H. Guo, Y. Lian, L. Yan, X. Qi, R. L. Smith, *Green Chem.*, **2013**, *15*, 2167-2174.

## Graphical Abstract

A novel hydrophilic heterogeneous cobalt catalyst for the Heck, Suzuki and Hiyama coupling reactions in neat water

Sara Sobhani,*Hadis Hosseini Moghadam

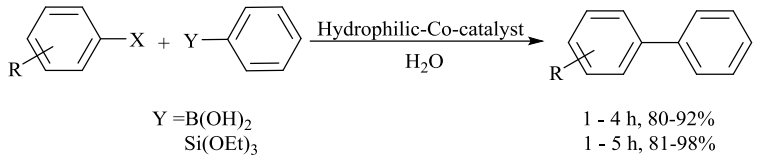


Y =$B(OH)_2$ 1 - 4 h, 80-92%
$Si(OEt)_3$ 1 - 5 h, 81-98%

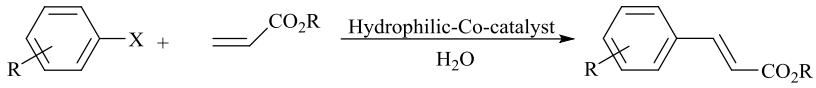


0.5 - 4 h, 62-98%

# Electrochemical catalyst an effective method for synthesis 2,3-dihydroquinazolin-4(1H)-one

**Mohammd Dodangeh [*a], Ali Ramazani[a], Malek-Taher Maghsoodlou[b], Monireh Rezaei[c]**

[a]*Department of Chemistry, University of Zanjan,P.O. BOX 19395-4697 Zanjan, Iran*

[b]*Chemistry Department, Faculty of Science, University of Sistan and Baluchistan, P. O. Box: 98135-674, Zahedan, Iran*

[c] *Chemistry Department, Imam Khomeini International University, Qazvin, Iran*

*Mohammad Dodangeh *E-mail: Mohammad.Dodangeh@yahoo.com

**Abstract**

A mild and efficient method was applied for the one-pot three-component synthesis of 2,3-dihydroquinazolin-4(1H)-one from the condensation between benzo[d]thiazol-2-amine, aryl aldehydes and 2H-benzo[d][1,3]oxazine-2,4(1H)-dione using electrochemical catalyst in an undivided cell in the presence of sodium bromide as an electrolyte. Electrochemical catalyst has many advantages such as clean work-up, fast, green process, green solvent and environment friendly method.

**Keywords**: 2H-benzo[d][1,3]oxazine-2,4(1H)-dione; Electrochemical catalyst; green chemistry.

## Introduction

In past decade electrosynthesis has been developed to be a strong synthesis tool and become increasingly attractive. [1] Organic electrosynthesis, enable to the replace of dangerous and toxic chemical catalyst by electrons, has received great attention as a strong tool for green synthesis.[2] Electro synthesis offers several economic, ecologic, green method, and practical advantage.[3] The multicomponent reactions (MCRs) have been used widely for synthesis, the active compounds in organic, combinatorial and medicinal chemistry.[4,5] MCRs are a convergent method in which three or more reactants are combined in one pot to render a product. These processes have been widely exploited in drug discovery and heterocyclic product synthesis. [6-8] 2,3-Dihydroquinazolin-4(1*H*)-one derivatives have a significant and important class of nitrogen heterocyclic. Quinazolin structure as the core unit to be useful in nature plant alkaloids and pharmacological compounds such as evodiamin, febriugine, isofebrifugine, metolazone, quinethazone, afloqualone, raltitrexed and nolatrexed. These derivatives have a lot of potential to use biological and pharmaceutical activities including anticonvulsant antibacterial anticancer antihypertensive and plant growth regulation. [9]

## Experimental

*General*

All reagents and solvents were obtained from Fluka and Merck and used without further purification. TLC was performed on Silica–gel Polygram SILG/UV 254 plates. Melting points and IR spectra were measured with an Electro thermal 9100 apparatus and a JASCO FT-IR-460 plus spectrometer. Controlled-current coulometer and preparative electrolysis were performed using a SAMA potentiostate/galvanostate (Zahedan, Iran), respectively. The 1H NMR spectra were obtained on Bruker DRX-300 advance instruments with DMSO.

**General procedure for synthesis of 3-(benzo[d]thiazol-2-yl)-2-(4-chlorophenyl)-2,3-dihydroquinazolin-4(1H)-one**

A mixture of 4-chlorobenzaldehyde (1 mmol), 2H-benzo[d][1,3]oxazine-2,4(1H)-dione (1mmol), benzo[d]thiazol-2-amine (1mmol ) and NaBr (0.05 g, 0.5 mmol ) in EtOH (20 mL) was stirred with a magnetic stirrer and electrolyzed in an undivided cell equipped with a graphite anode, and an iron cathode at ambient temperature under a constant current density of 10mA/cm2 ( electrodes square 5 cm2), until the catalytic quantity of 0.1 F/mol of electricity was passed. After electrolysis process, the mixture was filtered, then it was rinsed twice with cold ethanol to obtain corresponding product.

**Analytical data for the selected compounds**

***3-(benzo[d]thiazol-2-yl)-2-(4-chlorophenyl)-2,3-dihydroquinazolin-4(1H)-one (4b)***

IR (KBr, cm-1): 3334, 1635, 1609, 1506, 1405, 1251; 1HNMR (300 MHz, DMSO-d6): $\delta$ (ppm) = 6.81 (1H, t, 1CH *J= 7.6*), 6.96 (1H, d, 1CH *J= 7.5*), 7.30 (2H, d, 2CH *J=7.7*), 7.36 (1H, t, 1CH *J=7.5*), 7.38 (2H, d, 2CH *J=7.9*), 7.42 (1H, t, 1CH *J=7.1*), 7.46 (1H, t, 1CH *J=8.1*),7.54 (1H, d, 1CH *J=8.0*), 7.78 (1H, d, 1CH *J=7.9*), 7.79 (1H, d, 1CH *J=8.3*),8.06 (1H, d, 1CH *J=8.1*), 8.34 (1H, NH).

***3-(benzo[d]thiazol-2-yl)-2-(4-nitrophenyl)-2,3-dihydroquinazolin-4(1H)-one (4e)***

IR (KBr, cm-1): 3375, 1647, 1613, 1521; 1HNMR(300 MHz, DMSO-d6): $\delta$ (ppm) = 6.81 (1H, t, CH *J=7.6*), 7.00 (1H, d, CH *J=7.4*), 7.34(1H, t, CH *J=7.8*), 7.41 (1H, t, CH *J=7.2*), 7.44 (1H, t, 1CH *J=6.7*), 7.57 (2H, d, 2CH, *J=8.1*), 7.67 (1H, s,1CH), 7.77 (1H, d, 1CH, *J=7.8*), H7.81 (1H, d, 1CH, *J=8.4*), 8.05 (1H, d, 1CH, *J=7.9*), 8.15 (2H, d,2CH, *J=6.4*), 8.46 (1H, s, 1NH).

***3-(benzo[d]thiazol-2-yl)-2-(p-tolyl)-2,3-dihydroquinazolin-4(1H)-one (4f)***

IR (KBr, cm-1): 3342, 1630, 1612, 1503, 1432, 1251; 1HNMR (300 MHz, DMSO-*d6*): $\delta$ (ppm) = 2.17 (3H, s, CH3), 6.78 (1H, t, CH, *J=7.1*), 6.93 (1H, d, CH, *J=8.1*), 7.08 (2H, d, 2CH, *J=7.5*), 7.17 (2H, d, 2CH, *J=6.9*), 7.35 (1H, t, CH, *J=8.2*),7.38(1H, t, CH, *J=7.7*), 7.45 (1H, t, CH, *J=7.4*), 7.51(1H, d, CH, *J=7.8*), 7.77 (1H, t, CH, *J=7.8*), 7.79 (1H, d, CH, *J=7.9*), 8.04 (1H, d, CH, *J=7.2*), 8.30 (1H, s, NH).

***3-(benzo[d]thiazol-2-yl)-2-(4-methoxyphenyl)-2,3-dihydroquinazolin-4(1H)-one (4g)***

IR (KBr, cm-1): 3347, 1635, 1608, 1508, 1433, 1304, 1230; 1HNMR (300 MHz, DMSO-d6): $\delta$ (ppm) = 3.63 (3H, s, OCH3, *J=4.2*), 6.78 (1H, t, CH, *J=6.1*), 6.83 (2H, d, 2CH, *J=6.5*), 6.94 (1H, d,CH, *J=7.1*),7.21 (2H, d, 2CH, *J=6.5*), 7.34 (1H, t, CH, *J=7.2*), 7.39 (1H, t, CH, *J=7.2*), 7.44(1H, t, CH, *J=7.5*), 7.52 (1H, br s, CH), 7.78(1H, d, CH, *J=7.7*), 7.81 (1H, d, CH, *J=7.9*), 8.04 (1H, d, CH, *J=7.4*), 8.32 (1H, s, NH).

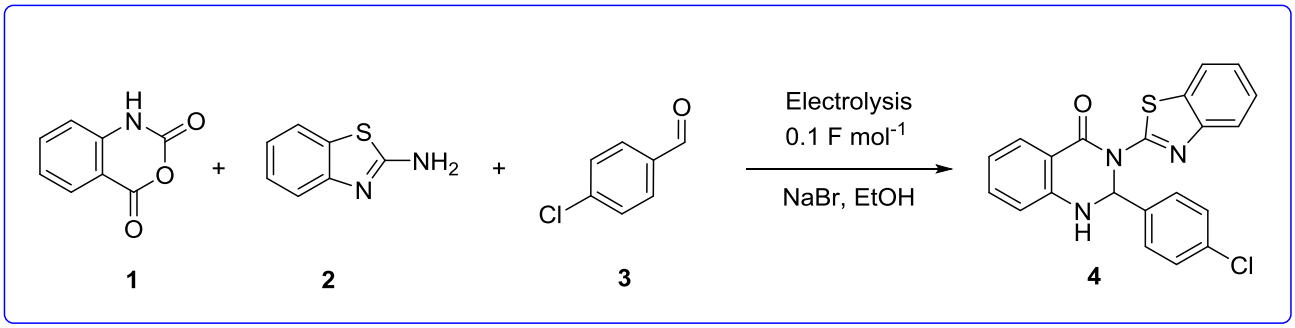


**Scheme 1. Synthesis 2,3-Dihydroquinazolin-4(1H)-one derivatives with an electrochemical cell**

## Results and discussion

To optimize the reaction conditions, the condensation between 4-chlorobenzaldehyde, 2H-benzo[d][1,3]oxazine-2,4(1H)-dione, benzo[d]thiazol-2-amine was chosen as model reaction. The reaction mixture was stirred at room temperature, and this progress was monitored by TLC. The reaction is performed in alcoholic solvents in the presence of sodium bromide as an electrolyte. Various current quantities were applied under the mentioned conditions. As can be seen in Table 1, excellent conversions of the starting materials were obtained under 15 mA/cm$^2$ current densities after 0.1 F/mol of electricity had passed. The current density of 15 mA/cm2, I = 60 mA, electrode surface Scheme 1.

Using mentioned optimized reaction, the reaction was explored for the synthesis of a wide variety of 2,3-Dihydroquinazolin-4(1*H*)-one derivatives using aromatic aldehydes, 2H-benzo[d][1,3]oxazine-2,4(1H)-dione and benzo[d]thiazol-2-amine. The results are summarized in Table 2. As shown in Table 2, the products were obtained in excellent yields.

Our proposed mechanism for the preparation of 2, 3-dihydroquinazolin-4 (1H) -one derivatives. First, deprotonation of an alcohol at the cathode leads to the formation of the alkoxide anion. It's subsequent reaction in solution with 2-aminobenzothiazole **2** gives rise to 2-

aminobenzothiazole anion **5**. Then the condensation of 2-aminobenzothiazole anion and isatoic anhydride **1**, produced intermediate **6** with the removal of CO2 molecules. Then, activated intermediate **7** was reacted with this ahdehyde **3** through an imine intermediate **9** synthesis. In the next step, intermediate **9** could be prepared by an intermolecular nucleophilic attack of the amide nitrogen on activated imine carbon, cyclisation, 1,5-proton transfer and tautomerization, affording the corresponding product **4** (Scheme 2).

**Table 1.** Optimization of Reaction Conditions for the Synthesis 3-(benzo[d]thiazol-2-yl)-2-(4-chlorophenyl)-2, 3-dihydroquinazolin-4(1H)-one

| Entry | I (mA) | Current density ($mA/cm^2$) | Time (min) | Electricity | Yield[a] (%) |
|---|---|---|---|---|---|
| 1 | **5** | 1 | 340 | 0.1 | 55 |
| 2 | **10** | 2 | 170 | 0.1 | 67 |
| 3 | **30** | 4 | 60 | 0.1 | 81 |
| 4 | **60** | 15 | 40 | 0.1 | 94 |
| 5 | **80** | 20 | 31 | 0.1 | 82 |

[a]Isolated yield.

**Table 2.** Preparation of 2, 3-dihydroquinazolin-4(1H)-one derivatives

| Enter | Aldehyde | Product | Time (min) | Yield (%) | MP(Obs) (°C) | MP(Lit) (°C) |
|---|---|---|---|---|---|---|
| 1 | 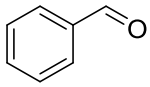 | 4a | 63 | 88 | 230-233 | 232-234[10] |
| 2 | 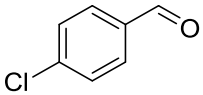 | 4b | 40 | 94 | 190-192 | 192-194[10] |
| 3 | 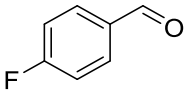 | 4c | 35 | 95 | 248-250 | 252-254[11] |
| 4 | 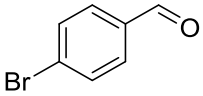 | 4d | 44 | 93 | 233-235 | 231-233[11] |

| | | | | | | |
|---|---|---|---|---|---|---|
| 5 | 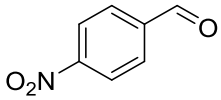 | 4e | 35 | 95 | 245-247 | 242-245[11] |
| 6 | 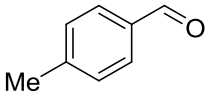 | 4f | 70 | 85 | 199-200 | 197-199[12] |
| 7 | 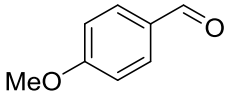 | 4g | 55 | 83 | 176-178 | 182-184[13] |
| 8 | 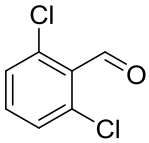 | 4h | 40 | 92 | 230-231 | 231-233[13] |
| 9 | 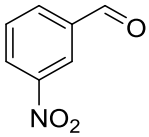 | 4i | 35 | 91 | 250-252 | 252-253[11] |

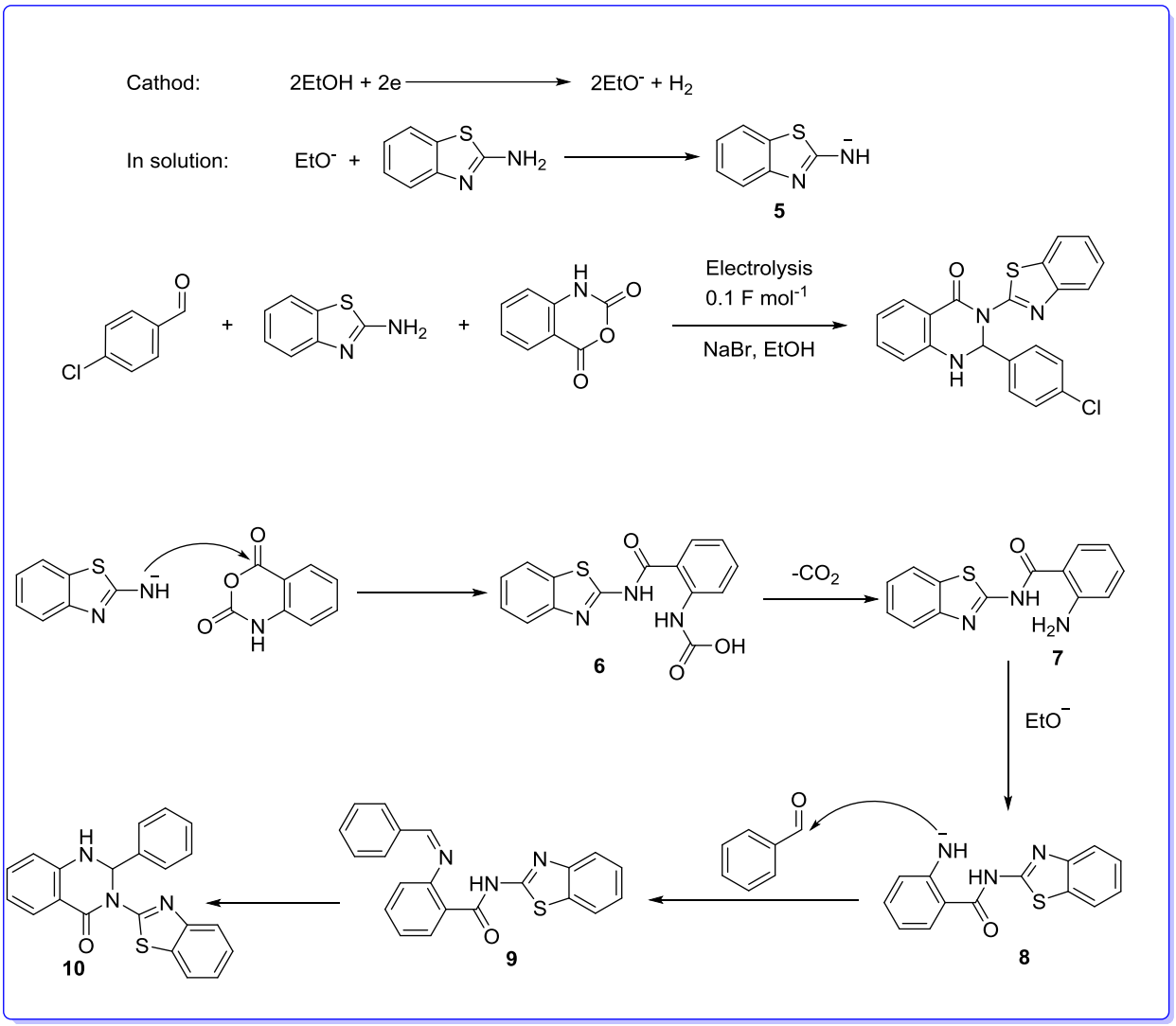


**Scheme 2. Proposed mechanism for the Synthesis 2,3-Dihydroquinazolin-4(1H)-one derivatives using electrolysis in the presence of sodium bromide as an electrolyte**

## Conclusion

The 2,3-Dihydroquinazolin-4(1H)-one derivatives were synthesized in the presence of sodium bromide as an electrolyte under neutral and mild conditions. The main advantages of this method are high yields, simple work-up, use of non- hazardous organic solvent and catalyst.

## Acknowledgments

We gratefully acknowledge financial support from the Research Council of the Zanjan University.

## References


[1] W. Liu, W. Huang, T. Lan, H. Qin and C. Yang, *Tetrahedron*, **2018**, *74*, 2298-2305.

[2] H. Wang, J. Zhang, J. Tan, L. Xin, Y. Li, S. Zhang and K. Xu, *Org Lett*, **2018**, *20*, 2505-2508.

[3] B. Schille, N.O. Giltzau and R. Francke, *Angewandte Chemie*, **2018**, *57*, 422-426.

[4] M.N. Elinson, V.M. Merkulova, A.I. Ilovaisky, F. Barba and B. Batanero, *Electrochimica Acta*, **2011**, *56*, 8219-8223.

[5] K. Khandan-Barani, M. Dodangeh, M. Kangani and M.-T. Maghsoodlou, *Oriental Journal of Chemistry*, **2016**, *32*, 1255-1260.

[6] H. Ahankar, A. Ramazani, K. Ślepokura, T. Lis and S.W. Joo, *Green Chem.*, **2016**, *18*, 3582-3593.

[7] P. Dastoorani, M.T. Maghsoodlou, M.A. Khalilzadeh and E. Sarina, *Tetrahedron Letters*, **2016**, *57*, 314-316.

[8] M. Ghorbani, B. Mohammadi, M. Saraii, B. Masoumi, M. Abbasian, A. Ramazani, K. Slepokura and T. Lis, *Org Lett*, **2016**, *18*, 4759-4761.

[9] Z.-B. Xie, S.-G. Zhang, G.-F. Jiang, D.-Z. Sun and Z.-G. Le, *Green Chemistry Letters and Reviews*, **2015**, *8*, 95-98.

[10] J.M. Khurana and S. Kumar, *Green Chemistry Letters and Reviews*, **2011**, *4*, 321-325.

[11] J. Chen, D. Wu, F. He, M. Liu, H. Wu, J. Ding and W. Su, *Tetrahedron Letters*, **2008**, *49*, 3814-3818.

[12] H.R. Shaterian, N. Fahimi and K. Azizi, *Research on Chemical Intermediates*, **2013**, *40*, 1879-1898.

[13] A. Moradi, R. Heydari and M.T. Maghsoodlou, *Research on Chemical Intermediates*, **2014**, *41*, 7377-7391.


## Graphical Abstract

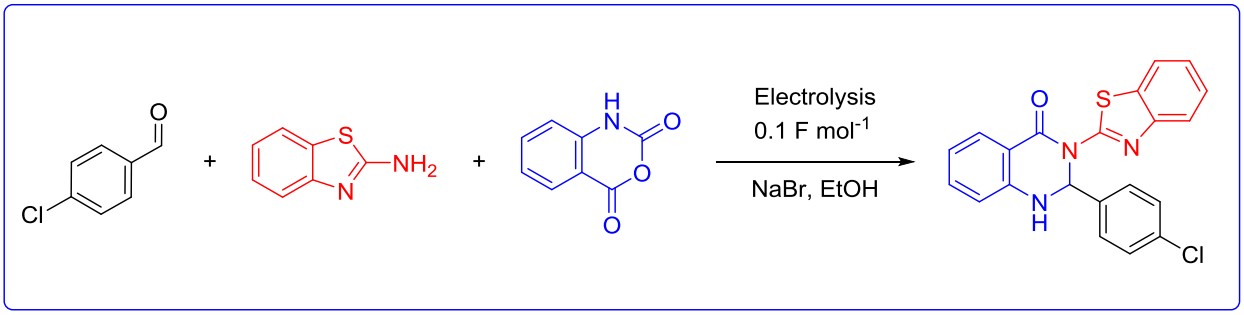

# Vitamin B12: a new catalytic system for the one-pot three-component synthesis of 2,3-dihydroquinazolin-4(1H)-one, 4H-pyrimidobenzothiazole and 2-aminobenzothiazolomethylnaphthol derivatives

**Mohammad Dodangeha*, Ali Ramazania and Malek-Taher Maghsoodlou[b]**

[a]*Department of Chemistry, University of Zanjan,P.O. BOX 19395-4697 Zanjan, Iran*

[b]*Department of Chemistry, Faculty of Science, University of Sistan and Baluchestan, P. O. Box: 98135-674, Zahedan, Iran, Tel: +985412416586; Fax: +985412416586;*

*E-mail: Mohammad.Dodangeh@yahoo.com

**Abstract**

For the first time vitamin B12 was applied as a catalyst for the one-pot three-component synthesis of 2,3-dihydroquinazolin-4 (1H) -one, 4H-pyrimidobenzothiazole and 2-aminobenzothiazolomethylnaphthol derivatives from the condensation between aryl aldehydes and 2-aminobenzothiazole with isatoic anhydride or β-naphthol or ethylacetoacetate. The use of catalytic amount of vitamin B12 with high yields is the most advantages of this research. The other advantages are: use of natural and biodegradable catalyst, easy work-up, short reaction times and neat reaction conditions.

**Keywords:** Vitamin B12; 2,3-dihydroquinazolin-4 (1H) -one; 4H-pyrimidobenzothiazole; aminobenzothiazolomethylnaphthol

**Introduction:**

Among many biologically important metals, Co, in the form of vitamin B12 (cyano-cobalamin 1), plays a unique role[1,2] . B12 coenzymes are indispensable for catalyzing enzymatic rearrangements (coenzyme B12, adenosylcobalamin) and methylation reactions (methylcobalamin)[1]. The special ability of vitamin B12 (1) and other corrinoids to form a Co–C bond, combined with its facility in furnishing alkyl radicals via homolysis, has attracted the interest of many researchers, because corrinoids can be used as catalysts for C–C-bond forming reactions, which belong to the most challenging processes in organic synthesis[3] . These catalytic reactions typically involve alkyl-cobalt complexes, which are formed in the reactions of Co (I) species and an electrophile or a Co (II) and a radical[4].

In modern organic synthesis, biologically active benzothiazoles are regarded as valuable building blocks. 2-Aminobenzothiazoles are unique structures that are widely used in medicinal and biological chemistry[5]. Their diverse functions range from facilitation of electron transfer in the firefly luciferine cycle[6], and, in pharmaceutical chemistry, antitumor[7] and antidiabetic activity [8], use as indicators of Alzheimer's disease[9], and anticancer activity[10]. Benzothiazoles are also commercially important as reactive dyes[11], hair dyes[12] agrochemical fungicides, insecticides, acaricides, herbicides, plant desiccants, and defoliants[13]. As a result of their importance as substructures in a broad range of natural and designed products, significant effort continues to be directed toward the development of new benzothiazole-based structures and new methods for their construction. Recently some methods have been reported for the synthesis of 2,3-dihydroquinazolin-4(1H)-one, 4H-pyrimidobenzothiazole and 2-aminobenzothiazolomethyl naphthol derivatives using CuO nanoparticles[14], Zr(HSO4)4[15] montmorillonite K-10[16], silicon sulfuric acid (SSA)[17], potassium trifluoromethanesulfonate (Ga(OTf)3) [18]heteropolyacids (HPAs)[19], Bi(NO3)3.5H2O[20], SrCl3.6H2O[21], ionic liquids [bmim]Br[22], LiCl[23], AlCl3[24], TBAHS[25], hydrotalcite[26], N,N-dichlorobis(2,4,6-trichlorophenyl) urea[27], FeF3[28], as catalyst.These routes, however, generally suffer from low yields of products, the requirement of longer reaction time and high temperature along. As Because of the biological activity of 2-aminobenzothiazoles, and as part of our ongoing program on green catalytic system[29-33], herein we report an eco-friendly, simple, and efficient method for the one-pot three-component synthesis of 2,3-dihydroquinazolin-4(1H)-one, 2-aminobenzothiazolomethylnaphthol and 4H-pyrimidobenzothiazole derivatives from the condensation between aryl aldehydes and 2-aminobenzothiazole with isatoic anhydride or β-naphthol or ethylacetoacetate in the presence of vitamin B12 (Figure 1) as green and biodegradable catalyst at ambient temprature in EtOH and H2O:EtOH media (Scheme 1).

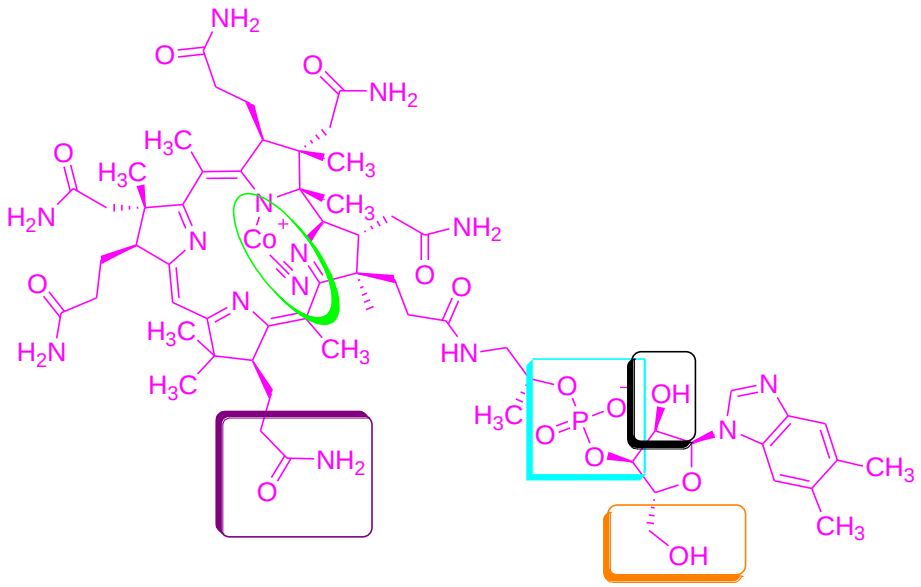


**Figure 1. The structure of vitamin B12**

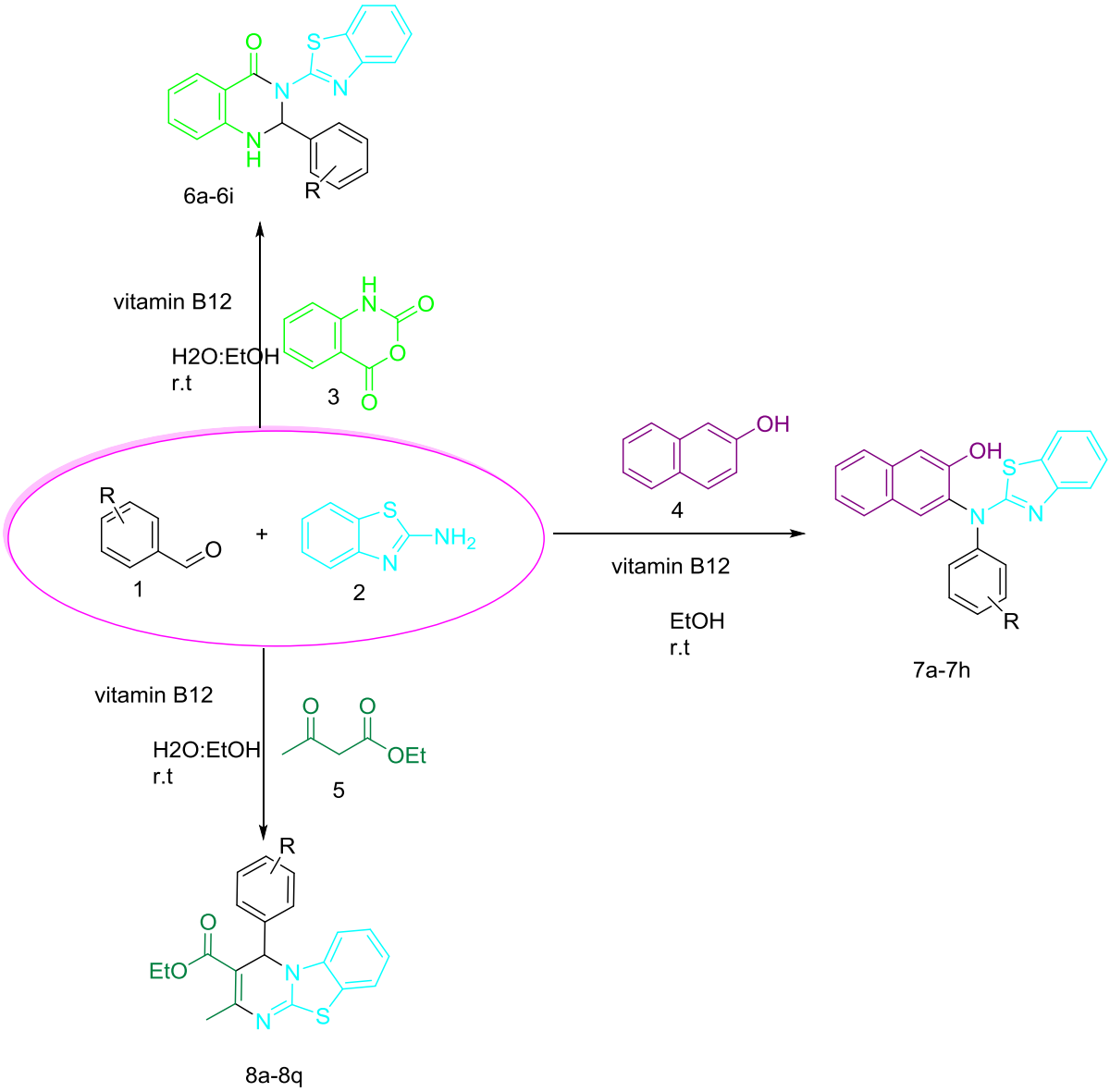


**Scheme 1.** Synthesis of 2,3-dihydroquinazolin-4(1H)-one, 4H-pyrimidobenzothiazole and 2-aminobenzothiazolomethylnaphthol derivatives in the presence of vitamin B12 as catalyst at ambient temperature

## Experimental

Materials and equipments all reagents were purchased from Merck, Fluka and Aldrich and used without further purification. The NMR spectra were recorded on a Bruker Avance DPX 300 MHz spectrometer using CDCl3 or DMSO, as solvent. Chemical shifts have been expressed in (ppm) downfield from TMS. IR spectra were recorded on a JASCO FT-IR 460 plus spectrophotometer. Melting points were

measured with an Electrothermal 9100 apparatus. All the reactions are monitored by thin layer chromatography (TLC), which was performed on silica-gel Poly Gram SIL G/UV 254 plates.

**General procedure for the synthesis of 3-(2'-benzothiazolyl)-2,3-dihydroquinazolin-4(1H)-one derivatives**

A mixture of an aromatic aldehyde **1** (1.0 mmol), 2-aminobenzothiazole **2** (1.0 mmol), isatoic anhydride **3** (1.0 mmol) and vitamin B12 (catalytic amount) in H2O:EtOH (3:1) was stirred at room temperature for appropriate time . The progress of the reaction was monitored by TLC. After completion of the reaction, the mixture was filtered and washed with water for separation of the product. The crude product was recrystallized from ethanol to afford the pure 3-(2'-benzothiazolyl)-2,3-dihydroquinazolin-4(1H)-one derivatives. The desired pure products were characterized by comparison of their physical data (melting point, IR and 1H NMR) with those of known compounds in the literature [14-22].

**General procedure for the synthesis of 1-((benzo[d]thiazol-2-ylamino)(aryl)-methyl)naphthalen-2-ol derivatives**

A mixture of an aromatic aldehyde **1** (1.0 mmol), 2-aminobenzothiazole **2** (1.0 mmol), β naphthol **4** (1.0 mmol) and vitamin B12 (catalytic amount) was added to 4 mL of EtOH. Then, the reaction mixture was stirred under room temperature for appropriate time. The progress of the reaction was monitored by TLC. After completion of the reaction, The mixture was filtered and then washed with water for separation of the product. The crude product was recrystallized from ethanol to afford the pure 1-((benzo[d]thiazol-2-ylamino)(aryl)-methyl)naphthalen-2-ol derivatives. The desired pure products were characterized by comparison of their physical data (melting points, IR and 1H NMR) with those of known compounds in the literature [23-24].

**General procedure for the synthesis of 4H-pyrimido(2,1-b](1,3]benzothiazoles.**

A mixture of an aldehyde **1** (1.0 mmol), 2-aminobenzothiazole **2** (1.0 mmol), ethyl acetoacetate **5** (1.0 mmol) and vitamin B12 (catalytic amount) in H2O:EtOH (1:1), was stirred at room temperature. The progress of the reaction was monitored by TLC. After completion of the reaction, The mixture was filtered, washed with water for separation of product. The crude product was recrystallized from ethanol to afford the pure 4H-pyrimido [2,1-b][1,3]benzothiazole derivatives. The desired pure products were characterized by comparison of their physical data (melting points, IR and 1H NMR) with those of known compounds in the literature [24-28].

**Some spectral data for selected products are represented below:**

***3-(benzo[d]thiazol-2-yl)-2-(4-chlorophenyl)-2,3-dihydroquinazolin-4(1H)-one (6b)***

IR (KBr, cm-1): 3334, 1635, 1609, 1506, 1405, 1251; 1HNMR (300 MHz, DMSO-d6): $\delta$ (ppm) = 6.81 (1H, t, 1CH *J= 7.6*), 6.96 (1H, d, 1CH *J= 7.5*), 7.30 (2H, d, 2CH *J=7.7*), 7.36 (1H, t, 1CH *J=7.5*), 7.38 (2H, d, 2CH *J=7.9*), 7.42 (1H, t, 1CH *J=7.1*), 7.46 (1H, t, 1CH *J=8.1*),7.54 (1H, d, 1CH *J=8.0*), 7.78 (1H, d, 1CH *J=7.9*), 7.79 (1H, d, 1CH *J=8.3*),8.06 (1H, d, 1CH *J=8.1*), 8.34 (1H, NH).

***3-(benzo[d]thiazol-2-yl)-2-(4-nitrophenyl)-2,3-dihydroquinazolin-4(1H)-one (6e)***

IR (KBr, cm-1): 3375, 1647, 1613, 1521; 1HNMR(300 MHz, DMSO-d6): $\delta$ (ppm) = 6.81 (1H, t, CH *J=7.6*), 7.00 (1H, d, CH *J=7.4*), 7.34(1H, t, CH *J=7.8*), 7.41 (1H, t, CH *J=7.2*), 7.44 (1H, t, 1CH *J=6.7*), 7.57 (2H, d, 2CH, *J=8.1*), 7.67 (1H, s,1CH), 7.77 (1H, d, 1CH, *J=7.8*), H7.81 (1H, d, 1CH, *J=8.4*), 8.05 (1H, d, 1CH, *J=7.9*), 8.15 (2H, d,2CH, *J=6.4*), 8.46 (1H, s, 1NH).

***3-(benzo[d]thiazol-2-yl)-2-(p-tolyl)-2,3-dihydroquinazolin-4(1H)-one (6f)***

IR (KBr, cm-1): 3342, 1630, 1612, 1503, 1432, 1251; 1HNMR (300 MHz, DMSO-*d6*): $\delta$ (ppm) = 2.17 (3H, s, CH3), 6.78 (1H,

t, CH, *J=7.1*), 6.93 (1H, d, CH, *J=8.1*), 7.08 (2H, d, 2CH, *J=7.5*), 7.17 (2H, d, 2CH, *J=6.9*), 7.35 (1H, t, CH, *J=8.2*),7.38(1H, t, CH, *J=7.7*), 7.45 (1H, t, CH, *J=7.4*), 7.51(1H, d, CH, *J=7.8*), 7.77 (1H, t, CH, *J=7.8*), 7.79 (1H, d, CH, *J=7.9*), 8.04 (1H, d, CH, *J=7.2*), 8.30 (1H, s, NH).

***3-(benzo[d]thiazol-2-yl)-2-(4-methoxyphenyl)-2,3-dihydroquinazolin-4(1H)-one (6g)***

IR (KBr, cm-1): 3347, 1635, 1608, 1508, 1433, 1304, 1230; 1HNMR (300 MHz, DMSO-d6): $\delta$ (ppm) = 3.63 (3H, s, OCH3, *J=4.2*), 6.78 (1H, t, CH, *J=6.1*), 6.83 (2H, d, 2CH, *J=6.5*), 6.94 (1H, d,CH, *J=7.1*),7.21 (2H, d, 2CH, *J=6.5*), 7.34 (1H, t, CH, *J=7.2*), 7.39 (1H, t, CH, *J=7.2*), 7.44(1H, t, CH, *J=7.5*), 7.52 (1H, br s, CH), 7.78(1H, d, CH, *J=7.7*), 7.81 (1H, d, CH, *J=7.9*), 8.04 (1H, d, CH, *J=7.4*), 8.32 (1H, s, NH).

***1-((Benzo[d]thiazol-2-ylamino)(4-chloro-phenyl)methyl)naphthalen-2-ol (7b)***

IR (KBr, cm-1): 3383, 1604, 1568, 1503, 1450 ;1H NMR (400 MHz, DMSO-d6): $\delta$ = 6.81 (1H, s, Ar), 6.89–6.91 (1H,m, Ar), 7.00–7.04 (1H, m, Ar), 7.19–7.30 (3H,m, Ar), 7.33 (1H, d, J = 5.2 Hz, Ar), 7.39 (2H, d, J = 8 Hz, Ar),7.46(1H, s, Ar), 7.67 (1H,d, J = 7.6 Hz, Ar), 7.80 (2H, t, J = 7.6 Hz,Ar), 8.00 (1H, d, J = 8 Hz, Ar),8.94 (1H,s, NH), 10.27 (1H,s, OH).

***1-((benzo[d]thiazol-2-ylamino)(4-bromophenyl)methyl)naphthalen-2-ol (7d)***

IR (KBr, cm-1): 3385, 1600, 1558, 1503, 1460 1H NMR (400 MHz, DMSO-d6): $\delta$ = 7.02 (1H, t, J = 7.6 Hz, Ar), 7.17–7.28 (6H,m, Ar), 7.38 (2H, d, J = 8 Hz, Ar), 7.46 (2H, d, J = 8.4 Hz, Ar), 7.67 (1H, d, J = 7.6 Hz, Ar), 7.79–7.82 (2H, m, Ar), 8.81 (1H, s, NH), 10.22 (1H,s, OH).

***1-((Benzo[d]thiazol-2-ylamino)(4-methoxy-phenyl)methyl)naphthalen-2-ol (7g)***

IR (KBr, cm-1): 3366, 1589, 1546, 1509, 1,451 cm-1; 1HNMR (300 MHz, DMSO-d6): d (ppm) = 3.68 (3H,s, OCH3), 6.82–7.81 (15H,m, 14Ar and CH–NH), 8.78 (1H, s, NH), 10.14 (1H, s, OH).

***1-((benzo[d]thiazol-2-ylamino)(3-bromophenyl)methyl)naphthalen-2-ol (7i)***

IR (KBr, cm-1): 3375, 1601, 1568, 1504, 1460 ,1H NMR (400 MHz, DMSO-d6): $\delta$ = 6.86 (1H,s, Ar), 7.00 (1H, t, J = 7.2 Hz,), 7.18–7.28 (5H, m, Ar),7.36–7.38 (3H,m, Ar), 7.65 (1H , d, J = 7.6 Hz), 7.75–7.80 (2H, m, Ar),7.99 (1H, s, Ar), 8.89 (1H,s, NH), 10.20 (1H, s, OH).

***2-Methyl-4-(2-chlorophenyl)-4H-pyrimido[2,1-b][1,3]benzothiazole-3-carboxylic acid ethyl ester (8c)***

IR (KBr, cm-1): 2935, 1680, 1596, 1516, 1383, 1182, 974, 827, 690; 1HNMR (300 MHz, $CDCl_3$): d (ppm) = 1.24 (3H, t, CH3), 2.44 (3H,s, CH3), 4.15 (2H,q, CH2), 6.74 (1H, s, CH), 7.08–7.16 (2H, m, Ar), 7.19–7.28 (2H,m, Ar), 7.39 (1H, d, Ar), 7.46 (2H,d, Ar), 7.62 (1H, d, Ar).

**Results and discussion**

For optimization the reaction conditions, a set of preliminary experiments with 2-aminobenzothiazole, benzaldehyde and isatoic anhydride or β-naphthol or ethylacetoacetate in different conditions were performed. The results obtained with the very least amount of catalyst at room temperature with high yields. Moreover, we tested the effects of two green solvents (H2O and EtOH), with various ratios and used alone . Among the screened solvent systems, (3:1) of H2O:EtOH for the 2,3-dihydroquinazolin-4(1H)-one, (4 mL) EtOH for the 4H-pyrimidobenzothiazole and (1:1) of H2O:EtOH for the 2-aminobenzothiazolomethylnaphthol was the solvent of choice. Since we wanted to present a green and environmentally benign protocol for this research we did not test organic solvents under these conditions.

Encouraged by the remarkable results obtained from above conditions, and in order to show the generality and scope of this protocol, the reaction were explored for the synthesis of a wide variety of substituted 3-(20-benzothiazolyl)-2,3-dihydroquinazolin-4(1H)-one, 1-((benzo[d]thiazol-2-ylamino)(aryl)-methyl)naphthalen-2-ol and 4H-pyrimido[2,1-

b][1,3]benzothiazoles using arylaldehydes, 2-aminobenzothiazole,isatoic anhydride or b-naphthol or ethyl acetoacetate. The results are summarized in Table 1.

**Table 1** Preparation of 3-(2'-benzothiazolyl)-2,3-dihydroquinazolin-4(1H)- one, 1-((benzo[d]thiazol-2-ylamino)(aryl)-methyl)naphthalen-2-ol and 4H-pyrimido [2,1-b][1,3]benzothiazole derivatives in the presence of vitamin B12 as biodegradable catalyst in green solvent at ambient conditions

| Enter | Aldehyde | Substrate | Product | Time (min) | Yeild (%) | Mp(Obs) (°C) | Mp(Lit) (°C) |
|---|---|---|---|---|---|---|---|
| 1 | 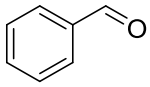 | 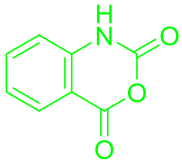 | 6a | 28 | 83 | 230-233 | 232-234[15] |
| 2 | 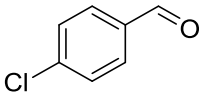 | 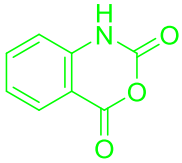 | 6b | 18 | 88 | 190-192 | 192-194[15] |
| 3 | 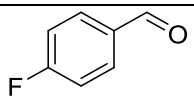 | 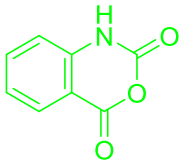 | 6c | 19 | 89 | 248-250 | 252-254[34] |
| 4 | 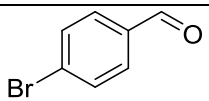 | 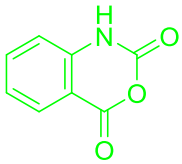 | 6d | 22 | 84 | 233-235 | 231-233[31] |
| 5 | 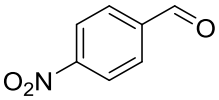 | 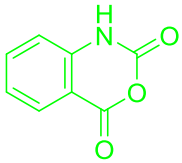 | 6e | 24 | 90 | 245-247 | 242-245[19] |

| | | | | | | | |
|---|---|---|---|---|---|---|---|
| 6 | 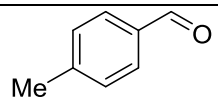 | 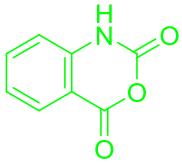 | 6f | 30 | 82 | 199-200 | 197-199[15] |
| 7 | 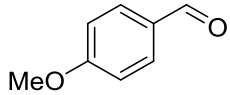 | 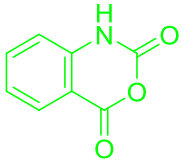 | 6g | 38 | 80 | 176-178 | 182-184[15] |
| 8 | 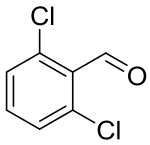 | 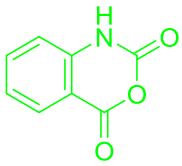 | 6h | 20 | 90 | 230-231 | 231-233[34] |
| 9 | 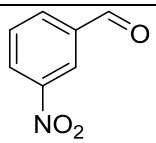 | 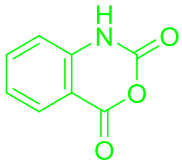 | 6i | 22 | 91 | 250-252 | 252-253[15] |
| 10 | 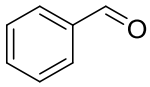 | 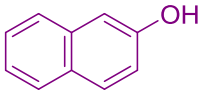 | 7a | 36 | 85 | 198-200 | 202-204[30] |
| 11 | 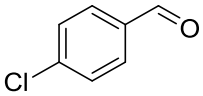 | 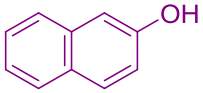 | 7b | 26 | 88 | 210-211 | 209-213[30] |
| 12 | 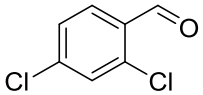 | 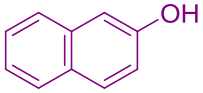 | 7c | 44 | 88 | 240-242 | 242[30] |
| 13 | 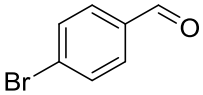 | 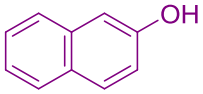 | 7d | 28 | 88 | 203-205 | 202-204[30] |
| 14 | 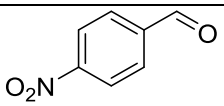 | 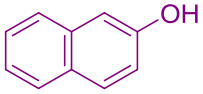 | 7e | 25 | 91 | 188-190 | 187-189[30] |

| | | | | | | | |
|---|---|---|---|---|---|---|---|
| 15 | 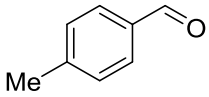 | 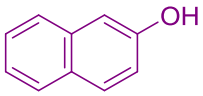 | 7f | 28 | 84 | 185-187 | 183-184[30] |
| 16 | 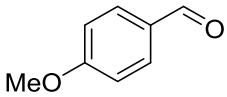 | 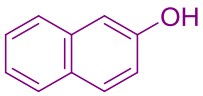 | 7g | 30 | 86 | 176-177 | 175-176[30] |
| 17 | 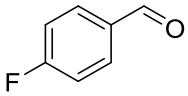 | 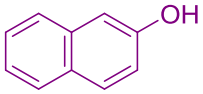 | 7h | 16 | 86 | 177-178 | 178-180[30] |
| 18 | 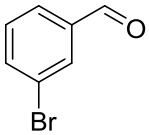 | 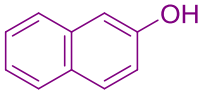 | 7i | 12 | 89 | 201-203 | 203-205[30] |
| 19 | 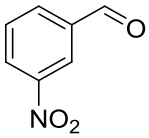 | 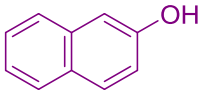 | 7j | 22 | 90 | 191-193 | 190-192[30] |
| 20 | 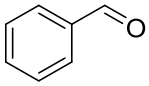 | 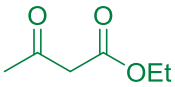 | 8a | 30 | 90 | 178-180 | 173-175[24] |
| 21 | 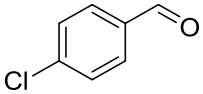 | 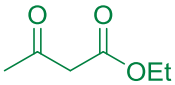 | 8b | 21 | 90 | 142-144 | 142-143[24] |
| 22 | 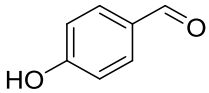 | 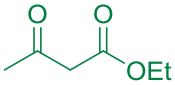 | 8c | 16 | 84 | 208-210 | 29-210[24] |
| 23 | 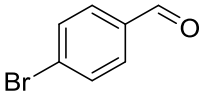 | 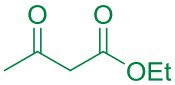 | 8d | 20 | 91 | 116-118 | 110-114[24] |
| 24 | 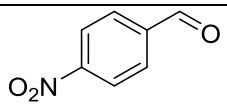 | 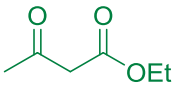 | 8e | 18 | 89 | 154-156 | 150-152[35] |
| 25 | 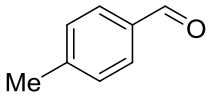 | 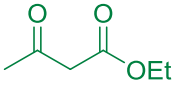 | | | | | |

| | | | | | | |
|---|---|---|---|---|---|---|
| | | 8f | 36 | 92 | 150-152 | 153-154[32] |
| 26 | 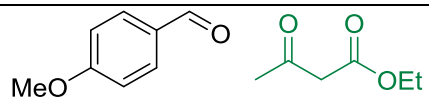 | 8g | 40 | 84 | 139-142 | 140-143[35] |

A suggested mechanism for this transformation is proposed in Scheme **2**. Reported in the literature [23,24], reaction of 2-naphthol with aldehydes in the presence of a catalyst is known to give ortho-quinone methides (o-QMs). The same o-QMs, generated in situ, have been reacted with 2-aminobenzothiazole via conjugate addition to form 1-(benzothiazolylamino)methyl-2-naphthols 4a–t. There is an alternative pathway, a Mannich-type reaction (Scheme 2).

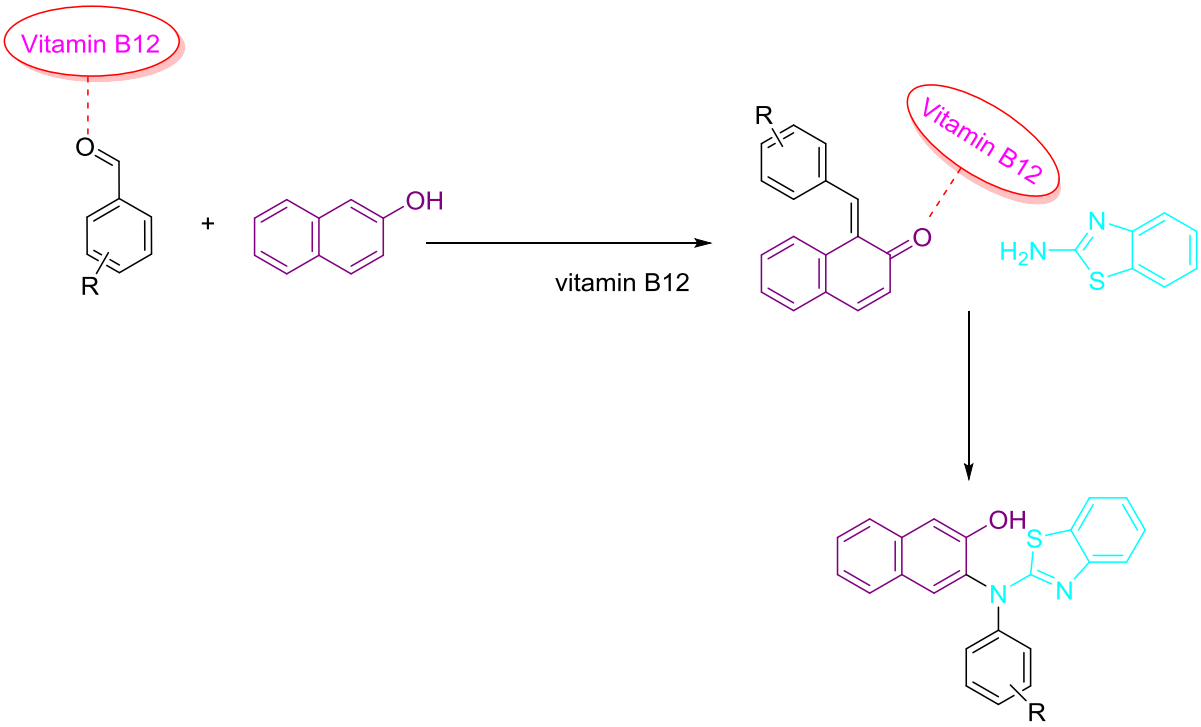

**Scheme 3. The suggested mechanism for the synthesis of 1-(benzothiazolylamino)methyl-2-naphthols based on o-QMs in the presence of vitamin B12 as catalyst**

## Conclusion

In summary, we report an eco-friendly and straightforward three-component, one-pot method for the synthesis of 2,3-dihydroquinazolin-4(1H)-one, 4H-pyrimidobenzothiazole and 2-aminobenzothiazolomethylnaphthol derivatives from the condensation between aryl aldehydes and 2-aminobenzothiazole with isatoic anhydride or β-naphthol or ethylacetoacetate derivatives in the presence of vitamin B12 as a highly effective and homogenous catalyst at ambient temperature. It is clear that vitamin B12 is an effective catalyst and provides a facility and green method to this synthesis. The catalyst shows environmentally friendly characters. Namely, it is inexpensive, clean, safe, nontoxic and easily obtained. Moreover, this method has several other advantages, including mild reaction conditions, higher yields, operational simplicity, clean and neutral reaction conditions, which makes it a useful and attractive process for the synthesis of a wide variety of biologically active compounds.

## References:

[1] R. Banerjee, *Wiley & Sons*, **1999**,
[2] D.A. Bernhard Krautler, Bernhard T. Golding, *Wiley-VCH*, **1998**,
[3] R. Scheffold, S. Abrecht, R. Orlinski, H.R. Ruf, P. Stamouli, O. Tinembart, L. Walder and C. Weymuth, *Pure and Applied Chemistry*, **1987**, *59*,
[4] Y. Hisaeda, T. Nishioka, Y. Inoue, K. Asada and T. Hayashi, *Coordination Chemistry Reviews*, **2000**, *198*, 21-37.
[5] A.R. Katritzky, D.O. Tymoshenko, D. Monteux, V. Vvedensky, G. Nikonov, C.B. Cooper and M. Deshpande, *The Journal of Organic Chemistry*, **2000**, *65*, 8059-8062.
[6] E.H. White, F. McCapra and G.F. Field, *Journal of the American Chemical Society*, **1963**, *85*, 337-343.
[7] C.G. Mortimer, G. Wells, J.P. Crochard, E.L. Stone, T.D. Bradshaw, M.F. Stevens and A.D. Westwell, *J Med Chem*, **2006**, *49*, 179-185.
[8] M.C. Van Zandt, M.L. Jones, D.E. Gunn, L.S. Geraci, J.H. Jones, D.R. Sawicki, J. Sredy, J.L. Jacot, A.T. Dicioccio, T. Petrova, A. Mitschler and A.D. Podjarny, *J Med Chem*, **2005**, *48*, 3141-3152.

[9] C. Rodriguez-Rodriguez, N. Sanchez de Groot, A. Rimola, A. Alvarez-Larena, V. Lloveras, J. Vidal-Gancedo, S. Ventura, J. Vendrell, M. Sodupe and P. Gonzalez-Duarte, *J Am Chem Soc*, **2009**, *131*, 1436-1451.
[10] S.T. Huang, I.J. Hsei and C. Chen, *Bioorganic & medicinal chemistry*, **2006**, *14*, 6106-6119.
[11] C.D. RD Naik, KR Desai, *Oriental Journal of Chemistry*, **2000**, *16*, 159-160.
[12] D.O. H. Moller, H. Hoeffkes, Ger. Offen, *Chem. Abstr*, **2001**, *134*, 168045c.
[13] H.G. U. Heinemann, P. Gerdes, B. Krueger, F. Maurer, M. Vaupel, A. Mauler-Machnik, U.Wachendorff-Neumann, G. Haenssler, K. Kuck, C. Erdelen, P. Loesel, Ger, **2017**,
[14] J. Zhang, D. Ren, Y. Ma, W. Wang and H. Wu, *Tetrahedron*, **2014**, *70*, 5274-5282.
[15] L. Wu, *E-Journal of Chemistry*, **2012**, *9*, 739-743.
[16] P. Salehi, M. Dabiri, M. Baghbanzadeh and M. Bahramnejad, *Synthetic Communications*, **2006**, *36*, 2287-2292.
[17] A. Shaabani, A. Rahmati and J.M. Rad, *Comptes Rendus Chimie*, **2008**, *11*, 759-764.
[18] M. Dabiri, P. Salehi, M. Baghbanzadeh, M.A. Zolfigol, M. Agheb and S. Heydari, *Catalysis Communications*, **2008**, *9*, 785-788.
[19] J. Chen, D. Wu, F. He, M. Liu, H. Wu, J. Ding and W. Su, *Tetrahedron Letters*, **2008**, *49*, 3814-3818.
[20] M. Wang, T.T. Zhang, Y. Liang and J.J. Gao, *Chinese Chemical Letters*, **2011**, *22*, 1423-1426.
[21] I. Mohammadpoor-Baltork, A.R. Khosropour, M. Moghadam, S. Tangestaninejad, V. Mirkhani, S. Baghersad and A. Mirjafari, *Comptes Rendus Chimie*, **2011**, *14*, 944-952.
[22] S. Allameh, M.M. Heravi, M.M. Hashemi and F.F. Bamoharram, *Chinese Chemical Letters*, **2011**, *22*, 131-134.
[23] A. Shaabani, A. Rahmati and E. Farhangi, *Tetrahedron Letters*, **2007**, *48*, 7291-7294.
[24] P.K. Sahu, P.K. Sahu, J. Lal, D. Thavaselvam and D.D. Agarwal, *Medicinal Chemistry Research*, **2011**, *21*, 3826-3834.
[25] L. Nagarapu, H.K. Gaikwad, J.D. Palem, R. Venkatesh, R. Bantu and B. Sridhar, *Synthetic Communications*, **2013**, *43*, 93-104.
[26] P.K. Sahu, P.K. Sahu, R. Jain, R. Yadav and D.D. Agarwal, *Catalysis Science & Technology*, **2012**, *2*, 2465.
[27] G.B.D. Rao, B.N. Acharya, S.K. Verma and M.P. Kaushik, *Tetrahedron Letters*, **2011**, *52*, 809-812.
[28] A.B. Atar and Y.T. Jeong, *Molecular diversity*, **2014**, *18*, 389-401.
[29] M.T. Maghsoodlou, S.M. Habibi-Khorassani, A. Moradi, N. Hazeri, A. Davodi and S.S. Sajadikhah, *Tetrahedron*, **2011**, *67*, 8492-8495.
[30] B. Adrom, M.T. Maghsoodlou, N. Hazeri and M. Lashkari, *Research on Chemical Intermediates*, **2014**,
[31] N. Hazeri, S.S. Sajadikhah, M.T. Maghsoodlou, M. Norouzi, M. Moein and S. Mohamadian-Souri, *Journal of Chemical Research*, **2013**, *37*, 550-552.
[32] A. Moradi, R. Heydari and M.T. Maghsoodlou, *Research on Chemical Intermediates*, **2014**,
[33] S.S. Sajadikhah and M.T. Maghsoodlou, *RSC Adv.*, **2014**, *4*, 43454-43459.
[34] J.M. Khurana and S. Kumar, *Green Chemistry Letters and Reviews*, **2011**, *4*, 321-325.
[35] A. Shaabani, A. Rahmati and S. Naderi, *Bioorganic & medicinal chemistry letters*, **2005**, *15*, 5553-5557.

## Graphical Abstract

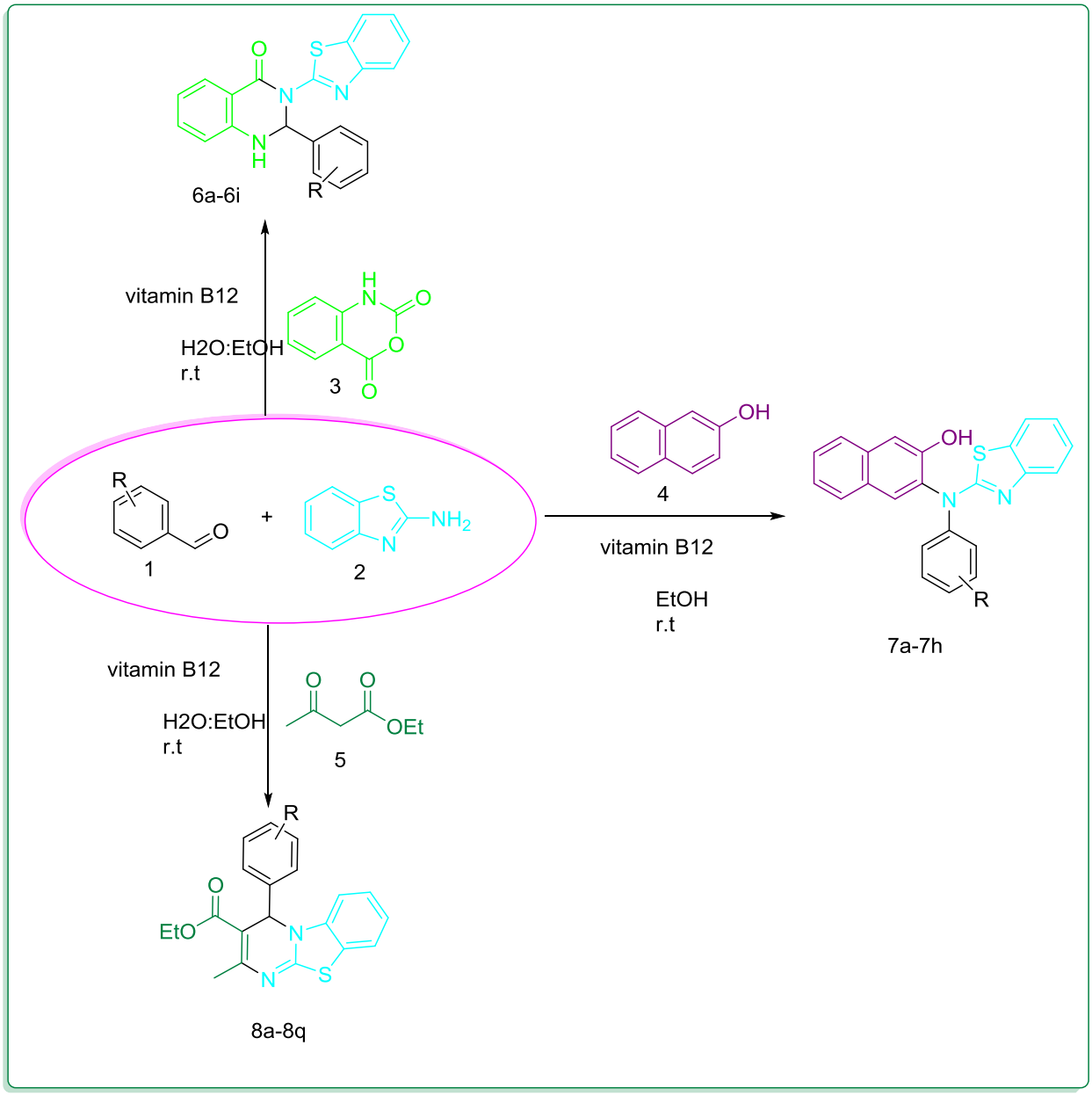

# Efficient, one-pot synthesis of xanthene derivatives using $Fe_3O_4$@$SiO_2$-Propyl-Pip-$SO_3H.HSO_4$ as a magnetically recyclable catalyst under solvent-free conditions

**Monireh Pourghasemi Lati,[a] Farhad Shirini,[b,*] Mokhtar Alinia-Asli,[a,*] and Mohammad Ali Rezvani[a]**

[a]*Department of Chemistry, College of Science, University of Zanjan, Zanjan, zip code 45195-313, Iran*

[b]*Department of Chemistry, College of Science, University of Guilan, Rasht, zip code 41335, I. R. Iran*

*Corresponding author

*E-mail: *shirini@guilan.ac.ir (F. Shirini)*
*m_aliniaaslir@znu.ac.ir (M. Alinia)*

**Abstract**

An efficient and green method has been introduced for the synthesis of xanthene derivatives through a one-pot condensation of aldehydes and dimedone in the presence of $Fe_3O_4$@$SiO_2$-Propyl-Pip-$SO_3H.HSO_4$ as a magnetically recyclable catalyst under solvent-free conditions with excellent yields. The catalyst is easily prepared and characterized using various techniques such as Fourier transform infrared (FT-IR), X-ray powder diffraction (XRD), Thermogravimetric analysis (TGA), Energy-dispersive X-ray spectroscopy (EDX) and Scanning electron microscopy (SEM). The catalyst was easily isolated from the reaction mixture by magnetic decantation using an external magnet and reused at least six times without significant degradation in the activity.

**Keywords**: Magnetic nanoparticles, Reusable catalyst, 1, 8-Dioxo-octahydro xanthenes, Aldehyde.

## Introduction

The synthesis of xanthenes has achieved significant attention in organic synthesis because of their wide range of remedial and biological properties, such as anti-inflammatory [1], antiviral activity [2], bactericide activity [3], photodynamic therapy activity [4], leuco-dyes [5], in laser technology [6] and p*H*-sensitive fluorescent materials for the visualization of biomolecular assemblies [7]. Thus, a broad utility range has made xanthenes principal synthetic candidates.

1, 8-Dioxo-octahydroxanthene derivatives are one of the important types of xanthenes that could be easily prepared from the reaction of aromatic aldehydes with dimedone or cyclohexadione. Various catalysts such as $SbCl_3/SiO_2$, $SiO_2$-R-$SO_3H$, MCM-41-$SO_3H$, $ZnCl_2$, ethylenediamine diacetate (EDDA), $SmCl_3$, SDS, CsF and heterogeneous catalysts like ZnO, $Yb(OTf)_3$-$SiO_2$, $FeCl_3.6H_2O$/TMSCl/[bmim][$BF_4$], $HClO_4$-$SiO_2$, L-Lysine Amberlyst-15 and trichloroisocyanuric acid (TCCA) have been reported by various authors [8-21].

However, these methods suffer from one or more disadvantages such as: long reaction times, low yields, the use of toxic solvents, requirement of excess of catalysts and harsh reaction conditions.

Magnetic nanoparticles (MNPs) are reagents with a wide range of usage in biomedicine/biotechnology [22], magnetic resonance imaging (MRI) [23], hyperthermia [24], fluid transport [25], drug delivery [26], environmental remediation [27], and catalysis [28, 29].

Magnetic nanoparticles (MNPs) are a highly valuable substrate for the attachment of homogeneous inorganic and organic containing catalysts.

In recent years supported-heterogeneous catalysts play a basic role in the development of modern organic synthesis [30]. magnetic supported catalysts have advantages over conventional ones, inexpensiveness, ease of preparation, including higher surface activity, and most importantly ease of separation from the reaction mixture employing an external magnet [31].

On the basis of this report we anticipated that $Fe_3O_4$@$SiO_2$-Propyl-Pip-$SO_3H.HSO_4$ can be used as an efficient solid acid catalyst for the promotion of the reactions which need the use of an acidic catalyst to speed-up. So we were interested to investigate the applicability of this reagent in the promotion of the synthesis of 1, 8-dioxo-octahydroxanthenes (Scheme 1).

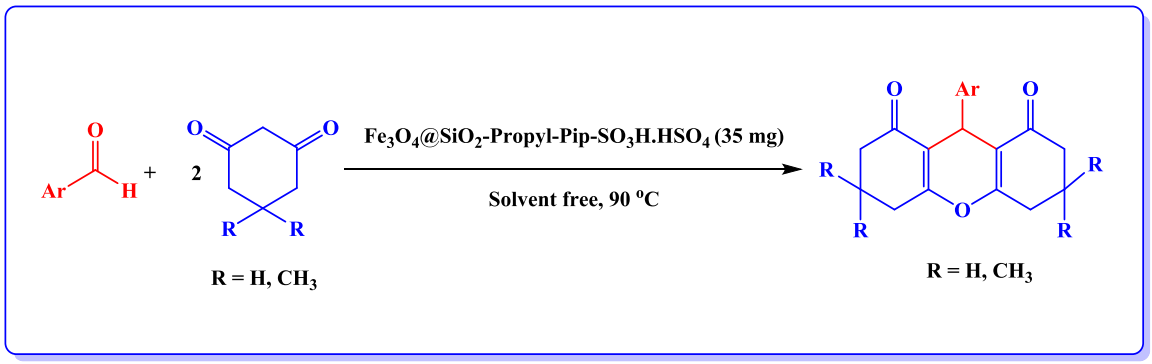


**Scheme 1.** Synthesis of 1, 8-dioxo-octahydro xanthenes derivatives catalyzed by $Fe_3O_4$@$SiO_2$-Propyl-Pip-$SO_3H.HSO_4$.

## Experimental

### *Material*

All chemicals, including iron (II) chloride tetrahydrate (99 %), iron (III) chloride hexahydrate (98 %) and aldehyde derivatives were purchased from Merck or Fluka Companies and were used without further purification. Water and other solvents were distilled before use. Yields refer to isolated products. The products were characterized by their physical constants, comparison with authentic samples and FT-IR, $^{1}H$ NMR and $^{13}C$ NMR spectroscopyies. The purity determination of the substrates and reaction monitoring were accomplished by TLC on silica-gel Polygram SILG/UV 254 plates.

### *Instrumentation*

The FT-IR spectra were run on a VERTEX 70 Brucker company (Germany). Thermogravimetric analyses (TGA) were performed on TG/DTA6300 All-Nanotechnology Company (Japan). Samples were heated from 25 to 700 °C at ramp 10 °C/min under $N_2$ atmosphere. Scanning election microphotographs (SEM) were obtained on a SEM-Philips XL30. Wide-angle X-ray diffraction (XRD) measurements were performed at room temperature on a Siemens D-500 X-ray diffractometer (Germany), using Ni-filtered Co-Kα radiation (λ=0.15418 nm). The surface morphologies were characterized by atomic force microscope (AFM, Ara nanoscope, Iran).

### *Preparation of 4-(4-propylpiperazine-1-yl)butane-1-sulfonic acid modified silica-coated magnetic nanoparticles ($Fe_3O_4$@$SiO_2$-Propyl-Pip-$SO_3H.HSO_4$)*[31]*:*

At first the magnetite ($Fe_3O_4$) nanoparticles in approximately 9-11 nm size were synthesized by a reported chemical co-precipitation technique [32]. In continue, the prepared $Fe_3O_4$-MNPs (4 g) were dispersed in a mixture of deionized water (48 mL) and ethanol (180 mL) by ultrasonication for 30 minutes. Subsequently, $NH_3.H_2O$ (4.0 mL, 25 %) and tetraethyl orthosilicate (TEOS, 2.4 mL) were charged to the reaction dish. After stirring at room temperature for 12 h, the silica-coated nanoparticles ($Fe_3O_4$@$SiO_2$) were collected by a permanent magnet followed by washing three times with EtOH and diethyl ether and dried at 40 °C in vacuum for 24 h.

Then the obtained brown precipitate (3.0 g) in dry toluene (40 mL) was sonicated for 30 min. After this time, 3-chloropropyl trimethoxysilane (1.0 mL) was added to the dispersed $Fe_3O_4$@$SiO_2$ in toluene and slowly heated to 105 °C. The reaction mixture was stirred at this temperature for 24 h. The residue was separated by an external magnet and washed three times with diethyl ether and dichloromethane and dried at 40 °C in vacuum for 24 h. After this step, piperazine (2.83 g) was added to a magnetically stirred mixture of the prepared $Fe_3O_4$@$SiO_2$-Propyl-Cl (2.78 g) in dry toluene (40 mL), and the mixture was stirred at room temperature for 36 h. The resulting solid material was separated by an external magnet, washed with diethyl ether and dichloromethane, and dried at 40 °C in vacuum to afford $Fe_3O_4$@$SiO_2$-Propyl-Pip MNPs.

In continue, the sulfonation of the obtained magnetic nanoparticales was executed using the reaction of $Fe_3O_4$@$SiO_2$-Propyl-Pip MNPs with 1,4-butane sultone. For this purpose, $Fe_3O_4$@$SiO_2$-Propyl-Pip MNPs (0.5 g) and 1,4-butane sultone (1.2 mL) were suspended in dry toluene (40 mL) and the colloidal solution was refluxed for 48 h, followed by instruction with one equivalent $H_2SO_4$ (0.62 mL) to yield the magnetically retrievable reagent ($Fe_3O_4$@$SiO_2$-Propyl-Pip-$SO_3H.HSO_4$) and the separation was repeated like last steps (Scheme 1).

Experiment should start as a continuation to introduction on the same page. All-

important materials used along with their source shall be mentioned. The main methods used shall be briefly described, with references. New methods or substantially modified methods may be described in sufficient detail. The statistical method and the level of significance chosen shall be clearly stated.

***General procedure for the synthesis of 1, 8-dioxo-octahydro xanthene derivatives***

A mixture of aldehyde (1 mmol), dimedone or cyclohexadione (2 mmol) and $Fe_3O_4$@$SiO_2$-Propyl-Pip-$SO_3H.HSO_4$ (35 mg) under solvent free condition was stirred at 90 °C for the appropriate time. After completion of the reaction, hot ethanol (2 mL) was added and the mixture, then the catalyst was separated by an external magnet from aqueous ethanol. The obtained products were characterized by FT-IR, $^1$H NMR, $^{13}$C NMR and by comparison of their melting points with the reported ones.

## Results and discussion

Herein and in continuation of these studies we wish to report the preparation of $Fe_3O_4$@$SiO_2$-Propyl-Pip-$SO_3H.HSO_4$ and its applicability, as a novel and efficient catalyst in the promotion of the synthesis of 1, 8-dioxo-octahydroxanthenes under mild conditions.

To optimize the reaction conditions, the reaction of 4-chlorobenzaldehyde (1 mmol) with dimedone (2 mmol) was studied in different solvents and under solvent-free conditions at different temperatures using various amount of the catalyst (Table 1). We tested different solvents including polar or non-polar ones and selected solvent-free conditions at 90 °C. This condition gave the best conversion and highest yield. The results are shown in Scheme. 1.

To recognize the efficiency of $Fe_3O_4$@$SiO_2$-Propyl-Pip-$SO_3H.HSO_4$ in the preparation of 1, 8-dioxo-octahydro xanthene derivatives, various aromatic aldehydes were reacted with dimedone or 1, 3-cyclohexanedione under the optimal reaction conditions (Table 2).

**Table 1.** Optimization of the reaction conditions for the synthesis of 1, 8-dioxo-octahydro xanthene derivatives using $Fe_3O_4$@$SiO_2$-Propyl-Pip-$SO_3H.HSO_4$.[a]

| Entry | Catalyst (mg) | Solvent | Temp. (ºC) | Time (min) | Conversion (%) |
|---|---|---|---|---|---|
| 1 | 35 | $H_2O$ | r.t. | 60 | _b |
| 2 | 35 | $H_2O$ | reflux | 60 | _b |
| 3 | 35 | EtOH | r.t. | 60 | _b |
| 4 | 35 | EtOH | reflux | 60 | _b |
| 5 | 35 | $CH_3CN$ | r.t. | 60 | _b |
| 6 | 35 | ----- | r.t. | 60 | _b |
| 7 | 25 | ----- | 90 | 7 | 100 |
| 8 | 45 | ----- | 90 | 3 | 100 |
| **9** | **35** | **-----** | **90** | **3** | **100** |

[a] Reaction conditions: 4-chlorobenzaldehyde (1 mmol), dimedone (2 mmol) and $Fe_3O_4$@$SiO_2$-Propyl-Pip-$SO_3H.HSO_4$ under different condition.

[b] The reaction is not completed.

**Table 2**. Preparation of 1, 8-dioxo-octahydro xanthene derivatives using $Fe_3O_4$@$SiO_2$-Propyl-Pip-$SO_3H.HSO_4$ as the catalyst. [a]

| Entry | Aldehyde | Product | Time (min) | Yield (%)[b] | M.p. (ºC) | |
|---|---|---|---|---|---|---|
| | | | | | Found | Reported [Ref.] |
| 1 | 4-$ClC_6H_4CHO$ | 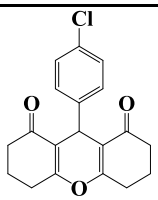 | 3 | 97 | 285-287 | 282-285 [33] |
| 2 | $C_6H_4CHO$ | 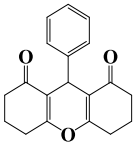 | 5 | 90 | 200-202 | 201-203 [34] |
| 3 | 2-$ClC_6H_4CHO$ | 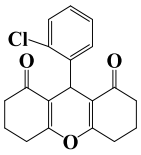 | 7 | 95 | 246-249 | 250-252 [33] |
| 4 | 4-$BrC_6H_4CHO$ | 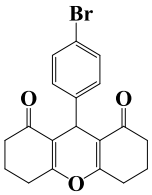 | 7 | 88 | 286-288 | 284-285 [35] |
| 5 | 4-$NO_2C_6H_4CHO$ | 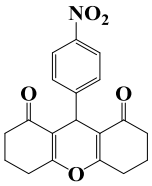 | 10 | 90 | 258-260 | 262–264 [35] |
| 6 | 3-$NO_2C_6H_4CHO$ | 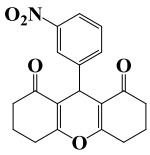 | 12 | 90 | 280-282 | 285-287 [33] |
| 7 | 2-$NO_2C_6H_4CHO$ | 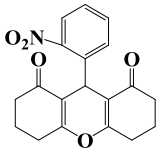 | 24 | 85 | 236-239 | 238-240 [33] |

| | | | | | | |
|---|---|---|---|---|---|---|
| 8 | 4-$OHC_6H_4CHO$ | 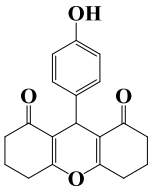 | 24 | 88 | 249-251 | 245-246 [35] |
| 9 | $C_6H_4CHO$ | 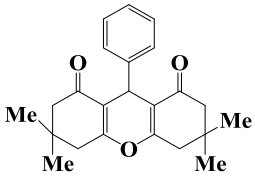 | 5 | 90 | 197-200 | 206-208 [33] |
| 10 | 4-$ClC_6H_4CHO$ | 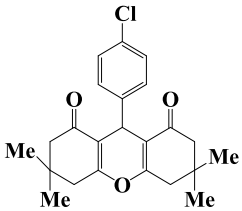 | 5 | 95 | 220-222 | 225-228 [35] |
| 11 | 2-$ClC_6H_4CHO$ | 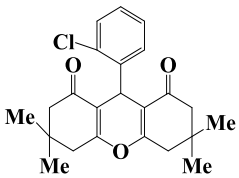 | 7 | 87 | 230-233 | 228-230 [36] |
| 12 | 4-$NO_2C_6H_4CHO$ | 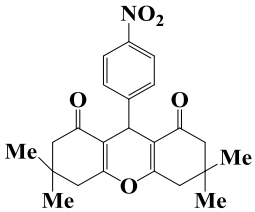 | 8 | 89 | 225-228 | 220-223 [33] |
| 13 | 3-$NO_2C_6H_4CHO$ | 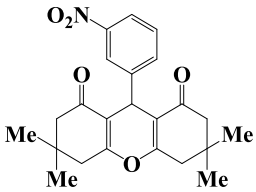 | 10 | 83 | 160-164 | 168-170 [37] |
| 14 | 4-$MeOC_6H_4CHO$ | 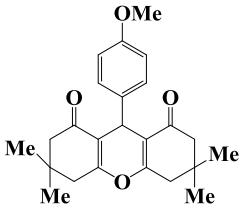 | 10 | 90 | 250-252 | 243-245 [36] |

| | | | | | | |
|---|---|---|---|---|---|---|
| 15 | 2-Naphtaldehyde | 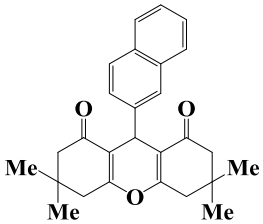 | 18 | 89 | 197-200 | 194-196 [36] |
| 16 | 4-$CHOC_6H_4CHO$ | 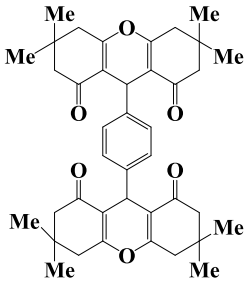 | 30 | 87 | >300 | >300 [33] |

[a]Isolated yield.

A plausible mechanism for the synthesis of 1, 8-dioxo-octahydro xanthene derivatives catalyzed by $Fe_3O_4$@$SiO_2$-Propyl-Pip-$SO_3H.HSO_4$ is shown in Scheme 2.

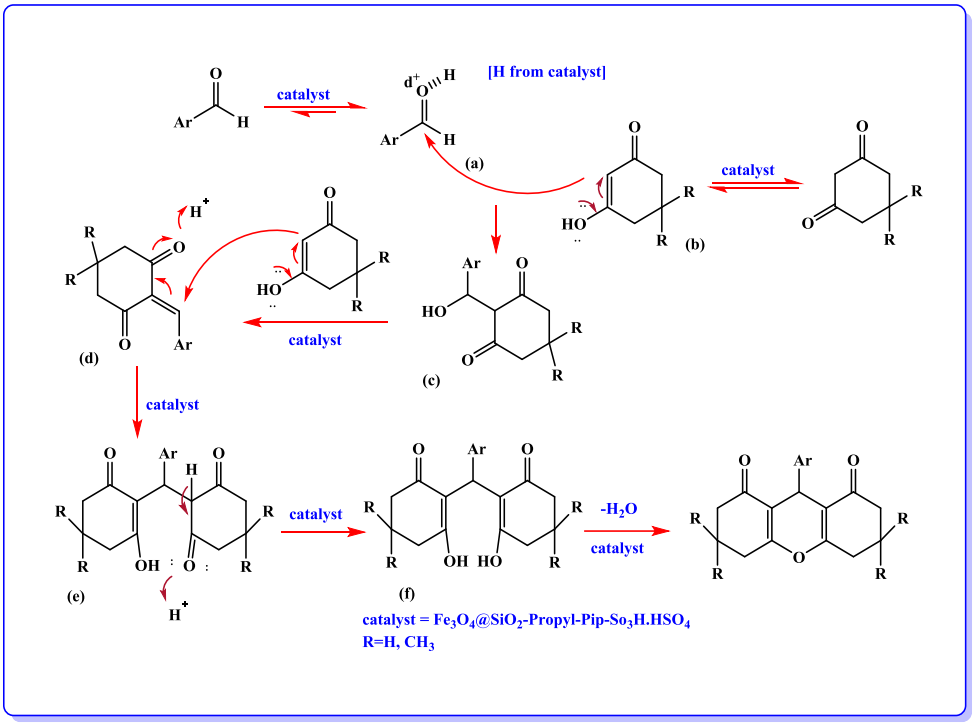


**Scheme 2.** Proposed mechanism for the synthesis of 1, 8-dioxo-octahydro xanthenes catalyzed by $Fe_3O_4$@$SiO_2$-Propyl-Pip-$SO_3H.HSO_4$.

The reusability of this catalyst is examined by the reaction of 4-chlorobenzaldehyde with dimedone under the optimized reaction conditions. This procedure was repeated six times and in each time with the least change in the reaction time and yield (Fig. 1).

In order to assess the efficiency of this methodology, the obtained result from the reaction of 4-chlorobenzaldehyde with dimedone have been compared with those of the previously reported methods using inorganic or organic catalysts (Tables 3).

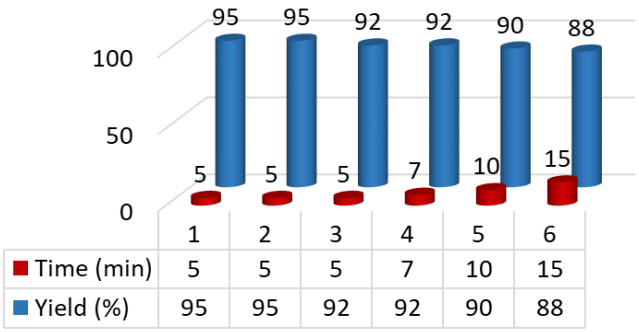


**Fig. 1**. Separation of $Fe_3O_4$@$SiO_2$-Propyl-Pip-$SO_3H.HSO_4$. by an external magnetic field.

**Table 3**. Comparison of the results obtained in the presence of $Fe_3O_4$@$SiO_2$-Propyl-Pip-$SO_3H.HSO_4$ with other catalysts reported in the literature in the synthesis of 9-(4-chlorophenyl)-3,3,6,6-tetramethyl-3,4,5,6,7,9-hexahydro-1*H*-xanthene-1,8(2*H*)-dione (Table 2, entry 10).

| Entry | Catalyst/Conditions | Time (min) | Yield(%)[a] | Ref. |
|---|---|---|---|---|
| 1 | DBSA (0.1 mol)/ $H_2O$/ reflux | 360 | 92 | [38] |
| 2 | ([Hmim]TFA) (0.0005 mol)/ solvent free/ 80 °C | 150 | 93 | [39] |
| 3 | ([TMPSA][$HSO_4$]) (0.0005 mol)/ solvent free/ 100 °C | 60 | 92 | [40] |
| 4 | $\beta$- cyclodextrin (0.001 mol)/ $H_2O$ / 60 °C | 720 | 90 | [35] |
| 5 | W-ZnO (0.56 mol)/ EtOH/ 80 °C | 15 | 98 | [41] |
| 6 | $Fe_3O_4$@$SiO_2$-Propyl-Pip-$SO_3H.HSO_4$ (35 mg)/ solvent free / 90 °C | 5 | 95 | This work |

[a] Isolated yields.

## Conclusion

It should stem directly from the data presented and no extra material should be introduced. It should be consistent with the introduction in fulfilling any promise made therein to the reader. The conclusion should also include negative results and recommendations based on the results. In such cases where the study has led to clear-cut finding, it is preferable to give the conclusions in the form of a series of numbered points.

## Acknowledgments

All acknowledgments should be typed in one paragraph directly preceding the reference section.

## References

[1] J. M. Jamison, K. Krabill, A. Hatwalkar, *Cell Biol. Int. Rep*, **1990**, *14*, 1075.

[2] R. M. Ion, D. Frackowiak, K. Wiktorowicz, *Acta Biochim*, **1998**, *45*, 833.

[3] T. Hideu, *Chem. Abstr.*, **1981**, *95*, 80922b.

[4] J. P. Poupelin, G. Saint-Ruf, O. Foussard-Blanpin, G. Narcisse, G. Uchida-Emouf, R. Lacroix, *Eur. J. Med. Chem*, **1978**, *13*, 67.

[5] Y. Kitahara, K. Tanaka, *Chem. Commun*, **2002**, 932.

[6] M. Ahmad, T. A. King, D. K. Ko, B. H. Cha, J. Lee, *J. Phys. D. Appl. Phys*, **2002**, *35*, 1473.

[7] C. G. Knight, T. Stephens, *J. Biochem*, **1989**, *258*, 683.

[8] Z. H. Zhang, Y. H. Liu, *Catal. Commun*, **2008**, *9*, 1715.

[9] G. H. Mahdavinia, M. A. Bigdeli, Y. S. Hayeniaz, *Chin. Chem. Lett*, **2009**, *20*, 539.

[10] S. Rostamizadeh, A. M. Amani, G. H. Mahdavinia, G. Amiri, H. Sepehrian, *Ultrason. Sonochem*, **2010**, *17*, 306.
[11] D. H. Jung, Y. R. Lee, S. H. Kim, W. S. Lyoo, *Bull. Korean Chem. Soc*, **2009**, 30,1989.
[12] A. Ilangovan, S. Malayappasamy, S. Muralidharan, S. Maruthamuthu, *Chem. Cent. J*, **2011**, *5*, 81.
[13] L. L. Bin, J. T. Shou, H. L. Sha, L. Meng, Q. Na, L. T. Shuang, *E-J. Chem*, **2006**, *3*, 117.
[14] K. P. Nandre, V. S. Patil, S. V. Bhosale, *Chin. Chem. Lett*, **2011**, *22*, 777.
[15] M. T. Maghsoodlou, S. M. H. Khorassani, Z. Shahkarami, N. Maleki, M. Rostamizadeh, *Chin. Chem. Lett*, **2010**, *21*, 686.
[16] V. K. Rao, M. M. Kumar, A. Kumar, *Indian J. chem*, **2011**, *50*, 1128.
[17] Fan, X. Sen, Li, Y. Z. Zhang, X. Y. Hu, X. Y. Wang, J. Ji, *Chin. J. Org. Chem*, **2005**, *25*, 1482.
[18] S. Kantevari, R. Bantu, L. Nagarapu, *J. Mol. Catal. A: Chem*, **2007**, *269*, 53.
[19] Y. Zhang, C. Sun, J. Liang, S. Zhicai, *Chin. J. Chem.* **2010**, *28*, 2255.
[20] B. Das, P. Thirupathi, I. Mahender, V. Saidi Reddy, Y. Koteswara Rao, *J. Mol. Catal. A: Chem*, **2006**, *247*, 233.
[21] M. A. Bigdeli, F. Nemati, G. H. Mahdavinia, H. Doostmohammadi, *Chin. Chem. Lett*, **2009**, *20*, 1275.
[22] U. C. Rajesh, D. S. Rawat, *RSC Adv*, **2014**, *4*, 41323.
[23] M. F. Casula, A. Corrias, P. Arosio, A. Lascialfari, T. Sen, P. Floris, I. J. Bruce, *J. Colloid Interface Sci*, **2011**, *357*, 50.
[24] S. Mornet, S. Vasseur, F. Grasset, E. Duguet, *J. Mater. Chem*, **2004**, *14*, 2161.
[25] A. H. Latham, M. E. Williams, *Acc. Chem. Res*, **2008**, *41*, 411.
[26] J. D. G. Duran, J. L. Arias, V. Gallardo, A. V. Delgado, *J. Pharm. Sci*, **2008**, *97*, 2948.
[27] A. Lu, W. Schmidt, N. Matoussevitch, H. Bonnemann, B. Spliethoff, B. Tesche, E. Bill, W. Kiefer, F. Schuth, *Angew. Chem*, **2004**, *116*, 4403.
[28] S. Rezayati, M. Torabi Jafroudi, E. Rezaee Nezhad, R. Hajinasiri, S. Abbaspour, *Res. Chem. Intermed*, **2016**, *42*, 5887.
[29] S. Z. Hejazi, A. F. Shojaei, K. Tabatabaeian, F. Shirini, *J. Serb. Chem. Soc*, **2015**, 80, 971.
[30] M. B. Gawande, A. K. Rathi, I. D. Nogueira, R. S. Varma, P. S. Branco, *Green Chem*, **2013**, 15, 1895.
[31] M. Pourghasemi Lati, F. Shirini, M. Alinia‐Asli, M. A. Rezvani, *J. Iran. Chem. Soc*, doi.org/10.1007/s13738-018-1364-5
[32] Z. Cheng, Z. Gao, W. Maa, Q. Sun, B. Wang, X. Wang, *Chem. Eng. J*, **2012**, *209*, 451.
[33] F. Shirini, Gh. H. Imanzadeh, M. Abedini, M. A. Dokhte-Ghaziani, P. Gh. Ghasemabadi, M. S. Langroodi, *Iran. J. Catal*, **2012**, *2*, 115.
[34] A. John, P. J. P. Yadav, S. Palaniappan, *J. Mol. Catal. A: Chem*, **2006**, *248*, 121.
[35] S. Kokkirala, N. M. Sabbavarapu, V. D. N. Yadavalli, *Eur. J. Chem.* **2011**, *2*, 272.
[36] Gh. H. Mahdavinia, *J. Iran. Chem. Res.* **2008**, *1*, 11.
[37] A. P. Chavan, *J. Korean Chem. Soc.* **2009**, *53*, 415.
[38] T. Sh. Jin, J. Sh. Zhang, J. Xiao, Ch. A. Q. Wang, T. Sh. Li, *Synlett*, **2004**, 0866.
[39] M. Dabiri, M. Baghbanzadeh, E. Arzroomchilar, *Catal. Commun.* **2008**, *9*, 939.
[40] D. Fang, K. Gong, Z. L. Liu, *Catal. Lett.* **2009**, *127*, 291.
[41] F. Shaabani Arbosara, F. Shirini, M. Abedini, H. Fallah Moafi, *J nanostruct chem*, **2015**, *5*, 55.

## Graphical Abstract

Efficient, one-pot synthesis of xanthene derivatives using $Fe_3O_4$@$SiO_2$-Propyl-Pip-$SO_3H.HSO_4$ as a magnetically recyclable catalyst under solvent-free conditions

Monireh Pourghasemi Lati,[a] Farhad Shirini,[b,*] Mokhtar Alinia-Asli,[a,*] and Mohammad Ali Rezvani[a]

[a]*Department of Chemistry, College of Science, University of Zanjan, Zanjan, zip code 45195-313, Iran*

[b]*Department of Chemistry, College of Science, University of Guilan, Rasht, zip code 41335, I. R. Iran*

*Corresponding author

*E-mail: *shirini@guilan.ac.ir (F. Shirini) m_aliniaaslir@znu.ac.ir (M. Alinia)*

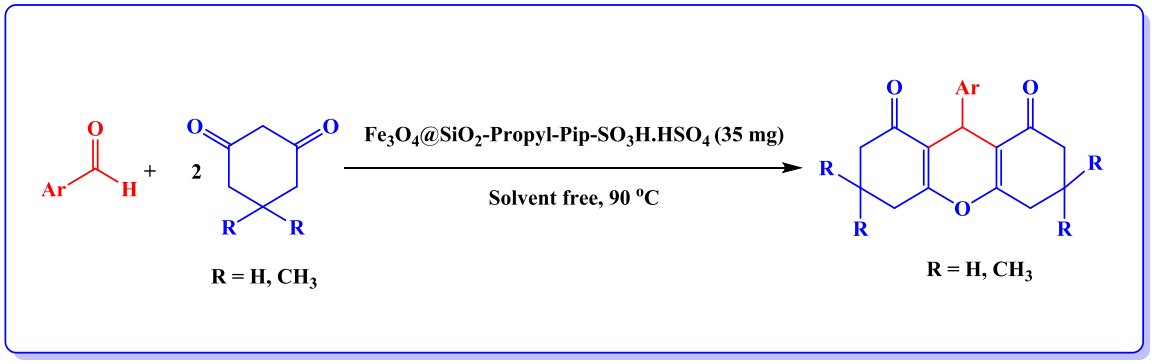

# Neural network analysis of proton exchange membrane fuel cell performance under different operation conditions

**Somayeh Majidi**[a]*, **Hussein Gharibi**[b]

[a] *Department of Chemistry, Faculty of Sciences, Najafabad Branch, Islamic Azad University, Najafabad, Iran*

[b] *Department of Chemistry, Faculty of Science, Tarbiat Modares University, P.O. Box, 14115-175, Tehran, Iran.*

*Corresponding author Tel.: +98 9127644750

*E-mail: somaye.majidi2010@gmail.com

## Abstract

The neural network can construct relationships between the control factors and responses in the PEMFC. This study proposes a feed forward neural network modelling for parametric analysis of proton exchange membrane fuel cell (PEMFC) performance. The neural network trained with Lederberg-Marquardt algorithm. Numerous parameters affecting the maximum power density of PEMFC are analysed, such as fuel cell operating temperatures, cathode and anode humidification temperatures and operating pressures. Experimental results are presented for identifying the proposed approach, which is useful to get deep knowledge of PEMFC behaviour.

**Keywords**: PEM fuel cell; Pt-catalyst; Operating condition; Artificial neural network.

## Introduction

A fuel cell is an electrochemical device that can convert the chemical energy into electrical and thermal energy [1]. It is environment friendly as the only byproducts are water and heat. During the last decade, several one-dimensional (1D) and multi-dimensional (MD) models have been developed to explain the electrochemical and/or thermodynamic phenomena inside the fuel cells [2,3]. However, some of these models require specific knowledge of parameters, i.e., membrane thickness and resistance which are either unknown or only known to the manufacturers. Therefore, the availability of the electrochemical equations or models may not be sufficient to accurately design the fuel cell system for the optimum performances. In addition, these models as described above are commonly very complicated for large-scale fuel cell systems. In the other hand, in most of control applications, the designer may be interested in relationship between inputs and outputs as well as the internal structure of the system. Such knowledge will provide the designers with the sufficient tool to control the inputs in order to reach the desired outputs, i.e., cell voltage and cell current for our particular application. Such a prediction may be performed by using artificial neural networks [4,5]. In this paper, we investigate the reliability of the neural networks for the fuel cell output prediction.

## Experimental

Two similar MEAs were used. The MEAs were prepared with a Nafion membrane sandwiched between two electrodes. Both anode and cathode catalyst was Pt/C 20%. Cell temperature was set at 75 $^{o}$C. The cathode and anode gas flows were 200 ml min–1 with 135 $kPa_{abs}$ pressure of gases. Anode relative humidity was 100%.

## Results and discussion

The neural network trained with Lederberg-Marquardt algorithm. Numerous parameters affecting the maximum power density of PEMFC are analyzed, such as fuel cell operating temperatures, cathode and anode humidification temperatures and operating pressures. Figure 1 shows the relationship among the cell temperatures, anode relative humidity and maximum electric power. Cathode relative humidity was set 80 oC and cell pressure was 1 atm. As shown in Figure 1a, the trends of PEMFC performance can clearly be presented. While both the operating temperature and RHa increase simultaneously with that, the other factors are at appropriate conditions, it is possible to improve the performance. Figure 1b shows relationship among the cell temperatures, cátodo relative humidity and maximum electric power. Anode relative humidity was set 80 oC and cell pressure was 1 atm. The performance increase, while both the operating temperature and RHc increase simultaneously until RHc 50%. After this condition, the performance decreases with increasing of RHc because of water flooding phenomena.

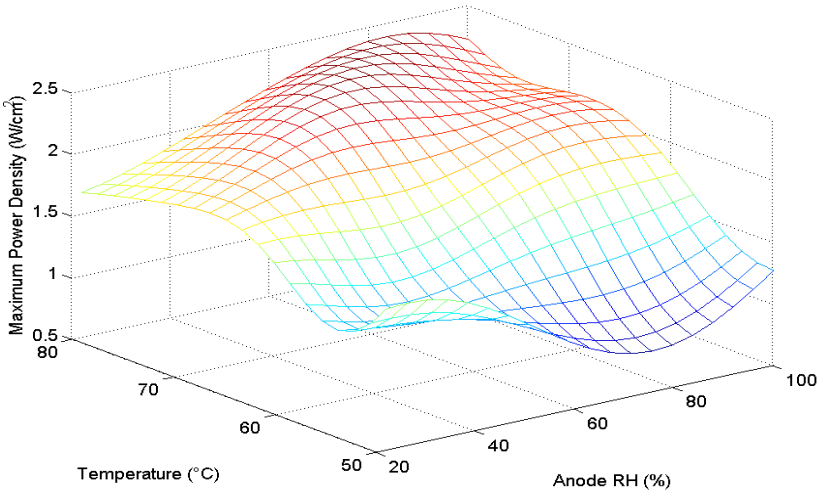


**Fig.**1. Maximum power density versus cell temperature and RHa at RHc of 80 % and pressure of 1 atm

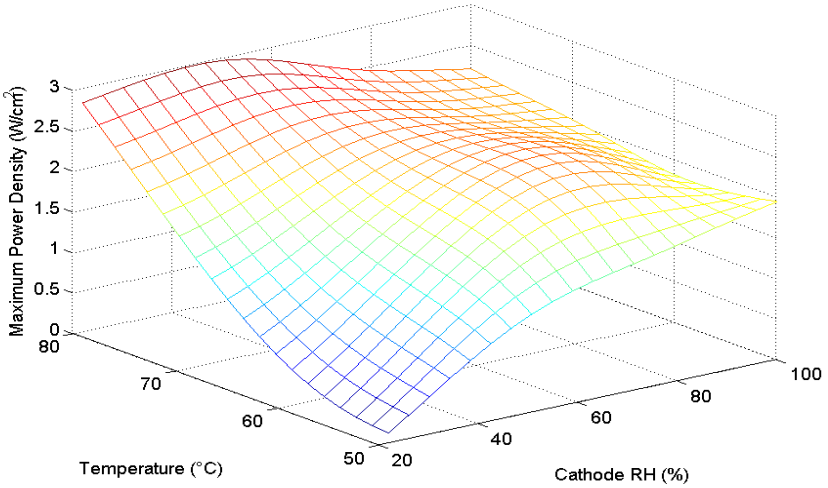


**Fig.**2. Maximum power density versus cell temperature and RHc at RHa of 80 % and pressure of 1 atm

## Conclusion

A neural network approach was employed for modeling, prediction, and analysis of PEMFC performance under various operating conditions. It was shown that the designed ANN is capable of modeling and predicting the performance for different input parameters including cell temperatures, cathode and anode humidification temperatures and operating pressures. The ANN provided a simple and direct means for the prediction of performance and was able to consider the effect of influencing parameters simultaneously. Results showed that when both the operating temperature and RHa increased simultaneously, the PEMFC performance improved. However, the PEMFC performance increased with increasing the operating temperature and RHc until RHc of 50%.

**Acknowledgments**
The support of Hydrogen and Fuel Cell laboratory of Tarbiat Modares University are acknowledged. We also gratefully acknowledge the financial support of Iranian Nanotechnology Initiative Council.

**References**

[1]J. Wu, X. Z. Yuan, H. Wang, M. Blanco, *Int J Hydrogen Energy*, **2008**, *33*, 1735.
[2] X. Liu, W. Tao, Z. Li, Y. He, *J. Power Sources*, **2006**, *158*, 25.
[3] S. Ou, L. Achenie, *J. Power Sources*, **2005**, *104*, 319.
[4] J.J. Baschuk, X. Li, *J. Power Sources*, **2004**, *142*, 134.
[5] R. Sousa Jr., E.R. Gonzalez, *J. Power Sources*, **2005**, *147*, 32.

## Graphical Abstract

Neural network analysis of proton exchange membrane fuel cell performance under different operation conditions

Somayeh Majidi*, Hussein Gharibi

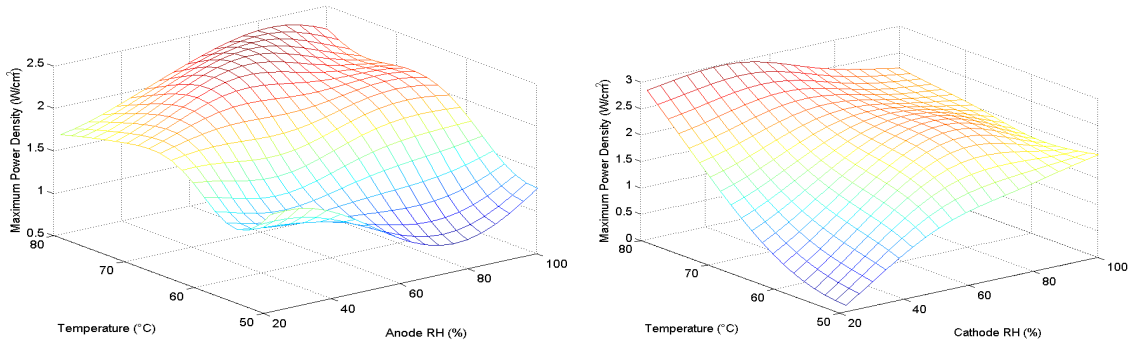

# Comparison of catalyst coated substrate and catalyst coated membrane MEAs performance in the PEM fuel cell under different operation conditions

**Somayeh Majidi**[a]*, **Hussein Gharibi**[b]

[a] *Department of Chemistry, Faculty of Sciences, Najafabad Branch, Islamic Azad University, Najafabad, Iran*

[b] *Department of Chemistry, Faculty of Science, Tarbiat Modares University, P.O. Box, 14115-175, Tehran, Iran.*

*Corresponding author Tel.: +98 9127644750

*E-mail: somaye.majidi2010@gmail.com

**Abstract**

In this study, the effect of the fabrication methods of the membrane-electrode assembly (MEA) on the proton exchange membrane fuel cell (PEMFC) performance after the MEA activation procedure was investigated. The MEA performance was analysed with polarization curves and electrochemical impedance spectroscopy (EIS).

The investigation of the CCS-MEA and CCM-MEA performance under different cathode relative humidity (RHC) and cell pressures indicates that the interfacial microstructure of CCS-MEA causes that MEA performance to be strongly influenced by the operation conditions.

**Keywords**: PEM fuel cell; Catalyst coated membrane; Catalyst coated substrate.

## Introduction

The polymer electrolyte membrane fuel cell (PEMFC) is an attractive power source for various applications such as backup power systems, stationary power systems, electrically powered vehicles, and distributed power generations [1]. Performance of the PEMFC is strongly affected by the membrane-electrode assembly (MEA) structure as well as MEA activation techniques, making these key issues in the development of the PEMFC [2]. Primarily two making process may be used to prepare MEAs, catalyst coated substrate (CCS) [3,4] and catalyst coated membrane (CCM) [5,6] methods. Tang H. and et al. [7] performed a comparative investigation on PEMFCs made with CCS and CCM MEAs under identical experimental conditions. Results demonstrated that a CCM can enhance the utilization efficiency and improve the catalyst layer and membrane interface of PEMFCs. In this paper, the performance of PEMFCs made with two MEA fabrication (CCS and CCM) methods was investigated after MEA activation under different operation conditions by electrochemical techniques such as polarization curve and electrochemical impedance spectroscopy (EIS).

## Experimental

The gas diffusion medium of MEA consisted of the carbon cloth (E-TEK-standard Teflon treated) and the diffusion layer containing 20 wt.% of Teflon. To prepare the MEA by the CCS method, the catalyst ink was sprayed onto the gas diffusion medium to form the electrode layer. The pretreated membrane and electrodes were bonded together in order to make CCS-MEA. For the preparation of MEA by the CCM method, the catalyst ink was deposited onto the pretreated membrane by spraying. The gas diffusion medium was placed on the both sides of the CCM to form the CCM-MEA.

The catalyst layer ink was prepared by directly mixing of Pt/C 20 wt.% (BASF) and Nafion solution 5 wt.% (Alderich) in distilled water and Isopropyl alcohol (Merck). The Pt loading was 0.4 mg cm-2 for anode and cathode sides of both CCS and CCM MEAs.

The prepared MEA was placed in a cell hardware (5 cm2, PaxiTech) and tested by a PEMFC test station (FCT, 150s). The performance of the MEA was evaluated by the polarization curve and EIS techniques under different operation conditions. The applied conditions were: low and high cathode relative humidity (RHC) (30% and 100%) and low and high cell pressure (100 and 200 kPaabs). In all of tests, cell temperature was set at 75 oC and anode relative humidity (RHa) was 100%. The polarization curve was obtained by scanning of the cell voltage from OCV to 0 mV. The impedance spectra were recorded in the frequency range from 10 kHz to 10 mHz.

## Results and discussion

Fig. 1 and 2 indicates I-V curves and EIS spectra of both MEAs under low (30%) and high (100%) $RH_C$, respectively. CCM-MEA showed higher performance compared to CCS-MEA in both low and high $RH_C$. When $RH_C$ decreased from 100% to 30%, MPD of CCM-MEA and CCS-MEA decreased by 20% (from 820 mW $cm^{-2}$ to 660 mW $cm^{-2}$) and 30% (from 490 mW $cm^{-2}$ to 350 mW $cm^{-2}$), respectively.

This fact demonstrates that in addition to water generated in the catalyst layer affecting the membrane hydration of CCS-MEA, there is another factor relevant to the relative humidity of gases [8,9]. Therefore, with increasing $RH_C$, the membrane hydration level of CCS-MEA more increased, thereby demanding the power output compared to CCM-MEA.

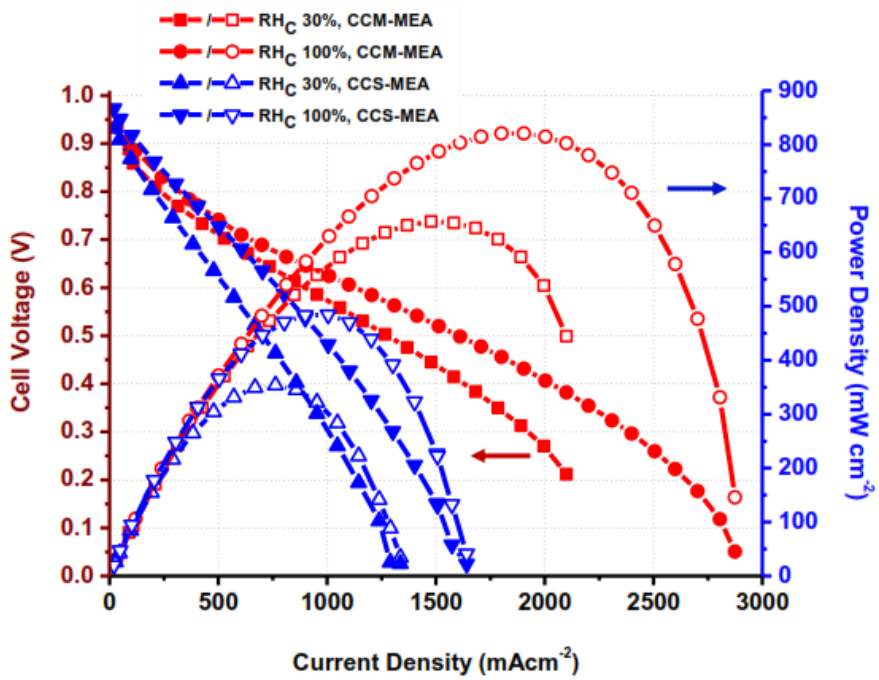


Fig. 1: Polarization curves of CCM-MEA and CCS-MEA after reaching the steady state at 75 ºC and 100 $kPa_{abs}$.

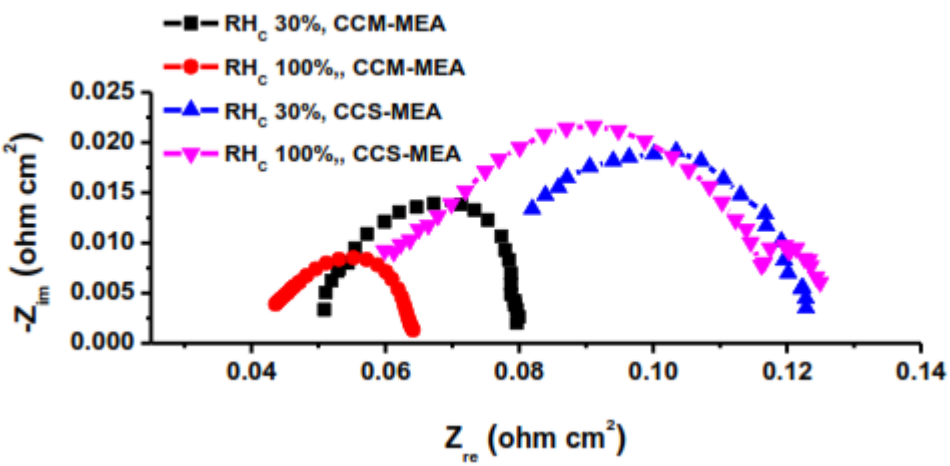


Fig. 2: EIS spectra of CCM-MEA and CCS-MEA at 0.7 V after reaching the steady state at 75 ºC and 100 $kPa_{abs}$.

Based on the impedance spectra shown in Fig. 2, charge transfer resistance (Rct), mass transfer resistance (Rmt), solution resistance (Rs) and constant phase element (CPE) were extracted using an expanded Randle's analogous circuit reported in Table 1. The Nyquist plots were fitted by Zview software. Table 1 indicates that CCM-MEA has lower values of different resistances compared to CCS-MEA, for example in 100% of RHC, Rs and Rct of CCM-MEA are 30% and 63% less than that of CCS-MEA, respectively. Unlike of CCS-MEA, there is no Rmt in CCM-MEA under 100% of RHC operation conditions.

Table 1: EIS spectra analysis of CCM-MEA and CCS-MEA under low and high $RH_C$ operation conditions, 100 $kPa_{abs}$.

| MEA | $RH_C$ (%) | $R_s$ (mΩ $cm^2$) | $R_{ct}$ (mΩ $cm^2$) | *CPE1* (mF) | $R_{mt}$ (mΩ $cm^2$) | *CPE2* (mF) |
|---|---|---|---|---|---|---|
| CCM-MEA | 30 | 50 | 32 | $22^{0.8}$ | - | - |
| | 100 | 42 | 22 | $45^{0.8}$ | - | - |
| CCS-MEA | 30 | 70 | 53 | $11^{0.76}$ | - | - |
| | 100 | 60 | 59 | $10^{0.8}$ | 47 | $700^{0.5}$ |

Further investigation of the results in Table 1 indicates that with increasing RHC from 30% to 100%, the mobility of protons increases, lead to a reduction in Rct of both MEAs [8,10]. When RHC increased, the water content in the membrane of both MEAs increased, this fact resulted in the reduction of Rs [11].

In order to investigate the effect of cell pressure on CCM-MEA and CCS-MEA performance, the experiments were performed under 100 kPaabs and 200 kPaabs of cell pressure. Fig. 3 and 4 illustrate the MEAs polarization curves and their Nyquist plots at 0.7 V, respectively. Generally, increasing the cell pressure enhanced the performance of CCM and CCS MEA by 5% (from 820 mW cm-2 to 864 mW cm-2) and 18% (from 490 mW cm-2 to 580 mW cm-2), respectively, but it was more highlighted for CCS-MEA.

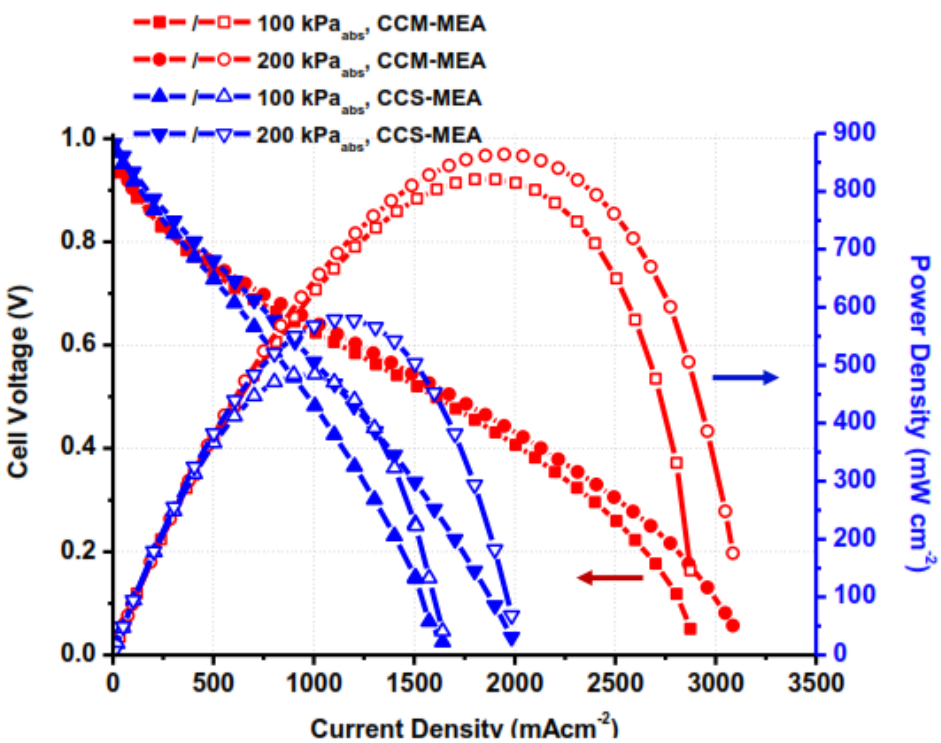


Fig. 3: Polarization curves of CCM and CCS at 0.7 V after reaching the steady state under $RH_C$ 100%.

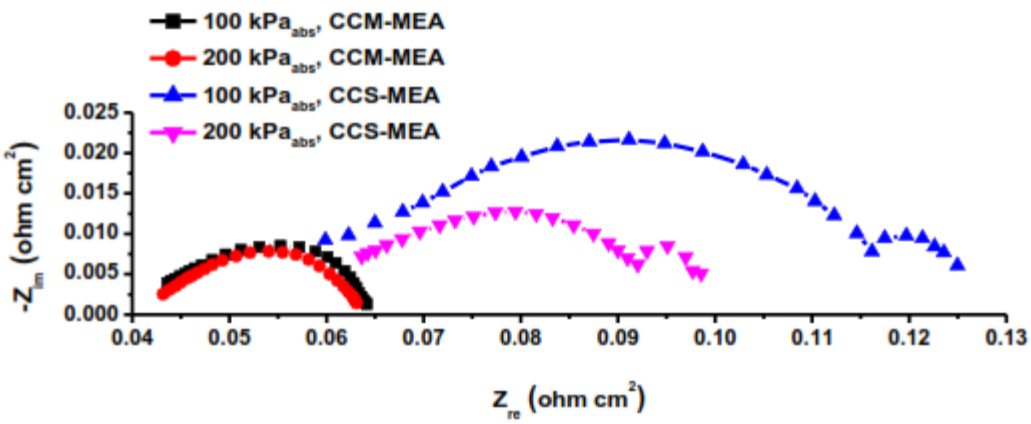


Fig. 4: EIS spectra of CCM and CCS at 0.7 V after reaching the steady state under $RH_C$ 100%

Nyquist's analysis results in Table 2 indicates that with increasing the cell pressure of CCS-MEA, the kinetic of ORR enhances and transportation of reactants onto the catalyst surface improves, significantly [12]. This behavior is explained by this fact that microstructure of catalyst layer of CCS-MEA leads to non-uniform distribution of reactants on the catalyst surface [13], especially in the low level of gas pressure, compared to CCM-MEA. Therefore, cell pressure enhancement from 100 $kPa_{abs}$ to 200 $kPa_{abs}$ could be chiefly affected $R_{ct}$ and $R_{mt}$ of CCS-MEA compared to CCM-MEA, demanding the power output.

Table 2: EIS spectra analysis of CCM-MEA and CCS-MEA under different operation pressures, 100% $RH_C$.

| MEA | P (kPa) | $R_s$ (mΩ cm$^2$) | $R_{ct}$ (mΩ cm$^2$) | *CPE*1 (mF) | $R_{mt}$ (mΩ cm$^2$) | *CPE2* (mF) |
|---|---|---|---|---|---|---|
| CCM-MEA | 100 | 42 | 22 | $45^{0.8}$ | - | - |
| | 200 | 43 | 20 | $55^{0.8}$ | - | - |
| CCS-MEA | 100 | 56 | 66 | $28^{0.7}$ | 22 | $220^{0.87}$ |
| | 200 | 58 | 40 | $51^{0.7}$ | 13 | $60^{1}$ |

**Conclusion**

Comparison between the steady state performances of CCM-MEA and CCS-MEA at the different operation conditions in terms of RHC and cell pressure indicated that CCM-MEA produced higher MPD than CCS-MEA. Analysis of EIS spectra demonstrated that CCM-MEA experienced considerable lower Rs, Rct and Rmt compared to CCS-MEA in different operation conditions. Results showed that Rs and Rct values of CCS-MEA were 30% and 63% higher than that of CCM-values in 100% of RHC, respectively. High catalyst utilization, close contact between the catalyst layer and membrane and mass transport facilitation in the CCM-MEA caused that it had higher performance after activation process compared to CCS-MEA under the different operation conditions.

**Acknowledgments**

The support of Hydrogen and Fuel Cell laboratory of Tarbiat Modares University are acknowledged. We also gratefully

acknowledge the financial support of Iranian Nanotechnology Initiative Council.

**References**

[1] K. Minsuk, P. Jin-Nam, K. Hyuk, S. Seongmin, L. Won-Ho, *Journal of Power Sources*, **2006**, *163*, 93.

[2] X.Z. Yuan., S. Zhang, J.C. Sun, H. Wang, *J Power Sources*, **2011**, *196*, 9097.

[3] X.M. Ren, P. Zelenay, S. Thomas, J. Davey, S. Gottesfeld, *J. Power Source*, **2000**, *86*,111.

[4] A. Lindermeir, G. Rosenthal, U. Kunz, et al., *J. Power sources*, **2004**, *129*,180.

[5] M.S. Wilson, S. Gottesfeld, *J. Appl. Electrochem*, **1992**, *22*,1.

[6] S.Q. Song, Z.X. Liang, W.J. Zhou, et al., *J Power sources*, **2005,** *145*,495.

[7] H. Tang, S. Wang, S.P. Jiang, M. Pan, *Journal of Power Sources*, **2007,** *170*, 140.

[8] M. Zhiani, S. Majidi, *Int. J. Hydrogen Energy*, **2013,** *38*,9819.

[9] T.J.P. Freire, E.R. Gonzalez. *J Electroanal Chem*, **2001,** *503*,57.

[10] X. Yan, M. Hou, L. Sun, D. Liang, Q. Shen, O. Xu, et al. *Int J Hydrogen Energy*, **2007,** *32*,4358.

[11] X. Yaun, C. Song, H. Wang, J. Zhang, Springer, New York, USA, **2010,** 263.

[12] L. Sun, R. Rah, G. Wang, Z. Shao, *Solid State Ionics*, **2008,***179*,960.

[13] H. Tang, S. Wang, M. Pan, S.P. Jiang, Y. Ruan, *Electrochimica Acta*,**2007,***52*, 3714.

## Graphical Abstract

Comparison of catalyst coated substrate and catalyst coated membrane MEAs performance in the PEM fuel cell under different operation conditions

Somayeh Majidi, Hussein Gharibi

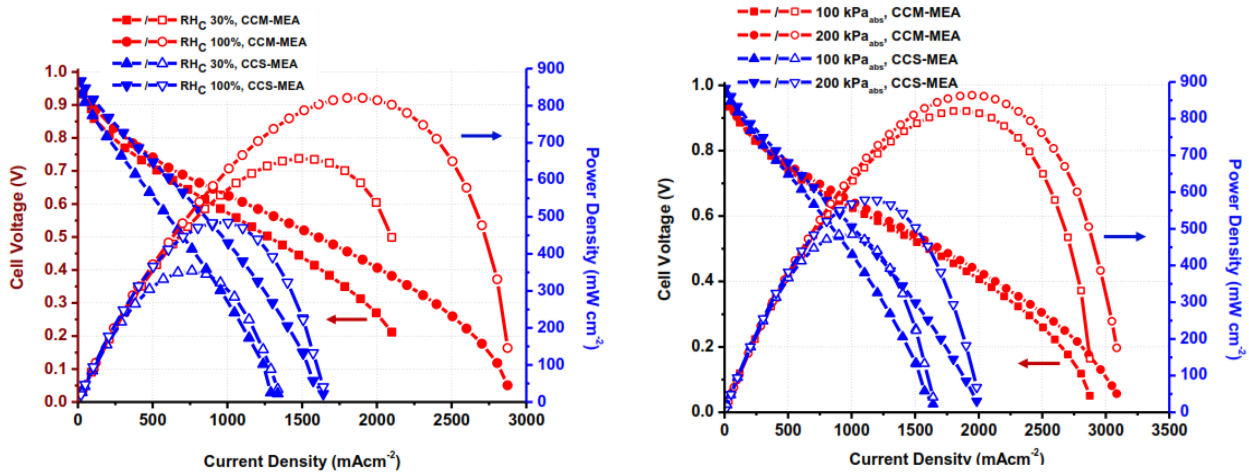

# Green, Transition-Metal-Free Catalysts:

# An Efficient Reusable Organocatalyst in Oxidation of Cylohexene by Oxaziridines

**Massomeh Ghorbanloo**[*a]

[a] *Department of Chemistry, Faculty of Science, University of Zanjan, 45371-38791 Zanjan, Iran,*

*Tel: +98 241 33054084; fax: +98 24 33052477*

[*]*E-mail: m_ghorbanloo@yahoo.com (M. Ghorbanloo)*

## Abstract

Interaction of 2-[(2-Hydroxy-benzylidene)-amino]-3-(4-hydroxy-phenyl)-propionic acid ligand with modified silica gel leads to immobilization of the ligand onto a modified silica gel surface, through the reactive (3-chloropropyl)-trimethoxysilane group. This heterogeneous catalyst was found to be an efficient heterogeneous catalyst for oxidation of cyclohexene in the presence of $H_2O_2$ as an oxidant and $CH_3CN$ as a solvent. The heterogeneous catalyst could be recovered easily and reused three times, without significant loss of its catalytic activity.

***Keywords*:** Transition-Metal-Free; Reusable; Organocatalyst; Oxidation; Oxaziridines; $H_2O_2$.

.

## Introduction

Metal-free organic catalysts have attracted much attention due to their exclusive greenness and also for their advantages such as high efficacy, environment friendliness and economy in many industrial catalytic processes [1].

Organic molecules containing N and P, electron-rich center, such as dendrimers, ionic liquids, *etc*., that have been extensively used in various homogeneous organic reactions for rearrangement reactions, cycloaddition, condensation and alkylation are diversity of organic metal-free catalysts [2-4]. Moreover, design and development of a green organocatalytic system for oxidation of olefins is the most significant challenging for catalytic chemists. For this purpose, imines are worthy compounds for using as organocatalysts in oxidation of olefins to related alcohols, ketones and epoxides.

For oxidation of olefins in the presence of imines, as catalysts, various oxidants such as organic peroxides or hydrogen peroxide are considered. The latter, hydrogen peroxide, in combination with nitriles (the R–CN/ $H_2O_2$ system) [5-6], acetic anhydride [7] and urea [8] have also been used to oxidation of unfunctionalized olefins.

The nitrile-hydrogen peroxide system has found good success in synthesis of epoxides from olefins [9-10]. It was previously used by Schirmann and Weiss[5] to prepare N-alkyloxaziridines from imines [11].

Thus, oxaziridines have been used as an oxygen transfer [12] reagents in synthetic organic chemistry.

The improvement of effective synthetic procedures for the preparation of oxaziridines, is an important goal and represents a considerable challenge [13]. But, most of these methods suffer from disadvantages like severe reaction conditions, formation of side products and difficult work-up trend. For overcoming to these problems, some of oxidative processes based on the activation of $H_2O_2$ by robust, efficient and reusable heterogeneous organocatalysts were developed [14]. Heterogeneous catalysts for oxidations are investigated because of advantages such as easy handling and product separation, catalyst recovery and less waste. Additionally in heterogeneous catalysts, inorganic materials with organic components are especially appealing due to the facility to combine the functional diversity of organic chemistry with the benefits of a thermal stable and robust inorganic substrate. Modified silica exhibits some advantages such as high surface area, high thermal and chemical stability.

In the current study, we would like to report an easy access to a new silica-supported organocatalyst based on Schiff base of L-tyrosine to achieve oxaziridine for oxidation of cyclohexene. Because in the literatures, oxaziridine was prepared during difficult procedures. For instance Hanquet and co-workers reported that oxaziridinium salt could be similarly prepared by methylation or oxidation method [15] and it was found to be highly reactive for epoxidation of olefins [16]. They further showed that the epoxi dation could be run with a catalytic amount of the corresponding iminium salt using oxone−$NaHCO_3$ in $CH_3CN$−$H_2O$ or mCPBA−$NaHCO_3$ in $CH_2Cl_2$ [17-18].

Our main purpose for the design of this reusable organocatalyst is to prepare a heterogeneous and more convenient catalytic system for application in oxidation reactions.

We are interested in using $H_3L$ (2-[(2-Hydroxy-benzylidene)-amino]-3-(4-hydroxy-phenyl)-propionic acid) and $H_2L/SiO_2$ as metal-free catalysts for the oxidation of cyclohexene in the presence of hydrogen peroxide. The heterogeneous structure of $H_2L/SiO_2$ was described by Ghorbanloo *et al.* [19].

## Experimental

*General*

The starting materials and all solvents were purchased from Merck and used as received. Silica gel (0.063–0.200 mm) was activated at 550 ºC for 6 hours before use. Aqueous 30% hydrogen peroxide (10.69 mol $L^{-1}$), was used and its exact concentration was determined before use by titration with standard $KMnO_4$. Elemental analyses were determined on a CHN Perkin-Elmer 2400 analyzer. FTIR spectra were recorded on a Perkin-Elmer 597 spectrometer. The reaction products of the oxidation were analyzed by an HP Agilent 6890 gas chromatography, equipped with a HP-5 capillary column (phenyl methyl siloxane 30 m × 320 µm × 0.25 µm) with flame-ionization detector. In addition, the reaction products of the oxidation were analyzed by GC-MS.

***Synthesis of $H_3L$***

The $H_3L$ ligand was synthesized according a literature procedure [18] as shown in scheme 1. A mixture of L-tyrosine (0.36 g, 2.0 mmol) and NaOH (0.08 g, 2.0 mmol) in toluene (10 mL), was added to a solution of salicylaldehyde (0.244 g, 2.0 mmol) in toluene (10 mL) and refluxed for 2 hours and then the resulting yellow solid was washed repeatedly with methanol, dried in air and characterized by IR spectroscopy, $^1$H NMR, $^{13}$C NMR and $^{13}$C CP-MAS NMR. Yield: 88.0%; m.p. 238 °C; Anal. Calcd. for $C_{16}H_{15}NO_4$: C, 67.36; H 5.30; N, 4.91 %. Found: C, 66.06, H, 4.94, N, 4.70 %; IR (KBr, $cm^{-1}$): 3208 (O–H stretching of phenolic and -COOH groups), 1612 (C=N strtching of azomethine group), 1609 (-COO asymmetric stretching of -COOH), 1514 (-COO symmetric stretching of -COOH); $^1$H NMR (500 MHz, DMSO-$d_6$, $\delta$ / ppm): 2.77 (1H, *dd*, *J* = 9.0 Hz, *J* = 13.5 Hz, Ar–C$\underline{H}_2$), 3.13 (1H, *dd*, *J* = 4.0 Hz, *J* = 15.0 Hz, $CH_2$–C$\underline{H}$–N), 3.74 (1H, *dd*, *J* = 4.0 Hz, *J* = 9.5 Hz, Ar–C$\underline{H}_2$), 6.56 (2H, *d*, *J* = 8.5 Hz, aromatic H), 6.63 (1H, *d*, *J* = 6.5 Hz, aromatic H), 6.69 (1H, *d*, *J* = 8.0 Hz, aromatic H), 6.90 (2H, *d*, *J* = 8.5 Hz, aromatic H), 7.16-7.20 (2H, *m*, aromatic H), 8.04 (1H, *s*, CH=N), 9.14 (1H, *s*, -COOH), 14.29 (1H, *s*, OH); $^{13}$C NMR (125.77 MHz, DMSO-$d_6$, $\delta$ / ppm): 36.96 ($CH_2$, overlapped by DMSO), 74.44 (CH), 114.84 ($2CH_{Ar}$), 116.30 ($CH_{Ar}$), 117.76 ($CH_{Ar}$), 117.99 ($C_{Ar}$), 129.93 ($2CH_{Ar}$), 130.23 ($C_{Ar}$), 131.60 ($CH_{Ar}$), 132.18 ($CH_{Ar}$), 155.27 ($C_{Ar}$), 163.31 (CH=N), 164.50 ($C_{Ar}$), 171.24 (COOH) ppm. $^{13}$C CP-MAS NMR (100.63 MHz, $\delta$ / ppm): 37.20 ($CH_2$), 56.53 (CH), 116.90 ($2CH_{Ar}$), 118.40 ($2CH_{Ar}$), 124.10 ($2C_{Ar}$), 131.2 ($4CH_{Ar}$), 156.00 ($2C_{Ar}$, also CH=N), 176.10 (COOH) [19].

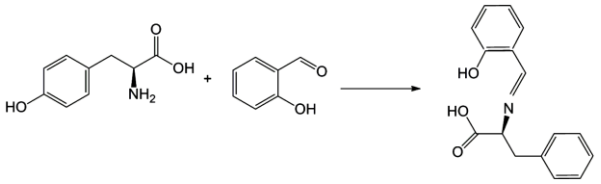


**Scheme 1.** Schematic representation of $H_3L$ synthesis procedure

***Grafting procedure***

Anchoring of the (3-chloropropyl)-trimethoxysilane, CPTM, as a linker on surface of silica gel was subjected to the experiment according to reported method [20]. Soxhlet extraction, with dichloromethane (for 12 h) yielded Cl-functionalized silica gel. The light cream powder, CPTM/$SiO_2$, was dried at room temperature and characterized by CHN analysis, IR spectroscopy and solid NMR. Linker loading = 1.16 mmol $g^{-1}$ silica gel, Anal. Calcd. for CPTM/$SiO_2$: C, 4.2; H 0.69%. Found: C, 4.27, H, 0.8%; IR (KBr, $cm^{-1}$) 3429 (O–H stretching of phenolic, –COOH and $H_2O$ of silica surface groups), 1086 (Si–O–Si asymmetric stretching of silicagel surface), 821 (Si–OH stretching of silicagel surface), 471 (δ Si–O–Si of silicagel surface); $^1$H MAS NMR (600 MHz, $\delta$ / ppm): 0.26 (protons of silica gel), 0.69 (Si-C$\underline{H}_2$-), 1.35 (Si-$CH_2$-C$\underline{H}_2$-), 2.98 (-C$\underline{H}_2$-Cl), 5.57 (-OH); $^{13}$C CP-MAS NMR (100.63 MHz, $\delta$ / ppm): 9.47 (Si-$\underline{C}H_2$), 26.01 (Si-$CH_2$-$\underline{C}H_2$-), 46.06 (-$\underline{C}H_2$-Cl); $^{29}$Si CP-MAS (as determined in $^1$H-$^{29}$Si HETCOR NMR experiment), (116.22 MHz, $\delta$ / ppm): –110.10 ($Q^4$ [siloxane, ($\underline{Si}O)_4Si$]), –102.10 ($Q^3$ [single silanol,$(SiO)_3\underline{Si}(OH)$]), –57.40 ($T^3$ [C-Si($O\underline{Si})_3$]), –50.50 ($T^2$ [C-Si($O\underline{Si})_2$(OH)]) [19].

### *Immobilization of the catalyst on a modified silica support*

Immobilization of the catalyst on a modified silica support was prepared according to reported method.[23] Briefly, suspension of freshly dried CPTM/$SiO_2$ (0.5 g) and $H_3L$ (0.25 g) in dry toluene was refluxed for 24 h, as shown in scheme 2. The yellow colored solid was separated, Soxhlet extracted with $CH_2Cl_2$ to remove the unreacted $H_3L$ ligand adsorbed on the external surface of CPTM/$SiO_2$. The yellow material, $H_2L/SiO_2$, was dried at room temperature and characterized by CHN analysis, IR spectroscopy and solid NMR. $H_3L$ loading = 0.84 mmol $g^{-1}$ silica gel; Anal. Calcd. for $H_2L/SiO_2$: C, 16.13; H 1.26; N, 1.18 %. Found: C, 17.30, H, 1.84, N, 1.17%; IR (KBr, $cm^{-1}$): 3477 (O–H stretching of phenolic, –COOH and $H_2O$ of silica surface groups), 1612 (C=N strtching of azomethine group), 1084 (Si–O–Si asymmetric stretching of silicagel surface), 811 (Si–OH stretching of silicagel surface), 474 (δ Si–O–Si of silicagel surface); $^1$H MAS NMR (600 MHz, $\delta$ / ppm): 0.26 (protons of silica gel), 1.36 (Si-$CH_2$), 2.38 ($CH_2$-O), 3.81 ($CH_{Ar}$), 5.97 ($CH_{Ar}$), 8.18 (-CH=N), 9.46 (-OH); $^{13}$C CP-MAS NMR (100.63 MHz, $\delta$ / ppm) 10.55 (Si-$CH_2$), 26.49 (Si-$CH_2$-$\underline{C}H_2$-), 37.06 ($CH_2$), 47.59 (-$CH_2$-Cl), 56.95 (CH), 115.51 (2$CH_{Ar}$), 118.60 (2$CH_{Ar}$), 123.96 (2$C_{Ar}$), 130.99 (4$CH_{Ar}$), 155.93 (2$C_{Ar}$, also CH=N), 175.78 (COOH) [19].

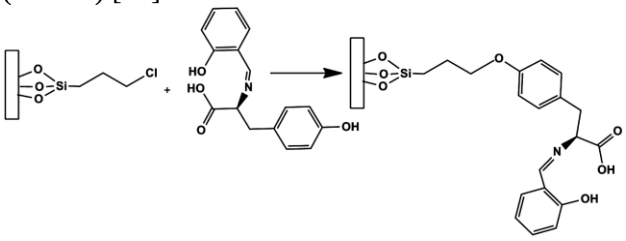


**Scheme 2.** Schematic representation of $H_2L/SiO_2$ synthesis procedure

### *General oxidation procedure*

We report here the oxidation of olefins by oxaziridines, in good yield. Cyclohexene oxidation by $H_2L/SiO_2$ and $H_3L$ carried out by heating an olefin with the oxaziridine at 60 °C in $CH_3CN$. Products were identified by comparison with authentic samples of the reaction mixtures. These oxides can be determined by gas chromatography.

Oxidation reactions were performed in a stirred round-bottom flask, fitted with a water-cooled condenser. The reactions were carried out under atmospheric pressure in air in an oil bath at 60 ± 1 ºC, with acetonitrile as a solvent and aqueous 30% $H_2O_2$ (10.69 mol $L^{-1}$) as an oxidant. In a typical experiment, a mixture of 5.0 mg as the heterogeneous catalyst, 2.0 mL $CH_3CN$ as a solvent, 1.0 mmol cyclohexene, were prepared in a 25 mL round bottomed glass flask, fitted with a water-cooled reflux condenser and placed in an oil bath. After the mixture was heated to 60 ºC, $H_2O_2$ was added. At appropriate intervals, aliquots were removed and analyzed immediately by GC. The oxidation products were identified by comparing their retention times with those of authentic samples. Yields are based on the added substrate and were determined by a calibration curve.

## Results and Discussion

### *Catalytic activity*

The heterogeneous ($H_2L/SiO_2$) catalyst were used in the oxidation of cyclohexene using 30% aqueous $H_2O_2$ as the oxidant and acetonitrile as the solvent, at 60 °C and the results are summarized in Table 1.

**Table 1** Oxidation of cyclohexene by $H_2L/SiO_2$[a]

| Entry | $[H_2O_2]/[C_6H_{10}]$ Molar ratio | Temperature, °C | Catalyst amount, g | Conversion, %[b] |
|---|---|---|---|---|
| 1 | 1 | 60 | 0.0020 | 38 |
| 2 | 2 | 60 | 0.0020 | 75 |
| 3 | 3 | 60 | 0.0020 | 97 |
| 4 | 3 | 40 | 0.0020 | 48 |
| 5 | 3 | 80 | 0.0020 | 88 |
| 6 | 3 | 60 | 0.001 | 13 |
| 7 | 3 | 60 | 0.0015 | 47 |
| 8 | 3 | 60 | 0.0025 | 79 |

[a] *Reaction conditions*: catalyst (($H_2L/SiO_2$); substrate, 1 mmol; Time, 4 h; $CH_3CN$, 2 mL; [b]) Based on substrate;

The results of control experiments revealed that the presence of the catalyst and the oxidant were essential to the oxidation process. The oxidation of cyclohexene in the absence of $H_2O_2$ did not occur, whereas in the absence of a catalyst the oxidation only preceded by up to 6% after 24 h. Also, the oxidation of cyclohexene with support $SiO_2$ or $CPTM/SiO_2$ did not occur.

In order to achieve suitable reaction conditions for maximum transformation of cyclohexene, the effect of $H_2O_2$ concentration (mol of $H_2O_2$ per mol of cyclohexene), temperature and catalyst amount were studied.

The effect of $H_2O_2$ concentration on the cyclohexene oxidation reaction is shown in Table 1, entries 1-3. The percentage of cyclohexene conversion increased with the increment of the ratio of $H_2O_2$ to cyclohexene ratio.

The temperature had remarkable effect on the conversion of cyclohexene in the range from 40 to 60 °C. The conversion increased from 48 to 97% when the temperature was elevated from 40 to 60 °C. The conversion decreased to 88% by further rising temperature to 80 °C. This seems likely that higher temperatures facilitate the decomposition of $H_2O_2$ [19].

Moreover, the amount of catalyst had a significant effect on the oxidation of cyclohexene. Four different amounts of catalyst were used. The results are shown in Tabel 1, entries 3,6-8 , indicating 13, 45, 97 and 79% conversion corresponding to 0.001, 0.0015, 0.0020 and 0.0025 g catalyst respectively. Lower conversion of cyclohexene with 0.001 g catalyst may be due to fewer catalytic sites. The maximum percentage of conversion was observed with 0.0020 g catalyst, but further increment of catalyst to 0.0025 g resulted in the lower conversion. This may be due to increased degradation of the oxidant at higher concentration of catalyst [21]. Therefore, it is clear that 0.0020 g of catalyst is adequate to obtain an optimum cyclohexene conversion of 97% in 4 h of contact time.

According to the results, the oxidation occurred on double bond and *cis*-cyclohexene-diol obtained as the sole product, (Figure S-1). It seems that the diol resulted from the epoxide ring opening under the aqueous acidic conditions. The same result is reported in the presence of RCN/UHP [22]. Cyclohexene is more prone to both epoxidation and allylic oxidation [23]. As shown in scheme 1, oxaziridines could produce only epoxides, as same as reported results in literatures [24-25].

Furthermore, the performance of the homogeneous catalyst was studied by running the oxidation of cyclohexene under the optimized conditions (i.e., 3:1 (mol $mol^{-1}$) mixture of $H_2O_2$ and substrate in acetonitrile at 60 °C).

Prominent difference in selectivity between $H_2L/SiO_2$ and $H_3L$ was seen in the oxidation of cyclohexene (Figure S-2). The cis-cyclohexene-diol weas achieved with $H_2L/SiO_2$ /$H_2O_2$ system, however its homogeneous counterpart produced only cyclohexene epoxide. That probably is caused by the presence of significant amounts of water in 30% $H_2O_2$, which can be responsible for the hydrolysis of

cyclohexene oxide to form related diol. Because in the presence of $SiO_2$, dismutation of $H_2O_2$ is occurred and amount of $H_2O$ in medium is higher than homogeneous catalytic system. Hydrolysis can also be promoted by Lewis acidity of $SiO_2$. Thus possibility of hydrolysis of epoxides in heterogeneous system is higher than homogeneous counterpart.

In addition $H_2L/SiO_2$ and $H_3L$ have chemical simplicity and easy synthesis procedure. Also, in order to evaluate the efficiency of the catalyst, our organocatalyst is being compared with the literature catalysts. Compared with the previously reported catalysts, both [$H_2L/SiO_2$ and $H_3L$ exhibited superior activity for the oxidation of cyclohexene. The previously reported N-hydroxyphthalimide-Anthraquinone and N-hydroxyphthalimide-1,4-diamino-2,3-dichloro-anthraquinone [26] showed lower catalytic activity for the oxidation of cyclohexene. Moreover, our catalysts showed higher catalytic activity than the 2-benzenesulfonyl-3-aryloxaziridines [24].

The catalyst and applied method in this paper have the advantages in terms of heterogeneous nature, high reusability, high conversions and selectivity of the catalyst.

### *Catalyst recycling and stability*

In order to investigate the possibility of several recycling runs for catalyst, the solid catalyst was separated from the reaction mixture by centrifugation. The supernatant was decanted and then the solid catalyst was washed two times by adding acetonitrile and centrifugation. The used and washed catalyst was then transferred to a flask and used again in a fresh reaction. The catalyst was recycled three times for cyclohexene oxidations. In general, no significant loss in the catalytic activity of the immobilized catalyst was observed compared with that of a fresh sample. Therefore, recycling is possible in the case of our heterogeneous catalyst. In addition, the recycled catalyst was separated from the reaction mixture after each experiment by simple filtration, washed with methanol, dried and characterized by FTIR, as shown in Fig. 1. According to this figure, the recycled catalyst has not been damaged and its spectrum is similar to fresh catalyst.

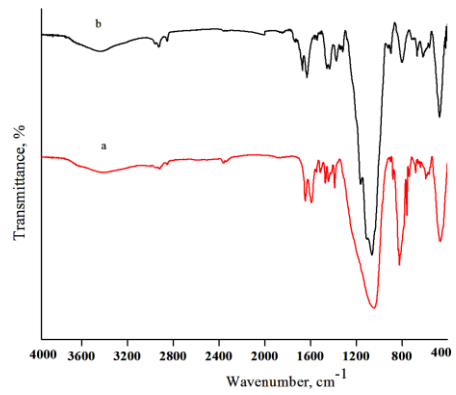


**Figure 1** FT-IR (KBr) spectra of a) fresh (red line) and b) recycled $H_2L/SiO_2$ catalyst

## Conclusion

In summary, we have developed an efficient homogeneous and heterogeneous catalyst system utilizing $H_2L/SiO_2$, and $H_3L$, for oxidation of cyclohexene. Good conversion with excellent selectivity was achieved. The solid catalyst material was easily separated from the reaction mixture via filtration. The $H_2L/SiO_2$, was reused in several catalytic runs, without significant loss of activity. During recycling, conversion of cyclohexene is identical to a fresh catalyst, in its first application.

This system could be useful for many base-catalyzed selective oxidations. This could open new application areas in free transition metal heterogeneous catalytic oxidation systems in the future.

Compared with a metal-based catalyst, our catalysts have the advantages of low cost, no heavy metal pollution and environmental friendliness, while showing high selectivity and long term stability under mild conditions in many catalytic processes. This literature focuses on the key issues of their synthesis, heterogenization, characterization and catalytic evaluation in oxidation of cyclohexene.

## SUPPLEMENTARY MATERIAL

It contains general procedure for the detailed GC measurement conditions, explanation to several phenomena, and GC–MS diagrams for all the products.

**Acknowledgements**

The authors are thankful to the University of Zanjan for support of this study.

**References**

[1] W. Adam, C. R. Saha-Moller, P. A. Ganeshpure, *Chem. Rev*. **2001**, ***101***, 3499.

[2] H. F. Jiang, Y. J. Wang, H. L. Liu, P. Liu, *Chin. J. Org. Chem*. **2004**, ***24***, 1513.

[3] G. Yang, Y. Ma, J. Xu, *J. Am. Chem. Soc*. **2004**, *126***,** 10542.

[4] D. J. Chen, Y. T. Wang, J. Klankermayer, *Angew. Chem. Int. Ed*. **2010**, ***49***, 9475.

[5] J. P. Schirmann, F. Weiss, *Tetrahedron. Lett*. **1972**, 633

[6] J. Kraiem, Y. Kacem, J. Khiari, B. B. Hassine, *Synth. Commun*. **2001**, *31*, 263.

[7] W. D. Emmons, *J. Am. Chem. Soc*. **1957**, *79*, 5739.

[8] J. Asgarian Damvandi, B. Karami, M. A. Zolfigol, *Synlett*. **2002**, 933.

[9] L. A. Arias, S. Adkins, C. J. Nagel, R. D. Bach, *J. Org. Chem*. **1983**, *48*, 888.

[10] G. B. Payne, P. H. Deming, P. H. Williams. *J. Org. Chem*. **1961**, *26*, 651.

[11] J. P. Schirmann, F. Weiss. *Tetrahedron. Lett*. **1972**, *13***,** 633.

[12] L. Bohe, M. Lusinchi, M. X. Lusinchi, *Tetrahedron* **1999**, *55*, 155.

[13] J. Aube, *J. Chem. Soc. Rev*. **1997**, *26*, 269

[14] A. Khalafi-Nezhad, E. Shaikhi Shahidzadeh, S. Sarikhani, F. Panahi, *J. Mol. Catal. A: Chem*. **2013**, *379*, 1.

[15] G. Hanquet, X. Lusinchi, P. Milliet, *Tetrahedron* **1993**, *49*, 423.

*[16] G. Hanquet, X. Lusinchi, P. Milliet,* Tetrahedron. Lett. ***1988***, 29, *3941*.

*[17] X. Lusinchi, G. Hanquet,* Tetrahedron ***1997***, 53, *13727*.

*[18] L. Bohé, M. Kammoun,* Tetrahedron. Lett. ***2004***, 45, *747*.

[19] M. Ghorbanloo, M. Jaworska, P. Paluch, G. D. Li, L. Zhou, *Transit. Metal. Chem*. **2013**, *38*, 511.

[20] S. Huh, J. W. Wiench, J. Yoo, M. Pruski, W. S. Y. Lin, *Chem. Mater*. **2003**, *15*, 14247.

[21] R. A. Sheldon, J. A. Vav Doorn, *J. Catal*. **1973**, *31*, 427.

[22] L. Ji, Y. N. Wang, C. Qian, X. Z. Chen, *Synthetic. Commun*. **2013**, *43*, 2256.

[23] A. J. Appleton, S. Evans, J. R. Lindsay Smith, *J. Chem. Soc.: Perkin. Trans*. **1995**, *2*, 281.

[24] F. A. Davis, N. F. Abdul-Malik, S. B. Awad, M. E. Harakal, *Tetrahedron. Lett.* **1981**, *22*, 917.

[25] A. Balsamo, G. Berti, P. Crotti, M. Ferretti, B. Machia, F. Macchi, *J. Org. Chem*. **1974**, *39*, 2596.

[26] X. Tong, J. Xu, H. Miao, G. Yang, H. Ma, Q. Zhang, *Tetrahedron* **2007**, *63*, 7634.

## Graphical Abstract

**Green, Transition-Metal-Free Catalysts:**

**An Efficient Reusable Organocatalyst in Oxidation of Cylohexene by Oxaziridines**

Massomeh Ghorbanloo

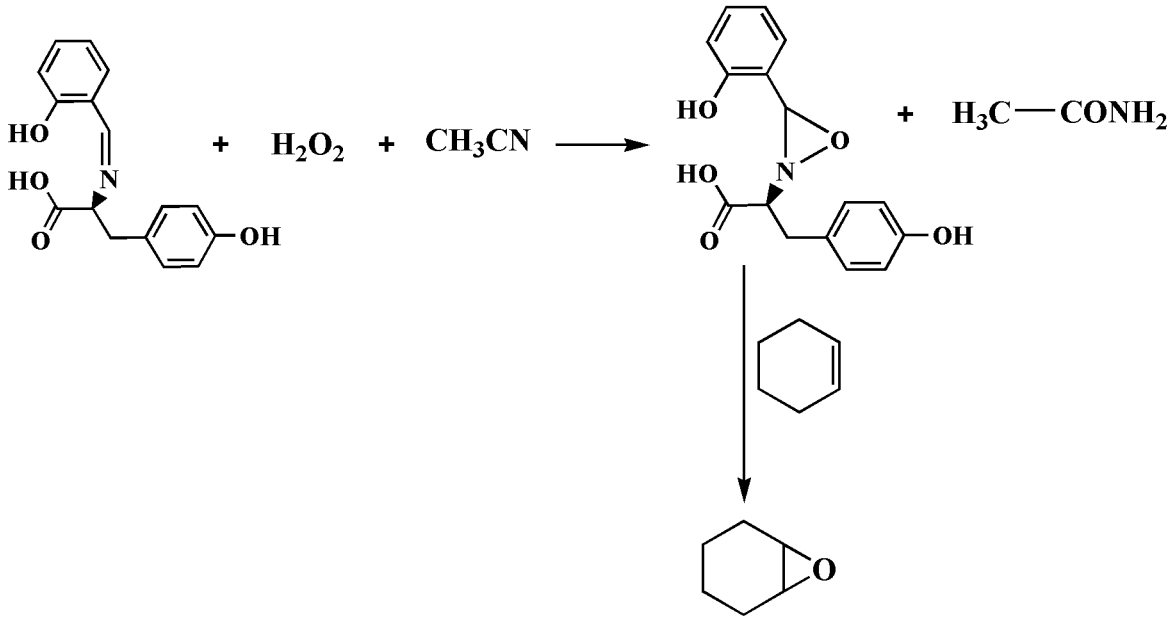

# SUPPLEMENTARY MATERIAL

## Green, Transition-Metal-Free Catalysts:

## An Efficient Reusable Organocatalyst in Oxidation of Cylohexene by Oxaziridines

Massomeh Ghorbanloo[1*a]

[a] Department of Chemistry, Faculty of Science, University of Zanjan, 45371-38791, Zanjan, Iran

Tel: +98 241 5154084; fax: +98 241 2283203

E-mail: m_ghorbanloo@yahoo.com (M. Ghorbanloo)

**Detailed GC Measurement conditions:**

Gas chromatography measurements were conducted using an HP model 6890 gas chromatograph with a flame ionization detector. TRB-5MS capillary column (30 m × 250 µm × 0.25 µm) was used to separate different products for the reaction with cyclohexene.

General GC conditions --- QD temperature: 150 ºC; Ion source temperature: 230 ºC; Injection volume: 1 microiliter; inlet temperature: 260 °C; Carrier gas: helium; the rate of carrier gas: 1.0 mL $min^{-1}$.; Oven ramp: (45 ºC) 3 min / 10 ºC $min^{-1}$ (200 ºC) 1 min 25 ˚C $min^{-1}$ (20080 ºC) 4 min.

[1] Corresponding author : Massomeh Ghorbanloo (m_ghorbanloo@yahoo.com)

**Correlative GC-MS spectra:**

1. Oxidation of cyclohexene in the presence of $H_2L/SiO_2$ as a catalyst

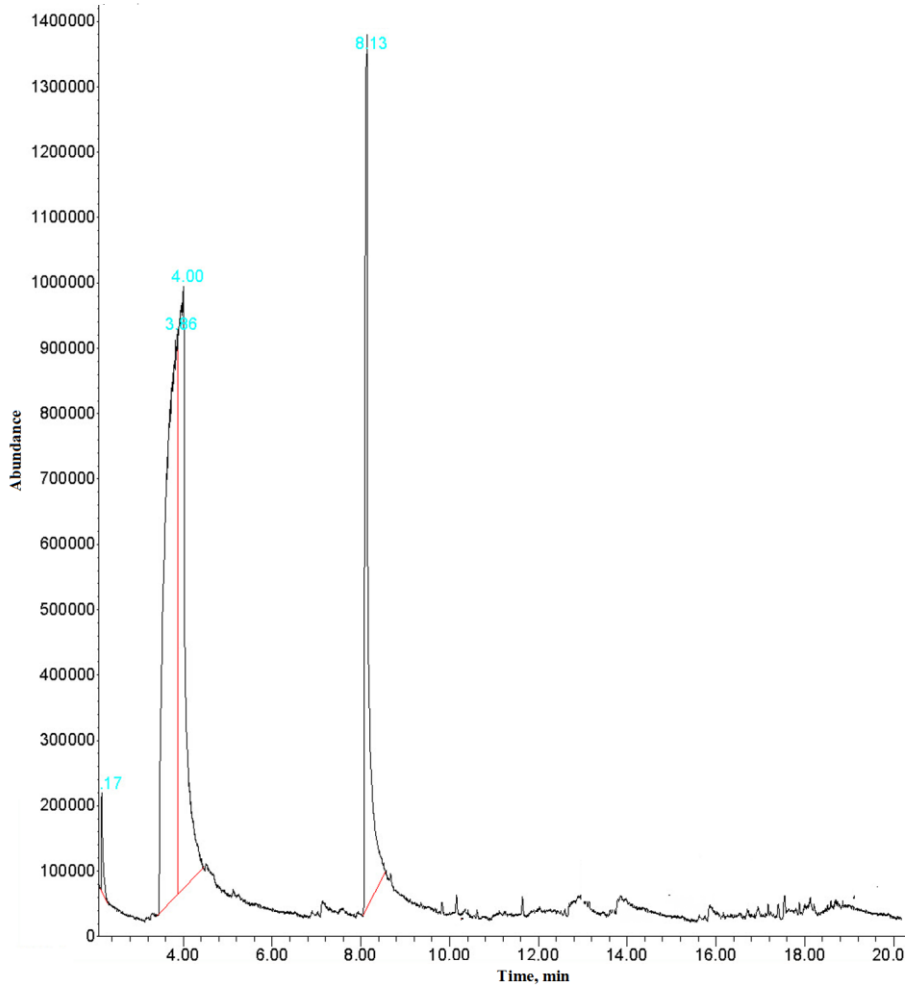


**Fig. S-1**. GC-MS of cyclohexene oxidation in the presence of $H_2L/SiO_2$ as a catalyst

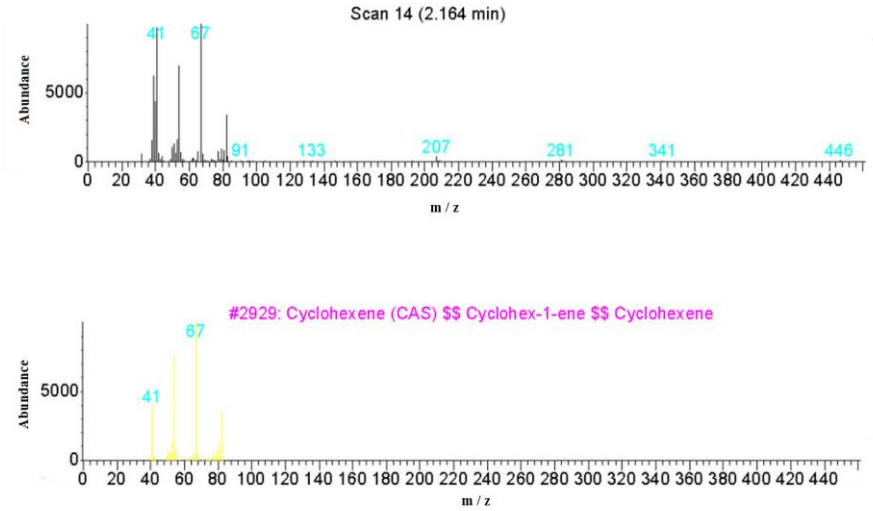


**Fig. S-1**-a

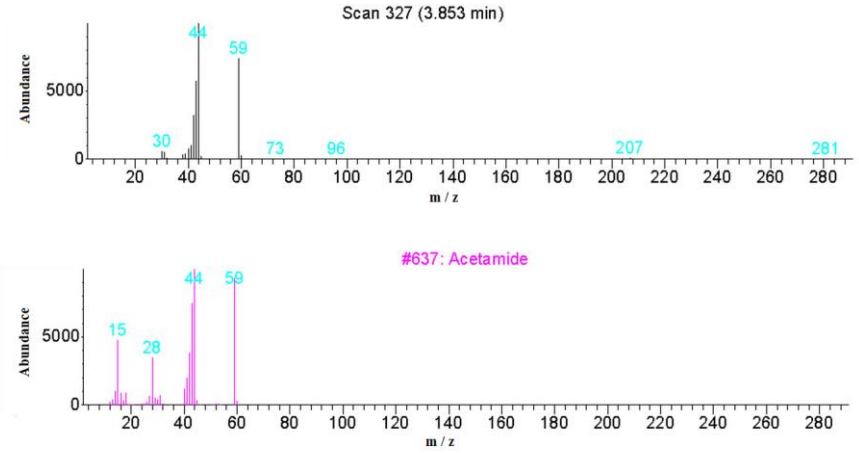


**Fig. S-1**-b

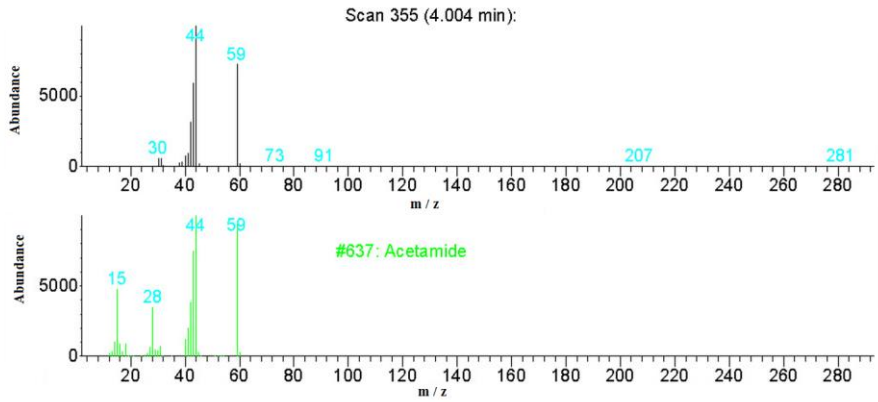


**Fig. S-1**-c

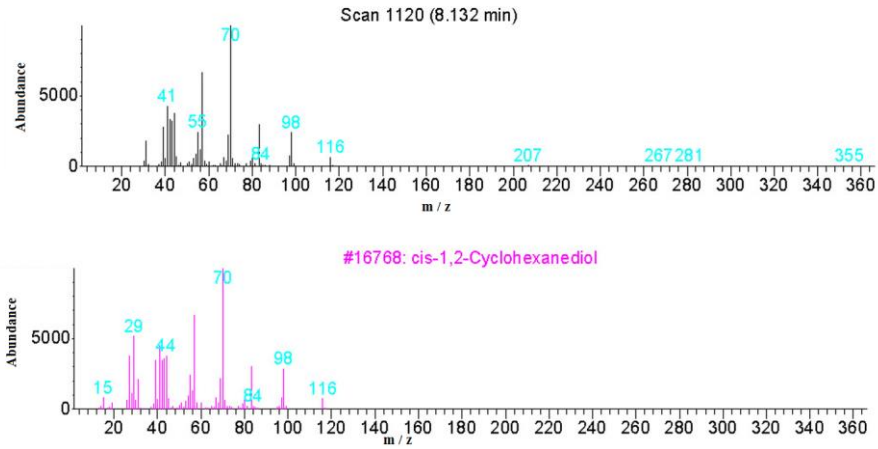


**Fig. S-1**-d

**Fig. S-1**. GC-MS of cyclohexene oxidation in the presence of $H_2L/SiO_2$ as a catalyst in comparison with references

## 2. Oxidation of cyclohexene in the presence of $H_3L$ as a catalyst

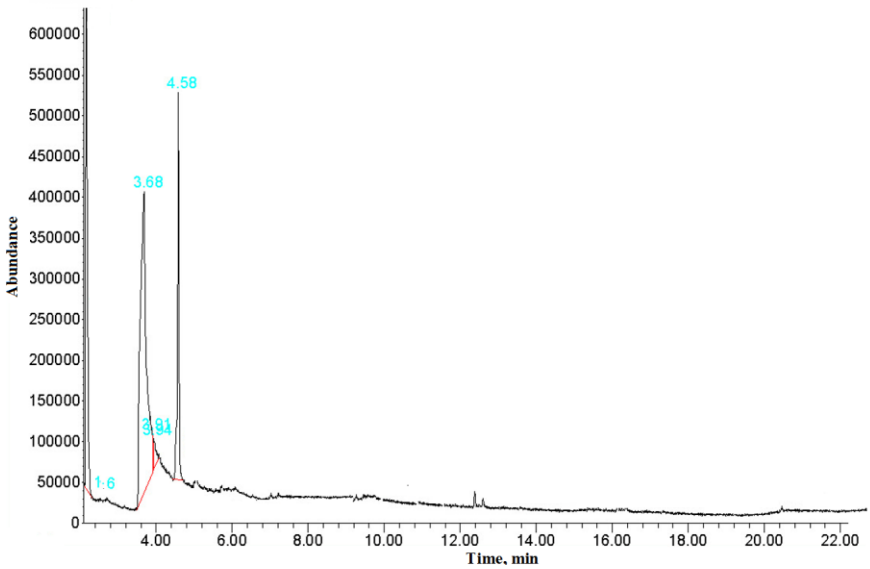


**Fig. S-2.** GC-MS of cyclohexene oxidation in the presence of $H_3L$ as a catalyst

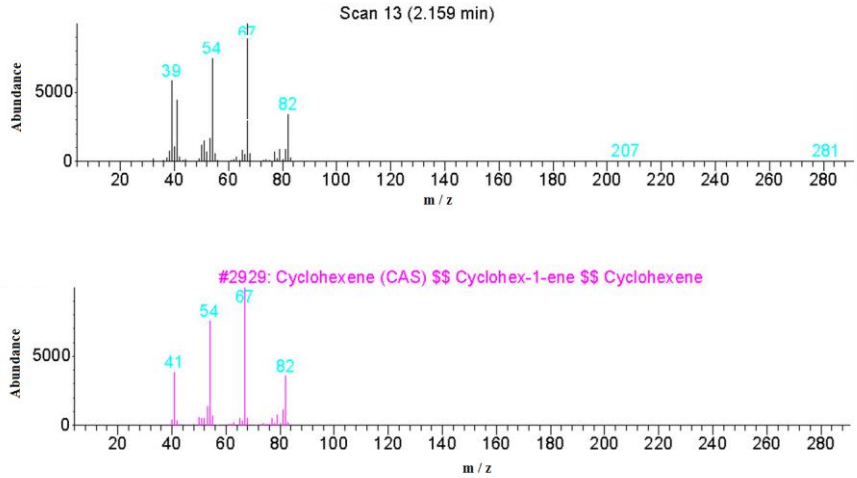


**Fig. S-2**-a

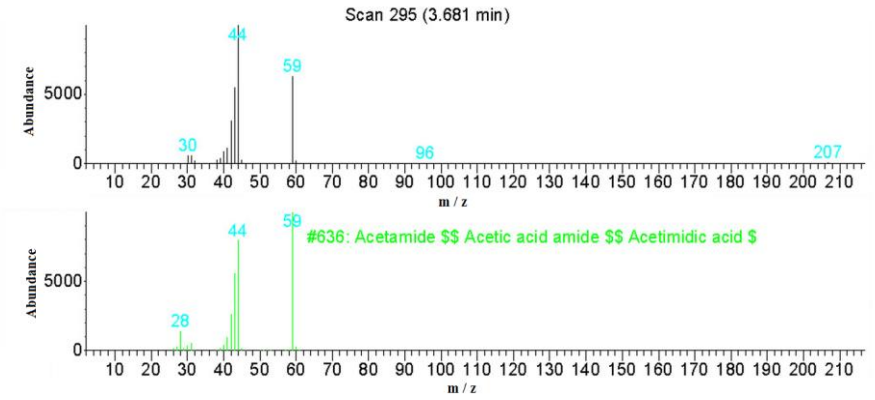


**Fig. S-2**-b

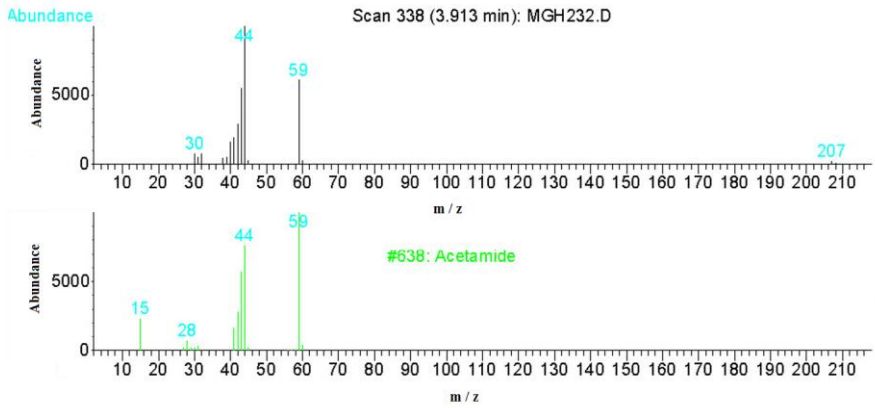


**Fig. S-2**-c

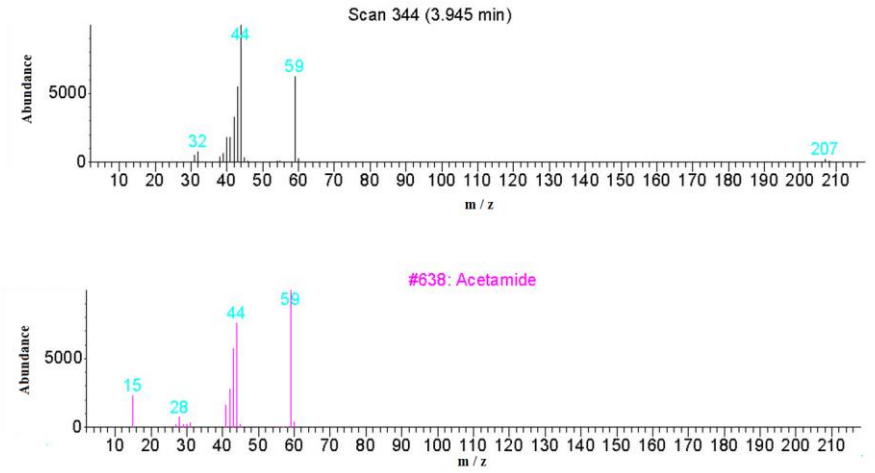


**Fig. S-2**-d

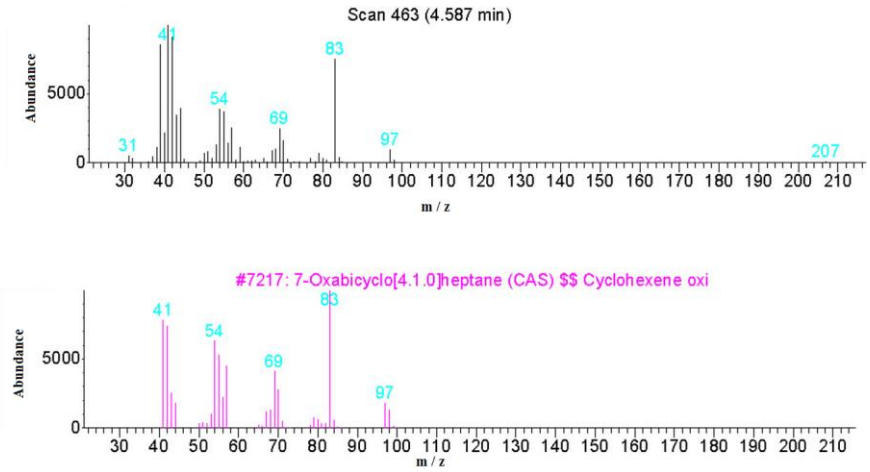


**Fig. S-2**-e

**Fig. S-2.** GC-MS of cyclohexene oxidation in the presence of $H_3L$ as a catalyst in comparison with references

# Topical Proton Affinities, Gas phase Basicities, Electron Affinity and Ionization Energy of ascorbic acid as a potential bio-catalyst

**Sharare Motamedi[1], Hamed Bahrami[1,*], Hamid Reza Shamlouei[2]**

[1] *Department of Chemistry, University of Zanjan, Zanjan, Iran*

[2] *Department of Chemistry, Lorestan University, Khorramabad, Iran*

*Corresponding author Tel.: +98 24 33052477; Fax number: +98 24 33052477

*E-mail: hbahrami@znu.ac.ir

**Abstract**

Ascorbic acid (vitamin C) has a role in lipid peroxidation reaction in living tissues. Therefore, thermodynamic quantities related to its ionization and proton transfer reactions have importance for its application for catalytic purposes. In this study, topical proton affinities, gas phase basicities, adiabatic and vertical ionization energies and electron affinities of ascorbic acid were calculated using DFT theoretical calculations. Topological analysis of atoms in molecules were used for studying the changes in molecular structures and chemical bond natures of protonated ascorbic acid isomers.

**Keywords:** Ascorbic acid; Thermodynamic properties; DFT calculations

## Introduction

Catalytic properties of ascorbic acid have long been proven. Ascorbic acid is strong catalyst in the oxidation of linoleate in aqueous solutions [1]. Iron and ascorbic acid appear to be the normal catalytic components responsible for the lipid peroxidation reaction in tissue homogenates [2]. It is found that ascorbic acid /copper dyad facilitates the oxidation of amines to carbonyl compounds [3]. Thermodynamically, ascorbic acid should be an antioxidant because of its oxidation-reduction potential and the stability of its oxidation products. Ascorbic acid functionalized polymers have implications for consumer-related applications like foods, pharmaceuticals, and personal care products [4]. Transition metal complexes of ascorbic acid encapsulated in fly ash based zeolite have been established as good catalyst [5].

Proton affinity (PA) and gas phase basicity are two important quantities which determine the capability of an atom or molecule to accept a proton in gas phase. PA is defined as -ΔH for the following reaction in the gas phase.

$$M(g) + H^+(g) \rightarrow MH^+(g) \quad (1)$$

The negative Gibbs free energy change of reaction (1) is called gas phase basicity [6]. There are different experimental techniques for determining the PA of compounds. For example, mass spectrometry and ion mobility spectrometry (IMS) can be used to measure the PA of M from the following proton-exchange reaction in gas phase,

$$M(g) + NH^+(g) \rightarrow MH^+(g) + N \quad (2)$$

Since experimental measurement of PA and GB is not easy to reach, recently there is much interest for computational methods to determine these quantities.

Adiabatic ionization energy, AIE, and electron affinity, AEA, are the energy difference between neutral molecule and its cation and anion when all species are in their ground electronic states, respectively [7]. The vertical electron affinity, VEA, is electronic energy difference between the ground states of the neutral molecule and its anion at the equilibrium geometry of the neutral molecule. IE and EA are useful quantities that make deep understanding of chemical and biological phenomena such as electron donor and acceptor abilities of DNA .

In this study, the above mentioned thermodynamic quantities of ascorbic acid were obtained computationally using DFT theoretical calculations. Topological analysis of atoms in molecules was used to check the length and the nature of the bonds in neutral and ionic structures.

## Methods

GAUSSIAN 09 program package was used to perform theoretical calculations in this study. all calculations were done using the B3LYP method and 6-311++(d,p) basis set. Topological analysis of atoms in molecules [8] using the AIM2000 series programs were used for studying the changes in molecular structures and chemical bond natures of protonated ascorbic acid isomers.

## Result and Discussion

The most stable structure of ascorbic acid reported in ref. [9] was used as initial structure and was re-optimized at B3LYP /6-311++(d,p) level of theory. Protonated isomers were constructed by adding proton to different sites in ascorbic acid and stable structure of all MH+ isomers were obtained.

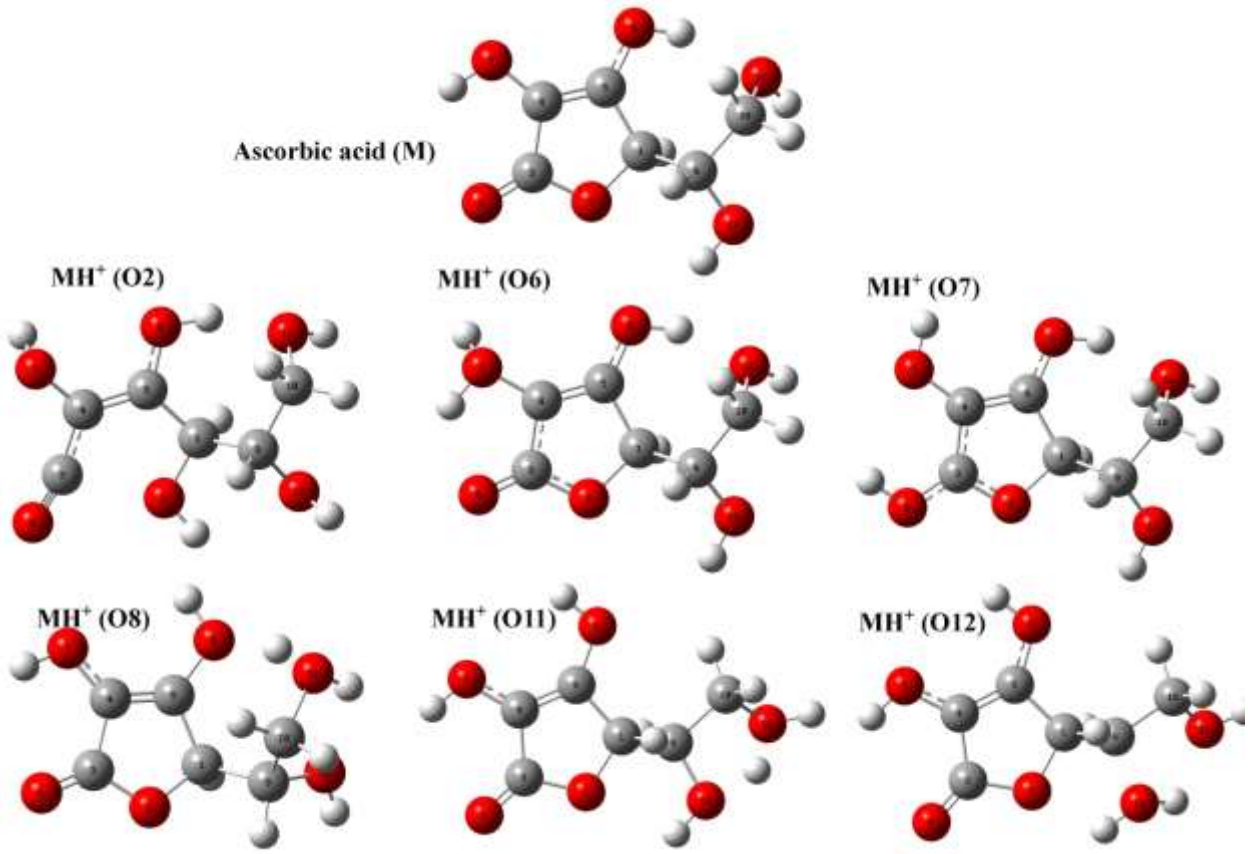


**Fig. (1).** Stable structure of ascorbic acid and its protonated isomers optimized at B3LYP/6-311++G(d,p) level of theory

The stable structures of neutral and protonated isomers of ascorbic acid is shown in Figure 1.

Proton affinity and gas phase basicities (GB) for protonation of each site was calculated and is reported in Table 1.

**Table 1.** TPA and TGB for protonation of selected sites of ascorbic acid to obtain different $MH^+$ isomers.

| Structure | PA(kJ/mol) | GB(kJ/mol) |
|---|---|---|
| M (O2) | 792.53 | 770.68 |
| M (O6) | 873.21 | 844.85 |
| M (O7) | 736.51 | 706.83 |
| M (O8) | 802.36 | 770.70 |
| M (O11) | 794.45 | 764.68 |
| M (O12) | 807.30 | 778.05 |

Some of the protonated output structures need further investigation regarding change in bond lengths. As seen in the Figure 1, protonation of O2 site has led to an increase of 0.89 Angstrom of the O2-C3 bond in comparison with neutral ascorbic acid. bond properties were examined by the AIM2000 program and the results are as follows. For this reason, critical point of bonds has been investigated, and characteristics of these points are reported in table 2. Critical points were numbered as shown in Figure 2. The parameters of O2-C3 bond critical point of neutral ascorbic acid is marked in Table 2.

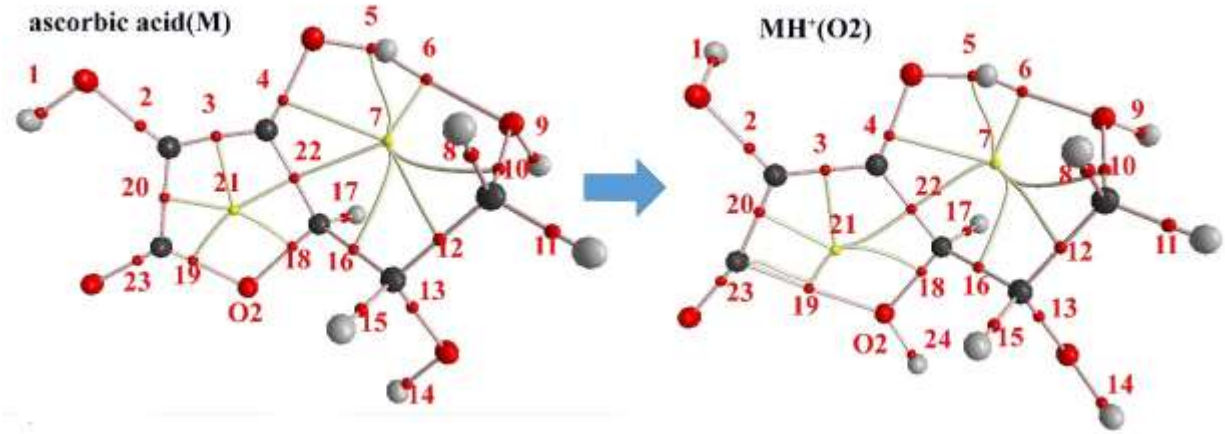


**Figure 2.** The AIM 2000 output structure of ascorbic acid and its O2 protonated isomer, MH+(O2), critical points are marked with the numbers.

**Table 2.** Specifications of critical points of chemical bonds of neutral ascorbic acid

| Critical point | $\lambda_1$ | $\lambda_2$ | $\lambda_3$ | $\rho_{(b)}$ | $\Delta^2\rho_{(b)}$ |
|---|---|---|---|---|---|
| 1 | -1.7901 | -1.7513 | 1.0287094 | 0.0358552 | -2.512828 |
| 2 | -0.621006 | -0.577945 | 0.80040 | 0.295071 | -3.98551 |
| 3 | -0.757469 | -0.523459 | 0.207109 | 0.33854 | -0.983816 |
| 4 | -0.643758 | -0.609326 | 0.876840 | 0.301718 | -0.362444 |
| 5 | -1.771531 | -1.73854 | 1.0439701 | 0.34765 | -2.4662 |
| 6 | -0.042275 | -0.041019 | 0.188104 | 0.029616 | 0.104808 |
| 7 | -0.002882 | -0.020137 | 0.033391 | 0.009918 | 0.050644 |
| 8 | -0.785353 | -0.755243 | 0.545629 | 0.285855 | -0.994964 |
| 9 | -1.79616 | -1.752353 | 1.03084 | 0.3637481 | -2.517675 |
| 10 | -0.4268377 | -0.417195 | 0.427151 | 0.2427905 | -0.416882 |
| 11 | -0.774318 | -0.747285 | 0.547837 | 0.2831655 | -973764 |
| 12 | -0.5014764 | -0.049374 | 0.378191 | 0.2549264 | -0.61702 |
| 13 | -0.4720652 | -0.462249 | 0.431138 | 0.2542709 | -0.502176 |
| 14 | -1.787074 | -1.743121 | 1.023422 | 0.3637215 | -2.506774 |
| 15 | -0.7607462 | -0.737031 | 0.54009 | 0.211255 | -0.957686 |
| 16 | -0.472922 | -0.463481 | 0.378923 | 0.244266 | -0.557480 |
| 17 | -0.774462 | -0.751434 | 0.553721 | 0.282885 | -0.972114 |
| 18 | -0.436004 | 0.4305491 | 0.399469 | 0.244699 | -0.467084 |
| 19 | -0.566823 | -0.575401 | 0.6319603 | 0.282962 | -0.52024 |
| 20 | -0.607691 | -0.5023015 | 0.373489 | 0.283654 | -0.7365028 |
| 21 | -0.040756 | 0.166995 | 0.173233 | 0.044333 | 0.299472 |

| | | | | | |
|---|---|---|---|---|---|
| 22 | -0.5224299 | -0.469463 | 0.3732043 | 0.258508 | -0.418689 |
| 23 | -1.122581 | -1.0279139 | 1.948151 | 0.419758 | -0.202344 |

The bonding profile was investigated at the critical point of the O2-C3 bond of O2 protonated ascorbic acid, the results are as follows: bond length= 2.26, electron density $\rho_{(b)}$ = 0.33415, $\lambda_1$= -0.337855, $\lambda_2$= -0.0303738, $\lambda_3$= 0.1761676, $\Delta^2\rho_{(b)}$, and Laplace density = 0.112009.

In the interactions that Laplace and Hamiltonian have positive sign in the critical point, the nature of the bond depends on the electron density in the critical point. According to the data and explanations provided, the interaction between C3-O2 after proton attachment to the O2 site is a weak interaction and has a Van der Waals character. This results suggests that attachment of proton to the O2 site can lead to dissociation of a chemical bond of this oxygen atom with the adjacent carbon atom. This can be the starting point to decomposition of protonated ascorbic acid.

Ionization energy and electron affinity of ascorbic acid as important thermodynamic values have been reported in previous studies. In the study on the structure of ascorbic acid by Abdoulamir et al., IE and EA was reported as 8.669 eV and 0.95 eV, respectively [10]. Also, Doco et al. Measured IE and EA in three computational methods as IE = -0.98, 1.14, 1.42 and EA=8.98, 8.49, 7.43 eV [11].

The vertical and adiabatic IE and EA calculated in this study are listed in table 2.

**Table 2.** IE and EA of ascorbic acid at B3LYP/6-311++G(d,p) level of theory, values are reported in both eV and kJ/mol.

| | Adiabatic(eV) | Vertical(eV) | Adiabatic(kJ/mol) | Vertical(kJ/mol) |
|---|---|---|---|---|
| IE | -0.295 | 8.73 | -28.46 | 842.78 |
| EA | -0.295 | 0.19 | -28.46 | 18.38 |

As can be seen in table 2, adiabatic values for both IE and EA are negative but vertical values are positive.

## Conclusion

Topical Proton Affinities, Gas phase Basicities, Ionization Energy and Electron Affinity of ascorbic acid was calculated in this study. The investigation of chemical bonds in protonated isomers of ascorbic acid showed that protonation of one of the oxygen sites can lead to decomposition of the structure of the molecule. Therefore, ascorbic acid can not be a desirable catalyst in cases where catalyst participation in proton transfer reactions is required.

## References

[1] G. Haase and W.L. Dunkley, *J. Lipid Res.*, **1969**, *10*, 555-560.
[2] A.A. Barber, *Lipids*, **1966**, *1*, 146-151.
[3] J. Srogl and S. Voltrova, *Org. Lett.*, **2009**, *11*, 843-845.
[4] A. Singh and D.L. Kaplan, *Adv. Mater.*, **2003**, *15*, 1291-1294.
[5] T.P. Amaladhas and S.S. Thavamani, *Adv Mat Lett*, **2013**, *4*, 688-6904.
[6] M. Tabrizchi and S. Shooshtari, *J. Chem. Thermodyn.*, **2003**, *35*, 863-870.
[7] J.C. Rienstra-Kiracofe, G.S. Tschumper, H.F. Schaefer, S. Nandi and G.B. Ellison, *Chem. Rev.*, **2002**, *102*, 231-282.
[8] F. Biegler-König and J. Schönbohm, *J. Comput. Chem.*, **2002**, *23*, 1489-1494.
[9] I. Peña, A.M. Daly, C. Cabezas, S. Mata, C. Bermúdez, A. Niño, J.C. López, J.-U.

Grabow and J.L. Alonso, *J. Phys. Chem. Lett.*, **2012**, *4*, 65-69.
[10] A.A. Al-Amiery, K.Y. Saour, D.L. A-Duhaidahawi, Y.K. Al-Majedy, A.A. Kadhum and A.B. Mohamad, *Free Radicals and Antioxidants*, **2017**, *7*, 31-35.
[11] R.C. Doco, M.K. Houngue and G.A. Kpotin, *J. Chem. Pharm. Res.*, **2017**, *9*, 231-236.

## Graphical Abstract

Topical Proton Affinities, Gas phase Basicities, Electron Affinity and Ionization Energy of ascorbic acid as a potential bio-catalyst

Sharare Motamedi, Hamed Bahrami*, Hamid Reza Shamlouei

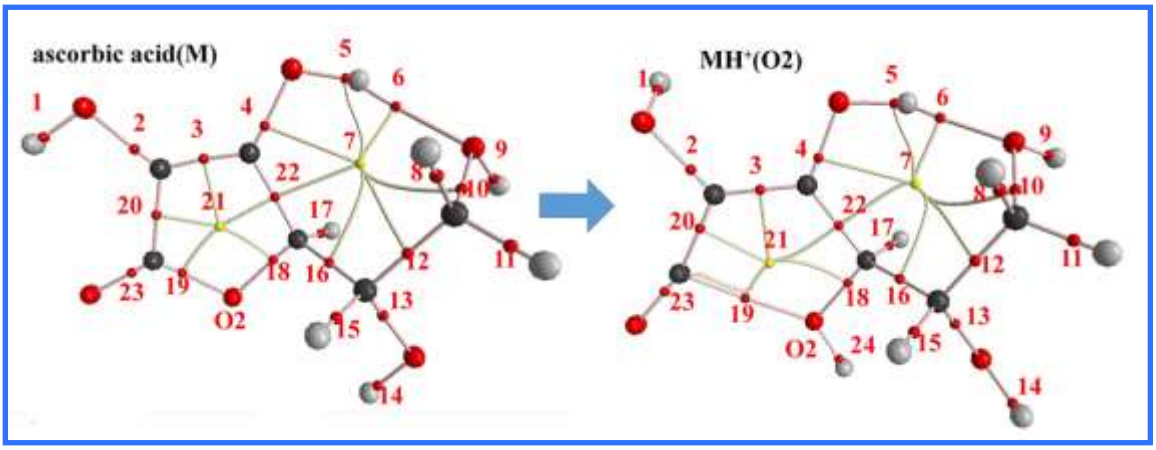

# The preparation and synthesis of the most well-known Nanoparticles and their applications in water contaminants removal

**Armin Zarei***

Young Researchers and Elite Club, Sanandaj Branch, Islamic Azad university, Sanandaj, Iran
*E-mail: zareie.ar@gmail.com

## Abstract

It is undeniable that magnetic nanoparticles and their magnificent dispersion properties in liquids are revealed to be more beneficial. Therefore over the last decade there have been, a number of longitudinal studies involving MNPs, which not only reported the hazardous influences on humans, but also on the environment. For this reason, the MNPs are drawing researchers' attraction for future scientific research. What is more, recent advances in the procedure of modern nanoparticles are never ignored in long-term. It should be noted that this study has systematically reviewed the critical role of MNPs in eliminating poisonous metals, which pose a threat to our health in aqueous environment. The most prevalent metallic substances could be Cd, Cr, Cu, Pb, Hg, and Ni. Sb, Pd, Pt, the diverse metallic species that are removed by the use of MNPs from wastewater and aqueous solutions.

***Keywords: magnetic nano particles, poisonous metals, aqueous solutions, Cd, Cr, Cu, Pb, Sb, Pd, Pt.***

## Introduction

The impact of water pollution on human's health and the nature has noxiously affected the environment so that some life forms are in danger of extinction. Today's world population is booming and we are witnessing the world's fast economic progress, gaining momentum. Therefore, it is going to have a critical role in urbanization and increasing population growth as well as industrialization. This has led the Earth to endure a growing number of dangerous challenges such as global warming, climate change, excessive waste producing, resulting in drastic environmental depreciation and making an imbalanced ecosystem that the planet has ever experienced.

In human's history, water has been thought to be a key factor in the flow of life. As time goes on, the needs of human beings for water seems more indispensable as the population is booming. Nonetheless, nowadays millions of citizens are unfortunately suffering from the lack of drinking water resources. What is more, over the past thirty years there has been increasingly rapid demand in the supply of pure and clean drinking water.

As a result, it is sometimes believed that one third of the global population are more likely to face famine and drought by the following twenty years because of the excessive consumption of ground water for agriculture aim, which could be ceased to exist at least to keep water resources for the next generations. Consequently, the water resources onto the planet are run out by over abuse, the poor policy of countries toward the water crisis and last but not least environmental contamination. The

principal fountainhead of water pollution should be attributed to release untreated water, dumping industrial waste as well as run-off from rural fields.

Moreover, threatening behavior of mankind on the planet towards the environment and his activities to manipulate the earth's resources, such as farming, the industrialization, booming population growth and increasing sewage production have all been detrimental impact on water quality. Unluckily, the quality of water suffers from these harmful activities.

Accordingly, in the present supercritical situation water impurity, affecting all species, has posed a serious threat to the human health that should never be taken for granted. It means that the water crisis has been turned into an international concern for the governments, scientists, scholars and environmentalists [1-3].

As life on the earth depends on clean water, preserving and protecting the aquatic environment and its resources against contaminants is a must and people should be educated to safeguard the nature to have a healthier life. To reach this goal, being dependent on traditional solutions, which are time-consuming and costly, seems inefficient. Specialists and scientists should come up with some ideas to address the problem. It is often asserted that robust and technological improvements are needed to tackle the sophisticated issue. Although such new methods for water purification have their own pros and cons, the benefits far outweigh the drawbacks, meaning that water filtration ought to be done economically and less chemicals/energy consumption, however environmental effects should be considered in the long-term. In comparison to existing treatment techniques, which can undermine the impacts on the environment, new technologies are more cost-effective so that they are in demand in the global market. Thus, the new and modern ways to overcome the global water pollution barriers are sedimentation, filtration, centrifugation, crystallization, precipitation, oxidation, floatation, solvent extraction, dissipation, refining, reverse osmosis, particle diffusion, gravity separation, adsorption, and so on. Adsorption is ascribable to the most appropriate water strategy owing to its terrific features like easy utilization and different ranges of high adsorption as well as scale segments [4].

The other applications of adsorption, which could be applied, are source recovery for consumable, mechanical and the other water purposes.

In spite of these facts, adsorption has its own demerits. For one thing, because of the lack of high adsorption capacity of adsorbents, it could never get the position at commerce levels. However, it is more likely to be one the most special water treatment in the near future. For this reason, over the past decade, most research done in the water treatment has emphasized the use of adsorption method.

Besides, activated carbon [5-8] was employed to remove heavy metals from water, using cost-effective adsorbing substances. The other forms of adsorbents namely fly ash [9-11], soya cake [12-13], and alumina [14-17] have been applied for the water pollutants removal.

It should never be repudiated that nanotechnology has become more lucrative and handy in relatively all branches of science. Today, nanotechnology is considered as a key factor for the water treatment. During the last ten years, a great deal of progress has been made to develop environmentally-friendly and cost-effective water refinement.

Thanks to nanotechnology scientists have been able to prepare nano-materials as adsorbents to omit poisonous and damaging combinations from water and wastewater. Water remediation via nanotechnology has attracted a great deal of attention among scientific community, so the aim of the present review is to highlight the projects which have been carried out over the last couple of years with the assertion of removing heavy metals from aqueous solutions.

**1.1. Adsorption**

Adsorption is the adhesion of atoms, ions or molecules from a gas, liquid or dissolved solid to a surface [19]. The process creates a film of the adsorbate on the surface of the adsorbent. Adsorption is a surface phenomenon, while absorption involves the whole volume of the material. The term sorption encompasses both Procedures, while desorption is the reverse of it similar to surface tension, adsorption is a consequence of surface energy. In a bulk material, all the bonding requirements (ionic, covalent or metallic) of the constituent atoms of the material are filled by other atoms in the material.

However, atoms on the surface of the adsorbent are not wholly surrounded by other adsorbent atoms and therefore can attract adsorbates. The exact nature of the bonding depends on the details of the species involved, but the adsorption process is generally classified as physic sorption (characteristic of weak van der Waals forces) or chemisorption (characteristic of covalent bonding). It may also occur due to electrostatic attraction [18].

**1.2. Synthesis of nanoparticles**

The preparation of NPs is observed as a critical stage in the water purification procedure. Generally, there are two steps in the preparing NPs: the bottom-up approach and the top-down one. The former way of NPs synthesis involves the arrangement of smaller molecules atom-by-atom or molecule-by-molecule into more complex assemblies and the latter way in which the nanoparticles from large

size (i.e., granular or micro-scale) are needed. Several methods for the NPs synthesis might be sol-gel process [20], precipitation [21] precipitation [22], catalytic growth [23], mechanical alloying/milling [24], mechano-chemical synthesis [25], impregnation [26], electro-deposition [27], laser ablation [28] and inert gas condensation [29]. These methods can be utilized for the surface Modification of NPs and applied in the wide ranges of areas. Furthermore, based on their shape and size, prepared NPs could be categorized into the followings: nano-particles, nano-tubes, nano-wires, nano-belts, nano-capsules, nano-fibres, nano-polymers, etc.

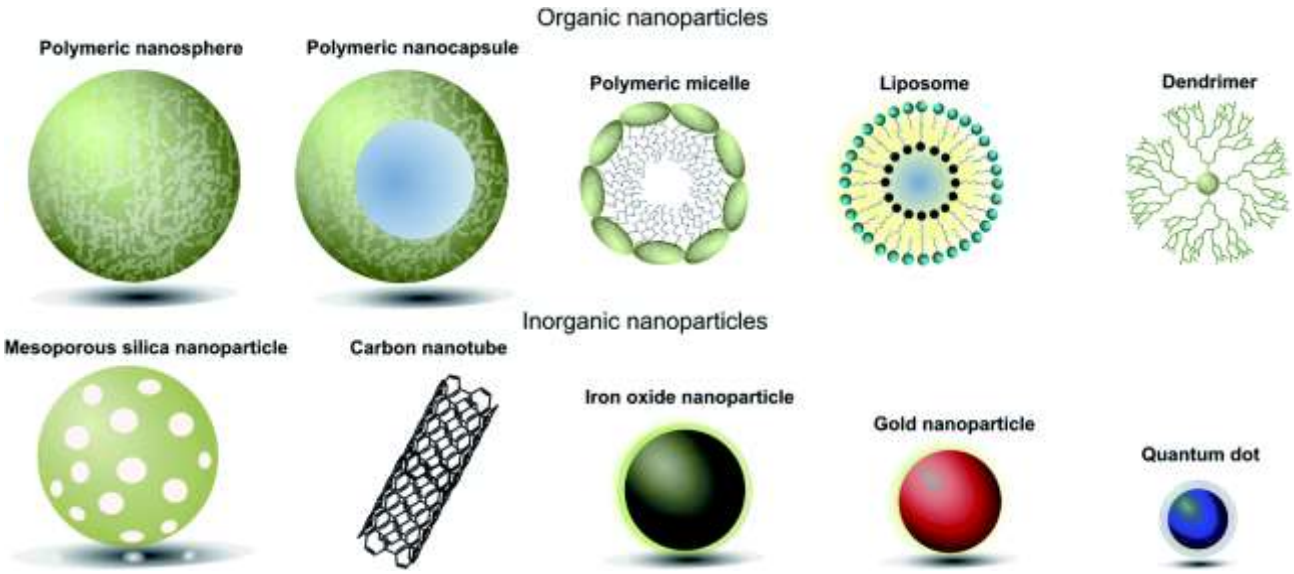


**Figure 1.** Organic nanoparticles

### 1.2. 1.3.Charcterization of nanoparticles

Special analytical techniques, such as X-ray diffraction (XRD), Fourier transform IR (FTIR) spectroscopy, scanning electron microscopy (SEM), transmission electron microscopy (TEM), and thermo-gravimetric analysis (TGA) are used for the

characterization of NPs, and the information altered over through these techniques illustrated in Table 1.

**Table 1**

Characterization techniques of nano-particles synthesized as an adsorbent for water treatment.

| Characteristics | Analytical techniques |
|---|---|
| Thermal properties | Thermo-gravimetric analysis (TGA) |
| Heavy Metal-NPs interaction | Extended X-ray absorption fine structure (EXAFS) spectroscopy |
| | X-ray absorption near edge structure (XANES) spectroscopy |
| | X-ray photoelectron spectroscopy (XPS) |
| | UV–Vis diffuse reflectance spectrometer |
| | Diffuse reflectance infrared Fourier transform (DRIFT) spectroscopy |
| | Fourier transform infrared (FTIR) spectroscopy |
| | Attenuated Total Reflectance infrared (ATR-IR) spectroscopy |
| | Raman spectroscopy |
| Particle size | Transmission Electron Microscope (TEM) |
| Crystal structure | X-ray diffraction (XRD) |

## 1.4. Nano-adsorbents

NPs are the engineered substances which have one dimension in nano-range, between 1 and 100 nanometers (nm), with a surrounding interfacial layer. The interfacial layer is an integral part of nanoscale matter, fundamentally affecting all of its properties [30].

It is no doubt true that these nano materials have enchanting features so that they are used in the broad range of scientific and technological branches including environment, electronics, medicines, drug delivery, gene delivery, cancer treatment and so on [31]. In comparison to macromolecules, these nanoparticles have attracted much attention as adsorbents due to their vital amount of surfaces. The reason why the water remediation is their excellent characteristics. The most distinctive features, that should be highlighted, are small size, catalytic potential, high reactivity, large surface area, ease separation and large number of active sites for interaction with different contaminants [32-33]. NPs are more likely to be modified because of the increasing electronic density at their edges, variety of surfactants and functional groups could be added to their surface to fortify their surface features like reactivity, affinity, capacity, and selectivity toward target pollutants in aqueous solutions [34]. Ttherefore, various NPs synthesized so far for water purification and their corresponding method of synthesis shown in Table 2.

**Table2**

Disparate approachess of NPs preparation applied as an adsorbent for water mitigation.

| Nanoparticles | Methods | Diameter(nm) | Starting materials | Ref. |
|---|---|---|---|---|
| Akaganiete | Precipitation method | 2.6 | Iron(III) chloride, ammonium carbonate | [35] |
| Alumina | Sol-gel method | 6-30 | ALCL3.6H2O | [36] |
| Anatase | Solvothermal method | 8-20 | Titanium (IV) ethoxide, ethanol | [37] |
| Iron oxide | Hydrothermal Synthesis | 14-25 | Iron sulfate, n-decenoic acid or n-decylamine | [38] |

## 1.5. Application of nano-adsorbents

### 1.5.1. detraction of inorganic pollutants

Some heavy metals that are most well-known toxic and venomous water polluters which cause different types cancers. One of these carcinogenic heavy metals could be arsenic, that is ascribed as direful metal because of its symptoms. Mercury (Hg), Lead (Pb), Cadmium (Cd), Chromium (Cr) and Selenium (Se) are the other metals with high serious toxic features. Although reasonable dose of various types of metals are crucial for the human body, by higher dose could be brought about terrible diseases, take as an illustration, permissive dose of Zinc is vital for the body ordinary development, but higher doses than allowable dose of Zinc cause mental pyrexia and poor development. Besides, queasiness, asthma, and carcinoma are considered to be caused by Cobalt. The surface and ground-waters at a few lands of various countries are less likely to be suitable for drinking purposes.

Since water resources have been contaminated by pestilent heavy metals, the scenario has been so complicated so that removal heavy metals from water resources should be put the first priority for nations. For water purification through adsorption process, the most commonplace applied nano adsorbents are iron oxides (FeO), silica (SiO2), manganese oxides (MnO2), aluminium oxides (Al2O3), and titanium oxides (TiO2) [39].

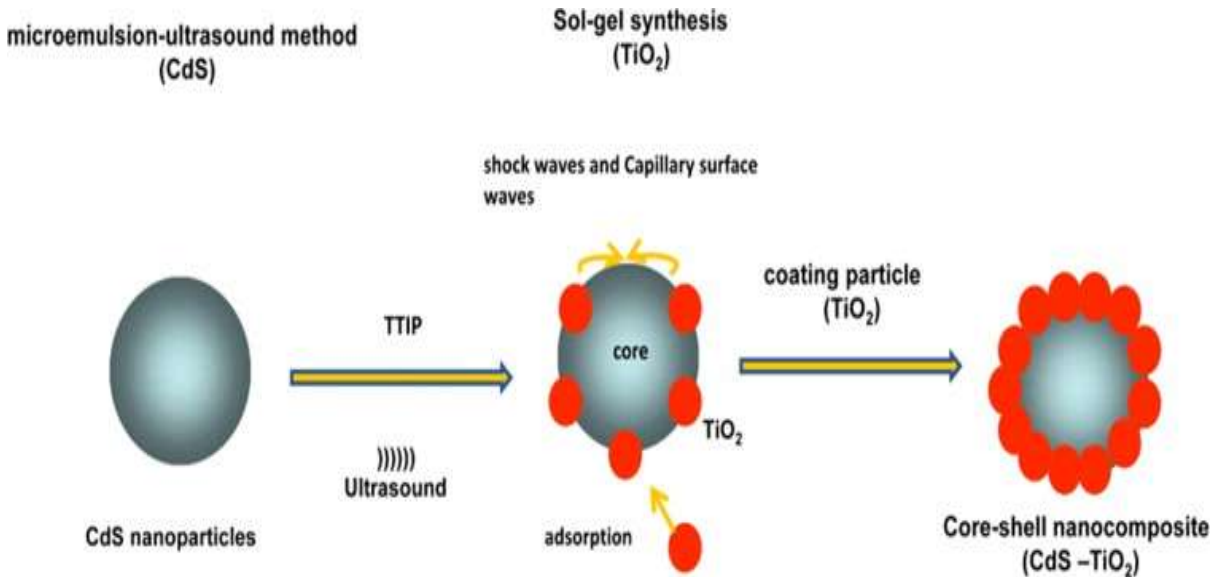


**Figure 2.Schematic illustration of various mechanisms of adsorption of metal ions by nanoparticles.**

## 1.6. Draw an analogy between adsorption capacity of nanoparticles and routine low-cost adsorbents

In recent years, there has been an increasing amount of literature on the removal heavy metals from water resources via nano adsorbents, yet nano substances commercial applications in water remediation have never been focused. Therefore, it means that the positive points of low cost adsorbents are greater than the nano particles, so this issue has attracted too much interests among scientific societies.

The most obvious advantage of the former over the latter is that the low-cost adsorbents have been used for the removal of almost all types of pollutants, in contrast to the nanoparticles that have been used in the removal of few, Besides, it is often asserted that make a comparison between these two is not so meaningful owing to applying various experimental conditions for the heavy metals elimination not only via nano adsorbents, but also via nano particles. A considerable amount of literature has been published to compare the adsorption capacities of both these two types of adsorbents for removal of certain heavy metals. Shanqin Ni et al. [40] argued the adsorption of toxic metals such as Cr, Zn, Cd and Pb on iron oxides during carbonate rock weathering process.
In their major study, Recillas et al. [41] used commercial activated carbon to determine the adsorption capacities of Cd (II) and Pb (II) ions respectively. Kumar and Jana [42] investigated the impact of $CeO_2$ NPs on Cr (VI) ions adsorption and they gained maximum adsorption capacity of 121.95 mg at 80 mg/L of initial Cr(VI) concentration [42].

Likewise, in the scenario of removing heavy metal ions, activated carbon played a significant role in a number of publications. However, in terms of performance toward toxic metal ions, NPs adsorbents should be

prioritized in comparison to activated carbons. There are some convincing reasons to this fact, first of all, NPs have a high ability under varied pH. Second of all, they are low dose requirements, time-consuming and faster removal.

## Conclusion

The review study has gone some way towards enhancing our understanding of the crucial efforts that have been done by a number of researchers for introducing new and advanced approaches to remove poisonous metallic species from water and wastewater. These projects show that nano-technology have been proved to be the first option in terms of water treatment. Although using NPs in this area has its own pros and cons, its benefits far out weight its drawbacks. The top and most significant advantages of NPs towards the other means of water remediation, are low dose requirement, separation easy, regeneration and reusability, fast removal and so on.

Besides, Regeneration and reuse capability of NPs makes their application economical. They are also capable of the inorganic pollutants removal at the variety ranges of pH and temperature. Consequently, it could be mentioned that the NPs are the best candidate for the water remediation due to their magnificent features in terms of removing contaminants from aqueous solutions.

## References

[1] T.A. Kurniawan, G.Y.S. Chan, W.H. Lo, S. Babel, Sci. Total Environ. 366 (2006) 407.

[2] S.S. Banerjee, D.H. Chen, J. Hazard. Mater. 147 (2007) 792.

[3] C.R. Yonzon, D.A. Stuart, X.Y. Zhang, A.D. McFarland, C.L. Haynes, R.P. Duyne,

Talanta 67 (2005) 438.

[4] G. Crini, Prig. Polym. Sci. 30 (2005) 38.

[5] D. Aggarwal, M. Goyal, R.C. Bansal, Carbon 377 (1999) 1989.

[6] M.M. Rao, A. Ramesh, G.P.C. Rao, K.K. Seshaiah, J. Hazard. Mater. 129 (2006) 129.

[7] K. Kadirvelu, K. Thamaraiselvi, C. Namasivayam, Sep. Purif. Technol. 24 (2001) 497.

[8] D. Mohan, V.K. Gupta, S.K. Srivastava, S. Chandra, Colloids Surf. A Physicochem.

Eng. Asp. 177 (2000) 177.

[9] M. Rao, A.V. Parwate, A.G. Bhole, Waste Manag. 22 (2002) 821.

[10] E. Diamantopoulos, S. Ioannidis, G. Sakellaropoulos, Water Res. 12 (1993) 1773.

[11] A. Kapoor, T. Viraraghavan, J. Environ. Eng. ASCE 122 (1996) 243.

[12] C.P. Covas, L.W. Alvarez, W.M. Argulles, J. Appl. Polym. Sci. 46 (1992) 1147.

[13] G.L. Rorrer, T.Y. Hsien, J.D. Way, Ind. Eng. Chem. Res. 32 (1993) 2170.

[14] T. Viraraghvan, A. Kapoor, Appl. Clay Sci. 9 (1994) 31.

[15] S.Q. Memon, N. Memon, S.W. Shah, M.Y. Khuhawar, M.I. Bhanger, J. Hazard.Mater.

139 (2007) 116.

[16] K. Vijayaraghavan, J. Jegan, K. Palanivelu, M. Velan, Sep. Purif. Technol. 44 (2005)

53.

[17] N. Daneshwar, D. Salari, S. Aber, J. Hazard. Mater. 94 (2002) 49.

[18] Ferrari, L.; Kaufmann, J.; Winnefeld, F.; Plank, J. (2010). "Interaction of cement model systems with superplasticizers investigated by atomic force microscopy, zeta potential, and adsorption measurements.

[19] "Glossary". The Brownfields and Land Revitalization Technology Support Center. Retrieved 2009-12-21.

[20] K. Phiwdang, S. Suphankij, W. Mekprasart, W. Pecharapa, Energy Procedia 34

(2013) 740.

[21] K. Petcharoen, A. Sirivat, Mater. Sci. Eng. B 177 (2012) 421.

[22] Y.H. Li, J. Ding, Z. Luan, Z. Di, Y. Zhu, C. Xu, D. Wu, B. Wei, Carbon 41 (2003) 2787.

[23] R. Arbain, M. Othman, S. Palaniandy, Miner. Eng. 24 (2011) 1.

[24] T. Tsuzuki, P.G. McCormick, J. Mater. Sci. 39 (2004) 5143.

[25] A. Kukovecz, Z. Balogi, Z. K'onya, M. Toba, P. Lentz, S.I. Niwa, F. Mizukami, A.

Moln'ar, J.B. Nagy, I. Kiricsi, Appl. Catal. A Gen. 228 (2002) 83.

[26] H. Park, P. Ayala,M.A. Deshusses, A. Mulchandani, H. Choi, N.V.Myung, Chem. Eng.

J. 139 (2008) 208.

[27] R.K. Thareja, S. Shukla, Appl. Surf. Sci. 253 (2007) 8889.

[28] K.K. Nanda, F.E. Kruis, H. Fissan, H. Acet. J. Appl. Phys. 91 (2002) 2315.

[29]Batista, Carlos A. Silvera; Larson, Ronald G.; Kotov, Nicholas A. (2015-10-09). "Nonadditivity of nanoparticle interactions". Science. 350 (6257): 1242477.

[30] Vert, M.; Doi, Y.; Hellwich, K. H.; Hess, M.; Hodge, P.; Kubisa, P.; Rinaudo, M.; Schué, F. O. (2012). "Terminology for biorelated polymers and applications (IUPAC Recommendations 2012)". Pure and Applied Chemistry. 84 (2)

[31] K. Hristovski, A. Baumgardener, P. Westerhoff, J. Hazard. Mater. 147 (2007) 265.

[32] A. Khaleel, P.N. Kapoor, K. Klabunde, J. Nanostruct. Mater. 11 (1999) 459.

[33] M.S. Mauter, M. Elimelech, Environ. Sci. Technol. 42 (2008) 5843.

[34] E.A. Deliyanni, K.A. Matis, Sep. Purif. Technol. 45 (2005) 96.

[35] W.M. Zeng, L. Gao, J.K. Guo, Nanostruct. Mater. 10 (1998) 543.

[36] Y. Gao, R.Wahi, A.T. Kan, J.C. Falkner, V.L. Colvin, M.B. Tomson, Langmuir 20 (2004) 9585.

[37] S. Takami, T. Sato, T. Mousavand, S.I. Ohara, M. Umetsu, T. Adschiri, Mater. Lett. 61 (2007) 4769.

[38] E.A. Deliyanni, N.K. Lazaridis, E.N. Peleka, K.A. Matis, Environ. Sci. Pollut. Res. 11 (2004) 18.

[39] T.A. Kurniawan, G.Y.S. Chan, W.H. Lo, S. Babel, Sci. Total Environ. 366 (2006) 407.

[40] Shanqin Ni, Yiwen Ju, Quanlin Hou , Shijie Wang, Qing Liu,
Yudong Wua, Lingling Xiao, Progress in Natural Science 19 (2009) 1133‑1139,

[41] S. Recillas, J. Colón, E. Casals, E. González, V.A. Puntes, S.X. Font, J. Hazard. Mater. 184 (2010) 425.

[42] A. Kumar, H.M. Jena, J. Env. Chem. Eng. 5 (2017) 2032.

# History of Coordination polymerization of olefins (From Ziegler Natta to Brookhart catalyst)

## Review Article

**Sohrab Rahmani *[a] and Peyman Atashi [b]**

[a,b]-*Laboratory of Polymer Synthesis, Department of Chemistry,*

*Faculty of Science, University of Zanjan, Zanjan, Iran*

*Corresponding author Tel.: +98 (24) 33052589; Fax number: +98 (24) 33052589

*E-mail: rahmani.sohrab@znu.ac.ir

---

Science progress and time passage make human look for methods to convert raw materials to advanced materials in order to broaden application and lower cost effect. Most of these materials are carbon based which their main source can be found in oil and natural gas. For this reason, catalysts that can convert light olefins to advanced polymers have been always at the forefront for the past 100 years since the first coordination polymerization in 1930 by Ziegler -Natta. In this article we review and highlight recent development of olefin coordination polymerization specially, designing of well-defined late metal catalysts which can open a new era in the polymer industry.

**Keywords**: Coordiantion polymerization, Ziegler Natta, Metallocene, late transition metal catalysts

---

## Introduction

polyethylene and poly propylene are the most important commercial polymers. As the most commonly used plastic in the word, poly ethylene is used for the fabrication of blow molded containers, extruded pipes, sheeting and packing materials, etc. On the other hand, many plastic items for medical or laboratory use can be made from polypropylene because it can withstand the heat in an autoclave. Food containers made from this polymer, do not melt during industrial hot filling processes [1]. The development of polyolefin dates back to the early 1930 with the production of low density polyethylene (LDPE) by free radical initiators. The reaction required elevated temperatures (200-400 $^{0}$C) and high pressure to produce LDPE containing both long and short chain branches. Due to the high pressure and rough conditions of the process and lack of control over the manufactured polyolefin, the process was recognized as an inefficient and dangerous process [2]. The identification of methods for achieving control of polymer structures and broadening their application, makes scientists Look for a new method of polymerization which was later called coordination polymerization. Historically, the design of new catalysts for olefin polymerization has mostly focused on early transition metals [3]. Recently, however, there has been advances and statements in the development of late transition metal based systems for homo and copolymerization of olefins [4]. The scope of this review is limited to late transition metal catalysts and their superiority over previous catalysts.

## Developments of olefin catalysts:

In 1950 Ziegler and Natta realized that certain combination of metal compounds and organometallic compounds polymerize ethylene at low temperature and pressure. The catalysts were effective with nonpolar monomers such as 1-alkene, dienes and alkynes. Although the discovery of these catalysts has been a major success, but there was still a drawback of low tacticity control on the manufactured polyolefin. This is due to the multiple catalytic sides in Ziegler Natta catalysts which lead to non-uniform incorporation of commoners and give different mixture of polypropylene with different tacticities [5]. In the late 1970, in Germany, Kaminsky discovered a new class of single side catalyst, based on metallocene /methyl alumin oxane. This new generation of catalyst showed higher activity with higher molecular weight and allows to produce polyolefins with stereo regular controllable structures and narrower PDI. After a while industrial and academic researchers were influenced by Kaminsky catalyst and were encouraged to develop the new catalyst for a wider range of new polymeric materials. Copolymerization of ethylene with polar monomers has been one of these developments which allows the polymer to grow its application in adhesive, miscibility and rheological properties. The high oxophilicity of early transition metal catalysts in metallocene (titanium, zirconium, hafnium,.), causes them to be easily deactivated and poisoned by electron pair on polar groups. So the reactivity of most polar groups toward the metal catalysts requires protection-deprotection strategies. Copolymerization of ethylene and propylene with different polar monomers such as methyl methacrylate and vinyl acetate with protection strategies by metallocene catalysts

has been reported. The disadvantageous of these catalysts were their difficult route of their synthesis and high cost of co-catalyst (MAO) that prevented them to be used in petrochemicals industry [6-11]. To overcome the limitation of early transition metal catalysts, especially their high oxophilicity, there has been a major shift of focus to late transition metal systems for the development of catalysts which can be used for copolymerization of ethylene with polar comonomers under mild conditions. Most prominent examples of catalysts in the late transition metal systems (Brookhart catalysts), are the Ni or Pd based α-diimine and phosphine imine, phenoxy imine and phosphine sulfonate chelating ligands (figures 1-4).

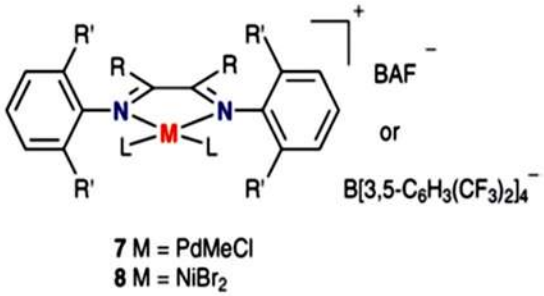


**Figure 1:** late transition metal catalysts based on Ni or Pd α-diimine chelating ligand

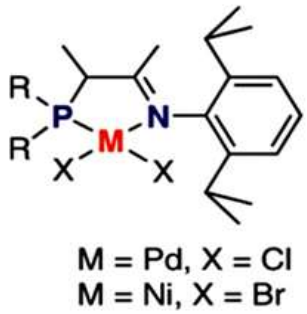


**Figure 2:** late transition metal catalysts based on Ni or Pd based phosphine imine chelating ligand

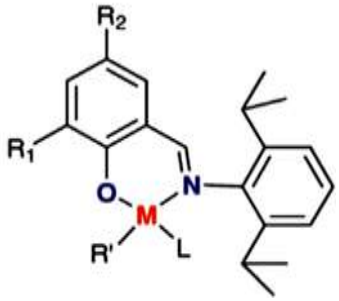

**Figure3:** late transition metal catalysts based on Ni or Pd based phenoxy imine chelating ligand

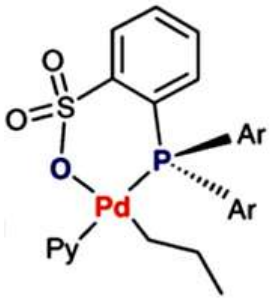

**Figure 4:** late transition metal catalysts based on Ni or Pd based phosphine sulfonate chelating ligand

## Late transition metals based on α-diimine nickel ligands

The α-diimine based Ni(II) and Pd(II) complex system is one of the most famous and highly active catalysts system which has reputation of great stability against solvent impurities or functional groups and high activity that can generate high molecular weight polymers [12,13]. All these features referred to the elegant and ingenious design of the catalyst which can be mentioned to the low Luis acidity of the palladium or nickel center, non-coordinating nature of the counter ion which can provide easy access of the incoming olefins to the coordination sites and finally and most importantly, the incorporation of the sterically bulky substituents on the α-diimine ligand that are

strategically blocking the axial sites of the metal center which is crucial for suppressing the associative chain transfer process (Figure 5) [14]. This system can be used for homopolymerization of ethylene which leads to branched poly ethylene and also copolymerization of ethylene with polar monomers such as Methyl acrylate and vinyl acetate [15,16]. Vinyl halides, acrylonitrile and vinyl ethers can be recognized as challenges for α-diimine catalysts. The tendency of these monomers to form a σ-coordination in combination with aggregation of insertion products prevent the copolymerization [17].

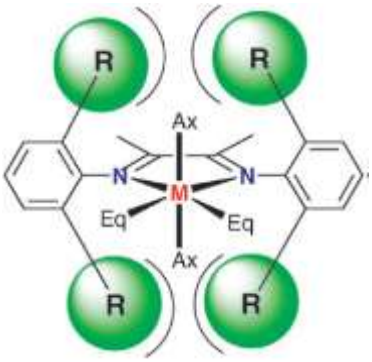


**Figure 5:** Axial and equatorial coordination sites of the α-diimine metal center and their steric interaction with the bis-aryl ortho substituents

Different parameters such as backbone structure, electronic effect, temperature and sterical factors have an influence on catalyst activity. In 2000 Johnson and Tempel had mechanistic studies on Pd (II) α-diimine ligands and revealed that in comparison with the Acenaphthyl α-diimine backbone, the Ni(II) complex having the methyl substituted ligand, gave higher molecular weight polymers with higher activity. Generally, the methyl a-diimine backbone is more effective in giving high MW PE and high activity. The Acenaphthyl backbone, however, exhibits more stability at higher temperatures [18]. In addition, an important parameter in catalyst design is the impact of ligand electronic effects on the catalytic activity. It has been proved that The more strongly electron-donating ligand exerts significant stability and longer lifetimes on the Ni(II) and Pd (II) catalysts towards ethylene polymerization. It also showed that introduction of electron donating groups led to a dramatic increase in polymer molecular weight [19,20]. As it was mentioned before, the design of α-diimine catalyst is intelligently and the critical point of this structure is appropriate steric and electronic effects to the metal center. An inherent limitation of these catalysts, is that the axial blocking ability can suffer at elevated temperature polymerization which is due to the rotational flexibility of the aryl-nitrogen bond (Figure 6)[21]. For this reason, at elevated polymerization temperatures, chain transfer or chain-transfer-to-monomer processes increase which leads to polymer molecular weight decrease.

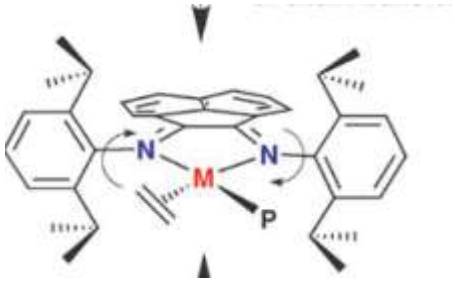


**Figure 6:** rotational flexibility of aryl-nitrogen bond at elevated temperatures

In order to avoid this rotation and further more prevent chain transfer processes to achieve high molecular weight polymers, scientists recommended some utilization on catalyst structure. Steric blocking the axial sites with aliphatic or aromatic bridges can be useful for this problem (figure 7)[22].

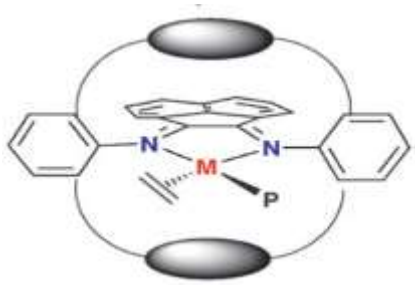


**Figure 7:** steric blocking the axial sites of α-diimine based catalysts

Another method which can avoid the rotation, and can be a barrier for chain transfer is to utilizing a tethered group that temporarily protect the most reactive 14 e intermediate via axial donation. These tethered groups are flexible enough so that when the coordination of next olefin is going to occur, the hemilabile ligand release from the metal and allow the metal active side to proceed with next insertion (figure 8)[23,24].

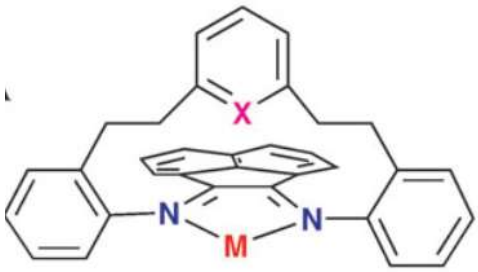


**Figure 8:** chemical structure of hemilabile complex

**New generation of catalysts based on chelating phosphine imine, phenoxy imine and phosphine sulfonate ligands**

A variety of late-metal polymerization catalysts have been designed in the last decade that utilize various chelating ligands [25-30]. One of the first ligands which was studied in this type was phosphine imine (P^N) ligands which the main strategy for synthesis of this catalyst was replacement of one imine site in the bis imine ligands with the better σ donating phosphine which leads to better thermal stability of Ni(II) and Pd(II) complexes but with lower activity (figure 2).polymers produced by these type of catalysts are highly branched and ,exhibiting even branch on branches structures [31]. Brookhart and coworkers designed phosphine imine (N^O) based Ni catalysts that allows them to control polymer crystallinity from linear semi crystalline to highly branched amorphous poly ethylene that depends on temperature and pressure of polymerization conditions (figure 3) and also let them copolymerize ethylene with highly polar functional monomers such as acrylonitrile which was a critical point of progress for theses catalysts in comparison to α-diimine based catalysts [32,33]. A unique catalyst that has attracted much attention recently is a series of Pd and Ni complexes based on phosphine sulfonate ligands (figure 4). Their main and exclusive feature of theses catalysts is that, according to their structure the chain walking process in these catalysts are much slower than chain growth which leads to linear copolymers. The catalysts also enable to copolymerize ethylene with CO and has great flexibility to copolymerize ethylene with different kind of polar comonomers such as methyl acrylates, vinyl ether, vinyl fluoride and pyrolydinnone (figure 4)[34-37]. A comparison of different catalysts and their specific features, from Ziegler Natta to different kind of late metal catalysts can be seen in table 1.

**Table 1**. Comparison of different catalysts performance

| Catalyst | Specific figure |
|---|---|
| Ziegler Natta | First catalyst which was used commercially for manufacturing HDPE, no control on tacticity, not useful for polar copolymerization |
| Metallocene | Single side catalyst, Produce polyolefin with stereo regular structures, difficult route to synthesis, high cost of cocatalyst (MAO), sensitive to polar groups, not useful for polar copolymerization |
| Late metals based on α-diimine | High activity, good resistance against moisture, suitable for copolymerization of ethylene with MA and VA, limitation for copolymerization of ethylene with AN, vinyl ethers and vinyl halides, inherent limitation in elevated temperatures |
| Late metals based on phosphine imine | Good thermal stability, lower activity, manufacture highly branched copolymers |
| Late metal based on phenoxy imine | Control polymer crystallinity from linear semi crystalline to highly branched amorphous depending on the polymerization conditions |
| Late metals based on phosphine sulfonate | Manufacture linear copolymers, Suitable for copolymerization of different kind of polar comonomers such as : MA, VA, AN, vinyl fluoride |

## Conclusion

According to the importance of cost effective, activity, wider application, less sensitivity and easier route of synthesis, scientists have been always looking for new catalysts for polymerization. These researches has been shifted from early transition metals to late transition metals because of their higher activity, better heat resistance and more stability against moisture and polar groups which prepare these catalysts suitable for polar copolymerizations and make them potential candidates for high performance materials. Also these catalysts able to control the tacticity and leads to manufacture polymers with controllable stereochemistry. As surveyed in this article α-diimine based late metal systems are particularly the first innovation in this research area, that with their flexible ligand structures, allowing to control the catalyst activity. In addition to α-diimine-based systems, significant progress has been made in the design of various other chelating ligands based on [N^O], [P^O] and [N^P] for late-metal polymerization catalysts. An interesting system among this family is a series of Pd–phosphine–sulfonate complexes. These catalysts are especially exciting because of their ability to copolymerize ethylene with a number of commercially relevant polar comonomers.

## Acknowledgments

The author wish to thank University of Zanjan for their national seminar

**References**

[1] C. Vasile, Handbook of Polyolefins, Marcel Decker Inc., New York, **2000**.

[2] E, Strom. S, Thomas, and Rasmussen. C., 100+ Years of Plastics: Leo Baekeland and Beyond. American Chemical Society, **2011**.

[3] AC Pinheiro, SM Da Silva, Roisnel T, Kirillov E, Carpentier JF, Casagrande OL. *New Journal of Chemistry*. **2018**;*42(2)*:1477-83.

[4] H Harakawa, S Patamma, AC Boccia, L Boggioni, DR Ferro, S Losio, K Nomura, I Tritto. *Macromolecules*. **2018**, *51(3)*, pp 853-863.

[5] H Sinn, W Kaminsky. Ziegler-Natta catalysis. In Advances in Organometallic Chemistry **1980** (*Vol. 18*, pp. 99-149). Academic Press.

[6] MI Tavares, GC Stael, MM Gorelova, De Menezes S.Journal of applied polymer science**. 2001***;80(11)*:2120-2.

[7] H Frauenrath, S Balk, H Keul, H Höcker. Macromolecular Rapid Communications. **2001** Oct 1;*22(14)*:1147-51.

[8] H Sinn, & W Kaminsky,. (**1980).** Ziegler-Natta catalysis. In Advances in Organometallic Chemistry (*Vol. 18*, pp. 99-149). Academic Press

[9] AF Galambos, inventor; Basell North America Inc, assignee. Propylene polymer yarn and articles made therefrom. United States patent US 5,455,305. **1995**.

[10] Ewen,. L. Haspeslach, J. L Atwood, & H.Zhang, **(1987)**. *Journal of the American Chemical Society*, *109(21)*, 6544-6545.

[11] JA.Ewen, *Journal of the American Chemical Society*. **1984**;*106(21):*6355-64.

[12] Z .Guan, PM.Cotts, EF.McCord, SJ.McLain. **1999**;*283(5410):*2059-62.

[13] DJ.Tempel, LK.Johnson, RL.Huff, PS .White,M.Brookhart.*Journal of the American Chemical Society*. **2000**;*122(28)*:6686-700.

[14] MD.Doherty, S.Trudeau, PS.White, JP .Morken,M.Brookhart.*Organometallics.* **2007**;*26(5)*:1261-9.

[15] DB .Culver, H.Tafazolian, MP.Conley. *Organometallics*. **2018**;*37(6)*:1001-6.

[16] BA.Riga, MD.Neves, AE.Machado, DM .Araújo, JR .Souza, OR.Nascimento, VT .Santana, CC.Cavalheiro, VP.Carvalho-Jr, Goi BE, *Inorganica Chimica Acta*. **2018**;*471*:620-9.

[17] K .Nozaki, S.Kusumoto, S.Noda, T .Kochi, LW.Chung, K.Morokuma, *Journal of the American Chemical Society*. **2010**;*132(45)*:16030-42.

[18] DJ.Tempel, LK.Johnson, RL.Huff, PS ,White, Brookhart M.*Journal of the American Chemical Society*. **2000**;*122(28)*:6686-700.

[19] C.Popeney, Z.Guan. *Organometallics.* **2005**;*24(6)*:1145-55.

[20] CS.Popeney, Z.Guan, *Macromolecules*. **2010**;*43(9):*4091-7.

[21] L.Deng, TK.Woo, L.Cavallo, PM .Margl, T.Ziegler, *Journal of the American Chemical Society*. **1997**;*119(26)*:6177-86.

[22] DP.Gates, SA.Svejda, E.Oñate, CM .Killian, LK.Johnson, PS.White, Brookhart M. *Macromolecules*. **2000**;*33(7):*2320-34.

[23] D.H.Leung, J.W. Ziller & Z Guan,. *Journal of the American Chemical Society*, **(2008)** *130(24)*, 7538-7539.

[24] DH.Camacho, Z.Guan. **2010**;*46(42)*:7879-93.

[25] D.Bézier, O.Daugulis, M.Brookhart. *Organometallics*. **2017**;*36(15)*:2947-51.

[26]O.Daugulis & M Brookhart,.*Organometallics*, **(2002)** *21(26)*, 5926-5934..

[27] B.Rieger, LS.Baugh, S.Kacker, S .Striegler, editors. John Wiley & Sons; **2006** Mar 6.

[28] S.Matsui, M.Mitani, J.Saito, Y.Tohi, H .Makio, N.Matsukawa, Y.Takagi, K.Tsuru, M .Nitabaru, T.Nakano, H.Tanaka. *Journal of the American Chemical Society*. **2001**;*123(28)*:6847-56.

[29] T.Kochi, S.Noda, K.Yoshimura, K .Nozaki. *Journal of the American Chemical Society*. **2007**;*129(29)*:8948-9.

[30] T.Kochi, K.Yoshimura, K.Nozaki. Dalton Transactions. **2006**(*1*):25-7.

[31] Z.Guan, WJ.Marshall. *Organometallics*. **2002** Aug 19;*21(17)*:3580-6.

[32] L.Zhang, M.Brookhart, PS.White. *Organometallics*. **2006**;*25(8)*:1868-74.

[33] X.Zhang, Z.Liu, J.Yi, F.Li, H.Huang, W .Liu, H.Zhen, Q.Huang, K.Gao, W.Yang. *Journal of Polymer Science Part A: Polymer Chemistry*. **2012**;*50(10)*:2068-74.

[34] A.Haras, GD.Anderson, A.Michalak, B .Rieger, T.Ziegler.*Organometallics*. **2006**;*25(19)*:4491-7.

[35] A.Berkefeld, S.Mecking.*Angewandte Chemie International Edition*. **2008**;*47(14)*:2538-42.

[36] S.Ito, K.Munakata, A.Nakamura, K .Nozaki. *Journal of the American Chemical Society*. **2009**; *131(41):*14606-7.

[37] T.Kochi, S.Noda, K.Yoshimura, K.Nozaki. *Journal of the American Chemical Society*. **2007**; *129(29)*:8948-9.

# Syndiospecific polymerization of styrene by Half-titanocene catalysts

## Review Article

**Sohrab Rahmani *[a] and Peyman Atashi [b]**

[a,b]-*Laboratory of Polymer Synthesis, Department of Chemistry,*

*Faculty of Science, University of Zanjan, Zanjan, Iran*

*Corresponding author Tel.: +98 (24) 33052589; Fax number: +98 (24) 33052589

*E-mail: rahmani.sohrab@znu.ac.ir

**Abstract**

Syndiotactic polystyrene has attracted much interest in scientific and industrial research after its first synthesis in 1985 and has led to a fast commercialization of this polymer. The catalyst systems used for this coordination polymerization of styrene are a key point in this development to provide high polymerization activities and syndiotacticities of the polymers obtained. In this article we review and highlight recent development of homogeneous and heterogeneous transition metal complexes for syndiospecific polymerization of styrene. It includes the polymerization activity of the catalysts itself, the syndiotacticity and other properties of the polymers received with these catalysts as well as the discussion of the relationships between structure and properties.

**Keywords**: syndiotactic polystyrene, transition metal catalysts, half-titanocene, supported catalysts, syndiospecific polymerization

## Introduction

One of the most important achievements in the field of polymerization catalysts has been the introduction of methyl alumoxanes as a new class of aluminum alkyl activators, produced by controlled hydrolysis of methyl aluminum alkyls, by Sinn and Kaminsky at the end of 1970s [1,2]. These cocatalysts led to an outstanding enhancement of the polymerization activity in combination with metallocenes as well as to an important increase in the uniformity of the molecular weight distribution of the polymers obtained. Metallocenes together with methyl alumoxanes allowed the synthesis of highly stereoregular and stereoblock polypropylenes, ethylene copolymers with a higher content of comonomer or higher a-olefins and styrene, cycloolefin polymers of high crystallinity and their copolymers [3–6] as well as polyethylenes with improved rheological properties by controlled long-chain branching [7–9]. A further key finding at the beginning of this time was the discovery of the first syndiotactic polystyrene synthesized by Ishihara et al. in 1985 using a homogeneous organometallic catalytic system on the basis of titanium compounds and methyl aluminoxane receiving a polymer with a 2-butanone insoluble part of 98 wt. %, a weight-average molecular weight of 82,000 g/mol, and a melting point of about 270 ◦C [10–13]. Because of its semicrystalline nature, syndiotactic polystyrene products exhibit performance attributes that are significantly different from those of amorphous styrenic materials. These properties include a high melting point, good chemical and moisture resistance, and a high degree of dimensional stability. Based on the first synthesis of syndiotactic polystyrene, tremendous studies have been done in this area that include:

Investigation of fundamental and application properties of the polymer and its compounds and blends.

Investigations on the synthesis of new half-metallocene transition metal catalysts in relation to their polymerization activity.

Mechanism of syndiospecific coordination polymerization [14–19].

## Mechanism of syndiospecific coordination polymerization

An overview on this mechanism is presented in Scheme 1.

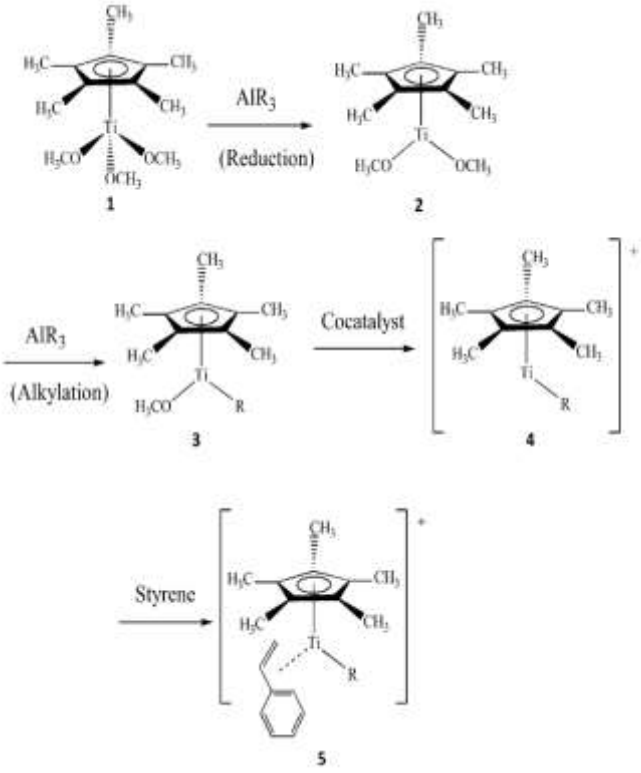


Scheme 1

The titanium transition metal complex of oxidation state (IV) 1 is reduced preferably by an aluminum alkyl AlR3 (e.g. trimethyl aluminum in methyl aluminoxane) to a titanium (III) complex 2 and is simultaneously alkylated by the formation of

a transition metal–carbon bond in 3. By the cocatalyst (methyl aluminoxane or an organic boron compound), the neutral compound 3 is transferred to the active titanium (III) cation with a free coordination site 4, and the cocatalyst anion (not shown here). A pre-coordination of the styrene monomer leads to the active species 5 for the syndiospecific polymerization by further insertion of styrene molecules into the active transition metal–carbon bond [20]. The stereochemical control of the propagation reaction of the syndiospecific polymerization is ensured by a secondary or 2,1-monomer insertion into the transition metal–carbon bond, a cis addition of the growing polymer chain to the double bond of the monomer, and a chain–end control mechanism of the propagation reaction. This section gives an overview of the catalytic systems for the syndiospecific polymerization of styrene.

**Transition metal complexes for syndiospecific styrene polymerization**

The transition metal complex is the most important part of the catalyst system providing syndiospecificity of the coordination propagation reaction during styrene polymerization. Depending on the structure of the transition metal complex, polystyrenes of atactic, syndiotactic-rich or highly syndiotactic structure can be obtained.

**Cyclopentadienyl and Pentamethylcyclopentadienyl titanium complexes**

The most often used cyclopentadienyl complex is the $\eta^5$-cyclopentadienyl titanium trichloride (Sheme 2).

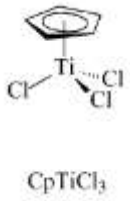


Scheme 2

$\eta^5$-Pentamethylcyclopentadienyl titanium trichloride and $\eta^5$-pentamethylcyclopentadienyl titanium trimethoxide are the most often used pentamethylcyclopentadienyl complexes. Based on the additional electron-releasing substituents at the cyclopentadienyl ligand, these complexes lead to higher polymerization activities in bulk with regard to the corresponding $\eta^5$-cyclopentadienyl titanium compounds suggesting a stabilization of the active polymerization site by electron-donating ligands, whereas the trichlorides are less active than the trimethoxide complexes. Furthermore, higher degrees of syndiospecificity and much higher molecular weights were achieved by pentamethylcyclopentadienyl-titanium complexes in comparison to cyclopentadienyl compounds (Scheme 3).

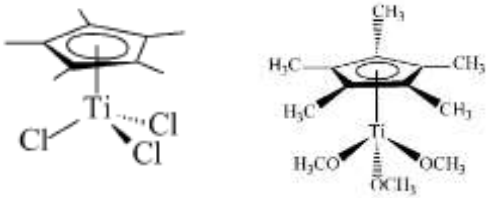


Scheme 3

**Bidentate cyclopentadienyl-titanium complexes**

Bidentate cyclopentadienyl complexes usually contain special groups attached to the cyclopentadienyl ring simultaneously interacting with the transition metal atom (Scheme 4).

Despite a broad application of such complexes as catalysts in the polymerization of α-olefins, also included by the term constrained geometry complexes [21], the importance of such complexes in the syndiospecific styrene polymerization is low

because of their poor catalytic activity. In bidentate cyclopentadienyl complexes, special groups are attached to the cyclopentadienyl ring, which simultaneously interact with the central metal atom. In the case of phenethyl groups, polymerization activity and molecular weight are significantly reduced, whereas the syndiospecificity is about the same. The reduced polymerization rate might be due to an interaction of the phenyl substituent with the electron deficient titanium active site by multihapto intramolecular coordination, thus competing with the coordination of a new styrene molecule and reducing the propagation rate, but without influence on the stereospecificity of the growing polymer chain. The lower molecular weight is a result of a promotion of b-hydride elimination by the bulky ligand [22, 23]. Substituents like methoxyethyl- or tetrahydrofurfuryl- as well as dimethylaminoethyl- and picolyl-groups result in a significant reduction in both, catalyst activity and stereoregularity. This seems to be due to decrease of electrophilicity of titanium by coordination of oxygen or nitrogen, destabilizing the active catalytic site and hindering the coordination and insertion of the styrene molecule. Furthermore, a coordination of the oxygen to the aluminum in MAO is possible.

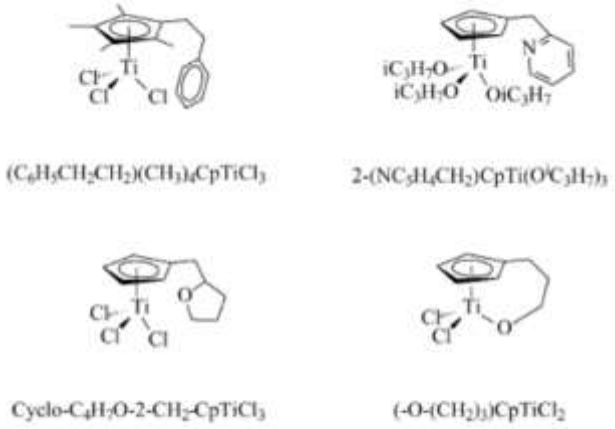


Scheme 4

**Metal complexes of other ring systems**

**Indenyl-titanium complexes**

Indenyl complexes are frequently investigated compounds of metal complexes of other ring systems in the syndiospecific coordination polymerization of styrene. In general, such complexes exhibit a higher polymerization activity than Cp and complexes because of a higher electron-donating ability of the indenyl moiety [24] (Scheme 5).

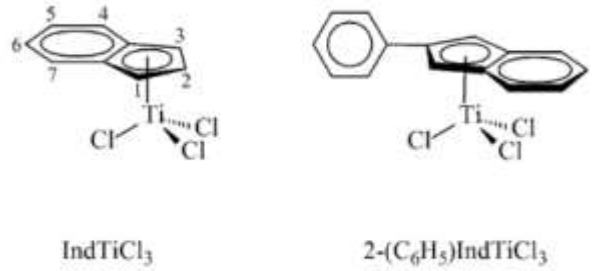


Scheme 5

Indenyl based complexes show increased long-term stabilities and the syndiotactic polystyrenes obtained generally demonstrate higher molecular weights than those produced with $CpTiCl_3$ [25]. In addition, $IndTiCl_3$ has been used in styrene homo and copolymerization with para-substituted styrenes [26-28].

**Fluorenyl-titanium complexes**

Besides indenyl complexes, fluorenyl (Flu) complexes are also components in efficient catalysts for the syndiospecific polymerization of styrene (Scheme 6). The fluorenyl complexes $[(\eta^1\text{-Flu})Ti(\mu\text{-}OiC_3H_7)(OiC_3H_7)_2]_2$, a dimer of $\eta^1\text{-FluTi}(OiC_3H_7)_3$, and the complex of different hapticities of the fluorenyl ligands $(\eta^5\text{-Flu})Ti(OiC_3H_7)_2(\eta^1\text{-Flu})$, were investigated in the syndiospecific polymerization of styrene with the MMAO

cocatalyst in toluene at 50 ◦C (Al/Ti = 500) and showed the following order of increasing polymerization activity in comparison to other half-metallocene catalysts $Cp*Ti(OiC_3H_7)_3$ < $IndTi(OiC_3H_7)_3$ < $[(\eta^1\text{-Flu})Ti(\mu\text{-}OiC_3H_7)(OiC_3H_7)_2]_2$ < $(\eta^5\text{-Flu})Ti(OiC_3H_7)_2(\eta^1\text{-Flu})$ indicating in particular the superior activity of the $\eta^5$-fluorenyl complex over the Cp* and indenyl compounds. This might be due to an easy homolytic breaking of the Ti-($\eta^1$-fluorenyl) bond producing active Ti (III) species or to the relatively high kinetic stability of the Ti-($\eta^5$-fluorenyl) moiety upon activation with MMAO [29] (Scheme 6).

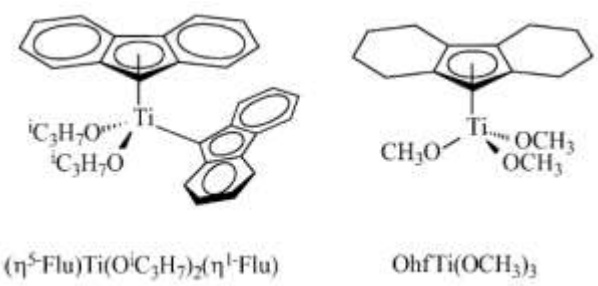


Scheme 6

**Supported catalysts**

The homogeneous catalytic systems for the syndiospecific styrene polymerization can also be used in a heterogeneous form if desirable, for example by supporting on an insoluble carrier. Such carriers can be inorganic compounds, organic polymers, or carriers based on mixed compounds. An inorganic carrier often used in catalysts for syndiotactic polystyrene is silica. It was applied in investigations with the catalytic systems $Ti(OC_4H_9)_4$ and $CpTiCl_3$ in combination with MAO demonstrating 50 ˚C as an optimal polymerization temperature considering an increase of activity and a drop of syndiotacticity with increasing temperature. The effects of MAO concentration and hydrogen were also investigated [30]. Investigating the different silica-supported half-metallocene titanium complexes $CpTiCl_3$, $Cp*TiCl_3$, and $IndTiCl_3$ with MAO as cocatalyst, the $Cp*TiCl_3$ supported catalyst was effective not only in terms of catalytic activity, but also with regard to the properties of the syndiotactic polystyrenes obtained, even at relatively low Al/Ti ratios of <300/1. The active polymerization sites formed of the supported catalysts appear to be more thermally stable than their homogeneous counterparts [31]. Supported catalyst system for the slurry phase polymerization of styrene in toluene was prepared by the immobilization of 2-methylindenyltrichlorotitanium on silica and activation of this catalyst was performed by Methylaluminoxane in polymerization media [32]. Organic polymers used as catalyst carriers comprise different styrene polymers. Crosslinked chloromethylated polystyrene beads served as a support for the $Cp*TiCl_3$/MAO catalyst system leading to higher polymerization activities [33]. On poly (styrene-co-hydroxystyrene) various amounts of titanium have been immobilized by reaction with $Cp*Ti(CH_3)_3$, resulting in catalysts of higher polymerization activities with decreasing amounts of supported titanium at a polymerization temperature of 55 ◦C with MAO as cocatalyst, and suggesting that the density of the active species in the polymer support seems to play an essential role in catalytic activity [34]. Syndiotactic polystyrene itself can be used as an organic polymer carrier by heterogenization or embedding the homogeneous catalyst system $Cp*Ti(OCH_3)_3$/MAO into syndiotactic prepolymer particles and additional activation with MAO/MMAO in a slurry

phase polymerization, obtaining catalyst activities and polymer syndiotacticities comparable to those of the homogeneous catalyst. The physical phase transitions and nascent morphology of syndiotactic polystyrene synthesized with such a catalyst in n-heptane slurry were also investigated in detail showing no global gelation in the reaction system [35, 36]. Syndiotactic poly (styrene-co-p-methylstyrene) has been functionalized with silylhydride groups. Tethering of half-titanocene complex on polymeric support was done by the hydrosilylation reaction of 1-allylindenyltrichlorotitanium with silyl-hydride functionalized copolymer in the presence of Karstedt catalyst as a coupling reagent. The polymer-supported catalyst was tested for syndiospecific polymerization of styrene using methylaluminoxane as a cocatalyst. The results of styrene polymerization showed that the polymer-supported catalyst exhibited high activity for syndiospecific polymerization of styrene (Scheme 7) [37].

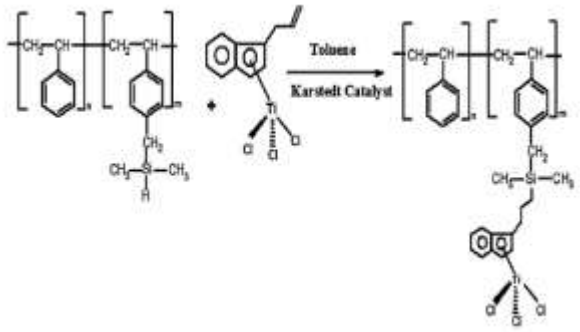


Scheme 7

In a resemble work, the cross-linked polystyrene beads were functionalized with silyl hydride groups. Two synthetic procedures has been employed to tether of indenyltrichlorotitanium ($IndTiCl_3$) on The functionalized polystyrene beads. In one approach (method A, Scheme 8) the half-titanocene catalyst bearing an allyl group (1-allylindenyltrichlorotitanium) was synthesized and covalently anchored on the functionalized polystyrene by using of hydrosilylation chemistry. In the second approach (method B, Scheme 9) the half-titanocene complex was synthesized on the functionalized polystyrene beads. The polymer-supported catalysts were tested for styrene polymerization using methylaluminoxane (MAO) as a cocatalyst. The obtained results revealed that the supported catalyst prepared with method (A) has higher catalytic activity and syndiotacticity than the supported catalyst obtained by method (B) [38].

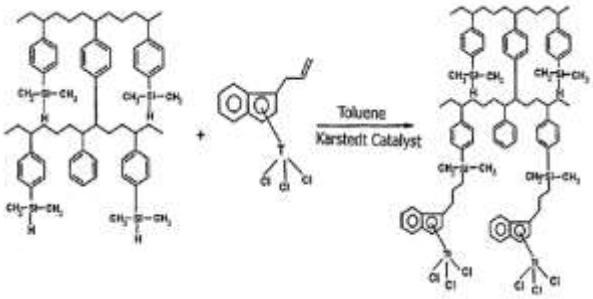


Scheme 8

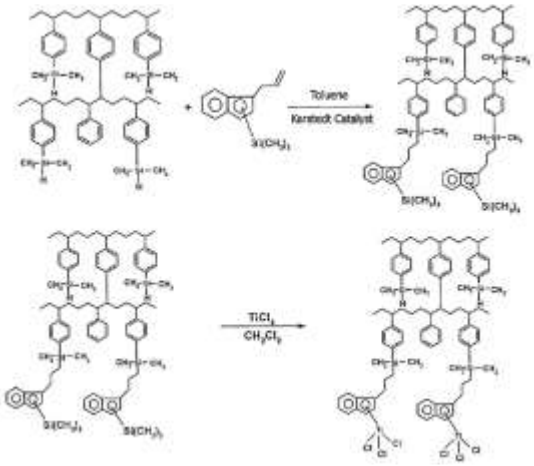


Scheme 9

**Acknowledgments**

The author wish to thank University of Zanjan for their national seminar.

**References**

[1] H. Sinn, W. Kaminsky, H-J Vollmer and R. Woldt, *Angew Chem*, **1980**, *92, 396*.

[2] H. Sinn, W. Kaminsky, *Adv Organomet Chem*, **1980**, *18, 99*.

[3] VK Gupta, S. Satish, IS. Bhardwaj, *J Macromol Sci, Rev Macromol Chem Phys* **1994**, *C34, 439*.

[4] SS Reddy, S. Sivaram, *Prog Polym Sci* **,** **1995**, *20, 309*.

[5] H-H Brintzinger, D. Fischer, R. Mu¨lhaupt, B. Rieger, R. Waymouth , *Angew Chem*, **1995**,*107,1255*.

[6] K. Soga, T. Shiono, *Prog Polym Sci* , **1997**, *22 ,1503*.

[7] AL McKnight, RM Waymouth , *Chem Rev*, **1998**, *98, 2587*.

[8] GM Benedikt, BL Goodall, *Norwich, NY: Plastics Design Library*, **1998**.

[9] J. Scheirs, W. Kaminsky, Metallocene-based polyolefins: preparation, properties and technology, 2, Chichester: Wiley, **2000**.

[10] N. Ishihara, M. Kuramoto, M. Uoi, Production of styrene polymer. JP 62187708; **1985**, assigned to Idemitsu Kosan Co. Ltd.

[11] N. Ishihara, M. Kuramoto, M. Uoi, Styrene polymers. EP 210615; **1986**, assigned to Idemitsu Kosan Co. Ltd.

[12] N. Ishihara, T. Seimiya, M. Kuramoto, M. Uoi, *Polym Prep Jpn* **1986**, *35, 240*.

[13] N. Ishihara, T. Seimiya, M. Kuramoto, M. Uoi, *Macromolecules*, **1986**, *19, 2464*.

[14] R. Po, N. Cardi, *Prog Polym Sci* , **1996,**

*21, 47*.

[15] N. Tomotsu, N. Ishihara, *Catal Surv Jpn*, **1997,** *1, 89*.

[16] N. Tomotsu, N. Ishihara, TH Newman, MT Malanga , *J Mol Catal A Chem* , **1998**, *128, 167*.

[17] C. Pellecchia, A. Grassi, *Top Catal* , **1999**, *7, 125*.

[18] M. Malanga, TH Newman, *Encyclopedia of polymer science and technology*. New York: John Wiley & Sons; **2001**,http://mrw.interscience.wiley.com/emrw/0471440264/home/.

[19] J. Schellenberg, N. Tomotsu, *Prog Polym Sci*, **2002**, *27, 1925*.

[20] TH Newman, MT Malanga, J *Macromol Sci Pure Appl Chem*, **1997**, *A34, 1921*.

[21] H. Braunschweig, FM Breitling, *Coordin Chem Rev*, **2006**, *250, 2691*.

[22] JC Flores, JS Wood, JCW Chien, MD Rausch, *Organometallics*, **1996**, *15, 4944*.

[23] TH Newman, KK Borodychuk, *Polym Prepr*, **1999**, *40(1), 387*.

[24] Y. Qian, J. Huang, MD Bala, B. Lian, H. Zhang, H. Zhang, *Chem Rev*, **2003**, 103, 2633.

[25] O. Stojkovic, W. Kaminsky, *Macromol Chem Phys*, **2004**, *205*, *357*.

[26] M. Geprags, G. McKee, JR Wunsch, *Polym Prep (Am Chem Soc, Div Polym Chem)* **1999**, *40(1)*, *389*.

[27] M. Auer, R. Nicolas, A. Rosling, C-E Wilen , *Macromolecules*, **2003**, *36*, *8346*.

[28] S. Rahmani, A. A. Entezami, *Macromolecular Research*, **2008**, 274, 43.

[29] O. Stojkovic, W. Kaminsky, *Macromol Chem Phys*, **2004**, 205, 357.

[30] V. Pasquet, R. Spitz, *Macromol Chem Phys* , **2001**, 202, 2346.

[31] J H. Yim, SK. Ihm, *J Appl Polym Sci*, **2006,** 102, 2293.

[32] S. Rahmani, R. Mohammadi, A.A. Entezami, Macromol. Symp., **2008**, 274, 43.

[33] W. Trakarnpruk , N. Apipanyasopon, *J Met Mater Miner*, **2003,** 12, 19.

[34] B. Kitiyanan, K. Nomura, *Stud Surf Sci Catal* , **2006,** 161, 213.

[35] JS. Chung, BG. Woo, KY. Choi, *Macromol Symp*, **2004**, 206, 375.

[36] HW. Lee, JS. Chung, KY. Choi, *Polymer*, **2005,** 46, 5032.

[37] S. Rahmani , A. A. Entezami, *Catal Lett*, **2011**, 141, 1625.

[38] S. Rahmani, A.A. Entezami, Journal of Molecular Catalysis A: Chemical, **2010**, 320, 27.

# Efficient synthesis of triazole derivatives using organocopper-based magnetically recoverable and reusable nanocatalysts

**Hamed Sadighian[a]*, Masume Hatami[a], Fatemeh Shahkarami[a], Saeid Taghavi Fardood[a]**

[a]*Affiliation (Department of Chemistry, University of Zanjan,P.O. BOX 19395-4697 Zanjan, Iran*

*E-mail: Hamed.sadighian@znu.ac.ir

**Abstract**

Recently several of efficient heterogeneous nanocatalysts designed and prepared for synthesis of Heterocyclic compounds such derivatives of triazole compounds under green conditions with excellent yields.

**Keywords**: nanocatalysts, organocopper, Magnetic nanoparticle, triazole.

## Introduction

The heterogeneous catalytic systems which developed recently are attracted to attention for their versatile and efficient properties. These catalytic systems have been employed in the synthesis of heterocyclic compounds. On the other hand, heterocyclic compounds especially treazole rings are important and attractive compounds particulary that comprise high potential in specific applied to biological approach to precision medicine targets [1-7]. For this reasons, designed and prepared of novel and versatile catalytic systems have been pay attended for the synthesis of triazole compounds. The nanocatalyst based organocoppers that supported by $Fe_3O_4$ nanoparticle with magnetically recoverable and reusable properties have been reported [8,9]. $Fe_3O_4$-supportedCu(II)-β-cyclo-dextrin, [MNPs@FGly][Cl] and MNPs@8-AQ-$CuCl_2$ are tree kinds of the nanocatalysts that was reported at recently. Each catalytic system is introduced with the examples of products.

In 2013, kaboudin et al. reported the efficient, recoverable and reusable magnetic nanoparticle-supported Cu(II)-β-cyclodextrin complex catalyst for the synthesis of 1,2,3-triazoles ( Scheme 1). They synthesized various derivatives of 1,2,3-triazole compounds from arylboronic acids under click condition using $Fe_3O_4$-supported Cu(II)-β-cyclo-dextrin in excellent yields (Scheme 2)[10].

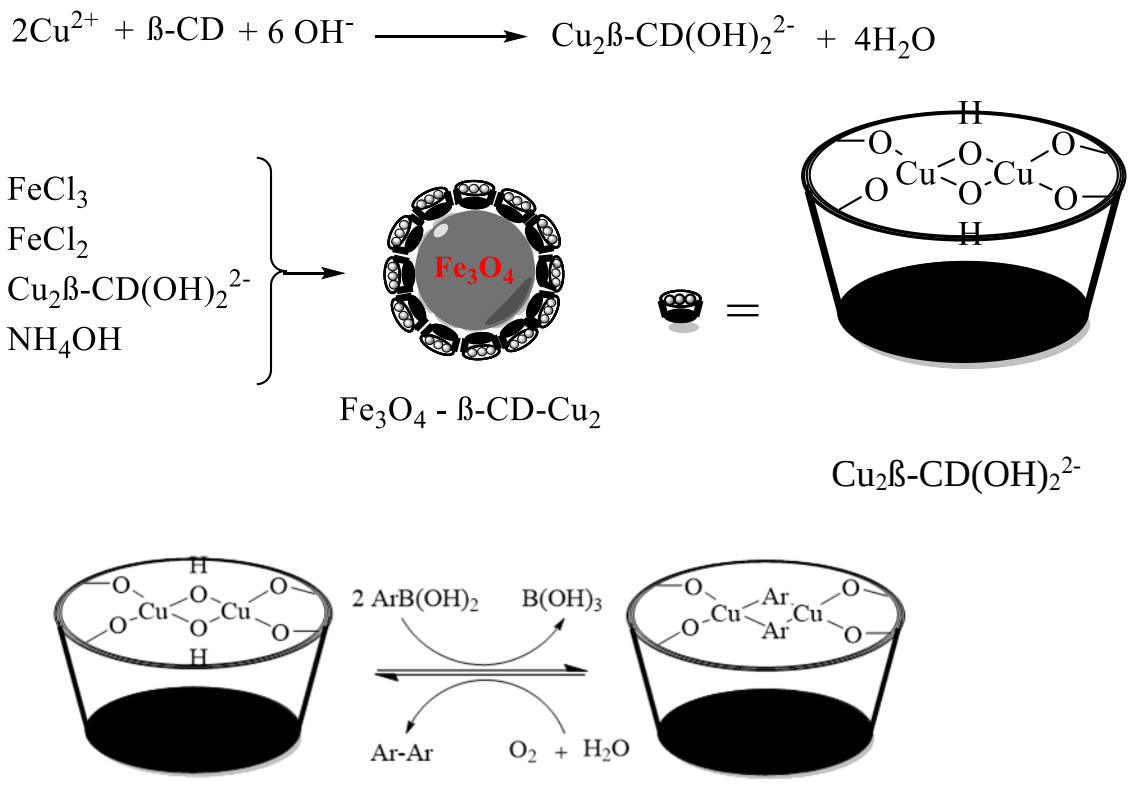


**Scheme 1.** Preparation of $Fe_3O_4$-supported Cu(II)-β-cyclo-dextrin nanoparticle-catalyzed homocoupling of aryl boronic acids.

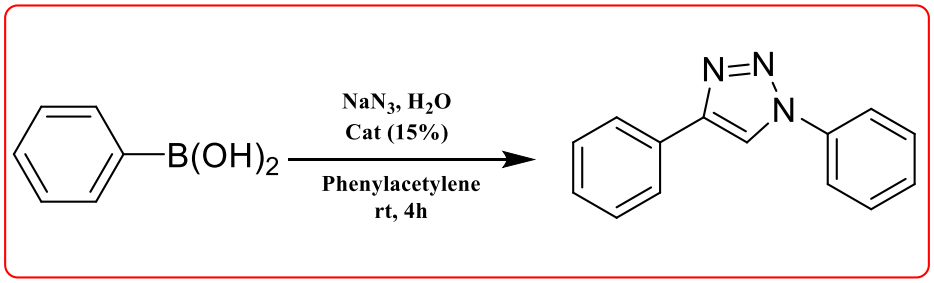


**Scheme 2.** Synthesis of triazole ring using Fe3O4-supported Cu(II)-β-cyclodextrin.

Matloubi et al. reported another class of organocopper-basedmagnetically recoverable and reusable nanocatalyst for high efficient synthesis of triazole derivatives by immobilization of copper ion onto the triazole functionalized $Fe_3O_4$ in 2015 (Scheme 3)[11]. In 2017, saeidian's group synthesized varied of novel derivatives of 1,2,3-triazole based sulfonamides compounds such bis(1,2,3-triazole)-based, N,N'-((propane-1,3-diylbis(1H-1,2,3-triazole) based sulfonamides and fluorine-bearing 1,2,3-triazole-based sulfonamides in the presence of [MNPs@FGly][Cl] nanocatalyst with excellent yields (Scheme 4)[12]. In 2017, matloubi's group designed novel heterogeneous organocopper nanocatalyst that was prepared by Immobilized of Copper (II) Ions onto Aminoquinoline-Functionalized Ferrite (Scheme 5). Alanine functionalized 1,2,3-triazoles was produced using MNPs@8-AQ-$CuCl_2$ in good yield (Scheme6)[13].

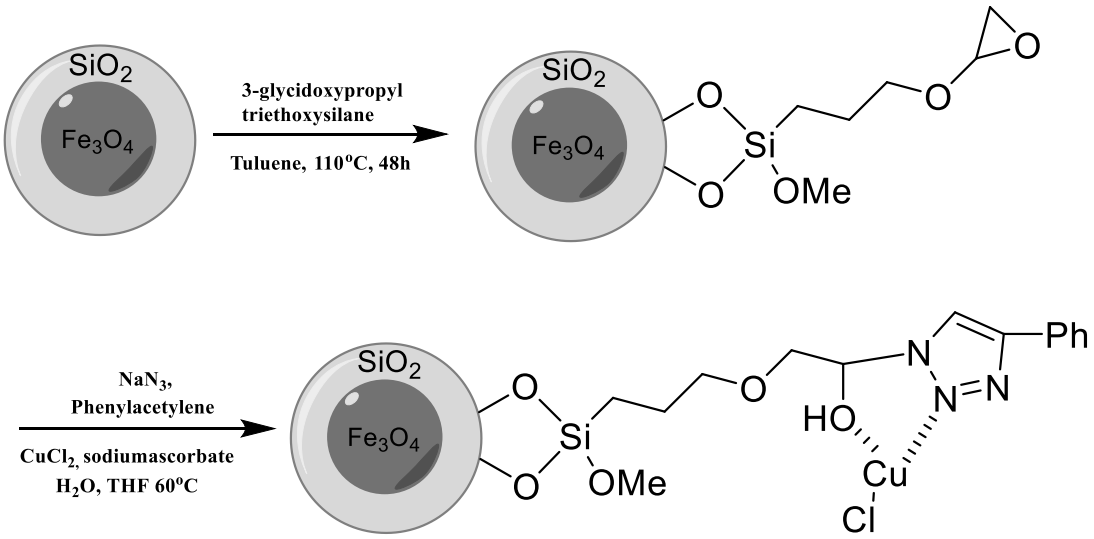


**Scheme3.** Immobilization and functionalization of 3-glycidoxypropyltrimethoxysilane on Fe3O4@SiO2 for the prepare of [MNPs@FGly][Cl]

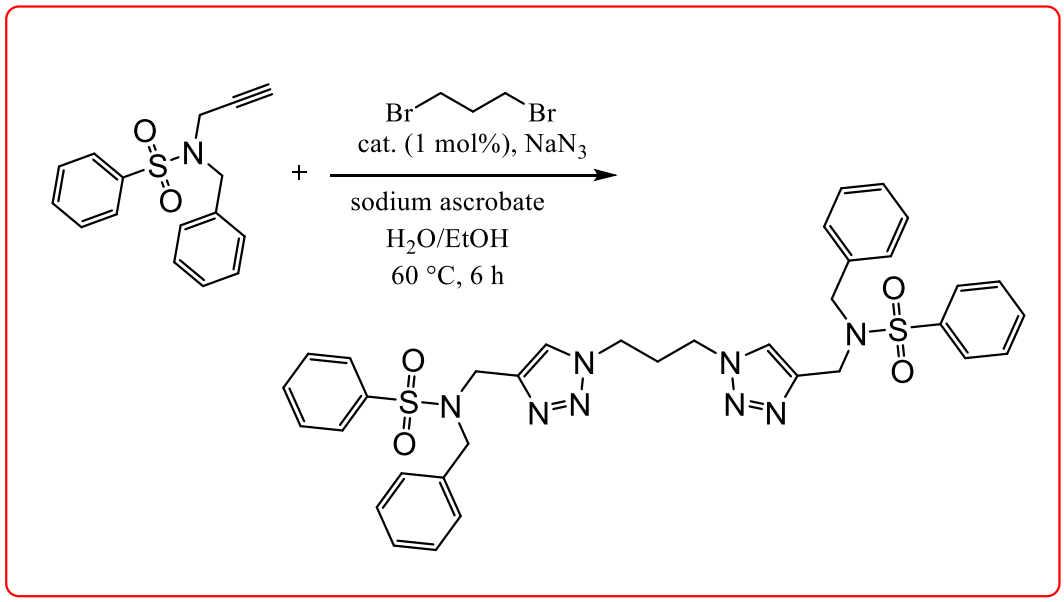


**Scheme 4.** Reaction of 1,3-dibromopropane with 2 equiv N-propargylsulfonamide using [MNPs@FGly][Cl]

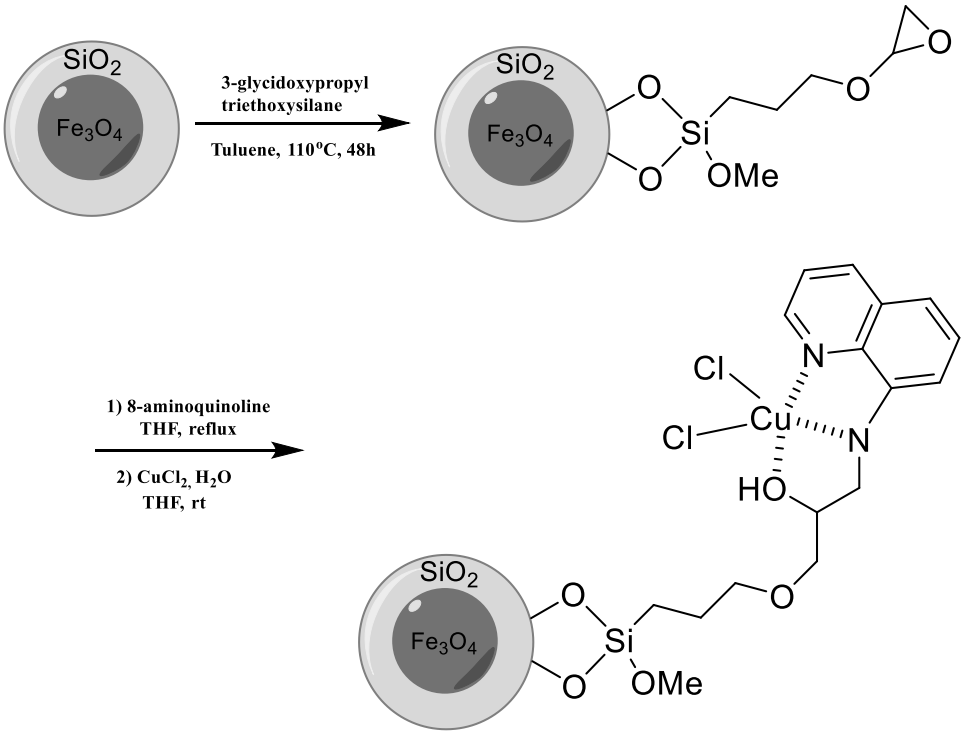


**Scheme 5.** The schematic pathway for the synthesis of MNPs@8-AQ-$CuCl_2$

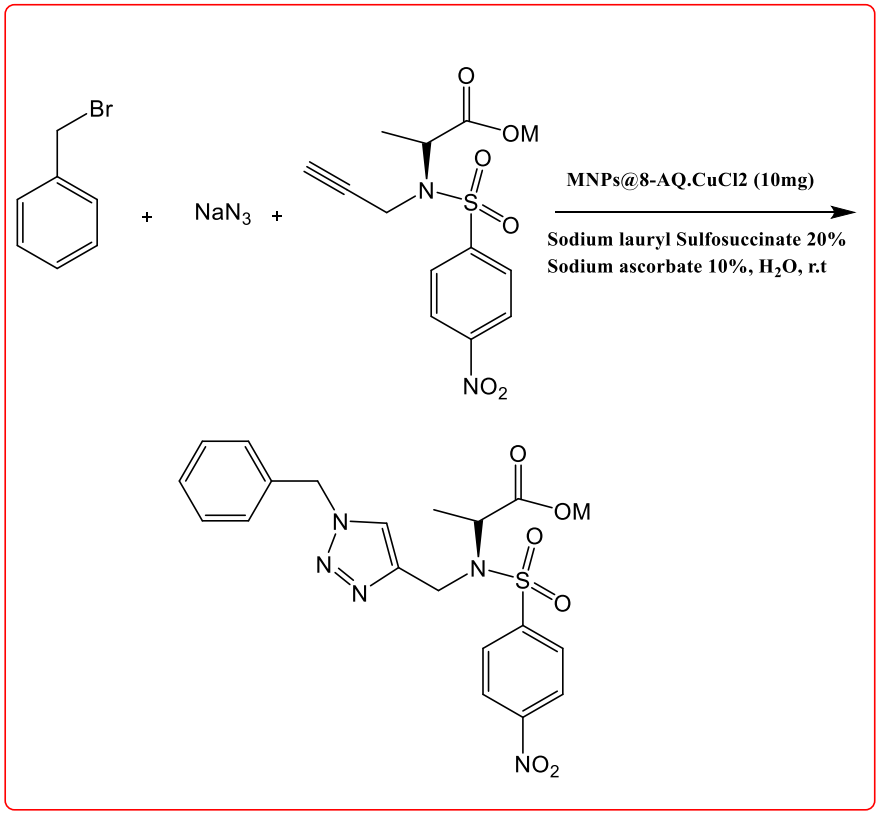


**Scheme 6.** Synthesis of amino acid functionalized-1,2,3-triazole with MNPs@8-AQ.$CuCl_2$.

## Conclusion

Magnetical nanocatalysts especially the organocopper which are supported by Fe3O4 nanoparticle have been developed as beloved catalytic systems in the synthesis of triazole compounds to biological targets. These catalytic systems have acceptable potential for their magnetically recoverable and reusable properties to click reactions.

## References

[1] H. Xiong and F. Seela, *J. Org. Chem.*, **2011**, *76*, 5584-5597.
[2] P. Thirumurugan, D. Matosiuk and K. Jozwiak, *Chem. Rev.*, **2013**, *113*, 4905-4979.
[3] W. Min, L. Jianmin, M. Jiping, Z. Zhe and W. Feng, *Angew. Chem. Int. Ed.*, **2015**, *54*, 14061-14065.
[4] H. Saeidian, H. Sadighian, M. Abdoli and M. Sahandi, *Journal of Molecular Structure*, **2017**, *1131*, 73-78.
[5] M.V. Papadopoulou, W.D. Bloomer, H.S. Rosenzweig, E. Chatelain, M. Kaiser, S.R. Wilkinson, C. McKenzie and J.-R. Ioset, *J. Med. Chem.*, **2012**, *55*, 5554-5565.
[6] Z. Mirjafary, L. Ahmadi, M. Moradi and H. Saeidian, *RSC Adv.*, **2015**, *5*, 78038-78046.
[7] Z. Mirjafary, H. Sadighian, S. Piri and H. Saeidian, *Journal of Sulfur Chemistry*, **2017**, *38*, 188-194.
[8] C.S. Radatz, L.d.A. Soares, E.R. Vieira, D. Alves, D. Russowsky and P.H. Schneider, *New J. Chem.*, **2014**, *38*, 1410-1417.
[9] Z. Zhang, P. Song, J. Zhou, Y. Chen, B. Lin and Y. Li, *Ind. Eng. Chem. Res.*, **2016**, *55*, 12301-12308.
[10] B. Kaboudin, R. Mostafalu and T. Yokomatsu, *Green Chem.*, **2013**, *15*, 2266-2274.

[11] F.M. Moghaddam and S.E. Ayati, *RSC Adv.*, **2015**, *5*, 3894-3902.
[12] H. Saeidian, H. Sadighian, M. Arabgari, Z. Mirjafary, S.E. Ayati, E. Najafi and F.M. Moghaddam, *Res. Chem. Intermed.*, **2018**, *44*, 601-612.
[13] F.M. Mogaddam, M. Eslami and S.E. Ayati, *ChemistrySelect*, **2017**, *2*, 11942-11948.

# Catalytic oxidative desulfurization of gasoline using organic-inorganic hybrid IMD-PWZn@NiO nanocatalyst

**Sahar Khandan, Mohammad Ali Rezvani***

*Department of Chemistry, Faculty of Science, University of Zanjan, Zanjan, Iran*

*Corresponding author Tel.: +98 (241) 5152477; Fax number: +98 (241) 5152617

*E-mail: marezvani@znu.ac.ir

**Abstract**

A new organic-inorganic hybrid nanocatalyst (IMD-PWZn@NiO) has been prepared by supporting the imidazolium salt of Zn-substituted phosphotungstate on nickel oxide particles. The synthesized materials were characterized by FTIR, XRD and SEM analysis techniques. The catalytic activity of the prepared composite was evaluated in the oxidative desulfurization (ODS) process of gasoline fuel. The ODS process was successfully developed on the basis of the catalytic oxidation of organosulfur compounds using $CH_3COOH/H_2O_2$ as an oxidizing agent. The removal of the sulfur content and mercaptan compounds of gasoline reached 97 and 96% at 35 °C after 1 h, respectively. The various experiments were taken into consideration to investigate the effects of catalyst amount and reaction temperature on sulfur removal efficiency. The nanocatalyst was found to give remarkable reusability for five times. The obtained data illustrated that IMD-PWZn@NiO/$CH_3COOH/H_2O_2$ oxidation system could be a convenient strategy for ODS of gasoline under moderate reaction conditions.

**Keywords**: Polyoxometalate, Nickel oxide, Nanocatalyst, Oxidative desulfurization, Gasoline

## Introduction

The removal of the sulfur attached to the heterocyclic or aliphatic hydrocarbons from liquid fuels is the most pressing issue of the petroleum industry recently. The high toxicity and corrosive nature of sulfur-containing compounds pose serious environmental problems during the combustion of the transportation fuel [1-3]. In view of the strict legislations about fuel quality in many countries, a lot of substantial research efforts have been focused on reducing the sulfur concentration of refined petroleum products [4,5]. To obtain low sulfur fuels, hydrodesulfurization (HDS) as the traditional process is often used in petroleum industry [6]. This technology has been proven to be a robust method in reducing thiol, sulfur mercaptan, sulfide, disulfide, thiophene and its derivatives [7]. Nevertheless, it is unsuccessful to obtain ultra-low-sulfur (<10 ppm S) because of the poor effect on refractory sulfide species such as thiophene, benzothiophene, dibenzothiophene, and their sterically hindered derivatives [8]. In addition, high temperature and high pressure conditions with large quantities of hydrogen are required during the HDS technology, which results in high costs and energy consumption [9]. Thus, there is an urgent need for inexpensive and energy-saving alternative methods to achieve ultra-deep desulfurization for the production of clean transportation fuels. A variety of alternative desulfurization techniques that have been studied include biodesulfurization, oxidative desulfurization (ODS), extraction and selective adsorption [10-13]. Among them, ODS has been widely recognized as one of the most cost-effective methods for deep desulfurization under moderate conditions (low temperature and ambient atmospheric pressure). According to this process, the organic sulfur-containing molecules are converted to their corresponding sulfoxide or sulfone in the presence of an oxidant and appropriate catalyst [14].

Polyoxometalates (POMs) are a unique class of negatively charged metal-oxygen clusters with remarkable catalytic properties, which have received extensive attention for catalyzing ODS reactions [15,16]. The application of bulk POMs as heterogeneous catalysts are limited because of their solubility in the aquatic and polar medium [17]. To overcome this undesirable obstacle, design and synthesis of heterogeneous catalysts have been explored in recent years by immobilization of POMs on appropriate supports [18]. Nickel oxide (NiO) particles has attracted more attention in catalysis due to its great physical and chemical properties, environmentally friendly nature, and low cost [19].

In this work, the IMD-PWZn@NiO nanocatalyst was synthesized and its catalytic activity evaluated for developing the ODS of gasoline. Also, the mixture of $CH_3COOH/H_2O_2$ was utilized as the oxidizing agent. After the oxidation step, the polar extraction solvent acetonitrile ($CH_3CN$) was used for extraction of oxidized sulfur compounds. The nanocatalyst was separated and reused at the end of the reaction for five times.

## Experimental

*Materials and methods*

All chemicals and solvents were commercially available and used as received. Hydrogen peroxide ($H_2O_2$, 30 vol.%), acetic acid ($CH_3COOH$, 99.7%), acetonitrile ($CH_3CN$), sodium tungstate dihydrate ($Na_2WO_4.2H_2O$), disodium hydrogen phosphate ($Na_2HPO_4$), and zinc nitrate hexahydrate ($Zn(NO_3)_2.6H_2O$) were purchased from Sigma–Aldrich without purification. Nickel nitrate hexahydrate ($Ni(NO_3)_2.6H_2O$), imidazolium bromide (IMDBr), and citric acid monohydrate ($C_6H_8O_7.H_2O$) were obtained from Merck.

Typical gasoline was used with the following specification: density of 0.7981 g/mL at 15 °C and total sulfur content of 0.4996 wt%.

The Fourier Transform Infrared spectroscopy (FTIR) studies were performed on a Thermo-Nicolet-iS 10 spectrometer, using KBr pellets technique with a measuring range of 400–4000 $cm^{-1}$. Powder X-ray diffraction (XRD) patterns were carried out on a D8 Bruker Advance powder X-ray diffractometer with a Cu Kα (λ = 0.154 nm) radiation source and the data were collected from 5 to 80° (2θ). The surface morphologies were examined by scanning electron microscopy (SEM) by LEO 1455 VP with an accelerating voltage of 26 kV. The total sulfur and mercaptan content of gasoline before and after treatment were determined using X-ray fluorescence with a TANAKA X-ray fluorescence spectrometer RX-360 SH.

***Synthesise of IMD-PWZn***

3.29 g of $Na_2WO_4.2H_2O$ was dissolved in 20 mL of distilled water. To this solution, 0.13 g of $Na_2HPO_4$ and 0.35 g of $Zn(NO_3)_2.6H_2O$ were added. The pH of the solution was adjusted to 4.5 under stirring, and the mixture was heated to 80-85 °C. Then, a solution of IMDBr 0.8 g in 10 mL HCl 1 M was added dropwise to above solution. The mixture was stirred to form a milky white precipitate. Finally, the obtained precipitate $[C_3H_4N_2]_3[PW_{11}ZnO_{39}]$ (abbreviated as IMD-PWZn) was filtered, recrystallized with acetonitrile and ether, and air dried.

***Synthesise of NiO particles***

1.90 g of $C_6H_8O_7.H_2O$ was dissolved in 15 mL of distilled water. This solution was added dropwise to the 15 mL of aqueous solution containing 2.90 g of $Ni(NO_3)_2.6H_2O$ under magnetic stirring at 70° C for 45 min to form a green gel. At last, the obtained gel was aged and dried at 80° C for 2 h and calcined at 400 ° C for 4 h.

***Synthesise of IMD-PWZn@NiO nanocatalyst***

The nanocatalyst was prepared as follows: 0.10 g of the prepared IMD-PWZn powder was dissolved in 10 mL boiling distilled water and then added slowly into the $Ni(NO_3)_2.6H_2O$ and $C_6H_8O_7.H_2O$ solutions during the formation of the green gel. The following steps were accomplished as same as the synthesis of NiO. After calcination step, the black powder (IMD-PWZn@NiO) was obtained.

***Catalytic oxidative desulfurization of gasoline***

In a typical run, a water bath was heated to 35 °C. Then, 50 mL of gasoline in a closed round-bottom flask equipped with a magnetic stirrer was heated to the reaction temperature. Afterward, 3 mL of $CH_3COOH/H_2O_2$ (in a volume ratio of 1/2) and 0.10 g of IMD-PWZn@NiO were added slowly to the reaction vessel. The ODS process was continued under stirring conditions (500 rpm) for 1 h. After the passage of this time, the above mixture was cooled to room temperature and 10 mL of $CH_3CN$ was added to extract the oxidized products. The formed immiscible phases (oil and water phases) were separated by a separation funnel and simple decantation technique. The total sulfur concentration after oxidation treatment was determined using the XRF spectrometer according to ASTM D-4294 and ASTM D-3227. The sulfur removal efficiency was calculated using Eq. (1), in which $S_i$ and $S_f$ are the initial and final concentration of sulfur compounds, respectively.

$$\text{Removal efficiency (\%)} = \left[\frac{S_i - S_f}{S_i}\right] \times 100 \quad (1)$$

## Results and discussion

*Characterization of materials*

The identification of specific chemical bonds and functional groups of the synthesized samples was characterized using FTIR to confirm their successful incorporation. The FTIR spectra of (a) NiO, (b) IMD-PWZn, and (c) IMD-PWZn@NiO are shown in Figure 1, respectively. As shown in Figure 1(a), a broad peak at 465 $cm^{-1}$ is caused by the vibration bond of Ni-O and the absorption band at 713 $cm^{-1}$ is assigned to Ni–O–H stretching bond. The absorption band at 1425 $cm^{-1}$ is due to dimeric O–H in-plane bending coupled C–O stretching vibrational in the structure of citric acid capping agent [20]. The unique characteristics peaks at 825, 883, 953, and 1052 $cm^{-1}$ are caused by the stretching modes of Keggin-type $[PW_{11}ZnO_{39}]^{3-}$ anions involving edge-sharing W–$O_c$–W, corner-sharing W–$O_b$–W, terminal W–$O_d$, and P–$O_a$ bond, respectively (Figure 1(b)) [21]. The peaks at 1383 and 1481 $cm^{-1}$ are attributed to C–N vibrations of in the structure of IMDBr. Furthermore, the absorption bands at 2853 and 2923 $cm^{-1}$ are ascribed to the symmetric and asymmetric stretching modes of $–CH_2$ groups [22]. FTIR spectra of IMD-PWZn@NiO composite exhibited characteristic peaks at 486, 830, 882, 934, 1434, 2853, and 2919 $cm^{-1}$ which showed some slight shifts compared to the bulk materials owing to the successful preparation of nanocatalyst.

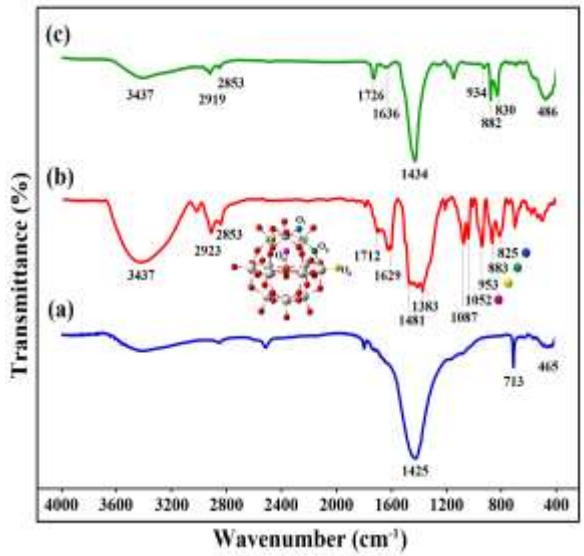


**Figure 1.** FT-IR spectra of (a) NiO, (b) IMD-PWZn, and (c) IMD-PWZn@NiO.

The materials were characterized by XRD technique in the scanning range 5° ≤ 2θ ≤ 80°. As shown in Figure 2(a), the XRD pattern of NiO is shown the unique sharp and narrow diffraction peaks at 2θ values of 37.3, 43.2, 62.8, 75.3, and 79.17°. These patterns are attributed to (101), (012), (110), (113), and (202) crystal planes, respectively (JCPDS, No. 04-0835). The XRD pattern of IMD-PWZn are shown in Figure 2(b), which displayed the broad amorphous in the range of 2θ= 5-10, 17-35, 40-45°. It is suggested the successful incorporation of IMDBr with PWZn. According to the pattern of IMD-PWZn@NiO nanocatalyst, it is shown that the absence of reflections characteristic of the POM due to the highly dispersion of IMD-PWZn particles on the surface of NiO (Figure 2(c)) [23].

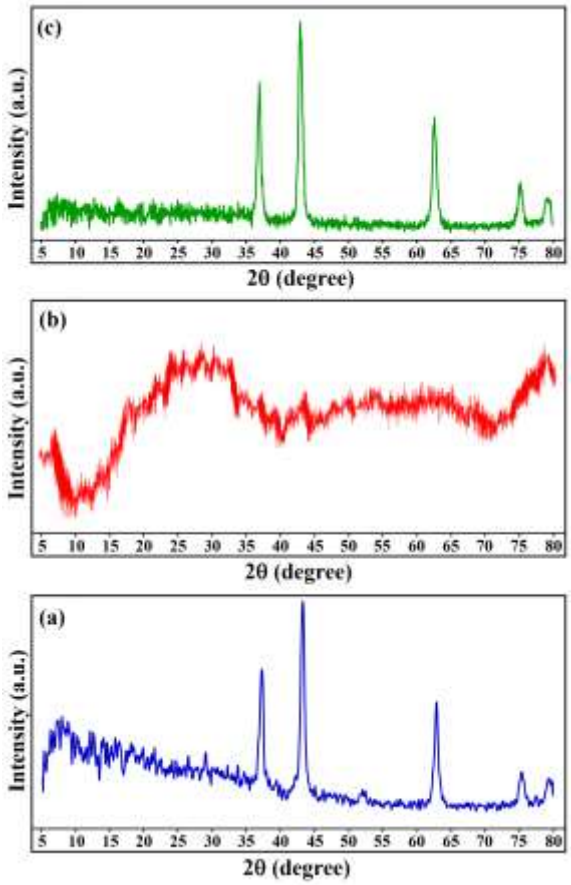


**Figure 2.** XRD pattern of (a) NiO, (b) IMD-PWZn, and (c) IMD-PWZn@NiO.

The surface morphology of samples was characterized by SEM technique. As depicted in Figure 3, the surface morphology of the synthesized materials was compared. As can be seen, the bulk NiO particles have an irregular shape (Figure 3(a)), while the SEM image of IMD-PWZn@NiO nanocatalyst is revealed the fine aggregation of nanoparticles in a spherical and homogeneous shape (Figure 3(c)). The SEM results are in good agreement with the results of XRD analysis.

**Table 2.** Effect of different temperatures on the ODS of gasoline.[a]

| Entry | Temperature (°C) | ODS efficiency (%) |
|---|---|---|
| 1 | 25 | 69 |
| 2 | 30 | 85 |
| 3 | 35 | 97 |
| 4 | 40 | 97 |

[a] Conditions of ODS: 50 mL of gasoline, 0.10 g of nanocatalyst, 3 mL of oxidant, 10 mL of extraction solvent, time = 1 h.

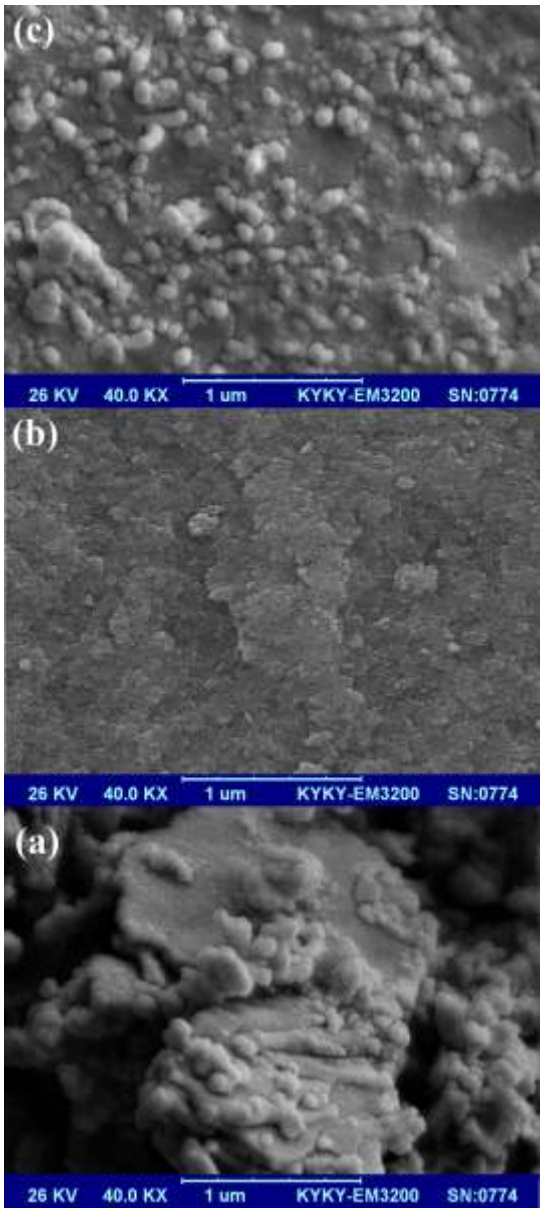


**Figure 3.** SEM image of (a) NiO, (b) IMD-PWZn, and (c) IMD-PWZn@NiO.

*Catalytic oxidative desulfurization results*

For investigation the sulfur oxidation of capability of IMD-PWZn@NiO nanocatalyst, ODS process was performed on typical gasoline under the mentioned condition in the experimental section. The attained results after oxidation treatment were reported in Table 1. According to the Entry 1, the total sulfur content of gasoline was reduced from 0.4996 % to 0.0140 wt.%. Also, the mercaptan compounds were much lowered from 94 to 4 ppm. It should be pointed out that the other specifications of gasoline were remained unchanged after ODS.

The effect of temperature was reported in Table 2. The experiments were carried out with IMD-PWZn@NiO nanocatalyst in the temperature range of 25-40 °C. It can be seen that the minimum reducing the concentration of sulfur compounds occurred at 25 °C. Increasing the temperature to 35 °C could be raised the ODS system efficiency above 90%, while the considerable changes were not obtained at 40 °C. Therefore, 35 °C was chosen as a favorable reaction temperature for IMD-PWZn@NiO/$CH_3COOH$/$H_2O_2$ catalytic system.

**Table 1.** The ODS test results of gasoline by IMD-PWZn@NiO nanocatalyst.

| Entry | Properties of gasoline | | Unit | Method | Before ODS | After ODS [a] |
|---|---|---|---|---|---|---|
| 1 | Total Sulfur by X-Ray | | wt.% | ASTM D 4294 | 0.4996 | 0.0140 |
| 2 | Mercaptans | | ppm | ASTM D 3227 | 94 | 4 |
| 3 | Density by hydrometer @ 15 °C | | g/mL | ASTM D 1298 | 0.7981 | 0.7980 |
| 4 | Salt | | ptb | ASTM D 3230 | 14 | 13 |
| 5 | Water Content by distillation | | vol. % | ASTM D 4006 | Nil. | Nil. |
| 6 | Distillation | Initial boiling point (IBP) | °C | ASTM D 86 | 48.6 | 48.1 |
| | | Final boiling point (FBP) | | | 209.1 | 208.8 |
| | | 10 | vol.% | | 69.9 | 69.2 |
| | | 50 | | | 118.3 | 117.5 |
| | | 90 | | | 187.8 | 187.2 |
| | | 95 | | | 208.5 | 208.1 |

[a] Conditions of ODS: 50 mL of gasoline, 0.10 g of nanocatalyst, 3 mL of oxidant, 10 mL of extraction solvent, time = 1 h, and temperature = 35 °C.

To assess the effect of nanocatalyst dosage on removal efficiency of sulfur compounds, various amount of organic-inorganic IMD-PWZn@NiO composite were used. According to the blank experimental results, 14% of the sulfur content of gasoline were removed. Also, it was found that the sulfur removal yield increased consecutively with an increased the dosage of nanocatalyst in the reaction medium. When the amount of nanocatalyst was further increased to 0.12 g, any noticeable change was not observed in the trend of increasing reaction efficiency. Therefore, the favorable dosage of IMD-PWZn@NiO nanocatalyst was 0.10 g for next oxidation runs.

**Table 3.** Effect of the nanocatalyst dosage on the ODS gasoline.[a]

| Entry | Nanocatalyst dosage (g) | ODS efficiency (%) |
|---|---|---|
| 1 | 0 (blank) | 14 |
| 2 | 0.02 | 26 |
| 3 | 0.04 | 42 |
| 4 | 0.06 | 64 |
| 5 | 0.08 | 82 |
| 6 | 0.10 | 97 |
| 7 | 0.12 | 97 |

[a] Conditions of ODS: 50 mL of gasoline, 3 mL of oxidant, 10 mL of extraction solvent, time = 1 h, and temperature = 35 °C.

After following each catalytic run, the IMD-PWZn@NiO nanocatalyst was regenerated by simple filtration, and washed with dichloromethane and dried at 90 °C for 1 h. Then, the recovered catalyst was used again for the subsequent process under similar oxidation conditions. The results of ODS process using reused nanocatalyst after the five regeneration cycles are shown in Figure 4. It was found that the removal efficiency of total sulfur content was dropped from 97 to 93%, which can be attributed to cover the active sites on the surface of nanocatalyst with sulfur-containing substrates or products.

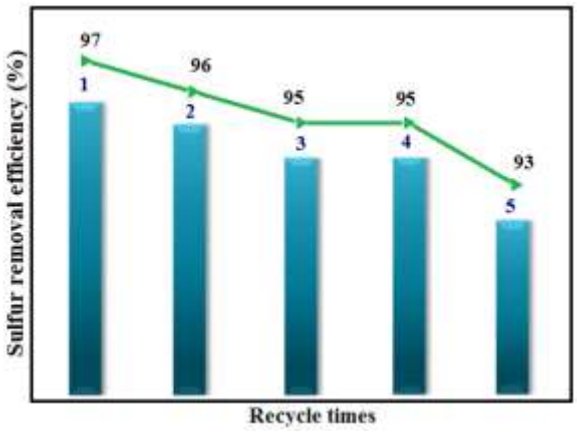


**Figure 4.** Reusability performance of IMD-PWZn@NiO nanocatalyst in ODS of gasoline.

## Conclusion

In summary, the new composite was designed by supporting of IMD-PWZn on NiO and employed as a nanocatalyst for ODS of gasoline. The characterization techniques were confirmed that the successful preparation of the nanocatalyst. The oxidation experimental results were demonstrated that the sulfur compounds could be efficiently removed from gasoline at 35 °C after 1 h. The reusability results of the organic-inorganic hybrid IMD-PWZn@NiO nanocatalyst indicated that the composite could be reused up to five cycles conveniently. This work was introduced as a facile method for the efficient ODS treatment to promote the quality of gasoline fuel.

## References

[1] C. Song, X. Ma, *Appl. Catal. B Environ.*, **2003**, *41*, 207-238.

[2] M. Zhang, W. Zhu, S. Xun, H. Li, Q. Gu, Z. Zhao, Q. Wang, *Chem. Eng. J.*, **2013**, *220*, 328-336.

[3] V. Perraud, J. R. Horne, A. S. Martinez, J. Kalinowski, S. Meinardi, M. L. Dawson, L. M. Wingen, D. Dabdub, D. R. Blake, R. B. Gerber, B. J. Finlayson-Pitts, *Proc. Natl. Acad. Sci. U. S. A.*, **2015**, *112*, 13514-13519.

[4] M. A. Rezvani, M. Shaterian, F. Akbarzadeh, S. Khandan, *Chem. Eng. J.*, **2018**, *333*, 537-544.

[5] M. A. Rezvani, S. Khandan, N. Sabahi, *Energy Fuels*, **2017**, *31*, 5472-5481.

[6] H. Li, W. Zhu, Y. Chang, W. Jiang, M. Zhanga, S. Yin, J. Xia, H. Li, *J. Mol. Graph. Model.*, **2015**, *59*, 40-49.

[7] B. Jiang, H. Yang, L. Zhang, R. Zhang, Y. Sun, Y. Huang, *Chem. Eng. J.*, **2016**, *283*, 89-96.

[8] M. Bagheri, M. Y. Masoomi, A. Morsali, *ACS Catal.*, **2017**, *7*, 6949-6956.

[9] G. Miao, D. Huang, X. Ren, X. Li, Z. Li, J. Xiao, *Appl. Catal. B Environ.*, **2016**, *192*, 72-79.

[10] I. Martínez, M. E. S. Mohamed, V. E. Santos, J. L. García, F. García-Ochoa, E. Díaz, *J. biotechnol.*, **2017**, *262*, 47-55.

[11] M. A. Rezvani, Z. Shokri Aghbolagh, H. Hosseini-Monfared, S. Khandan, *J. Ind. Eng. Chem.*, **2017**, *52*, 42-50.

[12] R. Abro, A. A. Abdeltawab, S. S. Al-Deyab, G. Yu, A. B. Qazi, S. Gao, X. Chen, *Rsc Adv.*, **2014**, *4*(67), 35302-35317.

[13] T. A. Saleh, G. I. Danmaliki, *Process Saf. Environ. Prot.*, **2016**, *102*, 9-19.

[14] M. A. Rezvani, M. A. Asli, S. Khandan, H. Mousavi, Z. S. Aghbolagh, *Chem. Eng. J.*, **2017**, *312*, 243-251.

[15] Y. Zhu, M. Zhu, L. Kang, F. Yu, B. Dai, *Ind. Eng. Chem. Res.*, **2015**, *54*, 2040-2047.

[16] H. Mirhoseini, M. Taghdiri, *Fuel*, **2016**, *167*, 60-67.

[17] D. E. Katsoulis, *Chem. Rev.*, **1998**, *98*, 359-388.

[18] Y. Ren, M. Wang, X. Chen, B. Yue, H. He, *Materials*, **2015**, *8*, 1545-1567.

[19] C. G. Morales-Guio, M. T. Mayer, A. Yella, S. D. Tilley, M. Grätzel, X. Hu, *J. Am. Chem. Soc.*, **2015**, *137*, 9927-36 .

[20] M. A. Rezvani, S. Khandan, M. Aghmasheh, *J. Taiwan Inst. Chem. Eng.*, **2017**, *77*, 321-328.

[21] E. Assady, B. Yadollahi, M. Riahi Farsani, M. Moghadam, *Appl. Organomet. Chem.*, **2015**, *29*(8), 561-565.

[22] F. M. Zonoz, A. Jamshidi, S. Tavakoli, *Solid State Sci.*, **2013**, *17*, 83-89.

[23] S. Boudjema, E. Vispe, A. Choukchou-Braham, J. A. Mayoral, R. Bachir, J. M. Fraile, *RSC Adv.*, **2015**, *5*, 6853-6863.

## Graphical Abstract

Catalytic oxidative desulfurization of gasoline using organic-inorganic hybrid IMD-PWZn@NiO nanocatalyst

Sahar Khandan, Mohammad Ali Rezvani*

# Novel synthesis of cone-like nanocomposite vanadium containing phosphomolybdovanadate@polyvinyl alcohol for oxidative desulfurization of gasoline

Nasrin Khalafi, Mohammad Ali Rezvani*, and Ziynab Maleki

Department of Chemistry, Faculty of Science, University of Zanjan, 451561319, Zanjan, Iran

*Corresponding author; E-mail: khalafi. nasrin @ znu.ac.ir and marezvani@znu.ac.ir Tel: +98 241 5152477 Fax: +98241 5152617.

**Abstract:**

To preparation of clean gasoline fuel our group synthesized a novel nanocatalyst by supported phosphomolybdovanadate on polyvinylalcohol (PVA) as an organic polymer. Organic polymers are suitable candidates as matrices for assembling polyoxometalates. Hence in this work, PVA is used to play this important role as great matrices. $(N(tBu)_4)_4HPMo_{10}V_2O_{40}$ (PMoV) was synthesized as our main polyoxometalate and then introduce PVA as polymer substrate. The structures of nanocomposite POM/PVA are characterized by FT-IR, UV-Vis, XRD and SEM. $(N(tBu)_4)_4HPMo_{10}V_2O_{40}$/PVA nanocomposite was shown be able to scavenge mercaptans and hydrogen sulfide (with high yield) in gasoline by $H_2O_2$ as an oxidant.

*Keywords:* polyoxometalate, polyvinylalcohol, nanocomposite, gasoline.

## 1. Introduction

Polyoxometalates (POMs) are well-defined oxoanionic clusters of early transition metals that have attracted growing interest for the development of advanced functional

materials [1]. POMs are a type of intriguing catalysts that can be applied for a wide range of technologically relevant applications owing to reasonably high thermal stability, and reversible electron transfer ability under mild conditions [2]. The evolution of this cluster`s chemistry is dependent upon the synthesis of new solids possessing unique structures and properties, although this still remains a challenge [3]. However, the application of this type of catalysts still suffers from some drawbacks, particularly the low surface area (1–10 $m^2/g$) leading to the low efficiency and the high solubility, causing recycling difficulty and environmental problem [4,5]. To overcome this disadvantage there is a need for the development of supported and heterogeneously active forms of POM [6]. Organic polymers are very easy to process due to their excellent toughness and durability and they are suitable candidates as matrices for assembling polyoxometalates. In this investigation, polyvinyl alcohol (PVA) is used to play this important and useful role as great matrices [7]. Nowadays many researches focus on the environmental safety to protect the world and its creatures. As refinery pollutants is one of the major problem in the world need to be concerned so in continuation of our group [8-11 ] $(N(tBu)_4)_4$ $HPMo_{10}V_2O_{40}$ synthesized as main keggin type polyoxometalate and then introduced to PVA as polymer substrate by uncommon method to be a proper step for progressing environmental safety. The structures of PMoV and PMoV/PVA are characterized by IR, UV-Vis, XRD and SEM. According to expressed resultant $(N(tBu)_4)_4$ $HPMo_{10}V_2O_{40}$/PVA nanoparticle was shown to be able to scavenge mercaptans and hydrogen sulfide (with high yield) in gasoline by $H_2O_2$ as an oxidant.

## 2. Experimental

### *2.1. Materials*

All solvents and reagents which are used in synthesized procedure are available commercially. The products characterized by analytical instrument FT-IR, UV-vis, XRD and SEM.

### *2.2. Preparation of catalyst*

$H_5PV_2Mo_{10}O_{40}$ synthesized according to published literature [9]. In summary, sodium metavanadate was dissolved by boiling in 50 ml of water and then mixed with $Na_2HPO_4$ .The solution cooled and concentrated sulfuric acid added, after obtaining a red color solution, $Na_2MoO_4 \cdot 2H_2O$ which was dissolved in 100 ml of water, added while it was stirring vigorously, followed by the slow addition of concentrated sulfuric acid. The hot solution cooled to room temperature and extracted with 500 mL of diethyl ether. For preparing $(N(tBu)_4)_4H\ PMo_{10}V_2O_{40}$, 1.0 g of $H_5PV_2Mo_{10}O_{40}$ dissolved in distilled water (10 ml). Potassium chloride (1.2 g) was added to the solution and let the mixture to stir for 15 min then filtered. Recrystallization of this solid was done from 20 ml of hot water and then dried under vacuum. Through stirring a solution from 2.0 g of potassium salt of $(PMo_{10}V_2O_{40})^{5-}$ in 55 ml of warm distilled water and a solution of 1.0 g of tetrabutyl ammonium bromide in 5.0 ml of $H_2O$ was prepared and added. The mixture was stirred at 60 °C for 3 h and filtered out the white precipitate. Then recrystallized with acetonitrile and ether, and air dried.

### *2.3. Preparation of cone-like nanocatalyst*

Preparation of $(N(tBu)_4)_4\ HPMo_{10}V_2O_{40}$/PVA is as follows :

0.1 g of PVA dissolved in 35 ml of hot distilled water and the temperature was fixed at 60 °C. Then 0.1 g of $(N(tBu)_4)_4 HPMo_{10}V_2O_{40}$ was added slightly to the solution and the mixture stirred for 2 h. The jelly solution dried at 50°C for 2h.

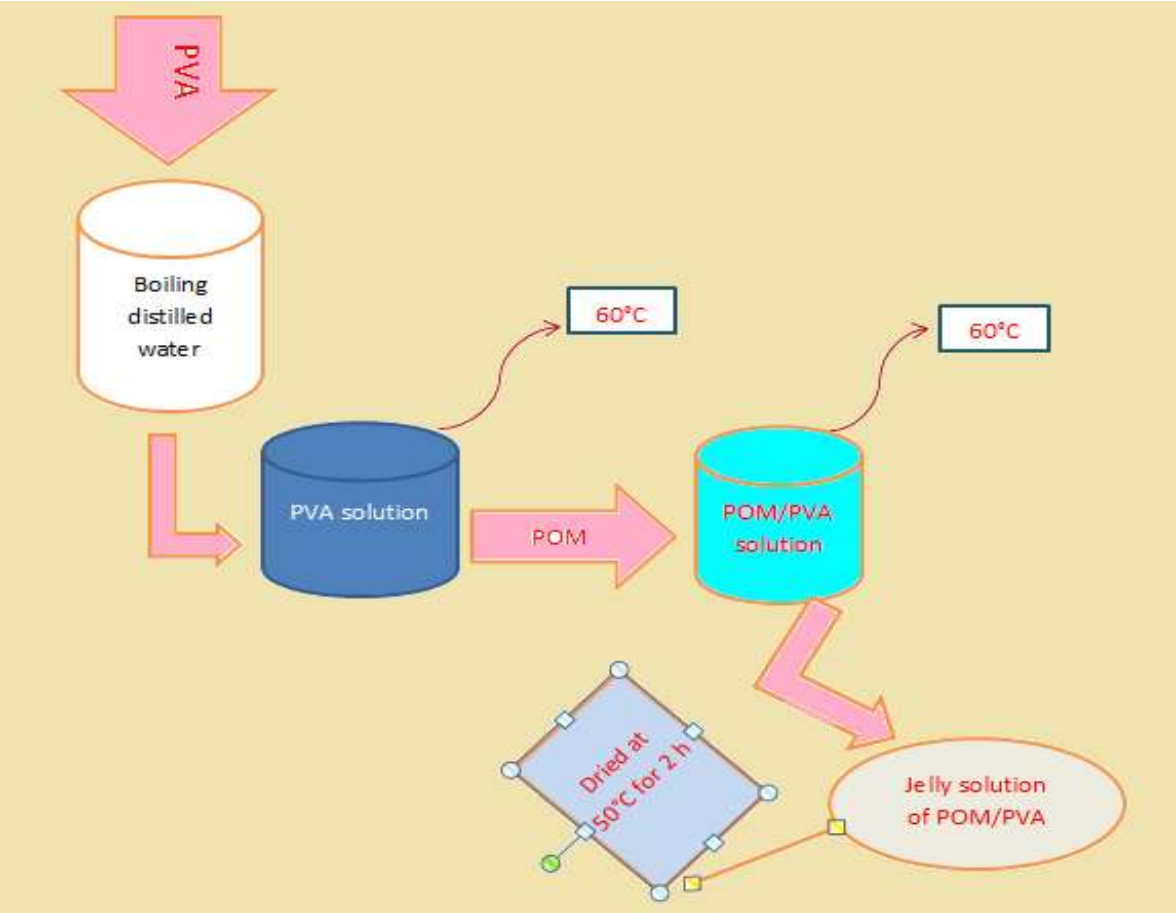


**Schem. 1.** Schematic of PMoV introduction to PVA

*2.4. Oxidation desulphurization (ODS) of gasoline:*

For oxidative desulfurization, gasoline (50ml) added to two-necked round flask while the temperature was at 65°C. Then 0.1 g of $PMo_{10}V_2O_{40}$/PVA added to the solution and strongly stirred by a magnetic stirrer. A mixture of acetic acid: $H_2O_2$ in ratio 1:2 dropwised through 2h.

After the oxidation finished the mixture was cooled down to room temperature and 10 ml acetonitrile (MeCN) for extraction of oxidized sulfur compounds. The acetonitrile/oil ratio used was 1/2 by volume. The biphasic mixture was separated by decantation. The oil phase was separated and weighed to calculate % recovery of gasoline (for three times reaction: %98, %97 and %96). The total sulfur and mercaptan sulfur content in gasoline before and after reaction were determined using X-ray fluorescence (a TANAKA X-ray fluorescence spectrometer RX-360 SH ASTM D-4294 method) and ASTM D-3227 Standard Test Method.

*2.5. Characterization methods*

FT-IR spectra were recorded by Thermo-Nicolet-is 10 and UV-vis spectra by UV-vis. Thermo-heylos in the range of 200-500 nm. X-ray diffraction (XRD) patterns was accomplished by D8 advance Brucker and radiation Cu kα (α = 1.54 nm) in the range of 0-60 (2θ). Scanning electron microscope (SEM) images were obtained on a LEO 1455VP with an accelerating voltage of 10.00 kV.

**3. Results and discussion**

*3.1. Characterization of synthesized catalysts*

From FT-IR spectra shown in Fig.1 can understand that there is a clear and notable difference between $PMo_{10}V_2$ powder, PVA and $PMo_{10}V_2$/PVA nanocomposite.

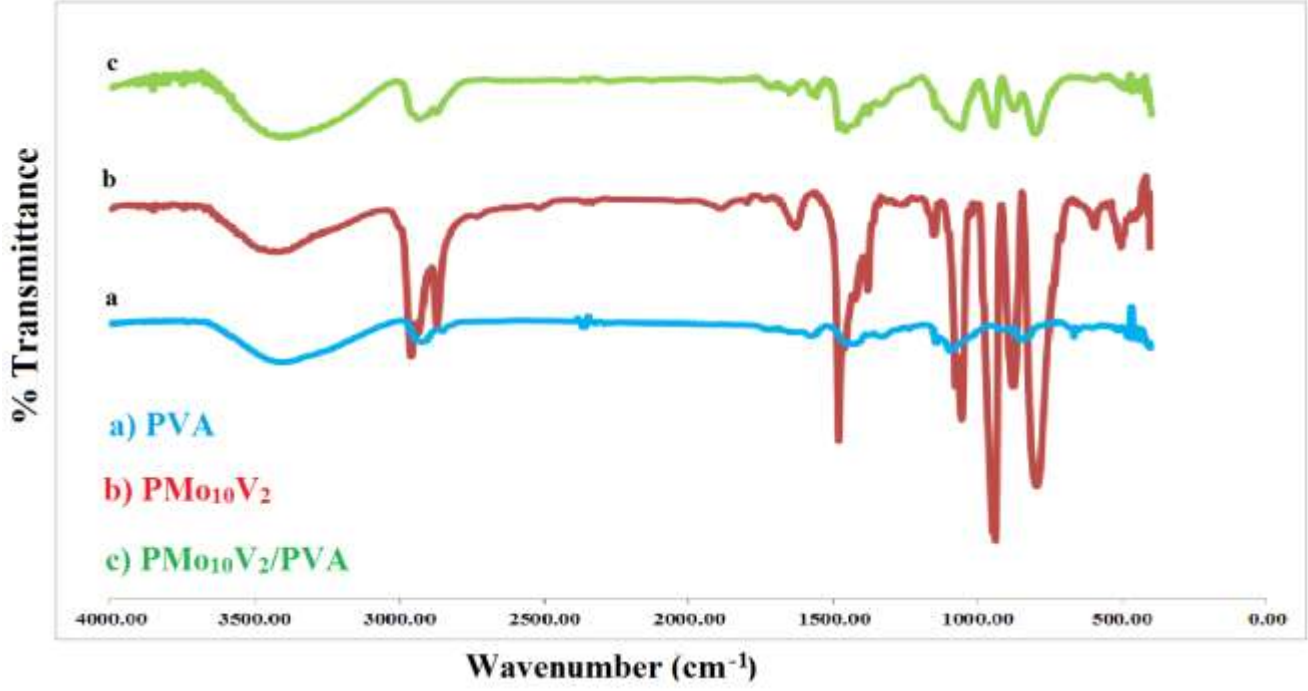


**Figure 1.** FT-IR spectra of: (a) PVA, (b) $(N(tBu)_4)_5PMo_{10}V_2O_{40}$ , (c) $N(tBu)_4)_5PMo_{10}V_2O_{40}$/PVA

According to characterization of nanocatalyst through 2h the band at 939.68 attributes to the asymmetric stretching vibration of the $M{=}O_d$ (M=Mo) terminal group that is shifted to 940.42 nm, the $M\text{-}O_b\text{-}M$ (M=Mo) corner- sharing band at 878.28 to 874.07 and the $M\text{-}O_c\text{-}M$ (M=Mo) stretching vibration band from 796.13 to 802.78, respectively ,when $PMo_{10}V_2$ introduced to PVA. These changes indicate that by introducing PMoV to PVA there are new types of interactions and the vibration of PMoV are distributed. These new interactions are created after PMoV assemblies and depict the existence of electrostatic and hydrogen-bond interactions with PVA. As presented in Table 1, characteristic bands of PMoV on PVA, compared to pure PMoV,

which present a blue- or red–shift indicate the electrostatic and hydrogen-bond interactions between PMoV and PVA. According to this table M-O corner – sharing band experiences a red shift, 4.21 nm, and show it is involved in the interaction with hydrogen on the PVA and formed a hydrogen bond.

**Table 1**
The assignments of FT-IR spectra of the $(N(tBu)_4)_5PMo_{10}V_2O_{40}$ solid.

| Entry | Assignments | PMoV/PVA | PMoV |
|---|---|---|---|
| 1 | $P\text{-}O_a$ antisym.str. | 1056 | 1056 |
| 2 | $M{=}O_d$ antisym.str. | 940 | 939 |
| 3 | $M\text{-}O_b\text{-}M$ antisym.str. | 874 | 878 |
| 4 | $M\text{-}O_c\text{-}M$ antisym.str. | 802 | 796 |

Fig. 2 shows the UV-vis spectra of pure PVA, $(N(tBu)_4)_5PMo_{10}V_2O_{40}$ and $(N(tBu)_4)_4$ $HPMo_{10}V_2O_{40}$/PVA as comparative data to confirm the changes on pure POM after introducing PVA. As the UV-vis spectra depicts, in (b) a band about 200 nm shows a charge transfer (CT) O Mo. By introducing POM on PVA, corresponding to (a, c), the intensity of bands decreased so can persuade us that interaction between them completed and spectra of PVA overlapped POM. That is what we expected and this confirmative state made us to use this nano catalyst during ODS.

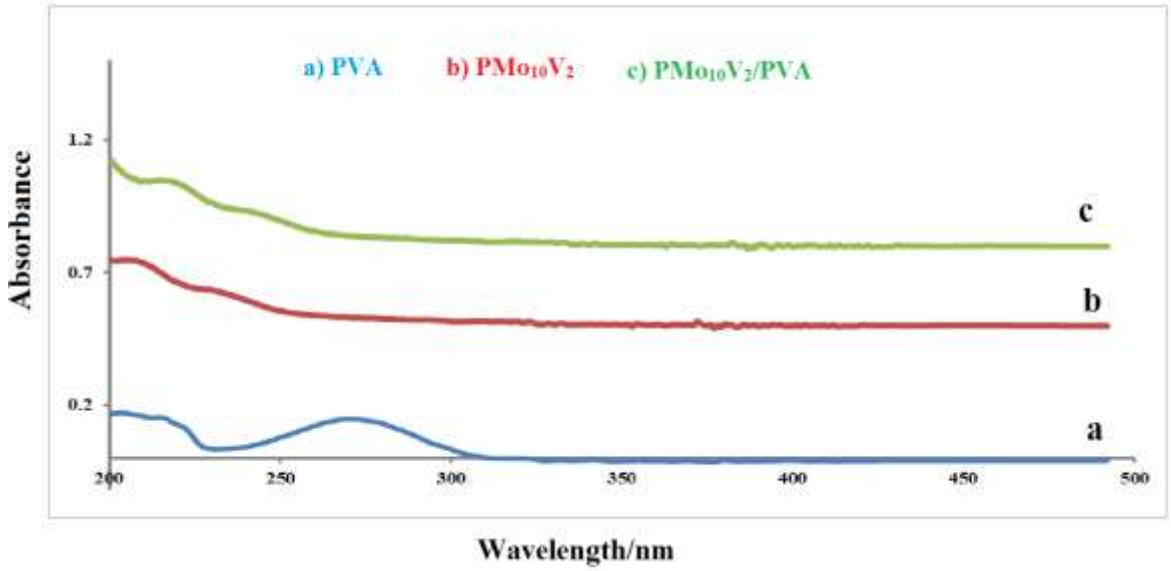


**Figure 2.** UV–vis spectra of: (a) PVA, (b) $(N(tBu)_4)_5PMo_{10}V_2O_{40}$ , (c) $(N(tBu)_4)_5PMo_{10}V_2O_{40}$/PVA

The SEM images, Fig. 3 (a, b, c and d), of $(N(tBu)_4)_4HPMo_{10}V_2O_{40}$/PVA present the self-assembly of polyoxometalate with PVA. The cone-like structures are a confirmative for enough stirring rate and exact temperature and are led to this appropriate nano shape. The presence of keggin type of POM on PVA, as substrate, indicates an interaction between them that was according to our expectations and can satisfy to be as an efficient catalyst for next project.

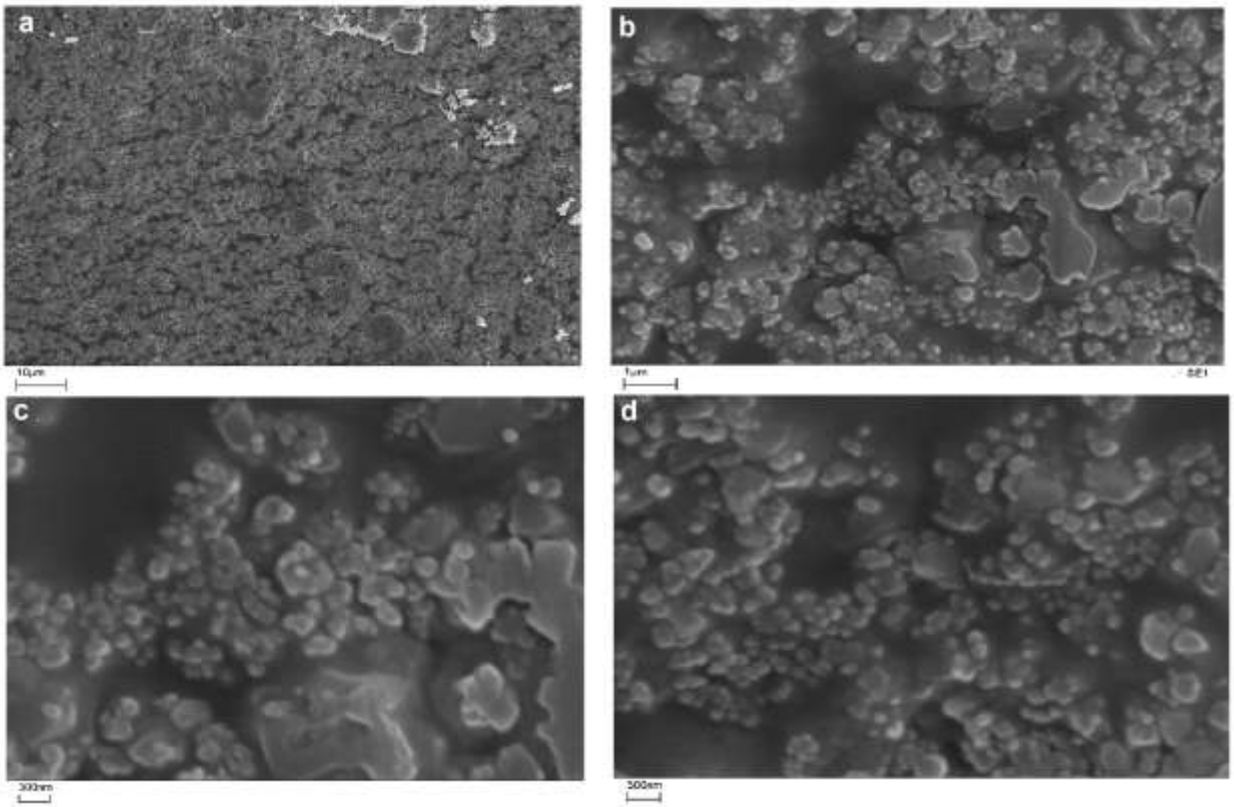


**Figure 3**. SEM images: ( a,b,c,d) $(N(tBu)_4)_5PMo_{10}V_2O_{40}$/PVA

The XRD patterns of $PMo_{10}V_2$/PVA are shown in Fig.4 and were collected in the range 0-60° 2θ. It is obviously seen that in the XRD patterns of keggin type polyoxometalat special peak have appeared. The existence of sharp peaks in 0-10° can prove the structure of synthesized PMoV as a keggin type. Beside, this focusing on 15-20° and 30° is important to be sure about the structure. According to previous reporting, the XRD pattern of pure PVA must have a sharp peak in 19.7° [12]. Fig. 4 consists of required information of PVA and PMoV. It can be seen that the

diffraction of PVA is overlapped by PMoV so the intensity around 20° decreased. Then PMoV introduced to PVA with a good interaction between them.

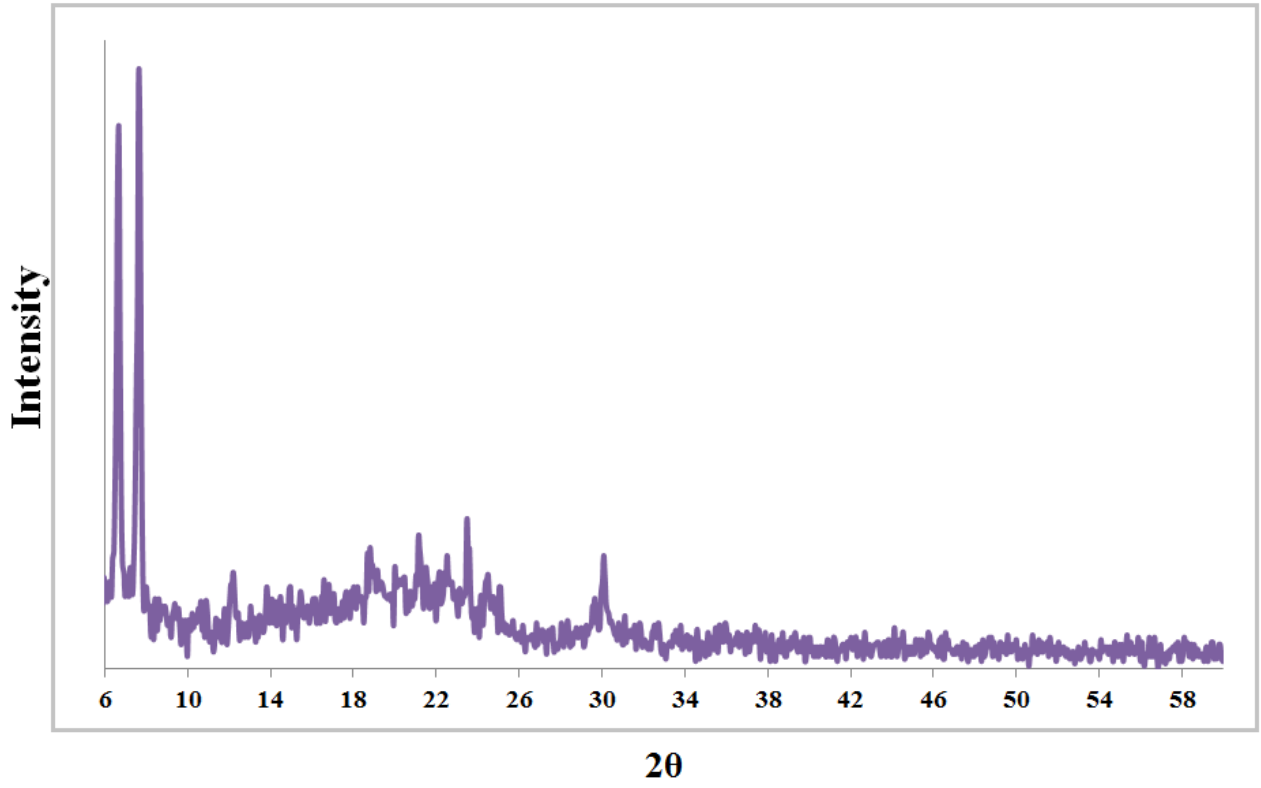


**Figure 4.** XRD pattern of $(N(tBu)_4)_5PMo_{10}V_2O_{40}$/PVA

*3.2. Catalytic results*

*3.2.1. General desulfurization process*

In the ODS process, gasoline is mixed with acetic acid/$H_2O_2$ and $(N(tBu)_4)_4HPMo_{10}V_2O_{40}$/PVA then the oxidation reaction takes place at 65 °C under atmospheric pressure. The $H_2O_2$ was used in the presence of acetic acid as oxidants because acetic acid as an organic acid, reacts with $H_2O_2$

to in situ produce peracid, which can efficiency convert organic sulfur to sulfones without forming a substantial amount of residual product. This is followed by a liquid extraction (acetonitrile) to obtain gasoline with low sulfur. $H_2O_2$ play a role as an oxidant which is the best one for being environmental friend. Its joining with polyoxometalate makes the best catalytic activity. At the first step $H_2O_2$ react with PMoV which bring $^{\bullet}OH$ and polyoxoperoxo that is so active. So alter convert organic sulfur to its solfoxide and solfune derivatives which stay in liquid phase that will be removed by extraction. Now the gasoline would be without sulfur and clean as purpose that is mention for desulfurization.

*3.2.2. Oxidation desulphurization of gasoline*

From the results of Table 2, after oxidation process, total sulfur content (Entry 2) and content of mercaptans (Entry 3) were much lower, while numerous other properties of gasoline showed in Table 2 remained unaffected. From the results obtained in this work, it was demonstrated that the nanomercaptan scavenger ,$(N(tBu)_4)_4HPMo_{10}V_2O_{40}$/PVA, can catalyze the oxidation desulphurization reaction in 2 h and can reduce total sulfur content (wt.%) of actual gasoline from 0.286 wt.% to 0.012 wt.% and also, reduce content of mercaptans from 38 ppm to 3 ppm.

**Table 2**. Oxidation desulphurization of gasoline by $(N(tBu)_4)_4HPMo_{10}V_2O_{40}$/PVA.

| Entry | Properties of gasoline | | Unit | Method | Before ODS | After ODS [a] |
|---|---|---|---|---|---|---|
| 1 | Density by hydrometer @ 15 $^0$C | | g/ml | ASTM D 1298 | 0.7863 | 0.7861 |
| 2 | Total Sulfur by X-Ray | | Wt.% | ASTM D 4294 | 0.286 | 0.012 |
| 3 | Mercaptans | | ppm | ASTM D 3227 | 38 | 3 |
| 4 | Water Content by distillation | | vol. % | ASTM D 4006 | Nil. | Nil. |
| 5 | Distillation | **IBP** | $^0$C | ASTM D 86 | **44.4** | **44.1** |
| | | **FBP** | | | **205.3** | **204.5** |
| | | 10 | Vol% | | 67.6 | 67.1 |
| | | 50 | | | 112.7 | 112.2 |
| | | 90 | | | 179.5 | 179.1 |
| | | 95 | | | 205.3 | 204.8 |

[a] Condition for desulphurization: 50 ml of gasoline, 0.1 g nano catalyst, 3 ml oxidant, 10 ml of extraction solvent, time = 2 h, and temperature = 65 °C.

## 4. Conclusion

In summary, we synthesized $(N(tBu)_4)_4$ $HPMo_{10}V_2O_{40}$ in mild temperature and with sol-gel method. For increasing the efficiency of POM, introduced to PVA and we tried to prepare a suitable situation for making a covalent interactions between them. The characterization data like FT-IR, UV-vis, SEM and XRD confirm our claim and show a self-assembly of keggin type POM which can work as an efficient and appropriate catalyst for oxidative desulfurization of gasoline.

**References**

[1] M. A. Rezvani, A. F. Shojaei, F. M. Zonoz, J. Serb. Chem. Soc. 79 (2014) 1099.

[2] N. M. Mahmoodi, M. A. Rezvani, M. Oveisi, A. Valipour, M. A. Asli, Mater. Res. Bull., 84 (2016) 422.

[3] M. A. Rezvani, M. Alinia Asli, M. Oveisi, R. babaei, K. Qasemi, S. Khandan, RSC Adv. 6 (2016) 53069.

[4] M. A. Rezvani, M. Alinia Asli, S. Khandan, H. Mousavi, Z. Shokri Aghbolagh, Chem. Eng. J. 312 (2017) 243.

[5] X. Sheng, Y. Zhoua, Y. Zhang, M. Xue, Y. Duan, Chem. Eng. J. 179 (2012) 295.

[6] Z. A. Abdalla, B. Li, Chem. Eng. J., 200 (2012) 113.

[7] W. Qi, L. Wu, Polym. Int., 58 (2009) 1217.

[8] M. A. Rezvani, A. F. Shojaie, M. H. Loghmani, Fuel Process. Technol. 118 (2014) 1.

[9] M. A. Rezvani, F. Mohammadi Zonoz, Ind. Eng. Chem. 22 (2015) 83.

[10] M. A. Rezvani, M. Shaterian, F. Akbarzadeh, S. Khandan, Chem. Eng. J. 333 (2018) 537.

[11] M. A. Rezvani, Z. S. Aghbolagh, H. H. Monfared, S. Khandan, J. Ind. Eng. Chem. 52 (2017) 42.

[12] G. Attia, M. F. H. Abd El-kader, Int. J. Electrochem. Sci., 8 (2013) 5672.

# A highly sensitive nano-structured sensor for electrocatalytic detection of pentoxifylline drug in environmental and biological samples

**Asma Khoobi[a,b,*], Abdol Mohammad Attaran[b], Morteza Enhessari[c], Masoud Yousofi[b]**

[a] *Department of Analytical Chemistry, Faculty of Chemistry, University of Kashan, Kashan, P.O. Box. 87317-51167, Islamic Republic of Iran*

[b] *Department of Chemistry, Payame Noor University, Delijan, Iran*

[c] *Department of Chemistry, Naragh Branch, Islamic Azad University, Naragh, Islamic Republic of Iran*

*Corresponding author Tel.: +98 (3155912383); Fax number: +98 (3155552930)

*E-mail: asma.khoobi@gmail.com

## Abstract

Lead titanate nano-sized powders were synthesized using citric acid gel method. The nanopowders were characterized using X-ray diffraction (XRD) and scanning electron microscopy (SEM). Then, a nanocomposite system based on lead titanate nanopowders and carbon paste electrode (CPE) was designed and applied for determination of pentoxifylline (PTX). The measurements were performed by cyclic voltammetry (CV) and differential pulse voltammetry (DPV) techniques. The prepared nanostructured electrode showd voltammetric responses with high sensitivity and selectivity for PTX. Analytical parameters such as repeatability, stability and linear dynamic range were also examined and a limit of detection of 2.1 nM was achieved. After investigation the effect of probable interferences in determination of PTX, it was found that the proposed method was free of the interferences. Finally, the proposed method was successfully applied for analysis of PTX in environmental and biological samples.

**Keywords**: Electrocatalytic *Detection; $PbTiO_3$ Nanopowders; Pentoxifylline; Environmental Analysis*

## Introduction

Nanostructured materials, because of their important characteristics have been the focus of serious interest for the last decade world-wide. In this field most of the novel and remarkable properties appear when the particle size ranges exist well below 100 nm [1]. Ferroelectric materials are a group of compounds that possess relatively low dielectric loss, high dielectric constants, moderate dielectric breakdown strength, high electrical resistivity and suitable electrooptical and electromechanical activates [2]. Ferroelectric materials with perovskite structure ($ABO_3$), such as lead titanate ($PbTiO_3$) and barium titanate ($BaTiO_3$), are the most studied ferroelectric oxide compounds due to their versatile characteristics for use in actuators, thin film capacitors, pyroelectric sensors, electronic transducers and nonlinear optics. The materials with nano-sized dimensions have received significant research attention because of the unconventional physical and chemical behaviour at the nanoscale dimensions [3-5]. Lead titanate ($PbTiO_3$) is usually used in numerous electronic devices due to a high pyroelectric coefficient and relatively low permittivity [6,7]. Some methods have been reported for preparation of $PbTiO_3$, such as sol-gel method [8], hydrothermal synthesis [9], dip-pennanolithography [10], liquid-solid-solution route [11] and solid-state reaction [12]. It is widely known that chemical synthesis methods can be provide precise composition, high chemical purity, uniform microstructures and without high formation temperature of the perovskite phase based on molecular scale mixing in the preparation of the precursor. The sol-gel method is a very usually applied chemical method for preparation of homogeneous large area thin films and uniform micrometer, sub-micrometer or nanometer sized powders. Additionally, the particles morphology can be easily controlled by changing in the synthesis factors [13,14].

Pentoxifylline (PTX, 3,7-Dimethyl-1-(5-oxohexyl)-3,7-dihydro-1H-purine-2,6-dione) a tri-substituted xanthine derivative is a hemorheologic agent applied for the treatment of peripheral arterial disease and intermittent claudication. The drug improves blood flow by peripheral circulation via reducing blood viscosity, inhibiting platelet aggregation, improving erythrocyte flexibility and decreasing fibrinogen concentration [15]. ]. Beside the well known hemorheological properties, it has been recognized to exert a wide range of immunological activities. It has been described that PTX disturbs polarization and migration of human leucocytes [16]. The compound also reduces leucocyte-endothelium interaction and shows a therapeutic role in inhibiting ischemia reperfusion injury in microsurgical operations [17]. PTX prevents atherosclerosis in diabetes mellitus and is a general phosphodiesterase inhibitor that decreases tumor necrosis factor gene transcription. The dug also can be prevented from strokes and used in managing sickle cell disease and increases blood flow to the brain [18,19]. Several methods for determination of PTX have been used, including spectrophotometry [20], high performance liquid chromatography [15], gas chromatography [21], thin layer chromatography [22] and electrochemistry [23]. Some of the methods suffer from problems such as complexity, time consuming and need expensive instrumentation along with sample preparation. Among the various methods reported for PTX determination, electrochemistry is often favorable method because of their high sensitivity, selectivity, rapid detection and free of sample preparation steps. Electrochemical techniques that use chemically modified electrodes are usually important methods in medicine and

biotechnology, environmental monitoring and industrial process control [24].

In the present study, a sol-gel method based on a metal-citrate complex system was used for synthesis of nano-sized $PbTiO_3$. Then, a sensitive and simple $PbTiO_3$ nanoparticle modified carbon paste electrode (PTN/CPE) was designed for determination of PTX. Primary investigation about the formation of the nanoparticles and modified electrode were perused. Then, analysis of PTX at the surface of the nanostructured electrode was performed by electrochemical methods.

## Experimental

### *Materials*

All solutions were freshly prepared by deionized water and chemicals used were of analytical grade. Citric acid (99.5 %), tetra-n-butyl titanate (98%), $H_20_2$ (30%), $Pb(N0_3)_2.6H_2O$ (98%), ammonia solution (25-28%), PTX, carbon graphite powder, paraffin oil and other chemicals were purchased from Merck and used without any further purification. Stock solutions of 0.2 M $H_3PO_4$, $CH_3COOH$, $H_3BO_3$ and a saturated solution of NaOH were used for preparation of 0.2 M Britton-Robinson (B-R) buffer solutions.

### *Preparation of $PbTiO_3$ nanostructures and working electrodes*

For synthesis of $PbTiO_3$ nano-sized powders, tetra-n-butyl titanate was added to stirred deionized water and the precipitation was observed. Then, the precipitate was filtered and washed with deionized water. An appropriate of citric acid and H202 was added and then, the solution became viscous and maroon in color. The pH value of the solution was adjusted to 6.0 by ammonia solution. For preparation of a water-soluble precursor for Ti(IV) continuous stirring and refluxing at 60°C was performed. Then, stoichiometric amount of $Pb(NO_3)_2$ was dissolved in 5.0 M citric acid solution with pH of 6.0 (adjusted by ammonia) and then, the Pb(II) precursor was mixed with the Ti(IV) precursor. The above mixture was refluxed at 60°C for 2 h with continuo's stirring. After drying in a furnace at 60°C for 24 h a porous citreous resin was formed. Then, the solid resin precursors were calcined at 500°C and 550°C for 2 h to obtain the $PbTiO_3$ nanopowders.

At the next step, the carbon paste electrode (CPE) was prepared by hand-mixing 0.50 g graphite powder with about 0.2 mL of paraffin oil in a pestle and mortar. For preparing the modified electrode, appropriate amount of $PbTiO_3$ nanopowders calcined at 550°C was dispersed in 5.0 mL deionized water by an ultrasound bath for 30 minutes and then was mixed into 0.50 g graphite powder in a small mortar. After vaporizing water, about 0.2 ml of paraffin oil was added to the above mixture.

### *Apparatus*

The X-ray diffraction (XRD) patterns of the nanopowders were recorded by a Model PI TS 3003 of SEIFERT diffractometer using Cu Kα radiation (k = 1.5418 Å) to examine the crystallization and structural properties of $PbTiO_3$ nanopowders. Scanning electron microscopy (SEM) micrographs were obtained using a KYKY-EM3200. Electrochemical experiments were carried out using an Autolab potentiostat-galvanostat PGSTAT 35 (Eco Chemie Utrecht, Netherlands), equipped with NOVA 1.6 software. The electrochemical cell was equipped with a three-electrode system containing a modified carbon paste, a platinum and an Ag/AgCl/KCl (3.0 M) as the working, counter and reference electrodes, respectively. A digital pH meter (Metrohm model 691) was applied for preparation of buffer solutions that served as a supporting electrolyte in the electrochemical experiments.

## Results and discussion

### *Structural and surface analysis*

The structural studies of the samples was investigated using XRD pattern of the $PbTiO_3$ nanopowders calcined at 500°C and 550°C. As can be observed in Fig. 1, at 500°C, the crystallization of tetragonal phase took place along with traces impurity phase [25]. But, at 550°C all peaks can be attributed to the $PbTiO_3$ crystals with a tetragonal structure (JCPDS: 78-0299). No impurity peak was found, indicating that a pure crystalline compound has been formed. The crystallite size (t) of the $PbTiO_3$ nanopowders calcined at the two temperatures could be achieved by the Scherrer's equation (Eq.(1)):

$$t = 0{:}9\lambda / \beta \cos\theta \qquad (1)$$

where λ, β and θ are wavelength of radiation, the peak width at its half maximum intensity and diffraction angle, respectively. Based on the data the crystallite size of $PbTiO_3$ nanostructures at 500°C and 550 °C were obtained 30.3 and 39.2 nm, respectively.

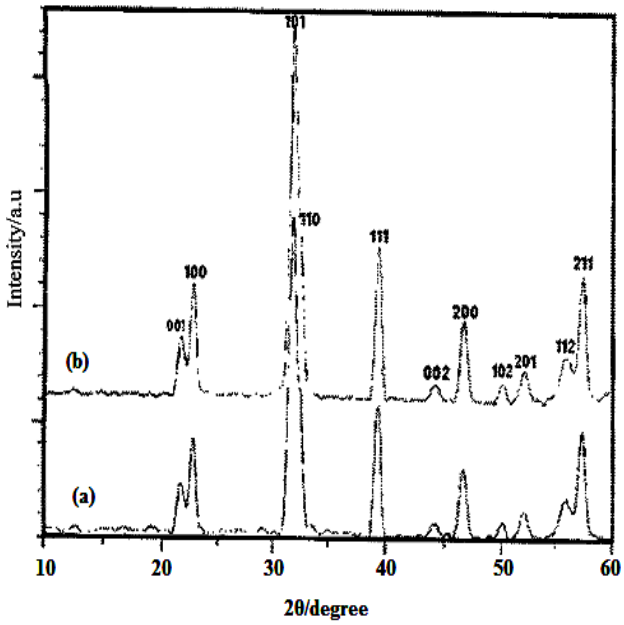


**Fig. 1.** XRD pattern of $PbTiO_3$ nanostructures calcined at (a) 500 °C and (b) 550°C for 2 h.

The morphologies and particle sizes of the $PbTiO_3$ nanopowders calcined at550°C have been investigated using SEM micrographs. Fig. 2 shows that $PbTiO_3$ nanopowders with the diameter in the range of 37 nm to 60 nm are uniformly distributed.

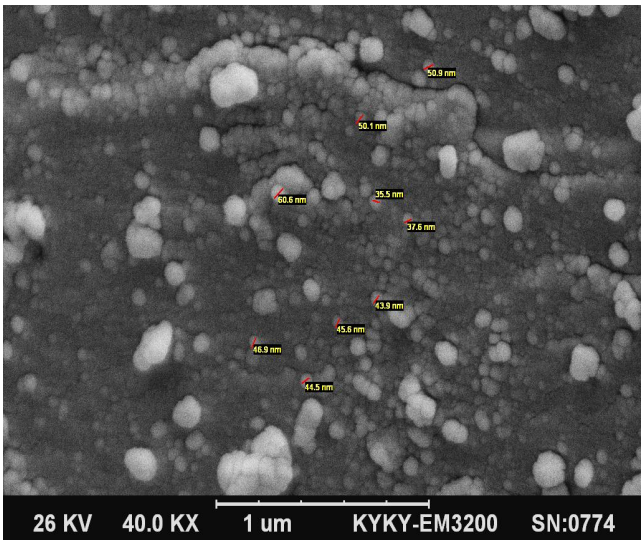


**Fig. 2.** SEM micrographs of $PbTiO_3$ nanostructures calcined 550 °C for 2 h.

Also for investigation of the CPE modification process SEM was used. Fig. 3 compares the morphological features of (a) CPE and (b) PTN/CPE.

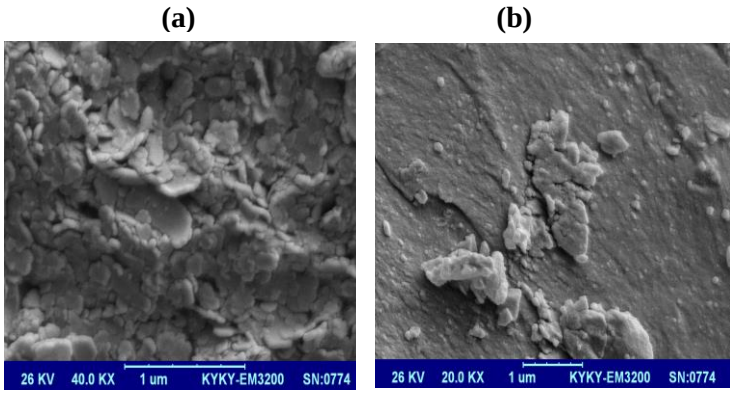


**Fig. 3.** SEM micrographs of (a) CPE and (b) PTN/CPE.

SEM was used to evaluate the physical appearance and surface characteristics of $PbTiO_3$ nanoparticles on the CPE surface. The SEM image of CPE was characterized

by a surface of irregularly shaped graphite particles that appeared to remain isolated (Fig. 3a). Whereas, the SEM micrograph of PTN/CPE (Fig. 3b), demonstrations different morphology than the CPE. The micrographs indicate that the modification of the CPE surface with $PbTiO_3$ nanoparticles has been well accomplished.

***Electrochemical properties of the PTN/CPE***

For investigation the catalytic activity of the PTN/CPE, differential pulse voltammetry (DPV) technique was used. The differential pulse voltammograms of PTX at the surface of bare CPE and PTN/CPE were recorded (Fig. 4). As can be observed, PTN/CPE shows a well-defined oxidation peak with magnification of about 3.0 times greater than the bare CPE. An enhancement in current response is clear evidence of the catalytic effect of the nanostructured modified electrode on the oxidation of PTX.

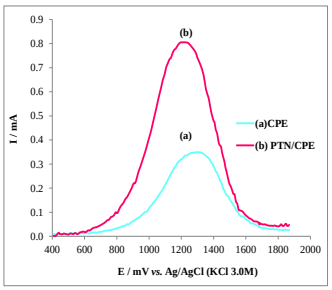


**Fig. 4.** Differential pulse voltammograms of PTX at the surface of (a) CPE and (b) PTN/CPE.

***Determination of PTX at the surface of PTN/CPE***

The main purpose of the work is designing a high sensitive method for determination of PTX. Since the charging current influence to background current is a limiting parameter in the determination of any electroactive species, experiments were performed using DPV. Also for achieving the best response of PTX at the surface of PTN/CPE, all effective factors on the oxidation peak current of the analyte was optimized. Therefore, the voltammograms were recorded in the presence of B-R buffer solutions (pH = 8.0), 10% of $PbTiO_3$ nanoparicles, a scan rate of 0.05 V s-1 and a modulation amplitude of 0.33 V. Fig. 5A shows the differential pulse voltammograms obtained for the oxidation of different PTX concentrations at the PTN/CPE. Also, Fig. 5B exhibits clearly that the plot of oxidation peak current versus PTX concentration is constituted of three linear segments, corresponding to three different ranges of analyte concentration. From the data, detection limit (3σ) of PTX was obtained 2.1 nM and linear range estimated to be 0.02-220.0 μM. A low detection limit for PTX is indicating the nanostructured modified electrode is an appropriate sensor for determination of PTX with high sensitivity. Therefore, the nanostructured electrode is a potential sensor for trace analysis of PTX in real samples.

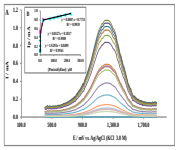

**Fig. 5.** (A) Differential pulse voltammograms of different concentrations of PTX at the surface of PTN/CPE and (B) Plots of peak current as a function of PTX concentration.

***Interference study***

The influence of several foreign species on the determination of PTX at the surface of PTN/CPE were studied. The tolerance limit DPV studies was considered as the maximum concentration of the interferenct which caused an about ±5% relative error in the analysis. The results showed that 20-fold of citric acid, lactic acid, dextrose, glucose, sucrose and starch did not show interference in the determination of PTX.

***The repeatability and stability***

The electrode ability for the generation of a reproducible surface was studied by DPV obtained from five separately prepared PTN/CPEs. The calculated relative standard deviation for various factors accepted as the criteria for a satisfactory surface reproducibility (1.2-3.8%). Furthermore, the long-term stability of the nanostructured modified electrode was evaluated over a 2-week period. Differential pulse voltammograms recorded in the period showed the peak potential for PTX was unchanged and the current signals reduced only less than 2.1%. These results indicate that the repeatability and stability of the nanostructured electrode is satisfactory.

***Application of the method in real sample analysis***

For evaluation the applicability of the proposed method, the method was used to the detection of PTX in industrial wastewater and biological samples (human blood plasma) by standard addition method. The recovery percentages of the method were obtained between 94.0-104.7% and 96.5-106.0% for industrial wastewater and biological samples, respectively. The results are listed in Tables 1. According to the results very good recoveries were obtained for the detection of PTX, which indicates that the nanostructured sensor can be applied for the analysis of the analyte in environmental and biological samples.

**Table 1.** Determination of PTX in wastewater and human blood plasma samples.

| Sample | Added ($\mu g\ L^{-1}$) | Found ($\mu g\ L^{-1}$) | Recovery (%) |
|---|---|---|---|
| ***Wastewater*** | 0.0 | 4.9 | – |
| | 10.0 | 15.6 | 104.7 |
| | 20.0 | 23.8 | 95.6 |
| | 30.0 | 32.8 | 94.0 |
| ***Plasma*** | 0.0 | Not detected | – |
| | 10.0 | 10.6 | 106.0 |
| | 20.0 | 19.3 | 96.5 |
| | 30.0 | 31.4 | 104.7 |

**Conclusions**

This work describes the designing of a novel $PbTiO_3$ nanostructures modified carbon paste electrode and its application for the determination of PTX. Characterization mechanisms showed the $PbTiO_3$ nanoparticles and nanostructured modified electrode were actually formed. The PTN/CPEs exhibited highly catalytic effect to the oxidations of the analyte. Also, the modified electrode showed high sensitivity in voltammetric measurements of PTX. Additionally, the nanostructures electrode was successfully used for the analysis of PTX in real complicated sample.

**Acknowledgments**

We are grateful to Payame Noor University (Delijan, Iran) and University of Kashan for supporting this work.

**References**

[1] J. Wang, J. Xu, M.D. Goodman, Y. Chen, and M. Cai, J. Shinar and Z. Q. Lin, *J. Mater. Chem.*, **2008**, *18*, 3270.
[2] J. Wang, X. Pang, M. Akinc, and Z. Lin, *J. Mater. Chem.*, **2010**, *20*, 5945.
[3] T. Shimada, T. Xu, Y. Uratani, J. Wang, and T. Kitamura, *Nano Lett.*, **2016**, *16*, 6774.
[4] T. Shimada, T. Xu, Y. Araki, J. Wang, and T. Kitamura, *Nano Lett.*, **2017**, *17*, 2674.
[5] Z.Q. Lin, *Chem. Eur. J.*, **2008**, *14*, 6294.
[6] G.Z. Wang, R. Saeterli, P. M. Rorvik, A.T.J. van Helvoort, R. Holmestad, T. Grande, and M.A. Einarsrud, *Chem. Mater.*, **2007**, *19*, 2213.
[7] S.M. Selbach, G.Z. Wang, M. A. Einarsrud, and T. Grande, *J. Am. Ceram. Soc.*, **2007**, *90*, 2649.
[8] B.A. Hernandez-Sanchez, K.S. Chang, and M.T. Seance, *Chem. Mater.*, **2005**, *17*, 5905.
[9] Y.G. Wang, G. Xu, L.L. Yang, Z.H. Ren, X. Wei, W.J. Weng, P.Y. Du, G. Shen, and G.R. Han, *J. Alloys Compd.*, **2009**, *481*, L27.
[10] J. Y. Son, Y.-H. Shin, S. Ryu, H. Kim, and H. M. Jang, J. *Am. Chem.Soc.*, **2009**, *131*, 14676.
[11] X. Wang, J. Zhuang, Q. Peng, and Y.D. Li, *Nature*, **2005**, *437*, 121.
[12] T. K. Manda,l and J. Gopalakrishnan, *J. Mater. Chem.*, **2004**, *14*, 1273.
[13] J.R. Zhang, and L. Gao, *J. Solid State Chem.*, **2004**, *177*, 1425.
[14] H.J. Zhang, X.L. Jia, and Y.J. Yan, *Mater. Res. Bull.*, **2004**, *39*, 839.
[15] B.G. Tsvetkova, I.P. Pencheva, and P.T. Peikov, *Der Pharma Chemica*, **2012**, *4*, 608.
[16]C. Dominguez-Jimenez, D. Sancho, M. Nieto, M. Montoya, O. Barriero, and F.S. Madrid, *J. Leucoc. Biol.*, **2002**, *71*, 588.
[17] C. Unal, C. Sen, D. Iscen, and H. Dalcic, *J. Surg. Res.*, **2007**, *138*, 259.
[18] M. Martos-Fernández, M. Saez-Barba, J. López-López, A. Estrugo-Devesa, J.María Balibrea-del-Castillo, and C. Bescós-Atín, *Oral Surgery, Oral Medicine, Oral Pathology and Oral Radiology*, **2018**, *125*, 431.
[19] K. Fukuta, Y. Shirakami, A. Maruta, K. Obara, S. Iritani, N. Nakamura, T. Kochi, M. Kubota, H. Sakai, T. Tanaka, and Masahito. Shimizu, *International Journal of Molecular Sciences*, 2017, *18*, 413
[20] A. Honda, and J. Magalhaes, *Braz. J. Pharm. Sci.*, **2001**, *37*, 165.
[21] G. Sadana, and A. Chogare, *Indian J. Pharm. Sci.*, **1991**, *53*, 159
[22]O. Grozdanovic, D. Antic, and D. Agbada, *J. Sep. Sci.*, **2005**, *28*, 575.
[23]J. Abbar, S. Malode, and S. Nandibewoor, *Bioelectrochemistry*, **2012**, *83*, 1.
[24] M. Taei, and M.S. Jamshidi, *Microchem. J.*, **2017**, *130*, 108.
[25] K. Zare, M.S. Sadjadi, M. Enhessari, and S. Khanahmadzadeh, *Journal of Physical and Theoretical Chemistry*, **2009**, *6*, 9.

# Graphical Abstract

**A highly sensitive nano-structured sensor for electrocatalytic detection of pentoxifylline drug in environmental and biological samples**

Asma Khoobi*, Abdol Mohammad Attaran, Morteza Enhessari, Masoud Yousofi

***PTN/CPE***

***PTX***

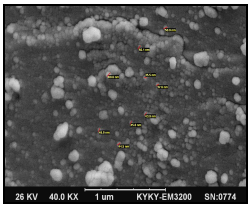


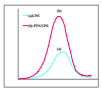

# Theoretical investigation of the $PX_3$ (X=F, Cl, Br) catalyst effect on the Nitroso–Diels–Alder Reaction

**Fereshteh Yaghoobi***

*School of Chemistry, Department of Science, University of Nahavand, P.O. Box:65931–39565, Hamadan, Iran*

*Email: Yaghoobifereshteh@gmail.com

**Tel:** (+98) 813 3493003

## Abstract

The Nitroso–Diels–Alder (NDA) cycloaddition reaction between $H_3C{=}NO$ and 1,3–butadiene catalyzed by a $PX_3$ (X = F, Cl, Br) Lewis acid was characterized using density functional theory calculations. Calculations showed that the smallest values of the activation energies belong to the reaction that catalyzed by $PCl_3$. The activation energy of the studied reactions was decreased within 8.96, 9.77 and 8.6 kcal.mol$^{-1}$ in the presence of $PF_3$, $PCl_3$ and $PBr_3$ catalysts, respectively. Investigations showed that the noncovalent bonding between the P atom of $PX_3$ and the O atom of $H_3C{=}NO$, is adequately capable to active the NDA reaction. The natural bond orbital (NBO) analysis were implemented to understand the nature of $C_{4,Cbut}\ldots O_{RNO}$ and $C_{1,Cbut}\ldots N_{RNO}$ bonds at the TS structures.

**Keywords**: Nitroso–Diels–Alder, Catalyst effect, Density functional theory, Activation energy

## Introduction

The Nitroso Diels–Alder (NDA) reaction has attracted remarkable attention in organic chemistry. The NDA reaction has been considered as one of the important methodologies for designing and synthesizing ring structures containing both nitrogen and oxygen atoms [1]. This useful reaction was first reported by Wichterle and Arbuzov in 1947 [2]. Their findings were later confirmed and extended as a general tool to synthesize a number of natural products and biologically active compounds. Kouklovsky and co-workers reported that Lewis acids could coordinate both nitrogen of nitroso and oxygen of acetoxy group in a-acetoxynitroso dienophiles. Thus, the reactivity was effectively enhanced in the presence of Lewis acids [3-4]. The numerous theoretical and experimental investigations have been carried out to understand the catalytic effect of lewis acids on the NDA reaction. In the present work the influence of $PX_3$ (X = F, Cl, Br) Lewis acid as catalyst on NDA reaction was investigated (Scheme 1). Our objective was to study this reaction in order to understand the role P-O bonding on activation energy of NDA reaction.

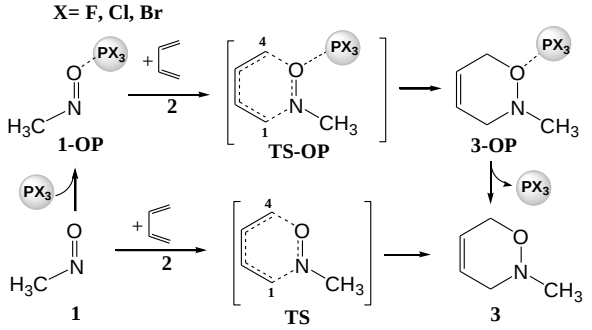


**Scheme 1.** NDA reaction between $H_3C{=}NO$ and 1,3–butadiene in the absence and the presence of $PX_3$

## COMPUTATIONAL DETAILS

All calculations reported in this study was performed using the Gaussian 09 software pakage [5] and structure of reactants, transition states, and products were fully optimized at the M06-2X/6-311++G** level of theory. The natural bond orbital (NBO) method [6] was performed inorder to analyz the natural charge in the transition structure. Zero-point energy corrections were applied for all of the reported energies.

## Results and discussion

The geometries of the all structures involved in NDA reaction between the $H_3C{=}NO$ (RNO) and 1,3–butadiene (BUT) in the absence and the presence of $PX_3$ (X = F, Cl, Br) as catalyst, was investigated. After approaching the BUT and RNO to each other, the reaction passes throught the TS state to generate a nitrogen- and oxygen-containing six memebered ring compound. In presence of $PX_3$ (X = F, Cl, Br), the first step is the formation of the IC structures between the $PX_3$ and the ONR which is presented as [$PX_3$…ONR]. In this step a P…O interaction is occured between the P atom of $PX_3$ and the O atom of RNO. The second step is the formation of the TS structures between BUT and [$PX_3$…ONR]. The structures of IC, TS and products (P) involved in the NDA reaction in the absence and the presence of $PX_3$ are shown in Scheme 2. As can be seen, the phosphorus atom of $PX_3$ is bonded to the oxygen atom of RNO. The P···O formed bond length for $PF_3$, $PCl_3$ and $PBr_3$ are 2.86, 2.93 and 3.05 Å in the IC structures, respectively. The comparison between IC and TS structures, in the presence of $PX_3$, show that the P···O bond length decreases in the TS structures. The P···O formed bond length for $PF_3$, $PCl_3$ and $PBr_3$ are 2.60, 2.66 and 2.70 Å in TS structures, respectively. In order to understand the the catalytic effect of $PX_3$ in above NDA reaction, the TS structures of the NDA reaction catalyzed by $PX_3$ compare with those of the uncatalyzed NDA reaction. The length of $C_{4,Cbut}$…$O_{RNO}$ and $C_{1,Cbut}$…$N_{RNO}$ bonds at the TS structures are

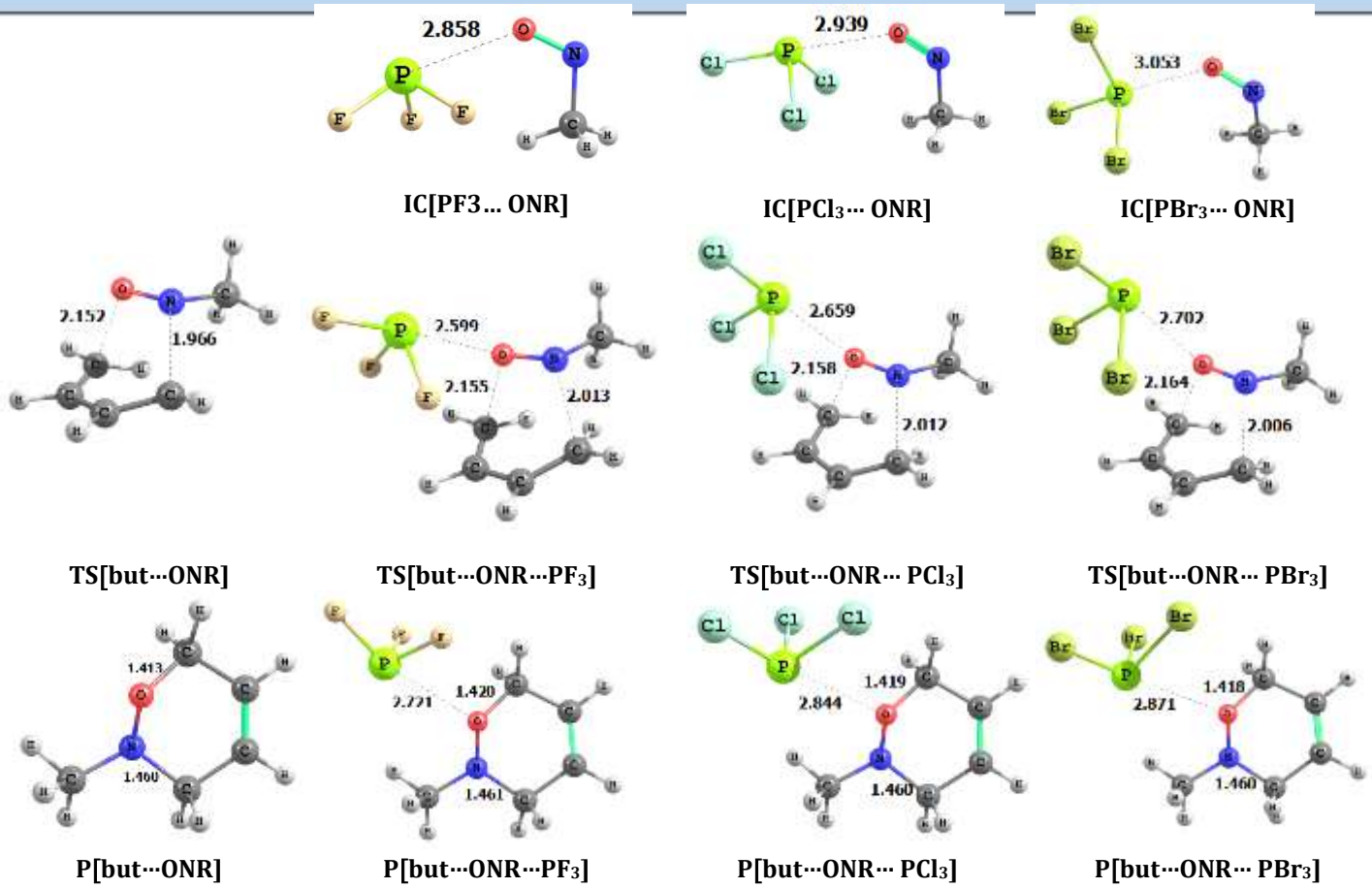


**Scheme 2.** The optimized structures of the intermediate complexes (IC), transition states (TS), and products (P) in the absence and the presence of $PX_3$ (X = F, Cl, Br) as catalyst.

slightly larger than those of the uncatalyzed reaction. The $C_{4,Cbut}\ldots O_{RNO}$ bond length in uncatalyzed reaction is 2.152 and in catalyzed reactions are 2.155, 2.158 and 2.164 Å, for $PF_3$, $PCl_3$ and $PBr_3$ respectively. Also, the $C_{4,Cbut}\ldots N_{RNO}$ bond length in uncatalyzed reaction is 1.966 and in catalyzed reactions are 2.013, 2.012 and 2.006 Å, for $PF_3$, $PCl_3$ and $PBr_3$ respectively.

The energy profiles related to the investigated reactions are presented in Scheme 3. As can be seen, the energy of RNO decreases after binding $PX_3$ by forming P···O bonding. The values of released energy for $PX_3\ldots$RNO are -4.59, -4.72 and -3.32 for X= F, Cl and Br, respectively.

The activation energies for the NDA reaction in TS state in the absence and the presence of $PX_3$ follow the order TS[but…ONR…$PCl_3$] <TS[but…ONR…$PF_3$] < TS[but…ONR…$PBr_3$] < TS[but…ONR].

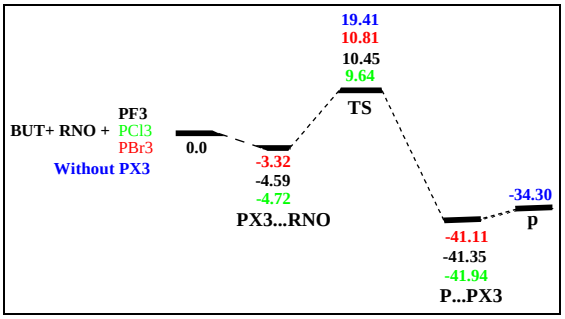


**Scheme 3.** Relative energy of the species involved in the NDA reaction between RNO and 1,3–butadiene BUT in the absence and the presence of $PX_3$.

By adding the $PX_3$ to the NDA reaction the activation energy was decreased between

8.6 and 9.77 kcal $mol^{-1}$. The activation energie diagram, illustrates that the energies of TS state, are considerably of stable compared to the uncatalyzed reaction. At the last step, after separating $PX_3$, about the 6 kcal/mol energy is released and product is formed.

## Natural bond orbital (NBO) analysis

In order to evaluate atomic charges, the charge–transfer analysis has been performed on the basis of the natural bond orbital (NBO) method. The natural population analysis corresponding to $C_{4,Cbut}\ldots O_{RNO}$ and $C_{1,Cbut}\ldots N_{RNO}$ interactions have also been reported in Table 1. As can be seen, the natural charge value of the O and N atoms increase after binding of $PX_3$ to RNO. The natural charge value of $C_{1,Cbut}$ at the TS structures are slightly smaller and for $C_{4,Cbut}$ are slighty larger than those of the uncatalyzed reaction

**Table 1**. Natural charges for atoms involved in the bonding interaction in the absence (Un–CA) and in the presence of $PX_3$ in TS structure.

| Atoms involved | UN-CA | $PF_3$ | $PCl_3$ | $PBr_3$ |
|---|---|---|---|---|
| $C_{1,Cbut}$ | -0.2740 | -0.2379 | -0.2419 | -0.2449 |
| $C_{4,Cbut}$ | -0.3149 | -0.3209 | -0.3198 | -0.3193 |
| $O_{RNO}$ | -0.3489 | -0.4184 | -0.4069 | -0.4049 |
| $N_{RNO}$ | -0.0147 | -0.0292 | -0.0274 | -0.0262 |

## Conclusion

In coclusion, a DFT based studies were done on the Nitroso–Diels–Alder (NDA) reaction between $H_3C{=}NO$ and 1,3–butadiene in the presence and absence of the $PX_3$ (X = F, Cl, Br) Lewis acid as the catalyst. The result show that $PCl_3$ more than $PF_3$ and $PBr_3$ effect upon the activation barrier of studied reaction in this work. In the presence of a $PCl_3$, the activation barriers is 9.77 kcal/mol less than those in the absence of a catalyst. The charge-transfer analysis was performed on the basis of the NBO method to evaluate the atomic charges. The NBO analysis showed that the value of natural charge of the O and N atoms increase in the presence of $PX_3$.

## References

[1] S. Carosso and M. J. Miller, *Org. Biomol. Chem*, **2014**, *12*, 7445.
[2] O. Wichterle, *Chem. Commun.*, **1947**, *12*, 292.
[3] B. S. Bodnar and M. J. Mille, *Angew Chem Int Ed Engl*. **2011**, *50*, 5630.
[4] H. Yamamoto, N. Momiyama, *Chem. Commun.*, **2005**, *0*, 3514.
[5] M. J. Frisch, G. W. Trucks, H. B. Schlegel, G. E. Scuseria, M. A. Robb, Cheeseman, J. R. Scalmani, G. Barone, V. B. Mennucci and G. A. Petersson, et al. Gaussian 09, Revision D.01, Gaussian, Inc.: Wallingford, CT, **2009**.
[6] E. Glendening, J. Badenhoop, A. Reed, J. Carpenter, J. Bohmann, C. Morales, C. Landis, and F. Weinhold, Natural Bond Orbital Analysis Program: NBO 6.0, *Theoret. Chem. Ins*. University of Wisconsin: Madison, WI, **2013**.

## Graphical Abstract

Theoretical investigation the catalyst effect of $PX_3$ (X=F, Cl, Br) on the Nitroso Diels–Alder Reaction

Fereshteh Yaghoobi

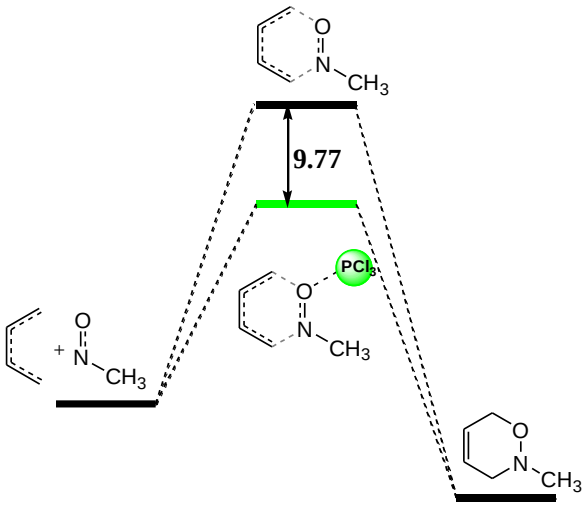

# The effect of the $PCl_3$ as a catalyst on the Hetero–Diels–Alder reaction between Urea or Iso–Urea with 1,3–butadiene

**Fereshteh Yaghoobi***

*School of Chemistry, Department of Science, University of Nahavand, P.O. Box:65931–39565, Hamadan, Iran*

*Email: Yaghoobifereshteh@gmail.com

**Tel:** (+98) 813 3493003

## Abstract

Using density functional theory (DFT), we show that $PCl_3$ is capable to catalyze the a Hetero–Diels–Alder (HDA) reaction between urea [$(NH_2)_2C=O$] or iso–urea [$NH_2OHC=NH$] with 1,3–butadiene. The $PCl_3$ through the pnicogen bonding between their P atom with the O atom of urea or the N atom of iso–urea catalyze the HAD reaction. The results show that pnicogen bonding of $PCl_3$ has more catalytic effects on activation energy of urea and 1,3–butadiene in comparison with iso–urea and 1,3–butadiene. The natural bond orbital (NBO) analysis on the TS structures were used to understand the nature of the interactions between urea and iso–urea with 1,3–butadiene in the presence and absence of the $PCl_3$ as catalyst.

**Keywords**: Hetero–Diels–Alder, Urea, Iso–Urea, Density functional theory, Activation energy

## Introduction

Those catalysts that interact with substrate through a noncovalent bond are widely developed and used [1]. In the last years, other noncovalent interactions such as halogen bonding or chalcogen bonding [2] have emerged as new concepts for the activation of substrates. The pnicogen bonding which is based on a attractive between a pnicogen atom (e.g., P or As ) and a Lewis base, is one of the newest members of the noncovalent interactions family [3]. Despite this interaction can be comparable in strength to other noncovalent interactions, there are only few studies published in this field. Recently, We have shown that $PHCl_2$ is able to catalyzed the Aza–Diels–Alder (ADA) cycloaddition between $X_2C{=}NNH_2$ (X= H, F, Cl, Br) and 1,3–butadiene [4]. In the present work the effect of pnicogen bonding as catalyst on HDA reaction was investigated. Therefore, we chose $PCl_3$ as pnicogon bond donor for the activation of two model reactions using density functional theory (schemes 1 and 2).

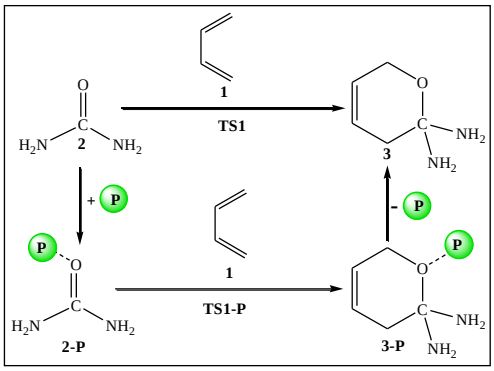


**Scheme 1.** The reaction between urea with butadiene in the presence and absence of the $PCl_3$

As can be seen in scheme 1, $PCl_3$ interact with the O atom of urea and in scheme 2, $PCl_3$ interact with the N atom of iso-urea. Therefore the effect of two kind of pnicogen bondind (P=O and P=N ) upon HAD reactions studied in this work was investigated.

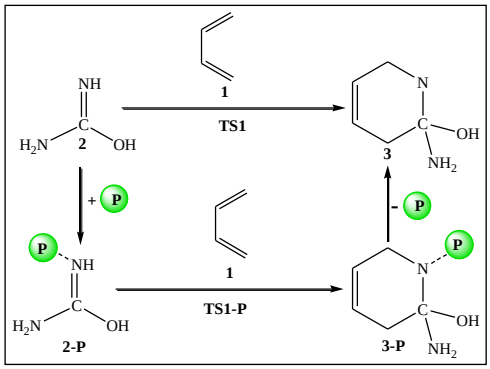


**Scheme 2.** The reaction between iso–urea with butadiene in the presence and absence of the $PCl_3$

## Computational details

All calculations reported in this study was performed using the Gaussian 09 software pakage [4] and structure of reactants, transition states, and products were fully optimized at the B3LYP/6-31G** level of theory. The natural bond orbital (NBO) method [5] was performed inorder to analyz the natural charge in the transition structure. Zero-point energy corrections were applied for all of the reported energies.

## Results and discussion

The geometries of the all structures involved in HDA reaction between the urea $[(NH_2)_2C{=}O]$ or iso–urae $[NH_2OHC{=}NH]$ and 1,3–butadiene (BUT) in the absence and the presence of $PCl_3$ as catalyst, was investigated. After approaching the BUT and urea or iso–urea to each other, the reaction passes throught the TS state to generate a oxygen– or nitrogen– containing six memebered ring compound, respectively.

In presence of $PCl_3$ the first step is the formation of the IC structures (2-P) between the $PCl_3$ and the urea or iso–urea which in this step a P…O or P…N interaction is occured between the P atom of $PCl_3$ and the O atom of urea or the N atom of iso–urea, respectively (schemes 1 and 2). The second step is the formation of the TS structures between BUT and (2-P) structures. In order to understand the the catalytic effect of $PCl_3$

in above HDA reaction, the TS structures of these reactions that catalyzed by $PCl_3$ compare with those of the uncatalyzed HDA reactions. All of structures involved in the HDA reactions studied here in the presence and absence of $PCl_3$ are shown in Scheme 3. As can be seen in Scheme 3, the phosphorus atom of $PCl_3$ is bonded to the oxygen atom of urea or nitrogen atom of iso–urea. The P···O formed bond length in urea is 2.79Å and the P···N formed bond length in iso–urea is 2.72Å. A comparison between TS structures of urea in the absence and presence of the $PCl_3$ show that the length of $C_{4,but}\cdots O_{urea}$ bond in the catalyzed reaction is shorter that its of uncatalyzed reaction. Opposite trend can be also seen for the $C_{1,but}\cdots C_{urea}$ bond where it is of the higher bond length in catalyzed reaction compared to its of the uncatalyzed reaction. A comparison between TS structures in the iso–urea show that the length of $C_{4,but}\cdots N_{Iso\text{-}urea}$ bond in the catalyzed reaction is higher that its of uncatalyzed reaction and the reverse trend was observed for the length of $C_{1,but}\cdots C_{Iso\text{-}urea}$ bond. It is also interesting to compare the structure of urea with iso–urea in the presence of catalyst. The results show that the $P\cdots O_{urea}$ bond lengths are larger than the $P\cdots N_{iso\text{-}urea}$ lengths.

In order to analyze in more detail the role of catalytic effects of the $PCl_3$ on the HDA reaction, the values of energies of the catalyzed and uncatalyzed reaction were investigated. The calculated energies profiles for reactions studied in this work are presented in Scheme 4. As can be seen, the energy of urea and iso–urea after interaction with the $PCl_3$ are decreased through the formation of the $P\cdots O_{urea}$ and $P\cdots N_{iso\text{-}urea}$ bonding, respectively. Then, the cycloaddition reaction can occure between activated urea or iso–urea and butadiene. The comparison between activation energy of urea and butadiene reaction in precence and

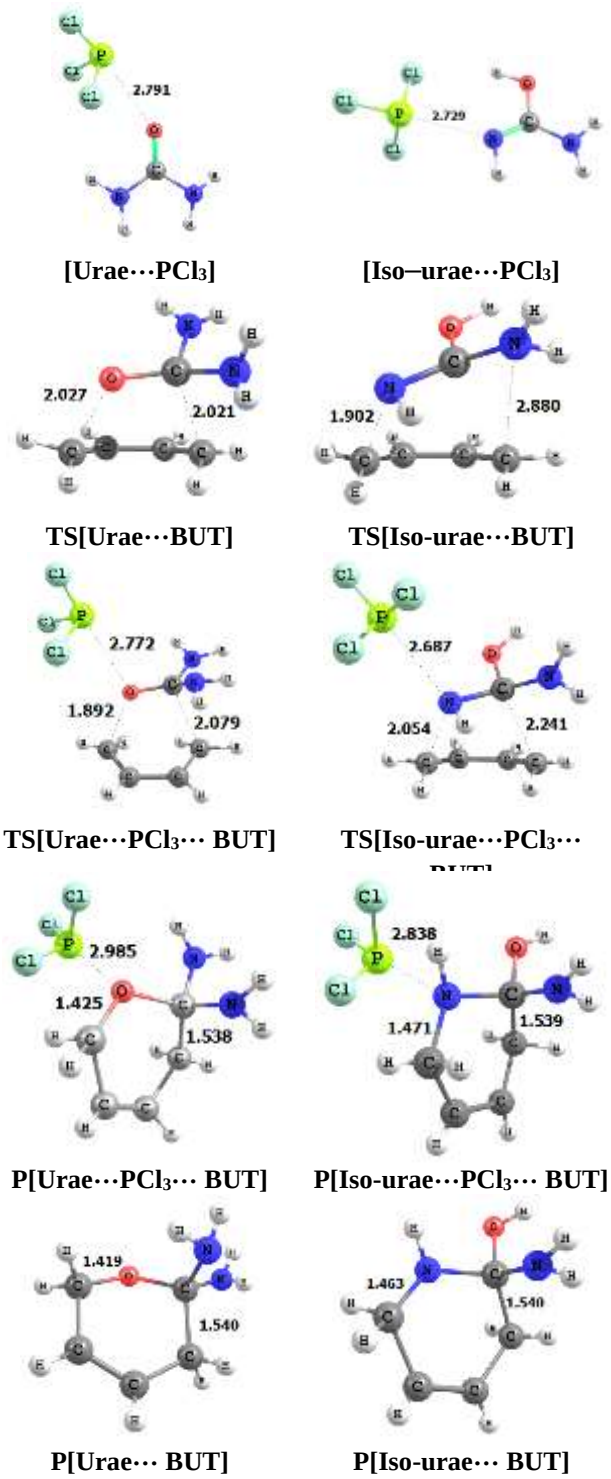


**Scheme 3.** All of structures involved in the HDA reactions studied here

absence $PCl_3$ reveal that activation energy is significantly reduced compare to the uncatalyzed reaction (Scheme 4-A). The

pnicogen bonding between $PCl_3$ and urea reduces the activation energy active reaction about 6.72 kcalmol$^{-1}$. As can be seen in Scheme 4-B, the activation energy of reaction between iso–urea and 1,3–butadiene in the presence of catalyst is reduced by 5.25 kcalmol$^{-1}$.

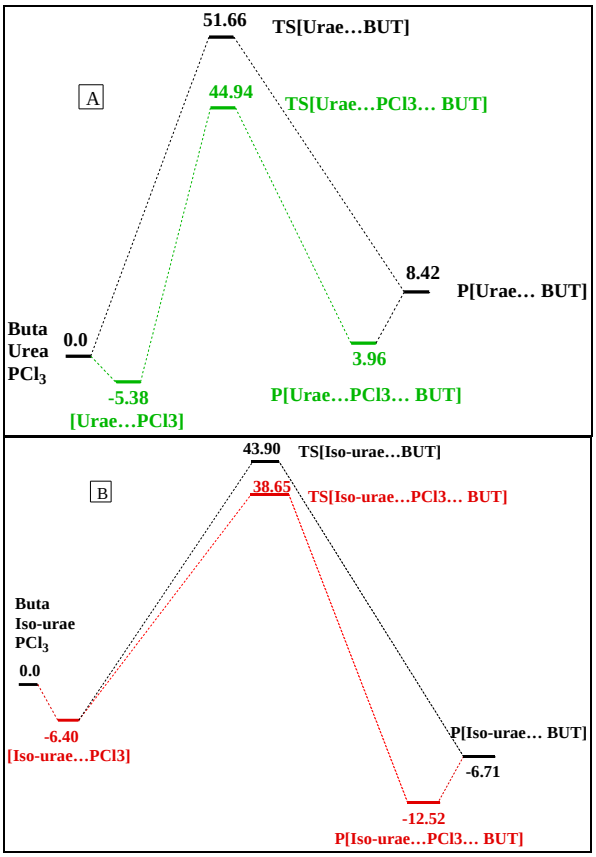


**Scheme 4.** Relative energy of the species involved in the HDA reaction between 1,3–butadiene and (A) Urea (B) Iso-Urea in the absence and the presence of $PCl_3$.

## Natural bond orbital (NBO) analysis

In order to evaluate atomic charges, the charge–transfer analysis has been performed on the basis of the natural bond orbital (NBO) method. In the $C_{1,Cbut}\cdots C_{urea}$ interaction, the charge values are -0.533 and -0.567 for the $C_{1,Cbut}$ atom, and 0.715 and 0.725 for $C_{urea}$ in the absence and the presence of $PCl_3$, respectinely. These trend in the $C_{4,Cbut}\cdots O_{urea}$ interaction are -0.238 and -0.204 for the $C_{4,Cbut}$ atom, and -0.630 and -0.635 for $O_{urea}$. Also, In the $C_{1,Cbut}\cdots C_{Iso\text{-}urea}$ interaction, the charge values are -0.574 and -0.540 for the $C_{1,Cbut}$ atom, and 0.689 and 0.696 for $C_{Iso\text{-}urea}$ in the absence and the presence of $PCl_3$, respectinely. These trend in the $C_{4,Cbut}\cdots N_{Iso\text{-}urea}$ interaction are -0.309 and -0.302 for the $C_{4,Cbut}$ atom, and -0.673 and -0.746 for $N_{Iso\text{-}urea}$. The obtained results are in good agreement with the calculated bond lenghs and the activation energies.

## Conclusion

We analyzed the catalytic effect of the $PCl_3$ through the pnicogen bonding on two different model of HDA reactions.

The activation energies of two HDA reactions in precence and absence $PCl_3$ are significantly reduced compare to the uncatalyzed reactions. The results show that the $PCl_3$ has more catalytic effect on reaction between urea and butadiene in comparision to iso–urea and butadiene.

## References

[1] A. Fu, W. Thiel, *J. Mol. Struct*, **2006**, *765*, 45.

[2] V. D. P. N. Nziko, S. Scheiner, *J. Org. Chem.*, **2016**, *81*, 2589.

[3] S. Scheiner, *Acc. Chem. Res.*, **2013**, *46*, 280.

[4] F. Yaghoobi, M. M. Sohrabi, *J. Phys. Chem. A*, **2018**, *122*, 2781.

[5] M. J. Frisch, G. W. Trucks, H. B. Schlegel, G. E. Scuseria, M. A. Robb, Cheeseman, J. R. Scalmani, G. Barone, V. B. Mennucci and G. A. Petersson, et al. Gaussian 09, Revision D.01, Gaussian, Inc.: Wallingford, CT, **2009**.

[6] E. Glendening, J. Badenhoop, A. Reed, J. Carpenter, J. Bohmann, C. Morales, C. Landis, and F. Weinhold, Natural Bond Orbital Analysis Program: NBO 6.0, *Theoret. Chem. Ins.* University of Wisconsin: Madison, WI, **2013**

## Graphical Abstract

The effect of the $PCl_3$ as a catalyst on the Hetero–Diels–Alder reaction between Urea or Iso–Urea with 1,3–butadiene

Fereshteh Yaghoobi

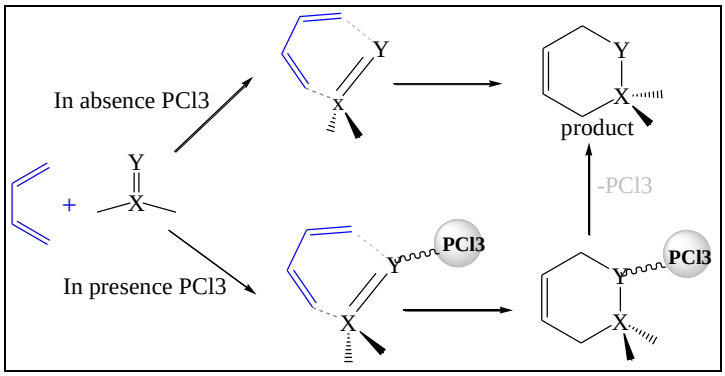

# Catalytic Epoxidation of Olfins with Graphene Oxide Supported Fe(III) Complex

**Ali Zarnegaryan[a], Majid Moghadam[b]**

[a]*Department of Chemistry, University of yasouj, yasouj, Iran*

[b]*Department of Chemistry, Catalysis Division, University of Isfahan Institution, Isfahan, Iran*

*Corresponding author Tel.: +98 (743100) 4128 ; Fax number: +98 (743100) 4128

*E-mail: zarnegaryana@yu.ac.ir

**Abstract**

Immobilization of metal complexes on solid supports is an efficient approach to remedy the drawbacks of homogeneous catalysis. In this study, an in situ strategy of synthesis and immobilization of a Fe(III) Complex complex onto graphene oxide (GO) support has been developed. The immobilized iron complex [Fe(III) (BAPTE)@GO] kept the two-dimensional sheetlike character of GO and was demonstrated to be highly effectivefor the epoxidation of Styrene. The present paper describes the preparation and characterization of Fe(III)complex immobilized onto graphene oxide. The structural and morphological characterization of the heterogeneous catalyst was carried out by different techniques such as Fourier transform infrared and diffuse reflectance UV–visible spectroscopies, X–ray diffraction, thermogravimetric analysis, nitrogen adsorption–desorption, transmission electron microscopy, field emission scanning electron microscopy and inductively coupled plasma atomic emission spectroscopy. The catalytic activity of the heterogeneous catalyst was studied in the epoxidation of olfins using *tert*–butyl hydroperoxide (TBHP) as an oxidant and it showed high selectivity and catalytic reactivity. The graphene–bound iron was successfully reused for several runs without significant loss of its catalytic activity.

**Keywords:** graphene oxide, heterogeneous catalyst, epoxidation

## Introduction

Epoxidation of alkenes catalyzed by metal complexes is an important reaction in organic synthesis because these compounds serve as useful intermediates that can be used for synthesis of a wide variety of other compounds[1]. In recent years, heterogenization of homogeneous catalysts has attracted much attention because they combine the best properties of both homogeneous and heterogeneous catalysts [2]. Nowadays, graphene has attracted much attention due to its novel and unique properties. Graphene oxide (GO), the product of oxidation of graphite, possesses abundant oxygen–containing functional groups, which not only render GO moderate water–dispersibility but also offer reactive sites for further modification [2]. Graphene oxide based materials have found various applications including sensors, solar cells, catalysis, and gas storage [3-6]. Covalent modification of graphene involves the reaction of functional molecules and the oxygenated groups on the GO surface such as carboxyl groups at the periphery, and epoxy, hydroxyl, and C=C groups in the basal plane of GO[7]. These characteristics make GO as the most promising supports to immobilize various homogeneous materials, including transition metal complexes[8-10]. For instance, Mungse et al. prepared oxo–vanadium Schiff covalently anchored onto graphene oxide sheets for oxidation of alcohols[11]. Su et al. reported GO supported transition metal Schiff base complexes as efficient and recyclable catalysts for epoxidation of styrene[12]. Zhao et al. prepared GO supported copper(salen) complex for epoxidation of different alkenes[13]. In this work, we wish to report the design and characterization of a Fe(III) BAPT complex supported on graphene oxide. Also, its catalytic activity was investigated in the epoxidation of Styrene with TBHP (Scheme 1).

## Experimental

### *Synthesis of BAPTE*

In a round-bottom flask, 4-aminothiophenol (2.5 g, 20 mmol) was added to absolute EtOH (20 ml) containing Na (0.46 g, 20 mmol). Then, 1,2-dibromoethane (0.86 ml, 10 mmol) in EtOH (5 ml) was added dropwise with constant stirring to the refluxing solution. The mixture was cooled and poured into $H_2O$ (300 ml). The solid was filtered off, washed with $H_2O$ and dried. The product was recrystallized from EtOH, and a yellowish residue was obtained. Yield: 68%, m.p. 79 °C.

$^1$H NMR (400 MHz, $CDCl_3$): $\delta$ = 7.19 (2H, d), 7.21 (2H, m), 6.60 (2H, m), 6.62 (2H, d), 3.73 (4H, m), 2.89 (4H, m). FT-IR (KBr) ($cm^{-1}$):3416(s), 2932 (w), 2280 (w), 1620 (w), 1592 (m), 1493(s),1283(s), 1176(m), 1117 (m), 819 (s).

### *Synthesis of GO-COCl*

Graphene oxide (GO) was oxidized from graphite powder by a modified Hummer method[14]. The obtained GO (3.0 g) was suspended in thionyl chloride (40 ml) and the mixture was stirred at 60 °C under nitrogen atmosphere for 6 h. The sample was filtered, washed repeatedly with toluene and dried. The dried sample was denoted as Cl–GO.

### *Preparation of $Fe^{III}$(BAPTE)$Cl_3$@GO catalyst*

The GO-COCl (1 g) was dispersed in anhydrous toluene (80 ml) using an ultrasonic bath. Then, 1,2-*bis*(4-aminophenylthio)ethane (100 mg) and triethylamine (4 ml) were added to this mixture and the resulting mixture was refluxed for 48 h under nitrogen atmosphere. After the reaction was completed, the mixture was filtered and washed with anhydrous toluene (4×10 mL) to remove the non-reacted BAPTE. In the final step, the prepared powder was

dispersed in ethanol (60 ml), $FeCl_3.4H_2O$ (250 mg) was added and the mixture was stirred under reflux conditions for 24 h. At the end of the reaction, $Fe^{III}$ (BAPTE) $Cl_3$@GO was filtered and washed with ethanol four times to remove the unreacted $FeCl_3.4H_2O$.

## Results and discussion

*Preparation and characterization of catalyst*

In brief, graphene oxide (GO) was prepared from oxidation of graphene powder by modified Hummers method[14].Prior to the immobilization of the iron catalyst, the GO was treated with $SOCl_2$ to convert the –COOH groups into –COCl groups. The GO-COCl was reacted with 1,2-*bis*(4-aminophenlythio)ethane (BAPTE) in the presence of triethylamine and the ligand was attached on GO-COCl via amide linkages. The final catalyst, $Fe^{III}$(BAPTE)$Cl_3$@GO, was prepared by the reaction of BAPTE@GO with $FeCl_3$. Covalent attachment of the $Fe^{III}$(BAPTE)$Cl_3$ to GO support provided a catalyst which is not soluble in common organic solvents. The structural and chemical nature of the catalyst was characterized by FT-IR and spectroscopies, FE-SEM microscopic techniques, XRD, TGA and ICP-AES analyses (Fig 1-4).

## Investigation of catalytic activity of $Cu^{II}$(BAPTE)$Cl_2$@GO in the epoxidation of olefins with TBHP

Initially, the catalytic activity of the prepared catalyst was investigated in the epoxidation of cyclooctene using TBHP as a model reaction under different conditions. To find optimum reaction conditions, the influence of different factors that may affect the conversion and selectivity of the cyclooctene epoxidation was investigated. To evaluate the oxidizing potential of other common oxidants, cyclooctene was subjected to the oxidation using different oxidants such as $H_2O_2$, TBHP and $NaIO_4$. The highest epoxide yield was obtained with TBHP while in the absence of oxidant; no conversion was observed. Under the optimized reaction conditions, the scope of this protocol was further investigated in the epoxidation of different olefins with TBHP. The results are summarized in Table 1.

## Conclusion

The surface of graphene oxide is rich of different functional groups which can be used for supporting of various catalysts. The $Fe^{III}$(BAPTE) grafted graphene nanosheets were prepared by covalent interaction between amino groups of BAPTE and acyl groups on the graphene oxide followed by reaction with $FeCl_3$. The prepared heterogeneous catalyst was used as a highly efficient catalyst in the epoxidation of various olefins with TBHP. Moreover, the catalyst was recovered easily and reused without significant loss in its catalytic activity.

## Acknowledgments

Partial support of this work by the research council of the University of yasouj and University of Isfahan is acknowledged.

## References

[1] R. A. Sheldon, J. K. Kochi, *Metal–Catalysed Oxidations of Organic Compounds*, Academic Press, New York, **1981**.

[2] D. E. De Vos, M. Dams, B. F. Sels and P. A. Jacobs, *Chem. Rev.*, **2002**, 102, 3615–3640.

[3] S. Stankovich, D. A. Dikin, G. H. B. Dommett, K. M. Kohlhaas, E. J. Zimney, E. A. Stach, R. D. Piner, S. T. Nguyen and R. S. Ruoff, *Nature*, 2006, **442**, 282–286.

[4] C. H. Lu, H. H. Yang, C. L. Zhu, X. Chen and G. N. Chen, *Angew. Chem., Int. Ed.*, **2009**, 48, 4785–4787.

[5] Y. H. Hu, H. Wang and B. Hu, *Chem. Sus. Chem.*, **2010**, **3**, 782–796.
[6] Mirkhani, V.; Moghadam, M.; Tangestaninejad, S.; Mohammadpoor- Baltork, I.; Rasouli, N. *Inorg. Chem. Commun.* **2007**, *10*, 1537.
[7] A. Lerf, H. He, M. Forster, J. Klinowski, *J. Phys. Chem. B*, **1998**, 102, 4477–4482.
[8] J. Pyun, *Angew. Chem., Int. Ed.*, **2011**, 50, 46–48.
[9] L. Dong, R. R. S. Gari, Z. Li, M. M. Craig and S. Hou, *Carbon*, **2010**, 48, 781–787.
[10] *T. A. Pham, B. C. Choi and Y. T. Jeong, Nanotech.*, **2010**, 21, *465603. H. P. Mungse,*
*[11] S. Verma, N. Kumar, B. Sain and O. P. Khatri, J. Mater. Chem.*, ***2012***, 22, *5427–5433.*
*[12]* H. Su, Z. Li, Q. I. Guo, J. I. Guang and Q. Kan, *RSC Adv.*, **2014**, 4, 9990–9996.
*[13]* Q. Zhao, C. Bai, W. Zhang, Y. Li, G. Zhang, F. Zhang, and X. Fan, *Ind. Eng. Chem. Res.* **2014**, 53, *4232–4238*.
*[14]* W. S. J. Hummers, R. E. Offeman, *J. Am. Chem. Soc.*, 1957, **80**, 1339

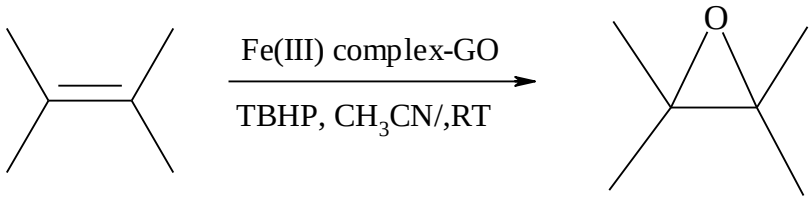


Schem 1. Epoxidation of alkenes

| Entry | Olefin | Product | Epoxide Selectivity (%) | Yield (%)[b] | TOF ($h^{-1}$) |
|---|---|---|---|---|---|
| 1 | 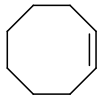 | 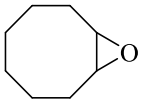 | 100 | 94 | 17.3 |
| 2 |  | 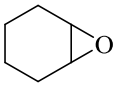 | 92[c] | 92 | 16.9 |
| 3 | 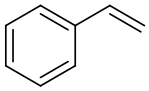 | 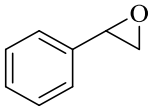 | 88[d] | 91 | 16.6 |
| 4 | 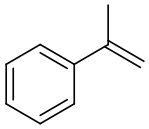 | 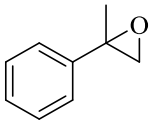 | 90[e] | 96 | 17.1 |
| 5 | 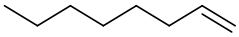 | 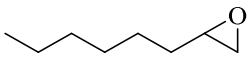 | 92 | 91 | 16. 8 |
| 6 | 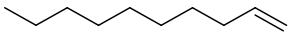 | 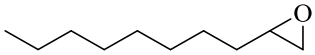 | 90 | 89 | 16.3 |

**Table 2.** Epoxidation of alkenes with *tert*-BuOOH catalyzed by heterogeneous Fe(III) complex under reflux -conditions.

[a]Reaction conditions: Alkene (1 mmol), TBHP (3 mmol) and catalyst (0.7 mol% based on Fe) in acetonitrile at 80 °C after 12 h.

[b]Determined by GC based on starting alkene.

[c]The by-product is cyclohex-2-ene-1-one.

[d]The by-product is benzaldehyde.

[e]The by-product is acetophenone.

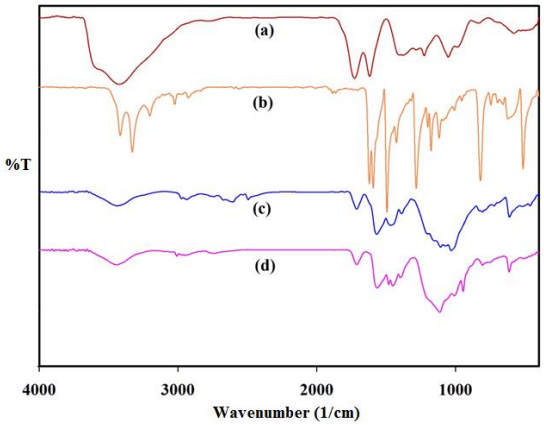


**Fig. 1.** FT- IR spectrum of: (a) GO, (b) BAPTE, (c) BAPTE@GO and (d) $Fe^{III}(BAPTE)Cl_3$@GO

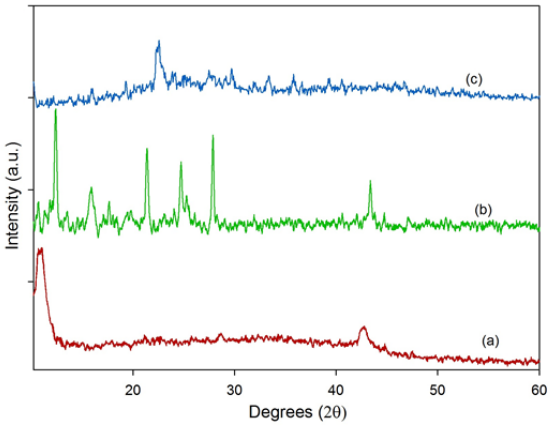


**Fig. 2** XRD pattern of: (a) graphene oxide, (b) BAPTE@GO, and (c) $Fe^{III}(BAPTE)Cl_3$@GO catalyst.

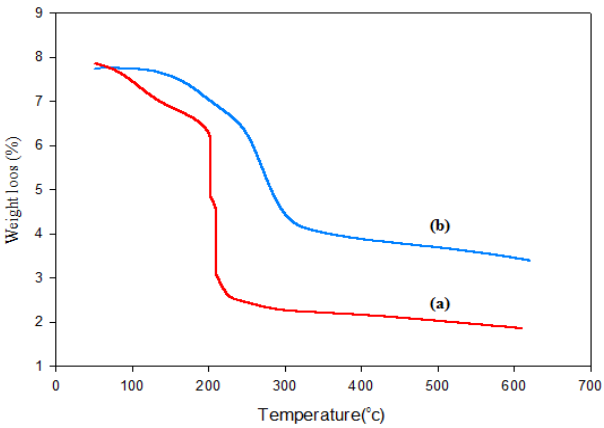


**Fig. 3.** Thermogram of: (a) graphene oxide; (b) $Fe^{III}(BAPTE)Cl_3$@GO catalyst

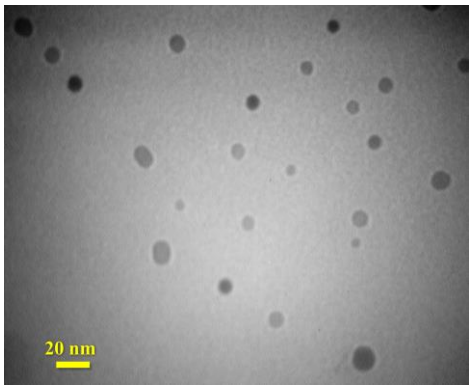


**Fig. 4.** TEM images of $Fe^{III}(BAPTE)Cl_3$@GO catalyst

# Eepoxidation reaction catalyzed heterogeneously by Fe(III)complex-Polyoxometalate compound

**Ali Zarnegaryan[a], Majid Moghadam[b]**

[a]*Department of Chemistry, University of yasouj, yasouj, Iran*

[b]*Department of Chemistry, Catalysis Division, University of Isfahan Institution, Isfahan, Iran*

*Corresponding author Tel.: +98 (743100) 4128 ; Fax number: +98 (743100) 4128

*E-mail: zarnegaryana@yu.ac.ir

**Abstract**

Nowadays, inorganic–organic hybrid materials based on polyoxometalates (POMs) are extensively attracted because of theirpotential applications in catalysis, gas storage, magnetism, photochemistry and electrochemistry.Their features of an oxygen-rich surface, high charge density and controllable size mean POMs are becoming popular inorganic building blocks. A hybrid complex based on covalent interaction between of 1,2-bis(p-aminophenylthio)ethane (BAPTE), and a Lindqvist type polyoxometalate, $Mo_6O_{19}^{2-}$, was prepared. This new hybrid catalyst, Fe(III) complex -POM, was characterized by $^1$H NMR, FT- IR, and UV-Vis spectroscopic methods and cyclic voltammetry. The catalytic activity of iron(III) complex -POM hybrid material was investigated for epoxidation reaction were produced in good to excellent yield. The reusability of this catalyst was also investigated.

**Keywords:** Lindqvist polyoxometalate, Inorganic–organic compound, epoxidation

## Introduction

In recent years, organic–inorganic hybrids have attracted an increasing interest due to the possibility of combining the different characteristics of the components to get unusual structures, properties, or applications [1]. Polyoxometalates (POMs) are a unique class of metal– oxygen clusters, whose molecular identity is maintained both in the solid state and in solutions [2].To date, two coordination approaches have been developed for the assembly of POMs into macrostructures: (1) Transition1. metal-substituted POMs are chosen as subunits and organic ligands as intermolecular linkers through coordinating with transition metal ions[3]. Modification of POMs is very important for their subsequent research and application. An effective way to achieve this goal is to modify the POMs with organic materials to obtain organic–inorganic hybrids. Lindqvist hexamolybdate cluster, $[Mo_6O_{19}]^{2-}$ (Scheme 1), as a unique class of metal oxide clusters, is an ideal building block for constructing the organic–inorganic hybrid assemblies. In recent years, we reported the application of different hybrid materials in catalysis. The $MoO_2$(salen)-POM, $MoO_2$-POM, Fe(salen)-POM, Ni(salen)-POM, and Co(salen)-POM hybrid systems have been studied in the oxidation of olefins or benzyl halide [4-8]. The goal of this research was to prepare a hybrid material based on the covalent attachment of Lindqvist $Mo_6O_{19}^{2-}$ to iron complex of (BAPTE) heterogeneous,. This heterogeneous catalyst, Fe(III)complex -POM, was applied in the epoxidation of olfines (Scheme 2).

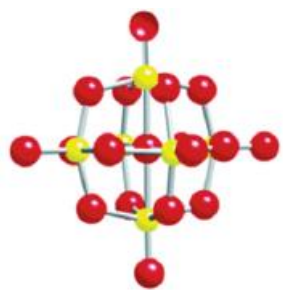

Scheme 1. The structure of hexamolybdate ion $[(n\text{-}C_4H_9)_4N]_2[Mo_6O_{19}]$

## Experimental

### *Synthesis of BAPTE*

In a round-bottom flask, 4-aminothiophenol (2.5 g, 20 mmol) was added to absolute EtOH (20 ml) containing Na (0.46 g, 20 mmol). Then, 1,2-dibromoethane (0.86 ml, 10 mmol) in EtOH (5 ml) was added dropwise with constant stirring to the refluxing solution. The mixture was cooled and poured into $H_2O$ (300 ml). The solid was filtered off, washed with $H_2O$ and dried. The product was recrystallized from EtOH, and a yellowish residue was obtained yield: 68%, m.p. 79 °C.

$^1$H NMR (400 MHz, $CDCl_3$): $\delta$ = 7.19 (2H, d), 7.21 (2H, m), 6.60 (2H, m), 6.62 (2H, d), 3.73 (4H, m), 2.89 (4H, m). FT-IR (KBr) ($cm^{-1}$):3416(s), 2932 (w), 2280 (w), 1620 (w), 1592 (m), 1493(s),1283(s), 1176(m), 1117 (m), 819 (s).

### *Synthesis of Fe(III)complex -POM*

In a round-bottom flask, BAPTE-POM (0.38 g, 0.13 mmol) and $FeCl_3.4H_2O$ (0.17 mmol) were dissolved in anhydrous DMF (10 mL) and heated to 100 °C under a dry atmosphere for 8h. The reaction was cooled to room temperature and filtered under vacuum into a flask containing dry ether (100 mL) and dry methanol (20 mL). A precipitate was formed and washed several times

with acetone and ether. The dried product was stored in a desiccator. IR ($cm^{-1}$): 941 (s), 995 (s), 807(s),717(s),1025 (m), 1151 (m), 1282 (m), 1482 (s), 1618 (s), 2870 (s), 2965 (w). UV-Vis (in DMF): ($\lambda_{max}$= 391 and 554 nm).

**Results and discussion**

The synthetic route for Fe(III) complex-POM , First, 4-aminothiophenol was reacted with 1,2-dibromoethane to produce BAPTE. Next, this ligand was hybridized with tetrbutylammonium hexamolybdate and BAPTE-POM was prepared. Usually, the association of a molecular unit to a POM is attained by electrostatic interaction. However, in order to increase the stability of the hybrid material, especially in polar solvents; a covalent linkage was stablished between POM and macrocyclic ligand. Initially, we developed a mild and efficient synthetic route for covalent attachment of BAPTE to a Lindqvist polyoxometalate. Finally, BAPTE-POM was reacted with $FeCl_3$ for preparation of $Fe^{III}$complex POM. $Mo_6O_{19}^{2-}$, to macrocyclic ligand was successfully carried out using dicyclohexylcarbodiimide (DCC) as a coupling agent.

The hybrid compound is soluble in polar, aprotic solvents such as DMSO and DMF. Several attempts for preparation of single crystals of this hybrid compounds were unsuccessful. Therefore, this new hybrid material was characterized by $^1$H-NMR (Fig 1) spectroscopic methods, and cyclic voltammetric studies. All these techniques provide more details for characterization of this polyoxometalate–iron complex hybrid material.

**Catalytic studies**

The catalytic activity of the Fe(III) complex-POM was studied in the epoxidation of alkenes with tert–BuOOH as an oxidant. First, the epoxidation of cyclooctene with tert–butyl hydroperoxide was chosen to optimize the reaction parameters such as catalyst amount and solvent. Excellent conversion and selectivity to the epoxide were obtained within 4 h. Cyclic olefins such as cyclohexene and cyclooctene were also epoxidized in high yields and selectivity. While in the case of the terminal C=C double bonds conjugated with an aromatic ring, the major product was the corresponding epoxide. This catalytic system showed slightly higher catalytic activity compared to previously reported system. This behaviour can be attributed to the presence of chloropropyl dangling groups and also the presence of supported ionic liquid moieties in which the heterogeneous catalyst acts as a quasi-homogeneous system.

**Conclusion**

In summary, a new Fe(III)complex –POM hybrid material was prepared via covalent interaction of (BAPTE), and a Lindqvist type polyoxometalate, $Mo_6O_{19}^{2-}$. This new hybrid material was characterized and used as a highly effective and recyclable catalyst for the epoxidation of olefins with TBHP. High yields, excellent selectivity and reusability of the catalyst are noteworthy advantages of this catalytic system

**Acknowledgments**

Partial support of this work by the research council of the University of yasouj and University of Isfahan is acknowledged.

**References**

[1] E. Coronado, C. J. GQmez-GarcRa, *Chem.Rev* . **1998**, 98, 273.

[2] Müller, A.; Das, S. K.; Kögerler, P.; Bögge, H.; Schmidtmann, M.; Trautwein, A. X.; Schunemann, V.; Krickemeyer, E.; reetz, W. *Angew. Chem., Int. Ed.* **2000**, 39, 3414.

[3] Mialane, P.; Dolbecq, A.; Se´cheresse, F. *Chem. Commun*, **2006**, 3477.

[4] M. Moghadam, V. Mirkhani, S. Tangestaninejad, I. M. Baltork and M. Moshref Javadi, *Polyhedron*, **2010**, 29, 648–654..

[5] M. Moghadam, V. Mirkhani, S. Tangestaninejad, I. M. Baltork and M. Moshref Javadi, *Inorg. Chem. Commun.*, **2010**, 13, 244–249.

[6] Mirkhani, V.; Moghadam, M.; Tangestaninejad, S.; Mohammadpoor- Baltork, I.; Rasouli, N. *Inorg. Chem. Commun.* **2007**, *10*, 1537.

[7] Mirkhani, V.; Moghadam, M.; ngestaninejad, S.; Mohammadpoor- Baltork, I.; Shams, E.; Rasouli, N. *Appl. Catal., A* 2008, *334*, 106.

[8] Mirkhani, V.; Moghadam, M.; Tangestaninejad, S.; Mohammadpoor- Baltork, I.; Rasouli, N. *Catal. Commun.* **2008**, *9*, 219.

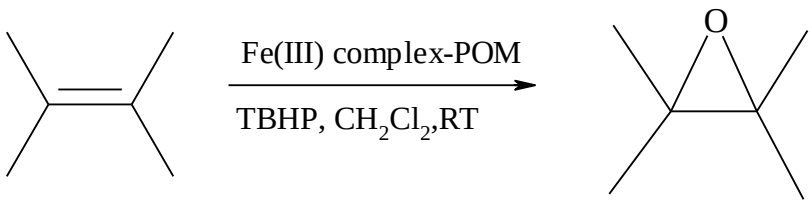


Scheme 2. Alkene epoxidation with TBHP catalyzed by $Fe^{III}(BAPTE)Cl_3$@POM

**Fig 1.** The FT-IR spectra of POM- BAPTE hybrid compound

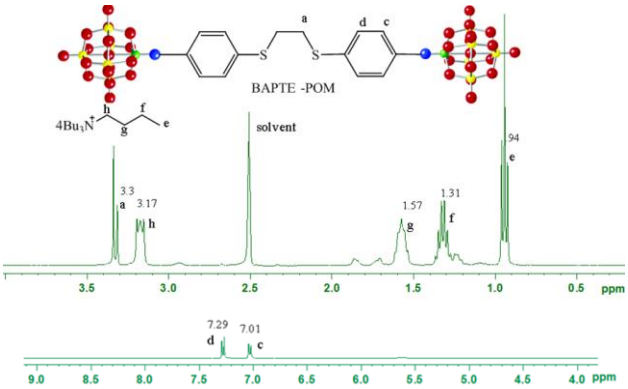

# Magnetic CNTs-supported Ni(II) complex as an efficient heterogeneous catalyst towards nitroaldol (Henry) reaction

**Seyed Jamal Tabatabaei Rezaei,[a,*] Shima Asghari[a], Hossein Khorramabadi[a], Davood Abdolahnezhadian,[a] Asemeh Mashhadi Malekzadeh[a], Ali Ramazani[a]**

[a] *Department of Chemistry, Faculty of Science, University of Zanjan, Zanjan, Iran*

*Corresponding author :

*E-mail: sjt.rezaei@znu.ac.ir

## Abstract

A novel heterogeneous support was developed based on hyperbranched poly(citric acid)-picolinic acid and $Fe_3O_4$ nanoparticles modified multi-walled carbon nanotubes (MWCNT/$Fe_3O_4$@PCA-Pic). Because of the surface modification of the magnetic carbon nanotubes with PCA-Pic, these hybrid nanomaterials are not only dispersible for a long time in a wide range of solvents but also are able to trap Ni(II) ions via complex formation of Pic functional end groups of the PCA-Pic dendrimer with metal ions. The morphology and structural feature of the catalyst was characterized using different microscopic and spectroscopic techniques such as FT-IR, UV-Vis, TGA, TEM, ICP and VSM. The catalyst was effectively used in the Henry (nitroaldol) reaction between nitroethane and a variety of aldehydes in an aqueous medium. Also, this catalyst can be recycled by applying an external magnetic field without significant loss of activity.

**Keywords**: Heterogeneous catalyst; Ni(II) complex; Henry reactions; Green synthesis.

## Introduction

When chemicals waste are released into our environment and disrupt the balance of our ecosystems, threatening our health, polluting the air we breathe and contaminating our food. Some of these chemicals waste include pesticides, fertilizers, pharmaceuticals, household chemicals, and a wide range of additional chemicals produced as byproducts of commercial and industrial activities [1,2]. In this context, the use of nanocatalysts during the past decade has attracted much attention for many applications in various industries, including water purification, fuel cell, chemical, biomedical and pharmaceutical products [3-6].

One of the most powerful tools available to the synthesis of organic compounds is carbon-carbon bond forming reactions. The number of reactions is wide and the reaction conditions are very variable [7]. Among these reactions, the Henry nitroaldol reaction is used to synthesize $\beta$-nitroalcohols from a nitroalkane and an aldehyde (or ketone) [8-10]. The obtained $\beta$-nitroalkanols are valuable and versatile starting materials for the synthesis of polyfunctionalized materials and biologically active compounds [11-14].

The Henry reaction is usually catalyzed by inorganic/organic base [13-15] or metal complexes. In these cases, a variety of metal complexes including iron [16], copper [17-20], zinc [16,21-23], lanthanum [24] and cobalt [25,26] displayed a high potential toward the nitroaldol reactions. Studies show that Ni(II) complexes have wide application in the general context of catalytic reactions such as, Mannich-type and Michael reactions [27,28], polymerization processes [29,30], in oxidation [31,32], alkene epoxidation [33] and asymmetric aldol reaction [34]. There are some reports on Ni(II) complexes which are catalytically active for the Henry reaction, but most of them are also homogenous catalysts [35], and only a few recyclable heterogeneous catalysts are found in the literature [36]. Although homogeneous systems show higher activity and selectivity than heterogeneous systems, their separation, recovery, and reusability are challenging.

The surface-modified carbon nanotubes (SMCNTs) have a high potential for use as a heterogeneous support due to its uniform size, large surface area, high catalyst loading and stability, and unique physical and chemical properties. However, SMCNTs remain dispersed in reaction solvents for extended periods, so the separation procedure for these systems is very difficult and time-consuming. It seems that an effective way of overcoming this defect and creating the ability to permanently heterogeneity is to incite the nature of magnetism to the SMCNTs. These catalytic systems are highly active and can be easily recovered using an external magnetic field [37-40].

In order to take advantage and properties of heterogeneous catalysts in achieving green chemistry goals and also as a part of our ongoing research program on the design of new catalysts for the development of useful and green synthetic methodologies [41-47], in the present work, we report a dendritic magneto Ni(II) complex based on factionalized CNTs for the Henry reaction of nitroethane with various aldehydes in aqueous medium. The catalyst is designed with an aim to combine the superior supporting property of factionalized MWCNTs to effectively immobilize and stabilize Ni(II) ions in an aqueous medium with the magnetic property of decorated $Fe_3O_4$ nanoparticles for simple catalyst separation and therefore to improve catalyst reusability (Scheme 1).

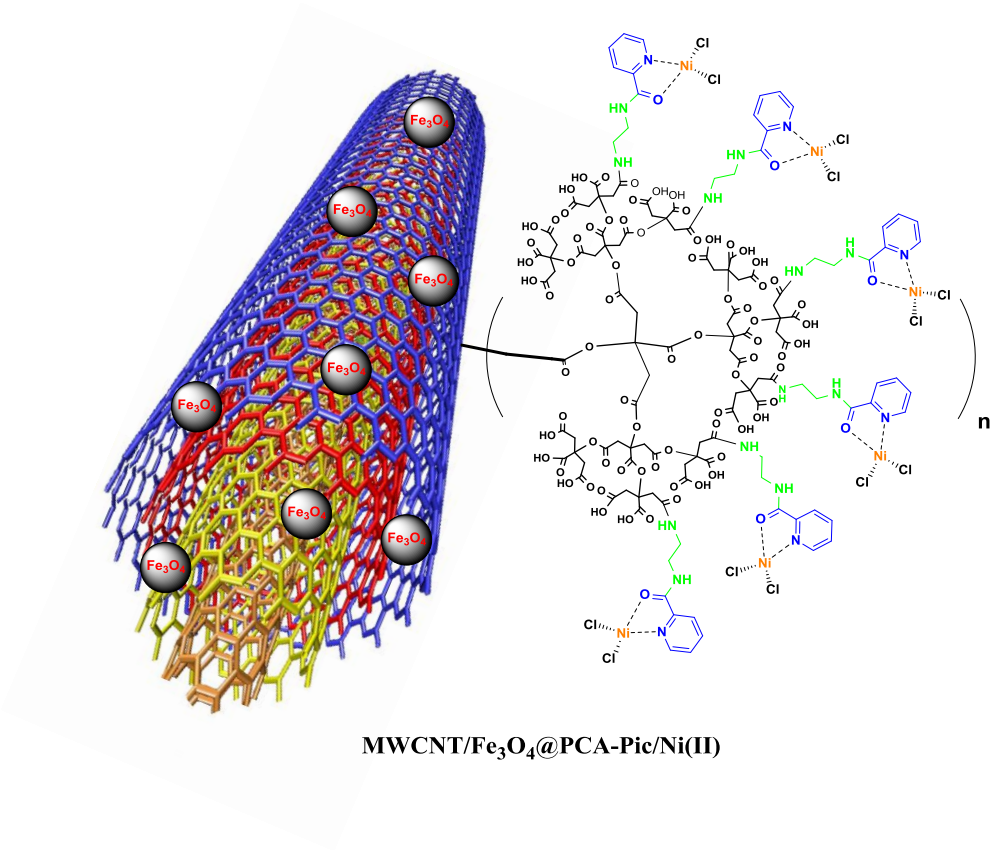


**Scheme 1.** Schematic chemical structure of MWCNT/$Fe_3O_4$@PCA-Pic/Ni(II) magnetic nanocatalyst

## 2.Experimental

### *2.1. Apparatus and reagents*

All chemicals were purchased from Sigma-Aldrich or Merck Chemical Companies. All the chemicals were of analytical grade and used without purification. Fourier transform infrared (FTIR) spectra were recorded by a Jasco 6300 FTIR spectrometer. The $^1$H NMR spectra were recorded on a Bruker (Karlsruhe, Germany) DRX-250 Avance spectrometer at 250.0 MHz, and deuterated chloroform was used as a solvent. The content of Ni in the magnetic catalyst was determined by inductively coupled plasma mass spectrometry (ICP-MS, Agilent ICP-MS 7500 Series) and thermogravimetric analysis (TGA) (STA 1500 instrument at a heating rate of 10 ºC/min in air). The magnetic properties of samples were detected at room temperature using vibrating sample magnetometer (VSM, Meghnatis Kavir Kashan Co., Kashan, Iran). The size and morphological characterization of the particles were carried out using a Zeiss-EM10C transmission electron microscope (TEM) operating at 80 kV. Ultrasonic generator was carried out on a TECNO-GAZ, S.p.A., Tecna 6, input: 50–60 Hz/305 W, and uniform sonic waves to disperse materials in solvents.

### *2.2. Synthesis of MWCNTs/$Fe_3O_4$@PCA*

The MWCNTs/$Fe_3O_4$@PCA was prepared in two steps according to our previous work[47].

### *2.3. Synthesis of MWCNTs/$Fe_3O_4$@PCA*

DCC and NHS were used to synthesize of MWCNTs/$Fe_3O_4$@PCA-EDA[48]. MWCNTs/$Fe_3O_4$@PCA (1.5 mmol, 1 g), NHS (7.5 mmol, 0.9 g) and DCC (7.5 mmol, 1.5 g) were dissolved in dry DCM (50 mL).

The reaction mixture was stirred at room temperature for 48 h. Then ethylenediamine (15 mmol, 1 ml) were added, and the reaction mixture was stirred at room temperature for another 24 h. The precipitated byproduct, dicyclohexylurea (DCU), was removed through final nanoparticle purified by using a permanent magnet and washed with DCM and the methanol.

### *2.4. Synthesis of MWCNTs/$Fe_3O_4$@PCA-Pic*

Picolinic acid (3 mmol, 0.4 g) and NHS (15 mmol, 1.7 g) were dissolved in dry DCM (50 mL), followed by addition of DCC (15 mmol, 3.1 g). The mixture was stirred at room temperature for 48 h and filtered to remove dicyclohexylurea (DCU). 1 g MWCNTs/$Fe_3O_4$@PCA-EDA was added and the reaction mixture was stirred at room temperature for 48 h. The particles were finally recovered by magnetic concentration and washed thoroughly with DCM and ethanol.

### *2.5. Synthesis of MWCNTs/$Fe_3O_4$@PCA-Pic/Ni(II)*

A solution of $NiCl_2 \cdot 6H_2O$ (1 g, 0.4 mmol) in 5 ml deionized water was added dropwise to a suspension of 0.5 g MWCNTs/$Fe_3O_4$@PCA-Pic dispersed in 10 ml deionized water. The resulting mixture was stirred at room temperature for 24 h. MWCNTs/$Fe_3O_4$@PCA-Pic/Ni(II) magnetic nanocatalyst washed with two further portions of water and ethanol. It was then dried under vacuum and used as such for the next step.

### *2.6. General procedure for Henry reaction catalyzed by MWCNTs/$Fe_3O_4$@PCA-Pic/Ni(II)*

The catalytic study was performed with the following conditions: a mixture of an aldehyde (1 mmol), nitroethane (2.00 mmol) and $Ni^{II}$-complex catalyst (1 mol% Ni) in 3 mL water contained in a capped glass vessel. The reaction mixture was stirred for the required time at the particular temperature. After the desired time, the catalyst was magnetically separated and the organic compounds were extracted from water by using dichloromethane. The organic phase was collected over anhydrous sodium sulfate and the solvent was removed under vacuum to obtain the crude product as a mixture of the β-nitroalkanol diastereoisomers (syn and anti *isomers*) which were analyzed by $^1H$ NMR. The yield of the β-nitroalkanol product (relatively to the aldehyde) was determined by $^1H$ NMR as reported previously [48-50]. The ratio between the *syn* and *anti* isomers was also determined by $^1H$ NMR spectroscopy (Supporting Information) [51].

## 3. Result and discussion

A new magneto Ni(II) complex based on magnetic carbon nanotubes (MWCNT/$Fe_3O_4$@PCA-Pic) were synthesized in order to prepare a suitable catalyst for Henry reaction. Scheme 1 shows the schematic chemical structure of $Fe_3O_4$@PCA- Pic/Ni(II) [52-54]. The prepared magneto Ni (II) complex was characterized by IR spectroscopy, thermogravimetric analysis (TGA), X-ray diffraction, vibrating sample magnetometer (VSM) and transmission electron microscopy (TEM).

Fig. 1 represented the FT-IR spectrum of MWCNT/$Fe_3O_4$, MWCNT/$Fe_3O_4$@PCA, MWCNT/$Fe_3O_4$@PCA-EDA and MWCNT/$Fe_3O_4$@PCA-Pic. In all four spectra, the characteristic absorption band of Fe3O4 has appears in 585 $cm^{-1}$. In Fig. 1b and c, the peaks in the range 1255–1443 $cm^{-1}$due to the C-O and absorbance band of carbonyl groups of carboxylic acid and esters has appeared in the range 1502–1722 $cm^{-1}$. In these spectra the peaks in the range

of 3050–3630 $cm^{-1}$ were attributed to acidic hydroxyl functional groups of grafted PCA. In Fig. 1c, the peak in the range 1535-1595 $cm^{-1}$ could be assigned to stretching mode of amide groups, indicating that the reaction between ethylenediamine (EDA) and Fe3O4@PCA have taken place. Also, in these spectra the bands at 2926 and 2848 $cm^{-1}$ are assigned to stretching mode of $CH_2$ in EDA and the broad peak at 3320 $cm^{-1}$ is due to free $NH_2$ groups stretching mode. All of the above evidence indicates the successful conjugation of ethylenediamine to the surface of $Fe_3O_4$@PCA. Functionalization of Fe3O4@PCA-EDA with picolinic acid (Pic) leads to the removal of the peak at 3320 $cm^{-1}$, as shown in Fig. 1d.

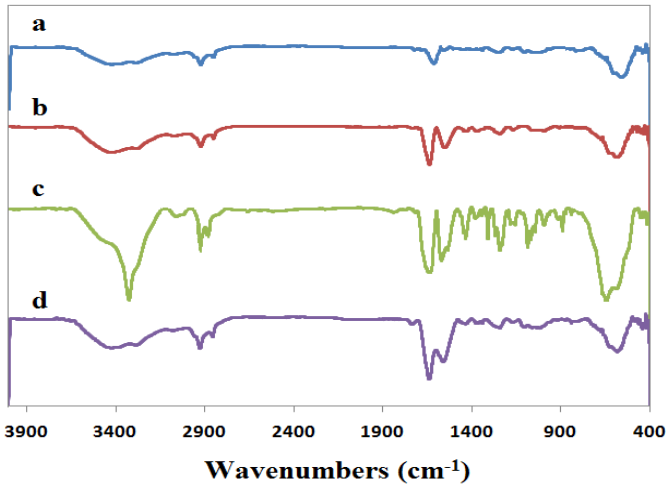


**Fig. 1.** FT-IR spectrum of MWCNT/$Fe_3O_4$ (a), MWCNT/$Fe_3O_4$@PCA (b), MWCNT/$Fe_3O_4$@PCA-EDA (c) and MWCNT/$Fe_3O_4$@PCA-Pic (d)

The morphology of magnetic nanocatalyst has been known to affected by several factors, including the reaction conditions and chemicals involved [55]. Fig. 2 shows TEM image of MWCNT/$Fe_3O_4$@PCA-Pic/Ni(II) and it could be observed that all nanospots (related to $Fe_3O_4$ and PCA-Pic/Ni(II)) on the outer surface of the nanotubes have a regular spherical shape with an average particle diameter of ~5-10 nm.

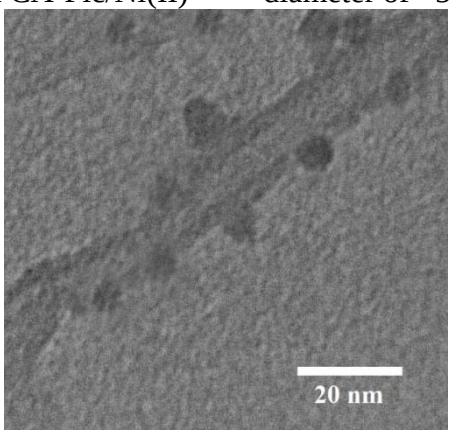

**Fig. 2.** TEM micrograph of MWCNT/$Fe_3O_4$@PCA-Pic/Ni(II)

UV–vis spectroscopy was employed to confirm the binding of picolinic acid ligand to the surface of MWCNT/$Fe_3O_4$@PCA-EDA. UV–vis absorption spectra of picolinic acid, MWCNT/$Fe_3O_4$@PCA-Pic and MWCNT/$Fe_3O_4$@PCA-EDA are presented in Fig. 3. The absorption peak of MWCNT/$Fe_3O_4$@PCA-Pic at 200-295 nm clearly indicated successful conjugation of picolinic acid. Note that MWCNT/$Fe_3O_4$@PCA-EDA exhibited no characteristic peak in this range (Fig. 3c).

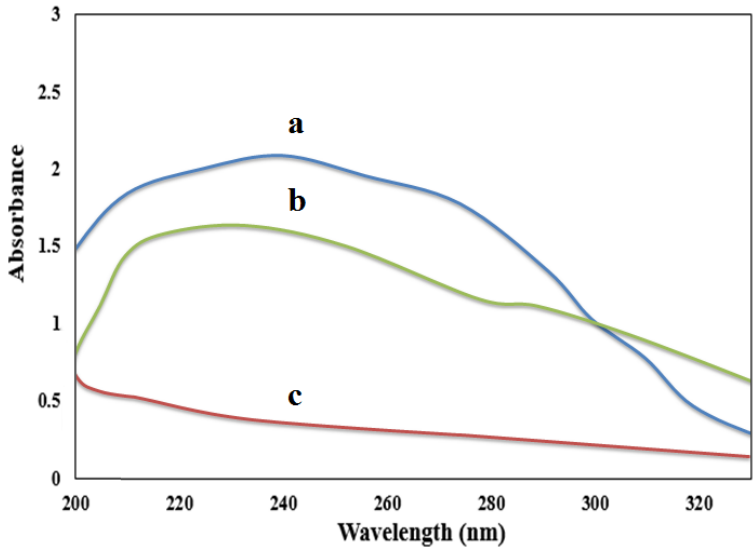


**Fig. 3.** UV–vis spectra of picolinic acid (a), MWCNT/$Fe_3O_4$@PCA-Pic (b) and MWCNT/$Fe_3O_4$@PCA-EDA (c)

The AAS technique was used to calculate the weight percent of nickel in magneto-complex. The data showed that the amount of nickel immobilized on MWCNT/$Fe_3O_4$@PCA-Pic is about 1.72 wt%.

Thermal gravimetric analysis (TGA) is a method of thermal analysis, which measures the amount of weight change of inorganic materials, metals, polymers and composite, either as a function of increasing temperature, in an atmosphere of nitrogen, helium, air, other gas, or in vacuum [56]. The TGA curve of MWCNT/$Fe_3O_4$, MWCNT/$Fe_3O_4$@PCA-Pic and MWCNT/$Fe_3O_4$@PCA-Pic/$Ni^{II}$ are presented in Fig. 4. Fig. 4a shows that the weight loss of MWCNT/$Fe_3O_4$ between 0 and 800 °C is about 5.5%, which might be because of the loss of residual water in the sample. In MWCNT/$Fe_3O_4$@PCA-Pic, the weight loss is about 15.1%, which reflects the amount of polymer layers on the surfaces of nanoparticles (Fig 4b). Comparing the curves (Fig. 4b and c) demonstrates that the amount of $Ni^{II}$ in the synthesized catalyst is about 1.82 wt%, which is consistent with the obtained results by the AAS technique.

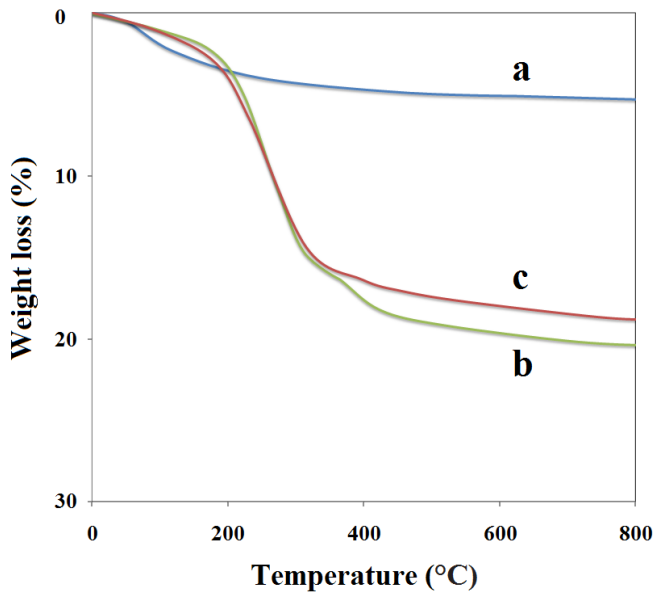


**Fig. 4.** TGA curves of MWCNT/$Fe_3O_4$ (a), MWCNT/$Fe_3O_4$@PCA-Pic (b) and MWCNT/$Fe_3O_4$@PCA-Pic/$Ni^{II}$ (c)

The magnetic properties of the MWCNT/$Fe_3O_4$@PCA-Pic/$Ni^{II}$ nanocatalyst were measured by Vibrating Sample Magnetometer (VSM) at room temperature (Fig. 5). The hysteresis loops that are characteristic of superparamagnetic behavior can be clearly observed for nanocatalyst. By plotting M versus H, the saturation magnetization value (Ms) of MWCNT/$Fe_3O_4$@PCA-Pic/$Ni^{II}$ nanocatalyst was found to be 15.9 emu $g^{-1}$, which means that this nanocatalyst has superparamagnetic properties and can be effectively aggregated at a special site by application of an external magnetic field.

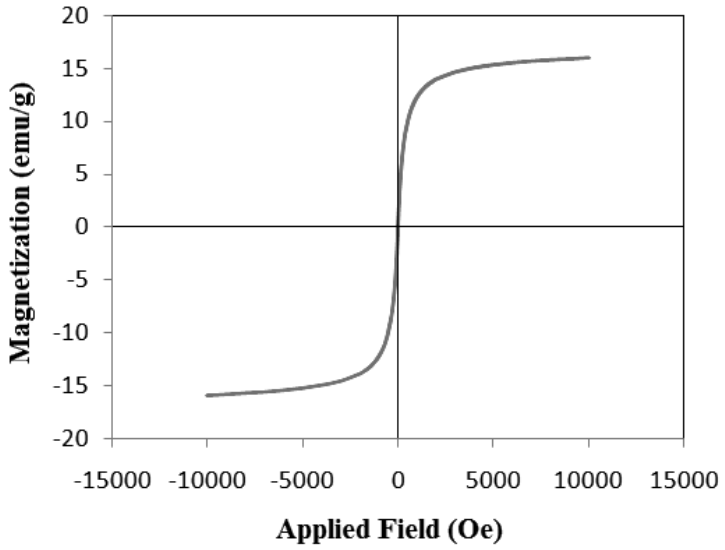

**Fig. 5.** VSM magnetization curve of the MWCNT/$Fe_3O_4$@PCA-Pic/$Ni^{II}$

**The Catalytic activity of the magneto Ni (II) complex in the Henry nitroaldol reaction**

We have tested the catalytic activity the newly prepared magneto Ni(II) complex as semi-heterogeneous catalysts in the Henry nitroaldol reaction of nitroethane with various aldehydes. At the first, the optimization of the reaction conditions (amount of catalyst, reaction time, temperature and solvent) was carried out in a model 4-nitrobenzaldehyde-nitroethane system with MWCNT/$Fe_3O_4$@PCA-Pic/$Ni^{II}$ as the catalyst precursor (Table 1). When 0.5 mol% of magneto Ni(II) complex is used as the catalyst at 60 °C, a conversion of 54% (*syn/anti*: 65/35) of nitrobenzaldehyde into *β*-nitroalkanol is achieved (entry 2, Table 1) after 48 h. Within 1 mol% of nickel, 90% yield of *β*-nitroalkanol was obtained (entry 6, Table 1). In contrast, increasing the amount of the catalyst to 2 mol% resulted in only a smaller or negligible effect on the yield (entry 2, Table 1).Thus, 1 mol % loading is the typical value. Blank test were carried out with nitrobenzaldehyde in the absence of a catalyst, at 60 °C in water (entry 1, Table 1). This test reaction gave 6% conversion of nitrobenzaldehyde into *β*-nitroalkanol, after a reaction time of 48 h. To create the optimized conditions, the variations of reaction time (24-72 *h*) and temperature (25-80 °C) were applied. The highest yield (90 %) with the good *syn/anti* molar ratio (68/32) was achieved (entry 6) at 60 °C, for 48 h, with 1 mol % of magneto Ni(II) complex. Studies show that use of protic solvents usually provides better results than aprotic ones [13,57,58], what is also observed in our case (Table 1, entries 6 and 9-11).The highest yield (90%) and selectivity (*syn/anti*: 68/32) are obtained in water (entry 6) at 60 °C. Thus, water was chosen as the sole solvent for further studies.

**Table 1.** Optimization of the parameters of the Henry nitroaldol reaction between 4-nitrobenzaldehyde and nitroethane with MWCNT/$Fe_3O_4$@PCA-Pic/$Ni^{II}$ as the catalyst system [a]

| Entry | Solvent | Catalyst amount (Ni(II) content, mol%) | Time (h) | Temp. (°C) | Yield [b](%) | Selectivity[c] (Syn/Anti) |
|---|---|---|---|---|---|---|
| 1 | $H_2O$ | - | 48 | 60 | 6 | 61/39 |
| 2 | $H_2O$ | 0.5 | 48 | 60 | 54 | 65/35 |
| 3 | $H_2O$ | 2 | 48 | 60 | 91 | 68/32 |
| 4 | $H_2O$ | 1 | 24 | 60 | 71 | 63/37 |
| 5 | $H_2O$ | 1 | 72 | 60 | 88 | 68/32 |
| 6 | $H_2O$ | 1 | 48 | 60 | 90 | 68/32 |
| 7 | $H_2O$ | 1 | 48 | 25 | 82 | 66/34 |

| | | | | | | |
|---|---|---|---|---|---|---|
| 8 | $H_2O$ | 1 | 48 | 80 | 90 | 71/29 |
| 9 | EtOH | 1 | 48 | 60 | 84 | 67/33 |
| 10 | $CH_3CN$ | 1 | 48 | 60 | 33 | 54/46 |
| 11 | THF | 1 | 48 | 60 | 50 | 58/42 |

[a] Reaction conditions: 1 mmol of 4-nitrobenzaldehyde and 2 mmol of nitroethane.

[b] Isolated yield.

[c] Calculated using $^1$H NMR.

We also examined the catalytic activity of MWCNT/$Fe_3O_4$@PCA-Pic/$Ni^{II}$ with different types of substituted aromatic aldehydes in the reaction with nitroethane (Table 2). In a typical reaction, a mixture of aldehyde (1 mmol), nitroethane (2 mmol), 1 mol% of magneto Ni(II) complex *catalyst* and 3 mL water contained in a capped glass vessel was stirred at 60 °C for 48 h. After a specific time, the catalyst was magnetically separated and *the organic compounds were extracted from water by using dichloromethane. After* evaporation of the solvent, obtained the crude product were analyzed using $^1$H NMR as a mixture of the *β*-nitroalkanol diastereoisomers (Supporting Information).

Generally, aromatic aldehydes with moderate or strong electron-withdrawing substituents without an exhibitive influence of the position of the substituents (entries 1, 2) were converted selectively into the corresponding *β*-nitroalkanol in very good yields (entries 1–3). Anyway, aromatic aldehydes with weak electron-withdrawing groups could be converted into the desired products, with lower yields (entries 6, 7). Nevertheless, the electron-donor substituents in the substituted aromatic aldehydes lead to lower yields (entries 4, 5). Remarkably, 4-pyridinecarboxaldehyde as a heteroaromatic system also led to 70% yield (entry 9).

**Table 2.** Henry reaction of various aldehydes and nitroethane with MWCNT/$Fe_3O_4$@PCA-Pic/$Ni^{II}$ as the catalyst system [a]

| Entry | Aldehyde | Yield [b] (%) | Selectivity [c] (Syn/Anti) |
|---|---|---|---|
| 1 | 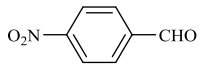 | 90 | 68/32 |
| 2 | 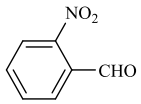 | 89 | 65/35 |

| | | | |
|---|---|---|---|
| 3 | 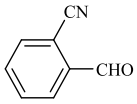 | 88 | 62/38 |
| 4 | 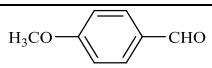 | 61 | 55/45 |
| 5 | 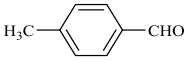 | 65 | 61/39 |
| 6 | 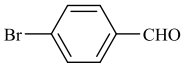 | 70 | 58/42 |
| 7 | 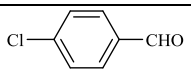 | 73 | 62/38 |
| 8 | 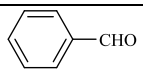 | 82 | 71/29 |
| 9 | 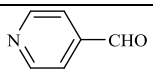 | 70 | 69/31 |

[a] Reaction conditions: 1 mmol of aldehyde, 2 mmol of nitroethane, 3 mL $H_2O$, MWCNT/$Fe_3O_4$@PCA-Pic/$Ni^{II}$ (1 mol % Ni(II)) at 60 ˚C for 48h.

[b] Isolated yield.

[c] Calculated using $^1$H NMR.

The stability and recyclability of semi-heterogeneous catalysts for the practical applications, especially in industry, are great importance. For this reason, the cyclic stability of the as-prepared MWCNT/$Fe_3O_4$@PCA-Pic/$Ni^{II}$ catalysts was also studied by monitoring the catalytic activity during successive cycles of the Henry nitroaldol reaction. Therefore, the reaction of 4-nitrobenzaldehyde and nitroethane was carried out in optimum condition up to 5 cycles. As shown in Fig. 6, MWCNT/$Fe_3O_4$@PCA-Pic/$Ni^{II}$ catalysts were still highly active with a average chemical yield 89.1% after 5 cycles that clearly illustrating the high stability and excellent reusability of the catalyst. Furthermore, in another test MWCNT/$Fe_3O_4$@PCA-Pic/$Ni^{II}$ was magnetically separated from the reaction mixture after ~50% conversion at the reaction temperature. Further reaction of the filtrate under optimum conditions did not proceed significantly. AAS of the filtrate also confirmed that the Ni content in the solution was below the detection limit. Therefore, we may conclude that any Ni(II) complexes that leached into the reaction mixture is not an active homogeneous catalyst and that the observed catalysis is truly heterogeneous in nature.

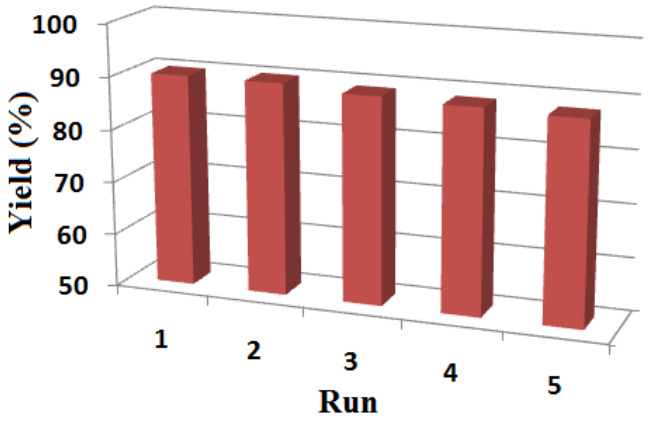


**Fig. 6** Effect of recycling on the catalytic efficiency of MWCNT/$Fe_3O_4$@PCA-Pic/$Ni^{II}$

## Conclusions

In this work, we have developed a novel magnetically retrievable nickel based semi-heterogeneous catalytic system (MWCNT/$Fe_3O_4$@PCA-Pic/$Ni^{II}$) for the diastereoselective Henry reactions in an environmentally friendly solvent. The modification of the $Fe_3O_4$ magnetic nanoparticles with hyperbranched polymers (PCA-EDA-Pic) was carried out to enhance the dispersibility of the magnetic nanocatalyst in polar solvents and stabilize the conjugated Ni(II) complexes via coordination with the picolinic acid. High stability and reusability of catalyst, short reaction times, easy purification and very low nickel leaching were other advantages of this green catalytic process. Further efforts to extend the application of this semi-heterogeneous system in other nickel transformations are currently in progress in our laboratory.

## Acknowledgements

We are grateful to University of Zanjan Research Council for partial support of this work.

## References

[1] G. Goodman, *Proc. R. Soc. Lond. B*, **1974**, *185*, 127-148.
[2] R. Höfer and J. Bigorra, *Green Chem.*, **2007**, *9*, 203-212.
[3] J.-S. Chang, J.-S. Hwang and S.-E. Park, *Res. Chem. Intermed.*, **2003**, *29*, 921-938.
[4] S. Chaturvedi, P.N. Dave and N. Shah, *Journal of Saudi Chemical Society*, **2012**, *16*, 307-325.
[5] G. Hutchings, *Nanocatalysis: Synthesis and applications*, John Wiley & Sons, (2013).
[6] R. Bharati and S. Suresh, in *Biofuels and Bioenergy (BICE2016)*, **2017**,25-32.
[7] M. Cannatelli and A. Ragauskas, *Organic Chemistry: Current Research*, **2013**, *2*, 1.
[8] L. Henry, *CR Hebd Acad Sci*, **1895**, *120*, 1265-1268.
[9] C.H. Heathcock, **1991**,
[10] T. Marcelli, R.N. van der Haas, J.H. van Maarseveen and H. Hiemstra, *Angew. Chem. Int. Ed.*, **2006**, *45*, 929-931.
[11] N. Ono, *The nitro group in organic synthesis*, John Wiley & Sons, (2003).
[12] A. Cwik, A. Fuchs, Z. Hell and J.-M. Clacens, *Tetrahedron*, **2005**, *61*, 4015-4021.
[13] A.G. Doyle and E.N. Jacobsen, *Chem. Rev.*, **2007**, *107*, 5713-5743.
[14] L. Yao, Y. Wei, P. Wang, W. He and S. Zhang, *Tetrahedron*, **2012**, *68*, 9119-9124.
[15] T. Ooi, K. Doda and K. Maruoka, *J. Am. Chem. Soc.*, **2003**, *125*, 2054-2055.

[16] H. Naïli, F. Hajlaoui, T. Mhiri, T.C. Mac Leod, M.N. Kopylovich, K.T. Mahmudov and A.J. Pombeiro, *Dalton Transactions*, **2013**, *42*, 399-406.
[17] C. Christensen, K. Juhl, R.G. Hazell and K.A. Jørgensen, *J. Org. Chem.*, **2002**, *67*, 4875-4881.
[18] S.-F. Lu, D.-M. Du, S.-W. Zhang and J. Xu, *Tetrahedron: Asymmetry*, **2004**, *15*, 3433-3441.
[19] D.-M. Du, S.-F. Lu, T. Fang and J. Xu, *J. Org. Chem.*, **2005**, *70*, 3712-3715.
[20] M.N. Kopylovich, A. Mizar, M.F.C. Guedes da Silva, T.C. Mac Leod, K.T. Mahmudov and A.J. Pombeiro, *Chemistry–A European Journal*, **2013**, *19*, 588-600.
[21] U. Köhn, M. Schulz, H. Görls and E. Anders, *Tetrahedron: Asymmetry*, **2005**, *16*, 2125-2131.
[22] C. Palomo, M. Oiarbide and A. Laso, *Angew. Chem. Int. Ed.*, **2005**, *44*, 3881-3884.
[23] M.N. Kopylovich, T.C. Mac Leod, K.T. Mahmudov, M.F.C.G. da Silva and A.J. Pombeiro, *Dalton Transactions*, **2011**, *40*, 5352-5361.
[24] A. Karmakar, S. Hazra, M.F.C.G. da Silva, A. Paul and A.J. Pombeiro, *CrystEngComm*, **2016**, *18*, 1337-1349.
[25] S. Wu, J. Tang, J. Han, D. Mao, X. Liu, X. Gao, J. Yu and L. Wang, *Tetrahedron*, **2014**, *70*, 5986-5992.
[26] D. Taura, S. Hioki, J. Tanabe, N. Ousaka and E. Yashima, *ACS Catalysis*, **2016**, *6*, 4685-4689.
[27] Z. Chen, K. Yakura, S. Matsunaga and M. Shibasaki, *Org. Lett.*, **2008**, *10*, 3239-3242.
[28] N.E. Shepherd, H. Tanabe, Y. Xu, S. Matsunaga and M. Shibasaki, *J. Am. Chem. Soc.*, **2010**, *132*, 3666-3667.
[29] Y. Dong, H. Pang, H.B. Yang, C. Guo, J. Shao, Y. Chi, C.M. Li and T. Yu, *Angew. Chem.*, **2013**, *125*, 7954-7958.
[30] W. Gao, B. Xiang, T.-T. Meng, F. Liu and X.-R. Qi, *Biomaterials*, **2013**, *34*, 4137-4149.
[31] K. Xavier, J. Chacko and K.M. Yusuff, *Appl. Catal., A*, **2004**, *258*, 251-259.
[32] T.F. Silva, B.G. Rocha, M.F.C.G. da Silva, L.M. Martins and A.J. Pombeiro, *New J. Chem.*, **2016**, *40*, 528-537.
[33] K. Gupta and A.K. Sutar, *Coord. Chem. Rev.*, **2008**, *252*, 1420-1450.
[34] S. Mouri, Z. Chen, S. Matsunaga and M. Shibasaki, *Chem. Commun.*, **2009**, 5138-5140.
[35] N.L. Nkhili, W. Rekik, T. Mhiri, K.T. Mahmudov, M.N. Kopylovich and H. Naïli, *Inorg. Chim. Acta*, **2014**, *412*, 27-31.
[36] A. Allahresani, *J. Iran. Chemi. Soc.*, **2017**, *14*, 1051-1057.
[37] S. Shylesh, V. Schünemann and W.R. Thiel, *Angew. Chem. Int. Ed.*, **2010**, *49*, 3428-3459.
[38] M.B. Gawande, A.K. Rathi, P.S. Branco and R.S. Varma, *Applied Sciences*, **2013**, *3*, 656-674.
[39] J. Govan and Y.K. Gun'ko, *Nanomaterials*, **2014**, *4*, 222-241.
[40] D. Wang and D. Astruc, *Chem. Rev.*, **2014**, *114*, 6949-6985.
[41] H. Aghahosseini, S.J. Tabatabaei rezaei, M. Tadayyon, A. Ramazani, v. amani, R. Ahmadi and D. Abdolahnjadian, *Eur. J. Inorg. Chem.*, **2018**, *22*, 2589-2598.
[42] S.J.T. Rezaei, Y. Bide and M.R. Nabid, *Tetrahedron Lett.*, **2012**, *53*, 5123-5126.
[43] S.J.T. Rezaei, *J. Iran. Chemi. Soc.*, **2017**, *14*, 585-594.
[44] S.J. Tabatabaei Rezaei, H. Khorramabadi, A. Hesami, A. Ramazani, V. Amani and R. Ahmadi, *Ind. Eng. Chem. Res.*, **2017**, *56*, 12256-12266.
[45] S.J. Tabatabaei Rezaei, A. Shamseddin, A. Ramazani, A. Mashhadi Malekzadeh and P. Azimzadeh Asiabi, *Appl. Organomet. Chem.*, **2017**, *31*, e3707.
[46] S.J. Tabatabaei Rezaei, A. Mashhadi Malekzadeh, S. Poulaei, A. Ramazani and H. Khorramabadi, *Appl. Organomet. Chem.*, **2018**, *32*, e3975.

[47] M.R. Nabid, Y. Bide and S.J.T. Rezaei, *Appl. Catal., A*, **2011**, *406*, 124-132.
[48] J.R. Dunetz, J. Magano and G.A. Weisenburger, *Org. Process Res. Dev.*, **2016**, *20*, 140-177.
[49] A. Karmakar, S. Hazra, M.F.C.G. da Silva and A.J. Pombeiro, *New J. Chem.*, **2014**, *38*, 4837-4846.
[50] M. Sutradhar, M.F.C.G. da Silva and A.J. Pombeiro, *Catal. Commun.*, **2014**, *57*, 103-106.
[51] M.A. Halcrow, *Chem. Soc. Rev.*, **2013**, *42*, 1784-1795.
[52] V.J. Bulbule, V.H. Deshpande, S. Velu, A. Sudalai, S. Sivasankar and V. Sathe, *Tetrahedron*, **1999**, *55*, 9325-9332.
[53] M.R. Nabid, Y. Bide, E. Aghaghafari and S.J.T. Rezaei, *Catal. Lett.*, **2014**, *144*, 355-363.
[54] A.M. Malekzadeh, A. Ramazani, S.J.T. Rezaei and H. Niknejad, *J. Colloid Interface Sci.*, **2017**, *490*, 64-73.
[55] X. Huang, L. Li, T. Liu, N. Hao, H. Liu, D. Chen and F. Tang, *Acs Nano.*, **2011**, *5*, 5390-5399.
[56] A. Coats and J. Redfern, *Analyst*, **1963**, *88*, 906-924.
[57] Y. Jung and R. Marcus, *J. Am. Chem. Soc.*, **2007**, *129*, 5492-5502.
[58] F. López, A.J. Minnaard and B.L. Feringa, *Acc. Chem. Res.*, **2007**, *40*, 179-188.

# Nanocrystalline copper(II) oxide-mediated Strecker reaction in water: An efficient and green method for preparation of α-aminonitriles

**Seyed Jamal Tabatabaei Rezaei,*** **Maryam bakhshalipour**

*1 Department of Chemistry, University of Zanjan, Zanjan, Iran*

**E-mail: sjt.rezaei@znu.ac.ir*

**Abstract**

An environmentally benign and highly efficient procedure for the synthesis of α-aminonitriles by a direct three component Strecker reaction has been developed under green conditions in water in the presence of copper oxide (CuO) nanoparticles as a catalyst. The results of these reactions showed that copper oxide nanoparticles are very active catalyst and are able to activate the reactant at ambient temperature. The catalyst was found to be reusable for five cycles without appreciable loss in activity. The obtained nanocatalyst was characterized by TEM, BET and XRD techniques.

**Keywords**: Copper(II) oxide nanoparticles; Strecker reaction; α-Aminonitriles; Green synthesis.; Heterogeneous catalyst

## Introduction

The Strecker reaction is one of the most efficient and straightforward methods for the synthesis of α-aminonitriles [1]. This approach involves a direct multi-component (three component) reaction using an aldehyde or ketone, an amine or its equivalent and a cyanide reagent to form α-aminonitriles, which can be subsequently converted to α-amino acids. α-Amino acids are also of great biological and economical importance due to their significance in chemistry and biology and as useful chiral building blocks [2,3]. Although, a variety of cyanating agents and methods such as alkaline cyanides [1-4], diethylphosphoro cyanidate [5] $Bu_3SnCN$ [6], and $Et_2AlCN$ [7] have been used to carry out the Strecker reaction, it has been shown that trimethylsilyl cyanide (TMSCN) is a very effective, relatively safe and easy-to-handle cyanide source for this purpose[8-16]. However, most of the existing TMSCN-based protocols involve the use of expensive or unrecoverable catalyst, toxic organic solvent, harsh acidic conditions, and tedious work-up procedure leading to copious amount of toxic wastes. Therefore, it seems that there is still much room to develop new improved and recyclable catalyst for this transformation, which works under economically appropriate conditions.

Although homogeneous catalysts are desirable because of their high activities and selectivity, the separation of homogeneous catalysts from the products of the reaction and/or recovery of the catalysts are problems inherent with them. Heterogeneous catalysis has the advantages, such as easy separations and efficient recycling and minimization of metal traces in the product. In recent years, there has been increasing emphasis on the use and design of environmentally friendly solid catalysts to reduce the amount of toxic waste. Nanocrystalline metal oxides have been efficiently used as adsorbents for gases

and destruction of hazardous chemicals and as catalysts for organic transformations. These high reactivities are due to high surface areas combined with unusually reactive morphologies [17-30]. Copper oxide nanoparticles have been of considerable interest due to the role of CuO in catalysis, in metallurgy, and in high-temperature superconductors [31,32] .

In recent decades, water has aroused considerable attention in synthetic community and proved to be a promising solvent in organic synthesis due to its economic, environmentally friendly and polar nature [33]. In relation to this, significant efforts have been dedicated to developing organic reactions in water with many inherent advantages over reactions in conventional organic solvents. Therefore, if the Strecker reaction can be developed to operate in water, it will be of practical value and contribute to the area of water chemistry.

In continuation of our interest in the application of new catalysts for development of useful synthetic methodologies [34-40], we herein report our results on the use of recoverable nanocrystalline CuO (nano CuO) catalyst for the Strecker reaction in water (Scheme 1).

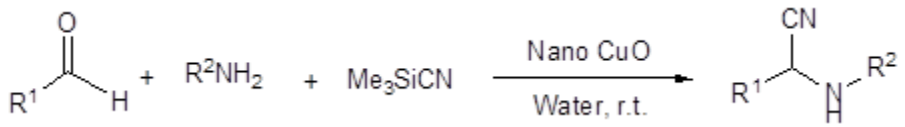


**Scheme 1.**

## EXPERIMENTAL

### Instruments and characterization

Melting points were measured on an Elecrtothermal 9200 apparatus and are uncorrected. $^{1}H$ and $^{13}C$ NMR spectra were recorded on a BRUKER DRX-300 AVANCE spectrometer at 300.13 and 75.47 MHz, respectively. IR spectra were recorded on a Bomem MB-Series FT-IR spectrophotometer. Surface area measurements were carried out by nitrogen adsorption on a Micromeritics ASAP 2010 instrument at an adsorption temperature of 77 K. The transmission electron microscopic studies were performed using a Phillips transmission electron microscope. X-ray powder diffraction (XRD) data were collected on an XD-3A diffractometer using Cu Kα radiation.

### Preparation of copper oxide (CuO) nanoparticles

600 mL of 0.02 M copper acetate aqueous solution was mixed with 2 mL glacial acetic acid in a round-bottomed flask equipped with a refluxing device. The solution was heated to 100 °C with vigorous stirring, and then about 1.6 g of NaOH solid (analytical grade) was rapidly added into the above boiling solution until the pH value of the mixture reached 6.5, where a large amount of black precipitate was simultaneously produced. After being cooled to room temperature, the precipitate was centrifuged, washed once with distilled water and three times with absolute ethanol, respectively, and dried in air at room temperature.

### General procedure for the preparation of α-aminonitriles

A mixture of aldehyde (2 mmol), amine (2 mmol), trimethylsilyl cyanide (2.4 mmol) and CuO nanoparticles (10 mol % with respect to aldehyde) in water (2 mL) was stirred at ambient temperature for an appropriate time (Table 3). The progress of the reaction was monitored by TLC. After completion, the reaction mixture was filtered to isolate the solid product. The solid product was diluted with chloroform, and the catalyst was removed by simple filtration (the catalyst is not soluble in chloroform). After evaporation of solvent, more purification was obtained by column chromatography (eluted with ethyl acetate–hexane, 1:9). All the products were characterized by spectral methods as well as by comparison of their spectral data with those reported earlier [8].

*Characterization Data for newly synthesized compounds:*

*2-p-tolyl-2-(piperidin-1-yl) acetonitrile* (Table 2, entry 15): FT-IR (KBr) ($\nu_{max}$/cm$^{-1}$): 3337, 2234; $^{1}H$ NMR (300 MHz, $CDCl_3$): $\delta_H$ 1.38 (m, 6H), 2.05 (s, 3H), 2.37 (m, 4H), 4.67 (s, 1H), 7.17–7.42 (m, 4H); $^{13}C$ NMR (75.4 MHz, $CDCl_3$): $\delta_c$ 21.4, 23.9, 44.5, 51.6, 62.1, 115.2, 118.1, 127.5, 132.0, 134.2. MS, *m/z* (%): 214 ($M^+$). Anal. Calcd. for $C_{14}H_{18}N_2$: C, 78.46; H, 8.47; N, 13.07%. Found: C, 78.42; H, 8.44; N, 13.11%.

*2-(4-fluorophenyl)-2-(piperidin-1-yl) acetonitrile* (Table 2, entry 16): FT-IR (KBr) ($\nu_{max}$/cm$^{-1}$): 2224; $^{1}H$ NMR (300 MHz, $CDCl_3$): $\delta_H$ 1.42 (m, 6H), 2.39 (m, 4H), 4.67 (s, 1H), 7.05–7.36 (m, 4H); $^{13}C$ NMR (75.4 MHz, $CDCl_3$): $\delta_c$ 23.6, 44.8, 50.6, 62.1, 114.9, 118.3, 128.6, 132.1, 134.4. MS, *m/z* (%): 218 ($M^+$). Anal. Calcd. for $C_{13}H_{15}FN_2$: C, 71.53; H,

6.93; N, 12.83%. Found: C, 71.57; H, 6.90; N, 12.78%.

**Results and discussion**

We first attempted synthesis of copper oxide nanoparticles by a simple precipitation method. After preparation of CuO nanoparticles and characterization by x-ray diffraction (XRD) and transition electron microscopy (TEM) techniques, the nanoparticles were employed as a recyclable catalyst for an efficient synthesis of α-aminonitriles (Scheme 1).

The XRD pattern of nano-sized is shown in Figure 1. All diffraction peaks of x-rays are indexed to the monoclinic crystal system of CuO. No characteristic peaks are observed for other possible impurities. Average size of the obtained CuO particles shown in Figure 2 is 10 nm. Surface areas of the catalysts were measured by BET surface area technique (Table 1). The results in Table 1 demonstrate that the nano form of CuO is preferable because of its high surface area compared with the bulk CuO and better accessibility of reactants to the active sites.

**Table 1.** BET surface area measurements of the catalysts

| Sample | particle size [nm] | BET surface area [$m^2g$-1] |
|---|---|---|
| Bulk CuO | - | 7 |
| Nano CuO | 5-10 | 106 |

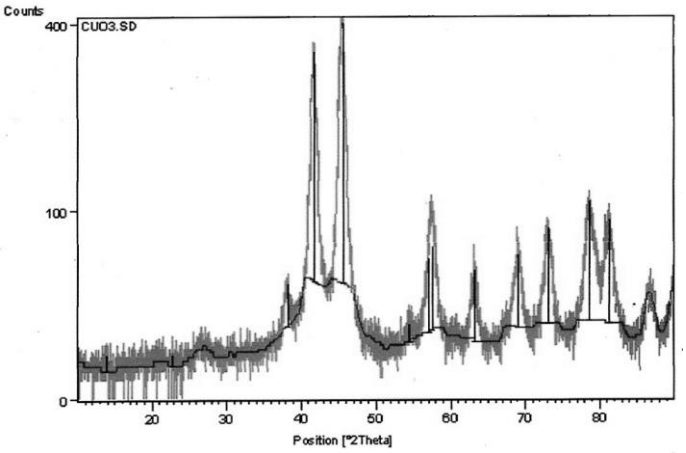


Figure 1. XRD pattern of CuO nanoparticles.

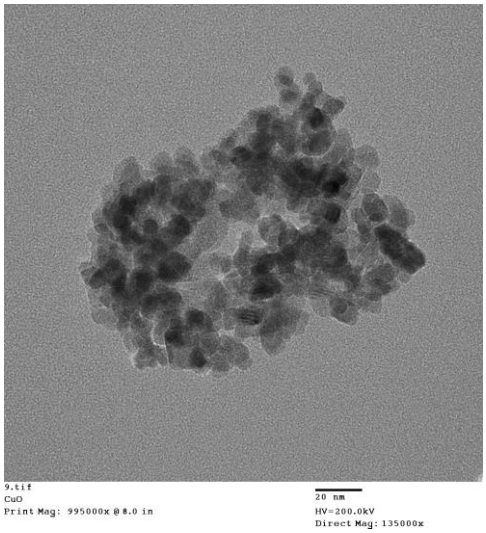


**Figure 2.** TEM image of CuO nanoparticles.

Initially, nano CuO as well as commercially available bulk CuO and $Cu_2O$ was evaluated for the Strecker reaction of benzaldehyde, aniline and TMSCN and the results are summarized in Table 2. The nano CuO was found to be a more active catalyst than the commercial CuO and $Cu_2O$. The high catalytic activity of nano CuO may be attributed to the higher surface area and a higher porosity compared to that of commercial CuO as well as the higher surface concentration of reactive sites. The use of solvents such as $CH_2Cl_2$, EtOH and THF was less effective in place of water (Table 2).

**Table 2.** Screening of reaction parameters

for Strecker reaction.[a]

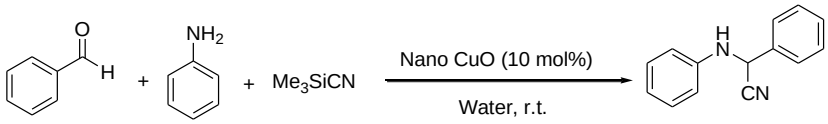


| Entry | Catalyst | Solvent | Yield[b](%) |
|---|---|---|---|
| **1** | Nano CuO | $CH_2Cl_2$ | 34 |
| **3** | Nano CuO | EtOH | 55 |
| **4** | Nano CuO | THF | 30 |
| **5** | Nano CuO | Water | 95 |
| **6** | Bulk CuO | Water | 48 |
| **7** | Bulk $Cu_2O$ | Water | 52 |
| **8** | None | Water | Trace |

[a] Reaction conditions: benzaldehyde (2 mmol), aniline (2 mmol), TMSCN (2.4 mmol), catalyst (10 mol % with respect to aldehyde), solvent (2 mL),for 20 min, at r.t.

[b] Isolated yields.

In order to evaluate the efficiency of this methodology, a series of α-aminonitriles were synthesized by using different aldehydes, amines and TMSCN in the presence of nano CuO (10 mol % with respect to aldehyde) in water. As shown in Table 2, all aldehydes could react effectively with aniline and TMSCN in water catalyzed by nano CuO to afford the corresponding products with excellent yields of 85–95%. The catalytic system also worked well with acid sensitive heterocyclic aldehydes such as 2-thiophenecarboxaldehyde and 3-pyridinecarboxaldehyde to generate the corresponding products with good yields of 95% and 86% (entries 5 and 6, Table 3). This method does not require any additives or stringent reaction conditions to proceed. The reaction conditions are mild enough to perform these reactions in the presence of either acid or base sensitive substrates. Enolizable aldehydes such as 2-phenylpropanal and decanal (entries 7 and 8, Table 3) also produced the corresponding α-aminonitriles.

Encouraged by above results, we continued our task to explore the reactivity of different amines with aromatic aldehydes and TMSCN under similar reaction conditions. As shown in Table 3, all aromatic amines could efficiently undergo reactions with different aldehydes and TMSCN to give the products in excellent yields (entries 9–17, Table 3). When it came to aliphatic amines such as benzyl amine, diethyl amine, and morpholine, relatively slow reaction rate occurred due to the unstable nature of the formed aliphatic imines in the presence of water (entries 12–17, Table 3). However, if the reaction time was prolonged to 5 h, moderate to good yields of the desired products could be obtained.

**Table 3.** Strecker reaction of TMSCN and various aldehydes and amines catalyzed by nano CuO [a]

| Entry | Aldehyde | Amine | Product | Time (h) | Yield[b](%) |
|---|---|---|---|---|---|
| **1** | 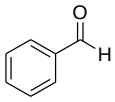 | 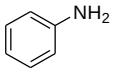 | 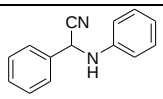 | 0.3 | 95 |
| **2** | 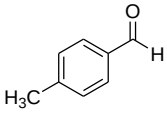 | 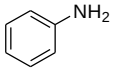 | 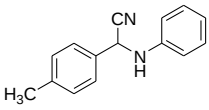 | 0.4 | 92 |
| **3** | 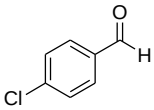 | 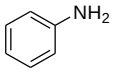 | 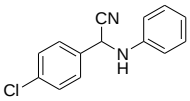 | 0.3 | 93 |

Table 3 (Continued )

| Entry | Aldehyde | Amine | Product | Time (h) | Yield[b](%) |
|---|---|---|---|---|---|
| **4** | 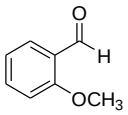 | 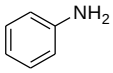 | 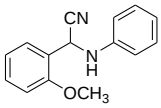 | 0.5 | 91 |
| **5** | 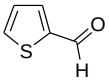 | 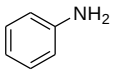 | 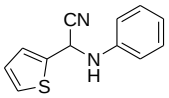 | 0.4 | 95 |
| **6** | 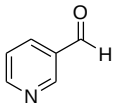 | 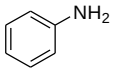 | 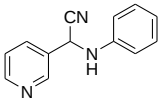 | 0.5 | 86 |
| **7** | 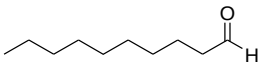 | 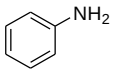 | 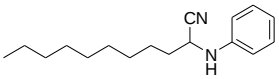 | 0.3 | 90 |
| **8** | 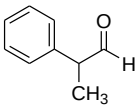 | 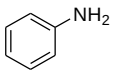 | 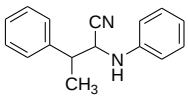 | 0.3 | 92 |
| **9** | 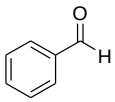 | 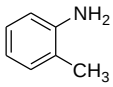 | 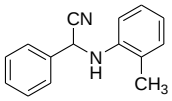 | 0.4 | 90 |
| **10** | 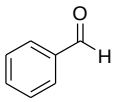 | 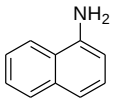 | 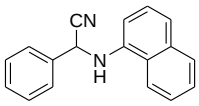 | 0.3 | 91 |
| **11** | 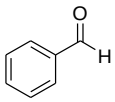 | 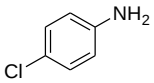 | 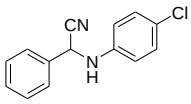 | 0.3 | 94 |
| **12** | 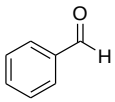 |  | 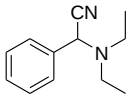 | 5 | 86 |
| **13** | 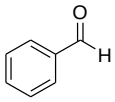 | 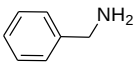 | 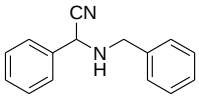 | 5 | 85 |

Table 3 (Continued )

| Entry | Aldehyde | Amine | Product | Time (h) | Yield[b](%) |
|---|---|---|---|---|---|
| **14** | 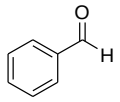 |  | 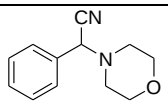 | 5 | 85 |
| **15** | 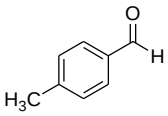 |  | 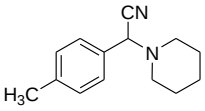 | 5 | 87 |
| **16** | 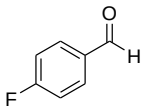 |  | 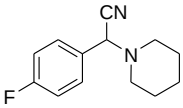 | 5 | 86 |
| **17** | 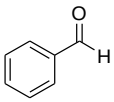 |  | 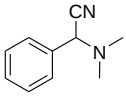 | 5 | 85 |

[a] Reaction conditions: aldehyde (2 mmol), amine (2 mmol), TMSCN (2.4 mmol), catalyst (10 mol % with respect to aldehyde), in water (2 mL).

[b] Isolated yield.

The three-component condensation is proposed to proceed via two-step reactions. Firstly, nano CuO serves as a Lewis acid to promote the formation of imine, which derived from the condensation of aldehyde and amine. Then the formed imine is further activated by nano CuO to produce a more electrophilic C=N intermediate, which facilitates the following attack of TMSCN to the carbon–nitrogen double bond, and thus forms the desired product α-aminonitriles after hydrolysis with water.

A flame atomic absorption spectroscopy (FAAS) experiment was designed to study the stability of the CuO catalyst during the reaction and the recycling process. Consequently, when a reaction mixture filtrate was subjected to FAAS analysis, only 0.3 ppm Cu was detected in the mixture which is equal to 0.1% of the starting CuO used for catalysis. This illustrates that CuO initiates a heterogeneous catalytic cycle and does not undergo degradation during the reactions allowing its successful reuse.

Also, the recyclability and reusability of the nano CuO catalyst was tested for the Strecker reaction of benzaldehyde, aniline and TMSCN up to four cycles. The results are showed in Fig. 3, demonstrating that after every run, the yield of product does not change, indicating the fair stability of nano CuO catalyst under experimental conditions.

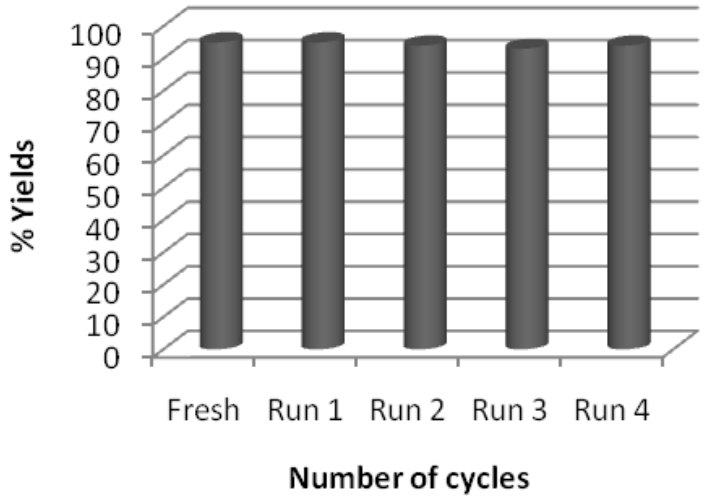


**Figure 3.** Reusability study of nano CuO for the Strecker reaction of benzaldehyde, aniline and TMSCN.

In summary, we have developed a mild, efficient and environmentally friendly method for the synthesis of α-aminonitriles via a three-component condensation of aldehydes, amines and TMSCN catalyzed by a catalytic amount of water-stable Lewis acid nanocrystalline CuO in water. This method is quite general and it works well with a wide variety of aldehydes and amines at room temperature. Recyclability of the catalyst with no loss in its activity, use of the very small quantity of catalyst, short reaction times, the simplicity of the reaction procedure and environmentally friendly feature made this approach distinctly superior over to many other protocols reported earlier.

## ACKNOWLEDGEMENT

We are grateful to University of Zanjan Research Council for partial support of this work.

**REFERENCES**

[1] A. Strecker, *Justus Liebigs Annalen der Chemie*, **1850**, *75*, 27-45.
[2] L.M. Weinstock, P. Davis, B. Handelsman and R.J. Tull, *The Journal of Organic Chemistry*, **1967**, *32*, 2823-2829.
[3] W. Matier, D. Owens, W. Comer, D. Deitchman, H. Ferguson, R. Seidehamel and J. Young, *Journal of medicinal chemistry*, **1973**, *16*, 901-908.
[4] S. Kobayashi and H. Ishitani, *Chemical Reviews*, **1999**, *99*, 1069-1094.
[5] S. Harusawa, Y. Hamada and T. Shioiri, *Tetrahedron Letters*, **1979**, *20*, 4663-4666.
[6] P. Vachal and E.N. Jacobsen, *Journal of the American Chemical Society*, **2002**, *124*, 10012-10014.
[7] S. Nakamura, N. Sato, M. Sugimoto and T. Toru, *Tetrahedron: Asymmetry*, **2004**, *15*, 1513-1516.
[8] B.B. Prasad, A. Bisai and V.K. Singh, *Tetrahedron Letters*, **2004**, *45*, 9565-9567.
[9] J. Yadav, B.S. Reddy, B. Eeshwaraiah and M. Srinivas, *Tetrahedron*, **2004**, *60*, 1767-1771.
[10] A. Heydari, P. Fatemi and A.-A. Alizadeh, *Tetrahedron letters*, **1998**, *39*, 3049-3050.
[11] J.-P. Leblanc and H.W. Gibson, *Tetrahedron letters*, **1992**, *33*, 6295-6298.
[12] T. Chakraborty, G. Reddy and K.A. Hussain, *Tetrahedron letters*, **1991**, *32*, 7597-7600.
[13] M.M. Heravi, K. Bakhtiari, V. Zadsirjan, F.F. Bamoharram and O.M. Heravi, *Bioorganic & medicinal chemistry letters*, **2007**, *17*, 4262-4265.
[14] I.V.P. Raj, G. Suryavanshi and A. Sudalai, *Tetrahedron Letters*, **2007**, *48*, 7211-7214.
[15] A. Majhi, S.S. Kim and H.S. Kim, *Applied Organometallic Chemistry*, **2008**, *22*, 466-470.
[16] A. Heydari, A. Arefi, S. Khaksar and R.K. Shiroodi, *Journal of Molecular Catalysis A: Chemical*, **2007**, *271*, 142-144.
[17] H. Itoh, S. Utamapanya, J.V. Stark, K.J. Klabunde and J.R. Schlup, *Chemistry of materials*, **1993**, *5*, 71-77.
[18] Y. Jiang, S. Decker, C. Mohs and K.J. Klabunde, *Journal of Catalysis*, **1998**, *180*, 24-35.
[19] J. Guzman and B.C. Gates, *Nano Letters*, **2001**, *1*, 689-692.
[20] B.M. Choudary, R.S. Mulukutla and K.J. Klabunde, *Journal of the American chemical Society*, **2003**, *125*, 2020-2021.
[21] B.M. Choudary, M.L. Kantam, K.V. Ranganath, K. Mahendar and B. Sreedhar, *Journal of the American Chemical Society*, **2004**, *126*, 3396-3397.
[22] F. Shi, M.K. Tse, M.M. Pohl, A. Brückner, S. Zhang and M. Beller, *Angewandte Chemie International Edition*, **2007**, *46*, 8866-8868.
[23] V. Polshettiwar and R.S. Varma, *Chemistry–A European Journal*, **2009**, *15*, 1582-1586.
[24] V. Polshettiwar, B. Baruwati and R.S. Varma, *Green Chemistry*, **2009**, *11*, 127-131.
[25] V. Polshettiwar, B. Baruwati and R.S. Varma, *Chemical Communications*, **2009**, 1837-1839.
[26] M.L. Kantam, S. Laha, J. Yadav and S. Jha, *Tetrahedron Letters*, **2009**, *50*, 4467-4469.
[27] S.J. Ahmadi, M. Hosseinpour and S. Sadjadi, *Synthetic Communications®*, **2011**, *41*, 426-435.
[28] M.L. Kantam, S. Laha, J. Yadav and S. Bhargava, *Tetrahedron Letters*, **2008**, *49*, 3083-3086.
[29] M.L. Kantam, T. Ramani, L. Chakrapani and K.V. Kumar, *Tetrahedron Letters*, **2008**, *49*, 1498-1501.

[30] S. Sadjadi, R. Hekmatshoar, S.J. Ahmadi, M. Hosseinpour and M. Outokesh, *Synthetic Communications®*, **2010**, *40*, 607-614.
[31] P.-O. Larsson and A. Andersson, *Journal of Catalysis*, **1998**, *179*, 72-89.
[32] B. Raveau, C. Michel, M. Hervieu and D. Groult, *Crystal Chemistry of High-Tc Superconducting Copper Oxides*, Springer Science & Business Media, (2013).
[33] C.-J. Li and T.-H. Chan, *Organic reactions in aqueous media*, Wiley, (1997).
[34] M.R. Nabid and S.J.T. Rezaei, *Applied Catalysis A: General*, **2009**, *366*, 108-113.
[35] S.J.T. Rezaei, M.R. Nabid, S.Z. Hosseini and M. Abedi, *Synthetic Communications*, **2012**, *42*, 1432-1444.
[36] S.J. Tabatabaei Rezaei, H. Khorramabadi, A. Hesami, A. Ramazani, V. Amani and R. Ahmadi, *Industrial & Engineering Chemistry Research*, **2017**, *56*, 12256-12266.
[37] M.R. Nabid, S.J.T. Rezaei and S.Z. Hosseini, *Materials Letters*, **2012**, *84*, 128-131.
[38] S.J.T. Rezaei, *Journal of the Iranian Chemical Society*, **2017**, *14*, 585-594.
[39] S.J. Tabatabaei Rezaei, A. Shamseddin, A. Ramazani, A. Mashhadi Malekzadeh and P. Azimzadeh Asiabi, *Applied Organometallic Chemistry*, **2017**, *31*, e3707.
[40] H. Aghahosseini, S.J. Tabatabaei rezaei, M. Tadayyon, A. Ramazani, v. amani, R. Ahmadi and D. Abdolahnjadian, *European Journal of Inorganic Chemistry*, **2018**, 22, 2589-2598

# An effective method for the synthesis of 2,3-dihydroquinazolin-4(1h)-ones using conducting polymer salts as catalyst

**Seyed Jamal Tabatabaei Rezaei,[*,1] Mohammad Reza Nabid,[2] Seyedeh Zahra Hosseini,[2] Mahshid Maleki [1]**

[1]*Department of Chemistry, University of Zanjan, Zanjan, Iran*

[2] *Department of Chemistry, Shahid Beheshti University, Tehran, Iran*

**E-mail: sjt.rezaei@znu.ac.ir*

**Abstract**

Conjugate polymer salts, polyaniline (PANI), polypyrrole (PPY) and poly (3, 4-ethylenedioxythiophene) (PEDOT), served as solid acid catalysts for the synthesis of 2,3-dihydroquinazolin-4(1H)-ones under mild conditions. Use of the polypyrrole and poly (3, 4-ethylenedioxythiophene) salts as solid acid catalyst is being reported for the first time. The reactions proceed in moderate to excellent yields in the presence of catalysts. The catalytic system could be efficiently recycled and reused.

**Keywords:** Conducting polymer salts, 2,3-Dihydroquinazolin-4(1H)-ones, Heterogeneous catalyst

## Introduction

2,3-Dihydroquinazolin-4(1H)-ones are an important class of heterocyclic compounds with a wide range of pharmacological and biological activities, such as diuretic properties, herbicide activity and plant growth regulation ability[٢,١] . Additionally, these compounds can easily be oxidized to their quinazolin-4(3H)-one analogu[٤,٣] , which are themselves important biologically active heterocyclic compounds[5-8]. Hence, there are considerable methods for the synthesis of these compounds. Some of the catalysts which have been developed in the past few years for this purpose include: p-toluenesulfonic acid[9], metallic samarium in the presence of iodine or $SmI_2$ [10], nickel boride[11], Low-valent titanium reagent [12], $SnCl_2$ [13], silica sulfuric acid [14], alum [15], Montmorillonite K-10 [16], ionic liquids [17], $Ga(OTf)_3$ [18]. Although there is progress for the synthesis of 2,3-Dihydroquinazolin-4(1H)-ones, developing economical and environmentally friendly procedures remains a challenge. Therefore, we are interested in the recyclable, green and metal-free catalysts for the production of these compounds.

The utilization of polymer-supported acids offers several advantages in preparative procedures. Of these, enhanced stability, higher selectivity, easier handling, simple workup procedures, nontoxicity, noncorrosiveness, mildness of the reaction conditions and the ease of recovery and reuse of the catalyst are the most important advantages [19-23]. Among several polymer-supported catalysts designed and used in organic reactions, polyaniline salts (PANI-Salts) are useful examples which has been performed as inexpensive polymer-based catalyst that can be easily separated, reused and are not contaminated by the products [24-28]. Herein we report an efficient and convenient procedure for the synthesis of 2,3-dihydroquinazolin-4(1H)-ones using PANI, PPY and PEDOT supported acid as reusable, green catalyst.

## Experimental

Polymer sample in the form of cylindrical pellet (10 mm diameter, 1-1.5 mm thickness) was obtained by subjecting the sample to a pressure of 400 MPa. Resistance measurement of the pellet was carried out using Keithley 213 Quad Voltage Source. Pellet density was measured from mass per unit volume of the pressed pellet. The amount of acid group present in the polymer chain was calculated based on the weight of redoped polymer salt and the weight of the used polymer-base. Melting points were measured on an Elecrtothermal 9200 apparatus and are uncorrected. $^{1}H$ and $^{13}C$ NMR spectra were recorded on a BRUKER DRX-300 AVANCE spectrometer at 300.13 and 75.47 MHz, respectively. IR spectra were recorded on a Shimadzu IR-470 spectrometer.

### Typical procedure for preparation of Catalysts:

In a 2 l round-bottomed flask, 100 ml of water was taken and 20 ml (1.0N) of acid solution was added slowly with stirring. To this mixture, 10 mmol of monomer was added and the solution was kept under constant stirring at room temperature. To this solution, 25 ml aqueous solution containing ammonium persulfate (2.28 g) was added for 15-20 min duration. The reaction was allowed to continue for 4 h at room temperature (except for 3,4-ethylenedioxythiophene; 10 h). The precipitated polymer salt was recovered from the polymerization vessel by filtration and then washed with distilled water until

the washing liquid was colorless. To remove oligomers and other organic by-products, the precipitate was washed with methanol until the methanol solution was colorless. Finally, the resulting polymer salt was washed twice with acetone and subsequently dried at 100°C until it achieved a constant mass. The physical and electrical properties of polymer salts are shown in Table 1.

**Table 1**:Physical and electrical properties of conjugate polymer salts

| Polymer Salt | Before reaction | | | After the third trial | | |
|---|---|---|---|---|---|---|
| | Conductivity (S/cm) | Dopant per monomeric unit | Density ($g/cm^3$) | Conductivity (S/cm) | Dopant per monomeric unit | Density ($g/cm^3$) |
| PANI–HCl | $0.5 \times 10^{-4}$ | 0.45 | 1.22 | $0.46 \times 10^{-4}$ | 0.42 | 1.22 |
| PANI–$H_2SO_4$ | $2.0 \times 10^{-2}$ | 0.30 | 1.22 | $1.94 \times 10^{-2}$ | 0.29 | 1.23 |
| PANI–$HNO_3$ | $1.3 \times 10^{-2}$ | 0.33 | 1.21 | $1.29 \times 10^{-2}$ | 0.31 | 1.22 |
| PPY-$H_2SO_4$ | $1.2\times 10^{-2}$ | 0.14 | 1.42 | $1.11\times 10^{-2}$ | 0.12 | 1.45 |
| PEDOT-$H_2SO_4$ | $0.8\times 10^{-2}$ | 0.13 | 1.47 | $0.73\times 10^{-2}$ | 0.10 | 1.48 |

**Typical procedure for the preparation of 2,3-dihydroquinazolin-4(1H)-one derivatives:**

Polyaniline-sulfate salt (10 wt. %, with respect to aldehyde) was added to a solution of isatoic anhydrides (1 mmol), ammonium acetate (1.1 mmol) or amines (1.1 mmol), and aldehydes (1 mmol) in ethanol (5 mL). The mixture was stirred at 70 ˚C for the specified period of time as indicated in Tables 3 and 4. The progress of the reaction was monitored by TLC. After completion, the reaction mixture was then allowed to cool at room temperature and water (5 mL) was added subsequently. The corresponding solid product was obtained through simple filtering, and recrystallized from ethanol. The spectral data of some selected products are listed below.

All the products were characterized by spectral methods as well as by comparison of their spectral data with those reported earlier [9-14,16,17,29].

**Spectroscopic Data of Few Selected Compounds:**

**Compound 2a**: White solid mp = 232–234 °C, IR (KBr): 3442 (NH), 1670 (C=O) $cm^{-1}$.

$^1$H NMR (300 MHz, DMSO-$d_6$): δ = 8.25 (s, 1 H), 7.62 (d, $J$ = 7.6 Hz, 1 H), 7.37 (d, $J$ = 8.0 Hz, 2 H), 7.18 – 7.25 (m, 3 H), 7.07 (s, 1 H), 6.75 (d, $J$ = 8.1 Hz, 1 H), 6.66 (t, $J$ = 7.6 Hz, 1 H), 5.73 (s, 1 H), 2.28 (s, 3 H). $^{13}$C NMR (75.47 MHz, DMSO-$d_6$): δ = 163.5, 148.0, 138.8, 137.7, 133.4, 128.9, 127.4, 126.9, 117.1, 115.0, 114.5, 66.5, 20.8.

**Compound 2g**: White solid mp = 187–188 °C, IR (KBr): 3433 (NH), 1675 (C=O) $cm^{-1}$. $^1$H NMR (300 MHz, DMSO-$d_6$): δ = 8.55 (d, *J* = 4.0 Hz, 1 H), 8.38 (s, 1 H), 7.83 (t, *J* = 7.6 Hz, 1 H), 7.60 (d, *J* = 8.0 Hz, 1 H), 7.49 (d, *J* = 7.6 Hz, 1 H), 7.20–7.36 (m, 3 H), 6.75 (d, *J* = 8.4 Hz, 1 H), 6.65 (t, *J* = 7.6 Hz, 1 H), 5.71 (s, 1 H). $^{13}$C NMR (75.47 MHz, DMSO-$d_6$): δ = 163.2, 160.2, 148.9, 147.3, 137.0, 133.2, 127.2, 123.4, 20.4, 117.0, 114.8, 114.4, 67.2.

**Compound 3a**: White solid mp =150-151 °C, IR (KBr): 3412 (NH), 1670 (C=O) $cm^{-1}$.

$^1$H NMR (300 MHz, DMSO-$d_6$): δ = 7.63 (dd, *J* = 1.6, 8.0 Hz, 1 H), 7.32–7.43 (m, 5 H), 7.19 (m, 1 H), 6.64 (m, 2 H), 5.87 (s, 1 H), 3.90 (m, 1 H), 2.74 (m, 1 H), 1.49 (m, 2 H), 1.27 (m, 2 H), 0.85 (t, *J* = 7.2 Hz, 3 H). $^{13}$C NMR (75.47 MHz, DMSO-$d_6$): δ = 162.0, 145.9, 140.2, 133.1, 132.8, 128.4, 127.9, 127.4, 117.2, 115.0, 114.2, 69.2, 44.1, 29.5, 19.4, 13.6.

**Compound 3b**: White solid mp =175-176 °C, IR (KBr): 3406 (NH), 1670 (C=O) $cm^{-1}$.

$^1$H NMR (300 MHz, DMSO-$d_6$): δ = 7.66 (d, *J* = 7.1 Hz, 1 H), 7.20–7.37 (m, 6 H), 7.14 (t, *J* = 6.8 Hz, 1 H), 6.64 (t, *J* = 7.3 Hz, 1 H), 6.58 (d, *J* = 7.9 Hz, 1 H), 5.78 (s, 1 H), 4.65 (m, 1 H), 1.60 (m, 2 H), 1.25 (m, 1 H), 0.79 (m, 5 H). $^{13}$C NMR (75.47 MHz, DMSO-$d_6$): δ = 162.3, 145.5, 142.9, 132.8, 128.1, 127.7, 127.5, 125.8, 117.1, 116.3, 114.4, 65.1, 49.8, 26.9, 18.3, 10.8.

## Result and discussion

As a part of our ongoing research program on the design of new catalysts for the development of useful and green synthetic methodologies [26,28,30-34], we herein report a practical method for the selective synthesis of 2,3-dihydroquinazolin-4(1H)-ones by employing isatoic anhydride, ammonium acetate (amines), and aldehydes in the presence of polyaniline, polypyrrole, and poly (3,4-ethylenedioxythiophene) salts as catalyst.

To find the standard experimental procedure, polyaniline salts were used as model catalysts. Isatoic anhydride, ammonium acetate and p-methylbenzaldehyde were treated with catalytic amounts of different polyaniline salts including polyaniline-hydrochloride, polyaniline-sulfate and polyaniline-nitrate salt in ethanol under reflux (Table 2). As a result it was found that polyaniline salts can effectively catalyze the reactions. Also, the results in Table 2 show that amongst these catalysts, polyaniline-sulfate salt is the best catalyst in terms of yield.

**Table 2:**Condensation of isatoic anhydride, p-methylbenzaldehyde, and ammonium acetate under various different reaction conditions[a]

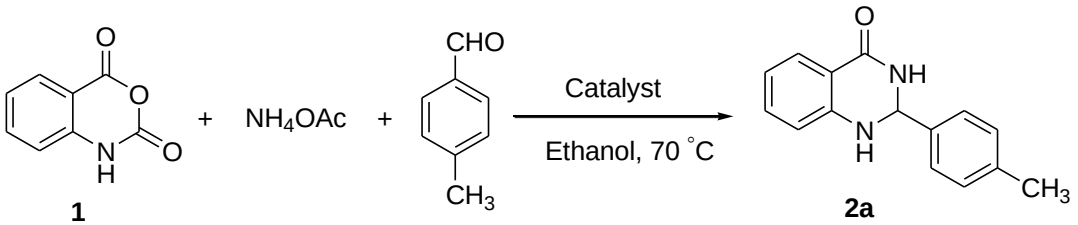

| Entry | Solvent | Catalyst (wt. %) | mmol $H^+$ | Yield[b](%) |
|---|---|---|---|---|
| **1** | EtOH | PANI–HCl(10) | 0.041 | 82 |
| **2** | EtOH | PANI–$HNO_3$(10) | 0.026 | 70 |
| **3** | EtOH | PANI–$H_2SO_4$(10) | 0.024 | 90, 88, 89[c] |
| **4** | $CH_2Cl_2$ | PANI–$H_2SO_4$(10) | 0.024 | 40 |
| **5** | $CH_3CN$ | PANI–$H_2SO_4$(10) | 0.024 | 55 |
| **6** | $H_2O$ | PANI–$H_2SO_4$(10) | 0.024 | 46 |
| **7** | THF | PANI–$H_2SO_4$(10) | 0.024 | 51 |
| **8** | EtOH | PANI–$H_2SO_4$(20) | 0.048 | 91 |
| **9** | EtOH | PANI–$H_2SO_4$(5) | 0.012 | 77 |
| **10** | EtOH | PPY-$H_2SO_4$(10) | 0.018 | 60, 58, 59[c] |
| **11** | EtOH | PPY-$H_2SO_4$(20) | 0.036 | 68 |
| **12** | EtOH | PPY-$H_2SO_4$(30) | 0.054 | 69 |
| **13** | EtOH | PEDOT-$H_2SO_4$(10) | 0.009 | 52, 50, 49[c] |
| **14** | EtOH | PEDOT-$H_2SO_4$(20) | 0.018 | 55 |
| **15** | EtOH | PEDOT-$H_2SO_4$(30) | 0.027 | 55 |
| **16** | EtOH | None | - | 10[d] |

[a] Reaction conditions: isatoic anhydride (1 mmol), ammonium acetate (1.1 mmol), p methylbenzaldehyde (1 mmol), catalyst (1–5.4 mol %), 70 ˚C , 85 min.

[b] Isolated total yield.

[c]The yields of three subsequent runs by using the same recovered catalyst.

[d] 70 ˚C for 3 h.

We investigated various conditions in the model reaction. Among all the solvents screened, such as dichloromethane, acetonitrile, ethanol, tetrahydrofuran, and water, ethanol is the best. Polyaniline-sulfate salt proved to be a superior catalyst among all the catalysts screened in this transformation. It should be noted that 10 wt. % (with respect to aldehyde) of polyaniline-sulfate salt was efficient enough to catalyze the reaction, and increasing the amount of catalyst did not improve the yield significantly (Table 2, entries 4 and 5). Finally, we achieved optimized conditions using 10 wt. % of polyaniline-sulfate salt as the catalyst in ethanol.

Also, we investigated the catalytic activity of the polypyrrole and poly (3,4-ethylenedioxythiophene) salts as solid acid catalysts under optimized condition for the synthesis of 2,3-dihydroquinazolin-4(1H)-ones. The results show that poly (3,4-ethylenedioxythiophene)-sulfate and polypyrrole-sulfate has a moderate activity in reactions compared to polyaniline-sulfate salt. Using more than 10 wt. % from these catalysts showed positive effect and increased the yield of the reaction (Table 2). However, polyaniline-sulfate is generally the best catalyst in terms of yield and time for various derivatives.

**Table 3:** Preparation of 2,3-monosubstituted-2,3-dihydroquinazolin-4(1H)-ones in the presence of polyaniline- sulfate salt under optimized conditions.

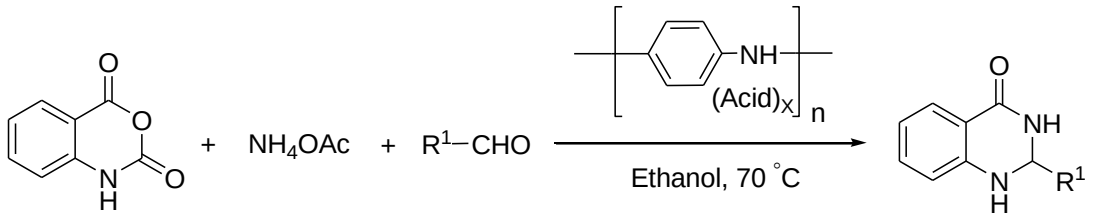


**1** **2**

| Entry | $R^1$ | Time(min) | Product | Yield[a](%) | Mp (°C) |
|---|---|---|---|---|---|
| **1** | p-$(CH_3)C_6H_4$ | 85 | **2a** | 90 | 232–234 |
| **2** | $C_6H_5$ | 90 | **2b** | 92 | 217–219 |
| **3** | p-$(OCH_3)C_6H_4$ | 80 | **2c** | 86 | 190–193 |
| **4** | p-$(Cl)C_6H_4$ | 85 | **2d** | 94 | 205–207 |
| **5** | p-$(NO_2)C_6H_4$ | 100 | **2e** | 96 | 213–215 |

| | | | | | |
|---|---|---|---|---|---|
| **6** | 2-Furyl | 85 | **2f** | 93 | 166–168 |
| **7** | 2- Pyridyl | 90 | **2g** | 91 | 187–188 |
| **8** | p-(F)$C_6H_4$ | 90 | **2h** | 90 | 198–200 |
| **9** | p-(OH)$C_6H_4$ | 90 | **2i** | 89 | 279–280 |
| **10** | m-(F)$C_6H_4$ | 90 | **2j** | 92 | 265–267 |

[a]Isolated yields.

Next, we studied the scope of this reaction (Table 3 and 4). As expected, this reaction proceeded smoothly and the desired products were obtained in good to excellent yields. A series of aldehydes with either electron-donating or electron-withdrawing groups attached to aromatic ring were investigated. The substitution groups on the aromatic ring had no obvious effect on the yield. On the other hand, we investigated the synthesis of 2,3-disubstituted-2,3-dihydroquinazolin-4(1H)-ones from isatoic anhydride, amines, and aldehydes under the optimized reaction conditions. The disubstituted products of 3a-h were obtained in high yield.

**Table 4:**Preparation of 2,3-disubstituted-2,3-dihydroquinazolin-4(1H)-ones in the presence of polyaniline- sulfate salt under optimized conditions.

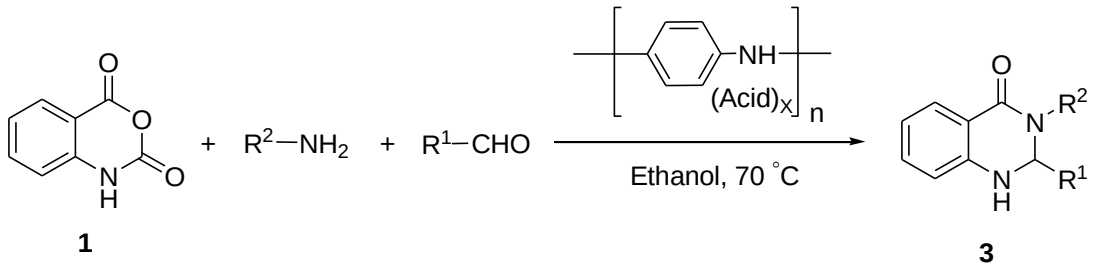

| Entry | $R^1$ | $R^2$ | Time(min) | Product | Yield[a](%) | Mp (°C) |
|---|---|---|---|---|---|---|
| **1** | p-(Cl)$C_6H_4$ | $^nBuNH_2$ | 90 | **3a** | 92 | 149–151 |
| **2** | $C_6H_5$ | $^sBuNH_2$ | 95 | **3b** | 88 | 174–176 |
| **3** | p-(Cl)$C_6H_4$ | $C_6H_5$ | 95 | **3c** | 90 | 218–220 |
| **4** | p-($NO_2$)$C_6H_4$ | $C_6H_5$ | 100 | **3d** | 91 | 195-196 |
| **5** | $C_6H_5$ | p-(Cl)$C_6H_4$ | 95 | **3e** | 80 | 214-216 |
| **6** | $C_6H_5$ | Me | 90 | **3f** | 88 | 161-163 |
| **7** | $C_6H_5$ | Et | 85 | **3g** | 87 | 135-137 |
| **8** | $C_6H_5$ | $C_6H_5$ | 90 | **3h** | 82 | 207-208 |

[a]Isolated yields.

One of the advantages of solid acid catalysts is their ability to perform as a recyclable reaction media. The feasibility of recyclable properties of the polyaniline-sulfate and other polymer supported acid catalysts was also examined through a series of sequential reaction of isatoic anhydride, ammonium acetate and p-methylbenzaldehyde as model substrates. In a typical reaction, the catalysts were simply filtered from the reaction and reused for three cycles (Table 2, entries 3, 6 and 9). The reaction proceeded smoothly with a good yield and this result indicates that the catalyst do not lose its activity and can be reused. After the tertiary trial, the catalyst was recovered and characterized by infrared, the amount of acid present in the polymer, and density measurements. A similar infrared pattern was observed for the polyaniline salt as prepared and the sample subjected after reaction (Fig. 1). Similarly, the value of the amount of acid group, density and conductivity of the polymer salt samples (before and after reaction) are almost the same (see Table 1).

In conclusion, we have demonstrated an alternative and simple procedure for the synthesis of 2,3-dihydroquinazolin-4(1H)-ones using polyaniline-sulfate salt as an eco-friendly, reusable, inexpensive and efficient catalyst. High yields, relatively short reaction times, simplicity of operation and easy work-up procedure are some advantages of this new protocol.

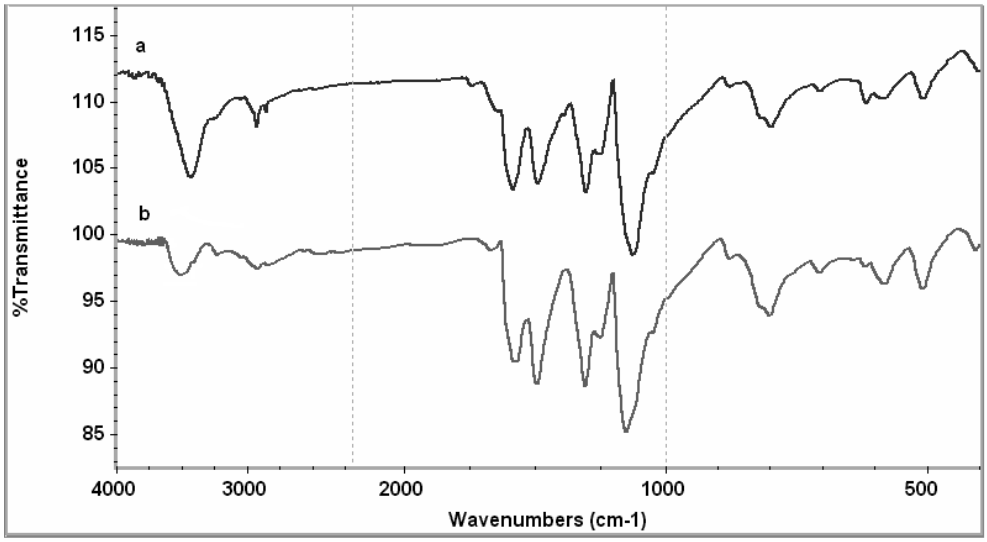


**Figure 1.** FTIR spectrum of polyaniline sulfate salt in KBr medium (a) as synthesized and (b) after three time recycling process.

## Acknowledgements

We gratefully acknowledge financial support from the Research Council of Zanjan University.

## References

[1] E. Hamel, C.M. Lin, J. Plowman, H.-K. Wang, K.-H. Lee and K.D. Paull, *Biochemical pharmacology*, **1996**, *51*, 53-59.

[2] M.-J. Hour, L.-J. Huang, S.-C. Kuo, Y. Xia, K. Bastow, Y. Nakanishi, E. Hamel and K.-H. Lee, *Journal of medicinal chemistry*, **2000**, *43*, 4479-4487.

[3] R.J. Abdel-Jalil, W. Voelter and M. Saeed, *Tetrahedron letters*, **2004**, *45*, 3475-3476.

[4] V. Rao, P. Hanumanthu and C. Ratnam, *INDIAN JOURNAL OF CHEMISTRY SECTION B-ORGANIC CHEMISTRY INCLUDING MEDICINAL CHEMISTRY*, **1979**, *18*, 493-496.

[5] E. Cohen, B. Klarberg and J.R. Vaughan Jr, *Journal of the American Chemical Society*, **1960**, *82*, 2731-2735.

[6] M.S. Malamas and J. Millen, *Journal of medicinal chemistry*, **1991**, *34*, 1492-1503.

[7] K. Matsuno, M. Ichimura, T. Nakajima, K. Tahara, S. Fujiwara, H. Kase, J. Ushiki, N.A. Giese, A. Pandey and R.M. Scarborough, *Journal of medicinal chemistry*, **2002**, *45*, 3057-3066.

[8] H.-R. Tsou, N. Mamuya, B.D. Johnson, M.F. Reich, B.C. Gruber, F. Ye, R. Nilakantan, R. Shen, C. Discafani and R. DeBlanc, *Journal of medicinal chemistry*, **2001**, *44*, 2719-2734.

[9] M. Baghbanzadeh, P. Salehi, M. Dabiri and G. Kozehgary, *Synthesis*, **2006**, *2006*, 344-348.
[10] W. Su and B. Yang, *Australian journal of chemistry*, **2002**, *55*, 695-697.
[11] J.M. Khurana and D. Magoo, *Tetrahedron Letters*, **2009**, *50*, 4777-4780.
[12] D. Shi, L. Rong, J. Wang, Q. Zhuang, X. Wang and H. Hu, *Tetrahedron letters*, **2003**, *44*, 3199-3201.
[13] C.L. Yoo, J.C. Fettinger and M.J. Kurth, *The Journal of organic chemistry*, **2005**, *70*, 6941-6943.
[14] M. Dabiri, P. Salehi, S. Otokesh, M. Baghbanzadeh, G. Kozehgary and A.A. Mohammadi, *Tetrahedron Letters*, **2005**, *46*, 6123-6126.
[15] P. Salehi, M. Dabiri, M. Baghbanzadeh and M. Bahramnejad, *Synthetic communications*, **2006**, *36*, 2287-2292.
[16] J. Chen, W. Su, H. Wu, M. Liu and C. Jin, *Green Chemistry*, **2007**, *9*, 972-975.
[17] J. Chen, D. Wu, F. He, M. Liu, H. Wu, J. Ding and W. Su, *Tetrahedron Letters*, **2008**, *49*, 3814-3818.
[18] M. Mahmoodi Hashemi and Y. Ahmadibeni, *Iranian Journal of Chemistry and Chemical Engineering (IJCCE)*, **2002**, *21*, 71-73.
[19] B. Clapham, T.S. Reger and K.D. Janda, *Tetrahedron*, **2001**, *57*, 4637-4662.
[20] B. Khumraksa, W. Phakhodee and M. Pattarawarapan, *RSC Advances*, **2014**, *4*, 20454-20458.
[21] K. Molvinger, M. Lopez and P. Chavant, *Applied Catalysis A: General*, **2002**, *231*, 91-98.
[22] S. Palaniappan, A. John, C.A. Amarnath and V.J. Rao, *Journal of Molecular Catalysis A: Chemical*, **2004**, *218*, 47-53.
[23] B. Tamami and B.K. PARVANAK, **2003**,
[24] A. John, P.J.P. Yadav and S. Palaniappan, *Journal of Molecular Catalysis A: Chemical*, **2006**, *248*, 121-125.
[25] C.N.S.S.P. Kumar, C.L. Devi, V.J. Rao and S. Palaniappan, *Synlett*, **2008**, *2008*, 2023-2027.
[26] M.R. Nabid and S.J.T. Rezaei, *Applied Catalysis A: General*, **2009**, *366*, 108-113.
[27] S. Palaniappan and A. John, *Current Organic Chemistry*, **2008**, *12*, 98-117.
[28] S.J.T. Rezaei, M.R. Nabid, S.Z. Hosseini and M. Abedi, *Synthetic Communications*, **2012**, *42*, 1432-1444.
[29] P. Salehi, M. Dabiri, M.A. Zolfigol and M. Baghbanzadeh, *Synlett*, **2005**, *2005*, 1155-1157.
[30] V.K.-Y. Lo, Y. Liu, M.-K. Wong and C.-M. Che, *Organic letters*, **2006**, *8*, 1529-1532.
[31] M.R. Nabid, S.J.T. Rezaei and S.Z. Hosseini, *Materials Letters*, **2012**, *84*, 128-131.
[32] S.J.T. Rezaei, *Journal of the Iranian Chemical Society*, **2017**, *14*, 585-594.
[33] S.J. Tabatabaei Rezaei, H. Khorramabadi, A. Hesami, A. Ramazani, V. Amani and R. Ahmadi, *Industrial & Engineering Chemistry Research*, **2017**, *56*, 12256-12266.
[34] S.J. Tabatabaei Rezaei, A. Shamseddin, A. Ramazani, A. Mashhadi Malekzadeh and P. Azimzadeh Asiabi, *Applied Organometallic Chemistry*, **2017**, *31*, e3707.

# Investigating the allelopathic potential of wild mustard (*Sinapis arvensis*) on germination components of wheat cultivars using Polyethylene Glycol 6000

**H.Rezvani [1*], J.Asghari[2], S.M.Ehteshami[3]**

[1]*Scientific Staff of Golestan Research and Education Center of Agricultural and Natural Resources Organization, Agricultural Research and Education Organization,Gorgan, Iran.*

[2,3] *Scientific Staff , Faculty of Agricultural Sciences, Guilan University , Rasht, Iran .*

*Corresponding author Tel.: +98 (911)370 5908

Fax number: +98 (017) 32150114

*E-mail: hosinrezvani@ yahoo.com

## Abstract

In order to evaluate the allelopathic effects of shoot and root water extract of wild mustard (*Sinapis arvensis*) on germination properties and seedling growth of wheat cultivars, an experiment was conducted in the form of completely randomized design with three replications at the physiology laboratory of Golestan Agriculture and Natural Resources Research Center in Iran in 2011. Experimental treatments were components of water extract wild mustard shoot and root (0, 2.5, 5 and 7.5%) and wheat cultivars (Morvarid, Moghan, Tajan and Arta). Also, in order to separate the osmotic effects of different concentrations of wild mustard water extract from allelochemicals effects was used the polyethylene glycol 6000. The results showed that with increasing the concentration of shoot and root water extract of wild mustard, percentage and rate of germination, shoot and root length, shoot and root dry weight and seedling dry weight of different wheat cultivars decreased significantly. So that in the highest concentration, Moghan and Morvarid cultivars showed the least influence and Tajan and Arta cultivars showed the highest influence. Furthermore the different concentrations of polyethylene glycol had no effect on the traits mentioned above. This confirms that the osmotic potential of extracts had no influence in to intensify of allelochemicals effects. Fitting of three-parameter logistic model provided a successful estimation of the relationship between different levels of water extract and germination percentage. Generally, wild mustard shoot showed more inhibitory effect than the root.

**Keywords**: Allelopathy; Water extract; Germination; Wild mustard, Wheat

## Introduction

One of the main reasons of yield loss in crops is weeds invasion. Weeds by competition for resources, to prevent from proper access of crop to these resources and thus to reduce crop production and increase its cost. According to FAO estimation, weeds damage to all of agricultural productions in 2009 alone is about 50 percent of global production (FAO, 2010). In most studies, the reduced product is attributed to different forms of competition between weeds and crops and allelopathic interactions between them are not considered. But scientific findings showed that interactions between crops and weeds are partly yield loss factors in crops (Wall et al., 2006). The more species of weeds on crops have deterrent effect, but some species of weeds to stimulate seed germination and growth of crops (Mason et al, 2005). Among the many species of weeds that can damage to wheat farms, wild mustard is one of the most common weed that reduces yield and increases production costs (Johnson et al., 2006). Wild mustard is an annual plant of Brassicaceae family that can reproduce only by seed. Approximately 2.5 to 3 months takes there is complete plant from a seed. This weed is compatible in a wide range of temperature (15 - 48 ºC) and is not destroyed easily by frost (Warwick et al., 2005). Wild mustard is a permanent and stable weed in most regions of the world. In Iran this weed is as the main broadleaf weed in fall cultivation (Zeinali and Ehteshami, 2003). In Iran 325 species of this family have been reported, which constitutes about 4% of the flora and have high dispersion (Ghahraman, 1994). Study on allelopathy has been particular importance in recent decades and includes several objectives such as the weed management, maintaining the species diversity, improvement and increasing of crop yield and protection of the environment (Mighani, 2003). What is important is the fundamental difference between the allelopathy and competition and separating of direct effects resulting from allelopathy from the indirect effects resulting from other organisms and environmental changes (Sisodia and Siddiqui, 2010). By definition, allelopathy includes any harmful or beneficial effects of directly or indirectly of plants and microorganisms on another plants through the production of chemicals materials (allelochemicals). Action mechanism of allelopathic substances is different on plants. These effects include preventing the germination, damaging the roots and other parts of meristematic, preventing the growth of seedlings, preventing the ATP production due to lack of free oxygen in chloroplast and Severe inhibition of mitochondrial activity and cellular respiration (Rice, 2002). Most species of weeds on crops have deterrent effects, but some species of weed to stimulate seed germination, growth and the production of crops. Ismail and Chong (2002) reported that the low concentrations of allelopathic substances may have positive or negative effects on the target plants, but in high concentrations always have deterrent effects. The weeds by releasing the phytotoxin (Toxins of plant origin) from seeds are affected damaged residues, washed material, secretory materials and volatile of crops. When susceptible plants are exposed to the allelochemical compounds, are affected their germination and growth (Bais and et al., 2003). Reduction of elongation in root and shoot of rice affected by water extract of

different parts of barnyard grass have been reported (Berenji et al., 2008). Several studies have been conducted on allelopathic effect of weeds on wheat. For example, there are reports on reduction of initial growth, seedling weight loss and a 21% reduction in wheat grain yield of triticale is extract (Wall et al., 2006). Also, studies have shown that some plants from cabbage family (Cruciferae )have allelopathic effects in inhibition of plants and microorganisms growth (Wall et al., 2006). Muller's studies (2002) showed that germination and growth of gramineae plants is reduced in the vicinity of black mustard (*Brasica nigra*). Many species of plants belonging to the mustard family include strong inhibitors of germination and growth. These compounds that are called mustard oil (allyl isothiocyanate and β phenethyl isothiocyanate) there are in the mustard tissues (*sinapis arvensis*) and are potential inhibitors of germination (Mason et al., 2005). Vicol and Dobrota (2008) founded that water extract of wild mustard can prevent from hollyhock growth (*Malva parviflora* L.). Also, they reported black mustard (*Brassica nigra* L.) on grounds of covered with annual weeds in southern california beaches prevented from germination and growth of other annual plants such as Bromus (*Bromus* Sp.) by releasing inhibitors from leaves and stems that were decomposing and would create a uniform vegetation. Mason et al., (2005) in greenhouse studies observed that the number of *sticky willy* (*Galium aparin* L.), wild spinach (*Chenopodium album* L.) and chamomile (*Matricaria inodora* L.) is reduced in the presence of wild mustard (*Sinapis alba* L.) strongly. Also, Muller (2002) in his study on the water extracts effect of dried remnants of several species of wild mustard on wheat observed that water extracts compared with the control can inhibit 57 to 91% coleoptile growth and 59 to 98% wheat roots growth. Identification of weeds with allelopathic property and its effect on germination and early growth of the products is important in any area. Whereas very little researches has been done on the allelopathic potential of wild mustard on wheat, therefore this research has been implemented in vitro in order to evaluate the allelopathic potential of four wheat cultivars in different concentrations of water extracts of wild mustard shoot and root and their effect on germination and seedling growth characteristics of wheat cultivars.

## Materials and Methods

In order to investigate the allelopathic effects of wild mustard shoot and root on wheat cultivars, a factorial experiment was conducted in the form of completely randomized design with three replications at the physiology laboratory of Golestan Agriculture and Natural Resources Research Center in Iran in 2011. Experimental treatments were components of water extract wild mustard shoot and root (0, 2.5, 5 and 7.5%) and wheat cultivars (Morvarid, Moghan, Tajan and Arta). Also, in order to separate the osmotic effects of different concentrations of water extract of wild mustard from allelochemicals effects was used polyethylene glycol 6000. Wild mustard organs were collected at flowering stage from farm of Golestan Agricultural and Natural Resources Research Center with the geographical location of 36° 45' N and 54° 25' E in March 2011. These organs washed

with water and then shoot and root were separated. Wild mustard segregated organs

were dried at room temperature and away from sunlight and then were powdered by an electric mill. To obtain 100% solution, was poured10 g of the powder in 100 ml water and was placed into the shaker for 24 hours. The prepared solution was passed through a filter paper. In this experiment was used petri dish in diameter 9 cm and was placed the sterile whatman filter paper at the bottom of that. In order to disinfect, the seeds were soaked for 30 seconds in hypochlorite 10% solution and were washed with distilled water immediately. Then, in each petri dish, 25 wheat seeds were placed and was added 6 ml water extract of wild mustard organs to each of them. Then they moved to germinator with 60% relative humidity and temperature in 25/20 day/night and length of 12 hours of light. Wheat germinated seeds were counted to determine germination rate daily. Germination criterion was exclusion of 2 mm radicle from seed. Counting the seeds continued until germinated seeds number in two consecutive days remained stationary in any sample. To measure the seeds germination rate used from the Maquer method (Hartmann et al., 1990):

$$R_s = \sum_{i=1}^{n} \frac{Si}{Di}$$

Eq. (1)

Where $R_s$ is germination rate of seeds, $S_i$ is germinated seeds number in i counting and Di is day number until i counting. Time to reach 50% of seeds maximum germination (D50) was calculated by Germin program. Also, in order to evaluate the wild mustard organs allelopathic potential in reducing of wheat cultivars germination percentage used from the three-parameter logistic model (Eq.2):

$$Y = a / [1 + (X/X_{50})^{b}]$$

Eq. (2)

Where Y is germination percentage at concentration of X water extract, a is maximum germination, X50 is concentration of water extract required for 50% inhibition of the maximum germination and b represents the slope of the decrease in germination because of the increase in concentration of water extract (Chuhan and et al., 2006 ). Also, for the separation of osmotic potential effects of different concentrations of wild mustard water extract from allelochemical material impacts used from polyethylene glycol 6000 by Michel method (Eq. 3):

Eq. (3 )

$$\varphi_s = -(1l18 \times 10^{-2})c - (1l18 \times 10^{-4})c^2 + (2/67 \times 10^{-4})ct - (8/39 \times 10^{-7})c^2$$

Where $\varphi_s$ is osmotic potential according to bar, c is amount of polyethylene glycol according to gram/liter, and t is the temperature according to degrees celsius.

At the end of experiment using ten random sample of each treatment were measured root and shoot dry weight, seedling dry weight and root and shoot length. Before data analysis, all data were assessed for normality. Data statistical analysis carried out using SAS software, and figures were drawn using Excel and Sigma Plot softwares.

## Results and discussion

### Results:

The results of data analysis showed that wild mustard shoot and root water extract and their interactions have significant effects on growth indices and germination components of wheat cultivars (Table 1). Also, different concentration of PEG didn't show significant

effect on mentioned traits (Table 2) which this confirms that osmotic potential of the extract was not involved in the exacerbation of allelochemicals effect and osmotic effect probability seems to be poor.

**Effect of shoot water extract of wild mustard on growth indices**

The results of variance analysis showed that shoot water extract of wild mustard reduced all the traits measured in the wheat cultivars significantly (Table 1). The concentrations of 5 and 7.5% shoot water extract showed greater inhibitory effect in the all of wheat cultivars. Ismail and Chong (2002) reported that allelopathic substances in low concentrations may have positive or negative effects on plants but in high concentrations always are inhibitors. Investigation the effect of different concentrations of shoot water extract of wild mustard showed that wheat cultivars growth indices in different concentrations had different inhibitory effects. According to Table (3) shoot length of wheat cultivars hadn't significant difference in 0 and 2.5% concentrations but with increasing the water extract concentration was determined inhibitory effect in different cultivars. Inhibitory effect of shoot water extract of wild mustard on shoot length of wheat cultivars at concentrations of 5 and 7.5% in Arta cultivar were 34.3 and 53.7% more than Moghan cultivar (23.4 and 31.6%) respectively. Also, root length with increasing the shoot water extract concentration of wild mustard reduced in wheat cultivars. In concentrations of 5 and 7.5% of shoot water extract, Moghan cultivar showed the lowest influence (33.16 and 43.35%) and Tajan cultivar showed the most influence than to control (49.7 and 61.2%). Reduce the root length than to shoot length in the same concentrations of shoot water extract of wild mustard may indicate that root cells elongation is impressed by blocking of gibberellin and indoleacetic acid actions via allelopathic substances extracted from the root and the shoot (Qasem, 2001). It can be expected, because the root is the first organ that absorbs allelopathic substances directly from environment and may be more influenced by these materials. The root, shoot and seedling dry weights with increasing the concentrations of shoot water extract showed a similar trend.

**Effect of root water extract of wild mustard on growth indices**

Influence of measured traits of wheat seedlings from view of concentrations of root water extract of wild mustard were similar to shoot (Table 1). Mean comparison of traits showed that at low concentrations between control and concentration of 2.5% was not significant difference statistically but with increasing the concentration of root water extract of wild mustard from 2.5 to 7.5% inhibition was increased in the measured traits. This reduced growth trend has been different in different wheat cultivars. So that shoot length of Tajan cultivar decreased 65.3% than to control with increasing the water extract concentration to 7.5%, while at the same concentration in Moghan and Morvarid cultivars reduced 46.3 and 48.5% respectively. Also seedling dry weight of wheat cultivars in the maximum concentration of root water extract of wild

mustard in Moghan and Morvarid cultivars showed the lowest influence (29.6 and 27.9%) and in Tajan and Arta cultivars showed the most influence (55.7 and 53.3%) respectively (Table 3). Johnson et al., (2006) introduced glucosinolate compounds produced in root of wild mustard as a biologic active inhibitor of germination and growth in other species and they believed that these compounds have more influence on the small grains. The results of this experiment are similar to reports of Turk and Tawaha (2002) and Chuhan et al., (2006).

**Effect of shoot and root water extract of wild mustard on germination components**

The results of variance analysis showed that organ type, water extract concentration and their interaction on the germination characteristics of wheat cultivars were significant at the 0.01% level (Table 1). The results showed that was significant difference between the germination rate of wheat cultivars in different concentrations (Table 3 and 4). So that at the highest concentration (7.5%), germination rate showed the most influence in Tajan and Arta cultivars (50.9 and 51.3%) respectively and showed the lowest influence in Morvarid cultivar compared with control at the same concentration (27.3%). The results of germination percentage were similar to germination rate in the different cultivars, so that in the highest concentration (7.5%), the germination percentage showed the most influence in Tajan and Arta cultivars (61.9 and 59.6%) respectively and showed the lowest influence in Morvarid cultivar compared with control at the same concentration (39.2%). Rizvi and et al., (2000) evaluated the allelopathic potential of wheat cultivars on wild oat and reported that wheat cultivars showed significant genetic differences in germination percentage and rate. Tawaha, and Turk (2003) reported that with increasing concentration of water extract in black mustard organs, reduced germination percentage in lentil and increased germination rate. Also, due to the was significant interaction between organs and various concentrations of water extract of wild mustard on germination components, the shoot and the root showed the most and the lowest inhibition respectively in all of the wheat cultivars (Table 1, Figure 1: a and b). This can indicate that the amount or type of allelopathic materials in shoot and root of wild mustard may be different. So that this difference can cause different effects. Chung et al., (2006) reported that the leaves are probably the main tank to produce allelochemical materials and roots have lower amounts of these compounds. Yurchak et al., (2005) observed that different parts water extract of turnip reduced corn and winter wheat germination and seedling growth (26.5 - 79.5%). In this study was determined that the shoot water extract (leaves and flowers) had greater inhibition effect and prevented from germination about 60 percent, but the root water extract inhibited from germination about 20 - 30%. In this case, probably leaves and flowers of wild mustard was produced more allelochemical materials to inhibit of wheat seed germination.

**Investigation of germination characteristics of wheat cultivars by regression analysis**

The importance of the final germination percentage in seed germination studies led to the influence of this index is studied by three-parameter logistic model (Chuhan et al., 2006).

$$Y=a / [1+(X/X_{50})^{b}]$$

In this model, well be justified the relationship between different levels of organs water extract of wild mustard and germination percentage of wheat cultivar. So that the determination coefficient ($R^2$) of model for shoot and root water extract of wild mustard was significant (Tables 5 and 6). $X_{50}$ parameter in model for different organs water extract showed that in concentration of 50% of shoot and root water extract of wild mustard, maximum germination percentage of wheat cultivars reduced 50% and wasn't any difference between the different organs extract. Parameter of b in model (which represents slope of decrease of germination percentage in increase of extract concentration) showed maximum and minimum in shoot and root respectively and this was shown in Tajan and Arta cultivars with more inhibition intensity and in Morvarid cultivar with less inhibition intensity. Increasing of this slope indicates stronger responses of germination to different levels of water extract and represents a greater sensitivity to the allelochemical materials. Time to reach 50% maximum germination (D50) in wheat cultivars increased when seeds faced with allelopathic substances, but the analysis of variance showed that the mean this time in concentration of 2.5% of different organs extract of wild mustard did not differ significantly with controls. D50 at concentrations of 5% root extract in Morvarid, Moghan and Arta cultivars was 72.15, 73.30 and 82.33 hours respectively. But when was used shoot extract, it was estimated 77.25, 83.14 and 94.25 hours in mentioned cultivars respectively. This index has an inverse relationship with the rate of seed germination and indicates decrease of seeds germination rate of wheat cultivars significantly when facing of cultivars with concentration of 50% shoot and root water extract of wild mustard.

**Discussion:**

The results showed that with increasing the extract concentration, the traits were significantly reduced that this could be due to the increase the amount of allelochemical materials and increase their toxicity on plant responses. However, osmotic potential of extract concentration may be involved in exacerbate of allelochemicals effect, but since concentrations used in this study were treated with polyethylene glycol 6000 and their effects at different concentrations were significant, so osmotic effect probability seems to be weak. Generally in all of wheat cultivars, root characteristics were inhibited more than shoot. These results confirm previous reports that based on the root is more sensitive than to shoot and the roots are more exposed to the allelopathic material effects. Also, Due to direct contact of plants root with the extracts this organ is more exposed to allelochemical materials and more is affected by inhibited direct and indirect effects. These results confirm findings of Mason et al., (2005) about the existence of allelopathic potential in wild mustard. This inhibition may be due to glucosinolates and

their derivatives (Isothiocyanates and other unknown compounds) that are soluble in water and there are in these plants and other plants of the *Brassica* family. Among the studied cultivars, Moghan and Morvarid cultivar showed the least influence. Also, it was observed that wild mustard shoot showed greater inhibitory effect on germination and growth of wheat cultivars than to root. The inhibitory effect of allelopathic materials (such as glucosinolates and Isothiocyanates) on characteristics such as germination percentage and rate of seeds, shoot length, root length and seedling dry weight in wheat cultivars reported by many researchers. Since that each of these known Isothiocyanates have different effects on the target plant, it seems for creation the inhibitory effect in physiological characteristics is required more concentrations of these materials or inhibition occur by some other secondary metabolites. Also, Kato-Noguchi (2004) found that among the secondary metabolites exited from plant in addition to Isothiocyanates that is proven their inhibitory effect, there are other substances with allelopathic properties that in low amounts have shown high inhibitory ability. Therefore, it is possible under field conditions and natural environment that include living or non living obstacles in surrounding of the plants and may decrease inhibitory effect, the inhibition also occur for other reasons. Generally, in four studied cultivars shoot showed higher inhibitory effect than to root and Morvarid cultivar showed the least influence to allelochemicals.

According to these results, it seems that plants of *Brassica* family due to negative allelopathic effects on seed germination and seedling growth have damaging effects in crop growth environments and since that plant establishment in the early stages of growth is very important, so these plants as soon as possible should be managed. However, it is possible the probability of existence the glucosinolates and Isothiocyanates in other plants of this family such as cabbage and indian mustard (major products of resulting from enzymatic degradation). Therefore is necessary that carry out comprehensive studies on the allelopathic potential to be provided possibility the use of them in agriculture such as control of weeds, plant pests and diseases, breeding of crop and horticultural plants and production of bioherbicides and biopesticides of environmentally friendly, safe, and analyzable.

Table1. Analysis of variance for water extract of wild mustard organs effects on germination and seedling growth of wheat cultivars

| | | Mean square | | | | | | | |
|---|---|---|---|---|---|---|---|---|---|
| S.o.v | Df | Germination percentage | Germination rate | D50 | Root length | Shoot length | Root dry weight | Shoot dry weight | Seedling dry weight |
| Rep | 2 | 0.00013$^{ns}$ | 0.00003$^{ns}$ | 0.0008$^{ns}$ | 0.000163$^{ns}$ | 0.0044$^{ns}$ | 0.00071$^{ns}$ | 0.000002$^{ns}$ | 0.000001$^{ns}$ |
| A (cultivar) | 3 | 439.47** | 5.31** | 452.72** | 39.71** | 16.39** | 0.00035** | 0.0054** | 0.00037** |
| B (wild mustard organ) | 2 | 414.57** | 3.12** | 519.37** | 185.03** | 121.11** | 0.0023** | 0.41** | 0.0069** |
| C (concentration) | 3 | 18296.7** | 123.12** | 4481.01** | 33.41** | 15.22** | 0.00039** | 0.0087** | 0.0011** |
| A×B | 6 | 58.18** | 0.635** | 14.04** | 1.871** | 0.316** | 0.000063** | 0.0091** | 0.00032** |
| A×C | 9 | 144.7** | 0.197** | 86.07** | 0.063** | 0.06** | 0.000027** | 0.85** | 0.000093** |
| B×C | 6 | 68.71** | 0.248** | 63.27** | 11.56** | 4.69** | 0.00015** | 0.94** | 0.0022** |
| A×B×C | 18 | 17.07** | 0.103** | 7.85** | 0.088** | 0.0041** | 0.0002** | 0.009** | 0.00015** |
| Error | 78 | 0.000031 | 0.00011 | 0.0007 | 0.002 | 0.0085 | 0.000061 | 0.000015 | 0.000011 |
| C.V | | 3.63 | 1.65 | 2.36 | 2.56 | 3.83 | 1.23 | 1.85 | 2.28 |

Ns = no significant ($p > 0.05$); * and ** = Significant ($p < 0.05$ and $p < 0.01$, respectively).

Table2. Analysis of variance for different concentrations of PEG 6000 effects on germination and seedling growth of wheat cultivars

| | | Mean square | | | | | | | |
|---|---|---|---|---|---|---|---|---|---|
| S.o.v | Df | Germination percentage | Germination rate | D50 | Root length | Shoot length | Root dry weight | Shoot dry weight | Seedling dry weight |
| Rep | 2 | 0.00001$^{ns}$ | 0.00002$^{ns}$ | 0.00071$^{ns}$ | 0.0044$^{ns}$ | 0.00014$^{ns}$ | 0.00001$^{ns}$ | 0.00003$^{ns}$ | 0.00013$^{ns}$ |
| A (cultivar) | 3 | 0.00037** | 0.0054** | 0.00035** | 16.39** | 39.71** | 32.72** | 5.31 | 39.47** |
| B (PEG concentration) | 3 | 0.63$^{ns}$ | 7.18$^{ns}$ | 0.023$^{ns}$ | 1.46$^{ns}$ | 0.64$^{ns}$ | 0.49$^{ns}$ | 0.23$^{ns}$ | 0.56$^{ns}$ |
| A×B | 9 | 0.716$^{ns}$ | 9.18$^{ns}$ | 0.57$^{ns}$ | 8.38$^{ns}$ | 0.23$^{ns}$ | 0.12$^{ns}$ | 0.54$^{ns}$ | 0.37$^{ns}$ |
| Error | 16 | 0.0062 | 0.0021 | 1.12 | 1.96 | 1.96 | 0.61 | 1.04 | 0.76 |
| C.V | | 2.94 | 2.94 | 8.81 | 14.65 | 4.65 | 8.30 | 12.96 | 7.65 |

Ns = no significant ($p > 0.05$); * and ** = Significant ($p < 0.05$ and $p < 0.01$, respectively).

Table3. Mean comparison for allelopathic effect of different concentrations of wild mustard root extract on germination components and seedling growth of wheat cultivars

| Cultivars | Extract concentration (%) | Germination percentage | Germination rate (seed. day) | D50 (h) | Root length(cm) | Shoot length(cm) | root dry weight(g) | Shoot dry weight(g) | Seedling dry weight(g) |
|---|---|---|---|---|---|---|---|---|---|
| Moghan | 0 | 95$^{a}$ | 8.52$^{a}$ | 59.11$^{c}$ | 7.41$^{a}$ | 9.06$^{a}$ | 0.034$^{a}$ | 0.038$^{a}$ | 0.071$^{a}$ |
| | 2.5 | 88.6$^{b}$ | 7.88$^{ab}$ | 62.25$^{c}$ | 6.91$^{ab}$ | 8.31$^{ab}$ | 0.031$^{ab}$ | 0.035$^{a}$ | 0.069$^{ab}$ |
| | 5 | 61.5$^{c}$ | 5.23$^{b}$ | 72.29$^{b}$ | 4.83$^{b}$ | 6.3$^{b}$ | 0.23$^{b}$ | 0.025$^{b}$ | 0.047$^{b}$ |
| | 7.5 | 48.4$^{d}$ | 3.63$^{c}$ | 77.66$^{a}$ | 3.12$^{c}$ | 4.11$^{c}$ | 0.018$^{c}$ | 0.20$^{c}$ | 0.035$^{c}$ |
| Morvarid | 0 | 93.4$^{a}$ | 8 $^{a}$ | 60.23$^{c}$ | 7.10$^{a}$ | 8.93$^{a}$ | 0.031$^{a}$ | 0.036$^{a}$ | 0.069$^{a}$ |
| | 2.5 | 88.7$^{ab}$ | 7.63$^{a}$ | 63.41$^{c}$ | 6.12$^{a}$ | 7.40$^{ab}$ | 0.029$^{ab}$ | 0.033$^{a}$ | 0.067$^{ab}$ |
| | 5 | 58.9$^{b}$ | 4.83$^{b}$ | 76.81$^{b}$ | 4.10$^{b}$ | 5.97$^{b}$ | 0.020$^{b}$ | 0.023$^{b}$ | 0.043$^{b}$ |
| | 7.5 | 45.6$^{c}$ | 2.86$^{c}$ | 83.57$^{a}$ | 2.30$^{c}$ | 3.98$^{c}$ | 0.016$^{c}$ | 0.018$^{c}$ | 0.031$^{c}$ |
| Arta | 0 | 91.5$^{a}$ | 7.25$^{a}$ | 61.53$^{c}$ | 6.93$^{a}$ | 8.79$^{a}$ | 0.029$^{a}$ | 0.032$^{a}$ | 0.061$^{a}$ |
| | 2.5 | 89$^{ab}$ | 6.76$^{ab}$ | 64.28$^{c}$ | 5.98$^{a}$ | 7.11$^{ab}$ | 0.025$^{ab}$ | 0.028$^{ab}$ | 0.059$^{a}$ |
| | 5 | 42.3$^{b}$ | 4.32$^{b}$ | 82.43$^{b}$ | 3.88$^{b}$ | 4.84$^{b}$ | 0.019$^{b}$ | 0.019$^{b}$ | 0.034$^{b}$ |
| | 7.5 | 29.1$^{c}$ | 2.55$^{c}$ | 92.65$^{a}$ | 1.93$^{c}$ | 2.73$^{a}$ | 0.014$^{c}$ | 0.014$^{c}$ | 0.024$^{c}$ |
| Tajan | 0 | 91.5$^{a}$ | 7.36$^{a}$ | 63.17$^{c}$ | 7.30$^{a}$ | 8.13$^{a}$ | 0.029$^{a}$ | 0.033$^{a}$ | 0.063$^{a}$ |
| | 2.5 | 86.4$^{ab}$ | 6.82$^{ab}$ | 65.25$^{c}$ | 6.87$^{a}$ | 7.22$^{ab}$ | 0.0257$^{ab}$ | 0.029$^{a}$ | 0.061$^{a}$ |
| | 5 | 40.3$^{b}$ | 4.21$^{b}$ | 82.11$^{b}$ | 3.86$^{b}$ | 4.83$^{b}$ | 0.017$^{b}$ | 0.021$^{b}$ | 0.036$^{b}$ |
| | 7.5 | 27.1$^{c}$ | 2.18$^{c}$ | 91.87$^{a}$ | 1.79$^{a}$ | 2.81$^{c}$ | 0.013$^{c}$ | 0.016$^{c}$ | 0.026$^{c}$ |

* Means followed by same letter, in same column, do not differ through LSD test at 5% and 1% probability

Table4. Mean comparison for allelopathic effect of different concentrations of wild mustard shoot extract on germination components and seedling growth of wheat cultivars

| Seedling dry weight(g) | Shoot dry weight(g) | root dry weight(g) | Shoot length(cm) | Root length(cm) | D50 (h) | Germination rate (seed. day) | Germination percentage | Extract concentration (%) | Cultivars |
|---|---|---|---|---|---|---|---|---|---|
| | 0 | 95$^{a}$ | 7.42$^{a}$ | 62.11$^{c}$ | 12.18$^{a}$ | 9.02$^{a}$ | 0.033$^{a}$ | 0.037$^{a}$ | 0.072$^{a}$ |
| Moghan | 2.5 | 82$^{ab}$ | 6.98$^{ab}$ | 65.65$^{bc}$ | 11.69$^{ab}$ | 7.98$^{ab}$ | 0.029$^{ab}$ | 0.035$^{ab}$ | 0.067$^{ab}$ |
| | 5 | 56$^{b}$ | 4.11$^{b}$ | 77.41$^{b}$ | 7.12$^{b}$ | 5.63$^{b}$ | 0.017$^{b}$ | 0.025$^{b}$ | 0.040$^{b}$ |
| | 7.5 | 41$^{c}$ | 2.59$^{c}$ | 82.12$^{a}$ | 4.18$^{c}$ | 3.68$^{c}$ | 0.015$^{c}$ | 0.018$^{c}$ | 0.028$^{c}$ |
| | 0 | 95$^{a}$ | 7$^{a}$ | 61.52$^{c}$ | 11.89$^{a}$ | 8.92$^{a}$ | 0.032$^{a}$ | 0.036$^{a}$ | 0.071$^{a}$ |
| Morvarid | 2.5 | 80$^{ab}$ | 6.59$^{a}$ | 64.43$^{c}$ | 10.95$^{ab}$ | 7.12$^{ab}$ | 0.027$^{ab}$ | 0.033$^{ab}$ | 0.062$^{ab}$ |
| | 5 | 53$^{b}$ | 3.73$^{b}$ | 80.15$^{b}$ | 6.41$^{b}$ | 5.16$^{b}$ | 0.017$^{b}$ | 0.023$^{b}$ | 0.037$^{b}$ |
| | 7.5 | 37$^{c}$ | 1.83$^{c}$ | 89.63$^{b}$ | 3.91$^{c}$ | 3.15$^{c}$ | 0.014$^{c}$ | 0.017$^{c}$ | 0.026$^{c}$ |
| | 0 | 93$^{a}$ | 6.23$^{a}$ | 64.12$^{c}$ | 10.78$^{a}$ | 8.89$^{a}$ | 0.028$^{a}$ | 0.032$^{a}$ | 0.060$^{a}$ |
| Arta | 2.5 | 75$^{ab}$ | 5.74$^{ab}$ | 67.27$^{c}$ | 9.11$^{ab}$ | 6.13$^{ab}$ | 0.023$^{ab}$ | 0.028$^{ab}$ | 0.055$^{ab}$ |
| | 5 | 37$^{b}$ | 3.21$^{b}$ | 92.21$^{b}$ | 5.43$^{b}$ | 4.14$^{b}$ | 0.014$^{b}$ | 0.019$^{b}$ | 0.029$^{b}$ |
| | 7.5 | 20$^{c}$ | 1.52$^{c}$ | 102.14$^{a}$ | 3.12$^{c}$ | 2.22$^{c}$ | 0.010$^{c}$ | 0.014$^{c}$ | 0.019$^{c}$ |
| | 0 | 94$^{a}$ | 6.33$^{a}$ | 63.17$^{c}$ | 10.71$^{a}$ | 8.18$^{a}$ | 0.026$^{a}$ | 0.030 | 0.061$^{a}$ |
| Tajan | 2.5 | 79$^{ab}$ | 5.79$^{ab}$ | 66.21$^{c}$ | 9.21$^{ab}$ | 6.94$^{ab}$ | 0.024$^{ab}$ | 0.026$^{ab}$ | 0.057$^{ab}$ |
| | 5 | 39$^{c}$ | 3.11$^{b}$ | 92.25$^{b}$ | 5.01$^{b}$ | 4.34$^{b}$ | 0.016$^{b}$ | 0.021$^{b}$ | 0.027$^{b}$ |
| | 7.5 | 22$^{d}$ | 1.15$^{c}$ | 103.7$^{a}$ | 2.75$^{c}$ | 2.25$^{c}$ | 0.010$^{c}$ | 0.012$^{c}$ | 0.029$^{c}$ |

* Means followed by same letter, in same column, do not differ through LSD test at 5% and 1% probability.

Table5. Parameters and the logistic equation coefficients for prediction of seeds germination percentage

| Cultivar | a ± se | b ± se | $X_{50}$ ± se | robability level | $R^2$ |
|---|---|---|---|---|---|
| Moghan | 2.15 ±92.23 | 0.045±2.53 | 0.128± 5.014 | 0.0089 | 0.92 |
| Morvarid | 2.24 ±90.31 | 2.24±3.31 | 0.117± 4.92 | 0.0001 | 0.96 |
| Arta | 2.392±85.64 | 0.0292±6.60 | 0.049± 4.63 | 0.0001 | 0.87 |
| Tajan | 0.017±79.1 | 0.017±5.66 | 0.042±4.57 | 0.0001 | 0.85 |

of wheat cultivars in different concentrations of shoot extract of wild mustard

Table6. Parameters and the logistic equation coefficients for prediction of seeds germination percentage

| Cultivar | a ± se | b ± se | $X_{50}$ ± se | robability level | $R^2$ |
|---|---|---|---|---|---|
| Moghan | 2.65± 97.23 | 0.0145±2.84 | 0.341±5.024 | 0.0091 | 0.88 |
| Morvarid | 1.89± 92.41 | 0.0124±3.19 | 0.213± 4.29 | 0.0001 | 0.92 |
| Arta | 2.31±89.24 | 0.0262 ±6.20 | 0.051±4.495 | 0.0001 | 0.97 |
| Tajan | 3.63± 84 | 0.22± 5.11 | 0.042±4.43 | 0.0001 | 0.92 |

of wheat cultivars in different concentrations of root extract of wild mustard

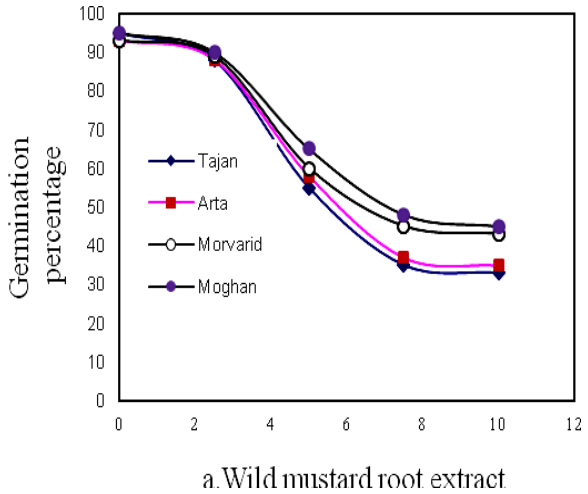

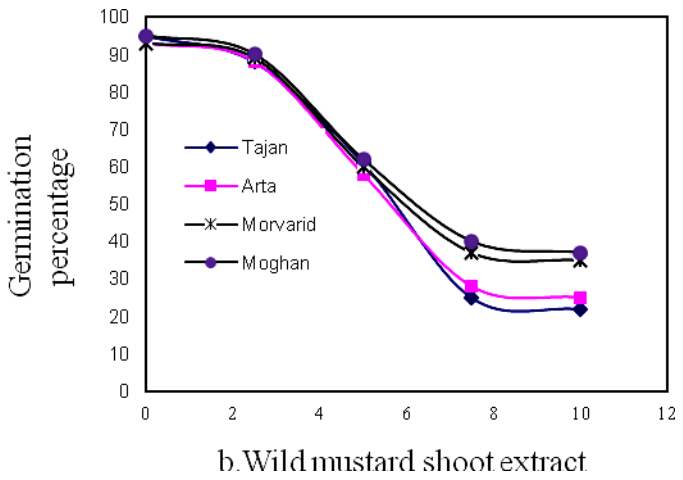


Figure1. The final germination percentage of wheat cultivars affected by different concentrations of root (a) and shoot (b) water extract of wild mustard

**References:**

[1] **Berenji, S., Asghari, B.J., and Matin, A.A. 2008.** Allelopathic potential of rice (Oryza sativa) varieties on seedling growth of barnyardgrass (*Echinochloa crus- galli*). J. Plant Interaction. 3: 175–180.

[2] **Bais, H.P., Vepachedu, R., Gilroy, S., Ragan, M., and Vivanco, M. 2003.** Allelopathy and exotic plant invasion, from molecules and genes to species interactions. Science, 31,1377-1380.

[3] **Chauhan, B.S., Gill, G., and Preston, C. 2006.** Factors affecting seed germination of annual sowthistle (*Sonchus oleraceus*) in southern Australia. Weed Sci. 54:854-860.

[4] **Chung, I.M., Kim, J., and Kim, S. 2006.** Evaluation of allelopathic potential and quantification of momilactone A, B from rice hull extracts and assessment of inhibitory bioactivity on paddy field weeds. J. Agric. Food Chem. 54: 25272536.

[5] **FAO. 2010.** The Lurking menace of weeds. Available at: http://www.fao.org/news /story/en/item/29402/icode/. 30.

[6] **Ghahreman, A. 1994.** Plant systematics. Chromophytes of Iran. (In Persian). Tehran University Press. Tehran. 2: 562 p.

[7] **Hartmann, H., Kester, D., and Davis, F. 1990.** Plant propagation, principle and practices. Hall Imitational Editions. 647p.

[8] **Ismail, B.S., and T.V. Chong. 2002.** Effect of aqueous extract and decomposition of mikania micrantha on selected agronomic crop weed Biol. Manage. 2:31-38.

[9] **Johanson, H., J. Ascard and W. Oleszek. 2006.** Brassicaceae as alternative plants for weed control in sustainable agriculture. In Allelopathy in pests management for sustainable agriculture. Eds. S.S. Narwal and P. Tauro. Scientific publishers, India. pp. 3-22.

[10] **Kato-Noguchi, H. 2004.** Allelopathic substance in rice root exudates: Rediscovery of momilactone B as an allelochemical. J. Plant Physiol. 161: 271-276.

[11] **Muller, C. H. 2002.** Allelopathy as a factor in ecological process. Vegetatio, 18: 348-357.

[12] **Mason-Sedun, W., R. S. Jessop and J. V. Lovett. 2005.** Differential phytotoxicity among species and cultivars of the genus brassica to wheat. I. Laboratory and field screening of species. Plant and Soil, 93: 3-16.

[13] **Mighani, F. 2003.** Allelopathy, concepts and aplications, Parto Vaghe Press. 256p.

[14] **Qasem, J.R. 2001.** Allelopathic Potential of White top and Syrian sage on Vegetable Crops. Agron. J. 93: 64-71.

[15] **Rice, E. L., 2002.** Allelopathy. 2nd ed. Academic press. Orlando, FL.

[16] **Rizvi, S. J. H., V. Rizvi, M. Tahir, M. H. Rahimian, P. Shimi and A. Atri, 2000.** Genetic variation in allelopathic activity of wheat (*Triticum aestivum* L.) genotypes. Wheat Information Service. Number 91: 25-29.

[17] **Sisodia, S., Siddiqui M.B. (2010).** Allelopathic effect by aqueous extracts of different parts of *Croton bonplandianum* Baill. on some crop and weed plants. J. Agri. Extension Rural Dev. 2, 22-28.

[18] **Tawaha, A. M. and Turk, M. A. 2003.** Allelopathic effects of black mustard (*Brassica nigra*) on germination and growth of wild barley (*Hordeum spontaneum*). Journal of Agronomy and Crop Science 189: 298-303.

[19] **Turk, M. A. and A. M. Tawaha, 2002;** Inhibitory effects of aqueous extracts of black mustard on germination and growth of lentil. Pak. J. Agri., 1: 28-30.

[20] **Vicol, A., Dobrota, C., 2008.** Lettuce, lambsquarters and country mallow callus culture bioassays in the study of allelopathy. Stud. Univ. Babes- Bolyai Bilo. 39(1): 69-73.

[21] **Warwick, S. I., H. J. Beckie, A. G. Thomas and T. Mcdonald. 2005**. The biology of canadian weeds. 8. *sinapis arvensis*. L. (updated). Canadian Journal of Plant Science, 55: 171-183.

[22] **Wall, D. A., G. H. Friesen and T. K. Bhati. 2006.** Wild mustard interference in traditional and semi-leafless field peas. Canadian Journal of Plant Science, 71: 473-480.

[23] **Yurchak, L .D., Uteush, Y.A., Omelchenko, T. V., 2005.** Microflora and specific allelopathic properties of fodder plants from the crocifera family in plant-microorganism interaction in phytocoenoses. Naukova Dumk. Kive, pp:161-168.

[24] **Zeinali, E., and Ehteshami, S. M. R. 2003.** Biology and Control of Important Weed Species. Gorgan University of Agricultural Sciences and Natural Resources Press, Iran, 412p.

# Preparation of $ZnFe_2O_4$ nanoparticles using honey and its use as catalyst for the synthesis of 3-amino-4-cyano-5-phenyl-1*H*-pyrrole-2-carboxamides

**Bagher Mohammadi*, Negin Shojaei, Hamid Saeidian**

*Department of Chemistry, Payame Noor University, P. O. Box 19395-3697, Tehran, Iran*

*Corresponding author Tel.: +98 (912) 5424292; Fax number: +98 (243) 5524028

*E-mail: bagher.mohammadi@yahoo.com

**Abstract**

This work described a green and useful method for the preparation of $ZnFe_2O_4$ nanoparticles using honey. This nano particles used as an efficient nanocatalyst for the synthesis of 3-amino-4-cyano-5-phenyl-1*H*-pyrrole-2-carboxamides. The synthesis was carried out *via* a simple three-component reaction between arylidenmalononitrile, malononitrile and hydroxylamine hydrochloride in the precense of nano $ZnFe_2O_4$ in solvent-free conditions. Eco-friendness method, short reaction times, excellent yields of products, inexpensive and readily available starting material, and time and energy saving are the main advantages of this method.

**Keywords**: Nano $ZnFe_2O_4$, . Pyrrole, Honey, Solvent-free.

## Introduction

Magnetic nanoparticles (MNPs) for example zinc ferrite magnetic nanoparticles could catalyze organic reactions in a mild and environment friendly manner. Furthermore these catalysts have many advantages such as use of minimum amount of reagent and energy, high yield of products easy reaction, simple work-up procedure and minimize byproduct, efficiency and recyclability are the main advantages of these catalysts. In recent decades there have been reported many papers regarding use of Magnetic nanoparticles in organic synthesis due to its low cost and efficacy [1-3].

Pyrroles, an important class of heterocyclic compounds, are of both natural and biological interest. They are part of a large number of highly significant natural products such as vitamin B12, chlorophyll, heme, Lamellarins, Pyrrolnitrin, dispacamide, oroidin, massadine and many others. Most of these compounds exhibit a biological activity, such as antitumor, antibacterial, anticancer, anti-HIV, antibiotic, anti-inflammatory, and antioxidant activities. They have been also used as estrogen receptor beta selective ligands [4-6].

As part of our current studies on efficient methods to prepare organic compounds from simple and readily available building blocks, herein we report a simple and efficient strategy for the synthesis of 3-amino-4-cyano-5-phenyl-1H-pyrrole-2-carboxamides *via* an unprecedented one-pot three-component reaction between arylidenmalononitrile, malononitrile and hydroxylamine hydrochloride in the presence of nano $ZnFe_2O_4$.and solvent-free conditions (Scheme 1).

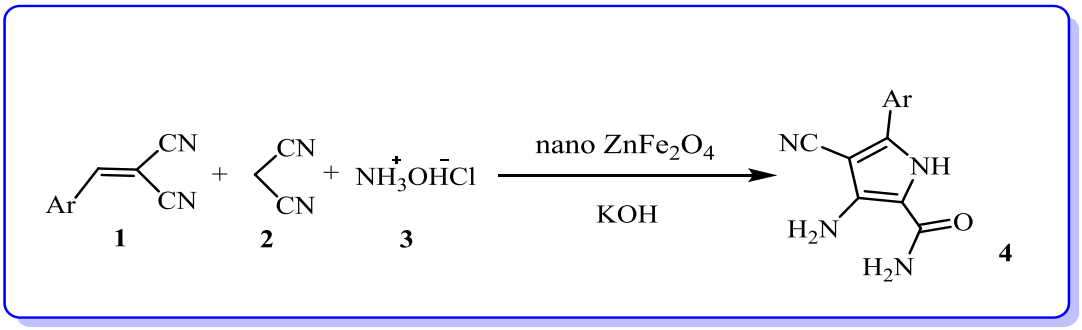


**Scheme 1.** Three-component synthesis of 3-amino-4-cyano-5-phenyl-1*H*-pyrrole-2-carboxamides **4** using nano $ZnFe_2O_4$.

## Experimental

*General*

All chemicals used in this study were purchased from Merck and used without further purification. Melting points were determined with an Electrothermal melting point apparatus and they are uncorrected. Infrared (IR) spectra were recorded with a Shimadzu 8400s FT-IR spectrometer using potassium bromide pellets. $^1$HNMR spectra (300 MHz) were recorded on a DRX-300 Advance Bruker spectrometer. The chemical shifts are reported in ppm ($\delta$-scale) relative to internal TMS and coupling constants are reported in DMSO-*d6*. Thin layer chromatography (TLC) was performed using 60 mesh silica gel plates visualized with short-wavelength UV light.

*Nano catalyst preparation*

In a typical synthesis, 4.16 g $Zn(NO_3)_2.6H_2O$ and 11.6 g $Fe(NO_3)_3.9H_2O$ were dissolved in 150 ml deionized water to obtain a mixed solution. The molar ratio of $Zn(NO_3)_2.6H_2O$ to $Fe(NO_3)_3.9H_2O$ was 1:2. An aqueous solution (150 ml) of 10 g honey was mixed with the metal-nitrate solution. The mixed solution was placed on a hot plate with continuous stirring at 100 $^oC$. During evaporation, the solution formed a very viscous gel, which is one of the roles of honey in this synthesis protocol. Then the gel was heated to 350 $^oC$ to initiate a self-sustaining combustion reaction and produce as-burnt ferrite powder. To confirm nano-$ZnFe_2O_4$ the SEM image of $ZnFe_2O_4$ magnetic nanoparticles was carried out in Figures 1.

***General procedure for the synthesis of 3-amino-4-cyano-5-phenyl-1H-pyrrole-2-carboxamide 4a***

The reaction was carried out by first mixing benzylidenmalononitrile **1a** (1 mmol), malononitrile **2** (1 mmol), hydroxylamine hydrochloride (1 mmol), saturated potassium hydroxide (0.1 ml) and nano $ZnFe_2O_4$ (0.17 mmol) in a 5 ml vial without any solvent. Then the reaction mixture was stirred at room temperature for 5 minutes. The TLC monitoring of the reaction mixture clearly indicated formation of 3-amino-4-cyano-5-phenyl-1*H*-pyrrole-2-carboxamide **4a** in excellent yield. Afterward the product was separated and purified by a silica gel column chromatography with ethyl acetate as eluent. The **4a** product was recrystallized as dark brown crystals from methanol.

.

***3-amino-4-cyano-5-phenyl-1H-pyrrole-2-carboxamide, (4a, $C_{12}H_{10}N_4O$)***

dark brown crystals; yield: 78 %; IR (KBr): 3455 (s), 3326 (m), 3281 (w), 3227 (s), 2268 (w), 2211 (s), 1678 (s), 1608 (s), 1450 (w), 1408 (m), 776 (m), 698 (m) and 530 $cm^{-1}$ (m); $^1H$ NMR (299.9 MHz, DMSO-$d_6$, 25°C, TMS): δ=5.73 (s, 2H; $NH_2$), 7.07 (s, 2H; $H_2NCO$), 7.48 (m, 3H, 3CH), 7.73 (d, *J*=7.2 Hz, 2H, 2CH), 11.32 ppm (br. s, 1H; NH); $^{13}C$ NMR (62.9 MHz, DMSO-$d_6$, 25°C, TMS): δ=80.45 (CCN), 107.94 (CN), 116.66(CCO), 126.42, 129.64 and 129.75 (5CH), 136.98 (CNH), 145.11 ($CNH_2$), 163.40 ppm (CO).

**Results and discussion**

Arylidenmalononitrile, malononitrile and hydroxylamine hydrochloride in the presence of $ZnFe_2O_4$ magnetic nano particles, produced 3-amino-4-cyano-5-phenyl-1*H*-pyrrole-2-carboxamides **4** in good to excellent yields (Table 1).

spectrum of **4c** showed absorption bands at 3458, 3333 and 3221 $cm^{-1}$ due to the presence of two $NH_2$ groups. The bands at 2215 $cm^{-1}$ indicated the presence of nitrile (CN) group. The band at 1661 $cm^{-1}$ was due to the presence of an amido group. $^1H$ NMR spectrum of **4c** exhibited a sharp singlet at 3.80 ppm due to the $OCH_3$ group and two broad singlets at 5.71 and 7.02 ppm indicated the presence of two $NH_2$ groups, along with two doublets with appropriate chemical shifts and coupling constants for the 4 aromatic H atoms. A distinct singlet at 11.22 ppm showed presence of NH group. The $^1H$-decoupled $^{13}C$ NMR spectrum of **4c** showed characteristic signal at 55.84 ppm due to the $OCH_3$ group. The signal at 107.29 ppm was due to the nitrile group and the signal at 163.41 ppm indicated the presence of an amido group. The other eight distinct resonances for 4CH and 4C were also in agreement with the expected structure.

To optimize this reaction, the **4a** preparation was selected as a model, and then the effects of nano-$ZnFe_2O_4$ amounts to the reaction yields were tested. The results of these experiments were displayed in Table 2. All of these tests were done in room temperature. As can be seen from Table 2, the highest yield was obtained in the presence of 17 mol% of nano-$ZnFe_2O_4$.

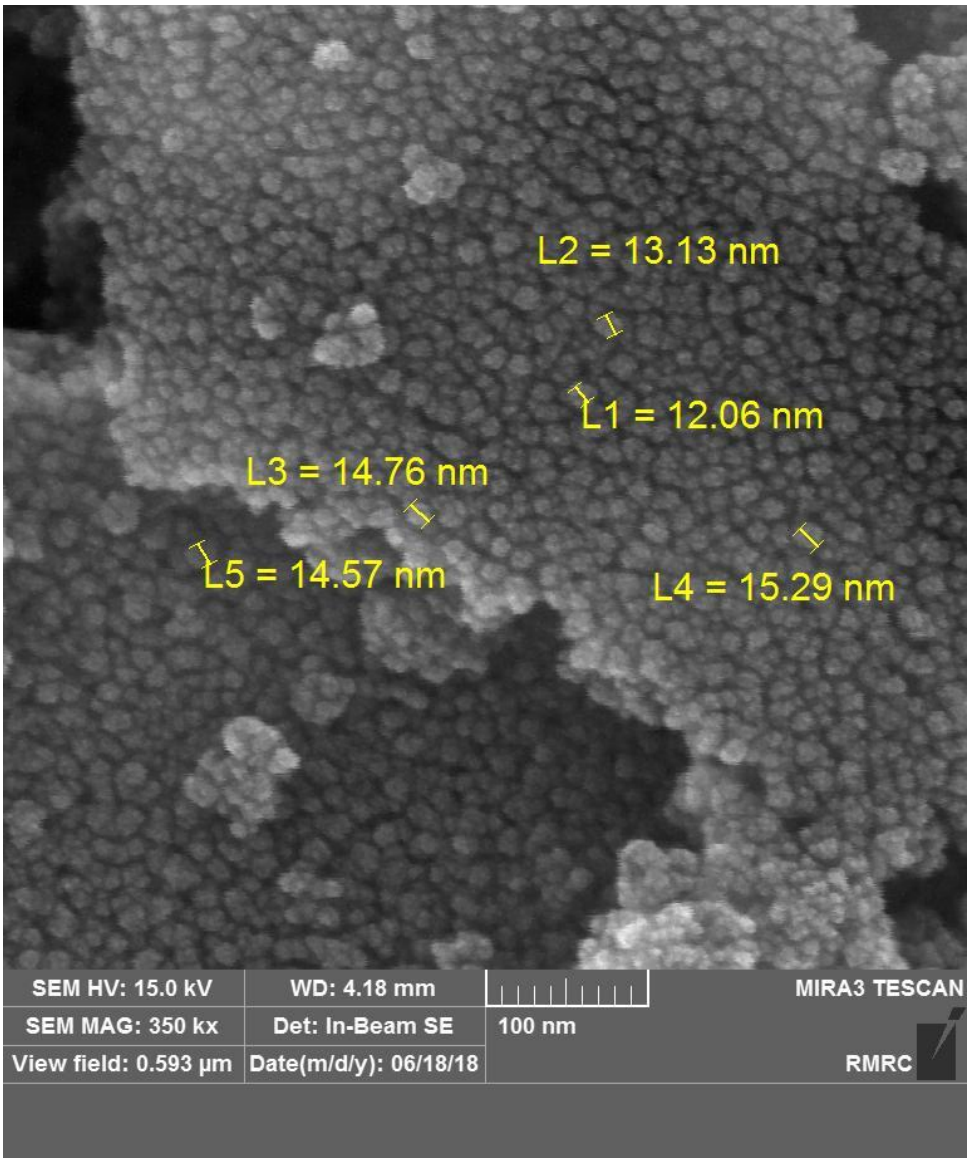


**Figure1.** SEM image of $ZnFe_2O_4$ magnetic nanoparticles. The average nano particle size is 14 nm.

**Table 1**. Solvent free synthesis of -amino-4-cyano-5-phenyl-1*H*-pyrrole-2-carboxamides **4a-d.**

| Entry | Ar | Yield[a] (%) | M.p. °C |
|---|---|---|---|
| a | Ph | 90 | 230-232 |
| b | 4-MePh | 85 | 245-247 |
| c | 4-OMePh | 87 | 238-240 |
| d | 3-MePh | 92 | 240-243 |

[a]Isolated yield.

**Table 2.** Synthesis of **4a** in the presence of various amount of nano-$ZnFe_2O_4$

| Entry | Catalyst Amount (mol%) | Time (min) | Yield[a] (%) |
|---|---|---|---|
| **1** | 0 | 5 | 22 |
| **2** | 2 | 5 | 38 |
| **3** | 5 | 5 | 45 |
| **4** | 8 | 5 | 60 |
| **5** | 11 | 5 | 75 |
| **6** | 14 | 5 | 82 |
| **7** | 17 | 5 | 90 |
| **8** | 20 | 5 | 90 |

[a]Isolated yield.

## Conclusion

In conclusion, we have developed a green, efficient and easy reaction for the synthesis of nano $ZnFe_2O_4$ and then 3-amino-4-cyano-5-phenyl-1*H*-pyrrole-2-carboxamides **4** *via* one pot three-component reaction method. The reaction is characterized by high yields of products, use of simple and available starting materials, high atom economy, eco-friendliness and mild reaction conditions.

## Acknowledgments

We gratefully acknowledge the financial support from the Research Council of Payame Noor University

## References

[1] S. V. Jadhav, K. M. Jinka and H. C. Bajaj *Catal. Today*, **2012**, *198*, 98.

[2] A. S. Singh, U. B. Patil and, J. M. Nagarkar, *Catal. Commun.*, **2013**, *35*,11.

[3] A. S. Singh, S. S. Shendage and J. M. Nagarkar, *Tetrahedron Lett*. **2013**, *54*,6319.

[4] I. S. Young, P. D. Thornton and A. Thompson, *Natural product reports*, **2010**, *27*, 1801.

[5] Nishio, Y.; Uchiyama, K.; Kito, M.; Nakahira, H. *Tetrahedron***2011**, *67*, 3124.

[6] Xu, Y.; Liu, X.-H.; Saunders, M.; Pearce, S.; Foulks, J. M.; Parnell, K. M.; Clifford, A.; Nix, R. N.; Bullough, J.; Hendrickson, T. F. *Bioorganic & medicinal chemistry letters***2014**, *24*, 515

## Graphical Abstract

Preparation of $ZnFe_2O_4$ nanoparticles using honey and its use as catalyst for the synthesis of 3-amino-4-cyano-5-phenyl-1*H*-pyrrole-2-carboxamides

Bagher Mohammadi,*, Negin Shojaeic

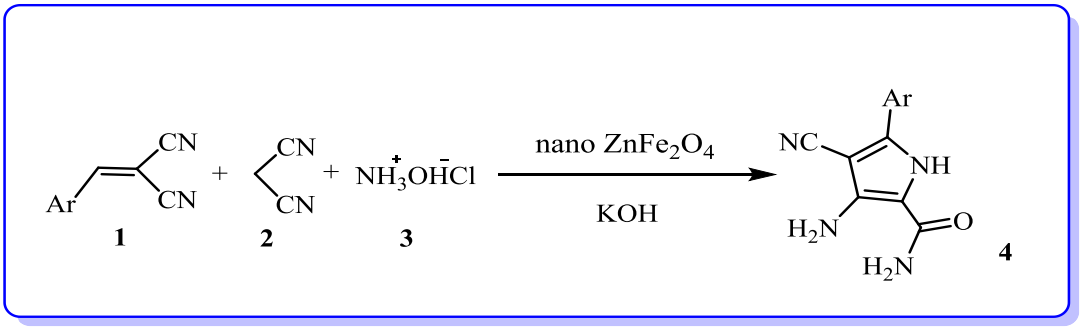

# Synthesis of a novel inorganic–organic hybrid nanocomposite, $(Bu_4N)_7H_3[P_2W_{18}Cd_4(Br)_2O_{68}]@TiO_2$, as a novel nano mercaptan scavenger in gasoline

**Masomeh Aghmasheh**[a], **Mohammad Ali Rezvani**[b,*]

[a] *Department of Chemistry, University of Zanjan, 19395-4697 Zanjan, Iran*

[b]*Department of Chemistry, Faculty of Science, University of Zanjan, 451561319, Zanjan, Iran*

*Corresponding author Tel.: +98 241 5152477; Fax number: +98241 5152617

*E-mail: marezvani@znu.ac.ir

**Abstract**

To preparation of clean gasoline fuel a novel inorganic–organic hybrid nanocomposite, $(Bu_4N)_7H_3[P_2W_{18}Cd_4O_{68}]@TiO_2$ was synthesized by supported sandwich-type polyoxometalate (STPOM) on $TiO_2$. $(Bu_4N)_7H_3[P_2W_{18}Cd_4O_{68}]@TiO_2$ nanocomposite has been synthesized by an unusual reaction of A-β-$Na_8HPW_9O_{34}$ with cadmium nitrate and titanium tetraisopropoxide.
The $(Bu_4N)_7H_3[P_2W_{18}Cd_4O_{68}]@TiO_2$ was exploited as a heterogeneous nanocatalyst for deep oxidative desulfurization (ODS) of gasoline and model oil. High desulfurization efficiency was achieved using hydrogen peroxide/acetic acid ($H_2O_2$/AcOH) as an oxidant at 35 °C after 60 min. On the basis of the suggested ODS system, the mercaptan and sulfur content of gasoline could be removed with 97% and 98% yield, respectively. The obtained results show that this sandwich-type nanocomposite be able to scavenge hydrogen sulfide and mercaptans with high yield. This system provides an efficient, convenient and practical method for scavenging of sulfur compound. Using toluene solutions of the model compounds, experiments were carried out to compare the reactivity of the different benzothiophenes in oxidation reactions, a key step for oxidative desulphurization.

**Keywords**: Oxidative desulphurization; Heteropolyacids; Nanocomposite; Scavenger; Mercaptan.

## Introduction

Heteropolyacids (HPAs) and their metal-substitute derivatives as versatile and efficient solid acid catalysts have been employed admirably in the acid-catalyzed reactions and desulfurization processes. The catalysts based on heteropolyacids (HPAs) have many advantages over liquid acid catalysts. They are not corrosive and environmentally benign, presenting fewer disposal problems [1]. Solid heteropolyacids have attracted much attention in organic synthesis owing to easy workup procedures, easy filtration, and minimization of cost and waste generation due to reuse and recycling of the catalysts [2]. Recently, supported heteropolyanions have been synthesized and applied as effective catalyst in organic reactions [3-6]. Supporting the heteropolyacids on solids with high surface areas improve their catalytic performance in various liquid–solid and gas–solid surface heterogeneous reactions [7-9]. The global economy requires fossil-derived fuels to function, from the generation of electrical power to transportation [10]. Liquid fuels contain a large variety of sulfur-containing impurities (e.g. mercaptans, sulfides, disulfides, thiophenes and its derivatives). The presence of organosulfur compounds in gasoline and diesel are found undesirable due to the emission of sulfur oxides during the combustion, which led to air pollution and acid rain [10-12]. Despite the increasing worldwide attention to environmental protection standards, sulfur molecules must be removed from fuels prior to their release into the atmosphere [7]. Hydrodesulfurization (HDS) is an industrial refining process, which can reduce the OSCs levels by hydrogenolysis at high temperature (300–400 °C) and high pressure (10–130

world population and rapid industrial development has increased the consumption of fossil fuel-derived oils. Deep desulfurization of transportation fuels has become an important research subject due to the increasingly stringent regulations and fuel specifications in many countries for environmental protection purpose [8]. Conventional hydrodesulphurization (HDS) process is difficult to remove alkyl substituted dibenzothiophenes like 4, 6-dimethyldibenzothiophene, which are refractive to HDS due to steric hindrance. In order to produce ultralow sulfur diesel fuel with HDS process, higher temperature, higher pressure, larger reactor volume, and more active catalysts are required [9]. In addition, the severe conditions lead to negative effects, such as the decrease of catalyst life, higher hydrogen consumption, and higher yield losses resulting in higher costs. Therefore, alternative desulfurization techniques have been investigated widely, among which oxidative desulfurization (ODS) is considered to be one of the promising new methods for super deep desulfurization of fuel oil [11]. In the ODS process, the refractory dibenzothiophene (DBT) and benzothiophene (BT) are oxidized to their corresponding sulfones under mild conditions, which are subsequently removed by extraction, adsorption, distillation, or decomposition [8-12]. Various oxidants have been used in ODS, among these oxidants, H2O2 is mostly chosen as an oxidant, only producing water as a byproduct [12-14]. Peracids produced in situ from organic acids catalysts and H2O2 are reported to be very effective for rapid oxidation of sulfur compounds in fuel oils under mild conditions. Scheme 1 illustrates a probable pathway for the oxidation reaction of BT to benzothiophene sulfone in the emulsion system.

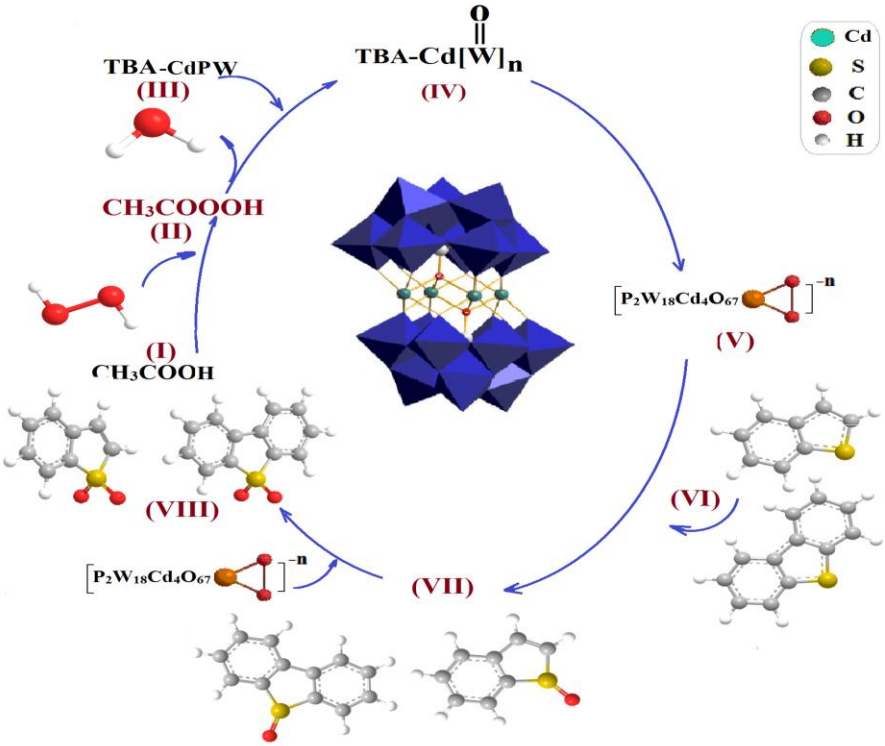


Scheme 1. The oxidation of model oil

## Experimental

*General*

All reagents and solvents used in this work are available commercially and were used as received, unless otherwise indicated. Model compounds and chemicals, including thiophene (Th), benzothiophene (BT), dibenzothiophene (DBT), 4-methyldibenzothiophene (4-MDBT), and 4,6-dimethyldibenzothiophene (4,6-MDBT), solvent (toluene) for experiments and analysis and hydrogen peroxide (30 vol%) were obtained from Aldrich Chemical Company. All NMR spectra were recorded on a Bruker BRX 500 AVANCE spectrometer. IR spectra were recorded on a Buck 500 Scientific Spectrometer (KBr Pellets). The sulfur content of original and treated oils was determined an X-ray fluorescence spectrometer (ASTM D4294). The test method is based on the ASTM D-4229 standards.

***Preparation of $(Bu_4N)_7H_3P_2W_{18}Cd_4O_{68}$***

1.0 g (0.35 mmol) of A-$PW_9$ in small portions was added to a stirred solution of 0.216 g (0.7 mmol) of $Cd(NO_3)_2.H_2O$ in 8 mL $H_2O$ (pH adjusted to 6 by HOAc). The solution was put into reactor vessel carefully. It is placed under microwave irradiation at 1000 watt for 5 min. This work keeps on for 6 times. It was necessary to recommend that each time; we repeated it was necessary to stir the solution vigorous magnetically. The solution cooled to room temperature. Potassium chloride (1.2 g) was added to the solution and the mixture was stirred for 15 min and filtered. This solid was recrystallized from 20 mL of hot water and dried under vacuum.

***Preparation of (Bu4N)7H3P2W18Cd4O68@TiO2 nanocatalyst***

In 10 mL of glacial acetic acid was added 0.5 g of titanium tetraisopropoxide with vigorous stirring. A solution of 0.3 g of $(Bu_4N)_7H_3P_2W_{18}Cd_4O_{68}$ in 5 mL of distillated water was drop wised in it. The mixture was stirred to dissolve any solid. Then, the sol was heated to 100 °C under oil bath condition until a homogenous $(Bu_4N)_7H_3P_2W_{18}Cd_4O_{68}@TiO_2$ hydrogel was formed. Finally, the gel was filtered, washed with deionized water–acetone and dried in oven at 50 °C overnight

***ODS process of model oil***

The experiment was conducted in a closed round-bottom flask which equipped with a magnetic stirrer and thermometer. Initially, a certain amount of thiophenic sulfur compounds, including BT, and DBT were dissolved in *n*-heptane with a corresponding sulfur content of 500 ppmw (parts per million by weight). The water bath was heated to the temperature of 25, 30, 35, and 40 °C in separate ODS runs. Afterward, 50 mL of prepared model oil was poured into the flask and heated to the reaction temperature under stirring conditions. The appropriate amount of (Bu4N)7H3P2W18Cd4O68@TiO2 nanocatalyst from 0.02 to 0.12 g was suspended in the mixture. The progress of the ODS was followed by the addition of 3 mL of H2O2/AcOH in the volume ratio of 1:1 to the reaction vessel. The treatment process was continued under vigorous magnetic stirring (600 rpm) for 5-60 min. After each oxidation step, the treated model oil was cooled to room temperature and 10 mL of MeCN extraction solvent was added to extract the oxidized thiophenic sulfur compounds from oil phase to the aqueous phase. The separation funnel was used for separation of the formed immiscible liquids. Finally, the synthesized heterogeneous $(Bu_4N)_7H_3P_2W_{18}Cd_4O_{68}@TiO_2$ nanocatalyst was separated from reaction system using simple filtration. The concentration of total sulfur after ODS process was determined via XRF spectrometer according to ASTM D-

4294 and D-3227. The removal efficiency of thiophenic sulfur compounds was calculated using Eq. (1), in which $T_i$ is the initial concentration and $T_f$ is the final concentration of thiophenic sulfur compounds in *n*-heptane phase after oxidation treatment.

$$\text{TSCs removal efficiency } (\%) = \left[1 - \frac{T_f}{T_i}\right] \times 100 \quad (1)$$

***ODS process of real gasoline***

The general procedure of ODS of real gasoline was carried out in the same manner as the ODS of model oil. The experiment was performed in a round-bottom flask coupled in a temperature-controlled water bath. Briefly, 50 mL of gasoline was heated to 35 °C. Then, 3 mL of $H_2O_2$/AcOH and 0.1 g of $(Bu_4N)_7H_3P_2W_{18}Cd_4O_{68}$@$TiO_2$ nanocatalyst were added to the flask. The reaction proceeded under vigorous stirring (600 rpm) at 35 °C for 60 min. The mixture was cooled to the room temperature and 10 mL of MeCN added to it. The oil phase was separated by decantation and analyzed using XRF method. The removal efficiency of the sulfur content of gasoline was expressed by Eq. (2), in which $S_i$ is the initial concentration and $S_f$ is the final concentration of sulfur content in gasoline after ODS.

$$\text{sulfur removal efficiency } (\%) = \left[1 - \frac{S_f}{S_i}\right] \times 100 \quad (2)$$

**Result and discussion**

XRD patterns of $TiO_2$, $(Bu_4N)_7H_3P_2W_{18}Cd_4O_{68}$ and $(Bu_4N)_7H_3P_2W_{18}Cd_4O_{68}$@$TiO_2$ are shown in Figure 1. XRD patterns (a) and (c) in Figure 1 are corresponded to pristine $TiO_2$ and $(Bu_4N)_7H_3P_2W_{18}Cd_4O_{68}$@$TiO_2$, respectively. The XRD pattern corresponding to pure $TiO_2$ was found to match with that of fully anatase phase. No peaks from any else impurities or rutile phase were observed, which indicates the high purity of the obtained powders.

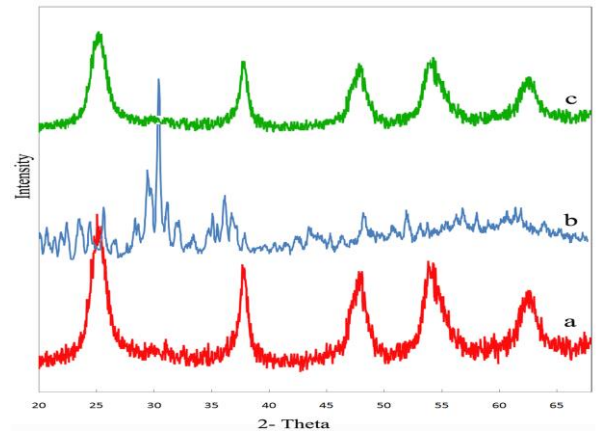


**Figure 1.** XRD pattern of (a) $TiO_2$ (b) $(Bu_4N)_7H_3P_2W_{18}Cd_4O_{68}$ and (c) $(Bu_4N)_7H_3P_2W_{18}Cd_4O_{68}$@$TiO_2$.

The sharp diffraction peaks manifest that the obtained $TiO_2$ have high crystallinity. When $Bu_4N)_7H_3P_2W_{18}Cd_4O_{68}$ is bound to the $TiO_2$ surface, $(Bu_4N)_7H_3P_2W_{18}Cd_4O_{68}$@$TiO_2$), all of signals corresponding to $Bu_4N)_7H_3P_2W_{18}Cd_4O_{68}$ is disappeared and the final pattern matched to fully anatase phase of $TiO_2$ (JCPDS No. 21-1272), which is most likely due to $Bu_4N)_7H_3P_2W_{18}Cd_4O_{68}$ forming only a thin coating on the $TiO_2$ surface and thus the majority of the observed signals are due to the crystal phases of anatase $TiO_2$. Using the Scherrer equation, the crystallite diameter of $Bu_4N)_7H_3P_2W_{18}Cd_4O_{68}$@$TiO_2$ is about 10 nm.

UV-vis spectra of $TiO_2$, $Bu_4N)_7H_3P_2W_{18}Cd_4O_{68}$ and $Bu_4N)_7H_3P_2W_{18}Cd_4O_{68}$@$TiO_2$ nanocomposite are shown in Figure 3. In

ultraviolet light regions, which are shorter than 350 nm, pure nano $TiO_2$ whose band gap energy equivalent to around 330nm (3.70 eV) shows the highest absorbance due to charge-transfer from the valence band (mainly formed by 2p orbitals of the oxide anions) to the conduction band (mainly formed by 3d $t_2g$ orbitals of the $Ti^{4+}$ cations) [9]. The CTA-POM-$TiO_2$ nanocomposite shows a red shift compared with the parent anatase, and a blue shift compared with CTA-POM. In addition, some hyper fine structure in the range from 310 to 350 nm observed in CTA-POM spectrum. The inset of the figure shows the UV-vis spectrum of the CTA-POM-$TiO_2$ indicating there are two peaks around 220 and 290 nm. The above UV–vis results indicate that introduction of CTA-POM into $TiO_2$ framework has an influence on coordination environment of $TiO_2$ crystalline [20].

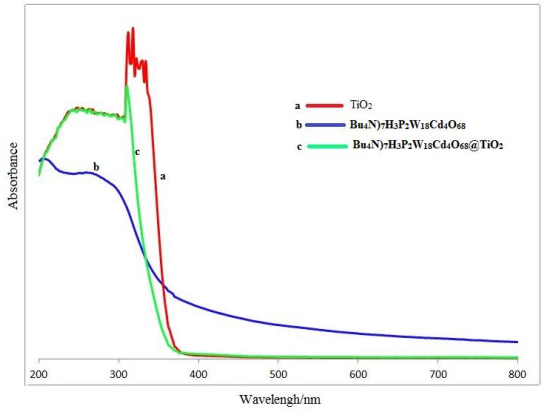


**Figure 2.** UV-vis spectra of (a) $TiO_2$ (b) $(Bu_4N)_7H_3P_2W_{18}Cd_4O_{68}$ and (c) $(Bu_4N)_7H_3P_2W_{18}Cd_4O_{68}@TiO_2$.

IR spectrum of the prepared catalyst in the range 700–1100 $cm^{-1}$ showed absorption bands at 1052, 984, 879 and 763 $cm^{-1}$, corresponding to the four typical skeletal vibrations of the Keggin polyoxoanions, which indicated that $(Bu_4N)_7H_3P_2W_{18}Cd_4O_{68}$ has been supported on $TiO_2$ (Fig. 3). These peaks could be attributed to ν(P–O), ν(W–O), ν(W–$O_b$–W) and ν(W–$O_c$–W) ($O_b$: corner-sharing oxygen, $O_c$: edge-sharing oxygen), respectively [11].

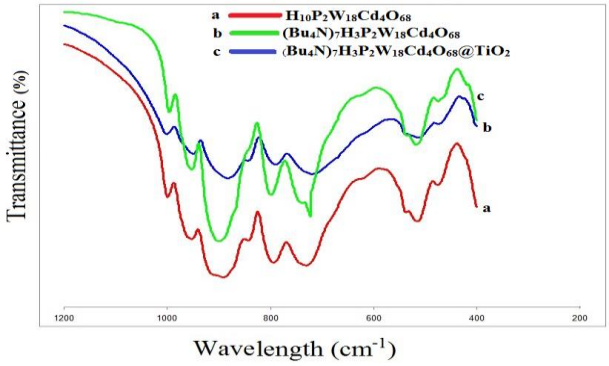


**Figure 3.** FT-IR spectra of (a) $TiO_2$ (b) $(Bu_4N)_7H_3P_2W_{18}Cd_4O_{68}$ and (c) $(Bu_4N)_7H_3P_2W_{18}Cd_4O_{68}@TiO_2$.

## Catalytic result

### *ODS results of gasoline and model oil*

For investigation the sulfur oxidation capability of $(Bu_4N)_7H_3P_2W_{18}Cd_4O_{68}@TiO_2$ nanocatalyst, the ODS process was performed on typical gasoline and model oil under the mentioned condition in the experimental section. The removal efficiency of the sulfur content of gasoline using as $TiO_2$ a catalyst was finally reached 36%. When the $(Bu_4N)_7H_3P_2W_{18}Cd_4O_{68}$ were supported on the $TiO_2$, the total sulfur content of gasoline was reduced 97% (Table 1). Also, the mercaptan compounds were much lowered from 97 ppm to 3 ppm (Entry 2). Further, the removal efficiencies of BT, Th and DBT were obtained 97, 98 and 99%, respectively. These results rendered the success of the catalytic $(Bu_4N)_7H_3P_2W_{18}Cd_4O_{68}@TiO_2/H_2O_2/AcOH$ system to capture and desulfurize the organic sulfur molecules.

**Table 1.** Oxidative desulphurization of gasoline by $(Bu_4N)_7H_3P_2W_{18}Cd_4O_{68}@TiO_2$.

| Entry | Properties of gasoline | | Unit | Method | Before ODS | After ODS [a] |
|---|---|---|---|---|---|---|
| 1 | Total Sulphur by X-Ray | | Wt.% | ASTM D 4294 | 0.468 | 0.046 |
| 2 | Mercaptans | | ppm | ASTM D 3227 | 97 | 3 |
| 3 | Density by hydrometer @ 15 $^0$C | | g/ml | ASTM D 1298 | 0.7875 | 0.7874 |
| 4 | Salt | | (ptb) | ASTM D 3230 | 18 | 17 |
| 5 | Water Content by distillation | | vol. % | ASTM D 4006 | Nil. | Nil. |
| 6 | Distillation | IBP | $^0$C | ASTM D 86 | 49.5 | 48.8 |
| | | FBP | | | 208.6 | 208.4 |
| | | 10 | Vol% | | 72.2 | 71.8 |
| | | 50 | | | 118.8 | 118.6 |
| | | 90 | | | 189.5 | 188.4 |
| | | 95 | | | 206.1 | 205.9 |

[a] Condition for desulphurization: 50 mL of gasoline, 0.1 g catalyst, 3 ml oxidant, 10 mL of extraction solvent, time = 1 h, and temperature = 35 °C.

### *Effect of nanocatalyst dosage on the ODS process*

To assess the effect of nanocatalyst dosage on removal efficiency of sulfur compounds, various amounts of organic-inorganic $(Bu_4N)_7H_3P_2W_{18}Cd_4O_{68}@TiO_2$ hybrid composite were used in the same conditions for all the dosage of catalyst (35 °C and 1 h). According to the blank experimental results, 2 22% of BT were removed [Fig. 4]. Also, it was found that the sulfur removal yield increased consecutively with an increase in the concentration of the nanocatalyst (active peroxo-molybdate complexes) in the reaction medium. When the amount of catalyst was further increased to 0.12 g, any noticeable change was not observed in the trend of increasing reaction efficiency. Therefore, the favorable dosage of $(Bu_4N)_7H_3P_2W_{18}Cd_4O_{68}@TiO_2$ nanocatalyst was 0.10 g for next oxidation runs.

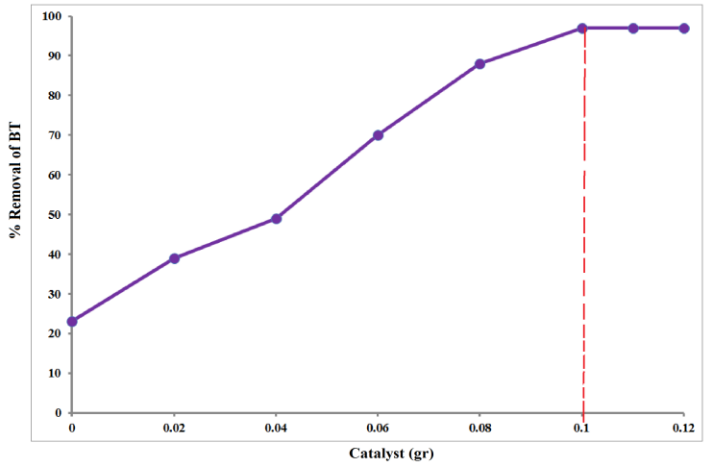

**Figure 4.** The effect of nanocatalyst dosage on removal efficiency of BT.

The $(Bu_4N)_7H_3P_2W_{18}Cd_4O_{68}@TiO_2$ nanocomposite was very active catalyst systems for the model compound oxidation, while other polyoxometalates systems were much less active. Oxidation reactivities decreased in the order of *thiophene>benzothiophene> dibenzothiophene> 4-methyldibenzothiophene> 4,6-dimethyldibenzothiophene*. However, the oxidation of the benzothiophenes was achieved under mild reaction conditions and it was easy to increase reaction temperature or reaction time to achieve high oxidation conversions, even for the least reactive 4,6-dimethyldibenzothiophene. This system has been used only for the desulfurization of gasoline, which usually has a sulfur content <1000 ppm.

## Conclusion

In conclusion, the new type of heterogeneous nanocatalyst $(Bu_4N)_7H_3P_2W_{18}Cd_4O_{68}@TiO_2$ was successfully prepared by sol-gel method. For the first time, the catalytic oxidation performance of this nanocomposite was evaluated in sulfur oxidation reactions to develop the moderate ODS process. The various experiments were performed for treating the gasoline and model oil using $H_2O_2$/AcOH as an oxidant. On the basis of the catalytic $(Bu_4N)_7H_3P_2W_{18}Cd_4O_{68}@TiO_2/H_2O_2$/AcOH system, the removal efficiency of the total sulfur and mercaptan content were 97 % at 35 °C after 60 min. At the end, the results of catalyst regeneration indicated that the heterogeneous nanocomposite could be reused up to five cycles with easy filtration. This work introduced as a new ODS system to promote the quality of gasoline fuel.

## References

[1] M. A. Rezvani, A. F. Shojaei, F. M. Zonoz, *J. Serb. Chem. Soc.*, **2014**, *79*, 1099.

[2] N. M. Mahmoodi, M. A. Rezvani, M. Oveisi, A. Valipour, M. A. Asli, *Mater. Res. Bull.*,**2016**, *84*, 422.

[3] M. A. Rezvani, M. Alinia Asli, M. Oveisi, R. babaei, K. Qasemi, S. Khandan, *RSC Adv.*, **2016**, *6*, 53069.

[4] M. A. Rezvani, M. Alinia Asli, S. Khandan, H. Mousavi, Z. Shokri Aghbolagh, *Chem. Eng. J.*, **2017**, *312*, 243.

[5] X. Sheng, Y. Zhoua, Y. Zhang, M. Xue, Y. Duan, *Chem. Eng. J.*, **2012**, *179*, 295.

[6] Z. A. Abdalla, B. Li, *Chem. Eng. J.*, **2012**, *200*, 113.

[7] W. Qi, L. Wu, *Polym. Int.*, **2009**, *58*, 1217.

[8] M. A. Rezvani, A. F. Shojaie, M. H. Loghmani, *Fuel Process. Technol.*, **2014**, *118*, 1.

[9] M. A. Rezvani, F. Mohammadi Zonoz, *Ind. Eng. Chem.*, **2015**, *22*, 83.

[10] M. A. Rezvani, M. Shaterian, F. Akbarzadeh, S. Khandan, *Chem. Eng. J.*,**2018**, *333*, 537.

[11] M. A. Rezvani, Z. S. Aghbolagh, H. H. Monfared, S. Khandan, *J. Ind. Eng. Chem.*, **2017**, *52*, 42.

[12] D.Wang, E.W. Qian, H. Amano, K. Okata, A. Ishihara, T. Kabe, *Appl. Catal. A* , **2003**, *253*, 91.

[13] T.V. Rao, B. Sain, S. Kafola, Y.K. Sharma, S.M. Nanoti, M.O. Garg, *Energy Fuels*, **2007**,*21*, 3420.

[14] S.Z. Liu, B.H.Wang, B.C. Cui, L.L. Sun, *Fuel*, **2008**, *87*, 422.

[15] P. De Filippis, M. Scarsella, *Ind. Eng. Chem. Res.*, **2008**, *47*, 973.

# Study on the effect of iron nanocatalysts for liquid fuel production from syngas

**Kaveh Kalantari**

*Department of Chemical engineering, University of Zanjan,P.O. BOX 19395-4697 Zanjan, Iran*

*E-mail: kalantari_k@yahoo.com

**Abstract**

In this paper the use of supported and unsupported iron nanocatalysts in liquid fuel production from syngas has been reviewed. The effect of support on iron nanocatalysts has been considered. Iron oxide nanoparticles as catalyst show high performance in contrast with supported iron catalysts for Fischer-Tropsch synthesis. Supported iron nanocatalysts and conventional supported iron catalysts have been compared.

**Keywords**: Fischer-Tropsch synthesis, iron nanoparticles, nanocatalyst.

## Introduction

Fischer-Tropsch synthesis (FTS) discovered in 1920s remains one of the major research topics within alternate fuels R&D [1]. FT reaction is the catalytic hydrogenation of carbon monoxide which yields a wide range of alkanes, alkenes, and oxygenated compounds. Iron and cobalt-based catalysts have been considered as practical FT catalysts [2]. Iron-based catalyst systems remain the preferred choice in commercial FTS plants due to their low cost and their propensity to yield high olefinic content in the hydrocarbon distribution [3,4].

Studies with highly dispersed metals as nanocatalysts are of interest because nanosizing increases surface area that exposes more catalytic sites. The use of nanosized metals could potentially enhance the activity of heterogeneous catalysts that dominate the field of catalysis [4-7]. In exothermic reactions such as CO hydrogenation, nanocatalysts are likely to be more effective and selective or show other interesting properties as the temperature is lowered [6,7].

This review will concentrate on the use of supported and unsupported nanocatalysts in FT synthesis and comparing their performance.

## Unsupported iron nanocatalysts in FT synthesis

The use of iron oxide nanoparticles have been considered in past years[6-8]. Mahajan et al. [6,7] used two nanosized $\propto$-$Fe_2O_3$ materials [NANOCAT (3 nm) and BASF (20-80 nm)] and UCI reference catalyst ($Fe_2O_3$= 69.6, $K_2O$ = 5.1, $SiO_2$ = 8.3, CuO = 2.6, MPD= 32.5 µm) to study the effect of nanosizing on catalytic activity during the FT synthesis reaction operating in slurry phase at a lower temperature of 240°C Slurries of supported UCI materials and iron nanoparticles in ethylflo-polyolefin-164 solvent were reduced with CO to generate catalyst for FT reaction. Table 1 shows the data of FT synthesis by nanocatalysts and supported UCI catalyst.

They reported the comparison between CO and Syngas ($H_2$:CO = 2:1) reductant with NANOCAT catalyst. Gas conversion data for Syngas reductant were far lower than those obtained with CO reductant. Consequently the space-time yield (STY) of hydrocarbons was lower by a factor of 4.

**Table 1.** Data summary of FTS runs[a] catalyzed by unsupported nano Fe particles (NANOCAT and BASF) and supported UCI systems [6]

| | NANOCAT | | | BASF | UCI |
|---|---|---|---|---|---|
| | 240°C | 260°C [b] | 260°C [c] | 240°C | 240°C |
| % conversion | | | | | |
| $H_2$ | 34.8 | 44.7 | 14.3 | 41.7 | 38.7 |
| CO | 42.9 | 52.1 | 16.2 | 55.9 | 65.4 |
| CO+$H_2$ | 40.5 | 46.8 | 14.9 | 48.5 | 47.4 |
| Hydrocarbon product distribution, wt% | | | | | |
| $C_1$ | 12.8 | 16.0 | 16.4 | 10.7 | 7.0 |
| $C_2$ | 8.9 | 11.2 | 11.4 | 8.5 | 5.2 |
| $C_3$ | 14.6 | 15.4 | 13.8 | 15.2 | 0.6 |
| $C_4$ | 9.3 | 11.4 | 8.8 | 9.6 | 5.1 |
| $C_5$-$C_{10}$ | 23.7 | 30.0 | 23.0 | 28.2 | 14.5 |
| $C_{11+}$ | 30.7 | 16.0 | 26.6 | 27.8 | 60.6 |
| Overall product distribution, wt% | | | | | |
| HC | 31.8 | 32.3 | 35.9 | 30.5 | 28.4 |
| $H_2O$ | 36.5 | 37.2 | 40.6 | 30.5 | 25.0 |
| $CO_2$ | 31.7 | 30.5 | 23.5 | 39.0 | 46.6 |
| STY, kg/kg-Fe/ h | | | | | |
| $C_1$–$C_4$ | 0.26 | 0.37 | 0.09 | 0.36 | 0.22 |
| $C_{5+}$ | 0.14 | 0.17 | 0.04 | 0.20 | 0.16 |

[a] Reaction conditions: catalyst loading = 4.6 wt %; Ethylflo-164 = 330 g; syngas: H2/CO = 66%/ 34%; *P* = 0.78 MPa; *V* = 4.5- 4.7 NL/ g-Fe/ h; run time = 120 h. The initial oxide catalyst precursor was initially reduced with CO in all cases. [b] At *P* = 2.77 MPa; SV = 5.78 NL/ g-Fe/ h. [c] Initially reduced with 67% H2/ 33% CO gas mixture. Syngas feed rates during FT

synthesis were 6.3 (24 h) and 4.4 (28 h) NL/ g-Fe/ h. Total run time = 52.5 h. Operating $P$ = 2.8 MPa.

For NANOCAT catalyst, the FT activity order was as follows: for CO-treated runs, 260°C > 240°C; at 240°C, CO-treated >> syngas-treated [6,7]. With NANOCAT, high STY at higher temperature and a higher rate with CO-treated catalyst were generally similar to those reported for the precipitated Fe-based catalysts [6,9]. Prior to this study they reported that FT synthesis could be achieved at a lower temperature of 220°C with nanosized particles of Fe in slurry phase [10]. The STY value unequivocally showed that BASF had a better activity for hydrocarbon synthesis than NANOCAT (0.56 kg/kg-Fe/ h versus 0.40 kg/kg-Fe/ h) [7]. The FT activities of the two unsupported nanocatalysts, NANOCAT and BASF, were compared with the micrometer-sized supported UCI catalyst. A direct comparison of the average CO conversion values at 42.9% (NANOCAT), 55.9% (BASF) versus 65.4% (UCI) in Table 1, suggested that UCI outperformed both nanocatalysts. This comparison is not borne out by the corresponding hydrocarbon STY data that show 0.40, 0.56, and 0.38 (kg/kg-Fe/ h) for NANOCAT, BASF, and UCI, respectively. This discrepancy was explained by the $CO_2$-produced values in Table 1. During CO conversion, any C in CO converted to hydrocarbons (or oxygenates) products is useful, whereas C conversion to $CO_2$ product is undesirable. The data in Table 1 show that the highest $CO_2$ produced (46.6%) offset the overall higher CO conversion (65.4%) for UCI in terms of STY. On the basis of solely STY at 240°C, the activity order for the CO-pretreated catalysts was BASF > NANOCAT ≈ UCI [6,7].

They discovered that of the three starting ∝-$Fe_2O_3$, all three materials either remained or transformed into nanoparticles of <50 nm size under FT synthesis conditions. The 3 nm NANOCAT showed a slight agglomeration to 10-20 nm; the BASF redistributed from 20-80 nm to 30-50 nm and surprisingly, the micrometer-sized (32500 nm) UCI catalyst transformed into a material with particle size of <10 nm [6]. Sarkar et al. [8] used an unpromoted ultrafine iron nano particle catalyst (∝-$Fe_2O_3$, MPD = 3 nm) for FT synthesis in slurry phase. They reported that particle size distribution (PSD) measurements indicated growth of individual catalyst particles, that is in agreement with Mahajan's report.

## Supported iron nanocatalysts in FT synthesis

### 1. Inorganic supports

Many inorganic oxides such as $Al_2O_3$, $SiO_2$, $TiO_2$ have been used as supports for improving the structural stability of iron-based catalysts [11]. Suslick et al. [12] reported the use of silica supported nanostructured iron generated by High-Intensity Ultrasound as a catalyst in FT synthesis. Figure 1 compares the activity (in terms of turnover frequency of CO molecules converted per catalytic site per second) of silica-supported nanophase iron and conventional silica-supported iron, as a function of temperature. The sonochemically produced iron on silica catalyst is an order of magnitude more active than the conventional supported iron at similar loading and dispersion. These nanocatalysts exhibit high activity at low temperature (<250°C), whereas the conventional catalyst exhibits no

activity. They believed that the dramatic difference in activity between these catalysts below 300°C may be due to the amorphous nature of iron and the inherently highly defected surface formed during sonolysis of $Fe(CO)_5$ when the amorphous state of iron is preserved. At higher temperatures, the activity decreases, which may be due to iron crystallization, surface annealing, or catalyst deactivation from surface carbon deposition.

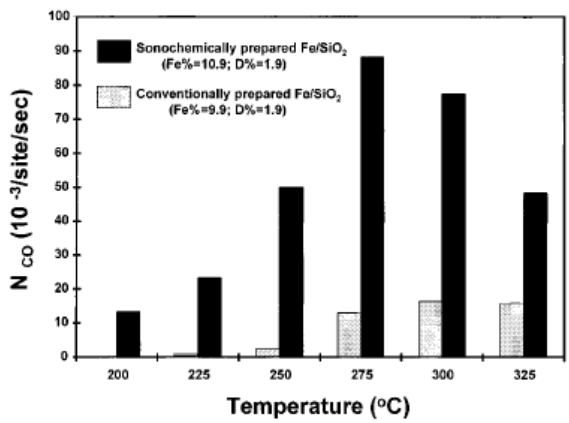


**Figure 1.** The catalytic activity of $SiO_2$ supported amorphous nanostructured iron sonochemically prepared from $Fe(CO)_5$ and $SiO_2$ slurry (iron loading = 10.94 wt %, and dispersion, *D*= 1.85%) and $SiO_2$-supported crystalline iron prepared by the incipient wetness method (iron loading = 9.91 wt %, *D* = 1.86%) as a function of temperature for FT synthesis (H2/CO = 3.48, 1 atm). [12]

Differences in selectivities of product distributions between sonochemically prepared supported iron catalyst and conventional supported catalyst were not substantial. Under reaction conditions, the major reaction products for both catalysts were short-chain $C_1$ to $C_4$ hydrocarbons and $CO_2$. At temperatures higher than 275°C, the reaction product distributions were similar for both type of catalyst. At temperature lower than 275°C, the nanocatalyst had a higher selectivity toward long-chain hydrocarbons ($C_{5+}$ ), whereas the conventional supported iron showed no activity at those temperatures [12].

O'Shea et al. [13] used iron oxide nanoparticles deposited on the surface of a silica substrate for FT reaction in a fixed-bed reactor. This nanocatalyst presented the highest activity at low reaction temperature, 220°C, and major selectivity to alcohols.

## 2. Organic supports

In recent years, supports with carbonaceous base in the form of activated carbon and carbon nanotubes (CNTs) have been investigated for FT reactions [14-19]. Marchetti et al. [14] reported that iron uniform size nanoparticles dispersed on MCM-41 (mesoporous carbon materials) showed a high CO conversion when it was used as catalyst in FT synthesis (14.3% at 1 hour of reaction time) mainly methane was formed. The high methane selectivity may be attributed to the very small size of the metallic crystals that cannot sustain the chain growth although the pores are big enough not to impose steric constrains.

Measurement of activity and selectivity were carried out in a fixed bed reactor at 270°C, $H_2$:CO ratio of 2:1 and atmospheric pressure. Table 2 shows the activity and selectivity results at different reaction time for Fe/MCM-41 catalyst.

Comparing Fe/MCM-41 with a good traditional catalyst, like $Fe/SiO_2$ [20] at similar reaction conditions, it can be seen that the former presents a CO conversion of about six times higher than the latter (7.8% vs. 1.4%, respectively). The exchange of the

support with alkaline cations will lead to an increase in the olefin production [14].

**Table 2.** Activity and selectivity tests in the FT synthesis [14]

| | Time (min) | | |
|---|---|---|---|
| | 66 | 1385 | 2474 |
| HC production (molec/g.s) $10^{-17}$ | 12.3 | 6.4 | 4.6 |
| Olefins/paraffins | 0.096 | 0.176 | 0.186 |
| $CH_4$ (%) | 83 | 82 | 85 |
| Conversion (%) | 14.3 | 7.8 | 5.4 |
| Schultz-Flory coefficient (α) | 0.187 | 0.159 | 0.150 |

Reaction conditions: 270°C, 1 atm, H2 : CO = 2 : 1 in a fixed bed reactor, using a mass catalyst of 460 mg and a space rate of 0.14 $s^{-1}$.
HC: hydrocarbon from $C_1$ to $C_5$.
$\alpha$: probability of hydrocarbon chain growth ($0 \leq \alpha \leq 1$).

Abbaslou et al. [15] studied the effect of electronic properties of inner and outer surface of carbon nanotubes (CNTs) on FT reactions. Catalytic activity and product selectivity of in-Fe/CNT and out-Fe/CNT catalysts were analyzed at different temperatures ranging from 260 to 285°C. Activity of both catalysts follows similar trends as reaction temperature increases. However, after a reaction period of 125 h, in-Fe/CNT catalyst shows higher CO conversion compared to out-Fe/CNT. They discovered that catalysts with iron nanoparticles inside the pores exhibit higher selectivity to heavier hydrocarbons. confinement of reaction intermediates inside the channels increases the contact time of the reactants with the active sites, resulting in production of heavier hydrocarbons. Another advantage of deposition of catalytic species inside the pores was the physical encapsulation of catalytic particles, which can reduce the site sintering.

Chen et al. [16] studied the confinement effect of iron particles inside the nanotubes channels for FT reactions. They used closed cap CNTs for deposition of iron particles on exterior surface of nanotubes using impregnation method. In order to prepare iron catalyst inside the nanotubes, they used strong acid pre-treatment to open the CNTs' cap. Therefore, their catalysts experienced different pretreatment procedure which may affect the catalyst performance. According to their report, the catalytic performance of the iron catalysts supported either inside or outside of the natotubes' channel is similar at pressure less that 2 MPa. However, at higher pressure (5MPa), the yield of $C_{5+}$ hydrocarbons over the encapsulated iron catalyst is twice that over iron catalyst outside CNTs [16].

## Conclusion

From this short review on the use of nanocatalysts for Fischer-Tropsch synthesis, it may be observed that the FT synthesis reaction conditions induce an environment in which, the formation and subsequent stabilization of the nanosized Fe particles are preferred. This plays a crucial role in promoting FT synthesis. The activity of the nanosized Fe particles is attributed to the oxide and/or carbide phases. Iron nanoparticles showed higher activity and STY than supported UCI catalysts. Silica supported nanostructured iron catalyst showed a high activity in comparison with the conventional silica-supported iron catalyst. Fe/MCM-41 catalyst exhibited a higher CO conversion than a good traditional

catalyst; $Fe/SiO_2$, at similar reaction conditions. Carbon nanotube supported catalysts with iron nanoparticles inside the pores exhibited a higher selectivity to heavier hydrocarbons. Finally, it may be concluded that iron nanocatalysts have a more favorable effect on product distribution in FT synthesis than that of the conventional iron catalysts.

**References**

[1] H Schulz, "Short history and present trends of Fischer–Tropsch synthesis", *Appl. Catal. A: Gen.*, 186 (1999) 3–12.

[2] M.A. Marvast, M. Sohrabi, S. Zarrinpashne, G. Baghmisheh, "Fischer–tropsch synthesis: Modeling and performance study for Fe-HZSM5 bifunctional catalyst", *Chem. Eng. Technol.*, 28 (1) (2005) 78–86.

[3] R. L. Espinoza, A. P. Steynberg, B. Jager, A. C. Vosloo, "Low temperature Fischer–Tropsch synthesis from a Sasol perspective", *Appl. Catal. A: Gen.*,186 (1999) 13–26.

[4] A. Tavakoli, M. Sohrabi, "Application of Anderson–Schulz–Flory (ASF) equation in the product distribution of slurry phase FT synthesis with nanosized iron catalysts", *Chem. Eng. J.*, 136 (2008) 358–363.

[5] C. Burda, X. Chen, R. Narayanan, M.A El-Sayed, "Chemistry and Properties of Nanocrystals of Different Shapes", *Chem. Rev.*, 105 (2005) 1025–1102.

[6] D. Mahajan, P. Gutlich, J. Ensling, K. Pandya, U. Stumm, P. Vijayaraghavan, "Evaluation of Nanosized Iron in Slurry-Phase Fischer–Tropsch Synthesis", *Energy Fuels*, 17 (2003) 1210–1221.

[7] D. Mahajan, P. Gutlich, U. Stumm, "The role of nano-sized iron particles in slurry phase Fischer–Tropsch synthesis", *Catal. Commun.*, 4 (2003) 101–107.

[8] A. Sarkar, D. Seth, A. K. Dozier, J. K. Neathery, H. H. Hamdeh, B. H. Davis, "Fischer–Tropsch Synthesis: Morphology, Phase Transformation and Particle Size Growth of Nano-scale Particles", *Catal Lett*, 117 (2007) 1–17.

[9] D. B. Bukur, L. Nowicki, R. K. Manne, X. Lang, "Activation studies with a precipitated iron catalyst for Fischer–Tropsch synthesis: II. Reaction studies", *J. Catal.*, 155 (1995) 366–375.

[10] D. Mahajan, A. Kobayashi, N.Gupta, "Fischer–Tropsch synthesis catalysed by ultrafine particles of iron: cessation of water-gas shift activity**",** *J. Chem. Soc., Chem. Commun***.,** (1994) 795.

[11] N. Lohitharn, J.G. Goodwin Jr, E. Lotero, "Fe-based Fischer–Tropsch synthesis catalysts containing carbide-forming transition metal promoters", *J. Catal.* 255 (2008) 104–113.

[12] K. S. Suslick, T. Hyeon, M. Fang, "Nanostructured materials generated by High-Intensity Ultrasound: Sonochemical synthesis and catalytic studies", *Chem. Mater.*, 8 (1996) 2172–2179.

[13] V. A. de la Pena O'Shea, M. C. Alvarez-Galvan, J. M. Campos-Martin, J. L. G. Fierro, "Fischer–Tropsch synthesis on mono- and bimetallic Co and Fe catalysts in fixed-bed and slurry reactors", *Appl. Catal. A: Gen.*, 326 (2007) 65–73.

[14] S. G. Marchetti et al., "Iron Uniform-Size Nanoparticles Dispersed on MCM-41 Used as Hydrocarbon Synthesis Catalyst", *Hyperfine Interactions*, 139/140 (2002) 33–40.

[15] R. M. Malek Abbaslou, A. Tavassoli, J. Soltan, A. K. Dalai, "Iron Catalysts Supported on Carbon Nanotubes for Fischer–Tropsch Synthesis: Effect of Catalytic Site Position", *Appl. Catal. A: Gen.*, (2009) doi:10.1016/j.apcata.2009.07.025

[16] W. Chen, X. Pan, X. Bao, "Tuning of Redox Properties of Iron and Iron Oxides via Encapsulation within Carbon Nanotubes", *J. Am. Chem. Soc.*, 129 (2007) 7421–7426.

[17] W. Ma, E. L. Kugler, J. Wright, and D. B. Dadyburjor, "Mo–Fe Catalysts Supported on Activated Carbon for Synthesis of Liquid

Fuels by the Fischer–Tropsch Process: Effect of Mo Addition on Reducibility, Activity, and Hydrocarbon Selectivity", *Energy Fuels*, 20 (2006) 2299–2307.

[18] E. van Steen, F. F. Prinsloo, "Comparison of preparation methods for carbon nanotubes supported iron Fischer–Tropsch catalysts", *Catal. Tod.*, 71 (2002) 327–334.

[19] M. C. Bahome, L. L. Jewell, D. Hildebrandt, D. Glasser, N. J. Coville, "Fischer–Tropsch synthesis over iron catalysts supported on carbon nanotubes", *Appl. Catal. A: Gen.*, 287 (2005) 60–67.

[20] N. G. Gallegos et al., "Selectivity to olefins of $Fe/SiO_2$ –MgO catalysts in the Fischer–Tropsch reaction", *J. Catal.*, 161 (1996) 132–142.

# $H_4SiW_{12}O_{40}$@$TiO_2$@CS Composite: High-Performance Catalyst for Degradation of Methylene Blue Dye

**Zahra Nouri, Mohamad Ali Rezvani, Zahra Shokri Aghbolagh***

*Department of Chemistry, Faculty of Science, University of Zanjan, 451561319, Zanjan, Iran*

**Corresponding author Tel.: Fax: +98241 5152617.*

**E-mails: mrezvani@znu.ac.ir, zahra.shokri@znu.ac.ir*

## Abstract

In this paper the nanocomposite was successfully synthesized by reaction of Silicotungstic acid ($H_4SiW_{12}O_{40}$), titanium dioxide ($TiO_2$) and chitosan (CS) at room temperature under sonication condition. A new compound, $H_4SiW_{12}O_{40}$@$TiO_2$@CS, has been prepared as an efficient and green catalyst for the removal of cationic dyes such as methylene blue (MB) from aqueous solution. The incorporation of the materials was confirmed by SEM, XRD and FT-IR spectroscopy. Results obtained indicate that $H_4SiW_{12}O_{40}$@$TiO_2$@CS could be employed as an efficient catalyst much more than the pure $H_4SiW_{12}O_{40}$, CS and $TiO_2$ powders for decolorization from water.

**Keywords**: Photocatalyst, Dye removal, Nanocomposite, Polyoxometalate, Methylene blue.

## Introduction

About 15% of the total world production of dyes in lost during the dyeing process and is released in the textile effluents [1]. There are many types of pollutant presented in wastewater. Dyes are one of the contaminant in the environment. Nowadays, these compounds widely used for a long time in many industrial fields, such as paper making, coating and textiles, leather, cosmetics, ink [2,3] to color their products. Many industries such as textile, plastics, and paper and pulp generate streams of wastes effluents which considerable amount of wastes effluents which considerable amount of organic dye [4,5]. All these techniques are versatile in nature and have their own pros and con. In order to improve the solar conversion efficiency, there are many attempts to study visible-light sensitive catalysts [6,7]. Photocatalysis is based on the reactive properties of photogenerated electron-hole pairs are gererated. The photocatalytic degradation pathway whit the identification of the main degradation metabolites has already been established in our laboratories for Methylene Blue dye [8]. The MB is an intensely colored compound which is use in dyeing and printing textiles and is a common water pollutant. Titanium dioxide mediated photolytic oxidation has been applied more extensively por dye studies. This is mainly because of its low cost, stable nature and its optical absorption in the UV region. The use of $TiO_2$ has also guaranteed good results in detoxification of water samples loaded with molecules like intensely, alcohols, and organochlorides [9,10].

## Experimental

*General*

AAll reagents and solvents used in this work are available commercially and were used as received, unless otherwise indicated. Methylene blue was supplied by a textile firm and used as received. All reagents and solvents used in this work are available commercially and were used as received, unless otherwise indicated and CS (low molecular weight with a degree of deacetylation of 75–85%) were purchased from Sigma–Aldrich. The products characterized by analytical instrument FT-IR, UV-Vis, XRD and SEM. Typical real gasoline (density 0.7784 g/ml at 15°C, total sulfur content 0.498 wt.%, and mercaptan 97 ppm) was used. X-ray diffraction (XRD) patterns was accomplished by D8 advance Brucker and radiation Cu kα (λ=1.54 nm) in the range of $5 \leq 2\theta \leq 40°$. Fourier transform infrared (FT-IR) spectra were recorded by Thermo-Nicolet-is 10 in the range of 400-4000 $cm^{-1}$. Ultraviolet-visible (UV-vis) spectra were studied with a double beam termo-heylos spectrophotometry in the range of 200-400 nm. Scanning electron microscope (SEM) images were obtained on a LEO 1455 VP with an accelerating voltage of 10.00 KV.

***Preparation of $H_4SiW_{12}O_{40}$@$TiO_2$@CS nanocatalyst***

In a typical synthesis, 0.05 gr chitosan was added into glacial acetic acid (2%) with stirring. And individually $H_4SiW_{12}O_{40}$@$TiO_2$@CS was prepared at 100℃ via sol- gel method. 0.05 gr $TiO_2$ was added into glacial acetic acid (2%) with stirring for 30 min and a solution of 0.05 gr $H_4SiW_{12}O_{40}$ in water was drop wised in it. The mixture was stirred to dissolve any solid. Then, the sol was heated to 100 ℃ under oil bath condition until a homogenous $H_4SiW_{12}O_{40}$@$TiO_2$ hydrogel was formed. And the solution was added into solution chitosan. This work keeps on for 6 min. finally, the gel was filtered. Washed with deionized water- acetone and dried in oven at 50℃ overnight.

***Decolorization test method***

In order to remove color from methylene blue, first place a 30 ml of methylene blue color at a concentration of 20 ppm to give

0.02g of $H_4SiW_{12}O_{40}$@$TiO_2$@CS catalyst and place it under UV light for 60 minutes. The light eliminates dyed, and the centrifuge can be used to separate the degraded paint from the water. Of course, this type of color removal is different from the catalyst in the visible light and the optimal condition is 0.02 grams of catalyst and placed under the UV light. Using UV-Vis spectrometry in the interval 400 to 800, the amount calculate the color removal, using the formula below, the percentage of removal of dyes was calculated using the following formula:

$$\text{Removal (\%)} = \left(\frac{C_i - C_f}{C_i}\right)\times 100$$

Where $C_i$ is the initial dye concentration and $C_f$ is the equilibrium dye concentration in mg $L^{-1}$.

**Results and discussion**

***Characterization of synthesized photocatalyst***

The synthesized quaternary ammonium salt based keggin-type polyoxometalate was characterized by XRD, SEM and IR technique. FT- IR patterns of $H_4SiW_{12}O_{40}$, $TiO_2$, CS and $H_4SiW_{12}O_{40}$@$TiO_2$@CS are shown in Figure 1. FT- IR spectrum of pour $TiO_2$ is showed at 1437 $cm^{-1}$ (O-Ti-O) and 668 $cm^{-1}$ (Ti-O). In the IR spectra (Figure 1), $H_4SiW_{12}O_{40}$@$TiO_2$@CS displays characteristic vibration patterns of the Keggin-type framework in low-wavenumber region (500< $\upsilon$ <1100 $cm^{-1}$). These, peak 1021, 924, 801 and 680 $cm^{-1}$ due to the fingerprint region of keggin structure. The vibration sharp peaks centered at approximately 924 $cm^{-1}$ are attributed to the $\upsilon_{as}$(W-$O_d$) and $\upsilon_{as}$(W-$O_b$-W), respectively, four bands in the range 600- 1030 $cm^{-1}$ which originate from the asymmetric stretching of the W-$O_c$-W [11], the frequencies at about 1021 $cm^{-1}$ ascribe to $\upsilon_{as}$(Si- $O_a$), which are derived from the characteristic vibration patterns of Keggin-type polyoxoanion. In the IR spectra for pour chitosan displays characteristic vibration patterns of C-H at 3000 $cm^{-1}$. The peaks at 1672 $cm^{-1}$ and 1593 $cm^{-1}$ are assigned to bending C-H and N-H.

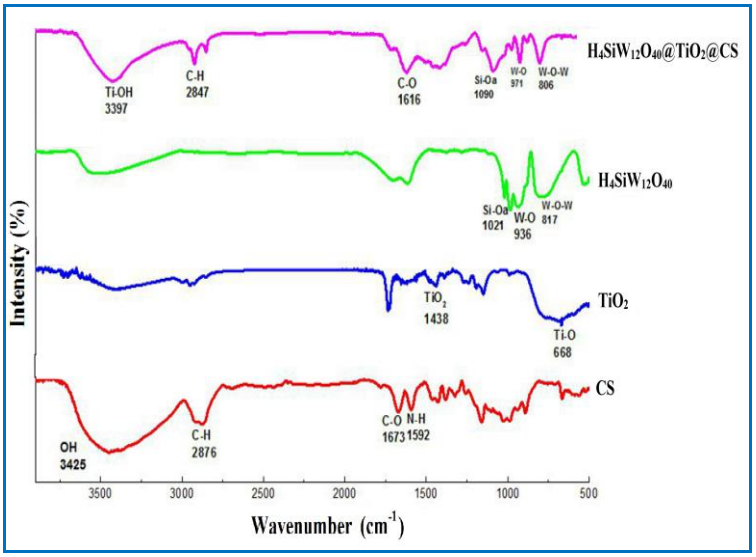


**Figure 1.** FT-IR spectroscopy analysis of $TiO_2$, CS, $H_4SiW_{12}O_{40}$, and $H_4SiW_{12}O_{40}$@$TiO_2$@CS.

The XRD Patterns of $H_4SiW_{12}O_{40}$@$TiO_2$@CS and $H_4SiW_{12}O_{40}$ are shown in Figure 2. The polyoxometalate pattern due to its sharp peaks indicates that it is a completely crystalline compound. The nanocomposite pattern shows that $H_4SiW_{12}O_{40}$ are well placed on the bed of titanium dioxide and chitosan, the peaks of nanocomposite are more like titanium dioxide peaks, which will show that titanium dioxide is most present in nanocomposites.

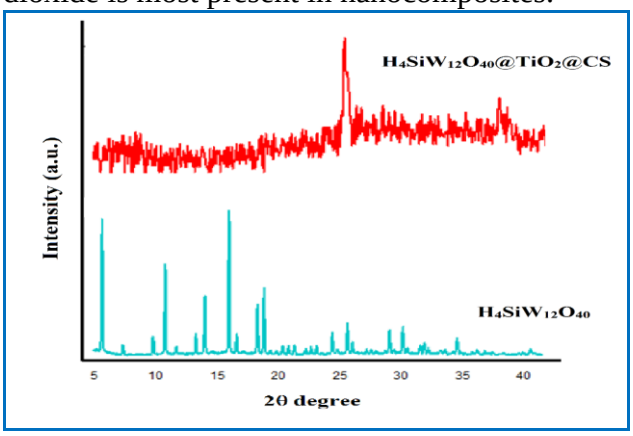


**Figure 2.** XRD of $H_4SiW_{12}O_{40}$ and $H_4SiW_{12}O_{40}$@$TiO_2$@CS.

The morphology and size of the resulting sample was investigated by SEM images. Figure 3 shows the images of the $H_4SiW_{12}O_{40}$@$TiO_2$@CS samples prepared in 2h that include agglomerated nanoparticles which have formed plated or layers. From Figure 3, shows the SEM image of nanocatalyst as crushed nanoleaf with average size of about 60 nm and the shape of the surface of the nanocomposite is a curved shape.

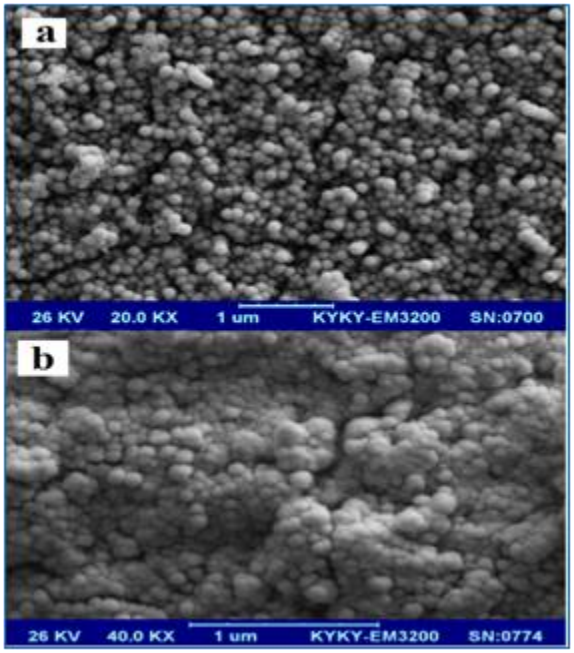


Figure 3. SEM images of a sample of (a) $H_4SiW_{12}O_{40}$, (b) $H_4SiW_{12}O_{40}$@$TiO_2$@CS.

***Effect of photocatalyst dosage on the removal of dye from aqueous solution:***

One important factor that should be concerned is the catalyst dosage. Consequently, knowledge on the effect of catalyst dosage is very important to the process optimization. From the results of Figure 4. It is evident that higher catalyst dosage leads to higher degradation dye efficiency. In order to obtain optimal conditions for the removal of methylene blue dye, the effect of increasing the concentration of synthesized catalyst was tested. The results show that by increasing the catalyst concentration and concentration, the color removal rate increases, so that the optimum concentration for color degradation is 0.02 gr. According to the calculations done, a color elimination of 98% was carried out in 60 minutes.

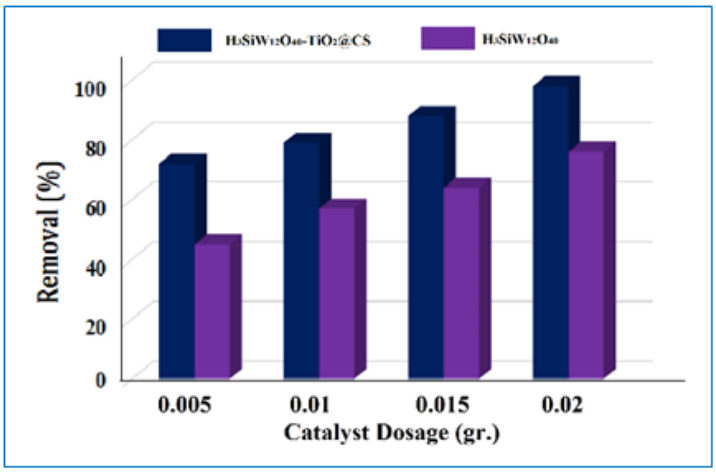


**Figure 4.** Effect of photocatalyst dosage on the removal of dye from aqueous solution

***Effect of reaction temperature and time on the removal of dye from aqueous solution***

The catalytic activities of the $H_4SiW_{12}O_{40}$@$TiO_2$@CS catalysts in the degradation of methylene blue dye at different times were compared and shown in Figure 5. The shorter the removal time will indicate that the effect of the catalyst has been greater. In this method, the color elimination value has been measured in the 15 minute intervals, the removal value has reached 98% in 60 minutes.

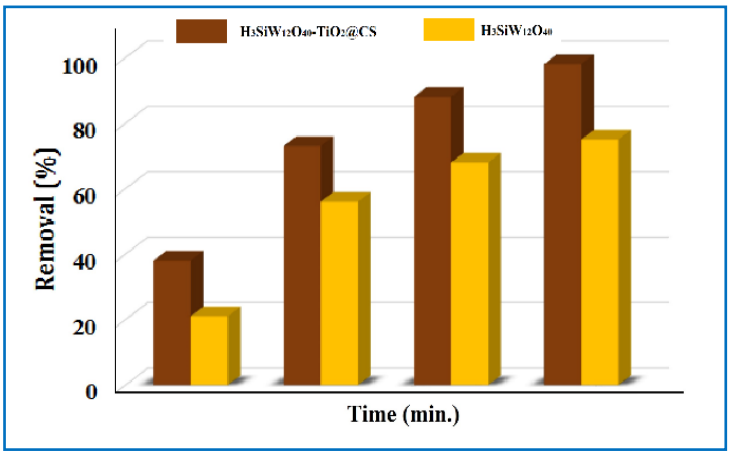


**Figure 5.** Effect of reaction time on the removal of dye from aqueous solution.

### *Investigation of the effect of light exposure on Degradation of methylene blue Dye*

Light irradiation is very effective in the destruction of color, which is very effective in this catalyst because of the presence of titanium dioxide which is very active in light UV conditions, has a significant effect on the removal of color, due to the presence of polyoxometalate, which is a polar material, the reaction speed Titanium dioxide has been enhanced to remove color.

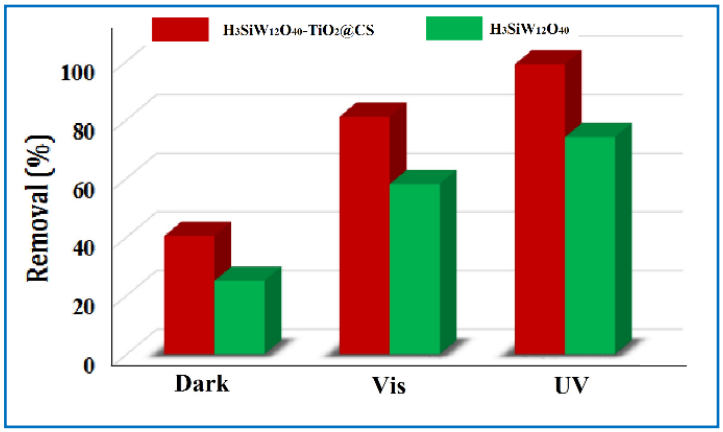


**Figure 6.** Investigation of the effect of light exposure

### *Recycling of the $H_4SiW_{12}O_{40}$@$TiO_2$@CS catalyst*

At the end of the degradation of methylene blue, the catalyst $H_4SiW_{12}O_{40}$@$TiO_2$@CS was filtered, washed with dichloromethane, in order to know whether the catalyst would ***succumb*** to poisoning and lose its catalytic activity during the reaction, we investigated the reusability of the catalyst. All products are soluble in dichloromethane but the catalyst is not. For this products in dichloromethane but the catalyst in not. For this purpose we carried out the degradation dye reaction of methylene blue in the presence of fresh and recovered catalyst (Figure 7). Even after seven runs for the reaction, the catalytic active of $H_4SiW_{12}O_{40}$@$TiO_2$@CS was almost the same as that freshly used catalyst. The results are summarized in Figure 7.

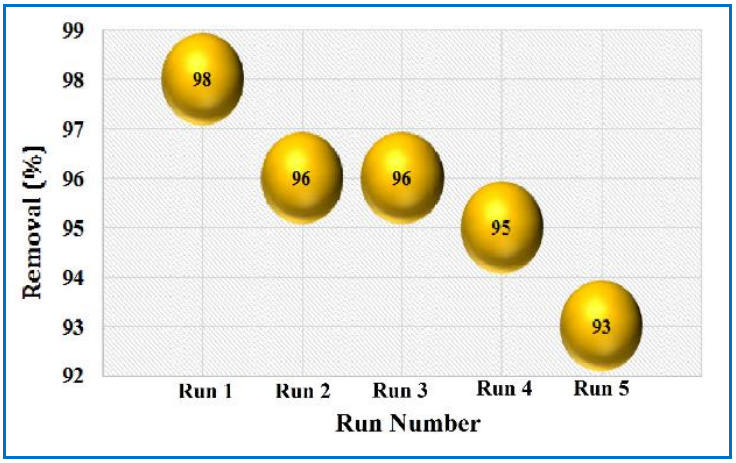


**Figure 7.** Recycling of the $H_4SiW_{12}O_{40}$@$TiO_2$@CS catalyst

## Conclusion

In this study, decolorization of methylene blue solution was performed by photocatalytic method. In this project, the polyoxometalate $H_4SiW_{12}O_{40}$, which is stabilized on $TiO_2$ and CS, $TiO_2$ substrates, is used as the $H_4SiW_{12}O_{40}$@$TiO_2$@CS

photocatalyst. The results prove that the synthetic catalyst has high chemical stability, so that for the fifth time, a slight reduction in the removal efficiency of the dye is observed.

**Acknowledgments**
The authors are grateful to the University of Zanjan for supporting this work.

**References**

[1] L. Dotto, L.A.A. Pinto, *Journal of Hazardous Materials*, **2011**, *187*, 164–170.
[2] H.Y. Zhu, R. Jiang, L. Xiao, W. Li, A, *J. Hazard. Mater*, **2010**, 179, 251–257.
[3] L. Fan, C. Luo, M. Sun, H. Qiu, X. Li, *Colloids Surf. B: Biointerfaces*, **2013**, 103, 601–607.
[4] S. Clemmensen, J. Jensen, N. Jensen, O.A. Meyer, K. Olsen, G. Würtzen, *Archives of Toxicology*, **1984**, 56, 43–45.
[3] S. Parsons, Advanced Oxidation Processes for Water and Waste Water, IWA Publishing, **2004**.
[5] C.T. Helmes, C.C. Sigman, V.A. Fung, K. Thompson, M.K. Doeltz, M. Mackie, T. E. Klein, D. Lent, *J. Environ. Sci. Health: A*, **1984**, 19, 97–231.
[6] M.M. Alnuaimi, M.A. Rauf, S.S. Ashraf, *Dyes Pigm*, **2007**, 72, 367–371.
[7] J. H. Sun, S.P. Sun, G.L. Wang, L.P. Qiao, *Dyes Pigm*, **2007**, 74, 647–652.
[8] A. Houas, H. Lachheb, M. Ksibi , E. Elaloui, C. Guillard, J. M. Herrmann, *Appl. Catal. B: Envron*, 2001, 31, 145–151.
[9] X. R. Xu, H. B. Li, J. D. Gu, *Chemosphere*, **2006**, 63, 254–260.
[10] D. Chatterjee, S. Dasgupta, *J. Photochem. Rev*, **2005**, 6, 186-205.
[11] Xinbo D, Danjun W, Kebin L, Yanzhong Z, Huaiming H, Ganglin H, Vanadium-substituted heteropolyacids immobilized on amine- functionalized mesoporous MCM-41: A recyclable catalyst for selective oxidation of alcohols with H2O Mater. Res. Bull., 2014, 57, 210-220.

# Removal of cationic dye (Methylorange) from aqueous solution using $PMnW_{11}$@PANI@CS composite

**Shima Hosseini, Mohamad Ali Rezvani*, Zahra Shokri Aghbolagh**

*Department of Chemistry, Faculty of Science, University of Zanjan, 451561319, Zanjan, Iran*

**Corresponding author Tel.: Fax: +98241 5152617.*

**E-mails: shima_hosseini@znu.ac.ir, mrezvani@znu.ac.ir, zahra.shokri@znu.ac.ir*

## Abstract

In this study a new nanocomposite, $PMnW_{11}$@PANI@CS has been synthesized as an efficient and green catalyst for the removal of cationic dyes such as Methylorange (MO) from aqueous solution. The nanocomposite was successfully prepared by reaction of mono Mn(II)-substituted Keggin-type polyoxometalate $Cs_5PMnW_{11}O_{39}$ ($PMnW_{11}$), Polyaniline (PANI), and chitosan (CS) at room temperature under sonication condition. The organic-inorganic hybrid characterized by FT-IR, UV–Vis, XRD, and SEM techniques. In this study the ability of $PMnW_{11}$@PANI@CS to remove of Methylorange (MO) from aqueous solution by adsorption was studied. Experiments were conducted by varying parameters of dye concentration of MO, photocatalyst concentration and temperature and contact time. The percentage of color removal decreased with the increase of initial dye concentration. Results obtained indicate that $PMnW_{11}$@PANI@CS nanocomposite could be employed as an efficient catalyst much more than the pure $PMnW_{11}$, CS and PANI powders for decolorization from water.

**Keywords**: Green catalyst, Dye removal, Methylorange.

## Introduction

Pigments and dyes are widely used in the industry, such as cosmetic, food, pulp, textile, rubber, paper, plastics, and leather, to co final products [1-2]. Therefore, release of dyes from the wastewater has been an important environmental concern to minimize the water and soil pollution [2]. Several methods such as precipitation, advanced oxidation, membrane filtration, electrochemical, ion-exchange, coagulation, and adsorption [3-8] are used for the release of dyes from wastewater. In this study new photocatalysis synthesized by reaction of $PMnW_{11}$with PANI and their immobilization on the surface of CS. The chemical characterization of this compound nanocomposite was accomplished by means of UV-Vis, FT-IR, XRD, and SEM techniques. The MO in different photocatalytic disinfection process and in visible light and took an early materials. The best possible value 0.01 gr of catalytic and put under the glare is light. Using UV-Vis spectroscopy in the range of 400 to 800 removal color is calculated.

## Experimental

*General*

All solvents and reagents which are used in this synthetic procedure are available commercially and were used as received, unless otherwise indicated. The products characterized by analytical instrument FT-IR, UV-Vis, XRD and SEM. Typical real gasoline (density 0.7784 g/ml at 15°C, total sulfur content 0.498 wt.%, and mercaptan 97 ppm) was used. X-ray diffraction (XRD) patterns was accomplished by D8 advance Brucker and radiation Cu kα (λ=1.54 nm) in the range of $10° \leq 2\theta \leq 35°$. Fourier transform infrared (FT-IR) spectra were recorded by Thermo-Nicolet-is 10 in the range of 400-4000 $cm^{-1}$. Ultraviolet-visible (UV-vis) spectra were studied with a double beam termo-heylos spectrophotometry in the range of 200-400 nm. Scanning electron microscope (SEM) images were obtained on a LEO 1455 VP with an accelerating voltage of 10.00 KV.

***Preparation of PANI***

In this method aniline and ammonium persulfate were used. In a typical procedure, 0.5 mL of pure aniline monomer was added to 10 mL of deionized water and the solution was stirred at room temperature. Then an ammonium persulfate solution was prepared by dissolving 1.1 gr of ammonium persulfate in 5 mL deionized water and then it was added drop-wise to the first solution. After that it was dispersed for 10 min by sonication, followed immediately by magnetic stirring for 30 min. The solution was then filtrated, upon filtering washed with 10 mL ethanol and 10 mL deionized water and dried at 80˚C for 3 h.

***Preparation of $PMnW_{11}$***

In a typical reaction, 0.3 gr of $PW_{12}O_{40}$ was dissolved in 5 mL of distilled water. To this solution, NaOH were added drop-wise till the pH was adjusted to 4.5 under stirring, and the mixture was heated to 90 ˚ C. 0.04 gr $MnNO_3$ dissolved in 5 mL distilled water was added to a.m. solution in 90˚C. Then 0.2 gr KCl were added to it and a yellow residue were obtained [9]. The formed solid was $PMnW_{11}$.

***Synthesis of $PMnW_{11}$@PANI***

A solution of $PMnW_{11}$was prepared by dissolving 0.05 gr of POM in 4 mL of deionized water. Then it was added drop-wise into the a.m. solution of PANI and it was stirred for 2 h. at last the solution was filtrated and washed with 10 mL of ethanol and 10 mL of deionized water.

***Synthesis of $PMnW_{11}$@PANI@CS***

An aqueous solution of chitosan (0.1 gr) was prepared by dissolving CS in 20 mL of aqueous acetic acid (2 wt%) and then it was stirred at 50˚ C for 1-2 h till it was become a concentrated gel. After that 0.04 gr of $PMnW_{11}$@PANI dissolved in 5 mL of acetic acid (2 wt%) was dispersed for 20 min and then was poured into the CS solution drop-wise while the whole solution was under sonication for 1h. then dried at 80 ˚C for 12h.

***Decolorization test method***

The adsorption of MO from aqueous solutions by $PMnW_{11}$@PANI@CS was tested as follows. The adsorption of dye was evaluated by adding different concentration of adsorbent/dye solution. After the agitation

at a rate of 2500 rpm for 30 min under 25˚C, the solution was centrifuged and small amounts of the liquid were taken to be analyzed. Methylorange concentration in supernatant after separation was monitored by UV–vis spectrophotometer at $\lambda_{max}$=465 nm. The amount of adsorbed dye $Q_e$ (mg/g) was calculated as follows:

$$Q_e=(\frac{C_i-C_f}{C_i})\times 100$$

Where $C_i$ is the initial absorption of dye and $C_f$ is the dye absorption after t (min) time.

## Results and discussion

### *Characterization of synthesized photocatalyst*

In order to support our observations, the FT-IR spectroscopy analysis of $PMnW_{11}$, PANI, CS, $PMnW_{11}$@PANI, and $PMnW_{11}$@PANI@CS shown in Figure 1. The perfect hybridization of $PMnW_{11}$ on modified PANI was proven by its characteristic stretching peaks of W-O terminal (W = $O_t$) and W-O bridging groups (W–$O_b$–W, W–$O_c$–W), at 942 $cm^{-1}$ and 871, 802 $cm^{-1}$ which confirm the presence of, respectively and single strong band at 1071 $cm^{-1}$ assigned to the P-$O_a$ stretching modes of the central $PO_4$ tetrahedron which are in agreement with literature data. These peaks has shown a red shift when compared with pure $PMnW_{11}$ peaks, to the strong interaction between the amine group on the PANI and $PMnW_{11}$ due to the strong adsorption *via* electrostatic binding between them [1].

The binding of $PMnW_{11}$@PANI@CS was also followed by UV-Vis spectroscopy. $PMnW_{11}$, PANI, CS and $PMnW_{11}$@PANI@CS samples were dispersed in ethanol solvent with different concentrations from 0.05 mg $mL^{-1}$ to 0.5 mg $mL^{-1}$. The absorption peak was showed at 215 nm correspond to ligand-to-metal charge transfer (LMCT) transition of $PMnW_{11}$, 221 nm for $PMnW_{11}$@PANI@CS which indicated red shifts in the modified $MnW_{11}$@PANI@CS hybrid nanocomposite. This shifts an evidence for the intermolecular electronic interactions between $PMnW_{11}$, PANI and CS [9].

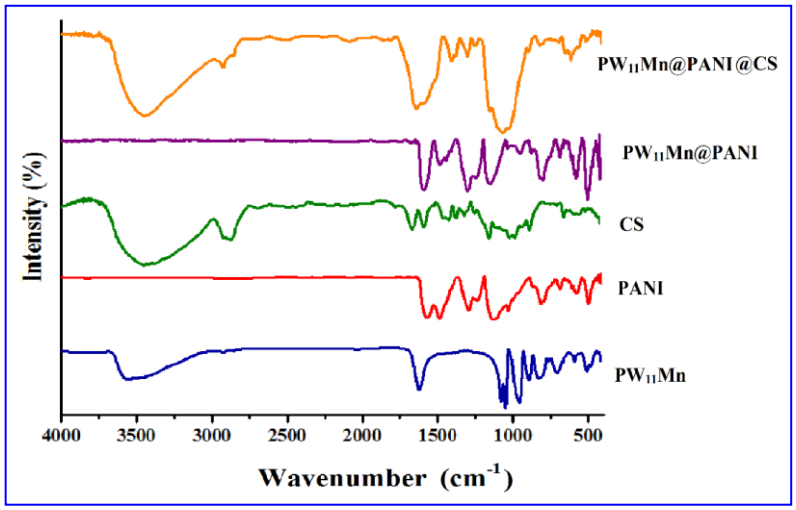


**Figure 1.** FT-IR spectroscopy analysis of $PMnW_{11}$, PANI, CS, $PMnW_{11}$@PANI, and $PMnW_{11}$@PANI@CS.

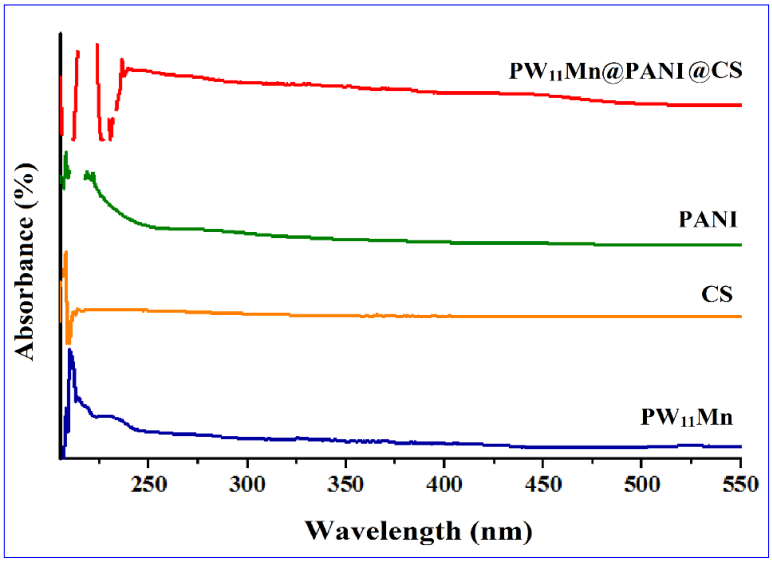


**Figure 2.** UV–vis spectra of spectra of $PMnW_{11}$, PANI, CS, and $PMnW_{11}$@PANI@CS.

The crystalline structure was accomplished using X-ray diffraction (XRD) methods and revealed the composition $PMnW_{11}$@PANI@CS. The patterns were collected in the scanning range 10° ≤ 2θ ≤

35° are shown in Figure 3. The peaks for pure $PMnW_{11}$ at 6°-10°, 25°-30° and 30-40 degrees indicated kegging type of polyoxometalate [9]. Investigation of the powder XRD data assigned the presence of the Keggin type polyoxometalate $Cs_5PMnW_{11}O_{39}$ ($PMnW_{11}$) on the PANI and CS, which had been formed in situ under milding conditions in the presence of PANI, CS and Keggin-type Cs salt of a mono Mn(II)-substituted phosphotungstate ($Cs_5PMnW_{11}O_{39}$, $PMnW_{11}$). There is a complex relationship between the dye removal efficiency and structure of catalyst, which provides an appropriate structure for elimination of MO molecules. It is suggested that the interactions of the $PMnW_{11}$ with PANI and the CS are important factors in catalytic activity in our reaction. The peaks for pure $PMnW_{11}$ at 25°-30° and 40°-60° degrees indicated kegging type of polyoxometalate [9]. The XRD pattern of $PMnW_{11}$@PANI@CS exhibited one broad peak around 2θ=11.5°, this peak with the decrease in intensity was similarly observed in diffraction patterns of the PANI [7-8].

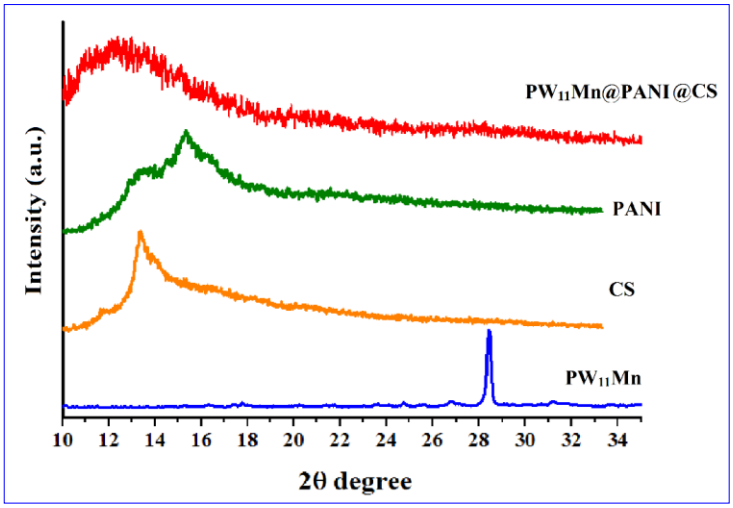


**Figure 3.** XRD of $PMnW_{11}$, PANI, CS, and $PMnW_{11}$@PANI@CS.

The morphology of the blank $PMnW_{11}$ (Figure 4a) PANI (Figure 4b), CS (Figure 4c) and $PMnW_{11}$@PANI@CS (Figure 4d) displays the withered morphology. Due to the sonication condition as in the preparation procedures, it is clear that the supports $PMnW_{11}$@PANI@CS photocatalyst showed the nanometer microspheres morphology with almost uniform size (Figure 6d). Therefore, this photocatalyst has appropriate structure for removal of dye from aqueous solution.

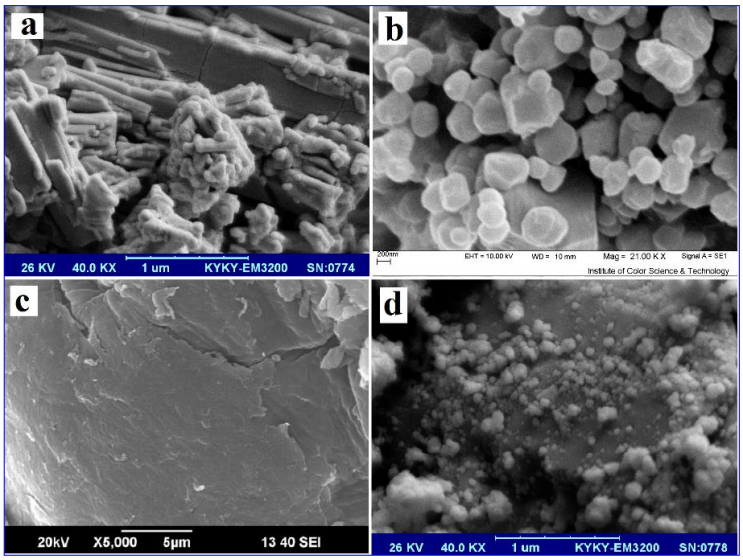


**Figure 4.** SEM images of a sample of $PMnW_{11}$@PANI@CS hybrid catalyst. The images of (a): $PMnW_{11}$, (b): PANI, (c): CS, and (d): $PMnW_{11}$@PANI@CS.

***Effect of photocatalyst dosage on the removal of dye from aqueous solution***

$PMnW_{11}$@PANI@CS samples (0.02, 0.015, 0.01, and 0.005 gr) were added to flasks containing 20 ml of MO solution of concentration 10 mg/L. The degradation results are shown in Figure 5. The adsorption decrease greatly with increasing amounts of catalyst. The elimination of MO dye using $PMnW_{11}$@PANI@CS composite at different initial concentrations (0.005-0.02 gr) was analyzed as a function of contact time to depict the equilibrium time. The rapid removal was observed during the first 30 min and gradually decreased with laps of time until equilibrium. The increased

activity at initial stage could be due to the availability of more adsorption sites on $PMnW_{11}$@PANI@CS surface, and gradual occupancy of these sites reduced the reaction rate and the adsorption becomes less efficient. The time required to attain this state of equilibrium was termed as equilibrium time, and the amount of dye adsorbed at the equilibrium time reflected the maximum adsorption capacity of the adsorbent under these particular conditions. It is evident from Figure 5 that the contact time needed to attain the equilibrium condition for MO was about 30 min.

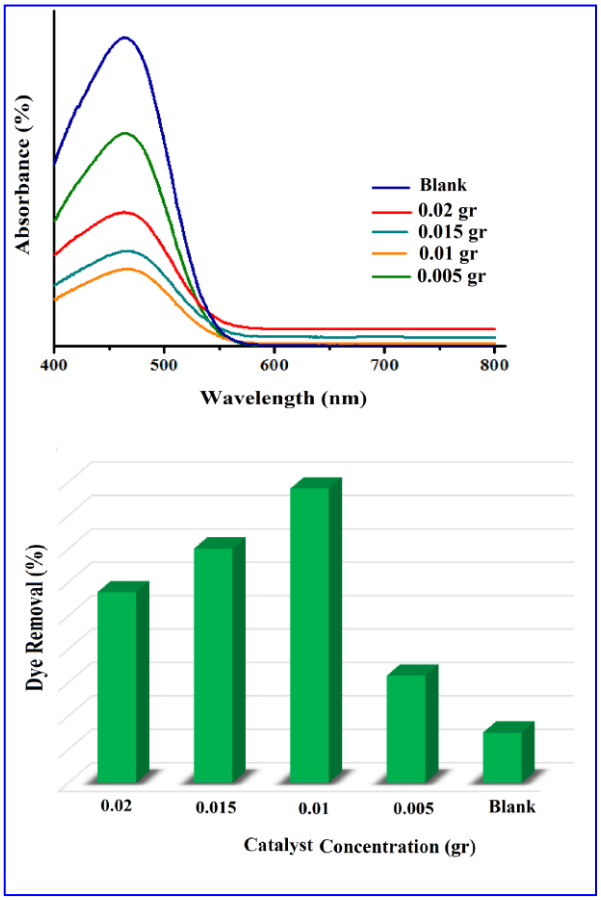


**Figure 5.** Effect of photocatalyst dosage on the removal of dye from aqueous solution

***Effect of reaction temperature and time on the removal of dye from aqueous solution***

The catalytic activities of the $PMnW_{11}$@PANI@CS in the degradation of MO dye at different temperature (Figure 6) and times (Figure 7) were compared and shown. The removal time will indicate that the effect of the catalyst has been greater. In this method, for study of effect of temperature the color elimination value has been measured in the 30 minute intervals, the removal value has reached 98%.

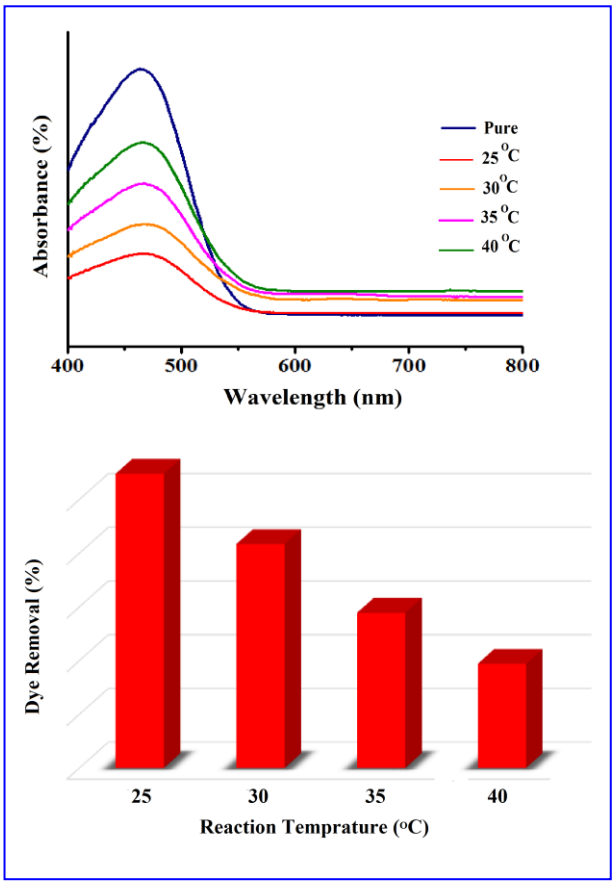


**Figure 6.** Effect of reaction temperature on the removal of dye from aqueous solution.

***Effect of dye dosage on the removal of dye from aqueous solution***

Methyl orange samples (10, 20, 30 and 40 ppm) were added to flasks containing 0.01 gr of synthesized catalyst. The degradation results are shown in Figure 8. The removal decrease with increasing amounts of dye. When 10 ppm of cationic dye (MO) were

used, it took less than 30 min the removal value to reach 98%.

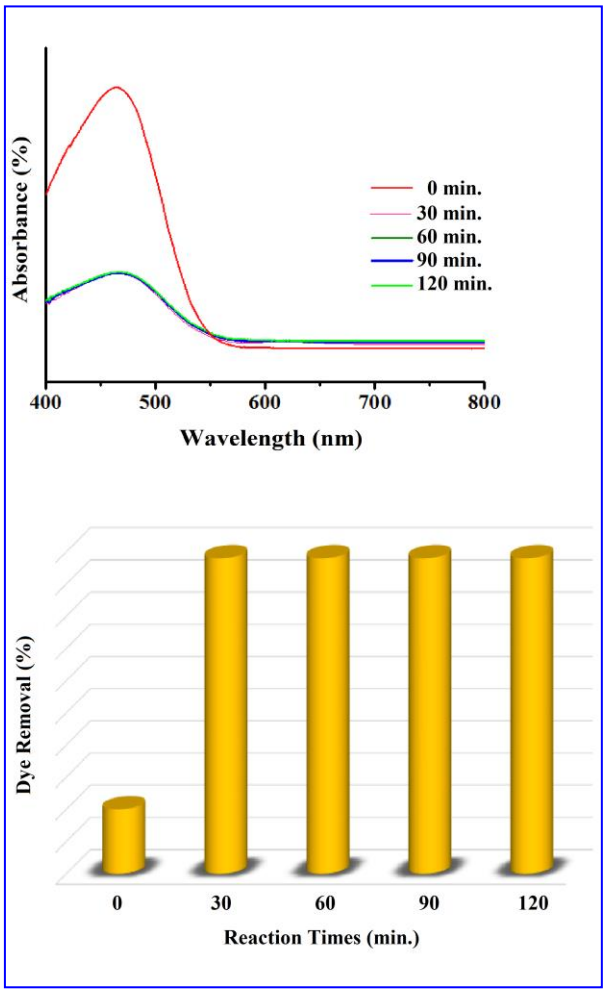


**Figure 7.** Effect of reaction time on the removal of dye from aqueous solution.

## Conclusion

In conclusion, the new type of phase transfer nanocatalyst $PMnW_{11}$@PANI@CS has been successfully prepared by modification of $PMnW_{11}$ clusters with PANI and their immobilization on the surface of CS. For the first time, the catalytic activity of the catalyst was tested on methylene blue from aqueous solution. The percentage of color removal decreased with the increase of initial dye concentration. Results obtained indicate that $PMnW_{11}$@PANI@CS nanocomposite could be employed as an efficient catalyst much more than the pure $PMnW_{11}$, CS and PANI powders for decolorization from water.

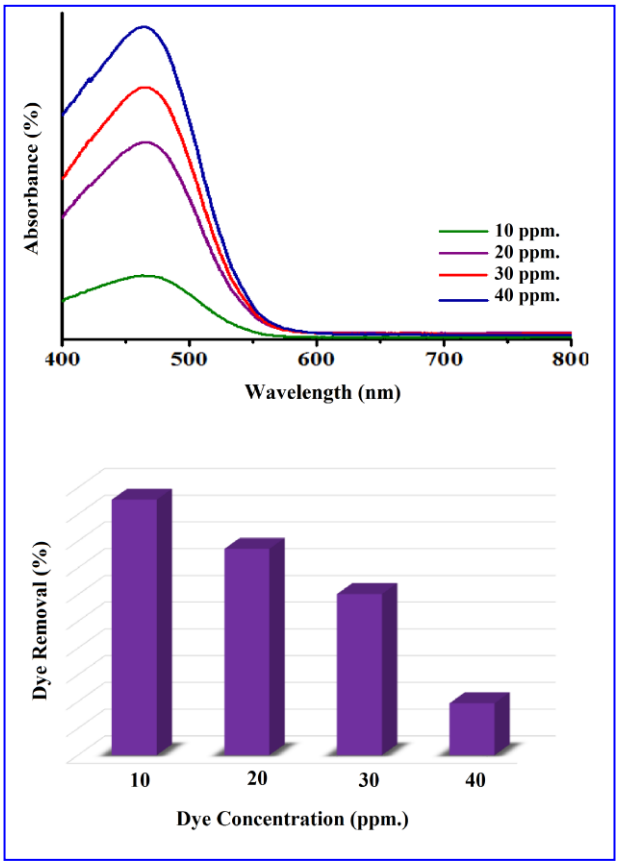


**Figure 8.** Effect of dye dosage on the removal of dye from aqueous solution.

## Acknowledgments

The authors are grateful to the University of Zanjan for supporting this work.

## References

[1] V. Janaki, Oh. Byung Taek, K. Shanthic, K. j. Lee, A.K. Ramasamy, K. K. Seralathan, *Synthetic Metals*, **2012**, *162*, 974–980.

[2] G. Annadurai, L.Y. Ling, J.F. Lee, *Journal of Hazardous Materials*, **2008**, *152*, 337–346.

[3] G.Z. Kyzas, N.K. Lazaridis, *Journal of Colloid and Interface Science*, **2009**, *331*, 32–39.

[4] G.L. Dotto, L.A.A. Pinto, *Journal of*

*Hazardous Materials*, **2011**, *187*, 164–170.
[5] M.M. Alnuaimi, M.A. Rauf, S.S. Ashraf, *Dyes Pigm*, **2007**, *72*, 367–371.
[6] J. H. Sun, S.P. Sun, G.L. Wang, L.P. Qiao, *Dyes Pigm*, **2007**, *74*, 647–652.
[7] D. Chatterjee, S. Dasgupta, *J. Photochem. Rev*, **2005**, *6*, 86-205.
[8] X. R. Xu, H.B. Li, J. D. Gu, *Chemosphere*, **2006**, *63*, 254-260.
[9] M. A. Rezvani, Z. S. Aghbolagh, H. H. Monfared, S. Khandan, *Journal of Industrial and Engineering Chemistry*, **2017**, *52*, 42–50.

# Vanadium containing keggin–type polyoxometalate supported on anatase as an efficient and reusable catalyst for oxidation of thiols

**Mohammad Mohammadi, Mohammad Ali Rezvani* and Majid Hadi**

*Department of Chemistry, Faculty of Science, University of Zanjan, 451561319, Zanjan, Iran*

*Corresponding author; E-mail: marezvani@znu.ac.ir Tel: +98 241 5152477 Fax: +98241 5152617.

## Abstract

In this manuscript, vanadium polysilicotangestate ($H_7SiV_3W_9O_{40}$) (SiVW) as a Keggin-type polyoxometalate was synthesized and immobilized on anatase TiO2 via sol-gel method. The materials characterized by XRD, UV-Vis, IR techniques. Catalytic activity of synthesized nanocomposite was tested on oxidative of thiols. This Keggin-type supported catalyst was shown to be able to have oxidative of thiols into the corresponding disulfides with high yield. The advantages of this method are nontoxic, mild condition and environmentally friendly. This system, SiVW@$TiO_2$/$H_2O_2$, provides an efficient and convenient method for oxidation of thiols.

**Keywords**: : nanocomposite; polyoxometalate; anatase; thiol; Keggin.

## Introduction

Disulfide plays an important role in biology and synthetic organic chemistry [1-3]. Disulfide is used as a protecting group under oxidative conditions for thiol, and can be regenerated by S-S bond cleavage. Disulfides have also found industrial applications as vulcanizing agent and are important synthetic intermediates in organic synthesis [4]. Various reagents and oxidants have been employed for conversion of thiols to disulfides. Some of these methods suffer from obvious disadvantages such as long reaction times, limited availability of the oxidant, toxicity of reagents and difficult isolation of products [5-9]. In continuation of our group research on the syntheses and application of polyoxometalates in organic syntheses [10-16] and due to the importance of derivatives of disulfides in biological and chemical processes, we hereby report the applicability of POM@TiO2 for efficient oxidation of thiols to the corresponding disulfides. We wish to report a very efficient and simple method for oxidative of thiols into the corresponding disulfides using hydrogen peroxide as an oxidizing reagent catalyzed by the H7SiV3W9O40@TiO2 (SiVW@TiO2) nanocomposite under mild conditions.The application of polyoxometalates(POMs) as catalytic materials is increasing continuously in the catalytic field. These compounds possess unique properties such as: well-defined structure, Brönsted acidity, possibility to modify their acid–base and redox properties by changing their chemical composition (substituted POMs), ability to accept and release electrons, high proton mobility, being environmentally benign and presenting fewer disposal problems [11-15]. Supporting the heteropolyacids on solids with high surface areas improve their catalytic performance in various liquid–solid and –solid surface heterogeneous reactions. Titanium dioxide is a wide-band-gap semiconductor material that has received intense scrutiny for a broad range of applications, thanks to its intriguing physical-chemical properties and cheap, abundant, and reasonably nontoxic nature [16-18]. TiO2, also a widely used catalyst support as well as a catalyst is known to enhance the catalytic activity in many cases because of the strong interaction between the active phase and the support [10-13]. We designed anatase TiO2 crushed nano leaf coupled by mixed-addenda vanadium-containing keggin type polyoxometalate at 100 °C via sol–gel method under oil-bath condition, as a nano catalyst for oxidative of thiols. The chemical characterization of this compound was accomplished by means IR, XRD, TEM and UV–vis techniques.

## 2. Experimental

### 2.1. Materials

All solvents and reagents used in this work are available commercially and were used as received, unless otherwise indicated. Previously reported methods were used to purify the thiols [15]. Preparation of mixed heteropolyacids and salts were based on a literature procedure with the following modifications [10-13]. Titanium (IV) tetraisopropoxide was obtained from Merck Chemical Company. All chemicals were purchased from Merck and used without purification. The 1H-NMR spectra were recorded on a FT-NMR Bruker 100 MHz Aspect 3000 with tetramethylsilane as an internal standard and CDCl3 as the solvent. The IR spectra were recorded on a Buck 500 Scientific Spectrometer in KBr pellets.

### 2.2. Synthesis of nanocatalyst SiVW@$TiO_2$

The $SiW_9V_3$@$TiO_2$ nanoparticle was prepared as following: First, titanium tetraisopropoxide was added into glacial acetic acid with stirring. Next, a solution of H7SiV3W9O40 [10] in water was drop wised in it. The mixture was stirred to dissolve any solid. Then, the sol was heated to 100 ° C under oil bath condition until a homogenous SiVW@TiO2 hydrogel was formed. Finally, the gel was filtered, washed

with deionized water-acetone and dried in oven at 50 º C overnight (Scheme 1).


**Scheme 1**. Chart of synthesis of nanocatalyst.

## 2.3.General procedure for oxidation of thiols

The SiVW@TiO2 (0.3 g, 0.1 mmol) was dissolved in the mixture of 17 mL of ethanol and 3 mL of H2O. The substrate, (thiol) (4 mmol) and 5 mL H2O2 were added to solution. The reaction mixture was stirred at 30 °C until thin layer chromatography, TLC, indicated the reaction was complete. The solvent was then removed and the resulting residue was then washed with CH2Cl2. After completion of the reaction, the solid product was filtered off and recrystallized. The products were isolated and identified by comparison of their physical and spectral data with authentic samples prepared according to a previous method [11].

### *2.4. Characterization methods*

By a D8 Bruker Advanced, X-ray diffractometer using Cu Kα radiation (α=1.54 A), X-ray diffraction (XRD) patterns were recorded. The patterns were collected in the range 20–70° 2θ and continuous scan mode. On a Philips CM10 transmission electron microscope with an accelerating voltage of 100 kV, transmission electron microscope (TEM) images were obtained. The electronic spectra of the synthesized catalysts were taken on a RAYLEIGH (UV-1800) ultraviolet–visible (UV–vis) scanning spectrometer. Infrared spectra were recorded as KBr disks on a Buck 500 scientific spectrometer.

### *3. Results and discussion*

### *3.1. Characterization of synthesized nanocatalysts*

XRD patterns of SiVW@$TiO_2$, H7SiV3W9O40 and TiO2 are shown in Figure 1. These patterns showed the uniform anatase structure. XRD patterns (a) and (b) in Figure 1 are corresponded to pristine $H_7SiV_3W_9O_{40}$ and $TiO_2$, respectively. The XRD pattern corresponding to pure $TiO_2$ was found to match with that of fully anatase phase. No peaks from any else impurities or rutile phase were observed, which indicates the high purity of the obtained powders. The sharp diffraction peaks manifest that the obtained TiO2 have high crystallinity. When $H_7SiV_3W_9O_{40}$ is bound to the TiO2 surface, SiVW@$TiO_2$, approximately all of signals corresponding to $H_7SiV_3W_9O_{40}$ is disappeared (Figure 1(c)) and the final pattern matched to fully anatase phase of $TiO_2$ (JCPDS No. 21-1272), which is most likely due to $H_7SiV_3W_9O_{40}$ forming only a thin coating on the TiO2 surface and thus the majority of the observed signals are due to the crystal phases of anatase $TiO_2$. Using the Scherrer equation, the crystallite diameter of SiVW@$TiO_2$ is about 8 nm. Also UV-visible spectroscopy of obtained powders was studied. UV-vis spectra of SiVW@TiO2 nanocomposite, SiVW ($H_7SiV_3W_9O_{40}$) and $TiO_2$ are shown in (Figure 1(d)). UV-vis spectra showed broad and strong absorption in range of 200-400 nm for SiVW@$TiO_2$ crystallite, which was different from original $H_7SiV_3W_9O_{40}$ and anatase $TiO_2$. The SiVW@$TiO_2$ nanocomposite shows a red shift compared with the parent anatase, and a blue shift compared with H7SiV3W9O40. In addition, some hyper fine structure in the range from 310 to 350 nm observed in $H_7SiV_3W_9O_{40}$ spectrum. The inset of the figure shows the UV-vis spectrum of the SiVW@$TiO_2$ indicating there are two peaks around 220 and 290 nm. The above UV–vis results indicate that introduction of $H_7SiV_3W_9O_{40}$ into $TiO_2$ framework has an influence on coordination environment of $TiO_2$ crystalline [10]. In ultraviolet light regions, which are shorter than 340 nm, pure nano $TiO_2$ whose band gap energy equivalent to around 335nm (3.70 eV) shows the highest absorbance due to charge-transfer from the valence band (mainly formed by 2p orbitals of the oxide anions) to the conduction band (mainly formed by 3d t2g orbitals of the $Ti^{4+}$ cations) [10].

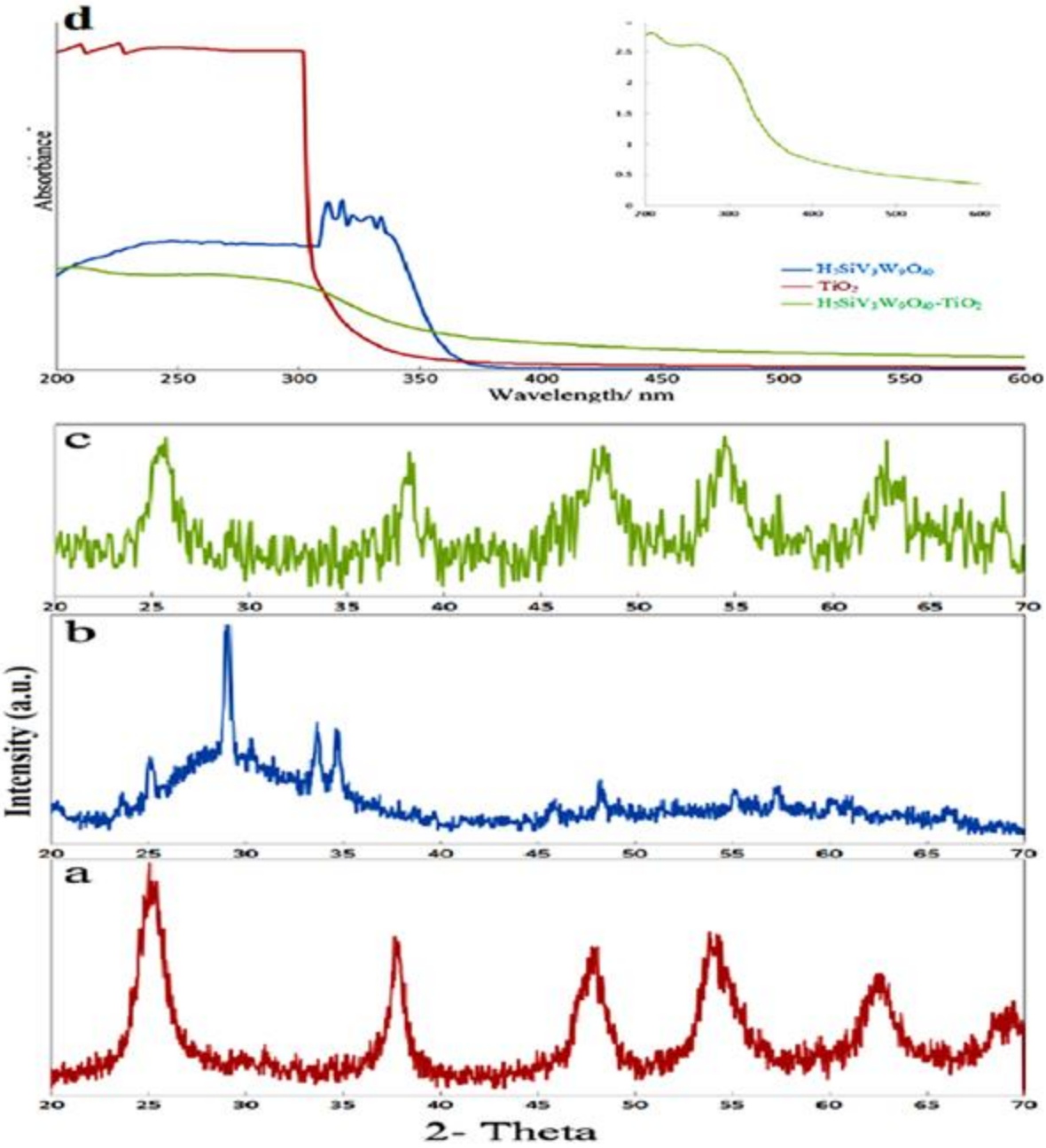


**Figure 1.** XRD pattern of (a) $TiO_2$ (b) SiVW and (c) SiVW@$TiO_2$ and (d) UV-vis spectra of obtained catalysts.

Figure 2 depicts the transmission electron micrographs of obtained powders. Figure 2(a) shows the TEM image of obtained fully anatase phase of $TiO_2$ as crushed nano leaf with average size of about 20 nm. It is observed from Figure 2(b) that after modification of anatase with $H_7SiV_3W_9O_{40}$ a significant change in size and morphology was occurred. It can be seen that in Figure 2(b), most of the obtained powders are smaller than that of parent $TiO_2$. As shown in TEM image of SiVW@$TiO_2$ most of nano particles formed in nano cluster shape and there is not significant agglomeration between grains. In order to investigate the structural evolution of catalysts in function of the temperature of thermal treatment, XRD patterns and FT-IR spectra were recorded after calcination at increasing temperatures from 100 to 600 $^0$C.

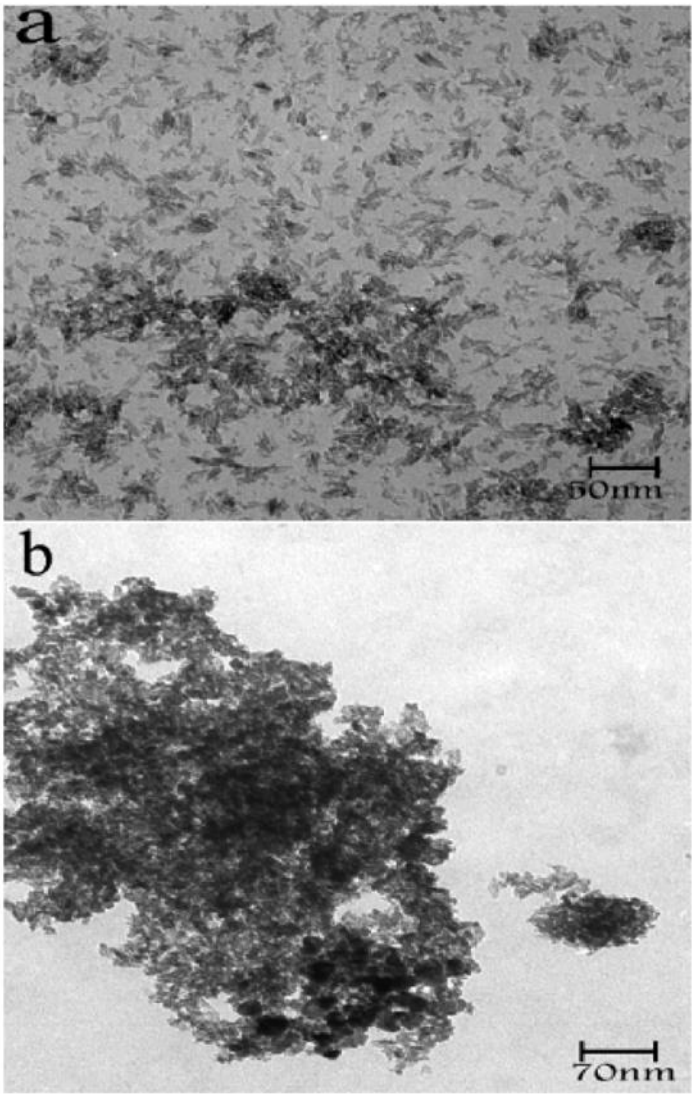


**Figure 2.** TEM image of (a) $TiO_2$ and (b) SiVW@$TiO_2$.

Figure 3 (a) and (b) show XRD patterns and IR spectra of $H_7SiV_3W_9O_{40}$ at 100-600$^0$C range, respectively. From Figure 3 (a), it can be seen that at 100 and 200 $^0$C XRD patterns of $H_7SiV_3W_9O_{40}$ are same. By increasing of temperature more than 300 $^0$C XRD patterns were changed. In spite of broadening of corresponding picks it is no observed significant change in position of picks. Indeed, it is not observed any additional picks respect to 100 $^0$C pattern. On the other hand, FT-IR spectra, Figure 3 (b), of $H_7SiV_3W_9O_{40}$ are not show any change in bands.

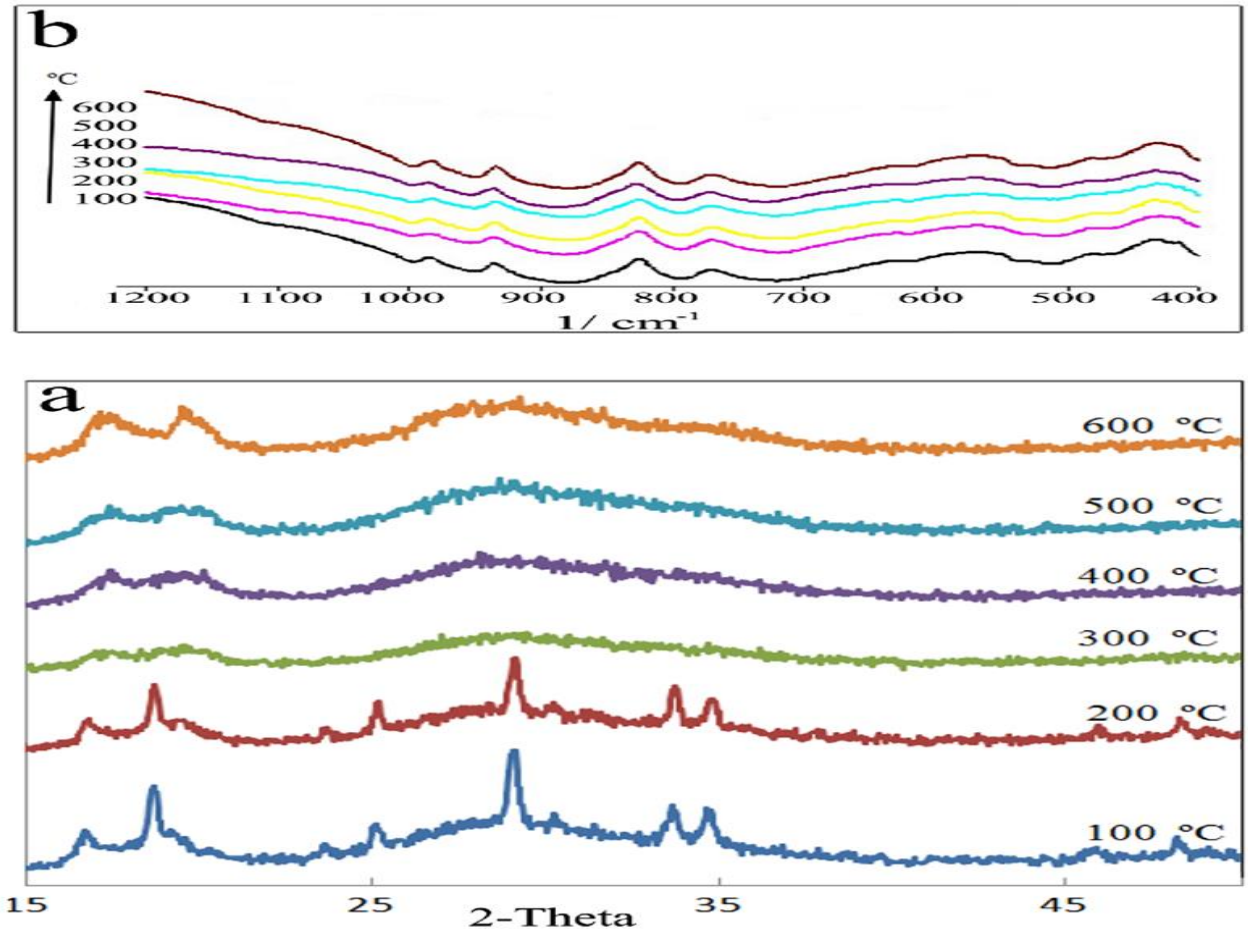


**Figure 3**. Effect of temperature on (a) XRD pattern and (b) IR spectra of SiVW.

### 3.2. Effects of the catalyst structure

Table 1 was shown effect of catalyst on oxidation of thiols by $H_2O_2$. 4-chlorothiophenol was taken as a model compound. The SiVW@$TiO_2$ nanoparticle was very active catalyst system for oxidative of thiols, while other polyoxometalates systems were much less active. It is shown that the oxidation reactivity order of the catalyst in the presence of hydrogen peroxide is: SiVW@$TiO_2$ > SiVW ($H_7SiV_3W_9O_{40}$) > $H_5PMo_{10}V_2O_{40}$ > $H_6PMo_9V_3O_{40}$ > $H_3PMo_{12}O_{40}$ > $H_3PW_{12}O_{40}$ > H4$SiW_{12}O_{40}$. The results show that the catalytic activity of SiVW@$TiO_2$ nanocomposite has presented much higher than other unsupported polyoxometalates. Supporting $H_7SiV_3W_9O_{40}$ on solid $TiO_2$ with high surface area improve their catalytic activity. The amount of each catalyst was constant throughout the series. The Keggin-type polyoxometalates led to more effective reactions in comparison with the Wells–Dawson type polyoxometalates.

**Table 1.** Effect of different catalyst in Oxidation of 4-Chlorothiophenol[a]

| Entry | Catalyst | Time (min.) | Temperature (ºC) | Yield (%) |
|---|---|---|---|---|
| 1 | SiVW@$TiO_2$ | 30 | 30 | 98 |
| 2 | SiVW ($H_7SiV_3W_9O_{40}$) | 60 | 60 | 95 |
| 3 | $H_5PMo_{10}V_2O_{40}$ | 60 | 60 | 94 |
| 4 | $H_6PMo_9V_3O_{40}$ | 60 | 60 | 94 |
| 5 | $H_3PMo_{12}O_{40}$ | 60 | 60 | 90 |
| 6 | $H_3PW_{12}O_{40}$ | 60 | 60 | 89 |
| 7 | $H_4SiW_{12}O_{40}$ | 60 | 60 | 87 |

[a] Condition for oxidation: 4 mmol substrate, 5 ml $H_2O_2$ as an oxidant, 1.0 mmol catalyst, 20 ml solvent 25 ml $CH_2Cl_2$ as an extraction solvent.

### 3.3. Effect of temperature

The reaction was carried out at different temperatures under the same conditions by SiVW@$TiO_2$ as a nanocatalysts and $H_2O_2$ system. 4-chlorothiophenol was taken as a model compound. The results are shown in Table 1 and 2. The results in Table 2 showed that yields of products are a function of temperature. The results show that yield increased as the reaction temperature was raised. % conversion of model compound increased with temperature and time (Fig. 4). In figure 4, % conversion of 1, 8-Octanedithiol at 60 ºC is higher than that at 50 ºC. 98% conversion of 1, 8-Octanedithiol ($SHCH_2(CH_2)_6CH_2SH$) was obtained at 60 ºC. The catalytic activities of the SiVW@$TiO_2$ nanocatalysts in the oxidation of 1, 8-octanedithiol at different temperatures, 10 - 60 ° C were compared.

**Table 2.** Effect of temperature on oxidation of different thiol and dithiol using SiVW@$TiO_2$ catalyst

| Entry | *Thiol* | Disulfide | *Time (min.)* | *Yield %* | M.P(°C) found | M.P(°C) literature |
|---|---|---|---|---|---|---|
| 1 | 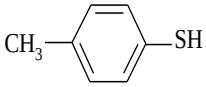 | 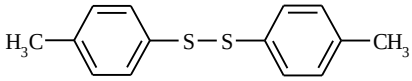 | 30 | 98 | 43-44 | 44-45 |
| 2 | 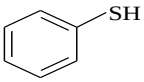 | 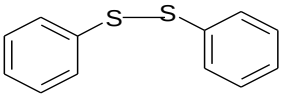 | 45 | 95 | 60-61 | 61 |
| 3 | 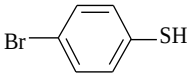 | 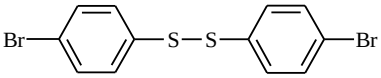 | 30 | 96 | 90-92 | 91-93 |
| 4 | 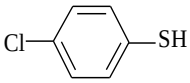 | 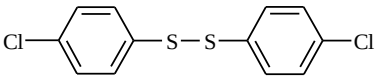 | 30 | 98 | 72-73 | 70-71 |
| 5 | 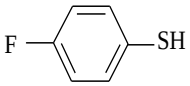 | 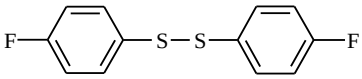 | 50 | 91 | liquid | -- |
| 6 | 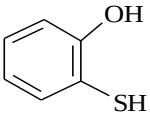 | 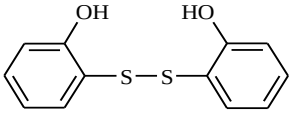 | 30 | 89 | liquid | -- |
| 7 | 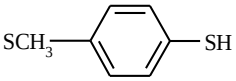 | 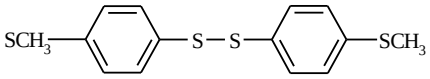 | 60 | 88 | 40-43 | 40-43 |
| 8 | 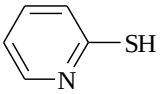 | 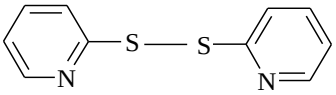 | 60 | 84 | 55-56 | 55-57 |
| 9 | 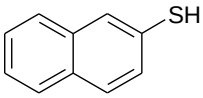 | 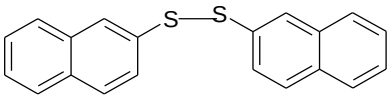 | 60 | 92 | 144-146 | 142-145 |

### 3.4. Effects of thiols substituent

The effects of various substituents on the yields of produced disulfides have been examined in the presence of SiVW@$TiO_2$ as a catalyst. As shown in Table 2, not only the nature of the substituent is important, but its position is so. As examples of electron-withdrawing groups, bromo, chloro and nitro substituted thiophene, were chosen and were converted to their corresponding disulfides. Thiols with electron-donation substituents were oxidized easier than the thiols with electron-withdrawing substituents.

### *3.5. Recycling of the catalyst*

At the end of the oxidation of thiols to disulfides, the catalyst was filtered, washed with dichloromethane, In order to know whether the catalyst would succumb to poisoning and lose its catalytic activity during the reaction, we investigated the reusability of the catalyst. All products are soluble in dichloromethane but the catalyst is not. Thus, it could be separated by a simple filtration and washed with dichloromethane and dried at 90 °C for 1 h, and reused in another reaction with the same substrate. Even after five runs for the reaction, the catalytic activity of SiVW@$TiO_2$ was almost the same as that freshly used catalyst. The results are summarized in Table 3.

**Table 3.** Reuse of the catalyst for oxidation of 4-Chlorothiophenol

| Entry | Isolated yield (%) |
|---|---|
| 1 | 96 |
| 2 | 94 |
| 3 | 94 |
| 4 | 92 |
| 5 | 91 |

## 4. Conclusion

Fixing of $H_7SiV_3W_9O_{40}$ into $TiO_2$ decreases the particle size of crushed nano leaf of anatase phase.The SiVW@$TiO_2$ nanoparticle was very active catalyst system for the models compound oxidation,while unmodified $H_7SiV_3W_9O_{40}$ showed much lower activity. This $TiO_2$ / polyoxometalates /$H_2O_2$ system provides an efficient, convenient and practical method for the syntheses of symmetrical disulfides.

**References**

[1] Y. Yang, Q. Wuc, Y. Guoa, C. Hu, (2005) J. Mol. Catal. A. 225: 203-208.

[2] N. Mizuno, M. Misono, (1998) Chem. Rev. 98: 199-204.

[3] T. Okuhara, N. Mizuno, M. Misono, (1996) Adv. Catal. 41: 113-118.

[4] T. Okuhara, T. Nishimura, H. Watanabe, (1992)J. Mol. Catal. 74: 247-153.

[5] W. Zhu, H. Li, X. He, Q. Zhang, H. Shu, Y. Yan, (2008) Catal. Commun. 9: 551-555.

[6] M. A. Rezvani, A. F. Shojaei, F. M. Zonoz, J. Serb. Chem. Soc. 79 (2014) 1099.

[7] N. M. Mahmoodi, M. A. Rezvani, M. Oveisi, A. Valipour, M. A. Asli, Mater. Res. Bull., 84 (2016) 422.

[8] M. A. Rezvani, M. Alinia Asli, M. Oveisi, R. babaei, K. Qasemi, S. Khandan, RSC Adv. 6 (2016) 53069.

[9] M. A. Rezvani, M. Alinia Asli, S. Khandan, H. Mousavi, Z. Shokri Aghbolagh, Chem. Eng. J. 312 (2017) 243.

[10] M. A. Rezvani, M. Shaterian, F. Akbarzadeh, S. Khandan, Chem. Eng. J. 333 (2018) 537.

[11] A. Fallah Shojaei, M.A. Rezvani, M. Heravi, J. Serb. Chem. Soc., 76 (2011) 1513.

[12] M.A. Rezvani, S. Khandan, M. Aghmasheh, J. Taiwan Inst. Chem. Eng. 77 (2017) 321.

[13] M. A. Rezvani, F. Mohammadi Zonoz, Ind. Eng. Chem. 22 (2015) 83.

[14] M. A. Rezvani, M. Shaterian, F. Akbarzadeh, S. Khandan, Chem. Eng. J. 333 (2018) 537.

[15] M. A. Rezvani, Z. S. Aghbolagh, H. H. Monfared, S. Khandan, J. Ind. Eng. Chem. 52 (2017) 42.

[16] M. A. Rezvani, A. Fallah Shojaie, M. H. Loghmani, Catal. Commun. 25 (2012) 36.

[17] A. Fallah Shojaei, M. A. Rezvani, M. H. Loghmani, Fuel Process. Technol. 118 (2014) 1.

[18] M. A. Rezvani, M. A. N. Asli, L. Abdollahi, M. Oveisi, J. Serb. Chem. Soc. 81 (2016)1.

# A highly efficient and green method for the synthesis of pranopyrazoles using Carbon-Based Solid Acid NanoCatalyst

**Maryam Pirhadi,[1] Seied Ali Pourmousavi,[1, 2] Zahra Hosainabadi[1]**

[1]School of Chemistry, Damghan University, Damghan, 36715-364, Iran

[2]Institute of Biological Science, Damghan University, Damghan, 36716-41167, Iran
E-mail: pourmousavi@du.ac.ir

**Abstract**

Carbon-based solid-acid Nanocatalyst (SPH-$SO_3H$) was prepared by the thermal treatment of sulfuric acid with starch and poly(vinyl chloride) at 180 °C in a sealed autoclave. Then the Nano catalyst was characterized by means of Field Emission Scanning Electron Microscope (FESEM) and Fourier-transform infrared spectra (FT-IR). SPH-$SO_3H$ Nanoparticles was used as an efficient catalysts for the one-pot synthesis of pranopyrazoles using hydrazinehydrate, ethylacetoacetate, malononitrile and aldehyde conditions at room temperature in high yields .

**Keywords**: carbon based solid acid, Multicomponent reaction, pranoprazoles**,** Nanocatalyst.

## Graphical Abstract:

**A Highly efficient and green method for thr synthesis of pyranopyrazoles using Carbon-based solid acid Nanocatalyst**

Maryam pirhadi, Seied Ali Pourmousavi, Zahra Hosainabadi

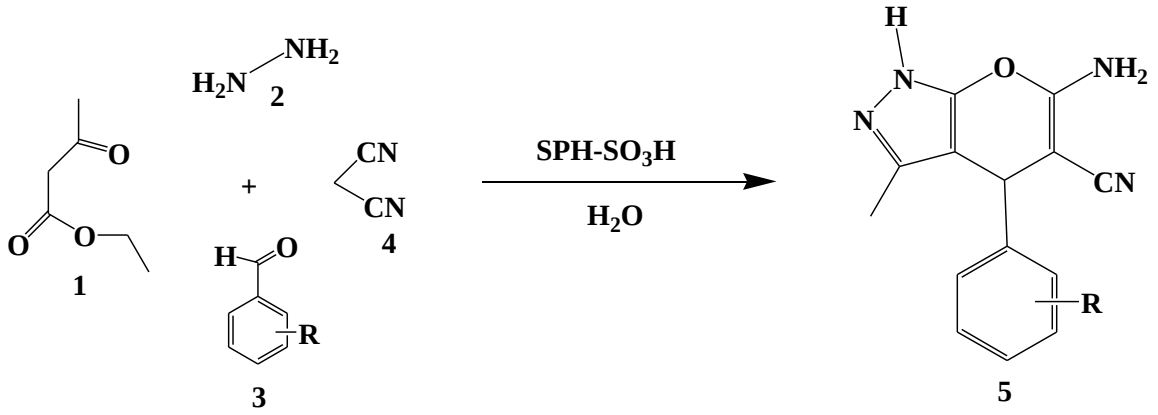

## Introduction

The increasing concerns about environmental issues have stimulated the research for recyclable strong solid acids to replace conventional toxic and corrosive acid catalysts, such as sulfuric acid [1]. Solid acid catalysts have received much attention for the potential substitution of the homogeneous acids with the advantages of easy separation and reusability [2]. Among them carbon-based solid acid catalysts have several advantages as solid catalysts because of the unique properties of carbon possessing sp, $sp^2$ and $sp^3$ bondings resulting in the ability to make different structures, such as layers, tubes and spheres. Carbon can be easily functionalized in amorphous to crystalline structures especially in the amorphous form [3–8].
$SO_3H$-bearing carbon materials have been reported to act as strong solid-acid catalysts. Hara's group first prepared sulfonated carbon catalysts via the sulfonation and carbonization of polycyclic aromatic hydrocarbons [9]. Recently, Hara et al. prepared a series of acidic carbon catalysts through the direct carbonization of raw materials such as sugar and cellulose followed by the sulfonation of the resulting carbons, and found that such acidic carbon materials exhibited good catalytic behavior [10].

The solid acid catalysts were generally prepared through two steps. In the first step, the carbonization of biomass was carried out to form polycyclic aromatic carbon sheets. Then, the aromatic carbon sheets were sulfonated to introduce the sulfonic acid groups. The carbonization process was taken at high temperature for a long period and large amount of wastes were produced during the process, which resulted in serious pollution. Efficient procedures for the synthesis of carbon-based solid acid through one-step hydrothermal carbonization have been developed [11].

Multi-component reactions (MCRs) are a specific batch of organic reactions in which the desired product is prepared during a single stage of the combination of raw materials.[12] This reaction was first introduced in 1850 by Stricker.[13] By using these reactions, complex organic molecules that have various functional groups can be synthesized. The advantages of these reactions include the ease of reaction, the shortening of the reaction time and the lower side effects. [14] In recent years, the pharmaceutical industry has been paying great attention to hybrid methods, and the development of heterogeneous reactions in the synthesis of heterocyclics has attracted many drug makers to making drug compounds reactive. [15] These structural kernel compounds are a myriad of active bioactive compounds that have anti-anxiety, fever, and honey properties.

These reactions, in addition to the pharmaceutical industry in research centers, are also very much considered. [16-20] One of the widespread applications of these reactions is the synthesis of piranopirazole derivatives. Pyranopyrazoles, the structural units of a series of natural products,[21] are known for their insecticidal[22] and anti-inflammatory activity,[23] molluscicidal activity,[24] and use in screening for chk 1 kinase inhibitor.[25] Pyrano[2,3-c] pyrazoles provide an interesting template for medicinal chemistry; some of the recent methods include synthesis in aqueous media,[26] in ethanol under reflux,[27] under microwave irradiation,[28] and under solvent-free conditions.[29] The reported methods offer some advantages and also suffer from disadvantages such as the requirement for excess solvent, longer reaction times, and poor yields. Therefore, development of a facile and efficient methodology for the synthesis of pyranopyrazoles is desired. In continuation of our endeavor to develop new methodologies for the synthesis of carbon-based solid acid. Here, we report for the first time a facile procedure for the synthesis of SPH-$SO_3H$ through the heat treatment of sulfuric acid and starch with poly(vinyl chloride). This catalyst showed good activity in the condensation reaction of aldehyde, ethyl aceto acetate, malononitrile and hydrazine hydrate to produce pyranopyrazoles derivatives.

## Experimental

*General*

All chemicals, unless specified, were purchased from commercial sources and were used without further purification. The products were characterized by comparison of their physical data with those of known samples or their spectral data. The development of reactions was monitored by thin layer chromatography (TLC), visualized by UV light. The mid-IR spectra were obtained in the 400-4000 $cm^{-1}$ region with a spectral resolution of 2 $cm^{-1}$ by averaging the results of 10 scans with a Perkin-Elmer RXI Fourier Transform spectrophotometer using KBr pellet technique. The NMR spectra were acquired at the ambient temperatures on a Brucker AVANCE DRX 400 MHz spectrophotometer using DMSO and $CDCl_3$ as the solvent and TMS as an internal standard. The particle morphology was examined by FESEM (Philips XL30 scanning electron microscope).

### *Catalyst preparation*

A mixture of 2 g of starch and 0.2 g of polyvinyl chloride and 10 mL of $H_2SO_4$ were combined in a 100-mL Teflon-sealed autoclave and maintained at 180 $^0$C for 24 h. The obtained black products were filtered and washed with hot distilled water and then oven-dried at 80 $^0$C overnight.

### *Solid acid titration*

The acid loading of the sulfonic, carboxylic and hydroxyl group functionalized SPH-$SO_3H$ (total acidity) was determined by titration. The total

acidity of catalyst was achieved by treating 40 mg of the sample with 40 ml of a (0.01 M) NaOH solution for 2 h at room temperature. The catalysts were separated with filteration, and the NaOH solution was saved. Then, two drops of a phenolphthalein solution were added to the NaOH solution. The solution was titrated to neutrality using a (0.01 M) HCl solution to determine the loading of acid sites of SPH-$SO_3H$ NPs. And so, The acid loading of the sulfonic group functionalized SPH-$SO_3H$ was determined by titration. The ionexchange reaction for the catalysts was achieved by treating 40 mg of the sample with 10 ml of a saturated (2 N) NaCl solution for 24 h at room temperature. The catalsts were separated , and the saturated NaCl solution was saved. Then, two drops of a phenolphthalein solution were added to the saturated NaCl solution. The solution was titrated to neutrality using a (0.01 M) NaOH solution to determine the loading of sulfonic acid group sites of SPH-$SO_3H$ NPs.

### *General procedure for the synthesis of pranoprazoles*

To a mixture of aldehyde (2 mmol), ethylacetoacetate (2 mmol), malononitrile (2 mmol), hydrazine hydrate (2.5 mmol) and SPH-$SO_3H$ (0.05 g) was added $H_2O$ (10ml) and the mixture was stirred at room temperature (scheme 1). The progress of the reaction was monitored by TLC. After completion, the reaction mixture was cooled to room temperature, and acetonitrile was added and shaken well for 5 min, then poured over crushed ice, stirred for 10 min, precipitated product was filtered, washed with water, dried and recrystallized from methanol.

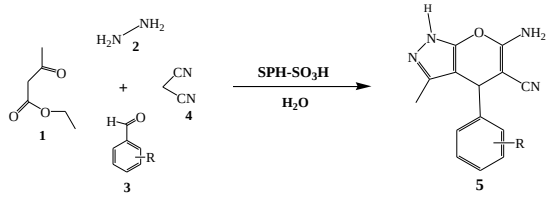


scheme 1 synthesis of pyrano pyrazole

## Results and discussion

### Characterization of catalyst:

***Acidity Test:***

If all the sulfur element in the catalysts was assumed to be –$SO_3H$ groups, the acid site densities of the catalysts were 0.5–2 mmol $H^+$/g depending on the synthesis conditions. But the acid titration experiments demonstrated much higher acid site densities than the estimations based on sulfur elemental analysis. The reason is that abundant phenolic –OH and –COOH groups were generated in the process of partial oxidation by concentrated sulfuric acid.

*FESEM*

The components of the Nano catalysts were analysis by using Field Emission Scanning Electron Microscope (FESEM) in Fig. 1. FESEM spectrums show that SPH-$SO_3H$ nanoparticles are nearly spherical with Nano dimension ranging from 11 to 20 nm in size and smoother surface.

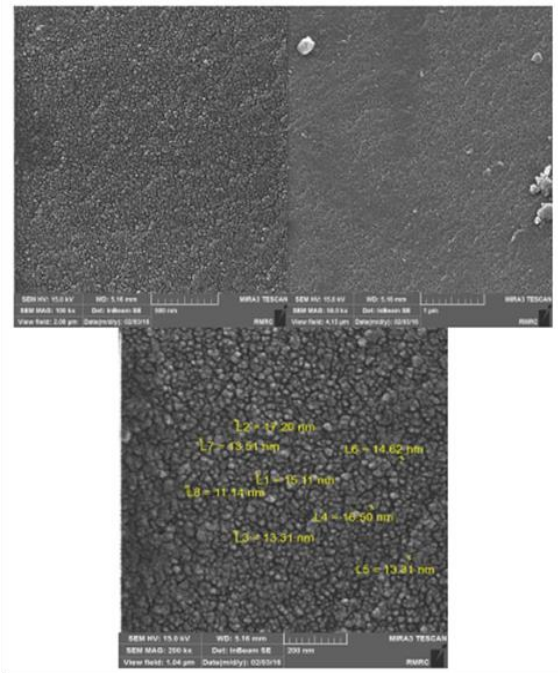

Fig. 1 The SEM image of SPH-$SO_3H$

FT-IR

The FT-IR spectra of SPH-$SO_3H$ are shown in Fig 2. The bands at 1179 ($SO_3^-$ stretching) and 1032 $cm^{-1}$ (O=S=O stretching in $SO_3H$) in the FT-IR spectrum indicate that the carbonaceous material possesses $SO_3H$ groups. This indicates that the $SO_3H$ groups were successfully incorporated into the carbon framework by adding $H_2SO_4$ in the synthesis system. On the other hand, the bands due to –OH stretching at 3420 $cm^{-1}$ and C=O stretching at 1710 $cm^{-1}$were observed.

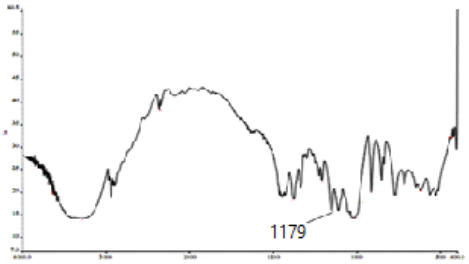


Fig. 2 The IR spectra of the SPH-$SO_3H$

### *Catalytic test of SPH-$SO_3H$ in the synthesis of of pranopyrazoles*

To optimize the reaction conditions, as a model reaction, the condensation between hydrazine hydrate (2.5 mmol), ethylacetoacetate (2 mmol), malononitrile (2 mmol) and benzalaldehyde (2 mmol) was studied in the presence of different amounts of SPH-$SO_3H$ and solvents at room temperature in the absence of solvent (Table 1).

**Table 1.** Effect of conditions on the reaction of hydrazine hydrate (2.5 mmol) with ethyl acetoacetate (2 mmol), malononitrile (2 mmol) and benzaldehyde (2 mmol).

| Entry | Catalyst Amount (mol%) | Solvent | Time (min) | Yield[a] (%) |
|---|---|---|---|---|
| **1** | - | water | 300 | 33 |
| **2** | 0.025 | Water | 5 | 60 |
| **3** | 0.05 | Water | 5 | 80 |
| **4** | 0.075 | Water | 5 | 80 |
| **5** | 0.05 | Water | 5 | 80 |
| **6** | 0.05 | EtOH | 120 | 50 |
| **7** | 0.05 | THF | 120 | 35 |
| **8** | 0.05 | Ethylacetate | 180 | 10 |
| **9** | 0.05 | n-Hexane | 260 | 25 |
| **10** | 0.05 | - | 300 | 30 |

[a]Isolated yield.

As it is shown in Table 1, the reaction was efficiently performed using 0.05gr of the catalyst at room temperature in the precence of $H_2O$ as solvent to give the desired product in high yield within short reaction time (Table 1, entry 3).

To assess the efficacy and generality of SPH-$SO_3H$ in the synthesis of 6-amino-4-(4-methoxyphenyl)-5-cyano-3-methyl-1-phenyl-1,4-dihydropyrano[2,3-c] pyrazoles, various arylaldehydes (including benzaldehyde, and arylaldehydes aldehydes possessing electron-releasing substituents, electron-withdrawing substituents and halogens on their aromatic ring) were reacted with hydrazine hydrate, ethyl acetoacetate and malononitrile under the optimal reaction conditions to afford the corresponding products in high yields and in short reaction times. The results are summarized in Table 2.

**Tabl 2.** The preparation of dihydropyranopyrazoles using SPH-$SO_3H$ (0.05 g) at room temperature in the precence of $H_2O$ (10 mL).

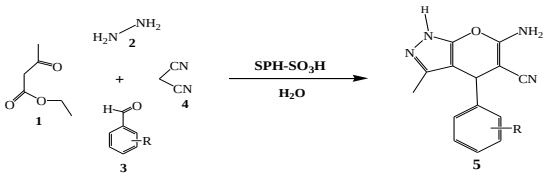


| Entry | R | Time (min) | Yield[a] (%) | M.p. °C (Lit.) |
|---|---|---|---|---|
| 1 | H | 5 | 80 | 242-246 (244-246)[33] |
| 2 | 2-$NO_2$ | 5 | 80 | 238-241 (222-224)[34] |
| 3 | 2-Cl | 5 | 82 | 146-148 (145-148) [35] |
| 4 | 4-OH | 5 | 83 | 223-224 (223-224) [37] |
| 5 | 3-OH | 5 | 84.3 | 239-244 (220-223)[36] |
| 6 | 3,4-MeO | 5 | 70.5 | ۱۷۰-۱۸۰ |
| 7 | 2-MeO | 5 | 74.5 | ۲۲۶-۲۳۸ |
| 8 | 4-MeO | 5 | 76.1 | ۲۱۰-۲۱۵ (۲۱۰-۲۱۲) [33] |
| 9 | 2-OH | 5 | ۸۳,۵ | ۱۹۸-۱۹۹ (۲۰۸-۲۰۹)[35] |
| 10 | 4-$NO_2$ | 5 | 81 | 250-252 (251-252)[33] |
| 11 | 4-$CH_3$ | 5 | 78.69 | 190-194 (206-208) [33] |
| 12 | 3-$NO_2$ | 5 | 81 | 190-193 (190-192)[34] |
| 13 | 4-F | 5 | 88 | 171-172 (170-171) [35] |
| 14 | 4-Cl | 5 | 85 | 241-243 (234-235)[33] |

**Mechanism:**

Formation of the product is suggested to involve the tandem reactions. Thus the benzylidenemalononitrile (7) containing the electron-poor C=C double bond is quantitatively produced by fast Knoevenagel reaction of malononitrile to the aromatic aldehyde. This reaction easily occurs in protic solvents including water without adding any catalyst, although it results in a net dehydration. [30] A similar rapid reaction between ethyl acetoacetate and hydrazine was instantaneously carried out in water to produce pyrazoles (6).[31] The second step that requires the presence of SPH-$SO_3H$ presumably involves, as also previously reported,[32] Michael addition of 6 to 7, and the hydroxyl tautomer group in pyrazolone undergoes fast nucleophilic addition to the CN moiety, producing the corresponding intermediate (9) subsequently rearranging in formation of the final 6-amino-4-(4-methoxpheayl)-5-cyano-3-methyl-1-phenyl-1,4-dihydropyrano[2,3-c] pyrazoles (5) (Scheme 2).

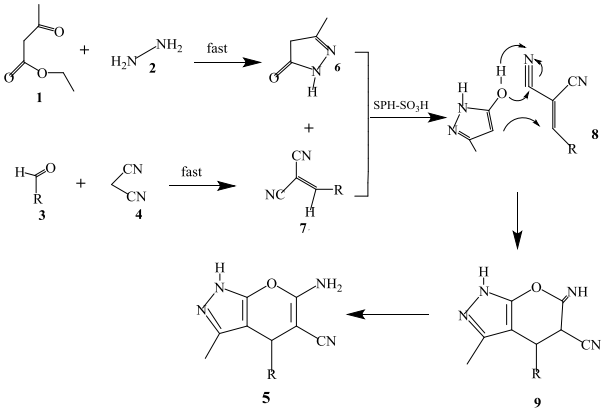


Scheme 2 Mechanism of pyrano pyrazoles

**Conclusion**

A new carbon-based solid acid has been synthesized through the simple heat treatment of sulfuric acid and starch in the precence of polyvinyl chloride. SPH-$SO_3H$ Nanoparticles was used as an efficient catalysts for the one-pot synthesis of pranopyrazoles using hydrazinehydrate, ethylacetoacetate, malononitrile and aldehyde at room temperature in good to high yields. All the reaction work easily for a variety of ahdehydes with both electron-donating and electron-withdrawing groups to give corresponding products in excellent yields.

**Acknowledgments**
Financial support from the Research Council of the Damghan University is gratefully acknowledged.

**References**

[1]. B. Zhang, J. Ren, X. Liu, Y. Guo, Y. Guo, G. Lu, Y. Wang. *Catalysis Communications*,**2010** ,*11(7)*,629-32.

[2]. Y. Lu, X. Liang, C. Qi.. *Bulletin of Materials Science*, **2012** ,*35(3)*,419-24.

[3]. X. Wang, R. Liu, M.M. Waje, Z. Chen, Y. Yan, K.N. Bozhilov, P. Feng, *Chemistry of Materials*, **2007**,*19(10)*,2395-7.

[4]. R. Liu, X. Wang, X. Zhao, P. Feng, *Carbon*,**2008**,*46(13)*,1664-9.

[5]. J. Janaun, N. Ellis, *Applied Catalysis A: General*,**2011** ,*394(1-2)*,25-31.

[6]. B. Chang, J. Fu, Y. Tian, X. Dong, J. Phys, *The Journal of Physical Chemistry C*, **2013**,*117(12)*,6252-8.

[7]. B. Chang, Y. Tian, W. Shi, J. Liu, F. Xi, X. Dong, *RSC Advances*,**2013**,*3(43)*,20999-1006.

[8]. B. Chang, J. Fu, Y. Tian, X. Dong,. *RSC Advances*, **2013**, *3(6)*, 1987-94.

[9]. X. Liu, M. Huang, H.L. Ma, Z.Q. Zhang, J.M. Gao, Y.L. Zhu, X.J. Han, X.Y. *Molecules*, **2010,** *15(10)*, 7188-96.

[10]. Y. Zhao, H. Wang, Y. Zhao, J. Shen, *Catalysis Communications*, **2010,** *11(9)*, 824-8.

[11]. L. Xuezheng, L. Chunqing, Q. Chenze, J. Mater. *Sci*, **2011,** *46*, 5345–5349

[12] A .Dömling, I. Ugi. *Angewandte Chemie International Edition*,**2000,** *39(18)*,3168-210.

[13] A. Strecker, *European Journal of Organic Chemistry*, **1850**, *75(1)*, 27-45.

[14] D. Tejedor, F. Garcia-Tellado , *Chemical Society Reviews*. **2007**, *36(3)*, 484-91.

[15] G. Vasuki, K. Kumaravel, *Tetrahedron Letters*, **2008,** *49(39)*, 5636-8.

[16] A. Dömling, *Current opinion in chemical biology*, **2002,** 6(3), 306-313..

[17] RV. Orru, M .de Greef, *Synthesis*, **2003,** *10(200)*, 1471.

[18] H .Bienaymé, C. Hulme, G .Oddon, P .Schmitt, *Chemistry–A European Journal*, **2000,** *6(18)*,3321-9.

[19] A. Dömling, *Chemical reviews*. **2006,** *106(1)*,17-89.

[20] M.Reactions, J .Zhu, H. Bienaymé, *Ed.; Wiley-VCH: Weinheim.* **2005**.

[21]. JM. Khurana, B. Nand, S. Kumar, *Synthetic Communications®*, **2011,** *41(3)*,405-10.

[22]. H. El-Sayed, A. Fakher, HM. BELAL, *Synthesis and biological activity of some pyrazole derivatives. Journal of the Serbian Chemical Society*. **1999 Jan 1**;64(1):9-18.

[23]. M. E. A. Zaki, , H. A. Soliman, O. A. Hiekal, A. E. Z. Rashad, *Naturforsch C*, **2006**, *61*, 1.

[24]. FM. Abdelrazek, P. Metz, NH. Metwally, SF. El-Mahrouky, *An International Journal Pharmaceutical and Medicinal Chemistry*, **2006,** *339(8),* 456-60.

[25]. N. Foloppe, LM. Fisher, R. Howes, A. Potter, AG. Robertson, AE. Surgenor, *Bioorganic & medicinal chemistry*, **2006,** *14(14)*,4792-802.

[26]. (a) D. Shi, J. Mou, Q. Zhuang, L. Niu, N. Wu, X. Wang. *Synthetic communications*. **2004,** *34(24)*, 4557-63.; (b) T. S. Jin, A. Q. Wang, Z. L. Cheng, J. S. Zhang, T. S. Li, *Synth. Commun*, **2005**, *35*, 137; (c) Y. Peng, G. Song, R. Dou, *Green Chemistry*, **2006**, *8(6)*, 573-5.; (d) G. Vasuki, K. Kumaravel, *Tetrahedron Letters*, **2008,***49(39)*, 5636-8.; (e) TS. Jin, RQ. Zhao, TS. Li, *Arkivoc*, **2006,** *11*, 176-82.

[27]. F. Lehmann, M. Holm, S. Laufer, *Journal of combinatorial chemistry*, **2008,** *10(3)*, 364-7.

[28]. JF. Zhou, SJ. Tu, HQ. Zhu, SJ. Zhi. *Synthetic communications*, **2002,** *32(21)*, 3363-6.

[29]. (a) SB. Guo, SX. Wang, JT. Li. *Synthetic Communications*, **2007,** *37(13)*, 2111; (b) Z.Ren, W.Cao, W.Tong, Z. Jin, *Synth.Commun*. **2005**, *35*, 2509.

[30]. F. Bigi, M. L. Conforti, R. Maggi, A. Piccinno, G. Sartori, *Green Chem.* **2000**, *2*, 101.

[31]. V. Polshettiwar, R. S. Varma, *Tetrahedron Lett*. **2008**, *49*, 397.

[32]. F. F. Abdel-Latif, J. Indian, *Chem.* **1990**, *29B*, 664.

[33].(a) H. Mecadon, M.D.R. Rohman, M. Rajbangshi, B. Myrboh, *Tetrahedron Lett*, **2011**, *52*, 2523; (b)P.P. Bora, M. Bihani, G.J.Mol. Bez, *catal.B: Enzym*. **2013**, *92*, 24.

[34]. M. Bihani, P.P. Bora, Gh. Bez, H. Askari, *Sust.Chem.Eng*. **2013**, *1*, 440.

[35]. K. Kanagaraj, K. Pitchumani, *Tetrahedron Lett.* **2010**, *51*, 3312.

[36]. M.M. Heravi, A. Ghods, F. Derikvand, K. Bakhtiari, F.F.J. *Bamoharram, Iran Chem. Soc.* **2010**, *7*, 615.

[37]. J.A. Makawana, D.C. Mungra, M.P. Patel, R. G. Patel, *Bioorg. Med. Chem. Lett*. **2011**, *21*, 6166.

# An Investigation into the Performance of the Steam Reforming of Methanol over Cu/ZnO/H-Mordenite Nanocatalyst

**Elham Sa'idi[a], Mahmoud Ziarati[a,*], Nahid Khandan[b], Seyed Morteza Alian Amiri[a]**

[a] *Department of Chemistry and Chemical Engineering, Malek_ Ashtar University of Technology(MUT), P.O. BOX 158751774 Lavizan, Tehran, Iran*

[b] *Department of Chemical Technologies, Iranian Research Organization for Science & Technology (IROST), P.O. BOX 33535111 Tehran, Iran*

*Corresponding author Tel.: +98 9122386289; Fax number: +98 2122962257

*E-mail: maziarati@mut.ac.ir

**Abstract**

This paper investigates the impacts of Cu/ZnO/H-Mordenite (40/40/20%) catalyst on the steam reforming of methanol (SRM) in a fixed bed reactor. The structure of the deposition-precipitation made catalyst was characterized by X-ray diffraction (XRD) patterns and scanning electron microscope (SEM) images. The GC–MS analysis confirmed that methanol fuel was converted mainly to $H_2$ and $CO_2$ compounds. Results showed that the methanol conversion and $H_2$ selectivity of Cu/ZnO/H-Mordenite (40/40/20%) were 80.48 % and 81.17 %, respectively and as a result its $H_2$ yield was 65.32%. The high performance of the Cu/ZnO/H-Mordenite (40/40/20%) catalyst may be attributed to the strong interaction of Cu/ZnO species which lead to high Cu/ZnO dispersion and smaller particle size.

**Keywords**: Cu/ZnO/H-Mordenite, Macropore Zeolite, Deposition- Precipitation Technique, Steam Reforming of Methanol.

## Introduction

Many researchers use Cu-based catalysts to produce hydrogen via steam reforming of methanol (SRM) [1-7]. Among these catalysts, Cu/ZnO has the most potential to use in SRM because of strong interaction between Cu and Zn which causes them to have high activity [8, 9].

Moreover, the general features of zeolites have led to their vast applications in different processes. Although there is no exact definition of the term "zeolite", some researchers have described zeolites as crystalline, hydrated aluminosilicates with a three-dimensional framework structure constructed of $SiO_4$ and $AlO_4$ tetrahedra linked through oxygen atoms [10, 11]. A general formula for zeolites as crystalline aluminosilicates would be the $M_v(A1O_2)_x(SiO_2)_y.ZH_2O$ in which M is either a monovalent or divalent cation [12].

The widespread usage of Cu/ZnO for SRM and prominent properties of zeolite supports encouraged us to combine these two materials as a unit catalyst system for SRM.

The aim of this paper is to investigate the impact of Cu/ZnO/H-Mordenite nanocatalyst on steam reforming of methanol (SRM). In the next sections of this paper, main results obtained from SRM over Cu/ZnO/H-Mordenite (40/40/20%) catalyst are reported and discussed.

## Experimental

### *Catalyst preparation*

In this paper, Cu/ZnO/H-Mordenite (20/20/40%) catalyst was prepared by deposition- precipitation technique. To do this, Cu $(NO_3)_2.3H_2O$ and Zn $(NO_3)_2.6H_2O$ were purchased from Merck Company (Germany) and H-Mordenite zeolite was purchased from Zeolist Company which its characteristics have been shown in Table 1 as follows.

**Table 1.** Typical properties of H-Mordenite powder as reported by manufacturer.

| Product | $SiO_2/Al_2O_3$ Mole Ratio | Nominal Cation Form | Surface Area $m^2/g$ |
|---|---|---|---|
| CBV 10A | 13 | Sodium | 425 |

$Na_2CO_3$ (1 M) was applied as precipitation agent and it was added dropwise to an aqueous solution of metal nitrates (1 M) at 60ºC. During precipitation, the solution was stirred continuously and its pH was measured by a pH meter. The $Na_2CO_3$ solution was added at a controlled rate in order to maintain the prescribed pH around 7± 0.2. After stirring by 700-1000 rpm, the solution was aged for 30min at room temperature and then filtered out three times and rinsed for 15min between each filtering to obtain precipitate. On the basis of the investigation and previous research, the reactions occurred during the deposition-precipitation technique can be simplified as follows:

$$Cu(NO_3)_2.3H_2O + Na_2CO_3 \rightarrow CuCO_3 + 2NaNO_3 + 3H_2O \quad (1)$$

$$Zn(NO_3)_2.6H_2O + NaCO_3 \rightarrow ZnCO_3 + 2NaNO_3 + 6H_2O \quad (2)$$

$NH_4NO_3$ was used to change the $Na^+$ cation of Mordenite zeolite to $NH_4$ cation. For this purpose, 0.1 M solution of $NH_4NO_3$ was prepared and then heated to 80ºC. The amount of 3gr of Mordenite zeolite was solved to it and stirred for 1h. Then obtained precipitate was washed 3 times until the $Na^+$ cation properly change into $NH_4$ cation.

To deposit the support on the catalyst, 2.4 gr of zeolite was added to the 320ml of deionized water and stirred in the room temperature to obtain a uniform solution. In the next step, the catalyst was added to it after 3 times of washing. The obtained solution was stirred 1h in order to the support is deposited on the catalyst suitably. The precipitate was then dried for 12h at 90ºC and calcinated by air flow for 4h at gradual temperature rise up to 400ºC. The reaction occurred during the calcination of the obtained precipitate has been shown in equation (3) and (4) as follows:

$$CuCO_3 \rightarrow CuO + CO_2 \quad (3)$$

$$ZnCO_3 \rightarrow ZnO + CO_2 \quad (4)$$

As shown in the equation (5) in the following, an exothermic reaction was occurred during the reduction of the catalyst.

$$CuO+H_2 \leftrightarrow Cu+H_2O+Q \quad (5)$$

To reduce the prepared catalyst, at first certain amounts of the catalyst were put in the reactor and then the temperature of the reactor was set on 250ºC. To exit the air from the reactor, $N_2$ flowed for 10min with the flow rate of 70cc/min to provide a suitable ambience in order that the catalyst is not oxidizing during reduction. Then, $H_2$ flows at 50cc/min for 50min at 250ºC to fill out the reduction process.

***Catalyst Characterization***

For characterization of the catalyst, X-ray diffraction (XRD) analyses was surveyed to assure the accuracy of the catalyst and to form valid phases. The pore size distribution and apparent morphology of the catalyst were determined by the SEM analyses of IROST (model of MORA II TESCAN).

The X-ray diffraction (XRD) is performed on a powder diffraction unit, subject to mono-chromatized Cu Kα radiation at 300 mA and 40 kV. The diffraction pattern was defined with respect to the joint committee of powder diffraction standards (JCPDS) database. Scanning electron microscope (SEM) analyses was run through a JEOL JSM-6340 microscope.

Figure 1 shows the XRD patterns of the prepared Cu/ZnO/H-Mordenite (40/40/20%) catalyst as follows.

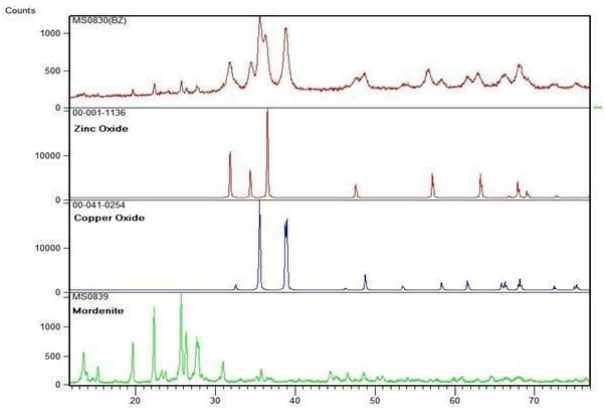


**Figure 1.** XRD patterns of the prepared Cu/ZnO/H-Mordenite (40/40/20%) catalyst.

As the X- ray diffraction (XRD) patterns of the Cu/ZnO/H-Mordenite (40/40/20%) catalyst shows in Figure 1, the phases of Cu oxide and Zn oxide in the catalyst were detectible in comparison to the standard XRD patterns of them.

As shown in Figure 2, Scanning electron microscope (SEM) images of the prepared catalyst presented the good sphericity and regular morphology of the crystals. Moreover, the particle sizes obtained from SEM for the prepared catalyst were smaller than 50nm.

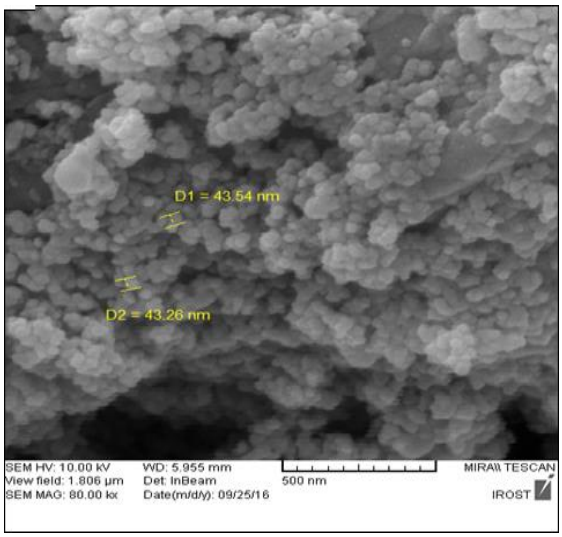


**Figure 2.** SEM image of the prepared Cu/ZnO/H-Mordenite (40/40/20%) catalyst.

***Catalytic Reactor Test***

To obtain the yield of the catalyst for SRM reaction, a fixed bed stainless steel reactor placed in a catalytic setup was applied. The weight of the catalyst fixed on 1gr for SRM reaction. The produced gas from the performance test is analyzed by on-line gas chromatographs (GC). A plot-Q column (3m×3mm i.d.), Helium carrier gas was applied to analyze $H_2$ and $CO_2$. Portable gas analysis equipment was applied to analyze CO. SRM reaction was performed in six periods of time by Cu/ZnO/H-Mordenite (40/40/20%) catalyst to perform reactor test.

The results have been summarized in Table (2) as follows.

## Results and discussion

The methanol conversion and $H_2$ selectivity of Cu/ZnO/H-Mordenite (40/40/20%) catalyst has been illustrated in Figure 3 and Figure 4, respectively.

As summarized in Table 3, the results of reactor test for the applied catalyst indicated the average yield of SRM was 65.32 percent.

**Table 2.** Selectivity and conversion percent of SRM reaction in the presence of Cu/ZnO/H-Mordenite (40/40/20%) catalyst.

| $H_2$ selectivity (%) | | Methanol conversion (%) | Time (min) |
|---|---|---|---|
| $H_2$ | $CO_2$ | | |
| 80.85 | 17.15 | 83 | 60 |
| 79.46 | 18.53 | 81 | 120 |
| 81.4 | 16.6 | 80 | 180 |
| 80.83 | 17.17 | 79 | 240 |
| 79.23 | 18.77 | 79 | 300 |
| 81.14 | 16.05 | 79 | 360 |

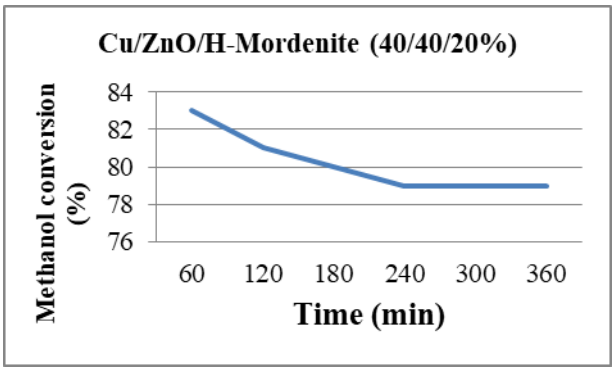


**Figure 3.** The diagram of the methanol conversion by Cu/ZnO/H-Mordenite (40/40/20%) catalyst.

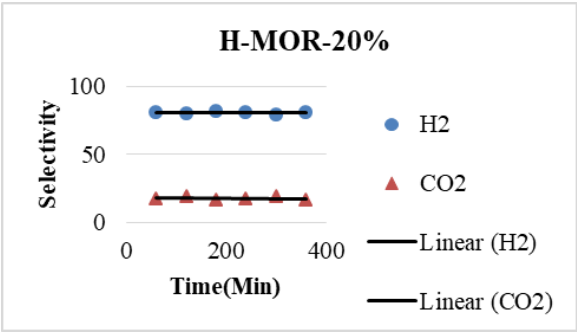


**Figure 4.** The diagram of the selectivity of $H_2$ and $CO_2$ by Cu/ZnO/H-Mordenite (40/40/20%) catalyst.

**Table 3.** The average $H_2$ selectivity, methanol conversion and yield percent of SRM reaction over the prepared catalyst.

| Catalyst | Methanol conversion | $H_2$ selectivity | Yield |
|---|---|---|---|
| Cu/ZnO/H-Mordenite | 81.17 | 80.48 | 65.32 |

## Conclusion

As the results shows, it can be concluded that Cu/ZnO/H-Mordenite (40/40/20%) catalyst enhances the performance of SRM which lead us to conclude that performing of steam reforming of methanol over Cu/ZnO supported on macropore zeolites is desirable for $H_2$ production. Furthermore, the size of spherical synthesized catalyst by deposition-precipitation technique was 40–45nm which leads to high Cu/ZnO dispersion.

## Acknowledgments

The authors acknowledge the department of chemistry and chemical engineering in Malek_Ashtar University of Technology (MUT) for funding.

## References

[1] M.M.Gunter, T. Ressler, R.E. Jentoft, and B. Bems, *J. Catal*., **2001**, 203, 133-149.

[2] B. Lindstrom, and L.J. Pettersson, *Int. J. Hydrogen Energy*, 2001, 26, 923-933.

[3] G.C. Shen, S. Fujita, S. Matsumoto, and N. Takezawa, *J. Mol. Catal. A: Chem*., **1997**, 124, 123-136.

[4] B. Lindstrom, L.J. Pettersson, and P.G. Menon, *Appl. Catal. A: Gen*., **2002**, 234, 111-125.

[5] P.H. Matter, and U.S. Ozkan, *J. Catal*., **2005**, 234, 463-475.

[6] T. Fuknaga, N. Ryumon, N. Ichikuni, and S. Shimazu, Catal. Commun., **2009**, 10, 1800-1803.

[7] X.R. Zhang, P.F. Shi, J.X. Zhao, M.Y. Zhao, and C.T. Liu, *Fuel Process. Technol*., **2003**, 83, 183-192.

[8] L.V.C. Rees, *Nature*, **1982**, 296, 491- 492.

[9] J.P. Shen, and C. Song, *Catalysis Today*, **2002**, 77, 89–98.

[10] D.W. Breck, *John Wiley & Sons, Inc*., New York, **1974**.

[11] R.M. Barrer, *Pure Appl. Chem.*, **1979**, 51, 1091-1100.

[12] J. Turkevich, *Catalysis Reviews: Science and Engineering*, **1968**, 1, 1-35.

## Graphical Abstract

An Investigation into the Performance of the Steam Reforming of Methanol over Cu/ZnO/H-Mordenite Nanocatalyst

Elham sa'idi[a] , Mahmoud Ziarati[a]*, Nahid Khandan[b], Seyed Morteza Alian Amiri[a]

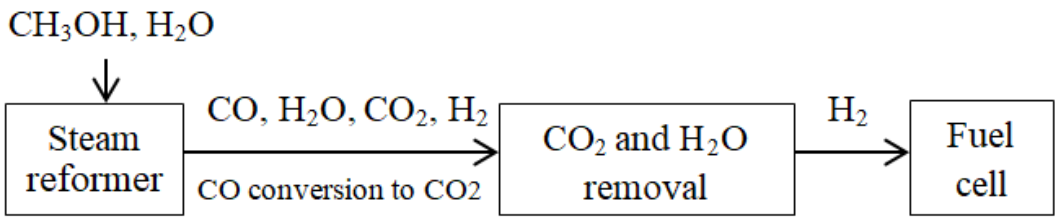


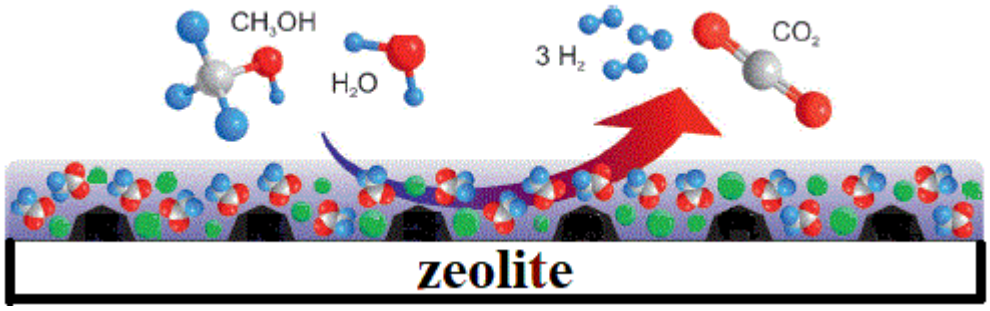

# Hydrogen Production by Steam Reforming of Methanol over Cu/ZnO/ ZSM-5 Catalyst

**Elham sa'idi[a], Mahmoud Ziarati[a,*], Nahid Khandan[b], Masoud Sabbaghi[a]**

[a] *Department of Chemistry and Chemical Engineering, Malek_ Ashtar University of Technology(MUT), P.O. BOX 158751774 Lavizan, Tehran, Iran*

[b] *Department of Chemical Technologies, Iranian Research Organization for Science & Technology (IROST), P.O. BOX 33535111 Tehran, Iran*

*Corresponding author Tel.: +98 9122386289; Fax number: +98 2122962257

*E-mail: maziarati@mut.ac.ir

**Abstract**

In this paper, steam reforming of methanol was studied over Cu/ZnO/ZSM-5 (40/40/20%) catalyst for production of hydrogen. The catalyst was synthesized by deposition- precipitation technique and its structure was characterized by X-ray diffraction (XRD) and scanning electron microscope (SEM). GC-MS analysis was applied in order to predict the rates of $CO_2$ and $H_2$ formation under the reaction conditions. Inappreciable amounts of CO by-product were formed in the reforming process at six periods of contact times and high methanol conversions. In fact, the percent of methanol conversion and $H_2$ selectivity of Cu/ZnO/ZSM-5 (40/40/20%) were 55.25 % and 75.57 %, respectively and as a result its yield was 41.75%. These results lead us to conclude that the presence of mesopore zeolite supports in Cu/ZnO catalyst exhibits superior SRM performance.

**Keywords**: Cu/ZnO/ZSM-5, Mesopore Zeolite, Deposition- Precipitation Technique, Steam Reforming of Methanol.

## Introduction

As an alternative source of clean energy and high potential applications, including the transportation sector and stationary power generation, hydrogen is currently receiving increasing interest. It traditionally is produced from fossil fuels by steam reforming of natural gas or heavy hydrocarbons; however recently, there is growing research and development activities on hydrogen produced from other sources, such as biomass, methanol (MeOH) and Dimethyl Ether (DME) [1, 2]. Steam reforming of methanol (SRM) is particularly attractive for hydrogen production because of the lower production of carbon monoxide compared to other options [3].

$$CH_3OH+H_2O \rightarrow CO_2+3H_2 \quad (1)$$

Some other considerable advantages of methanol are high hydrogen to carbon ratio and low soot formation due to the absence of carbon-carbon bonds which lead catalyst not to be deactivated [4-9]. Because of liquid state at ambient temperature, it is easy to store and transport methanol in comparison to preserving $H_2$ in cryogenic conditions or under high pressure [10, 11]. There is appreciable number of published research papers on methane and methanol steam reforming processes, however there is less focus on SRM over high efficient catalysts particularly in fixed bed reactors.

Selecting a proper catalyst system plays an important role in hydrogen production via SRM into hydrogen.

As many studies show, Cu based catalysts are among the most applicable catalysts for production of pure hydrogen through SRM [12–18].

Often, the SRM catalysts are applied by the promoter and support to improve the redox characterizations of the copper phases, increase the surface area, prevent sintering of the Cu, etc. One of the suitable promoters for this purpose is ZnO.

Zeolites, e.g. ZSM-5, are proper supports for a variety of reactions owing to their activity, shape selectivity, ion-exchanging properties and special pore structure, such as the tridimensional mesopore topology and large specific surface area in ZSM-5 [19-24]. They play an important role in the hydrogen production process, especially in the processes that are under development or improvement in order to meet the requirements for more efficient technologies. One of the objectives of the present study is to gain increased understanding of the impacts of Cu/ZnO/ ZSM-5 on SRM process. In this study, mainly results obtained from SRM over Cu/ZnO/ZSM-5 (40/40/20%) catalyst are reported and discussed.

## Experimental

### *Catalyst preparation*

Cu/ZnO/ZSM-5 (40/40/20%) catalyst was prepared using deposition-precipitation technique. To do this, Cu $(NO_3)_2.3H_2O$ and Zn $(NO_3)_2.6H_2O$ were purchased from Merck Company and ZSM-5 zeolite was purchased from Zeolist Company. Data on ZSM-5 zeolite properties provided by the manufacturer have been given in Table 1 as follows.

**Table 1.** Typical properties of ZSM-5 powder as reported by the manufacturer.

| Product | $SiO_2/Al_2O_3$ (Mole Ratio) | Nominal Cation Form | Surface Area ($m^2/g$) |
|---|---|---|---|
| CBV 2314 | 23 | Ammonium | 425 |

The required amounts of materials to produce 5 gr of Cu/ZnO/ZSM-5 (40/40/20%) catalyst have been calculated as shown in the following equations. Then the amounts of each slat as precursor of the catalyst were calculated

separately using stoichiometric ratio according to the following values.

$$Cu = 5 \times 0.4 = 2\ gr$$
$$ZnO = 5 \times 0.4 = 2\ gr$$
$$zeolite = 5 \times 0.2 = 1\ gr$$

To precipitate the catalyst, $Na_2CO_3$ (1 M) was added dropwise to an aqueous solution of stirred metal nitrates (1 M) at 60ºC. The pH of solution was controlled around 7± 0.2. The stirring rate was 700-1000 rpm during the precipitate production. Then the solution was aged for 30 min at the room temperature while stirred at 300 rpm. After this step, the aged solution was filtered in three times. To deposit the support on the catalyst, 1 gr of zeolite was solved in the 320ml of deionized water and stirred in the room temperature to form a uniform solution. In the next step, the catalyst was added to the performed solution. The obtained solution was stirred 1hr in order to deposit the support on the catalyst suitably. The precipitate was then dried for 12 h at 90 ºC and calcinated by air flow for 4 h at the temperature gradually rise up to 400 ºC.

To reduce the prepared catalyst, initially certain amounts of catalyst were placed in the reactor and then the temperature of the reactor set on 250ºC. To exit the air from the reactor, $N_2$ flowed for 10min to provide a suitable ambience not to oxidize catalyst during reduction. Then, $H_2$ flowed at 50 cc/min for 50min at 250ºC to do the reduction process.

***Catalyst Characterization***

Some analysis such as XRD was surveyed to assure the calcination of the catalyst and formation valid phases. To determine the particle sizes and apparent morphology of catalyst, the SEM analysis of IROST Company (model of MORA II TESCAN) was applied.

The X-ray diffraction (XRD) was performed on a powder diffraction unit, subject to mono-chromatized Cu Kα radiation at 300 mA and 40 kV. The diffraction pattern was defined with respect to the joint committee of powder diffraction standards (JCPDS) database. Scanning electron microscope (SEM) analysis was run through a JEOL JSM-6340 microscope.

***Catalytic Reactor Test***

To obtain the yield of the catalyst for SRM reaction, a fixed bed stainless steel reactor placed in a catalytic setup was applied. The weight of the catalyst fixed on 1gr for SRM reaction. The produced gas from the performance test was analyzed by on-line gas chromatographs (GC). A plot-Q column (3m×3mm i.d.), Helium carrier gas was applied to analyze $H_2$ and $CO_2$. Portable gas analysis equipment was applied to analyze CO. SRM reaction was performed in six periods of time by Cu/ZnO/ZSM-5 (40/40/20%) catalyst to perform reactor test. The results have been summarized in Tables (2) as follows.

**Table 2.** Methanol conversion and $H_2$ selectivity of SRM reaction in the presence of Cu/ZnO/ZSM-5 (40/40/20%) catalyst

| Selectivity (%) | | Methanol conversion (%) | Time (min) |
|---|---|---|---|
| $H_2$ | $CO_2$ | | |
| 75.42 | 22.58 | 53.20 | 60 |
| 75.62 | 22.38 | 57.50 | 120 |
| 75.12 | 22.88 | 56.60 | 180 |
| 75.42 | 22.58 | 54.20 | 240 |
| 76.11 | 21.89 | 55.40 | 300 |
| 75.71 | 22.29 | 54.60 | 360 |

## Results and discussion

The X- ray diffraction (XRD) patterns of Cu/ZnO/ZSM-5 (40/40/20%) catalyst are presented in Figure 1. It is seen that the phases of Cu oxide and Zn oxide were formed in the

catalyst. The peak of applied ZSM-5 in the catalyst in comparison to the standard zeolite XRD was also observable in Figure 1.

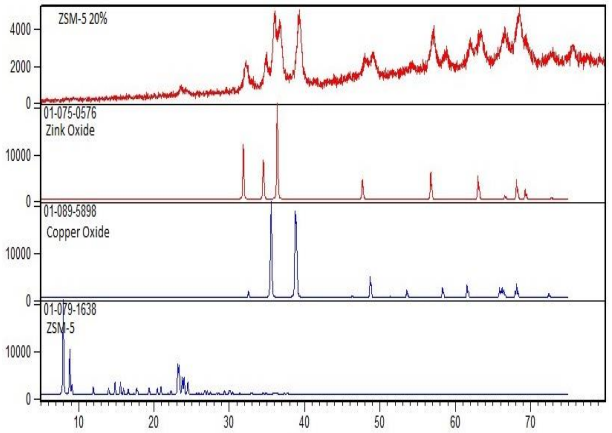


**Figure 1.** XRD patterns of the prepared Cu/ZnO/ZSM-5 (40/40/20%) catalyst, standard ZnO, CuO and ZSM-5 (from top to down).

According to the scanning electron microscope (SEM) image of the catalyst indicated in Figure 2, the particles tend to be spherical and their sizes are approximately in nanometer scale. However, as shown in the Figure 2 the Cu/ZnO/ZSM-5 (40/40/20%) particles had the diameter between 70 to 90 nanometer.

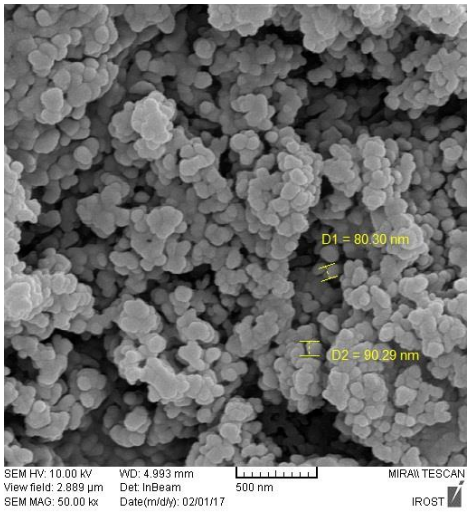


**Figure 2.** SEM image of the Cu/ZnO/ZSM-5 (40/40/20%) catalyst.

The diagrams of the methanol conversion and $H_2$ selectivity of Cu/ZnO/ ZSM-5 (40/40/20%) catalyst have been illustrated in Figure 3 and Figure 4, respectively.

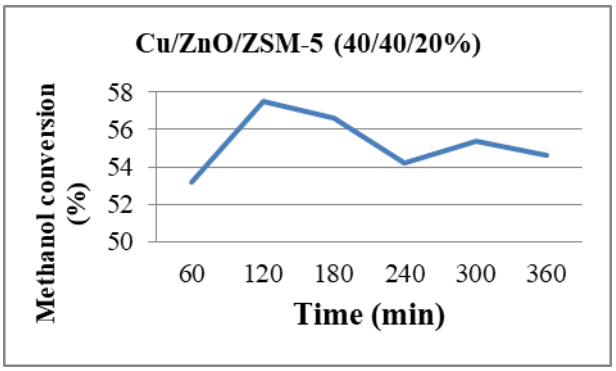


**Figure 3.** The diagram of the methanol conversion by Cu/ZnO/ZSM-5 (40/40/20%) catalyst.

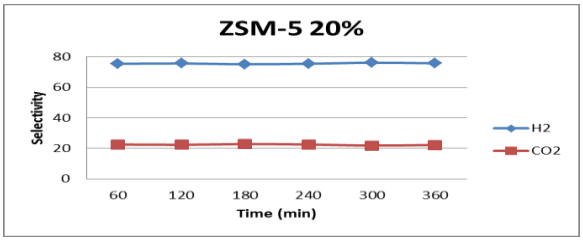


**Figure 4.** The diagram of the selectivity of $H_2$ and $CO_2$ in the presence of Cu/ZnO/ZSM-5 (40/40/20%) catalyst.

The results of reactor test for the applied catalyst have been summarized in the Table 3 as follows.

**Table 5.** The average methanol conversion, $H_2$ selectivity and yield percent of SRM reaction in the presence of the prepared catalyst.

| Catalyst | Methanol conversion | $H_2$ Selectivity | Yield |
|---|---|---|---|
| Cu/ZnO/ZSM-5 | 55.25 | 75.57 | 41.75 |

The results of reactor test showed that the average $H_2$ selectivity of the Cu/ZnO catalyst with ZSM-5 support for SRM process is 75.57% and the average percent of methanol conversion was 55.25% and as the results the yield of the catalyst was 41.75%.

## Conclusion

Production of $H_2$ by SRM was studied over the prepared Cu/ZnO/ZSM-5 catalyst and the

structure of catalyst was characterized with XRD and SEM. This is the first reported application of Cu/ZnO catalyst supported on ZSM-5 for SRM performed in a fixed bed reactor.

The SRM over Cu/ZnO/ZSM-5 catalyst was found to produce satisfactory accurate data within a reasonable time. As the results show, the yield of Cu/ZnO/ZSM-5 is 41.75% while the yield of catalyst without support is 36.38%. The CO production is also negligible in this process. It lead us to conclude that the performance of Cu/ZnO/ZSM-5 (40/40/20%) catalyst is more than Cu/ZnO catalyst and as a result, application of zeolite supports for Cu/ZnO catalyst increases the performance of the steam reforming of methanol.

**Acknowledgments**

The authors acknowledge the department of chemistry and chemical engineering in Malek_Ashtar University of Technology (MUT) for funding.

**References**

[1] X. E. Verykios, *Int J Hydrogen Energy*, **2003**, 28, 1045-1063.

[2] A. F. Elewuwa, Y. T. Makkawi, *International Journal of Hydrogen Energy*, **2015**, 40, 15865- 15876.

[3] K. Liu, Ch. Song, and V. Subramani, *A John Wiley & Sons Inc. Publication, New Jersey*, **2010**, 65-77.

[4] S. K. Kamarudin, W. R. W. Daud, M. A. Som, M. S. Takriff, and A. W. Mohammad, *J. Power Sources*, **2006**, 157, 641-649.

[5] B. D. McNicol, D. A. J. Rand, K. R. Williams, *J. Power Sources*, **2001**, 100, 47-59.

[6] B. Emonts, J. Bogild Hansen, T. Grube, B. Hohlein, R. Peters, H. Schmidt, *J. Power Sources*, **2002**, 106, 333- 337.

[7] B. Lindstrom, L.J. Pettersson, *J. Power Sources*, **2002**, 106, 264-273.

[8] L. J. Pettersson, and R. Westerholm, *Int. J. Hydrogen Energy*, **2001**, 26, 243-264.

[9] B. Lindstrom, and L.J. Pettersson, *Catal. Lett.*, **2001**, 74, 27- 30.

[10] D.R. Palo, R.A. Dagle, and J.D. Holladay, *Chem. Rev.*, **2007**, 107, 3992- 4021.

[11] M. L. Cubeiro, J. L. G. Fierro, *J.Catal.*, **1998**, 1, 150- 162.

[12] M. M. Gunter, T. Ressler, R. E. Jentoft, and B. Bems, *J. Catal.*, **2001**, 203, 133-149.

[13] B. Lindstrom, and L.J. Pettersson, *Int. J. Hydrogen Energy*, 2001, 26, 923-933.

[14] G. C. Shen, S. Fujita, S.Matsumoto, and N. Takezawa, *J. Mol. Catal. A: Chem.*, **1997**, 124, 123-136.

[15] B. Lindstrom, L. J. Pettersson, and P.G. Menon, *Appl. Catal. A: Gen.*, **2002**, 234, 111-125.

[16] P. H. Matter, and U. S. Ozkan, J. Catal., **2005**, 234, 463-475.

[17] T. Fuknaga, N. Ryumon, N. Ichikuni, and S. Shimaz, *Catal. Commun.*, **2009**, 10, 1800-1803.

[18] X. R. Zhang, P. F. Shi, J. X. Zhao, M. Y. Zhao, and C. T. Liu, *Fuel Process. Technol.*, **2003**, 83, 183-192.

[19] G. Bellussi, P. Pollesel, *Stud. Surf. Sci. Catal.* 158, **2005**, 1201–1212.

[20] J. Thomas, F. Degnan, *J. Catal.* 216, **2003**, 32–46.

[21] C. R. Marcilly, *Top. Catal.* 13, **2000**, 357–366.

[22] E.J. Creyghton, R.S. Downing, *J. Mol. Catal. A: Chem*. 134, **1998**, 47–61.

[23] M. S. Rigutto, R. van Veen, L. Huve, in: J. Cejka, H. van Bekkum, A. Corma, F. Schueth (Eds.), *Introduction to Zeolite Science and Practice*, **2007**, 855–913.

[24] J. S. Jung, J. W. Park, G. Seo, *Appl. Catal. A: Gen.* 288, **2005**, 149–157.

## Graphical Abstract

Hydrogen Production by Steam Reforming of Methanol over Cu/ZnO/ ZSM-5 Catalyst

Elham sa'idi[a], Mahmoud Ziarati[a]*, Nahid Khandan[b], Masoud Sabbaghi[a]

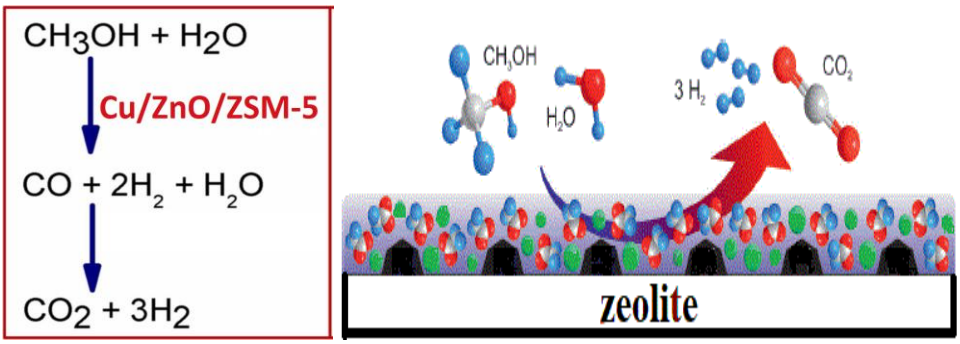

# Synthesis of sulfonated carbon-based solid acid as a novel and efficient Nanocatalyst for the synthesis of 2-amino-7-hydroxy-4H-chromene

**Beheshte Hamidi,[1] Seied Ali Pourmousavi,[1,2*] and Zahra Hoseien Abadi[1]**

[1] *School of Chemistry, Damghan University Damghan, Iran*
[2] *Institute of Biological Science, Damghan University Damghan, Iran*

**Email: pourmousavi@du.ac.ir*

## Abstract

A novel carbon-based solid-acid nanocatalyst (SCP-$SO_3H$) was simply prepared for the first time by the the one-step hydrothermal reaction of Starch as carbohydrate source and p-toluenesulfonic acid as sulfonating in the presence of citric acid.The catalytic activities of SCP-$SO_3H$ as efficient and reusable catalyst were investigated by the condensation reaction of aldehyde, malononitrile and resorcinol for the synthesis of 2-amino-7-hydroxy-4H-chromene in water as a green solvent at 70 ºC in excellent yields. The prepared catalytic system was characterized by X-ray diffraction, transmission electron microscopy, scanning electron microscopy.The catalyst could be quantitatively recovered from the reaction mixture by simple filtration and reused at least three times with almost consistent acticity.

**Keywords**: Carbon-based solid-acid nanocatalyst, aldehyde, malononitrile, resorcinol, 2-amino-7-hydroxy-4H-chromene.

## Introduction

Heterogeneous catalysts have found considerable interest in organic reactions, since these catalysts can be recoverd and reused several times after the reaction without noticeable loss of reactivity. Reactions with these catalysts are generally clean and selective and give high yields of products [1-4]. Among the heterogeneous solid acid catalyst in organic synthesis, Carbon base solid acids (CBSAs), which are important materials with many practical and research application [5-7], This catalysts have rececived much attention for green catalytic procedures because several advantages as solid catalysts such as no pollution, easy separation and reusability [8-10]. Recently, new various sulfonated carbon-based solid acid have been reported. These material show the higher catalytic performance and higher stabilitiy versus other solid acides such as sulfonated mesoporous silica's [11-15].

2-amino-4H-chromenes and their derivatives are of significant importance as they possess a wide range of biological activities, such as antimicrobial [16], antiproliferative [17], sex pheromone [18], antitumor [19] ones; they can be used in cancer therapy, and are beneficial to the central nervous system [20]. Several methods have been reported for the synthesis of 2-amino-4H-chromene derivatives using malononitrile, resorcinol and aldehydes.Various catalysts,such as piperidine[21], cetyltrimethylammonium bromide(CTABr)[22], TFE[23], $Ca(OH)_2$[24], MgAl/HT[25] and tungstic acid functionalized mesoporous SBA-15[26] have been used for these reactions.

However, some of these catalysts suffer from the drawback of green chemistry such as prolonged reaction times, low yields and toxicity. Therefore, introducing clean processes and utilizing eco-friendly and green catalysts which can be simply recycled at the end of reactions have been under permanent attention.

## Experimental

All chemical were purched from Merck company and used without further purification. The development of reactions were monited by TLC on Merck pre-coated silica gel 60 F254 aluminum sheets, visualized by UV light. Products were characterized by comparison of their physical data, IR and $^1$H NMR spectra of known samples. All $^1$H-NMR spectra were recorded at 500 MHz in DMSO relative to TMS (0.00 ppm). IR spectra were recorded on Perkin-Elmer Spectrum RXI FT-IR spectrophotometer. X-ray diffraction (XRD) patterns of samples were taken on a Philips X-ray diffract meter Model PW 1840. The particle morphology was examined by FESEM (Philips XL30 scanning electron microscope).

*Preparation of SCP-$SO_3H$ catalyst*

A mixture of Starch (5.0 g), p-toluenesulfonic acid (2.0 g), citric acid (2.5 g) and $H_2O$ (40 mL) was transferred into a 100 mL sealed Teflon-lined autoclave and kept at 180º C for 9 h. After cooling to room temperature, the resulting black solid was washed with hot deionized water and ethanol several times until sulfate ions were no longer detected, then dried at 60ºC in an oven under vacum for 12 h. The as-prepared catalyst is denoted as SCP-$SO_3H$.

*General procedure for the synthesis of 2-amino-7-hydroxy-4H-chromene derivatives*

A 25 mL flask was charged with aldehyde (1 mmol), malononitrile (1 mmol) and resorcinol (1mmol) SCP-$SO_3H$ catalyst (0.05 g) and then stirred in water (5.0 mL) at 70 ºC. After completion of the reaction the catalyst was separated from the reaction mixture and

the crude product was filtered. Further purification was achieved by crystallization in ethanol.

## Results and discussion

*Synthesis and Characterization of Catalyst:*

The hydrothermal carbonization and sulfonation of Starch in the precenc of citric acid and p-toluenesulfonic acid was achieved in a 100 mL Teflon-Lined Autoclave Reactor. The resulted sulfonic acid-functionalized nanoparticles were denoted as SCP-$SO_3H$ (Scheme 1).

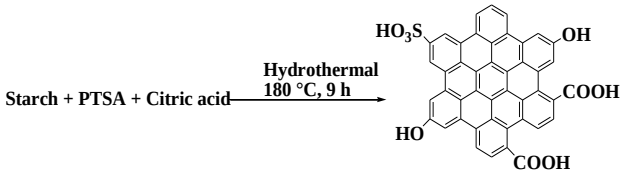


**Scheme 1**.synthesis of SCP-$SO_3H$

The amount of introduced sulfonic acid (-$SO_3H$) groups was 2.5 mmol $g^{-1}$, which was quantified by an ion-exchange of $H^+$ ions of the sulfonic acid with NaCl, followed by titration of the resulting filtrate with NaOH. The acidity shows that the number of the sulfonic acid group attached to carbon sheet is higher than the reported carbon-based solid acid. The number of $H^+$ determined by acid–base titration was 6.5 mmol $H^+$ $g^{-1}$ for total acidity include –$SO_3H$, -COOH and phenolic -OH groups based on reaction with NaOH and then back-titration by HCl solution.

Crystal structure of the SCP-$SO_3H$ was determined using XRD. The XRD patterns are shown in Fig. 1. The XRD diffraction pattern showed broad and diffuse diffraction peaks at 2θ = 20-30◦ and 2θ = 40-50◦ respectively. The broad C (0 0 2) and (1 0 0) diffraction peak indicated that the peak could be attributed to amorphous carbon structures, which was important for the catalytic activity.

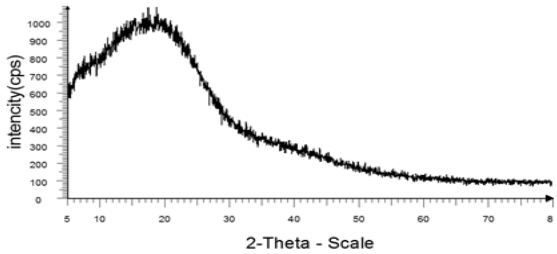


**Fig. 1**: XRD patterns of SCP-$SO_3H$

FT-IR patterns of SCP-$SO_3H$ in the wave length of 400-4000 $cm^{-1}$ are shown in Fig. 2. The carbonization process successfully endows as shown by the FT-IR spectrum of the catalyst. The $-SO_3H$ groups were giving rise to the sharp peaks at 1030 and 1150 $cm^{-1}$ due to asymmetric and symmetric stretching vibrations of $-SO_2-$ groups.

As especially visible in the FT-IR pattern of the catalyst, the bands point to the presence of −OH in COOH carboxylic and phenolic OH groups, signified by the broad band around 3600 to 2600 $cm^{-1}$Also, existing band at 1600 $cm^{-1}$ to 1700 $cm^{-1}$ is due to C=O of COOH and C=C of the poly-aromatic rings of hydrocarbon in the base.

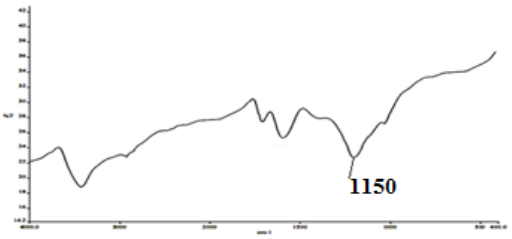


**Fig 2.** Fourier-transform infrared spectra (FT-IR) spectra for SCP-$SO_3H$ NPs.

Structural analysis of catalyst was carried out using FE-SEM, and representative images are illustrated in Fig. 3. Lots of porous and irregular structures appeared after the incomplete carbonization process which caused the dehydration of carbohydrates. SCP-$SO_3H$ was found to be composed of nonspherical and irregular grains of \30 nm in size. The sample was gold-coated before scanning, which could be considered as

evidence that the catalyst had a large surface area contributing to its catalytic activity.

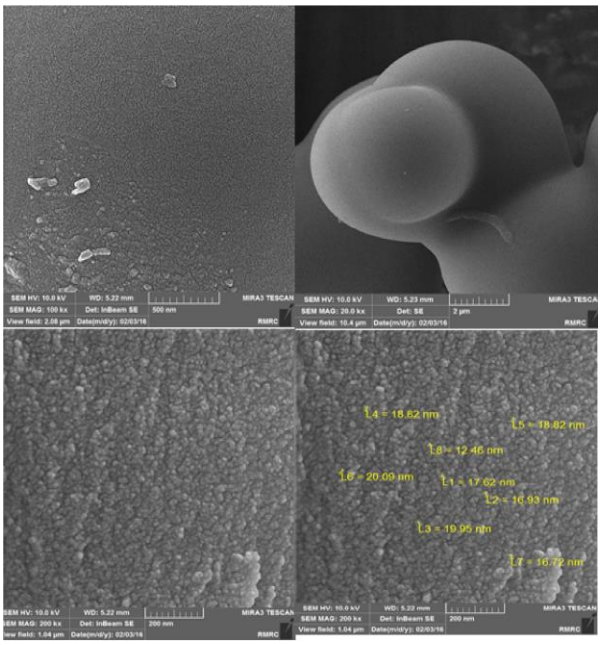

Fig 3. Scanning electron microscope (SEM) images of SCP-$SO_3H$ NPs.

*Catalytic Activity of Catalyst:*

After characterization of the solid acid catalyst, the catalytic activity of nanoparticles was tested in the synthesis of of 2-amino-7-hydroxy-4H-chromene derivatives.

To exploit a method for the preparation of 2-amino-7-hydroxy-4H-chromene derivatives, the reaction of benzaldhyde (1 mmol), malononitrile (1 mmol) and resorcinol (1 mmol) in the presence of SCP-$SO_3H$ catalyst was chosen as a model and its behavior was studied under a variety of conditions (Table 1).

**Table 1.** Optimization of the reasction conditions for the synthesis of 2-amino-7-hydroxy-4H-chromene derivatives

| Entry | Catalyst amount (g) | Solvent | T. °C | Time (min) | Yield[a] (%) |
|---|---|---|---|---|---|
| 1 | - | $H_2O$ | 70 | 300 | Trace |
| 2 | 0.025 | $H_2O$ | 70 | 60 | 40 |
| 2 | 0.05 | $H_2O$ | 70 | 60 | 82 |
| 3 | 0.075 | $H_2O$ | 70 | 60 | 80 |
| 4 | 0.1 | $H_2O$ | 70 | 60 | 80 |
| 5 | 0.05 | - | RT | 120 | Trace |
| 6 | 0.05 | EtOH | Ref. | 60 | 60 |
| 7 | 0.05 | DMF | 70. | 120 | 20 |
| 8 | 0.05 | *n*-Hexan | Ref. | 120 | 20 |
| 9 | 0.05 | MeCN | 70. | 120 | 30 |
| 10 | 0.05 | $CH_2Cl_2$ | Ref. | 120 | - |
| 11 | 0.05 | $MeCO_2Et$ | Ref. | 120 | 20 |

[a] Isolated yield

The best result was obtained when the reaction of benzaldehyde (1 mmol) with malononitrile (1 mmol) and resorcinol (1 mmol) was carried out at 70 °C in the presence of 0.05 g of SCP-$SO_3H$ in $H_2O$ as solvent (Scheme 2).

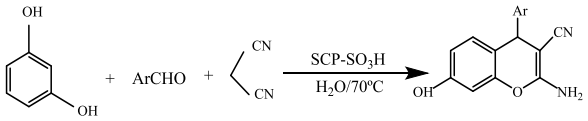


**Scheme 2**. Synthesis of 2-amino-7-hydroxy-4H-chromene

To extend the scope of this protocol for the synthesis of 2-amino-7-hydroxy-4H-chromene derivatives other benzaldehyde derivatives were applied in the three-component synthesis. The results, listed in Tables 2 show that these three-component reactions with catalyst gave the desired products successfully.

**Table 2**. Synthesis of 2-amino-7-hydroxy-4H-chromene derivatives using SCP-$SO_3H$

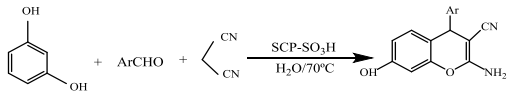


| Entry | Ar | Time (min) | Yield[a] (%) |
|---|---|---|---|
| 1 | $C_6H_5$ | 60 | 82 |
| 2 | 4-$MeC_6H_5$ | 180 | 77 |
| 3 | 4-$MeOC_6H_5$ | 240 | 80 |
| 4 | 4-$ClC_6H_5$ | 80 | 80 |
| 5 | 2,4-$Cl_2C_6H_3$ | 90 | 85 |
| 6 | 4-$FC_6H_5$ | 80 | 85 |
| 7 | 4-$NO_2C_6H_5$ | 80 | 85 |
| 8 | 3-$HOC_6H_5$ | 130 | 72 |
| 9 | 2- $ClC_6H_5$ | 90 | 80 |
| 10 | 2- $NO_2C_6H_5$ | 100 | 80 |

[a]Isolated yeild

Several aromatic aldehydes was converted to chromene derivatives using malononitrile, and resorcinol the presence of the catalyst at 70 °C in $H_2O$. The nature of the substituent on the aromatic ring of aldehyde seems to have no relevant effect on the reaction.

## Conclusion

In conclusion, for the first time, the synthesis of SCP-$SO_3H$ as a novel carbon-based solid acid nanocatalyst from starch is reported. Synthesis of SCP-$SO_3H$ was carried out through one-step hydrothermal carbonization and sulfonation in the presence of sulfuric acid and citric acid. This new heterogeneous nanocatalyst has been efficiently used for a direct one-pot synthesis of 2-amino-7-hydroxy-4H-chromene derivatives starting from ahdehydes, malononitrile and resorcinol. Various aldehyde applied to this synthetic protocol. The excellent catalytic performance, easy preparation from cheap starting materials and separation of the catalyst make it a good nanocatalyst for organic transformations.

## Acknowledgments

Financial support from the Research Council of the Damghan University is gratefully acknowledged.

.

## References

[1] Gyerard, V.S. notheisz, *F. Heterogeneous Catalyst in Organic Chemistry*. San Diago:Elsevier**, 2000**.
[2] K. Wilson, J. H. Clark, Pure *Appl* Chem, **, 2000,** 72:1313.
[3] N. Seifi, M. H. Zahedi-Niaki, M. R. Barzegari, A. Davoodnia. R. Zhiani, A. A. Kaju, J Mol *Catal* A, **2006,** 260:77.
[4] M .Z. Dastmalbaf, A. Davoodnia, M. M. Heravi, N. Tavakoli-Hoseini, A. Khojastehnezhad, H. A. Zamani,.*Bull Korean Chem Soc*, **2011,** *35*: 656.
[5] Y. Lu, X. Liang, C. Qi, Bull. *Master. Sci.*, **2012,** 35, 419.
[6] X.Wang, R.Liu, M.M Waje, Z.Chen, Y.Yan, K.N.Bozhilov, P.Feng, *Chem. Master*. **2007,** 19, 2395.
[7] R.Liu, X.Wang, X.Zhao, P.Feng, *Carbon* 46,1664-1669**(2008)**.
[8] J. Janaun, N. Ellis, *Appl. Catal*.A **2011,** 394, 25.
[9] B.Chang, J.Fu, Y .Tian, X.Dong, *J.Phys. Chem.* **2013.** C117,6252.
[10] B.Cheng, Y.Tian , W.Shi, J.Liu, F.Xi, X.Dong, *RSC Adv*. **2013,** 3, 20999.
[11] B.Cheng, J.Fu, Y.Tian , X.Dong, *RSC Adv*. **2013,** 3,1987.
[12] X. Liu, M. Huang, H. L. Ma, Z. Q. Zhang, J. M. Gao, Y. L. Zhu, X. J. Han, X. Y. Guo, *Molecules*, **2010,** *15*,7188.
[13] Y. Zhao, H. Wang, Y. Zhao, J. Shen, *Catal. Commun*. **2010,** 11, 824.
[14] L. Xuezheng, L.Chunqing, Q.Chenze, *J. Mater. Sci*. **2011,** 46, 5345.
[15] D. L. Klass, *Biomass for Renewable Energy,Fuels,and Chemicals,Academic Press*,San Diego **(1998)**.

[16] M. M Khafagy, A. H. El-Wahas, F. A Eid, A. M. El-Agrody, *Faramaco*, **2009,** 57 715.
[17] C. P. Dell, *C. W.* Smith, *European Patent Appl, EP537949, Chem*. Abstr. **1993,** 119, 139102d.
[18] G. Bianchi, A. Tava, *Agric. Biol. Chem.*, **1987,** 51, 2001.
[19] S. J. Mohr, M. A. Chirigos, F. S. Fuhrman, J. W. Pryor, *Cancer Res*, **1975,** 35, 3750.
[20] D. R. Anderson, S. Hegde. E. Reinhard, L. Gomez, W. F. Vernier, L. Lee, S. Liu, A. Sambandam, P .A. Snider, L. Masih, Bioorg. *Med. Chem. Lett*. **2005,** 15, 1587.
[21] H. M. Al-Matar, K. D. Khalil, H. Meter, H. Meter, H. Kolshorn, M. H. Elnagdi, *ARKI-VOC*, **2008,** 16, 288.
[22] J. Tong-Shou, J. C.Xiao, S.J.Wang, T.S.Li, *Ultrason.Sonochem*. **2004,** 11,393.
[23] S. Khaksar, A. Rouhallahpour, S. Mothammadzadeh Talesh, *J. Fluorine Chem*, **2012**. *141*, 11.
[24] S. R. Kolla, Y. R. Lee, *Tetrahedron*, ***2011***,67, 8271.
[25]S. R. Kale, S. S. Kahandal, A. S. Burange, M. B. Gawande, R. V. Jayaram, *Catal. Sci. Technol*. **2013,** 3**,** 2050.
[26] S.K.Kunda, J.Mondal, A.Bhaumik, *Dalton Trans*. **2013,** 42, 10515.

## Graphical Abstract

**Synthesis of sulfonated carbon-based solid acid as a novel and efficient Nanocatalyst for the synthesis of 2-amino-7-hydroxy-4H-chromene**

Beheshte Hamidi, Seied Ali Pourmousavi and Zahra Hoseien Abadi

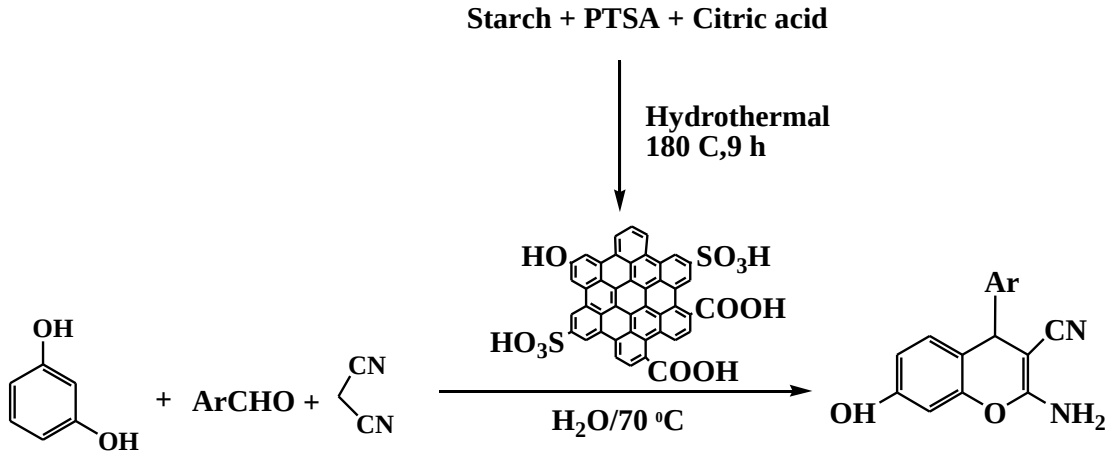

# Ultra-deep desulfurization of gasoline through mono Mn(II)-substituted phosphotungstate@CuO@PANi as a high-performance nanocatalyst

**Parvin Rahmani, Mohammad Ali Rezvani * and Fatemeh Parchegani***

*Department of Chemistry, Faculty of Science, University of Zanjan, 451561319, Zanjan, Iran*

*Corresponding author: Fax: +98245152617, E-mail: marezvani@znu.ac.ir, f-parchegani94@phd.araku.ac.ir*

**Abstract**

This paper describes the oxidation of several sulfur containing molecules with hydrogen peroxide in a two liquid–liquid (L–L) phase system with a phase transfer catalyst under atmospheric pressure. Polyoxometalates with favorable oxidation potentials and reactive transition metal centers are useful for electron transfer oxidation reactions. So, the oxygenation of sulfides to the corresponding sulfoxides catalyzed by a novel lacunary polyoxometalate, under the dual protection functions of polyaniline and cuper oxide.

The material ($PW_{11}Mn$@CuO@PANi) was characterized by FT-IR and UV-Vis spectroscopy. Catalytic activity of synthesized nanocomposite was tested on oxidative desulphurization of actual gasoline. The advantages of this method lie in its mild condition, low cost, large scale, simplicity and environmentally friendly route.

**Keywords**: Polyoxometalate, Nanocomposite, Gasoline, Oxidative Desulfuriz

## Introduction

Production of ultra-clean fuel oil with a low concentration of sulphur content is an extremely important task of refiners for environmental safety that has become a major challenge in recent years. The various types of sulfur compound in petroleum products emit $SO_x$ gases during the combustion. These atmosphere pollutants are not only causing corrosion, but also contributing to acid rain, photochemical smog, global warming and human diseases [1–3]. Also, the strict regulations regarding the environment safety and improvement of transportation fuels quality are the most pressing issues of the world recently. In this respect, lots of substantial research efforts have been conducted to reduce the sulfur levels in refined petroleum products to less than 10 ppmw [4,5]. The most important method for removing sulfur compounds from fuel is hydrodesulfurization (HDS) but a part of organic sulfur compounds is not easily removed and very high temperature and pressure conditions should be used to remove these recalcitrant sulfur compounds [2]. Alternative desulfurization strategies are currently envisaged and oxidative desulfuration (ODS) is one of the most interesting. Many efforts have been devoted to the development of processes using robust and recyclable catalysts [6]. In the same vein, Polyoxometalates (POMs) as well-known metal-oxygen inorganic compounds have received extensive attention in catalysis area over the past decade. Among the different varieties of their structures, transition metal-monosubstituted polyoxoanion in the primary Keggin structure, $[XM_{11}TMO_{39}]^{n-}$ (X= P, Si, B; M= W, Mo; TM= transition metal), is favored for the synthesis of POM-based catalysts due to their variable structures, tunable solubility, reversible redox transformations, and high catalytic activity [7]. Therefore, broader exploitation of POM compounds requires the development of vigorous and efficient synthetic protocols for their integration into hybrid architectures and devices. Polyaniline (PANi), a conducting polymer, has emerged as a promising 1D material that is particularly attractive for electronic devices due to its facile synthesis, environmental stability, unique electronic properties, and simple acid/base doping/dedoping chemistry [8]. Copper oxide (CuO) is a semiconducting compound with a monoclinic structure. CuO has attracted particular attention because it is the simplest member of the family of copper compounds and exhibits a range of potentially useful physical properties such as high temperature, super conductivity, electron correlation effects and spin dynamics [9]. Herein, a new mono substituted phosphotungstate supported polyaniline and CuO was investigated and demonstrated to be effective for desulfurization.

## Experimental

Mono substituted phosphotungstate $H_3[PW_{11}Mn]$ and CuO nanoparticles were synthesized according to a reported procedure [10]. During the formation of the milky gel from $Cu(NO_3)_2{\cdot}6H_2O$ and $C_6H_8O_7H_2O$ solutions, the $PW_{11}Mn$ aqueous solution was added slowly. The above solution was heated at 70 °C for 45 min, under vigorous stirring. The product finally dried at 50°C for 3 h. The resultant white powder nanocomposite was designated as $PW_{11}Mn$@CuO. After that, during the formation of polyaniline polymer, the $PW_{11}Mn$@CuO solution was added drop-wise to polyaniline solution under stirring for 2h. The precipitate was filtered and washed with 10 mL distilled water and 10 mL ethanol. The dark green product dried in oven 80 °C for 3h. The final ($PW_{11}Mn$@CuO@PANi) composite was characterized through FT-IR spectroscopy.

UV/Vis spectra of solutions were recorded with a Shimadzu 160 spectrophotometer.

## Results and discussion

The identification of specific chemical bands and functional groups of the synthesized samples was characterized using FT-IR spectroscopy to confirm their successful incorporation. The FT-IR spectra of (a) $PW_{11}Mn$, (b) CuO, (c)PANi, and (d) $PW_{11}Mn$@CuO@PANi nanocatalyst are depicted in Figure 1. According to Figure 1(a), the unique characteristics peaks at 784, 869, 967, and 1067 $cm^{-1}$ are caused by the stretching modes involving edge-sharing W–$O_b$–W, corner-sharing W–$O_c$–W, terminal W=$O_d$, and P-O bond in the Keggin-type $PW_{11}Mn$ respectively. Figure 1(b) is exhibited characteristics peaks at 1421, 881, and 534 $cm^{-1}$. The absorption bond at 881 $cm^{-1}$ is assigned to Cu–O–H stretching bond. A peak at 534 $cm^{-1}$ is caused by the vibration bond of Cu–O. The spectrum of PANi Figure 1(c), the presence of sharp peaks near 1501 and 1584 $cm^{-1}$ are attributed to C=C stretching of the benzenoid and quinoid rings respectively. The appearance of characteristic absorption band around 1241 $cm^{-1}$ is related to the C–N stretching in PANi structure.

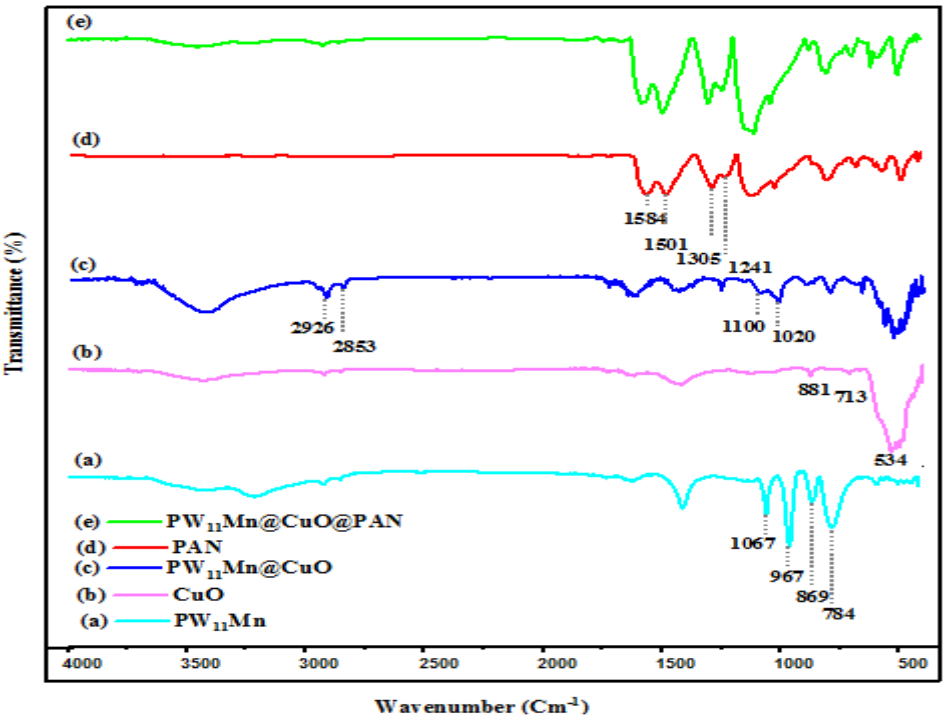


**Figure1**. FT-IR spectrum of the synthesized nanomaterials (a) $PW_{11}Mn$, (b) CuO, (c) PANi and (d) $PW_{11}Mn$@CuO@PANi

In order to further investigate the interactions between, PANi and CuO, the electron transformation was also followed by UV–vis spectroscopy. In ultraviolet light regions, the spectrum of $PW_{11}Mn$ indicated a strong band at 220 and 245 nm. assigned to the O→P transition and an $O^{2-}\rightarrow W^{6+}$ charge transfer transition of polyoxoanion, where W atoms are positioned in $W–O_c–W$ intra bridges between edge-sharing. (Fig.2c). The absorption band around 200 nm in Fig.2(a) is likely related to the formation of CuO nanoparticles. The peaks at 345 and 800 nm are attributed to benzenoid rings and quinoid rings of PANi, respectively (Fig.2b). UV-vis spectra of the composite display essentially the same absorptive characteristics as that of pristine PANi, $PW_{11}Mn$ and CuO (Figure 2a,b).

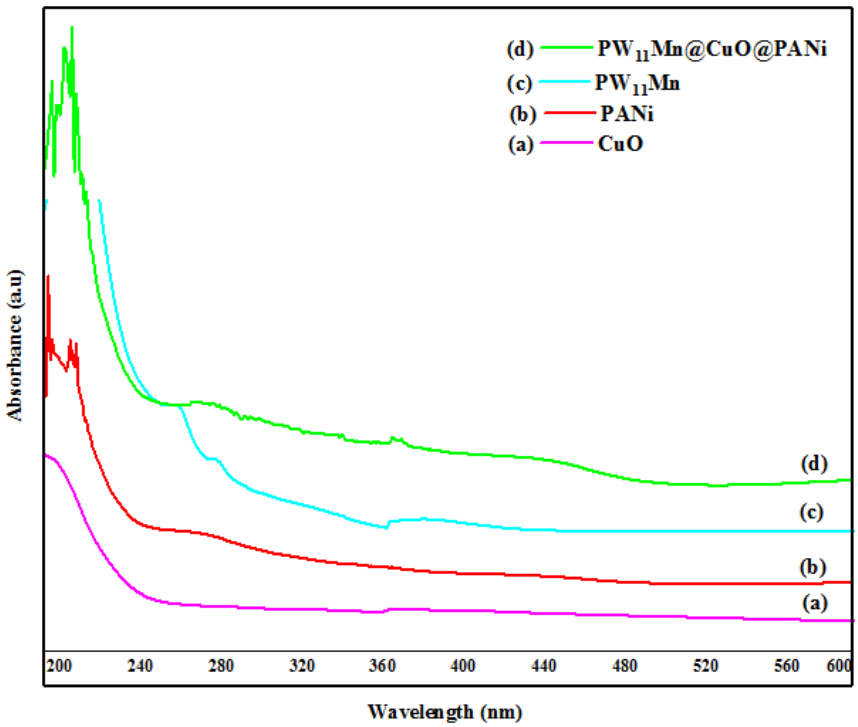


**Figure 2.** UV-vis spectra of (a) CuO, (b) PANi, (c) $PW_{11}Mn$, and (d) $PW_{11}Mn$@CuO@PANi

The effect of the nature of the catalyst on the oxidative desulphurization of gasoline using acetic acid/$H_2O_2$ as the oxidant is shown in Table 1. The percent conversion in actual gasoline in the presence of $PW_{11}Mn$@CuO@PANi was found 97 % after 60 min and the desulfurization efficiency increased rapidly with increasing catalyst dosage. It is noteworthy that other properties of fuel remained unchanged during the oxidation reactions.

## Conclusion

A highly efficient, new, simple and rapid method in synthesis of $PW_{11}Mn$@CuO@PANi nanocomposite is successfully developed. The organic sulfur compounds were removed using the peroxo-metal intermediate complex as a catalytic enhancer in the presence of $H_2O_2/CH_3COOH$ as oxidant. The results indicated that the

removal of mercaptans and total sulfur content could be reduced to 96% and 97%, respectively.

**Table 1.** Oxidative desulphurization of gasoline by $PW_{11}Mn@CuO@PANi$

| Entry | Properties of gasoline | | Unit | Method | Before ODS | After ODS [a] |
|---|---|---|---|---|---|---|
| 1 | Total Sulfur by X-Ray | | Wt.% | ASTM D 4294 | 0.4987 | 0.0132 |
| 2 | Mercaptans | | ppm | ASTM D 3227 | 98 | 3 |
| 3 | Density by hydrometer @ 15 $^0$C | | g/ml | ASTM D 1298 | 0.7996 | 0.7994 |
| 4 | Salt | | (ptb) | ASTM D 3230 | 17 | 17 |
| 5 | Water Content by distillation | | vol. % | ASTM D 4006 | Nil. | Nil. |
| 6 | Distillation | **IBP** | $^0$C | ASTM D 86 | **49.8** | **49.7** |
| | | **FBP** | | | **208.4** | **208.2** |
| | | 10 | Vol% | | 68.5 | 68.4 |
| | | 50 | | | 119.4 | 119.3 |
| | | 90 | | | 187.2 | 187.1 |
| | | 95 | | | 207.3 | 207.2 |

Condition for desulphurization: 50 mL of gas oil, 0.1 g of $PMo_{11}V@PbO@PANi$ nanocatalyst, 6 ml of oxidant, 10 mL of extraction solvent, time = 2 hours, and temperature = 35 °C.

## References


[1] M. A. Rezvani, A. F. Shojaei, F. M. Zonoz, J. Serb. Chem. Soc, **2014**, 79, 1099.

**[2]** N. M. Mahmoodi, M. A. Rezvani, M. Oveisi, A. Valipour, M. A. Asli, Mater. Res. Bull, **2016**, 84, 422.

**[3]** M. A. Rezvani, M. Alinia Asli, M. Oveisi, R. babaei, K. Qasemi, S. Khandan, RSC Adv, **2016**, 6 530.

[4] M. A. Rezvani, M. Alinia Asli, S. Khandan, H. Mousavi, Z. Shokri Aghbolagh, Chem. Eng. J, **2017**, 312, 243.

[5] X. Sheng, Y. Zhoua, Y. Zhang, M. Xue, Y. Duan, Chem. Eng. J, **2012**, 179, 295.

[6] Z. A. Abdalla, B. Li, Chem. Eng. J, **2012**, 200, 113.

[7] M. A. Rezvani, A. F. Shojaie, M. H. Loghmani, Fuel Process. Technol, **2014**, 118, 1.

[8] M. A. Rezvani, F. Mohammadi Zonoz, Ind. Eng. Chem, **2015**, 22, 83.

[9] M. A. Rezvani, M. Shaterian, F. Akbarzadeh, S. Khandan, Chem. Eng. J, **2018**, 333, 537.

[10] M. A. Rezvani, Z. S. Aghbolagh, H. H. Monfared, S. Khandan, J. Ind. Eng. Chem, **2017**, 52, 42.

## Graphical Abstract

**Ultra-deep desulfurization of gasoline through mono Mn(II)-substituted phosphotungstate@CuO@PANi as a high-performance nanocatalyst**

Parvin Rahmani, Mohammad Ali Rezvani, and Fatemeh Parchegani

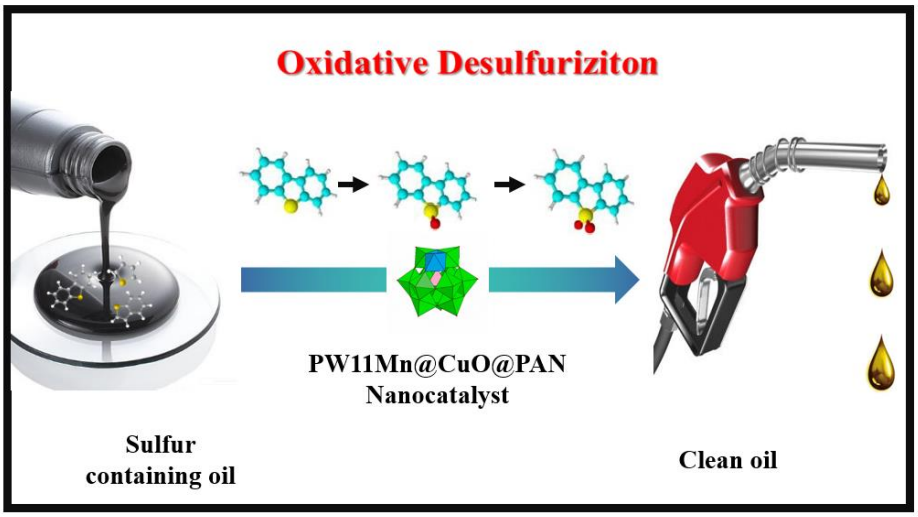

# Fabrication and characterization of novel Polymer/MetalOxide/Polyoxometalate(PMP) Compositeand its highly catalytic performance for the oxidative desulfurization

**Omid FegheMiri, Mohammad Ali Rezvani* and Fatemeh Parchegani***

*Department of chemistry, Faculty of science, university of zanjan, PO Box:451561319, Zanjan, Iran*

*Corresponding author: Fax: +98245152617, E-mail: marezvani@znu.ac.ir, f-parchegani94@phd.araku.ac.ir

**Abstract**

With the increasing aim of deep desulfurization of fuel, a kind of novel Polymer/Metal Oxide/Polyoxometalate (PMP) composite was successfully synthesized. This catalyst was exploited to act as a stable heteropolyacid-based one, under the dual protection functions of polyaniline and lead oxide. Structure was characterized by Fourier transform infrared (FT-IR) and scanning electron microscopy (UV-Vis). Our contribution demonstrates a new way of fuel desulfurization, namely selective oxidation of organic sulfur(S)-compounds present in fuels to water-soluble sulfur compounds followed by in-situ extraction of the latter into an aqueous phase.The results of oxidative desulfurization (ODS) revealed that PMP composite was an excellent catalyst capable of removing more than 90% of sulfure content compounds to less than 10 ppmw, after 60 minutes.

**Keywords**:Polyoxometalate, oxidative desulfurization, catalyst, fuel.

## Introduction

The removal of sulfur compounds in fuel is a significant tool for the environmental protection, since the combustion process produces $SO_x$derivatives that affect the stability of the atmospheric ozone layer, increasing the formation of acid rains[1].Deep desulfurization of diesel fuel has received vast research attention due to more severe environmental regulations forced over the last two decades. In the oil refinery industry, the hydrodesulfurization (HDS) process has been used for quite a lot of decades to reduce the sulfur content to a level of 500 ppm. To further reduce the sulfur to a level below 50 ppm, the HDS process has to be operated under even severer conditions (high temperature and high pressure), which are energy intensive and require hydrogen consumption. In searching for other alternatives, oxidative desulfurization(ODS) has been considered to be a complementary route to the HDS process for deep desulfurization, due to its moderate operating conditions and facil integrationto existing refineryplants.[2,3].In the ODS process,in the presence of an oxidant,sulfur-containing compounds are oxidized to sulfones and sulfoxides.These oxidized sulfur compounds have higher polarities

than their parent sulfur compounds and the other hydrocarbons and can be removed by a variety of separation processes such as adsorption and solvent extraction.To date, avariety of different oxidizing agents have been studied for the ODS process including$O_2$,tert-butyl hydroperoxide (TBHP), $H_2O_2$ and superoxides. $H_2O_2$ due to its low price and important oxidation property has been extensively used with plentiful homogenous and heterogeneous catalysts [4]. Polyoxometalates (POMs) are anionic all-inorganic molecular metal oxides with greatly varied structures that reach in size nanoscopic dimensions. This class of compounds exhibits abroad structural diversity in relationship with their notable chemical and physical properties that make them useful for applications in areas ranging from materials science and energy conversion to catalysis and medicine. Therefore, broader exploitation of POM compounds requires the development of vigorous and efficient synthetic protocols for their integration into hybrid architectures and devices [5,6]. Polyaniline (PANi), a conducting polymer, has emerged as apromising 1D material that is particularly attractive for electronic devices due to its facile synthesis, environmental stability,unique electronic properties, and simple acid/base doping/dedoping chemistry [7]. Regarding to the physical properties, lead has low melting temperature, tensile strength, the composites with a higher content of orthorhombic PbO show higher desulfurization up to 90%.Herein, a new mono substituted molybdophosphoric acid supported polyaniline and PbO was investigated and demonstrated to be effective for desulfurization.

## Experimental

Mono substituted molybdo phosphoric acid $H_3[PMo_{11}V]$and PbO nanoparticles were synthesized according to a reported procedure [8,9]. During the formation of the milky gel from Pb $(NO_3)_2{\cdot}6H_2O$ and $C_6H_8O7H_2O$ solutions, the $PMo_{11}V$ aqueous solution was added slowly. The above solution was heated at 70 °C for 45 min,under vigorous stirring. The product finally dried at 50°C for 3 h.

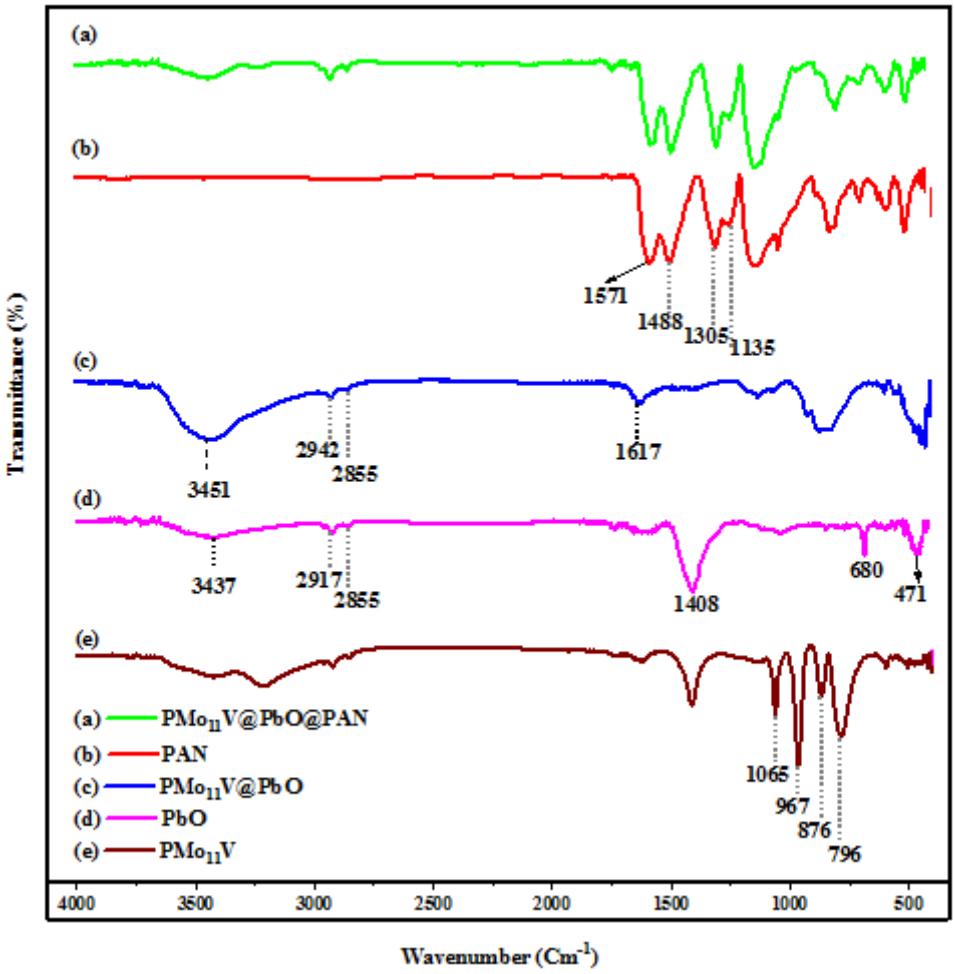


**Figure. 1**. FT-IR spectrum of the synthesized nanomaterials (a)PMP composite, (b)PAN, (c)$PMo_{11}V$@PbO, and (d) PbO (e) $PMo_{11}V$

The resultant white powder nanocomposite was designated as $PMo_{11}V$@PbO. After that, during the formation of polyaniline polymer, the $PMo_{11}V$@PbO solution was added drop-wise to polyaniline solution under stirring for 2h. The precipitate was filtered and washed with 10 mL distilled water and 10 mL ethanol. The dark green product dried in oven 80 °C for 3h. The final PMP ($PMo_{11}V$@PbO@Pani) composite was characterized through FT-IR spectroscopy. UV/Vis spectra of solutions were recorded with a Shimadzu 160 spectrophotometer

## Results and discussion

FT-IR spectra of the synthesized are shown inFig.1. FT-IR spectra give characteristic peaks at 1571, 1488, 1305, and 1135 $cm^{-1}$ corresponding to quinoid,benzenoid, C-N aromatic amine, and —N=quinoid=N—(electron-like band) stretching modes of PANi (Fig 1b).[5]Figure 1d is exhibited characteristics peaks at 1408, 680, and 471 $cm^{-1}$. The absorption bond at 680 $cm^{-1}$ is assigned to Pb–O–H stretching bond. A peak at 471 $cm^{-1}$ is caused by the vibration bond of Pb–O.Figure 1(e), the unique characteristic peaks at 796, 876, 967, and 1065 $cm^{-1}$ are caused by the stretching modes involving edge-sharing Mo–Ob–Mo, corner-sharing Mo–Oc–Mo, terminal Mo=$O_d$, and P-O bond in the Keggin-type $PMo_{11}V$, respectively.In order to further investigate the interactions between $PVMo_{11}$, PANi and PbO, the electron transformation was also followed by UV–vis spectroscopy.In ultraviolet light regions, the spectrum of $PVMo_{11}$ indicated a strong band at 215 and 235 nm. assigned

to the O→P transition and an $O^{2-}$→$Mo^{6+}$ charge transfer transition of polyoxoanion, where Mo atoms are positioned in Mo–$O_c$–Mo intra bridges between edge-sharing. (Fig.2c).The absorption band around 200 nm in Fig.2(d) is likely related to the formation of PbO nanoparticles. The peaks at 345 and 800 nm are attributed to benzenoid rings and quinoid rings of PANi, respectively (Fig.2b). UV-vis spectra of the PMP composite displayessentially the same absorptive characteristics as that of pristine PANi, $PVMo_{11}$ and PbO(Figure 2a,b).

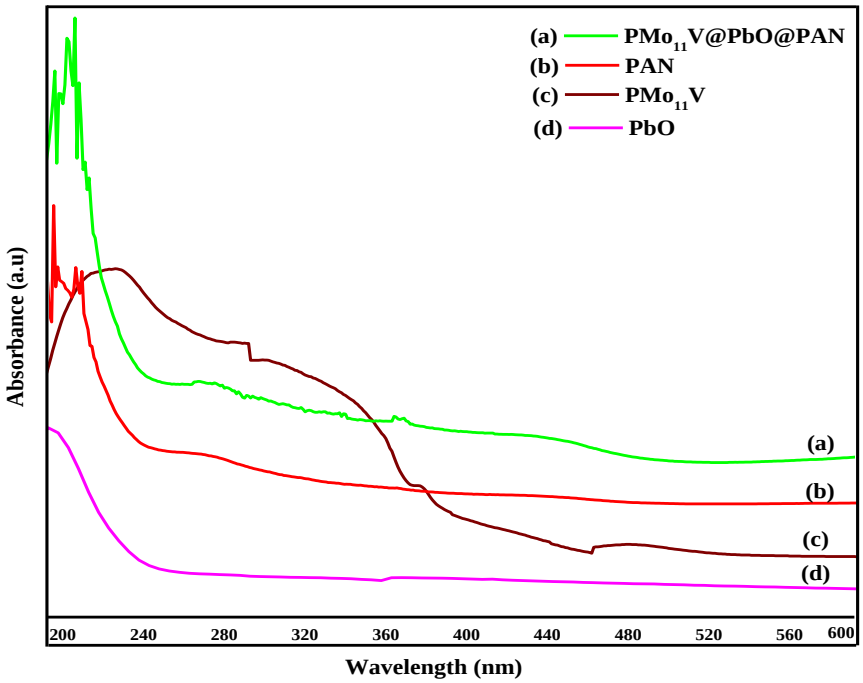


**Figure 2.**UV-vis spectra of (a) $PMo_{11}V$@PbO@PAN, (b) PAN, (c) $PMo_{11}V$ , and (d)PbO

Highly interestingly, the degree of desulfurization of actual gasoline reaches 95% in the presence of a aforesaid catalyst and $H_2O_2/CH_3COOH$ aoxidant. The explanation for this behavior is that, $H_2O_2$ as oxidant reacts with acetic acid to in-situ formation of peracetic acid (AcOOH). Peracetic acid (AcOOH) can act as an opulent fount of active oxygen, which can transmute organic sulfur to corresponding sulfones after 60 min. Furthermore, mercaptans concentration reached to 5 ppm at short reaction time according to Table 1. Obviously, our new heterogeneous catalyst $PMo_{11}V$@PbO@PANi enables the desulfurization of the real gasoline fuel oil greatly. It is noteworthy that other properties of fuel remained unchanged during the oxidation reactions.

## Conclusion

In conclusion, lacunary polyoxometalate was modified with polyaniline and lead oxide for use in ultra-deep desulfurization of gasoline. The results of the study of the catalyst indicated that the presence of PANiand PbOspecies in $PMo_{11}V$ enhanced the activity for the desulfurization of gasoline through ODS.

**Table 1.** Oxidative desulphurization of gasoline by $PMo_{11}V$@PbO@PANi

| Entry | Properties of gasoline | | Unit | Method | Before ODS | After ODS [a] |
|---|---|---|---|---|---|---|
| 1 | Total Sulfur by X-Ray | | Wt.% | ASTM D 4294 | 0.4989 | 0.0213 |
| 2 | Mercaptans | | ppm | ASTM D 3227 | 97 | 5 |
| 3 | Density by hydrometer @ 15 $^0$C | | g/ml | ASTM D 1298 | 0.7996 | 0.7994 |
| 4 | Salt | | (ptb) | ASTM D 3230 | 18 | 17 |
| 5 | Water Content by distillation | | vol. % | ASTM D 4006 | Nil. | Nil. |
| 6 | Distillation | **IBP** | $^0$C | ASTM D 86 | **49.6** | **49.4** |
| | | **FBP** | | | **208.4** | **208.3** |
| | | 10 | Vol% | | 68.8 | 68.7 |
| | | 50 | | | 119.8 | 119.5 |
| | | 90 | | | 187.6 | 187.4 |
| | | 95 | | | 206.5 | 206.3 |

[a]Condition for desulphurization: 50 mL of gas oil, 0.1 g of $PMo_{11}V$@PbO@PANi nanocatalyst, 6 ml of oxidant, 10 mL of extraction solvent, time = 2 hours, and temperature = 35 °C.

## References


[1] M. A. Rezvani, A. F. Shojaei, F. M. Zonoz, J. Serb. Chem. Soc, **2014**, 79 1099.

[2] N. M. Mahmoodi, M. A. Rezvani, M. Oveisi, A. Valipour, M. A. Asli, Mater. Res. Bull., **2016**, 84, 422.

[3] M. A. Rezvani, M. Alinia Asli, M. Oveisi, R. babaei, K. Qasemi, S. Khandan, RSC Adv, **2016**, 6, 53069.

[4] M. A. Rezvani, M. Alinia Asli, S. Khandan, H. Mousavi, Z. Shokri Aghbolagh, Chem. Eng. J, **2017**, 312, 243.

[5] M. A. Rezvani, A. F. Shojaie, M. H. Loghmani, Fuel Process. Technol, **2014**, 118, 1.

[6] M. A. Rezvani, F. MohammadiZonoz, Ind. Eng. Chem, **2015,** 22, 83.

[7] M. A.Rezvani, M. Shaterian, F. Akbarzadeh, S.Khandan, Chem. Eng. J, **2018**, 333, 537.

[8] M. A. Rezvani, Z. S. Aghbolagh, H. H. Monfared, S. Khandan, J. Ind. Eng. Chem, **2017**, 52, 42

[9] G. Attia, M. F. H. Abd El-kader, Int. J. Electrochem. Sci, **2013**, 8, 5672

**Graphical Abstract**

**Fabrication and characterization of a novel Polymer/Metal Oxide/Polyoxometalate (PMP) Composite and its highly catalytic performance for the oxidative desulfurization**

**Mohammad Ali Rezvani, Omid Feghe Miri**

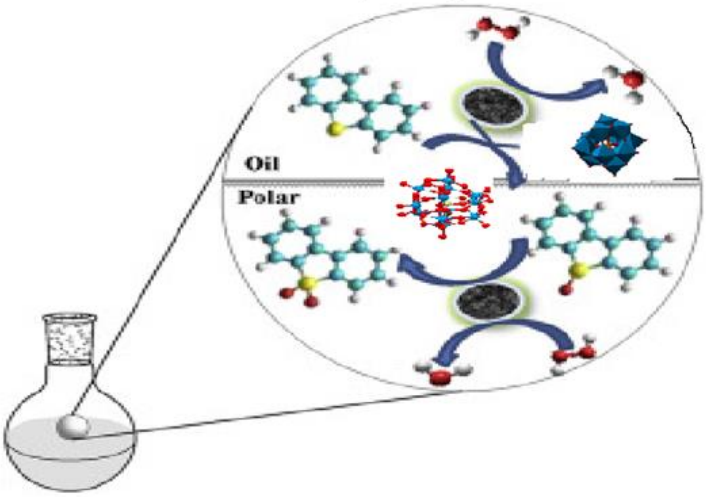

# Immobilized polyoxometalate on PANi and ZnO as an efficient and reusable photocatalyst for dye degradation

**Parvin Rahmani, Mohammad Ali Rezvani*, and Fatemeh Parchegani***

*Department of Chemistry, Faculty of Science, University of Zanjan, 451561319, Zanjan, Iran*

Corresponding author: Fax: +98245152617, E-mail: marezvani@znu.ac.ir, f-parchegani94@phd.araku.ac.ir

**Abstract**

A literature review showed that dye removal using the immobilized POM onto the ZnO and polyaniline (PANi) nanoparticle as a photocatalyst. The immobilized mono substituted tungstophosphoric acid onto the ZnO and PANi nanoparticle as an environmentally friendly catalyst was used for photocatalytic dye degradation. The synthesized nanocomposite $PW_{11}Mn$@ZnO@PANi was characterized using FTIR. Basic red was used as model dyes.

**Keywords**: Keggin-type polyoxometalate, Nanocomposite, Dye degradation, Photocatalysts

## Introduction

The discharge of toxic colored wastewaters without effective treatment into environment has severe influence on the aquatic organisms. Thus the process must be developed that can remove pollutants prior to discharging into the environment. The used traditional processes to remove dyes include physical, biological, and chemical methods. Several materials as adsorbent are used to uptake dyes. The dye removal capacity of some adsorbents increases by surface modification using organics such as surfactants. In addition surfactants have corrosion inhibition effect. Photocatalytic degradation method as an advanced oxidation process is an efficient procedure to degrade dyes and it includes irradiation of semiconductors as photocatalysts. Nano-materials such as titania, zinc oxide and polyoxometalates (POMs) have been the primary interest as photocatalysts. (Dr 5,2)
Polyoxometalates (POMs) as metal–oxygen anionic cluster can undergo to a reversible reduction without changing its structure. They have numerous applications in a multitude of areas ranging from catalysis to pharmacology and remain of continuous interest, especially in the areas of design and synthesis of functional nanomaterials. In addition, POM as an electron shuttle is known to resist oxidation and to catalyze redox reactions. Several researchers indicate that the polyoxoanion acts as a molecular acceptor by interactions with the nitrogen and oxygen atoms of the organic donor(Dr 6,1).
Polyaniline (PANi), a conducting polymer, has emerged as a promising 1D material that is particularly attractive for electronic devices due to its facile synthesis, environmental stability, unique electronic properties, and simple acid/base doping/dedoping chemistry (PANI 2014/). Zinc oxide thin films and nanoparticles have applications in luminescent devices, photocatalysis, photoelectrochemistry and nonlinear optical devices (ZnO). Herein, a new mono substituted phosphotungstate supported polyaniline and ZnO was investigated and demonstrated to be effective for dye degradation.

## Experimental

Mono substituted phosphotungstate $H_3[PW_{11}Mn]$ and ZnO nanoparticles were synthesized according to a reported procedure [Dr.9]. During the formation of the milky gel from $Zn(NO_3)_2{\cdot}6H_2O$ and $C_6H_8O_7H_2O$ solutions, the $PW_{11}Mn$ aqueous solution was added slowly. The above solution was heated at 70 °C for 45 min, under vigorous stirring. The product finally dried at 50°C for 3 h. The resultant white powder nanocomposite was designated as $PW_{11}Mn$@ZnO. After that, during the formation of polyaniline polymer, the $PW_{11}Mn$@ZnO solution was added drop-wise to polyaniline solution under stirring for 2h. The precipitate was filtered and washed with 10 mL distilled water and 10 mL ethanol. The dark green product dried in oven 80 °C for 3h. The final ($PW_{11}Mn$@ZnO@PANi) composite was characterized through FT-IR spectroscopy.
UV/Vis spectra of solutions were recorded with a Shimadzu 160 spectrophotometer.

## Results and discussion

The identification of specific chemical bands and functional groups of the synthesized samples was characterized using FT-IR spectroscopy to confirm their successful incorporation. The FT-IR spectra of (a) $PW_{11}Mn$, (b) ZnO, (c) $PW_{11}Mn@ZnO$, (d) PANi and (e) $PW_{11}Mn@ZnO@PANi$ nanocatalyst are depicted in Figure 1. According to Figure 1(a), the unique characteristics peaks at 830, 896, 957, and 1051 $cm^{-1}$ are caused by the stretching modes involving edge-sharing W–$O_b$–W, corner-sharing W–$O_c$–W, terminal W=$O_d$, and P-O bond in the Keggin-type $PW_{11}Mn$ , respectively. Figure 1(b) is exhibited characteristics peaks at 1421, 881, and 534 $cm^{-1}$. The absorption bond at 881 $cm^{-1}$ is assigned to Zn–O–H stretching bond. A peak at 534 $cm^{-1}$ is caused by the vibration bond of Zn–O. The spectrum of PANi Figure 1(d), the presence of sharp peaks near 1501 and 1584 $cm^{-1}$ are attributed to C=C stretching of the benzenoid and quinoid rings, respectively.

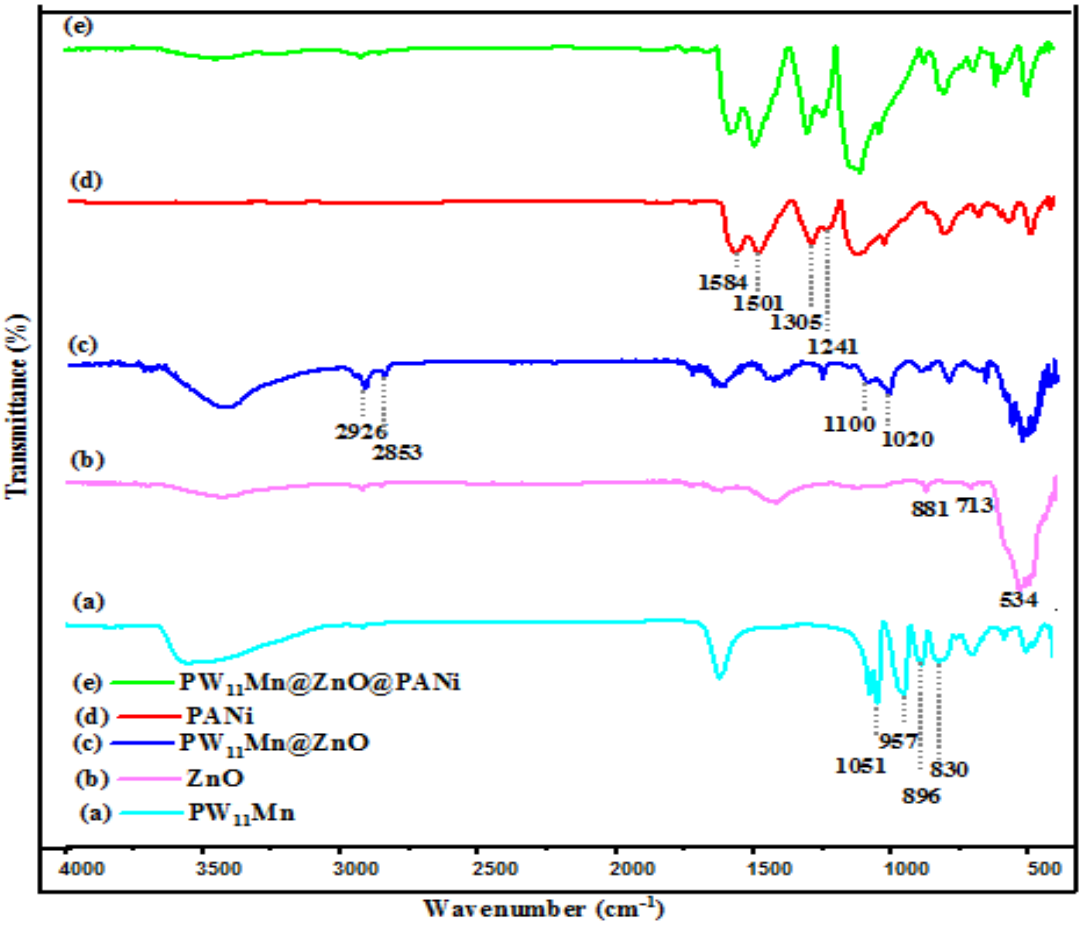


**Figure1**. FT-IR spectrum of the synthesized nanomaterials (a) $PW_{11}Mn$, (b) ZnO, (c) $PW_{11}Mn@ZnO$ (d) PANi (e) $PW_{11}Mn@ZnO@PANi$

.

The photocatalytic activity of as-obtained samples was estimated through the photodegradation of basic red. Typically, 20 mg of PW11Mn@ZnO@PANi composites was dispersed into 20 mL basic red (20 ppm) aqueous solution( pH=7). Prior to irradiation, the mixture solution was stirred in darkness for 30 min to obtain the saturated absorption of basic red molecules onto the catalysts, then above solution was illuminated under UV light irradiation, every 30 min, 1 mL of the suspension was withdrawn, centrifuged subsequently, and measured at the maximum absorption wavelength of 531 nm.

## Conclusion

In this paper, POM was synthesized and its surface was modified through zinc oxide and PANi. The 12-tungstophosphoric acid as a POM was immobilized on ZnO and PANi nanoparticles. $PW_{11}Mn$@ZnO@PANi was used as an environmentally friendly catalyst for photocatalytic dye degradation. The results showed dye degrada- tion increased by IPMCF dosage and decreased dye concentration.

## References

[1] M. A. Rezvani, S. Khandan, N. Sabahi, Energy Fuels, **2017**, 31, 5472−5481.

[2] M. A. Rezvani, A. Fallah Shojaie, M. H. Loghmani, Catal. Commun, **2012**, 25, 36–40.

[3] M. A. Rezvani, M. A. Asli, L. Abdollahi, M. Oveisi, J. Serb. Chem. Soc. **2016**, 81, 91–101.

[4] M. A. Rezvani, M. Oveisi, M. A. N. Asli, J.Mol. Catal. A: Chem. **2015**, 410, 121–132.

[5] M. A. Rezvani, A. Fallah Shojaei, F. Mohamadi Zonoz, J. Serb. Chem. Soc. **2014,** 79, 1099–1110.

[6] M. A. Rezvani, Z. S. Aghbolagh, H. H. Monfared, S. Khandan, J. Ind. Eng. Chem. **2017,** 52, 42–50.

[7] M. A. Rezvani, M. Alinia Asli, M. Oveisi, R. babaei, K. Qasemi, S. Khandan, RSC Adv. **2016**, 6, 53069–53079.

[8] M.. Rezvani, S. Khandan, M. Aghmasheh, Taiwan. Inst. Chem. Eng. J. **2017**, 77, 321–328.

## Graphical Abstract

**Immobilized polyoxometalate on PANi and ZnO as an efficient and reusable photocatalyst for dye degradation**

Parvin Rahmani, Mohammad Ali Rezvani, and Fatemeh Parchegani

# Application of Two Cobalt-Based Metal−Organic Frameworks as Oxidative Desulfurization Catalysts

**Behnam Gharib[a], Mohammad Yaser Masoomi[a], Ali Morsali[a,*]**

[a] *Department of Chemistry, Faculty of Sciences, Tarbiat Modares University, P.O. Box 14117-13116, Tehran, Islamic Republic of Iran*

*Corresponding author Tel.: +98 (21) 82884416; Fax number: +98 (21) 82884416

*E-mail: morsali_a@modares.ac.ir

**Abstract**

Two new porous cobalt-based metal−organic frameworks ,$[Co_6(oba)_5(OH)_2(H_2O)_2(DMF)_4]_n\cdot 5DMF$ (**TMU-10**) and $[Co_3(oba)_3(O)(Py)_{0.5}]_n\cdot 4DMF\cdot Py$ (**TMU-12**) have been synthesized by solvothermal method using a nonlinear dicarboxylate ligand. Under mild reaction conditions, these compounds exhibited good catalytic activity and reusability in oxidative desulfurization (ODS) reaction of model oil which was prepared by dissolving dibenzothiophene (DBT) in n-hexane. FT-IR and Mass analysis showed that the main product of DBT oxidation is its corresponding sulfone, which was adsorbed on the surfaces of catalysts. The activation energy was obtained as 13.4 kJ/mol.

**Keywords**:
Metal-Organic Frameworks, MOF, Catalysis.

## INTRODUCTION

Metal−organic frameworks (MOFs) are organic−inorganic hybrid materials, which have extremely large surface area and can be synthesized by choosing proper organic ligands and inorganic secondary building units (SBUs).[1−4] As they are designable and available for functionalization, MOFs are very useful for gas storage/separation, catalysis, drug delivery, ion exchange and sensing.[5−11] In some MOF materials, unsaturated metal sites having Lewis acidity can be obtained by removal of the solvent molecules, which are coordinated to metal sites.[12]
One of the most important duties of oil refining industry is removal of sulfur from diesel fuel, because consuming oil with high sulfur content leads to production of SOx, which is the precursor of acid rains. Thus, in many countries the sulfur level in oil must be below 15 ppm because of environmental regulations.[13,14] Many attempts have been made to degrade diesel engine's harmful sulfur emissions including hydrodesulfurization, biodesulfurization, adsorptive desulfurization, extractive desulfurization, and photo-oxidation.[15−17] Among them, oxidative desulfurization (ODS) is an efficacious process that operates at mild reaction conditions (at atmospheric pressure and below 100 °C) and offers high sulfur removal efficiency. Using this technology, oil organic sulfur is oxidized to strong polar matter, which can be simply separated from nonpolar oil phase by absorption or extraction.[18] Up until now, various catalysts, such as mixed metal oxides, ionic liquids, alkali metal salts, particularly, hetropolyacids, have been reported for ODS reactions.[19−28] A few reports are available on using MOFs as catalyst in ODS process.[29,30] Other studies focus on MOF@ heteropoly acid systems as ODS catalysts in which MOFs have been used as effective supports for improvement of catalytic activities in heterogenizated heteropoly acid without any certain catalytic activity.[31,32]
In this study, two new cobalt-based MOFs, **TMU-10** and **TMU-12**, have been used as catalysts in ODS reaction. These two MOFs have been synthesized based on an oxygen donor ligand ($H_2$oba = 4,4-oxybisbenzoic acid).

## EXPERIMENTAL SECTION

### Materials and Physical Techniques.

All reagents and materials for the synthesis and analysis were commercially available from Aldrich and Merck Company and used as received. Melting points were measured on an Electrothermal 9100 apparatus. IR spectra were recorded using Thermo Nicolet IR 100 FT-IR. PL-STA 1500 apparatus was used for measurement of thermal behavior with the rate of 10 °C min−1 in a static atmosphere of nitrogen. Philips X'pert diffractometer with monochromated Cu Kα radiation was applied for X-ray powder diffraction (XRD) measurements. Elemental analyses were collected on a CHNS Thermo Scientific Flash 2000 elemental analyzer. Mass spectra were recorded with an Agilent-5975C mass spectrometer operating at an ionization potential of 70 eV. Crystallographic measurements were made at 100(2) K for **TMU- 10** using a Bruker APEX-II CCD area detector, Mo Kα radiation, λ =0.71073 Å. Also data collection for **TMU-12** was performed at 180(2) K on a Bruker APEX-II CCD X-ray diffractometer with graphite monochromated Mo Kα radiation (λ = 0.71073 Å), operating at 50 Kv and 30 mA over 2θ ranges of 4.32−52.00°. The structures were solved by direct methods and refined by refinement of F2

against all reflections. Structure solution and refinement were accomplished using SHELXL97 and WinGX.[33–37]

*Synthesis of* $[Co_6(oba)_5(OH)_2(H2O)_2(DMF)_4]_n{\cdot}5DMF$ ***(TMU-10)***. Single Crystals. In a typical procedure, $Co(NO_3)_2.6H_2O$ (0.289 g, 1 mmol) and $H_2oba$ (0.254 g, 1 mmol) ($H_2oba$ = 4,4′-oxybisbenzoic acid) in 10 mL of DMF were placed in 25 mL Teflon-lined autoclave, which was heated gradually to 145 °C and maintained at this temperature for 48h. The mixture was then cooled to ambient temperature at 3.5 °C/min. As a result blue crystals of **TMU-10** suitable for X-ray diffraction formed. Yield: 0.215 g (45% based on oba). d.p. > 300 °C. IR data (KBr pellet, ν/cm−1): 658(m), 780(m), 872(m), 1012(w), 1097(m), 1160(m), 1237(vs), 1399(vs-br), 1501(m), 1560(s), 1603(vs), 1662(vs), 2931(w), and 3427(w-br). Elemental analysis (%) calculated for $[Co_6(C_{14}O_5H_8)_5(OH)_2(H_2O)_2\text{-}(C_3NOH_7)_4]{\cdot}(C_3NOH_7)_5$: C, 49.3; H, 4.7; N, 5.3. Found: C, 49.8; H, 4.2; N, 5.6.

*Powder*. In a typical experiment powder sample of **TMU-10** was obtained by mixing oba (2 mmol) and $Co(NO_3)_2{\cdot}6H_2O$ (0.578 g, 2 mmol) in 40 mL of DMF in a round-bottom flask at 145 °C for 72 h. The resulted powder was isolated by centrifugation, washed with DMF 4 times, and dried in air for characterization. Yield: 0.841 g (89% based on oba). IR data (KBr pellet, ν/cm−1): 658(m), 782(m), 873(m), 1012(w), 1098(m), 1160(m), 1237(vs), 1398(vs-br), 1504(m), 1558(s), 1603(vs), 1661(vs), 2928(w), and 3417(w-br). Elemental analysis (%) calculated for $[Co_6(C_{14}O_5H_8)_5(OH)_2(H2O)_2\text{-}\ (C_3NOH_7)_4]{\cdot}(C_3NOH_7)_5$: C, 49.3; H, 4.7; N, 5.3. Found: C, 49.5; H, 4.5; N, 5.1.

*Synthesis of* $[Co_3(oba)_3(O)\ (Py)_{0.5}]_n{\cdot}4DMF{\cdot}Py$ ***(TMU-12)***. Red crystals of **TMU-12** together with purple powder were synthesized using a similar solvothermal reaction as for **TMU-10** in the presence of pyrazine (0.040 g, 0.5 mmol); otherwise conditions are identical. Yield: 0.367 g (80% based on oba). d.p. > 300 °C. IR data (KBr pellet, ν/cm−1): 653(m), 700(w), 780(m), 872(m), 1011(w), 1088(w), 1158(s), 1235(vs), 1396(vs-br), 1503(m), 1603(vs-br), 1674(vs), 2926(w), 3067(w), and 3431(w-br). Elemental analysis (%) calculated for $[Co_3(C_{14}O_5H_8)_3(O)(C_4H_4N_2)_{0.5}]{\cdot}(C_3NOH_7)_4$: C, 49.0; H, 4.0; N, 5.1. Found: C, 49.7; H, 4.2; N, 5.3.

**Activation Method**. All samples were heated in oven at 140 °C for 72 h under vacuum. The frameworks of these two MOFs remain intact after removal of guest molecules

*Evaluation of Catalytic Activity*. In a typical run, solution of dibenzothiophene (DBT) in n-hexane was used as simulated diesel oil, containing 500 mg L−1 sulfur. The oxidative desulfurization experiment was performed in a three-necked 100 mL round-bottomed flask including 25 mL of DBT solution, 100 mg of catalyst (**TMU-10** and **TMU-12**), and 0.11 mL of 70 wt % tert-butyl hydroperoxide (TBHP). The reaction was done by stirring mixture at a constant speed (1000 rpm) by a magnetic agitator at 60 °C at a given time. After that, the oil phase was analyzed by gas chromatography coupled with a flame ionization detector (GC-FID (Echrom GC A90) and UV−vis spectroscopy (UV−vis 2100 spectrophotometer (Shimadzu)). Fourier transform infrared spectroscopy (FT-IR) and mass spectrometry (MS) were used to identify the oxidation products. To examine reusability of the catalyst, it was several times washed by methanol, then dried at 110 °C for 12 h and then was used in the next run.

*Sulfur Adsorption*. The removal percentage of DBT was calculated as

$$\text{DBT removal (\%)} = ((A_0 - A_t)/A_0)*100$$

where $A_0$ is the initial concentration of sulfur (DBT) in the hexane solution and At is the sulfur concentration of the oil phase after any certain time (t).

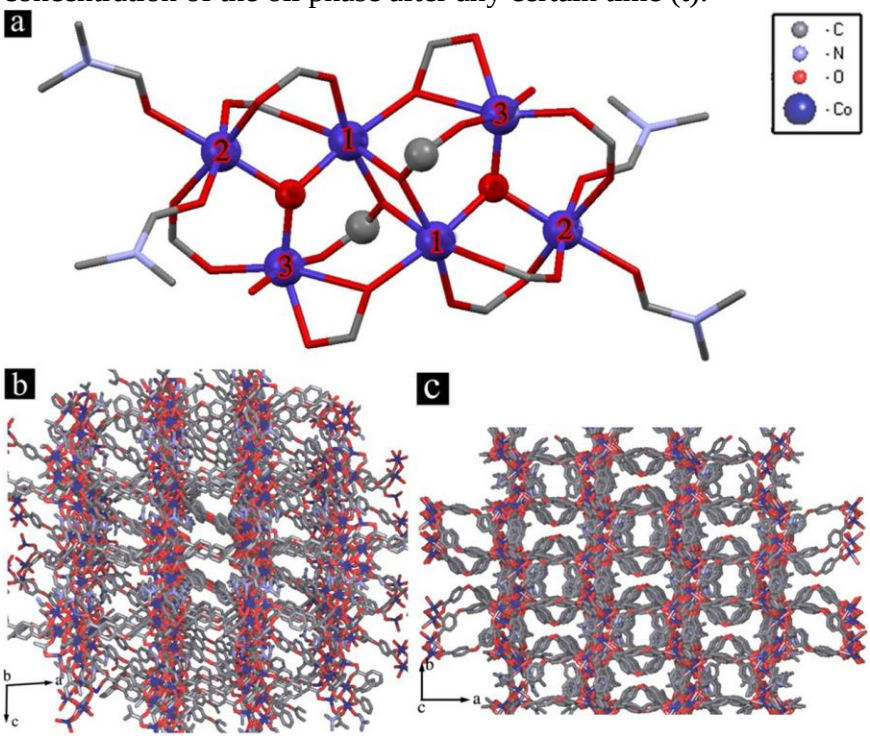


Figure 1.

## RESULTS AND DISCUSSION

Two new 3D porous cobalt based metal−organic frameworks, $[Co_6(oba)_5(OH)_2(H_2O)_2(DMF)_4]_n \cdot 5DMF$ (**TMU-10**; TMU stands for Tarbiat Modares University) and $[Co_3(oba)_3(O)\cdot(Py)_{0.5}]_n \cdot 4DMF \cdot Py$ (**TMU-12**) have been synthesized by solvothermal reaction of a mixture of $Co(NO_3)_2 \cdot 6H_2O$, $H_2oba$, and pyrazine. The IR spectra of these MOFs show the symmetric $\nu_{sym}(COO)$ and asymmetric $\nu_{as}(COO)$ vibrations of the carboxylate groups around 1400 and 1600 cm−1, respectively. Also the characteristic absorption peak (νC□O = ∼1673 cm−1) of DMF molecules are present in the IR spectra of these MOFs .**TMU-10** with higher yield was also synthesized via reflux method by mixing oba and $Co(NO_3)_2 \cdot 6H_2O$ at 145 °C for 72 h. A comparison between XRD of simulated and crystal or powder samples of **TMU-10** confirms that it can be synthesized in large scale by refluxing of initial reagents.

The structure of **TMU-10** is comprised of a hexanuclear secondary building unit (SBU), $Co_6(CO_2)_{10}(O)_2(O)_4$, in which there are three crystallographically independent six coordinate Co(II) centers (Figure 1a). Co(1) binds to five O atoms from five oba ligands and one $\mu_3$-O atom of $OH^-$ anion, whereas Co(2) binds to three O atoms from three oba ligands, one $\mu_3$-O atom of $OH^-$ anion and two O atoms from two DMF molecules. Also Co(3) is coordinated to four O atoms from three oba ligands, one $\mu_3$-O atom of $OH^-$ anion and one O atom of $H_2O$ molecule (Figure 1a). In **TMU-10** oba ligands adopt three different coordination modes: chelating-bridging coordination mode and two $\mu_2$ and $\mu_3$ bridging modes.

The oba ligand with V-shaped orientation (C−O−C =116.7° and 114.9°) acts as an important factor in the linkage of the SBUs resulting in a three-dimensional framework with pores running along the *b*- and *c*-axes (aperture size = 6.2×6.1 and 9.6 × 4.3 Å, respectively, taking into account the van der Waals radii; 32.7% void space per unit cell)[38] (Figure 1b and c). Similar to previously reported MOFs,[11,39] **TMU-10** is nonporous toward N2 at 77 K and 1 bar while it is porous to $CO_2$ at 195 K and 1 bar (BET surface area 129.8 $m^2/g$). This may be attributed to existence of structural changes during gas adsorption ($N_2$ at 77 K) and/or the existence of structural defects.

**TMU-12** is based on hexanuclear secondary building units (SBUs), $Co_6(CO_2)_{12}(O)_2(N)_2$,[40] in which there are three crystallographically independent cobalt centers. Co(1) has distorted octahedral geometry and coordinate to one $\mu_3$-O atom, four O atoms from four oba ligands and one N atom of pyrazine ($Co(1)O_5N$). Co(2) is coordinated to one $\mu_3$-O atom and four O atoms from four fully deprotonated oba ligands ($Co(2)O_5$). Finally, Co(3) has distorted octahedral geometry and coordinate to one $\mu_3$-O atom and five O atoms from five oba ligands ($Co(3)O_6$) (Figure 2a).

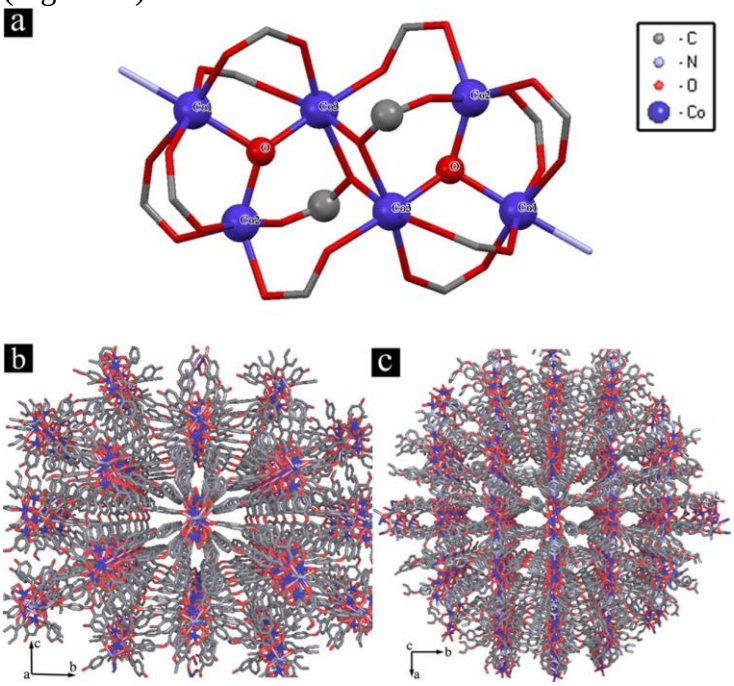


Figure 2.

In the framework, two types of bridging modes, $\mu_2$ and $\mu_3$, is available for oba ligands and each nonlinear (117°) dicarboxylate oba ligand binds four cobalt atoms from two different units. In MOF **TMU-12**, the V-shaped coordination of the oba ligands (C−O−C = 117.5°, 117.6°, and 117.0°) in combination with pyrazine result in a three-dimensional framework containing nano channel running along a axis (aperture size = 3.1 × 3.6 Å, taking into account the van der Waals radii), and two channels running along the *c* axis (aperture size = 8.5 × 2.6 Å and 7.1 × 8.2 Å, taking into account the van der Waals radii; 43.0% void space per unit cell)[38] that occupied by DMF guest molecules (Figure 2b and c). The $N_2$ isotherm collected at 77 K and 1 bar on the **TMU-12** revealed that $N_2$ molecules could not transpire within its pores under these conditions .

Thermogravimetric analysis (TGA) of **TMU-10** and **TMU-12** between 25 and 600 °C ascertained a weight loss in the temperature range of 50−255 °C (19.5%, expected 15.4%), and 100−351 °C (24.3%, expected 27.1%), respectively, attributed to the loss of guest DMF

molecules. Also **TMU-10** shows a second weight loss in the temperature range of 255− 397 °C that may be attributed to loss of remaining coordinated DMF molecules. **TMU-10** and **TMU-12** are thermally stable up to 375 and 379 °C, and they begin to decompose after that.

*Catalytic Performance*. *Evaluation of Adsorption Efficiency* in **TMU-10** and **TMU-12**. Type, amount of absorbent and temperature are crucial factors in adsorption reactions. Results show that the percentage of adsorption for **TMU-12** is more than that for **TMU-10** at 60 °C. This outcome is probably related to different coordination environments in two MOFs. This is attributed to larger aperture size and void space in **TMU-12**. In addition, the removal efficiency is enhanced by increasing the amount of catalyst. However, with further increasing in catalyst weight (>100 mg), the sulfur adsorption is not increased significantly. Further experiments were carried out using **TMU-12** as the best adsorbent. As the results show, sulfur adsorption is increased along with the reaction time until 30 min and remains constant afterward.

*Optimizing the ODS Reaction Conditions in the Presence of **TMU-12***. TBHP was chosen as oxidant for its better dispersion in organic reactants phase, which impedes formation of interface between catalyst and reactants that subsequently cause the higher oxidation efficiency.[41] The O/S is described as molar ratio of the amount of TBHP to the total amount of sulfur in initial solution of DBT. Sulfur removal from model oil increases upon adding oxidant to reaction mixture. Thus, these MOFs play an effective role as catalysts in ODS process. The finest conversion occurs when O/S ratio is 3 but by further increasing the ratios no considerable changes in the ODS efficiency occur (Table 1). It is noteworthy that there are no competitive reactions between the oxidation of DBT and the self-decomposition of TBHP up to 150 °C.[42] Thus, the O/S ratio of 3 is proper for the requirement of desulfurization. The amount of catalyst is an important factor in ODS reactions. As can be seen in Table 2, there is no change in the concentration of sulfur in absence of catalyst. Also, sulfur removal of the ODS reaction with various amounts of catalysts is increased continuously. When 50 mg catalyst is employed, sulfur removal of DBT reaches 27% within 120 min. As the amount of catalyst increases up to 100 mg, the removal of DBT reaches 35.5% under the same reaction conditions. However, by adding more catalyst (>100 mg), the sulfur removal is not increased significantly. Hence, 100 mg is chosen as the suitable amount of catalyst in the experiments.

Since reaction temperature greatly influences catalytic activity of the catalyst, it is one of the greatest factors that could not be ignored in the desulfurization process. Sulfur removal enhances with increasing reaction temperatures at the beginning of each experiment (Figure 3). Although the removal of DBT is up to 17% and 21.3% at 30 and 40 °C, respectively, within 120 min, the conversions increase significantly with increasing the temperature after that. Thus, 60 °C is chosen as the suitable reaction temperature in the following experiments.

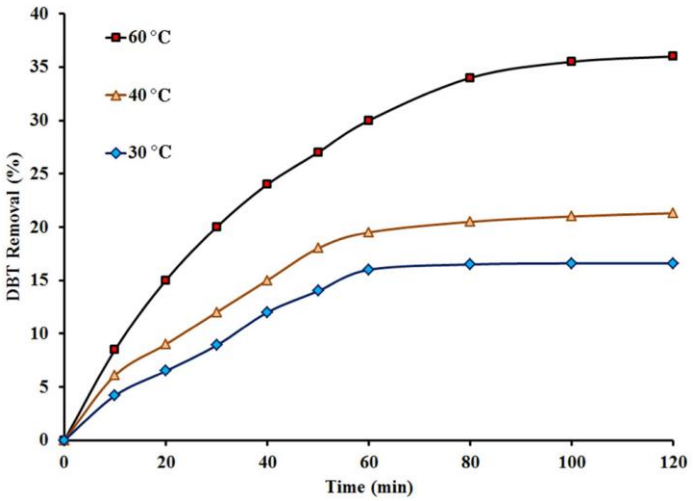


Figure 3.

Table 1.

| entry | O/S molar ratio | sulfur remained (ppm) | sulfur removal (%) |
|---|---|---|---|
| 1 | 0 | 392 | 21.6 |
| 2 | 2 | 369.5 | 26.1 |
| 3 | 3 | 332 | 33.6 |
| 5 | 5 | 328 | 34.4 |

Table 2.

| entry | catalyst dosage (mg) | sulfur remained (ppm) | sulfur removal (%) |
|---|---|---|---|
| 1 | 0 | ~500 | ~0 |
| 2 | 50 | 365 | 27 |
| 3 | 100 | 322.5 | 35.5 |
| 4 | 150 | 320 | 36 |
| 5 | 200 | 318 | 36.4 |

*Comparison of **TMU-10** and **TMU-12** Catalysts in ODS Reaction*. Desulfurization performances of activated **TMU-10** and **TMU-12** in removal of DBT under optimum conditions up to 8 h are investigated. Sulfur removal efficiency in the presence of **TMU-12** is nearly 2 times greater than that for **TMU-10**. Regarding structures of the two MOFs, a probable reason for the higher oxidation of DBT using **TMU-12** may be related to unsaturated coordination number around Co(2), which is responsible for more adsorption and oxidation of DBT in the presence of TBHP, while in the case of **TMU-10** there are no unoccupied positions around Co centers. There is only one $H_2O$ molecule coordinated to Co(3), which can be removed by activation in vacuum to create open metal site around Co(3). Also, larger void space of **TMU-12** causes more adsorption of DBT molecules in the framework and higher removal efficiency. Moreover, lower catalytic performance of these two MOF materials compared with other ODS catalysts may be attributed to difficulty in diffusion of DBT molecules into the pores of MOFs.

*Kinetics of Sulfur Removal*. Different types of kinetics orders are attempted to know the kinetics of DBT removal in model oil catalyzed by **TMU-10** and **TMU-12**. The values of $R_0$, $R_1$, and $R_2$ represent the correlation coefficients of zero-, first-, and second-order rate equations, respectively. It confirms that $R_1$ has the best correlation for different orders. Thus, the DBT removal in *n*-hexane solution suspended on two MOFs obeys from first order reaction kinetics. The apparent rate constants in the removal of DBT are 0.001 and 0.003/min over **TMU-10** and **TMU-12**, respectively. The half-times ($t_{1/2}$), at which $[A] = [A]_0/2$, are also calculated by equation $t_{1/2} = 0.693/k$, as 693 and 231 min at 60 °C for **TMU-10** and **TMU-12**, respectively. The activation energy ($E_a$ = 13.4 kj/mol) for DBT removal process catalyzed by **TMU-12** is also obtained by using Arrhenius equation at two different temperatures of 40 °C (k = 0.0022) and 60 °C (eqs 1 and 2)

$$k = Ae^{-Ea/RT} \quad (1)$$

$$\log(k_1/k_2) = -E_a/2.303R((T_2 - T_1)/T_1T_2) \quad (2)$$

where *A* is the frequency factor for the reaction, *R* is the universal gas constant, *T* is the temperature (in Kelvin), and *k* is the rate constant, while subscripts 1 and 2 show the reactions are done at temperatures 40 and 60 °C, respectively. The reusability of the catalysts is studied as the main parameter in the DBT removal. After each catalytic run, **TMU-12** catalyst was recovered by washing with methanol five times, and dried at 100 °C for 6 h. During the third cycle of the reaction in the presence of the recovered **TMU-12**, a slight decrease in the DBT removal is observed (Figure 4a); however, the catalytic activity is nearly retained during the later runs. The XRD pattern of **TMU-12** catalyst before and after repeating reaction shows stability of the catalyst (Figure 4b).

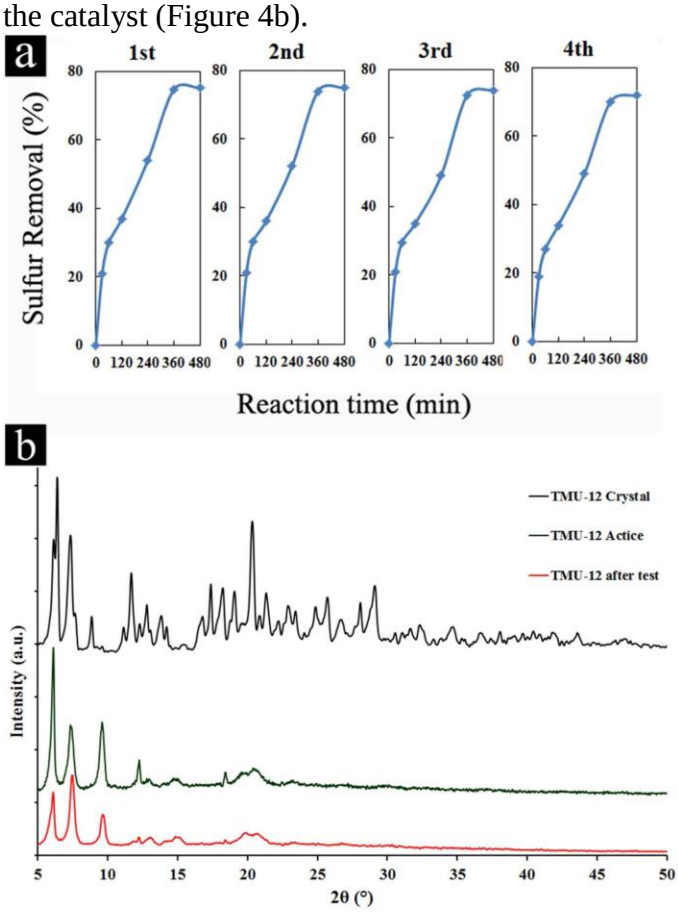


Figure 4.

*Product Characterization*. Regarding Tables 1 and 2, the concentration of sulfur does not change without any catalyst (blank). Sulfur adsorption efficiency enhances upon adding proper amounts of catalyst up to 30 min and remains constant after that. However, addition of TBHP as oxidant leads to increase in sulfur removal efficiency, indicating the efficient role of MOFs (especially **TMU-12**) as catalyst in ODS reaction. Oxidative desulfurization reaction in the presence of an oxidant occurs through two consecutive stages:[43,44] at first stage, DBT is oxidized to dibenzothophene sulfoxide (DBTO), and then, the formed DBTO is rapidly converted to dibenzothophene sulfone ($DBTO_2$). In GC chromatograms, by DBT removal from the fluid phase the height of DBT peak is declined without appearance of any new peak. For further investigation, **TMU-12** catalyst was washed with methanol, and the used solvent was decanted and the product was obtained after methanol evaporation at room temperature. A comparison between FT-IR spectra of the produced crystal and DBT are shown in Figure 5a. Both compounds show almost identical bands, except that in the spectrum of the mentioned crystal, two bands with strong intensity are observed at around 1295 and 1155 $cm^{-1}$ that can be attributed to the asymmetrical and symmetrical stretching vibration modes of O=S=O, respectively. In addition, mass analysis of obtained crystal shows production of sulfone of DBT. However, the peaks belonging to DBT (*m/z* = 184.0) and DBTO2 (*m/z* = 216.3) were detected after 6 h in which abundance of $DBTO_2$ is higher than that of DBT (Figure 5b). So the sulfone is adsorbed on the catalyst pore walls, probably because of its polarity characteristic derived from ether oxygen groups. Therefore, sulfone adsorption is an accomplisher step for sulfur removal from model oil. As reported in the literature, cobalt(II) salts and cobalt oxide can act as catalysts in oxidative desulfurization process.[45,46] Although, further study is needed to understand dependence of catalytic properties of MOF open metal sites in the presence of a proper oxidant on ODS process.

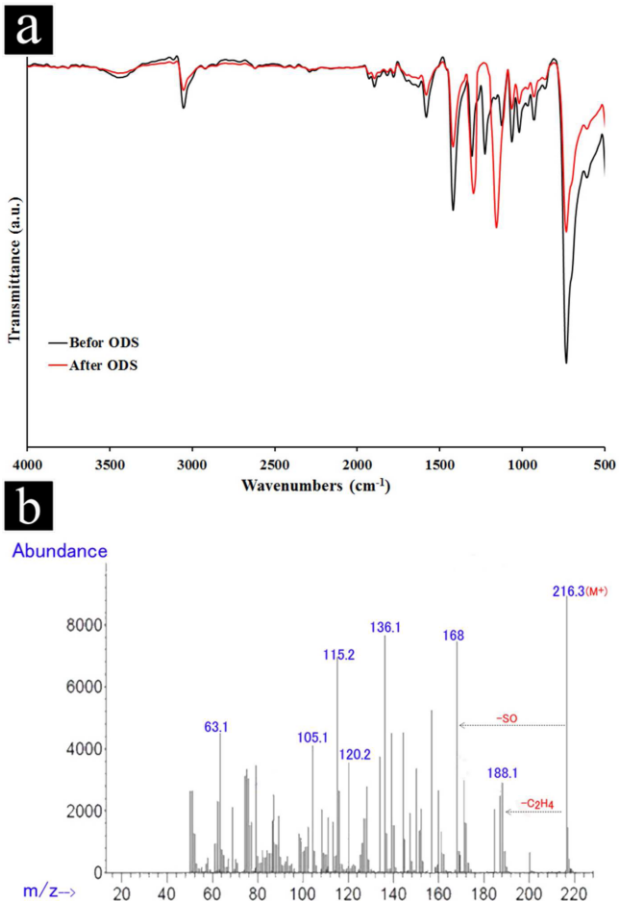


Figure 5.

## CONCLUSIONS

As novel oxidative desulfurization catalysts, two new porous cobalt based metal−organic frameworks, $[Co_6(oba)_5(OH)_2(H_2O)_2(DMF)_4]_n \cdot 5DMF$ (**TMU-10**) and $[Co_3(oba)_3(O)(Py)]_n \cdot 4DMF \cdot Py$ (**TMU-12**) were successfully synthesized via solvothermal method and characterized by X-ray crystallography. **TMU-10** and **TMU-12** consist of different structural topologies and pore sizes where **TMU-12** is constructed from two oba and pyrazine ligands whereas the structure of **TMU-10** is built of only oba ligand. **TMU-12** showed higher catalytic activity compared to **TMU-10** possibly because of a difference in their coordinate Co centers and void space. Desulfurization process is nearly completed under optimized conditions after 6 h. The adsorption of main product in the oxidation of DBT, dibenzothiophene-S,S-dioxide, on pore walls of MOF is an accomplisher step for sulfur removal from model oil. The kinetic studies show a pseudo-first-order reaction for ODS process. This study can be simply extensible to the synthesis of other MOF catalysts for ODS process in nonpolar media.

## ACKNOWLEDGMENTS

Support of this investigation by Tarbiat Modares University and the Iran National Science Foundation are gratefully acknowledged.

**REFERENCES**

(1) James, S. L. *Chem. Soc. Rev*. **2003**, *32*, 276−288.
(2) Long, J. R.; Yaghi, O. M. *Chem. Soc. Rev*. **2009**, *38*, 1213−1214.
(3) Stock, N.; Biswas, S. *Chem. Rev*. **2011**, *112*, 933−969.
(4) Masoomi, M. Y.; Morsali, A. *Coord. Chem. Rev*. **2012**, *256*, 2921−2943.
(5) Masoomi, M. Y.; Morsali, A. *RSC Adv*. **2013**, *3*, 19191−19218.
(6) Murray, L. J.; Dinca, M.; Long, J. R. *Chem. Soc. Rev*. **2009**, *38*,1294−1314.
(7) Allendorf, M. D.; Bauer, C. A.; Bhakta, R. K.; Houk, R. J. T.*Chem. Soc. Rev*. **2009**, *38*, 1330−1352.
(8) Lee, J.; Farha, O. K.; Roberts, J.; Scheidt, K. A.; Nguyen, S. T.; Hupp, J. T. *Chem. Soc. Rev.* **2009**, *38*, 1450−1459.
(9) Li, J.-R.; Kuppler, R. J.; Zhou, H.-C. *Chem. Soc. Rev*. **2009**, *38*, 1477−1504.
(10) Ingleson, M. J.; Heck, R.; Gould, J. a.; Rosseinsky, M. J. *Inorg. Chem*. **2009**, *48*, 9986−8.
(11) Tahmasebi, E.; Masoomi, M. Y.; Yamini, Y.; Morsali, A. *Inorg. Chem*. **2015**, *54*, 425−433.
(12) Kim, J.; Kim, S.-N.; Jang, H.-G.; Seo, G.; Ahn, W.-S. *Appl. Catal.*, A **2013**, *453*, 175−180.
(13) Juan, Z.; Dishun, Z.; Liyan, Y.; Yongbo, L. *Chem. Eng. J*. **2010**, *156*, 528−531.
(14) Arellano, U.; Shen, J. M.; Wang, J. A.; Timko, M. T.; Chen, L. F.; Vázquez Rodríguez, J. T.; Asomoza, M.; Estrella, A.; González Vargas, O. A.; Llanos, M. E. *Fuel* **2015**, *149*, 15−25.
(15) Zhang, B.; Jiang, Z.; Li, J.; Zhang, Y.; Lin, F.; Liu, Y.; Li, *C. J. Catal*. **2012**, *287*, 5−12.
(16) Song, H.; Wan, X.; Dai, M.; Zhang, J.; Li, F.; Song, H. *Fuel Process. Technol*. **2013**, *116*, 52−62.
(17) Shu, C.; Sun, T.; Zhang, H.; Jia, J.; Lou, Z. *Fuel* **2014**, *121*, 72−78.
(18) Stanislaus, A.; Marafi, A.; Rana, M. S. *Catal. Today* **2010**, *153*, 1−68.
(19) Hasan, Z.; Jeon, J.; Jhung, S. H. J. *Hazard. Mater*. **2012**, *205−206*, 216−221.
(20) Zhang, S.; Zhang, Q.; Zhang, Z. C. *Ind. Eng. Chem. Res*. **2004**, *43*, 614−622.
(21) Wan, M.-W.; Yen, T.-F. *Appl. Catal., A* **2007**, *319*, 237−245.
(22) Zhang, M.; Zhu, W.; Xun, S.; Li, H.; Gu, Q.; Zhao, Z.; Wang, Q. *Chem. Eng. J*. **2013**, *220*, 328−336.
(23) Zhu, W.; Wu, P.; Chao, Y.; Li, H.; Zou, F.; Xun, S.; Zhu, F.; Zhao, Z. *Ind. Eng. Chem. Res.* **2013**, *52*, 17399−17406.
(24) Zhu, W.; Huang, W.; Li, H.; Zhang, M.; Jiang, W.; Chen, G.; Han, C. *Fuel Process. Technol*. **2011**, *92*, 1842−1848.
(25) Ding, W.; Zhu, W.; Xiong, J.; Yang, L.; Wei, A.; Zhang, M.; Li, H. *Chem. Eng. J*. **2015**, *266*, 213−221.
(26) Zhu, W.; Dai, B.; Wu, P.; Chao, Y.; Xiong, J.; Xun, S.; Li, H.; Li, H. *ACS Sustainable Chem. Eng*. **2015**, *3*, 186−194.
(27) Zhu, W.; Wang, C.; Li, H.; Wu, P.; Xun, S.; Jiang, W.; Chen, Z.; Zhao, Z.; Li, H. *Green Chem*. **2015**, *17*, 2464−2472.
(28) Zhu, W.; Wu, P.; Yang, L.; Chang, Y.; Chao, Y.; Li, H.; Jiang, Y.; Jiang, W.; Xun, S. *Chem. Eng. J*. **2013**, *229*, 250−256.
(29) McNamara, N. D.; Hicks, J. C. *ACS Appl. Mater. Interfaces* **2015**, *7*, 5338−5346.
(30) McNamara, N. D.; Neumann, G. T.; Masko, E. T.; Urban, J. A.; Hicks, J. C. *J. Catal*. **2013**, *305*, 217−226.
(31) Liu, Y.; Liu, S.; Liu, S.; Liang, D.; Li, S.; Tang, Q.; Wang, X.; Miao, J.; Shi, Z.; Zheng, Z. *ChemCatChem* **2013**, *5*, 3086−3091.

(32) Rafiee, E.; Nobakht, N. *J. Mol. Catal. A: Chem*. **2015**, *398*, 17−25.
(33) Sheldrick, G. M. SHELX97 *Program for Crystal Structure Solution and Refinement;* University of Göttingen: Göttingen, Germany, 1997.
(34) Sheldrick, G. *Acta Crystallogr., Sect. A: Found. Crystallogr*. **2008**, *64*, 112−122.
(35) Bruker. APEX2 software package; Bruker AXS Inc., 2005.
(36) Sheldrick, G. M. *SADABS*, version 2.01; Bruker/Siemens Area Detector: Madison, WI , 1998.
(37) *Absorption Correction Program*; Bruker AXS: Madison, WI, 1998.
(38) Spek, A. L. *J. Appl. Crystallogr*. **2003**, *36*, 7−13.
(39) Masoomi, M. Y.; Stylianou, K. C.; Morsali, A.; Retailleau, P.; Maspoch, D. *Cryst. Growth Des.* **2014**, *14*, 2092−2096.
(40) Low, D. M.; Brechin, E. K.; Helliwell, M.; Mallah, T.; Riviere, E.; McInnes, E. J. L. *Chem. Commun*. **2003**, 2330−2331.
(41) Chica, A.; Corma, A.; Dómine, M. E. *J. Catal.* **2006**, *242*, 299−308.
(42) Morse, B. K. *J. Am. Chem. Soc*. **1957**, *79*, 3375−3380.
(43) Zhu, W.; Zhu, G.; Li, H.; Chao, Y.; Zhang, M.; Du, D.; Wang, Q.; Zhao, Z. *Fuel Process. Technol*. **2013**, *106*, 70−76.
(44) Torres-García, E.; Galano, A.; Rodriguez-Gattorno, G. *J. Catal.* **2011**, *282*, 201−208.
(45) Murata, S.; Murata, K.; Kidena, K.; Nomura, M. *Energy Fuels* **2004**, *18*, 116−121.
(46) Sampanthar, J. T.; Xiao, H.; Dou, J.; Nah, T. Y.; Rong, X.; Kwan, W. P. *Appl. Catal., B* **2006**, *63*, 85−93

**Graphical Abstract**

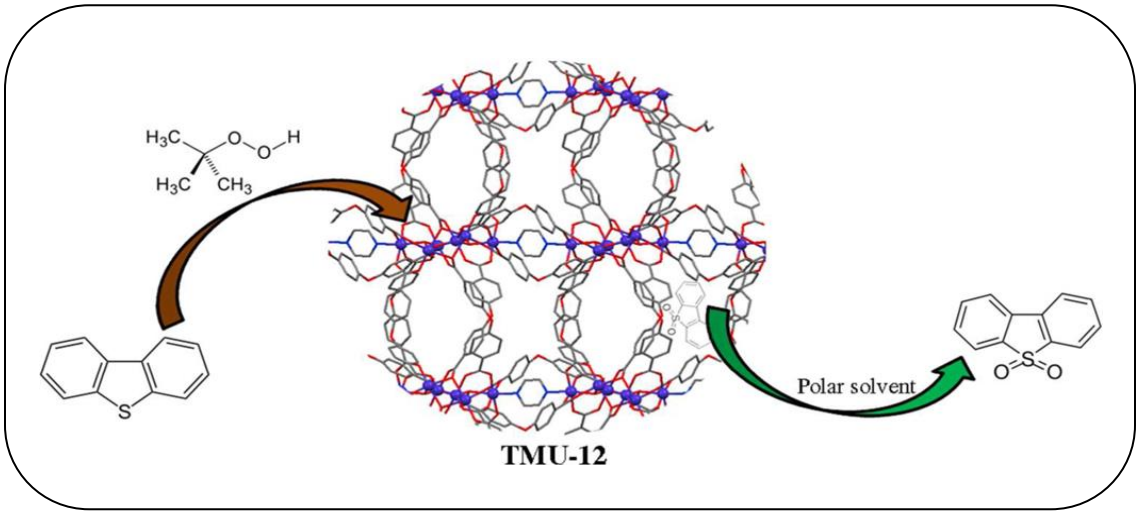

# Synthesis of tropolone derivatives in the presence of MgO Nanoparticles

**Issa Amini**[a]*

[a] *Department of Chemistry, Payame Noor University, P.O. BOX 19395-4697 Tehran, Iran*

*Corresponding author Tel.: +98 (24) 35233556; Fax number: +98 (24) 35226932

*E-mail: issa_amini@ymail.com

## Abstract

The use of Smiles rearrangement in Passerini-type couplings with tropolone allows very straightforward multicomponent formation of tropolone derivatives. The three-component addition of cyclohexyl isocyanide to tropolone (2-hydroxy-2,4,6-cycloheptatrien-1-one) and aldehyde in the presence of MgO Nanoparticles proceeds easily in methanol at 60 $^{o}$C, followed by reflux for 24 h to form titled compounds in a new Passerini- Smiles-type reaction.

**Keywords**: Passerini-Smiles-type reaction; Smiles rearrangement; MgO Nanoparticles; tropolone.

## Introduction

In recent years, nanoparticles (NP) have attracted tremendous attention in catalysis because of their improved efficiency under mild and environmentally benign conditions in the context of ecological (Green) synthesis. Due to their enormously large and highly reactive surface area, nanoparticles have potential to exhibit superior catalytic activity in comparison to bulk counterparts[1].

recently, we have established a one-pot method for the preparation of organic compounds. As part of our ongoing program to develop efficient and robust methods for the synthesis of heteroatom-containing compounds[2-4], we wish to report the preparation of a new class of tropolone derivatives **4a-b** by a novel three-component condensation reaction of aldehydes **1**, cyclohexyl isocyanide **2** and tropolone **3** in the presence of MgO nanoparticles in excellent yields (Scheme 1).

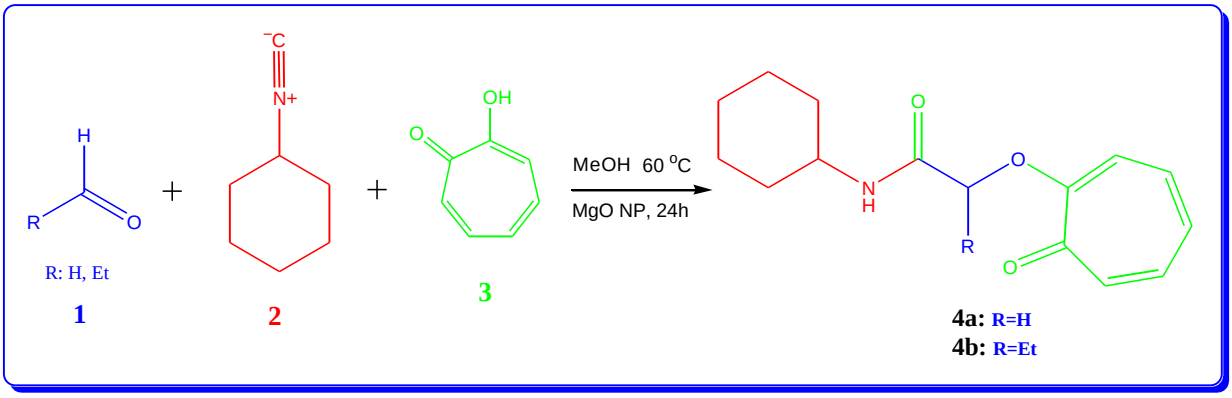


**Scheme 1** Synthesis of tropolone derivatives in the presence of MgO Nanoparticles

## Experimental

*General*

Starting materials and solvents were obtained from Merck (Germany) and Fluka (Switzerland) and were used without further purification. The methods were used to follow the reactions are TLC and NMR. TLC and NMR indicated that there is no side product. IR spectra were measured on a Jasco 6300 FTIR spectrometer. $^{1}H$ and $^{13}C$ NMR spectra ($CDCl_3$) were recorded on a BRUKER DRX-250 AVANCE spectrometer at 400.22 and 100.63 MHz, respectively. Preparative thin layer chromatography was prepared from Merck silica gel powder.

***General procedure for the synthesis of Compounds 4***

MgO nanoparticles (0.3 g) were added to a mixture of aldehyde (1 mmol), tropolone (1 mmol) and cyclohexyl isocyanide (1 mmol) in 7 mL of $CH_3OH$ at 60 °C, followed by reflux for 24 h. MgO nanoparticles were isolated from the reaction mixture by simple filtration and washed with methanol (3 ml). The solvent was removed under reduced pressure and the viscous residue was purified by preparative thin layer

chromatography (silica gel; petroleum ether–ethyl acetate (2:1)). The solvent was removed under reduced pressure and the products **(4a-b)** were obtained.

## Results and discussion

The aldehyde **1** is trapped by the cyclohexyl isocyanide **2** and tropolone **3** in the presence of MgO nanoparticles in methanol at 60 $^{o}$C over 24h, leads to the formation of tropolone derivatives **4** (Scheme 1). The reaction proceeds smoothly and cleanly under mild and neutral conditions and no side reactions were observed.

MgO nanoparticles were found to catalyze the synthesis of tropolone derivatives from aldehydes **1**, cyclohexyl isocyanide **2** and tropolone **3** in methanol at 60 $^{o}$C with high efficiency (Scheme 1). We also have used MgO powder (Merck) instead of MgO nanoparticles in this reaction, but increasing of reaction times and decreasing of α-aryloxy amide yields were observed (Scheme 1 and Table 1). The use of just 0.3 g of MgO nanoparticles per mmol of reactants is sufficient to push the reaction forward. Higher amounts of MgO nanoparticles (0.4 g) did not improve the result to a great extent (Table 1, entries 4-7).

In order to investigate the effects of other reaction media in this reaction, we carried out the described condensation in MeOH, $H_2O$ and solvent-free (neat) systems (Table 1, entries 1-3).

**Table 1**. Synthesis of tropolone **4a** from the reaction of formaldehyde, cyclohexyl isocyanide and tropolone under various conditions.

| Entry | Catalyst) [a] or solvent | Temp ($^{o}$C) | Time (h) | Yield (%)[b] |
|---|---|---|---|---|
| **1** | MeOH | 60 | 72 | 35 |
| **2** | $H_2O$ | 90 | 72 | 27 |
| **3** | Neat | 90 | 72 | 25 |
| **4** | MeOH MgO powder(Merck) (1g) | 60 | 48 | 61 |
| **5** | MeOH / MgO NP (0.1 g) | 60 | 24 | 70 |
| **6** | MeOH / MgO NP (0.3 g) | 60 | 24 | 80 |
| **7** | MeOH / MgO NP (0.4 g) | 60 | 24 | 80 |

[a])Amount of MgO catalyst per mmol of reactants. [b])Yields of isolated **4a**.

.

## Conclusion

We believe that the reported method offers a mild, simple, and efficient route for the preparation of tropolone derivatives **4** from aldehydes **1**, cyclohexyl isocyanide **2** and tropolone **3** in the presence of MgO Nanoparticles. Its ease of work-up, high yields and fairly mild reaction conditions make it a useful addition to modern synthetic methodologies.

## Acknowledgments

This work was supported by the Peyam Noor University.

## References

[1] D. Astruc, F. Lu, and J. R. Aranzaes, *Angew. Chem. Int. Ed*, **2005**, *44*, 7852-7872.

[2] A. Massoudi, I. Amini, A. Ramazani, F. Zeinali Nasrabadi *and Y. ahmadi*, *Bull. Korean. Soc*, **2012**, *33*, 39-42.

[3] A. Massoudi, I. Amini, A. Ramazani and F. Zeinali Nasrabadi, *Turk. J. Chem*, **2012**, *36*, 537-544.

[4] A. Massoudi, I. Amini, A. Ramazani and F. Zeinali Nasrabadi, *Turk. J. Chem*, **2012**, *36*, 779-787.

## Graphical Abstract

Synthesis of tropolone derivatives in the presence of MgO Nanoparticles

Issa Amini,*

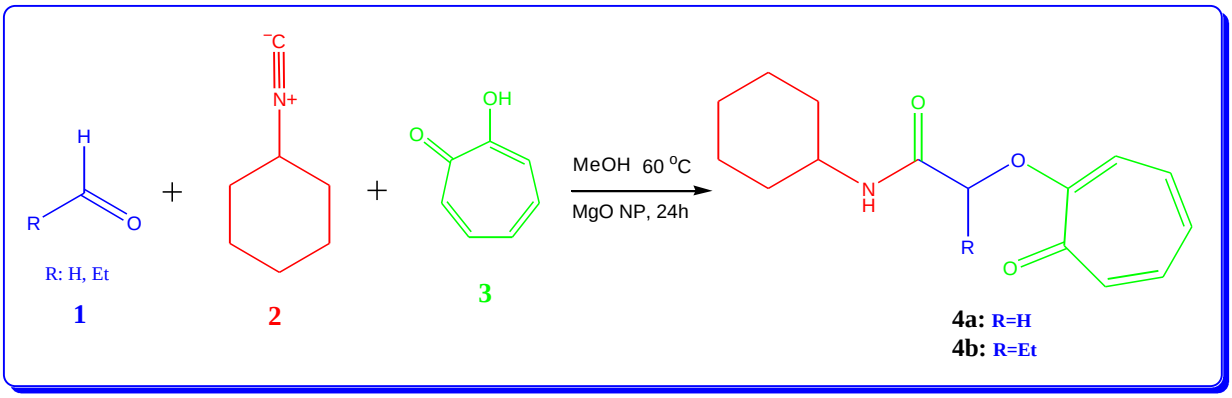

# $SiO_2$ Nanoparticles catalyzed Synthesis of alkyl 2-dinaphtho[2,1-*d*:1,2-*f*][1,3]-dioxepin-2-ylacetate from stabilized phosphorus ylides

**Issa Amini**[a]*

[a] *Department of Chemistry, Payame Noor University, P.O. BOX 19395-4697 Tehran, Iran*

*Corresponding author Tel.: +98 (24) 35233556; Fax number: +98 (24) 35226932

*E-mail: issa_amini@ymail.com

**Abstract**

Protonation of the highly reactive 1:1 intermediates, produced in the reaction of triphenylphosphine and alkyl acetylenecarboxylates, by 1,1-binaphthyl-2,2'-diol leads to vinyltriphenylphosphonium salts, which undergo Michael addition reaction to produce the corresponding stabilized phosphonium ylides. $SiO_2$ Nanoparticles was found to catalyze the conversion of the stabilized phosphonium ylides to alkyl 2-dinaphtho[2,1-*d*:1,2-*f*][1,3]- dioxepin-2-ylacetate under solvent-free conditions using microwave (0.18 KW, 0.5 min) and thermal (70 $^0$C, 30 min) conditions.

**Keywords**: $SiO_2$ Nanoparticles; 1,1-binaphthyl-2,2'-diol; Michael addition; acetylenic esters; vinyltriphenylphosphonium salt.

## Introduction

*β*-Additions of nucleophiles to the vinyl group of vinylic phosphonium salts leading to the formation of new alkylidenephosphoranes have attracted much attention as a convenient and synthetically useful method in organic syntheses. Silica gel as an additive promotes the Wittig reactions of phosphorus ylides with aldehydes, including sterically hindered aldehydes to increase the rate and yields of alkenes[1-3]. In the past we have established a convenient, one-pot method for the preparation of stabilized phosphonium ylides utilizing *in situ* generation of the phosphonium salts[1-3]. In this article, we report on the catalytic role of $SiO_2$ Nanoparticles in the conversion of stabilized phosphonium ylides to alkyl 2-dinaphtho[2,1-*d*:1,2-*f*][1,3]- dioxepin-2-ylacetate under solvent-free conditions using microwave (0.18 KW, 1 min) and thermal (70 $^0$C, 30 min) conditions (**SCHEME 1**).

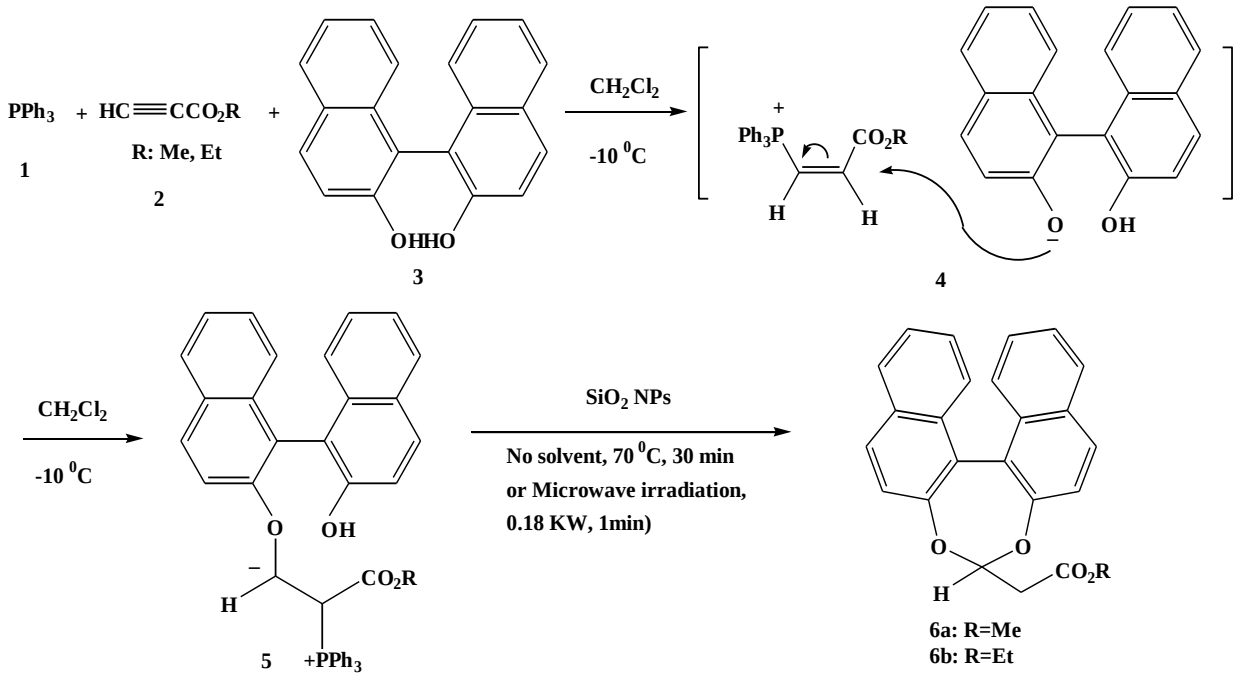


**Scheme 1.** $SiO_2$ Nanoparticles catalyzed of alkyl 2-dinaphtho[2,1-*d*:1,2-*f*][1,3]- dioxepin-2-ylacetate from stabilized phosphorus ylides

## Experimental

*General*

The starting materials and solvents were obtained from Merck (Germany) and Fluka (Switzerland) and were used without further purification. The methods used to follow the reactions were TLC and NMR. TLC and NMR indicated that there were no side products. IR spectra were measured on a Jasco 6300 FTIR spectrometer. $^1$Hand $^{13}$C-NMR spectra ($CDCl_3$) were recorded on a BRUKER DRX-400 AVANCE spectrometer at 400.22 and 100.63 MHz, respectively. Elemental analyses were performed using a Heraeus CHN-O-Rapid analyzer. Mass spectra were recorded on a FINNIGAN-MATT 8430 mass spectrometer operating at an ionization potential of 70 eV.

***General procedure for the synthesis of Ylides 5 and Compounds 6a, b***

To a magnetically stirred solution of triphenylphosphine **1** (1 mmol) and 1,1-

binaphthyl-2,2'-diol **3** (1 mmol) in $CH_2Cl_2$ (4 mL) was added dropwise a mixture of alkyl acetylenecarboxylates **2** (1 mmol) in $CH_2Cl_2$ (3 mL) at –10 $^0$C over 15 min. The mixture was allowed to warm up to room temperature to afford intermediate **5**. $SiO_2$ Nanoparticles (0.2 g) was added and the solvent was evaporated. The mixture was heated at 70 $^0$C for 30 min or irradiated in a microwave oven for at microwave power 0.18 KW for 1 min and then placed over a column of silica gel powder (12 g). The column was washed with ethyl acetate-light petroleum ether (1:10) as the eluent. The solvent was removed under reduced pressure and the products were obtained (**6a, b**).

## Results and discussion

The ylides **5** may result from initial addition of triphenylphosphine **1** on the acetylenic esters **2** and concomitant protonation of the 1:1 adducts by 1,1-binaphthyl-2,2'-diol **3,** followed by Michael addition reaction of the vinyltriphenylphosphonium salts **4** so formed. TLC indicated the formation of the ylides **5.** $SiO_2$ Nanoparticles was found to catalyze conversion of the stabilized phosphonium ylides **5** to alkyl 2-dinaphtho[2,1-*d*:1,2-*f*][1,3]- dioxepin-2-ylacetate **6** under solvent-free conditions using microwave (0.18 KW, 1 min) or thermal conditions (70 $^0$C, 30 min) (**SCHEME 1**). The use of just 0.2 g of silica NPs per 1 mmol of reactants is sufficient to push the reaction forward. Higher amounts of silica NPs (0.3 g) did not improve the result to a great extent (Table 1, entries 2-4). In order to investigate the effects of other reaction media in this reaction, we also carried out the described condensation in solvent-free (neat) systems (Table 1, entries 1). **(SCHEME 1)**.

**Table 1**. Synthesis of alkyl 2-dinaphtho[2,1-*d*:1,2-*f*][1,3]- dioxepin-2-ylacetate **6a,b** under various conditions.

| Entry | Catalyst | MW(kw)/ Time (min) | Temp (°C)/ Time (h) | Yield (%)[a] |
|---|---|---|---|---|
| **1** | Neat | 0.18/3 | 90/48 | 40 |
| **2** | $SiO_2$ powder (Merck) (1g) | 0.18/1 | 70/0.5 | 70 |
| **3** | $SiO_2$ NPs (0.2 g) | 0.18/1 | 70/0.5 | 90 |
| **4** | $SiO_2$ NPs (0.3 g) | 0.18/1 | 70/0.5 | 90 |

[a]Isolated yield.

## Conclusion

In summary, the reported method offers a mild, simple, and efficient route for the preparation of alkyl 2-dinaphtho[2,1-*d*:1,2-*f*][1,3]- dioxepin-2-ylacetate **6a,b** from triphenylphosphine **1**, alkyl acetylenecarboxylates **2** and 1,1-binaphthyl-2,2'-diol **3** in the presence of silica NPs under solvent-free conditions using microwave (0.18 KW, o.5 min) and thermal (70 $^0$C, 30 min) conditions. Its ease of work-up, high yields, and fairly mild reaction conditions make it a useful addition to modern synthetic methodologies.

## Acknowledgments

This work was supported by the Peyam Noor University.

## References

[1] A. Ramazani, I. Amini, and A. Massoudi, *Phosphorus, Sulfur, and Silicon*, **2006**, *181*, 2373-2376.

[2] A. Ramazani, S. Salmanpour, and I. Amini, *Phosphorus, Sulfur, and Silicon*, **2008**, *184*, 699-704.

[3] V.J. Patil, and U. Mavers, *Tetrahedron Lett*, **1996**, *37*, 1281.

## Graphical Abstract

$SiO_2$ Nanoparticles catalyzed Synthesis of alkyl 2-dinaphtho[2,1-*d*:1,2-*f*][1,3]- dioxepin-2-ylacetate from stabilized phosphorus ylides

Issa Amini,*

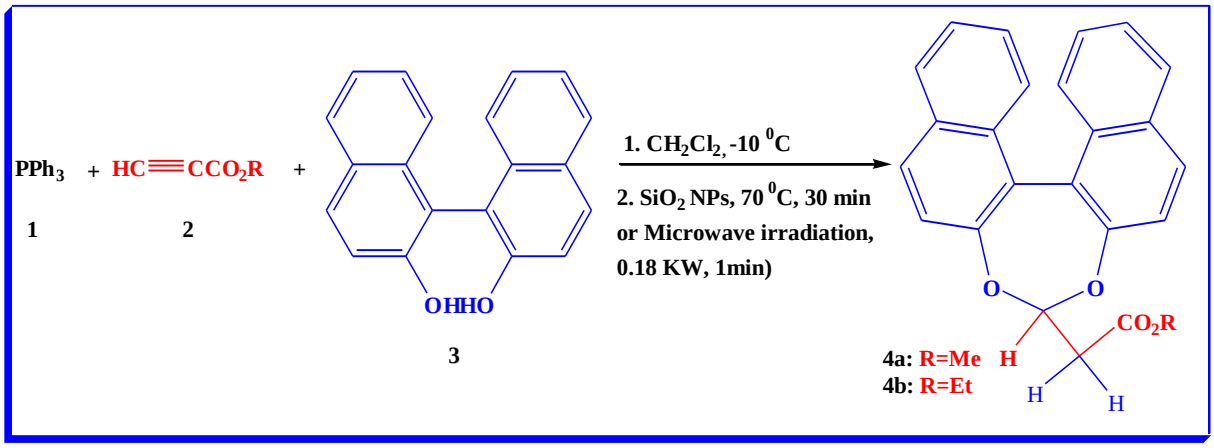

# Synthesis and characterization of new organic-inorganic hybrid $[C_{16}H_{33}N(CH_3)_3]_7H_3[P_2W_{18}Mn_4O_{68}]$-$TiO_2$ composite as an efficient nanocatalyst for oxidative desulphurization of gas oil

**Majid Hadi, Mohammad Ali Rezvani* and Mohammad Mohammadi**

*Department of Chemistry, Faculty of Science, University of Zanjan, 451561319, Zanjan, Iran*

**Corresponding author; E-mail: marezvani@znu.ac.ir Tel: +98 241 5152477 Fax: +98241 5152617.*

## Abstract

The oxidative desulphurization of gas oil and model fuel has been studied using $[C_{16}H_{33}N(CH_3)_3]_7H_3[P_2W_{18}Mn_4O_{68}]$-$TiO_2$ as a new nanocatalyst. The nanocatalyst was synthesized by an unusual reaction with titanium tetraisopropoxide at 100 ºC *via* sol–gel method under oil-bath condition. The materials characterized by $^{31}P$ NMR, XRD, FTIR and UV–vis techniques. The prepared composite was shown to be able to scavenge hydrogen sulphide and mercaptans in high yields. The addition of hydrogen peroxide/acetic acid enhanced the conversion. This system provides an efficient, convenient and practical method for scavenging sulphur compounds.

**Keywords**: heteropolyacid, desulphurization, anatase, nanocatalyst.

## Introduction

The catalytic function of heteropolyacids (HPAs) has attracted much attention, because of their ability to uncommon acceptance of electron without deformation of structure and reversible reduction. HPAs have several advantages such environmentally benign, reusability, non-corrosive and fewer disposal problems as catalysts which make them economically and environmentally attractive. Heteropolyacids, especially sandwich-type, have received great attention among the acid catalysts, because of their high acid strength and selectivity properties [1-4]. Deep desulphurization of transportation fuels has become an important research subject due to the increasingly stringent regulations and fuel specifications in many countries for environmental protection purpose [5-7]. Conventional hydrodesulphurization (HDS) process is difficult to remove alkyl substituted dibenzothiophenes, which are refractive to HDS due to steric hindrance. In order to produce ultralow sulfur diesel fuel with HDS process, high temperature, high pressure, larger reactor volume, and more active catalysts are required [6]. Therefore, alternative desulphurization techniques have been investigated widely. Among them, oxidative desulphurization (ODS) is considered to be one of the promising new methods for super deep desulphurization of fuel oil [6-8]. Peracids produced *in situ* from organic acids catalysts and $H_2O_2$ are reported to be very effective for rapid oxidation of sulfur compounds in fuel oils under mild conditions. Homogeneous catalysts cannot be separated from the reaction media and subsequently, cannot be reused. Immobiliztion of the homogeneous catalysts onto a solid support may be a strategy to overcome this problem. Recently, supported heteropolyacids have been synthesized and applied as effective catalyst in organic reactions [11]. Titanium dioxide is a wide-band-gap semiconductor material that has received intense scrutiny for a broad range of applications, thanks to its intriguing physical-chemical properties and cheap, abundant, and reasonably nontoxic nature. $TiO_2$, also a widely used catalyst support as well as a catalyst is known to enhance the catalytic activity in many cases because of the strong interaction between the active phase and the support [12]. In this article, we describe the synthesis and crystal structure of a new manganese-containing heteropoly compound, where two lacunary $PW_9O_{34}$- units sandwich the four manganeses. In continuation of our group research on the synthesis and application of polyoxometalates (POMs), we designed anatase $TiO_2$ crushed nano leaf coupled by sandwich type polyoxometalate at 100 ºC *via* sol–gel method under oil-bath condition [11-18]. The chemical characterization of this compound was accomplished by means of elemental analysis, FTIR, XRD, TEM and $^{31}P$ NMR spectroscopy. The catalytic performance of the catalyst tested on oxidation desulphurization of the model sulfur compounds such as benzothiophene (BT), dibenzothiophene (DBT), 4-methyldibenzothiophene (4-MDBT), and 4,6-dimethyldibenzothiophene (4,6-MDBT), and gas oil using acetic acid/hydrogen peroxide as oxidizing agent. POM-$TiO_2$ nanocomposite has presented much higher catalytic activity than that of the unsupported polyoxometalates. The catalyst easily separated and reused at the end of reaction without a significant loss of its catalytic activity, which suggests that the catalyst is stable under different conditions.

## 2. Experimental

### 2.1. Materials

All reagents and solvents used in this work are available commercially and were used as received, unless otherwise indicated. Model compounds and chemicals, including BT, DBT, 4-MDBT and 4, 6-MDBT, solvent (n-heptane) for experiments and analysis and hydrogen peroxide (30 vol%) were obtained from Aldrich Chemical Company. The compound of A-β-$Na_8HPW_9O_{34}.24H_2O$ (abbreviated as A-PW9) and other catalysts were prepared as previously described [10,11]. Titanium (IV) tetraisopropoxide and glacial acetic acid were obtained from Merck chemical company. Gas oil (density 0.8361 g/mL at 15ºC, Total sulfur content 0.98 Wt %) was supplied from the terminal of North Iranian Oil Company (Table 1). Tetra butyl ammonium (TBA) and cetyl tri methyl ammonium bromide (CTAB) are chosen as the countercation for organic phase reactions.

### 2.2. Preparation of $(Bu_4N)_7H_3[P_2W_{18}Mn_4O_{68}]$

To a stirred solution of $Mn(NO_3)_2.H_2O$ (0.207 g) in 8 mL $H_2O$ (pH adjusted to 6 by acetic acid), 1.0 g of A-$PW_9$ was added. The solution was put into reactor vessel carefully. It is placed under microwave irradiation at 1000 W for 5 min. This work keeps on for 6 times. The solution cooled to room temperature. Potassium chloride (1.2 g) was added to the solution and the mixture was stirred for 15 min and filtered. This solid was recrystallized from 20 mL of hot water and dried under vacuum. Then, to a stirred solution of 2.0 g of potassium salt of $[P_2W_{18}Mn_4(H_2O)_2O_{68}]^{10-}$ in 55 ml of warm distilled water was added a solution of 1.0 g of tetrabutyl ammonium bromide ($Bu_4N$) in 5.0 ml of $H_2O$. The mixture was stirred at 60 °C for 3 hours and then the precipitation was separated out by filtration. White precipitate filtered off, recrystallized with acetonitrile and ether, and air dried [10].

**Table 1.** Properties of actual gas oil

| Entry | Properties of gas oil | Method | Results |
|---|---|---|---|
| 1 | Specific gravity @ 60/60 °F | ASTM D1298 | 0.8365 |
| 2 | Density @ 15 °C | ASTM D1298 | 0.8361 |
| 3 | API GR. @ 60/60 °F | Calculated | 37.66 |
| 4 | Flash point (°F) | ASTM D93 | 142 |
| 5 | Water content vol. % | ASTM D4006 | 0.025 |
| 6 | Total sulfur content % Wt | ASTM D4294 | 0.98 |
| 7 | Cloud point (°C) | ASTM D2500 | -4 |
| 8 | Color test | ASTM D156 | 1.5 |
| 9 | Viscosity KIN @ 50 °C. CST. | ASTM D445 | 2.8 |
| 10 | Pour point (°C) | ASTM D97 | -9 |
| 11 | Mercaptans ppm | ASTM D3227 | 286 |
| 12 | Distillation (°C) | ASTM D86 | |
| 13 | Initial Boiling Point (I.B. P.) (°C) | ASTM D86 | 157.8 |
| 14 | 10 % Distillation (°C) | ASTM D86 | 194.6 |
| 15 | 20 % Distillation (°C) | ASTM D86 | 213.4 |
| 16 | 50 % Distillation (°C) | ASTM D86 | 268.6 |
| 17 | 90 % Distillation (°C) | ASTM D86 | 353.9 |
| 18 | Final boiling point (F.B.P) (°C) | ASTM D86 | 384.9 |
| 19 | Residue vol. % | ASTM D86 | 1.5 |
| 20 | Loss vol. % | ASTM D86 | 1 |
| 21 | Recovery vol. % | ASTM D86 | 97.5 |

Abbreviation: API GR.; API gravity (API – American Petroleum Institute); API = 141.5/Specific gravity – 131.5. Viscosity KIN; Kinematic viscosity.

### 2.3. Preparation of nanocatalyst $(Bu_4N)_7H_3[P_2W_{18}Mn_4O_{68}]$-$TiO_2$

Titanium tetraisopropoxide was added into glacial acetic acid with stirring and a solution of $(Bu_4N)_7H_3[P_2W_{18}Mn_4O_{68}]$ in water was drop wised in it. The mixture was stirred to dissolve any solid. Then, the sol was heated to 100 ºC under oil bath condition until a homogenous$(Bu_4N)_7H_3[P_2W_{18}Mn_4O_{68}]$-$TiO_2$ hydrogel was formed. Finally, the gel was filtered, washed with deionized water-acetone and dried in oven at 50 ºC overnight [10].

### 2.4. Preparation of $[C_{16}H_{33}N(CH_3)_3]_7H_3[P_2W_{18}Mn_4O_{68}]$

To a stirred solution of (0.207 g, 0.7 mmol) Mn $(NO_3)_2.H_2O$ in 8 ml $H_2O$ (pH adjusted to 6 by acetic acid), 1.0 g (0.35 mmol) of A-$PW_9$ was added. The solution was refluxed for 1 h and then cooled to room temperature. Then an aqueous solution of cetyltrimethyl ammonium bromide (CTAB) 8.20 g in water (20 ml) was added drop-wise, with contineous stirring at 85 °C to the mixture. The solid formed was filtered off, recrystallized with acetonitrile and ether, and air dried. The resultant $[C_{16}H_{33}N(CH_3)_3]_7H_3[P_2W_{18}Mn_4O_{68}]$. 20 $H_2O$ solid is designated as CTA-MnPOM.

### 2.5. Preparation of $[C_{16}H_{33}N(CH_3)_3]_7H_3[P_2W_{18}Mn_4O_{68}]$-$TiO_2$

Titanium tetraisopropoxide was added into glacial acetic acid with stirring and a solution of CTA-MnPOM in water was drop wised in it. The mixture was stirred to dissolve any solid. Then, the sol was heated to 100 ºC under oil bath condition until a homogenous CTAB-MnPOM-$TiO_2$ hydrogel was formed. Finally, the gel was filtered, washed with deionized water-acetone and dried in oven at 50 º C overnight.

### 2.6. Oxidative desulfurization of model fuel by acetic acid/$H_2O_2$ system

The water bath was first heated up and stabilized to the desired reaction temperature (25-80 °C). The model sulfur compound (BT, DBT, 4-MDBT or 4, 6-DMDBT was dissolved in *n*-heptane to make a stock solution with a sulfur content of 500 ppm. Then, 5 mL of the model sulfur compound, mixed with 2 mL acetic acid/$H_2O_2$ (acetic acid/hydrogen peroxide molar ratio of 1 into the flask). The flask was immersed in the heating bath and stirred at 500 rpm for 2 hours. The biphasic mixture was separated by decantation. It reached the reaction temperature in about 15 min. After withdrawing the first sample, 0.1 gr of nano catalyst (CTAB-MnPOM-$TiO_2$) was added to the flask to initiate the reaction.

**Table 2.** Oxidation desulphurization of gas oil by CTA-MnPOM-$TiO_2$ nanocatalyst

| Entry | Properties of gas oil | Before ODS | After ODS[a] | After ODS[b] |
|---|---|---|---|---|
| 1 | Total sulfur content Wt. % | 0.98 | 0.052 | 0.058 |
| 2 | Density @ 15 °C | 0.8361 | 0.8359 | 0.8363 |
| 3 | Mercaptans ppm | 286 | 8 | 10 |
| 4 | Flash point (°F) | 142 | 142 | 142 |
| 5 | Water content vol. % | 0.025 | 0.025 | 0.025 |
| 6 | Pour point (°C) | -9 | -9 | -9 |
| 7 | Distillation (IBP °C) | 157.8 | 155.9 | 156.5 |
| 8 | Distillation (FBP °C) | 384.9 | 383.6 | 384.0 |

[a] Condition for desulphurization: 5 ml of gas oil (2300 ppm S), 0.1 g nanocatalyst, 2 ml oxidant, 5 ml of extraction solvent, time = 2 hours, and temperature = 80 °C.
[b] Reuse of the catalyst in the desulphurization of gas oil.

### 2.7. Oxidation desulphurization of gas oil by acetic acid/$H_2O_2$ system

The water bath was first heated up and stabilized to the desired reaction temperature (25-80 °C). 5 mL of the gas oil was mixed with 2 mL acetic acid/$H_2O_2$ (acetic acid/hydrogen peroxide molar ratio of 1 into the flask). The flask was immersed in the heating bath and stirred at 500 rpm for 2 hours. The biphasic mixture was separated by decantation. It reached the reaction temperature in about 15 min. After withdrawing the first sample, 0.1 gr of nano catalyst (CTAB-MnPOM-$TiO_2$) was added to the flask to initiate the reaction. Sulfur concentration of sample was determined using a TANAKA SIENTIFIC RX-360 SH X-ray fluorescence spectrometer (ASTM D-4294 method and D-3227). Results are showed in Table 2.

### 2.8.Characterization methods

X-ray diffraction (XRD) patterns were recorded by a D8 Bruker Advanced, X-ray diffractometer using Cu Kα radiation (α=1.54 A). The patterns were collected in the range 20–70° 2θ and continuous scan mode. The electronic spectra of the synthesized catalysts were taken on a RAYLEIGH (UV-1800) ultraviolet–visible (UV–vis) scanning spectrometer. Infrared spectra were recorded as KBr disks on a Buck 500 scientific spectrometer.

### 2.9. Recycling of the catalyst

All at the end of the oxidation desulphurization of the model sulphur compounds and gas oil, the catalyst was filtered, washed with dichloromethane. In order to know whether the catalyst would succumb to poisoning and lose its catalytic activity during the reaction, we investigated the reusability of the catalyst. For this purpose we carried out the desulphurization reaction of gas oil and model compounds in the presence of fresh and recovered catalyst (Table 3). Even after three runs for the reaction, the catalytic activity of (CTAB-MnPOM-$TiO_2$) was almost the same as that freshly used catalyst. The results are summarized in Table 3.

**Table 3**. Reuse of the catalyst for oxidation of BT

| Entry | Isolated yield (%) |
|---|---|
| 1 | 97 |
| 2 | 96 |
| 3 | 95 |

## 3.RESULT AND DISCUSSION

### 3.1. Characterization of synthesized catalysts

XRD patterns of $TiO_2$, CTAB-MnPOM and CTAB-MnPOM-$TiO_2$ are shown in Figure 1. XRD patterns (a) and (b) in Figure 1 are corresponded to pristine $TiO_2$ and CTA-MnPOM, respectively. The XRD pattern corresponding to pure $TiO_2$ was found to match with that of fully anatase phase. No peaks from any else impurities or rutile phase were observed, which indicates the high purity of the obtained powders. The sharp diffraction peaks manifest that the obtained $TiO_2$ have high crystallinity. When CTA-MnPOM is bound to the $TiO_2$ surface, (CTAB-MnPOM-$TiO_2$), all of signals corresponding to CTA-MnPOM is disappeared and the final pattern matched to fully anatase phase of $TiO_2$ (JCPDS No. 21-1272), which is most likely due to CTA-MnPOM forming only a thin coating on the $TiO_2$ surface and thus the majority of the observed signals are due to the crystal phases of anatase $TiO_2$. Using the Scherrer equation, the crystallite diameter of CTAB-MnPOM-$TiO_2$ is about 9 nm.

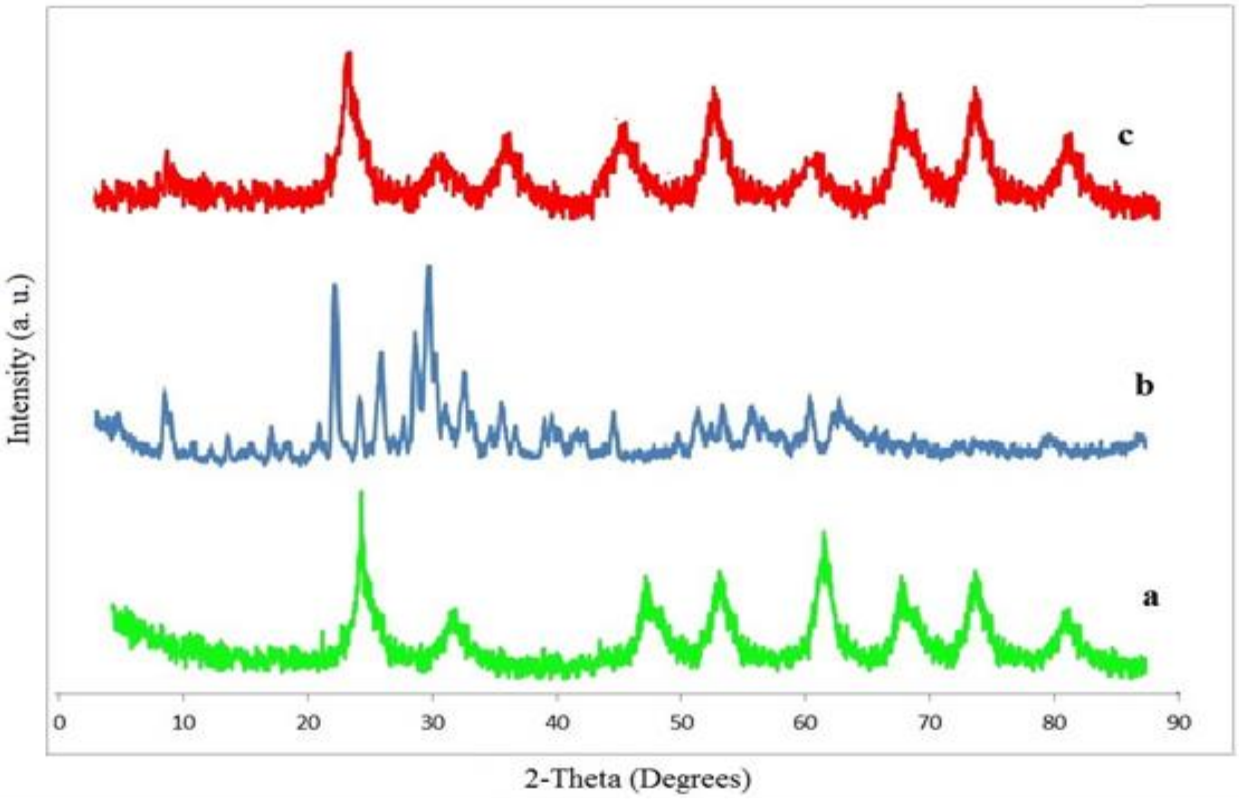


**Figure 1**. XRD pattern of (a) $TiO_2$ (b) CTA-MnPOM and (c) CTAB-MnPOM-$TiO_2$.

Also, UV-visible spectroscopy of obtained powders was studied. UV-vis spectra of TiO2, CTA-MnPOM and CTAB-MnPOM-TiO2 nanocomposite are shown in Figure 3. In ultraviolet light regions, which are shorter than 350 nm, pure nano $TiO_2$ whose band gap energy equivalent to around 330nm (3.70 eV) shows the highest absorbance due to charge-transfer from the valence band (mainly formed by 2p orbitals of the oxide anions) to the conduction band (mainly formed by 3d $t_2g$ orbitals of the $Ti^{4+}$ cations).[15] The CTAB-MnPOM-$TiO_2$ nanocomposite shows a red shift compared with the parent anatase, and a blue shift compared with CTA-MnPOM. In addition, some hyper fine structure in the range from

310 to 350 nm observed in CTA-MnPOM spectrum. The inset of the figure shows the UV-vis spectrum of the CTAB-MnPOM-$TiO_2$ indicating there are two peaks around 220 and 290 nm. The above UV–vis results indicate that introduction of CTA-MnPOM into $TiO_2$ framework has an influence on coordination environment of $TiO_2$ crystalline [10].

The $^{31}P$ NMR spectrum of the CTA-MnPOM exhibits a single line at -11.53 ppm upfield from the external standard, i.e. 85% $H_3PO_4$ (Fig. 4), indicating that the dimeric complex contains only one type of phosphorus. Also, this pattern indicates that a single product with high purity is obtained under the reaction conditions. This band is assigned to the central $PO_4$ unit of the polyoxotungstate.[17] The $^{31}P$ NMR spectrum of CTA-MnPOM also indicates small broadening near the baseline.

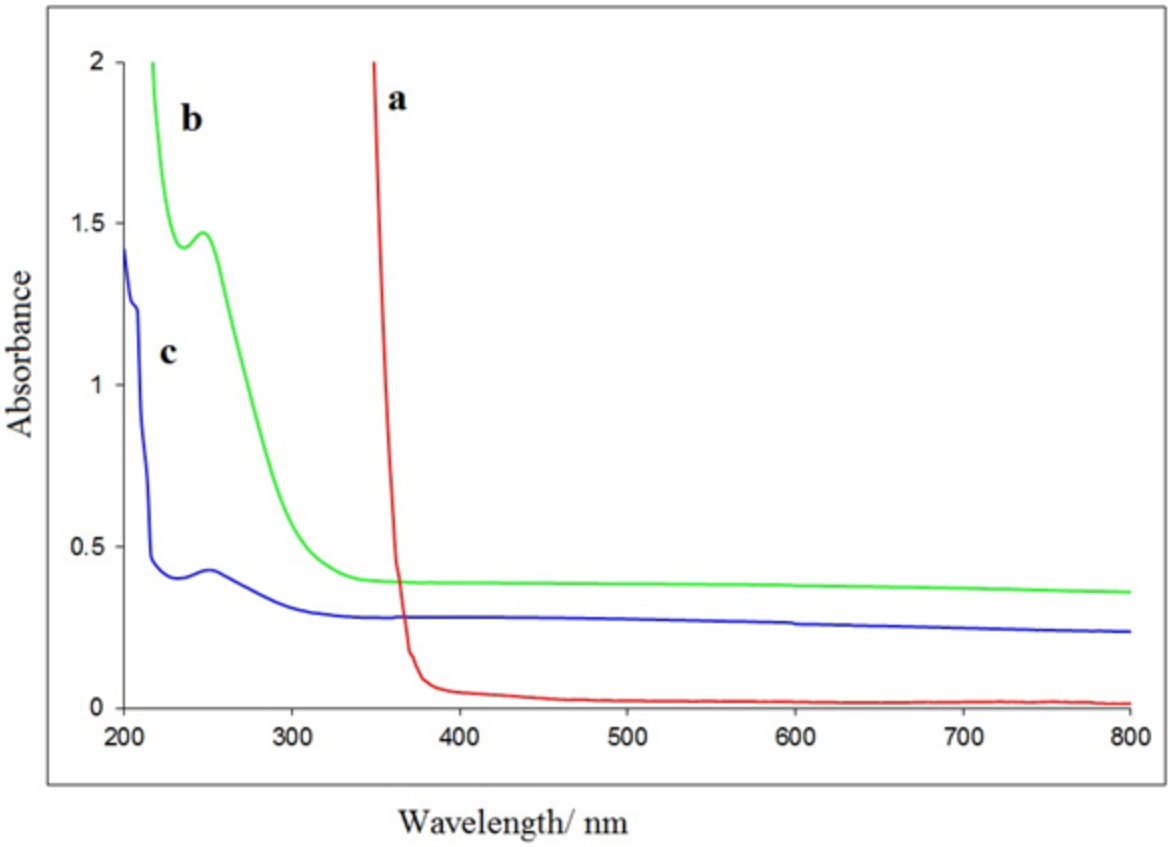


**Figure 2**. UV-vis spectra of obtained catalysts.

The $^{31}P$ NMR spectrum of the CTA-MnPOM exhibits a single line at -11.53 ppm upfield from the external standard, i.e. 85% $H_3PO_4$ (Fig. 4), indicating that the dimeric complex contains only one type of phosphorus. Also, this pattern indicates that a single product with high purity is obtained under the reaction conditions. This band is assigned to the central $PO_4$ unit of the polyoxotungstate.[17] The $^{31}P$ NMR spectrum of CTA-MnPOM also indicates small broadening near the baseline.

IR spectrum of the prepared catalyst in the range 700–1100 cm-1 showed absorption bands at 1052, 984, 879 and 763 cm -1, corresponding to the four typical skeletal vibrations of the Keggin polyoxoanions, which indicated that CTA-MnPOM has been supported on $TiO_2$ (Fig. 5). These peaks could be attributed to ν(P–O), ν(W–O), ν(W–Ob–W) and ν(W–Oc–W) (Ob: corner-sharing oxygen, Oc: edge-sharing oxygen), respectively [17].

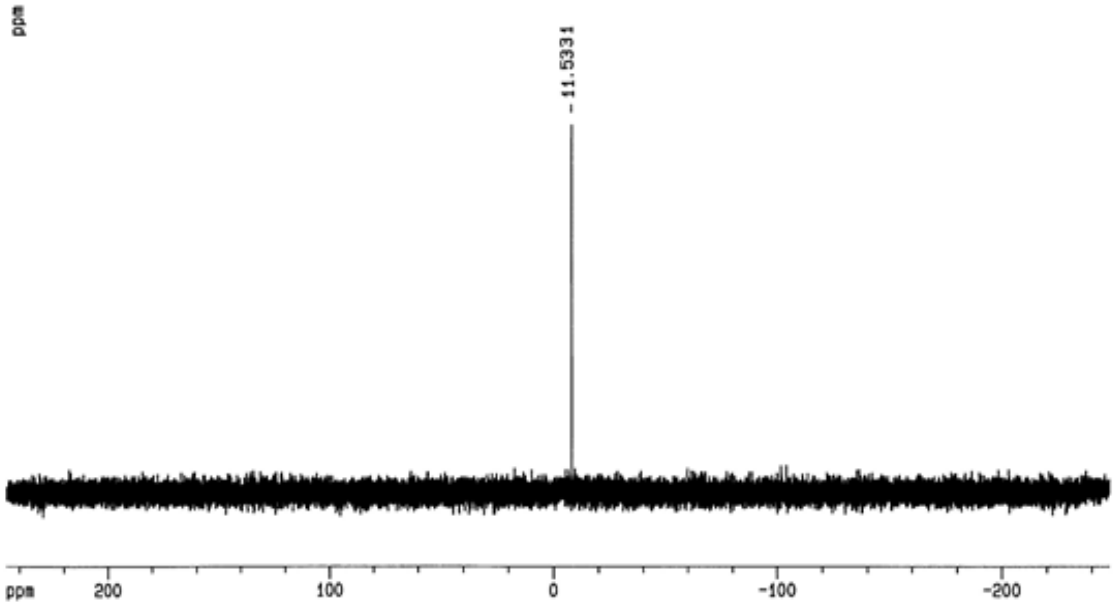


**Figure 3**. 31P NMR spectrum of the CTAB-MnPOM-$TiO_2$

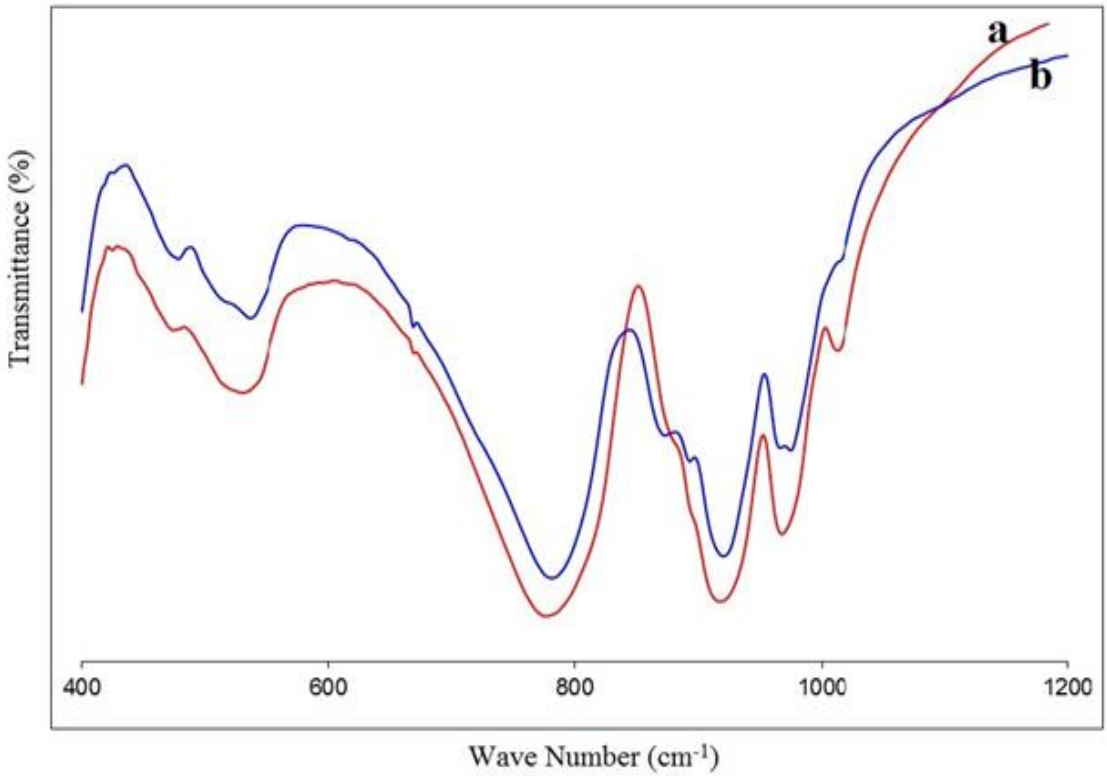


**Figure 4**. IR spectrum of (a) CTA-MnPOM and (b) CTAB-MnPOM-$TiO_2$

### 3.2. Catalytic results

#### 3.2.1. General desulfurization process

At first, should be noted that during the oxidation desulfurization (ODS) process, the $H_2O_2$ was used in the presence of acetic acid as oxidants because acetic acid as an organic acid, react with $H_2O_2$ to in situ produce peracid, which can efficiency convert organic sulfur to sulfones without forming a substantial amount of residual product, Scheme 1. Gas oil is mixed with acetic acid/$H_2O_2$ and nanocatalyst (CTAB-MnPOM-$TiO_2$) then the oxidation reaction takes place at 80 °C
under atmospheric pressure. This is followed by a liquid extraction (acetonitrile) to obtain gas oil with low sulfur.

### Conclusion

CTAB-MnPOM-$TiO_2$ nanocomposite has been synthesized at low temperature *via* sol–gel method under oil-bath condition. Fixing of CTA-MnPOM on $TiO_2$ decreases the particle size of crushed nano leaf of anatase phase. The CTAB-MnPOM-$TiO_2$ nanocomposite was very active catalyst systems for the model compound oxidation, while unmodified CTA-MnPOM much less active. The oxidation reaction is selective as only sulfone was detected. For this polyoxometalates/$H_2O_2$/acetic acid system, oxidation reactivity decreased according to the following order: DBT>4,6-DMDBT>4MDBT>BT. The percent conversion increases when the amount of oxidant and catalyst is increased. The addition of acetic acid enhanced the conversion.


**Scheme 1**. Mechanism oxidation desulfurization of simulated gas oil

**References**

[1] M. A. Rezvani, A. F. Shojaei, F. M. Zonoz, J. Serb. Chem. Soc. 79 (2014) 1099.
[2] N. M. Mahmoodi, M. A. Rezvani, M. Oveisi, A. Valipour, M. A. Asli, Mater. Res. Bull., 84 (2016) 422.
[3] M. A. Rezvani, M. Alinia Asli, M. Oveisi, R. babaei, K. Qasemi, S. Khandan, RSC Adv. 6 (2016) 53069.
[4] M. A. Rezvani, M. Alinia Asli, S. Khandan, H. Mousavi, Z. Shokri Aghbolagh, Chem. Eng. J. 312 (2017) 243.
[5] X. Sheng, Y. Zhoua, Y. Zhang, M. Xue, Y. Duan, Chem. Eng. J. 179 (2012) 295.
[6] Z. A. Abdalla, B. Li, Chem. Eng. J., 200 (2012) 113.
[7] W. Qi, L. Wu, Polym. Int., 58 (2009) 1217.
[8] M. A. Rezvani, A. F. Shojaie, M. H. Loghmani, Fuel Process. Technol. 118 (2014) 1.
[9] M. A. Rezvani, F. Mohammadi Zonoz, Ind. Eng. Chem. 22 (2015) 83.
[10] M. A. Rezvani, M. Shaterian, F. Akbarzadeh, S. Khandan, Chem. Eng. J. 333 (2018) 537.
[11] M. A. Rezvani, Z. S. Aghbolagh, H. H. Monfared, S. Khandan, J. Ind. Eng. Chem. 52 (2017) 42.
[12] D.Wang, E.W. Qian, H. Amano, K. Okata, A. Ishihara, T. Kabe, Appl. Catal. A 253(2003) 91.
[13] T.V. Rao, B. Sain, S. Kafola, Y.K. Sharma, S.M. Nanoti, M.O. Garg, Energy Fuels 21(2007) 3420.
[14] S.Z. Liu, B.H.Wang, B.C. Cui, L.L. Sun, Fuel 87 (2008) 422.
[15] P. De Filippis, M. Scarsella, Ind. Eng. Chem. Res. 47 (2008) 973.
[16] A. Fallah Shojaei, M.A. Rezvani, M. Heravi, J. Serb. Chem. Soc. 76 (2011) 955.
[17] A. Fallah Shojaei, M.A. Rezvani, M. Heravi, J. Serb. Chem. Soc. 76 (2011) 1513-1522.
[18] M. A. Rezvani, M. Shaterian, and F. Akbarzadeh, S. Khandan, Chem. Eng. J. 333 (2018)537–544.

# $FeCl_3$ catalyzed one-pot solvent-free synthesis of 1-phenyl-1, 2-dihydro-3H-naphtho [1, 2-e] [1, 3] oxazin-3-one

**Saeid Taghavi Fardood**[a,*], **Ali Ramazani** [a], **Morteza Ayubi**[a], **Shahin Abdpour**[a]

[a]*Department of Chemistry, University of Zanjan, P O Box 45195-313, Zanjan, Iran*

[b]*Research Institute of Modern Biological Techniques (RIMBT), P O Box 45195-313, University of Zanjan, Zanjan, Iran*

**E-mail: saeidt64@gmail.com*

*Corresponding author Tel.: +98 (912) 2423919

*E-mail: aliramazani@gmail.com

**Abstract**

Over the past few decades, chemistry has become a major science scholar for chemists. On the other hand, chemical reactions have long been caused the environmental problems. To overcome these problems and facilitate chemical reactions, alternative energy sources such as UV or microwave are used. Iron is one of the most abundant metals on Earth and $FeCl_3$ (Iron (III) chloride) is an efficient catalyst in modern organic synthesis, environmentally friendly and atom-economical organic transformations that can increase the yield and speed of the reaction. In this study, for the first time, a FeCl3 catalyst, instead of a ferrites catalyst, will be used to synthesize 1-phenyl-1, 2-dihydro-3H-naphtho [1, 2-e] [1, 3] oxazin-3-one in the microwave. According to the results of synthesis and analysis of the composition of the catalyst can be used for other multicomponent reactions.

**Keywords**: *Iron (III) chloride, catalyst, Solven free.*

## Introduction

Microwave (MW) irradiation as a novel, efficient and harmless method for reagent activation in the synthesis of organic compounds, and in special heterocyclic compounds, has been applied to achieve and milder reaction conditions [1].

Multicomponent reactions (MCRs) constitute a particularly attractive synthetic strategy due to the fact that the products are made in a single step while diversity can be promoted only by varying the reacting components [1-4]. Furthermore, multicomponent reactions (MCRs) by virtue of their convergence, productivity, ease of implementation and generally higher yields of products have attracted considerable attention in the area of combinatorial chemistry [5,6]. The first MCR was described by Strecker in 1850 for the synthesis of amino acids [7]. Yet, in the past decade, there have occurred tremendous developments in three- and four-component reactions and great attempts are continually being prepared to develop new MCRs [8,9].

Recently, various chemical transformation processes by catalysts under mild condition has more attention in organic synthesis. One of those acidic catalysts is $FeCl_3$ which has been explored as powerful catalyst for various organic transformations such as synthesis of Tetrasubstituted Imidazoles [10], α-amino phosphonates [11] , quinoline derivatives [7], 3,4-dihyropyrimidinone derivatives [9] and synthesis of dihydropyrimidinones [8]. The reported route is an efficient, convenient and novel method for the condensation of aldehyde with β-naphthol and urea in the presence of $FeCl_3$ to afford condensed 1,3-oxazin-3-one derivatives in good yields.

In this study, for the first time, a $FeCl_3$ catalyst, instead of a ferrites catalyst, will be used to synthesize 1-phenyl-1, 2-dihydro-3H-naphtho [1, 2-e] [1, 3] oxazin-3-one in the microwave.

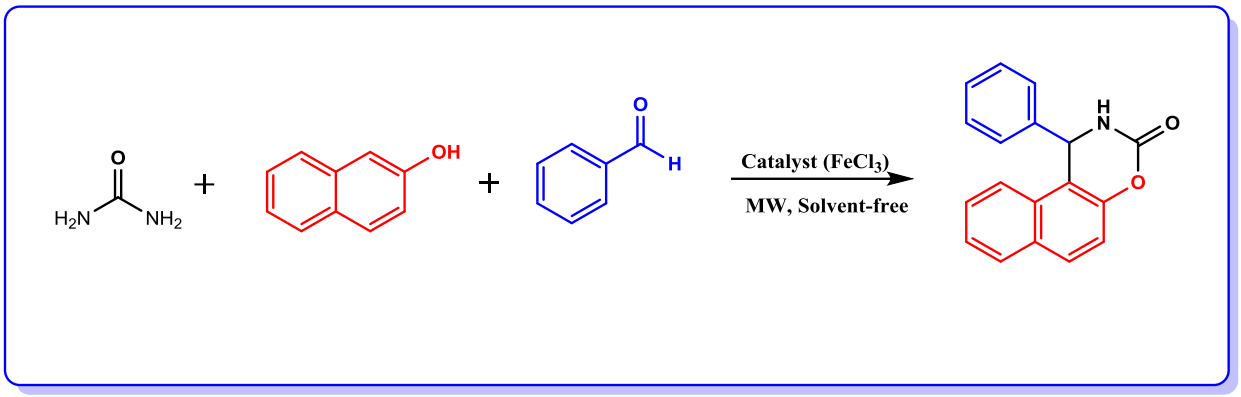


***Scheme 1**. Synthesis of 1-phenyl-1, 2-dihydro-3H-naphtho [1, 2-e] [1, 3] oxazin-3-one*

## Experimental

### *General*

Experiment should start as a continuation to introduction on the same page. All important materials used along with their source shall be mentioned. The main methods used shall be briefly described, with references. New methods or substantially modified methods may be described in sufficient detail. The statistical method and the level of significance chosen shall be clearly stated.

***General procedure for the synthesis of quinoxaline and 2,3-dihydropyrazine in ethanol***

A mixture of Urea 1 (1 mmol), 2-Naphthol 2 (1 mmol), Benzaldehyde 3 (1 mmol), and $FeCl_3$ anhydrous (0.02g) under solvent-free condition was placed for 15 min with the power of 500 W in microwave. The progress of the reaction was checked by TLC (petroleum ether: EtOAc, 10:2). After completion, the resulting product was heated in ethanol., then add 7 ml of cold water and apply a white deposition using a filter and dry.

## Results and discussion

Today, the use of catalysts in multi-component reactions is significant. Although the use of $Fecl_3$ as a catalytic role has been proven, the catalytic role of $FeCl_3$ in multiparticulate reactions in free-solvent reactions was investigated in this study and was confirmed according to the NMR and IR assays. In this work, a wide range of aldehydes, urea and β-naphtol were subjected to undergo three-component condensation in the presence of $FeCl_3$ under solvent free conditions (Table 1). Then, various aromatic aldehydes carrying electron-donating and electron-withdrawing groups on the aromatic ring in the ortho, meta, and para positions and heterocyclic aldehydes were evaluated. Yields of the all reactions were good to excellent.

## Conclusion

According to the results of synthesis and analysis of the composition of the catalyst can be used for other multicomponent reactions. It can also be said that the method used in this synthesis is green chemistry, optimal and inexpensive.

**Table 1** $FeCl_3$ catalyzed the synthesis of 1-phenyl-1, 2-dihydro-3H-naphtho [1, 2-e] [1, 3] oxazin-3-one

| Entry | Ar | Product | Time (min) | Yield (%)[a] | M.P. (°C) | M.P. (°C) [Ref.] |
|---|---|---|---|---|---|---|
| 1 | Ph | **4a** | 15 | 90 | 223-225 | 220-222 [12] |
| 2 | 3-Cl–$C_6H_4$ | **4b** | 15 | 88 | 193-195 | 194-196 [13] |
| 3 | 4-Cl–$C_6H_4$ | **4c** | 15 | 90 | 208-210 | 210-212 [13] |
| 4 | 2-$NO_2$–$C_6H_4$ | **4d** | 15 | 84 | 197-199 | 195-197 [12] |
| 5 | 4-$NO_2$–$C_6H_4$ | **4e** | 15 | 89 | 189-192 | 188-190 [12]n |
| 6 | 4-Me-$C_6H_4$ | **4f** | 15 | 92 | 165-167 | 164-166 [14] |

Reaction conditions: aldehyde **1a–f** (1mmol), β-naphtol **2** (1mmol), urea **3** (1 mmol) and 20 mg of catalyst under microwave irradiation (500 W) in solvent-free conditions.

[a] Isolated yields.

## References


[1] S. Taghavi Fardood, A. Ramazani, P. Azimzadeh Asiabi, Y. Bigdeli Fard and B. Ebadzadeha, *Asian J. Green Chem.*, **2017**, *1*, 34-40.

[2] S. Taghavi Fardood, A. Ramazani and S. Moradi, *J. Sol-Gel Sci. Technol.*, **2017**, *82*, 432-439.

[3] M. Bahrami, A. Ramazani, Y. Hanifehpour, N. Fattahi, S. Taghavi Fardood, P.A. Asiabi and S.W. Joo, *Phosphorus, Sulfur Silicon Relat. Elem.*, **2016**, *191*, 1368-1374.

[4] A. Ramazani, Y. Ahmadi, N. Fattahi, H. Ahankar, M. Pakzad, H. Aghahosseini, A. Rezaei, S. Taghavi Fardood and S.W. Joo, *Phosphorus, Sulfur Silicon Relat. Elem.*, **2016**, *191*, 1057-1062.

[5] S. Maddila, S. Rana, R. Pagadala, S. Kankala, S. Maddila and S.B. Jonnalagadda, *Catal. Commun.*, **2015**, *61*, 26-30.

[6] A. Domling, W. Wang and K. Wang, *Chem. Rev.*, **2012**, *112*, 3083-3135.

[7] J. Wang, X. Fan, X. Zhang and L. Han, *Can. J. Chem.*, **2004**, *82*, 1192-1196.

[8] V. Choudhary, V. Tillu, V. Narkhede, H. Borate and R. Wakharkar, *Catal. Commun.*, **2003**, *4*, 449-453.

[9] H.A. Oskooie, M.M. Heravi, N. Karimi and M.H. Monjezy, *Synth. Commun.*, **2011**, *41*, 826-831.

[10] M.M. Heravi, F. Derikvand and M. Haghighi, *Monatshefte für Chemie/Chemical Monthly*, **2008**, *139*, 31-33.

[11] J. Wu, W. Sun, W.Z. Wang and H.G. Xia, *Chin. J. Chem* . **2006**, *24*, 1054-1057.

[12] R. Hunnur, R. Kamble, A. Dorababu, B.S. Kumar and C. Bathula, *Arabian J. Chem.*, **2017**, *10*, S1760-S1764.

[13] M. Dabiri, A.S. Delbari and A. Bazgir, *Synlett*, **2007**, *2007*, 0821-0823.

[14] G.D. Rao, M. Kaushik and A. Halve, *Tetrahedron Lett.*, **2012**, *53*, 2741-2744.

## Graphical Abstract

$FeCl_3$ catalyzed one-pot solvent-free synthesis of 1-phenyl-1, 2-dihydro-3H-naphtho [1, 2-e] [1, 3] oxazin-3-one

Saeid Taghavi Fardood*, Ali Ramazani, Morteza Ayubi, Shahin Abdpour

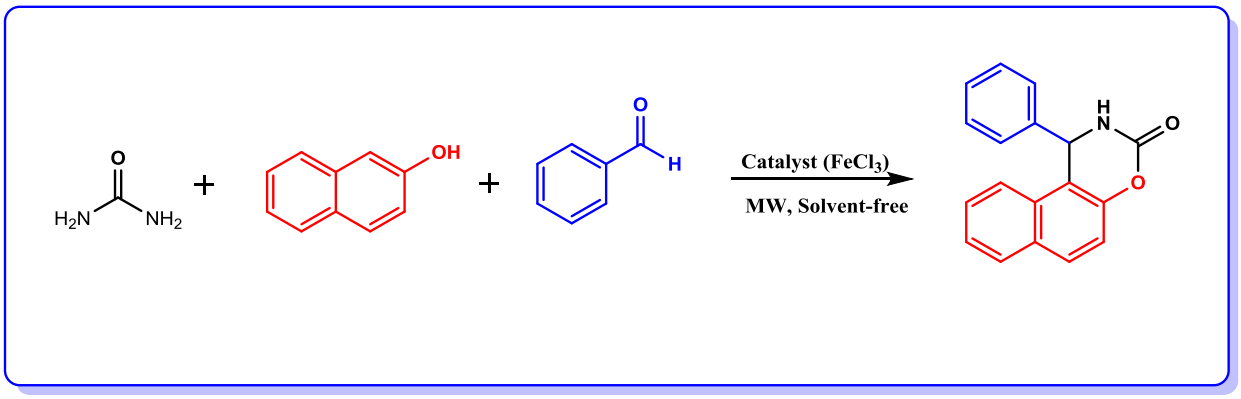

# Phosphotungstic acid immobilized on magnesium oxide ($PW_{12}O_{40}$@MgO) as an efficient nanocatalyst for oxidative desulfurization of gasoline

**Nahid Jafari, Mohammad Ali Rezvani***

*Department of Chemistry, Faculty of Science, University of Zanjan, Zanjan, Iran*

*Corresponding author Tel.: +98 (241) 5152477; Fax number: +98 (241) 5152617

*E-mail: marezvani@znu.ac.ir

## Abstract

In this manuscript, Keggin-type phosphotungstic acid ($H_3PW_{12}O_{40}$) was immobilized on magnesium oxide (MgO) to prepare $PW_{12}O_{40}$@MgO nanocomposite. The synthesized materials were characterized by FT-IR, UV-vis, XRD and SEM analysis techniques. The catalytic activity of the prepared composite was evaluated in the oxidative desulfurization (ODS) process of gasoline fuel. The ODS process was successfully developed on the basis of the catalytic oxidation of organosulfur compounds using $CH_3COOH/H_2O_2$ as an oxidizing agent. The removal of the sulfur content and mercaptan compounds of gasoline reached 98 and 97% at 35 °C after 1 h, respectively. The various experiments were taken into consideration to investigate the effects of catalyst amount and reaction temperature on sulfur removal efficiency. The nanocatalyst was found to give remarkable reusability for five times. This system is suggested as an effective strategy with a great potential in the preparation of clean gasoline fuel.

**Keywords**: Polyoxometalate, Magnesium oxide, Nanocatalyst, Oxidative desulfurization, Gasoline

## Introduction

Nowadays catalysts play an important role in desulfurization process, a promising process for producing clean fuels for transport. The various types of sulfur compounds in petroleum products emit SOx gases during the combustion. These atmosphere pollutants are causing damage to the environment in some different ways [1-3]. Ultra-low-sulfur-fuel (ULSF) is a fuel with substantially lowered sulfur content. Many countries have established regulations to restrict the sulfur content in petroleum products to zero level [4,5]. To obtain low sulfur fuels, hydrodesulfurization (HDS) as the traditional process is often used in petroleum industry [6]. This technology has been proven to be a robust method in reducing thiol, sulfur mercaptan, sulfide, disulfide, thiophene and its derivatives [7]. Nevertheless, it is unsuccessful to obtain ultra-low-sulfur (<10 ppm S) because of the poor effect on refractory sulfide species such as thiophene, benzothiophene, dibenzothiophene, and their sterically hindered derivatives [8,9]. In addition, high temperature and high pressure conditions with large quantities of hydrogen are required during the HDS technology, which results in high costs and energy consumption [10-13]. Alternatively, the ODS provides selective removal of those refractory sulfur compounds at proper temperatures and pressure. The organic sulfur-containing molecules are converted to their corresponding sulfoxide or sulfone in the presence of an oxidant and appropriate catalyst [14].

Heteropolyoxometalates (HPOMs) have received much attention as oxidative catalysts due to an unique combination of properties, including thermal and oxidative stability, tuneable acidity, redox potentials, solubility, etc [15,16]. One of the important aspects of HPOM clusters is their low specific surface areas (1–10 $m^2/g$) and high solubility in a variety of aqueous solution [17]. To overcome this undesirable obstacle, design and synthesis of heterogeneous catalysts have been explored in recent years by immobilization of HPOMs on appropriate supports. Metal oxide nanoparticles has attracted more attention in catalysis due to its great physical and chemical properties, environmentally friendly nature, and low cost [18-20].

In this work, the $PW_{12}O_{40}$@MgO nanocatalyst was synthesized and its catalytic activity evaluated for developing the ODS of gasoline. Also, the mixture of $CH_3COOH/H_2O_2$ was utilized as the oxidizing agent. After the oxidation step, the polar extraction solvent acetonitrile ($CH_3CN$) was used for extraction of oxidized sulfur compounds. The nanocatalyst was separated and reused at the end of the reaction for five times.

## Experimental

*Materials and methods*

All chemicals and solvents were commercially available and used as received. Hydrogen peroxide ($H_2O_2$, 30 vol.%), acetic acid ($CH_3COOH$, 99.7%), acetonitrile ($CH_3CN$), and phosphotungstic acid ($H_3PW_{12}O_{40}$) were purchased from Sigma–Aldrich without purification. Magnesium nitrate hexahydrate ($(Mg(NO_3)_2.6H_2O$) and citric acid monohydrate ($C_6H_8O_7.H_2O$) were obtained from Merck. Typical gasoline was used with the following specification: density of 0.7994 g/mL at 15 °C and total sulfur content of 0.4996 wt%.

The Fourier Transform Infrared spectroscopy (FTIR) studies were performed on a Thermo-Nicolet-iS 10 spectrometer, using KBr pellets technique with a measuring range of 400–4000 $cm^{-1}$. Ultraviolet–visible (UV–vis) spectra were recorded with a double beam termo-heylos spectrometer. Powder X-ray diffraction (XRD) patterns were carried out on a D8 Bruker Advance powder X-ray

diffractometer with a Cu Kα (λ = 0.154 nm) radiation source and the data were collected from 5 to 80° (2θ). The surface morphologies were examined by scanning electron microscopy (SEM) by LEO 1455 VP with an accelerating voltage of 26 kV. The total sulfur and mercaptan content of gasoline before and after treatment were determined using X-ray fluorescence with a TANAKA X-ray fluorescence spectrometer RX-360 SH.

***Synthesise of MgO nanoparticles***

In a typical synthesis, 0.20 g of citric acid was dissolved in 10 mL of water. The solution of citric acid was added drop-wise to a solution of magnesium nitrate 1.02 g in 30 mL of water at 70 °C. The mixture was magnetically stirred for 45 minutes to form milky-white gel. The gel was dried in the oven at 95 °C for 2.5 hours and calcined in the furnace at 900 °C for 2 hours, respectively.

***Synthesise of $PW_{12}O_{40}$@MgO nanocatalyst***

The 0.02 g of prepared MgO was dispersed in 10 mL of water in ultrasonic bath for half an hour to be completely uniform. The solution of 0.02 g $PW_{12}O_{40}$ in 1 mL of ethanol was added to the MgO solution and sonicated for 1 hour. The suspension is precipitated by centrifugation at 2000 rpm for 10 minutes. The obtained solid was then dried in oven at 95 °C for 2 hours and designed as a $PW_{12}O_{40}$@MgO nanocatalyst.

***Catalytic oxidative desulfurization of gasoline***

In a typical run, a water bath was heated to 35 °C. Then, 50 mL of gasoline in a closed round-bottom flask equipped with a magnetic stirrer was heated to the reaction temperature. Afterward, 3 mL of $CH_3COOH/H_2O_2$ (in a volume ratio of 1/2) and 0.10 g of $PW_{12}O_{40}$@MgO were added slowly to the reaction vessel. The ODS process was continued under stirring conditions (500 rpm) for 1 h. After the passage of this time, the above mixture was cooled to room temperature and 10 mL of $CH_3CN$ was added to extract the oxidized products. The formed immiscible phases (oil and water phases) were separated by a separation funnel and simple decantation technique. The total sulfur concentration after oxidation treatment was determined using the XRF spectrometer according to ASTM D-4294 and ASTM D-3227. The sulfur removal efficiency was calculated using Eq. (1), in which $S_i$ and $S_f$ are the initial and final concentration of sulfur compounds, respectively.

$$\text{Removal efficiency (\%)} = \left[\frac{S_i - S_f}{S_i}\right] \times 100 \quad (1)$$

## Results and discussion

*Characterization of materials*

***FT-IR analysis***

In the FT-IR spectrum of MgO, two peaks at 3450 and 1620 $cm^{-1}$ are assigned to the O–H stretching and bending vibrations, respectively (Fig. 1a). The peak at 450 $cm^{-1}$ is assigned to the stretching vibration of Mg–O band which in the third diagram shifts to 480 $cm^{-1}$. The bands between 2950 and 2850 $cm^{-1}$ are assigned to the stretching vibration of C–H of alkyl chain [21]. The FT-IR spectrum of $PW_{12}O_{40}$ is characterized by four prominent bands at 1080 ν(P–O), 995 ν(W–O terminal), 896 ν(W–$O_c$–W octahedral corner-sharing), and 790 $cm^{-1}$ ν(W–$O_b$–W, octahedral edge-sharing), which are characteristic of the Keggin units (Fig. 1b) [22]. In addition, the bands that are present around 3440 and 1620 $cm^{-1}$ are ascribed to the vibration bands of hydroxyl groups. The product spectrum verified that the POM was successfully immobilized on MgO support (Fig. 1c).

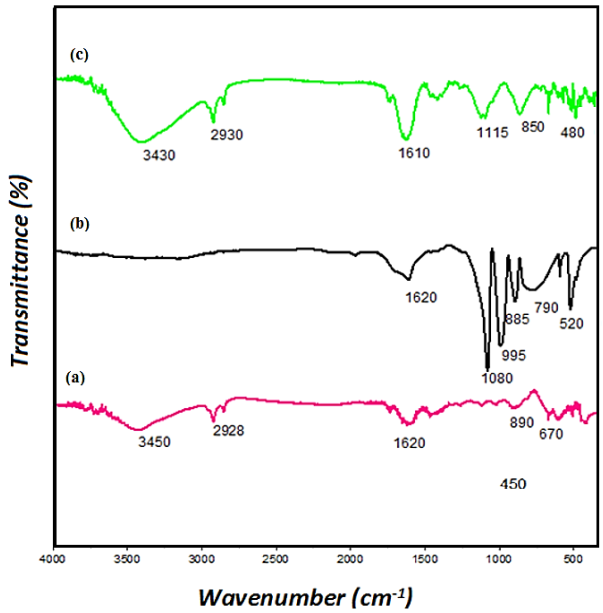


**Fig. 1.** FT-IR spectra of (a) MgO, (b) $PW_{12}O_{40}$, and (c) $PW_{12}O_{40}$@MgO nanocatalyst.

***UV–vis analysis***

The following figure shows UV–vis spectra of various materials, which was an appropriate method to evaluate the charge transfer behavior of synthesized materials. MgO nanoparticles exhibited strong absorption between 200 and 230 nm, which were corresponded to the excitation of four-fold coordinated $O^{2-}$ anions in the edges and corners. In the other spectra, two major adsorption bands could be observed in the region of 200–400 nm, which were attributed to the electronic properties of the center-metal in the structure of Keggin anion and ligand to metal charge transfer [23].

***XRD analysis***

The powder nanostructures were investigated by X-ray diffraction (XRD) measurement. Based on the obtained results, the main reflections of the MgO nanoparticles are observed at 2θ values of 38, 43.2, 62.8, 75.3, and 79.17. These patterns are attributed to (111), (200), (220), (311), and (222) crystal planes, respectively [21].

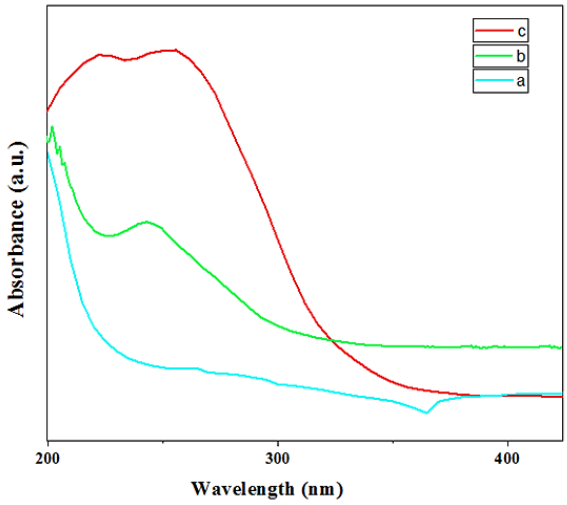


**Fig. 2.** UV-vis spectra of (a) MgO, (b) $PW_{12}O_{40}$, and (c) $PW_{12}O_{40}$@MgO nanocatalyst.

In Fig. 3b, the peak positions at 2θ values of 24.8, 29.2, 34.6, 45.1, 48.5, 53.2, 58.1, and 75.5° are corresponded to the $PW_{12}O_{40}$ polyoxometalate [22]. In addition, the most peaks of $PW_{12}O_{40}$@MgO attributed to the crystal of MgO. This indicates the highly $PW_{12}O_{40}$ dispersed of $PW_{12}O_{40}$ on the surfaces of MgO support, which is in good agreement with the results of SEM.

***SEM analysis***

As depicted in Fig.4, the surface morphology of the synthesized materials was compared. As can be seen, the bulk MgO nanoparticles have an regular spherical shape (Fig.4a). Also, the agglomerated paricles of $PW_{12}O_{40}$ is shown in Fig. 4b. The SEM image of $PW_{12}O_{40}$@MgO nanocatalyst is revealed the fine aggregation of nanoparticles in a spherical and homogeneous shape (Fig. 4(c)).

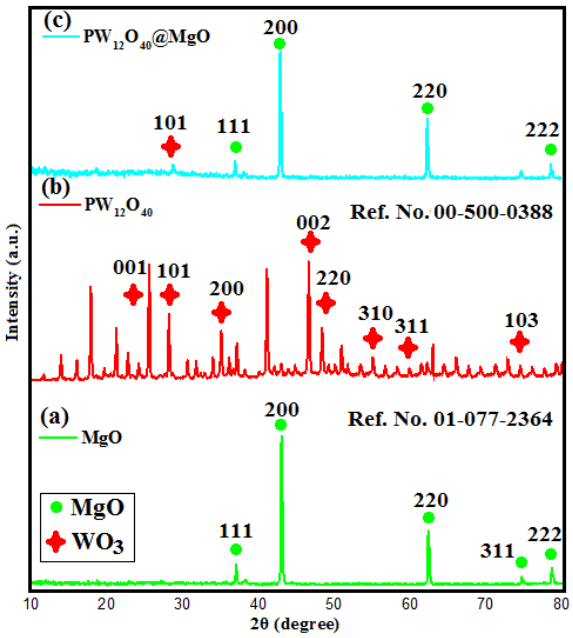


**Fig. 3.** XRD patterns of (a) MgO, (b) $PW_{12}O_{40}$, and (c) $PW_{12}O_{40}$@MgO nanocatalyst.

*Catalytic oxidative desulfurization results*

For investigation the sulfur oxidation of capability of $PW_{12}O_{40}$@MgO nanocatalyst, ODS process was performed on typical gasoline under the mentioned condition in the experimental section. The attained results after oxidation treatment were reported in Table 1. According to the Entry 1, the total sulfur content of gasoline was reduced from 0.4996 % to 0.0267 wt.%. Also, the mercaptan compounds were much lowered from 98 to 4 ppm. It should be pointed out that the other specifications of gasoline were remained unchanged after ODS.

*Reusability of $PW_{12}O_{40}$@MgO nanocatalyst*

After following each catalytic run, the $PW_{12}O_{40}$@MgO nanocatalyst was regenerated by simple filtration, and washed with dichloromethane and dried at 90 °C for 1 h. Then, the recovered catalyst was used again for the subsequent process under similar oxidation conditions. The results of ODS process using reused nanocatalyst after the five regeneration cycles are reported in Table2. It was found that the removal efficiency of total sulfur content was dropped from 98 to 94%, which can be attributed to cover the active sites on the surface of nanocatalyst with sulfur-containing substrates or products.

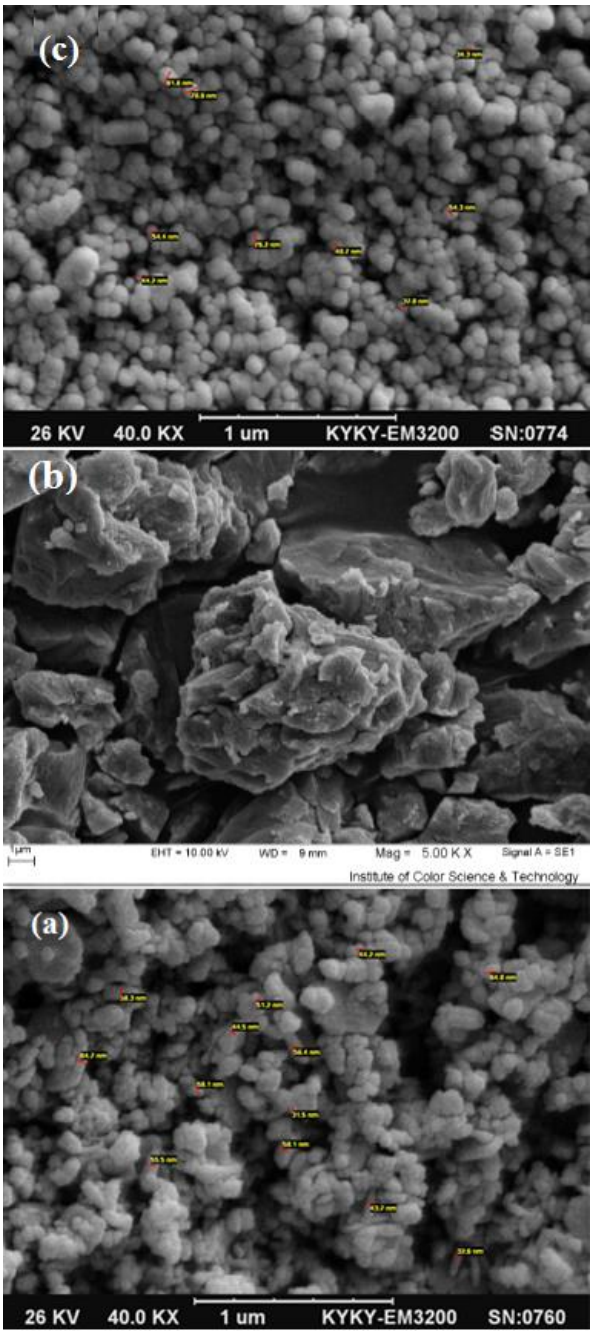


**Fig. 4.** SEM image of (a) MgO, (b) $PW_{12}O_{40}$, and (c) $PW_{12}O_{40}$@MgO nanocatalyst.

**Table 1.** The ODS test results of gasoline by $PW_{12}O_{40}$@MgO nanocatalyst.

| Entry | Properties of gasoline | | Unit | Method | Before ODS | After ODS [a] |
|---|---|---|---|---|---|---|
| 1 | Total Sulfur by X-Ray | | wt.% | ASTM D 4294 | 0.4996 | 0.0267 |
| 2 | Mercaptans | | ppm | ASTM D 3227 | 98 | 4 |
| 3 | Density by hydrometer @ 15 °C | | g/mL | ASTM D 1298 | 0.7981 | 0.7980 |
| 4 | Salt | | ptb | ASTM D 3230 | 14 | 13 |
| 5 | Water Content by distillation | | vol. % | ASTM D 4006 | Nil. | Nil. |
| 6 | Distillation | Initial boiling point (IBP) | °C | ASTM D 86 | 48.6 | 48.1 |
| | | Final boiling point (FBP) | | | 209.1 | 208.8 |
| | | 10 | vol.% | | 69.9 | 69.2 |
| | | 50 | | | 118.3 | 117.5 |
| | | 90 | | | 187.8 | 187.2 |
| | | 95 | | | 208.5 | 208.1 |

[a] Conditions of ODS: 50 mL of gasoline, 0.10 g of nanocatalyst, 3 mL of oxidant, 10 mL of extraction solvent, time = 1 h, and temperature = 35 °C.

## Conclusion

In summary, the new composite was designed by supporting of $PW_{12}O_{40}$ on MgO and employed as a nanocatalyst for ODS of gasoline. The characterization techniques were confirmed that the successful preparation of the nanocatalyst. The oxidation experimental results were demonstrated that the sulfur compounds could be efficiently removed from gasoline at 35 °C after 1 h. The reusability results of the $PW_{12}O_{40}$@MgO nanocatalyst indicated that the composite could be reused up to five cycles conveniently. This work was introduced as a facile method for the efficient ODS treatment to promote the quality of gasoline fuel.

## References

[1] C. Song, X. Ma, *Appl. Catal. B Environ.*, **2003**, *41*, 207-238.

[2] M. Zhang, W. Zhu, S. Xun, H. Li, Q. Gu, Z. Zhao, Q. Wang, *Chem. Eng. J.*, **2013**, *220*, 328-336.

[3] V. Perraud, J. R. Horne, A. S. Martinez, J. Kalinowski, S. Meinardi, M. L. Dawson, L. M. Wingen, D. Dabdub, D. R. Blake, R. B. Gerber, B. J. Finlayson-Pitts, *Proc. Natl. Acad. Sci. U. S. A.*, **2015**, *112*, 13514-13519.

[4] M. A. Rezvani, M. Shaterian, F. Akbarzadeh, S. Khandan, *Chem. Eng. J.*, **2018**, *333*, 537-544.

[5] M. A. Rezvani, S. Khandan, N. Sabahi, *Energy Fuels*, **2017**, *31*, 5472-5481.

[6] H. Li, W. Zhu, Y. Chang, W. Jiang, M. Zhanga, S. Yin, J. Xia, H. Li, *J. Mol. Graph. Model.*, **2015**, *59*, 40-49.

[7] B. Jiang, H. Yang, L. Zhang, R. Zhang, Y. Sun, Y. Huang, *Chem. Eng. J.*, **2016**, *283*, 89-96.

[8] M. Bagheri, M. Y. Masoomi, A. Morsali, *ACS Catal.*, **2017**, *7*, 6949-6956.

[9] G. Miao, D. Huang, X. Ren, X. Li, Z. Li, J. Xiao, *Appl. Catal. B Environ.*, **2016**, *192*, 72-79.

[10] I. Martínez, M. E. S. Mohamed, V. E. Santos, J. L. García, F. García-Ochoa, E. Díaz, *J. biotechnol.*, **2017**, *262*, 47-55.

[11] M. A. Rezvani, Z. Shokri Aghbolagh, H. Hosseini-Monfared, S. Khandan, *J. Ind. Eng. Chem.*, **2017**, *52*, 42-50.

[12] R. Abro, A. A. Abdeltawab, S. S. Al-Deyab, G. Yu, A. B. Qazi, S. Gao, X. Chen, *Rsc Adv.*, **2014**, *4*(67), 35302-35317.

[13] T. A. Saleh, G. I. Danmaliki, *Process Saf. Environ. Prot.*, **2016**, *102*, 9-19.

[14] M. A. Rezvani, M. A. Asli, S. Khandan, H. Mousavi, Z. S. Aghbolagh, *Chem. Eng. J.*, **2017**, *312*, 243-251.

[15] Y. Zhu, M. Zhu, L. Kang, F. Yu, B. Dai, *Ind. Eng. Chem. Res.*, **2015**, *54*, 2040-2047.
[16] H. Mirhoseini, M. Taghdiri, *Fuel*, **2016**, *167*, 60-67.
[17] D. E. Katsoulis, *Chem. Rev.*, **1998**, *98*, 359-388.
[18] Y. Ren, M. Wang, X. Chen, B. Yue, H. He, *Materials*, **2015**, *8*, 1545-1567.
[19] C. G. Morales-Guio, M. T. Mayer, A. Yella, S. D. Tilley, M. Grätzel, X. Hu, *J. Am. Chem. Soc.*, **2015**, *137*, 9927-36 .
[20] M. A. Rezvani, S. Khandan, M. Aghmasheh, *J. Taiwan Inst. Chem. Eng.*, **2017**, *77*, 321-328.
[21] M. Y. Nassar, T. Y. Mohamed, I. S. Ahmed, I. Samir, *J. Mol. Liq.* **2017**, *225*, 730-740.
[22] P. M. Rao, A. Wolfson, S. Kababya, S. Vega, M. V. Landau, J. Catal. 2005, *232*(1), 210-225.
[23] X. M. Yan, P. Mei, J. Lei, Y. Mi, L. Xiong, L. Guo, *J. Mol. Catal. A: Chem.* **2009**, *304*(1-2), 52-57.

## Graphical Abstract

Phosphotungstic acid immobilized on magnesium oxide ($PW_{12}O_{40}$@MgO) as an efficient nanocatalyst for oxidative desulfurization of gasoline

Nahid Jafari, Mohammad Ali Rezvani*

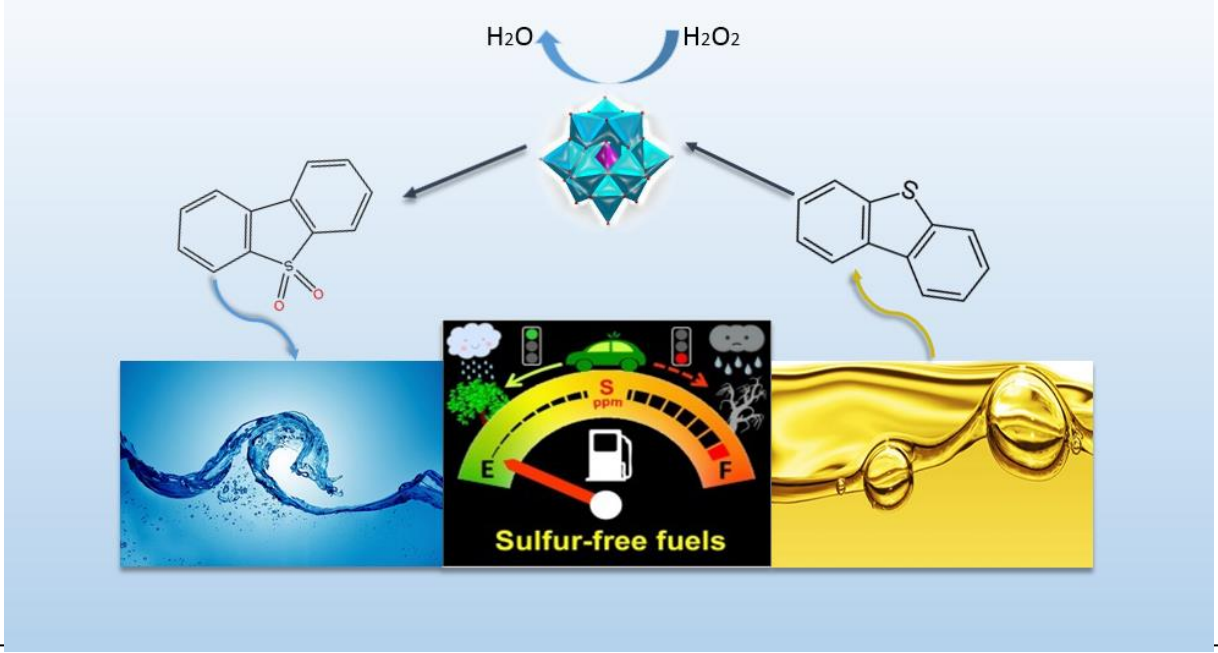

# Green synthesis and characterization of spinel $ZnMn_2O_4$ nanoparticles by tragacanth gel and studies of its photocatalytic activity for degradation of Congo red dye under visible light irradiation

**Saeid Taghavi Fardood[1,*], Farzaneh Moradnia[1], Ali Ramazani[1,2]**

[1]*Department of Chemistry, University of Zanjan, P O Box 45195-313, Zanjan, Iran*

[2]*Research Institute of Modern Biological Techniques (RIMBT), P O Box 45195-313, University of Zanjan, Zanjan, Iran*

**E-mail: saeidt64@gmail.com*

**Abstract**

In this work, $ZnMn_2O_4$ spinel nanoparticles was successfully synthesized by tragacanth gel through the easy and inexpensive novel sol-gel method. This technique has many strong points such as facile, economical, non-toxic and quickness in comparison with other methods. The magnesium manganite nanoparticles characterized by powder X-ray diffraction (XRD), field emission scanning electron microscopy (FESEM), Fourier transforms infrared spectroscopy (FTIR), and percent of dye degradation which was followed by UV–Visible spectroscopy. The XRD pattern confirmed the formation of spinel tetragonal structure of $ZnMn_2O_4$ nanoparticles with crystallite size of 14 nm. The $ZnMn_2O_4$ NPs expressed high photocatalytic activity for degradation of Congo red dye at room temperature in aqueous solution so that 96% of Congo red was degraded in 15 min.

**Keywords**: *spinel nanoparticles, tragacanth gel, Congo red dye, Photocatalytic activity.*

## Introduction

About 15% of the total world manufacture of dyes is lost during the dyeing process and is released in the textile sewerages [1]. The release of those colored wastewaters in the ecosystem is a demonstrative source of non-aesthetic pollution, eutrophication and perturbations in the aquatic life. As international environmental standards are becoming more stringent (ISO 14001, October 1996), technological systems for the removal of organic pollutants, such as dyes have been recently expanded. between them, physical methods, such as biological methods (biodegradation) [2], adsorption [3], and chemical methods (chlorination, ozonation [4]) are the most frequently used. Photocatalysis is considered as one of the important and efficient approaches to dismiss the dyes in wastewater [5-7]. Different methods have been provided for the synthesis of nanoparticles such as chemical, physical and green methods [8,9]. Lately, researchers focus on green chemistry methods to provide metal nanoparticles with favorable size and morphology and the results of this method are significant and important [10-12]. Photocatalysis is considered as one of the important and efficient approaches to dismiss the dyes in wastewater [6,7,13]. In the last decade, preparing the nanocatalyst via photocatalytic capability by using the green synthesis methods has been a idea for researchers. Plant extracts for the biological synthesis of nanoparticles have received more attention, because it is inexpensive, simple, environmentally safe and non-toxic. Further, most of the the plant extracts are fortified by the variety of biomolecules like alkaloids, phenols, terpenoids, flavonoids, etc. [14-18]. In this work, we report the synthesis spinel $ZnMn_2O_4$ NPs via novel biological way and use the tragacanth gel to provide sol-gel. We have studied the photocatalytic activity of $ZnMn_2O_4$ using followed degradation of Congo red as the industrial dye in aqueous solution under visible irradiation. XRD, FTIR and FE-SEM are the techniques that we used for characterization of biosynthesized $ZnMn_2O_4$. The chemical structure of Congo red is shown in Fig.1.

.

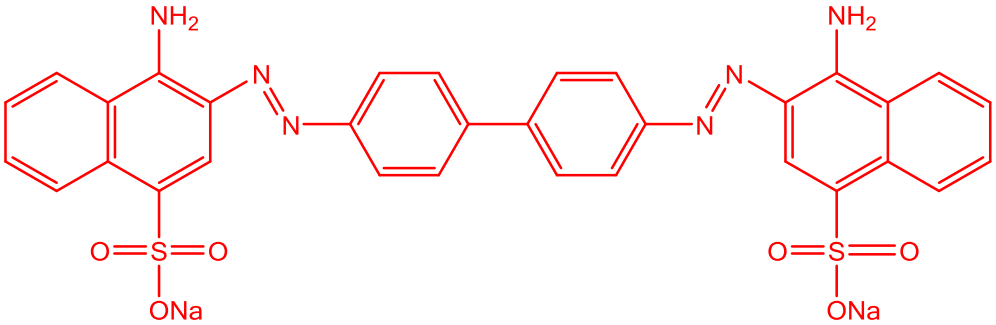


**Figure 1.** *Structure of Congo red*

## Experimental

*General*

The tragacanth gum (TG) was prepared from a native health food store. The $Zn(NO_3)_2.6H_2O$ and $Mn(NO_3)_2.4H_2O$ were purchased from Merck. Congo red was purchased from Merck and had used without further refinement. The structural properties of $ZnMn_2O_4$ NPs were confirmed by X-ray powder diffraction (XRD) technique on X'Pert-PRO advanced diffractometer using Cu (Kα) radiation (wavelength: 1.5406 Å), operated at 40 kV and 40 mA at room temperature in the range of 2θ from 10 to 80. The external structure of this the sample was determined by a Jasco 6300 Fourier transform infrared (FT-IR) spectroscopy. The FT-IR spectrum was collected between the wave number of 400 and 4000 $cm^{-1}$. Measurements were accomplished with KBr technique. UV–Vis absorption spectra were prepared on a Metrohm (Analytical Jena-Specord 205) double-beam instrument. The compound morphology and size of the sample surfaces were studied by scanning electron microscope (Zeiss EVO 18, Germany).

***Synthesis of spinel $ZnMn_2O_4$ NPs***

$Zn(NO_3)_2.6H_2O$ and $Mn(NO_3)_2.4H_2O$ were used as starting materials for the synthesis of $ZnMn_2O_4$ NPs. In the first step, 0.2 g of the tragacanth gum (TG) was blended and dissolved in 40 ml of deionized water and stirred for 80 min at 70 °C. Next step, 2 mmol $Mn(NO_3)_2.4H_2O$ and 1 mmol $Zn(NO_3)_2.6H_2O$ were added to the TG solution. After that, the container contains the gel was moved to a sand bath. The sand bath temperature was stabled at 75 °C and stirring was consecutive for 12 h. The product of this step was the brown color resin. In next step, this resin was calcined in air at 600 °C for 4 h to obtain spinel $ZnMn_2O_4$ NPs.

***Photocatalytic reactor***

Experiments were carried out in a batch mode photoreactor. The irradiation origin was a fluorescent lamp (λ> 400 nm, 90 W, Parmis, Iran), which was put above the batch photoreactor. The reaction was manufactured in conditions: Congo red = 20 mg/L, catalyst = 0.03 g, pH = natural and room temperature.

***Photocatalytic dye degradation***

Congo red was selected for check the photocatalytic dye degradation of $ZnMn_2O_4$ NPs. this experiment was investigated under the visible light. Degradation of Congo red was followed in the presence and absence of visible light in aqueous solution. Hereon, 50 ml solution of dye with 20 mg/L concentration was ready and 0.03 g of NPs sample was dispersed in it. The solutes above nanophotocatalyst were taken out from the reaction environment at regular time cycles. Centrifuge was used for separating the $ZnMn_2O_4$ NPs from solution and the absorbance alteration was followed at a maximum wavelength ($\lambda_{max}$) of dye (500 nm) by UV–Vis spectrophotometer (Analytical Jena-Specord 205). Following equation was used for calculation of degradation percentages.

$$\% \text{ Degradation} = (A_0 - A_t)/A_0 \times 100$$

## Results and discussion

Fourier transform infrared spectrometer (FTIR) spectra were registered in solid phase using the KBr pellet technique in the range of 400–4000 $cm^{-1}$. This technique was exploited to stabilize the formation of metal-metal (M-M) bonds and metal-oxygen (M-O) in the spinel structure of the sample. Figure 2 display FTIR absorption spectra of $ZnMn_2O_4$ NPs calcined at 600 °C for 4 h. The FT-IR spectrum analysis demonstrates two ranges of the absorption bands: In the range of 400–1000 $cm^{-1}$, two absorption bands for the spinel structure of the $ZnMn_2O_4$ $\nu_1$ at 621 $cm^{-1}$ and $\nu_2$ at 507 $cm^{-1}$ were observed. The band, $\nu_1$, suggests the stretching vibrations of the metal (Mn ↔ O) and the $\nu_2$ is attributed to stretching vibrations of the metal (Zn ↔ O) [19]. The bands at 2922 and 1646 $cm^{-1}$ are characteristic for hydroxyl group (O–H). These are the first evidence of $ZnMn_2O_4$ formation.

The phase and structural determination of the spinel $ZnMn_2O_4$ nanoparticles was confirmed by XRD technique. The XRD pattern of the $ZnMn_2O_4$ nanoparticles shows in Figure 3. As shown in Fig. 3, the diffraction peaks at 2θ of 18.31°, 29.45°, 31.27°, 33.02°, 36.44°, 38.96°, 44.81°, 50.90°, 52.12°, 54.66°, 56.85°, 59.08°, 60.88°, 65.36°, 71.17°, 75.15° and 77.57° are corresponded to (101), (112), (200), (103), (211), (004), (220), (204), (105), (312), (303), (321),

(224), (400), (305), (413) and (422) planes of the tetragonal spinel $ZnMn_2O_4$ NPs respectively. All the diffraction peaks were readily indexed to a pure phase tetragonal spinel structure (JCPDS Card no.**77-0470**)

. No diffraction peaks of other impurities were detected. The crystallite size of resulted sample was calculated from the value of full width at half maximum (FWHM) of the (311) diffraction peak applying the Scherer formula and it was found to be 14 nm. The average crystallite size of $ZnMn_2O_4$ nanoparticles was distinguished from the full width at half maximum (FWHM) of the (211) diffraction peak using the Scherrer formula:

$D = 0.9\lambda/\beta \cos \theta$

Hither D is the crystallite size (nm), β is the full width at half maximum of the peak, λ is the X-ray wavelength of Cu Kα=0.154 nm and θ is the Bragg angle [20]. Using the above manner, we gained an average crystallite size of 14 nm for $ZnMn_2O_4$NPs.

Figure 4 shows the FESEM images of green synthesized $ZnMn_2O_4$ NPs that calcined at 600 °C for 4 h. It can be seen from the SEM image, the $ZnMn_2O_4$ NPs have narrow size distributions and fairly uniform spherical shape.

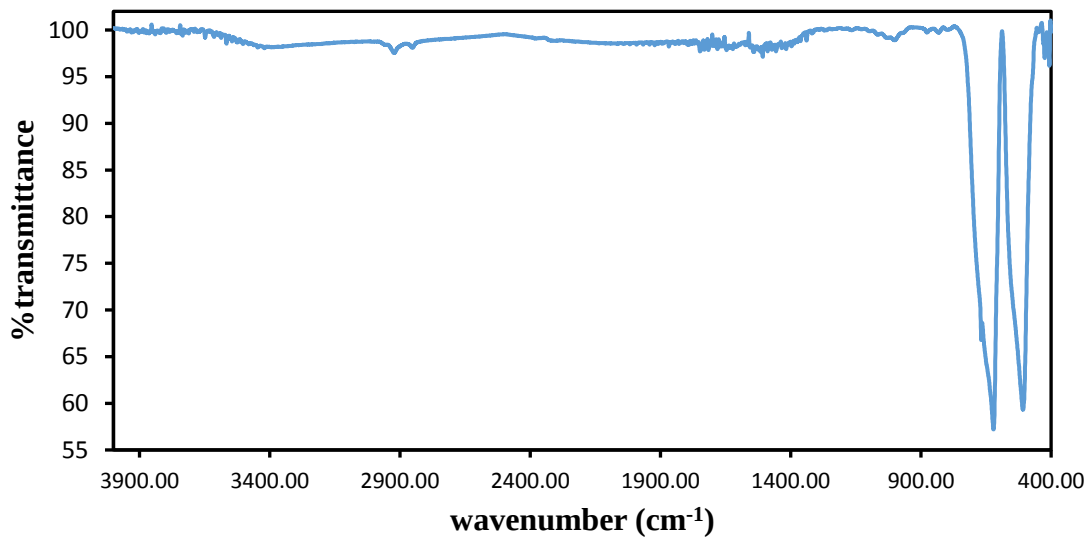


**Fig. 2.** FT-IR spectrum of $ZnMn_2O_4$ NPs.

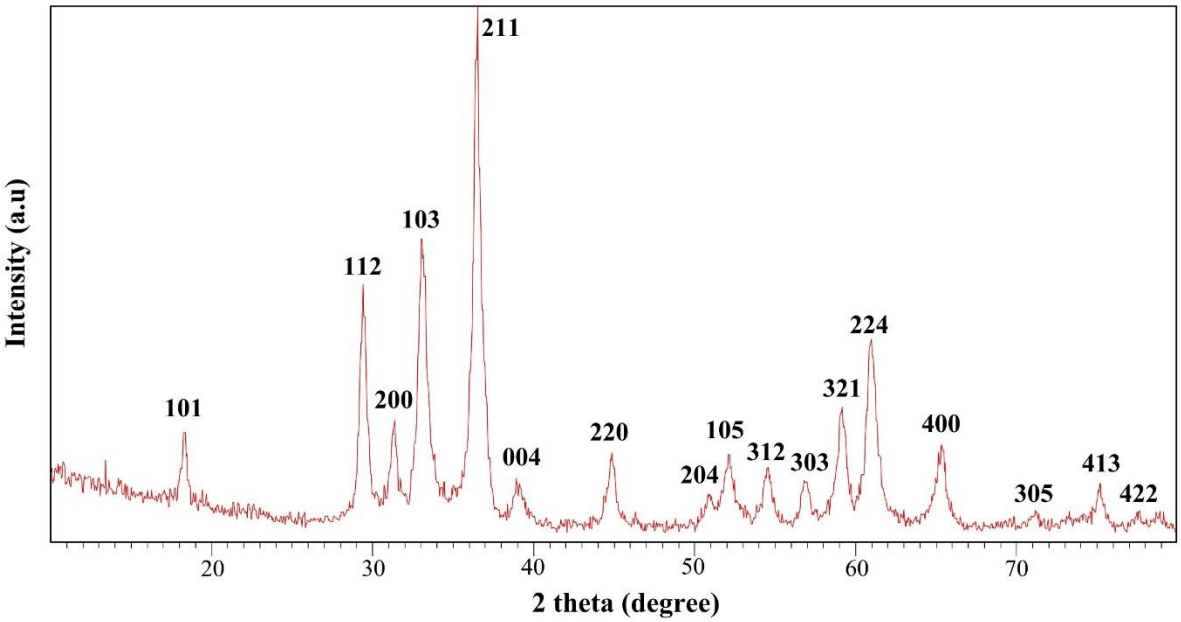


**Fig. 3**. XRD pattern of $ZnMn_2O_4$ NPs

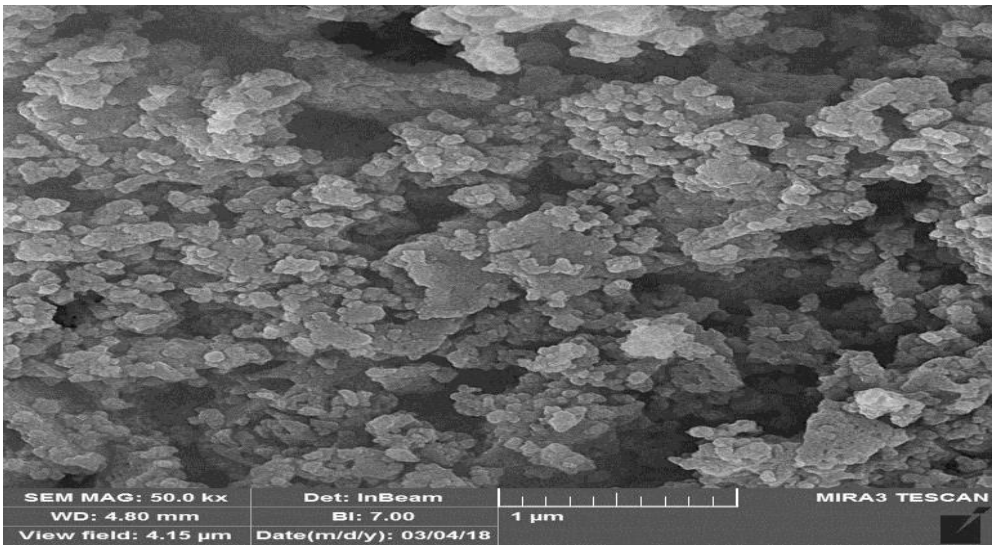


**Fig. 4.** SEM micrograph of the $ZnMn_2O_4$NPs.

The synthesized $ZnMn_2O_4$ NPs were considered as a photocatalyst for degradation of the Congo red dye in the presence of visible light irradiation and air at room temperature**.**

***Effect of visible light irradiation and $ZnMn_2O_4$ NPs catalyst***

In this work, the photocatalytic activity of $ZnMn_2O_4$ on degradation Congo Red dye was measured under Three conditions; nanophotocatalyst under visible light irradiation, nanophotocatalyst under dark and visible light irradiation without $ZnMn_2O_4$. In the state without none catalyst, we don't have any degradation. So long as using $ZnMn_2O_4$catalyst under dark condition, we see degradation of 41%. Fig. 6 shows when light and catalyst are applied at the same time, 96% of Congo red dye was degraded at 15 min.

***Effect the time on degradation of Congo red***

The UV-Vis spectra of the Congo Red was considered for following degradation process in present of $ZnMn_2O_4$ NPs as the photocatalyst at different time gap under the visible irradiation. Clearly, the maximum absorption peak of Congo red is found at 500 nm, that obvious diminution in intensity with raising irradiation time (Fig. 6). Approximately 96% of Congo red is degraded in 15 min. This evidence illustrates important result which can be expressed $ZnMn_2O_4$ NPs has a particular visible-light photocatalytic activity in degradation of the Cong red dye.

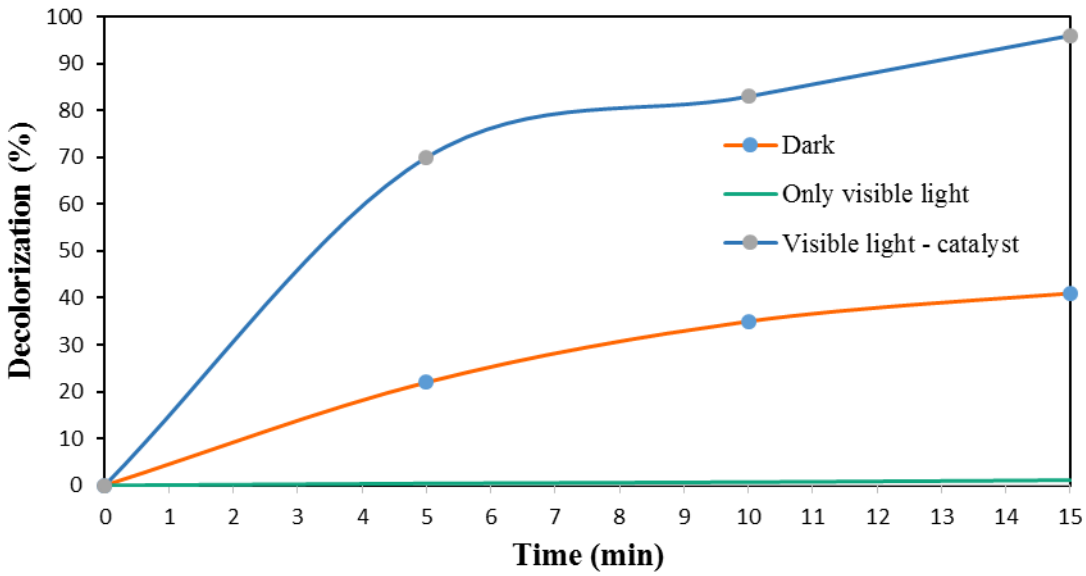


**Fig. 5.** Effect of visible light irradiation on the decolorization efficiency (%). Reaction conditions: Congo red =20 mg/L, catalyst= 0.03 g, pH=natural and room temperature

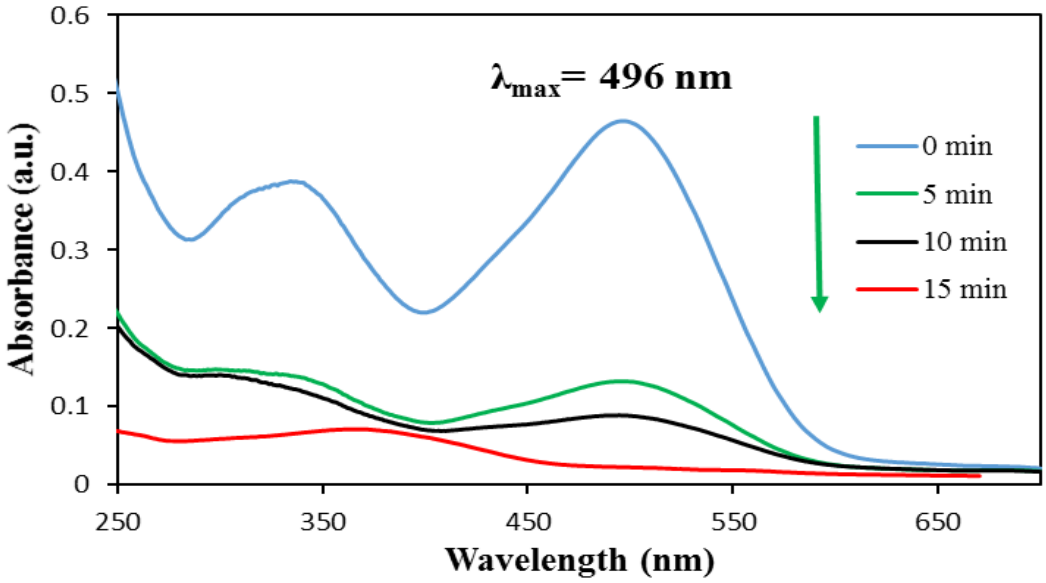


**Fig. 6.** Absorption spectra of Congo red solutions (20 mg/L) in the presence of 0.03 g of $ZnMn_2O_4$ photocatalyst under visible light radiation

## Conclusion

In present work, we worked on a useful green method for synthesis of $ZnMn_2O_4$ NPs via sol-gel method using tragacanth gel. The results of the analysis confirm the synthesis of $ZnMn_2O_4$ in spinel structure with a single phase after calcination for 4h at 600° C. In addition, the proposed method has significant advantages such as inexpensive, non-toxic, easy, environmentally friendly, free from any organic solvents and surfactant, non-toxic and it also show that the final NPs have favorable size and morphology. The aqueous solution of Congo red is selected for considering the unique photocatalytic activity of $ZnMn_2O_4$ NPs. UV-Vis spectrophotometric studies confirm that 96% of Congo red dye is degraded after 15 min in natural pH, room temperature and under the visible light irradiation. The obtained consequence states that this photocatalyst may be used to purify the water in various industries.

## References

[1] A. Houas, H. Lachheb, M. Ksibi, E. Elaloui, C. Guillard and J.-M. Herrmann, *Appl. Catal., B*, **2001**, *31*, 145-157.

[2] S.S. Patil and V.M. Shinde, *Environ. Sci. Technol.*, **1988**, *22*, 1160-1165.

[3] P.B. DeJohn and R.A. Hutchins, *Textile Chemist & Colorist*, **1976**, *8*,

[4] Y.M. Slokar and A. Majcen Le Marechal, *Dyes Pigm.*, **1998**, *37*, 335-356.

[5] L. Zhao, X. Li and J. Zhao, *Appl. Surf. Sci.*, **2013**, *268*, 274-277.

[6] Menaka, M. Qamar, S.E. Lofland, K.V. Ramanujachary and A.K. Ganguli, *Bull. Mater. Sci.*, **2009**, *32*, 231-237.

[7] M. Ramezani, S.M. Hosseinpour-Mashkani, A. Sobhani-Nasab and H. Ghasemi Estarki, *J. Mater. Sci. Mater. Electron.*, **2015**, *26*, 7588-7594.

[8] K. Atrak, A. Ramazani and S. Taghavi Fardood, *J. Mater. Sci. Mater. Electron.*, **2018**, *29*, 8347-8353.

[9] S.V. Bangale and S.R. Bamane, *J. Mater. Sci. Mater. Electron.*, **2013**, *24*, 277-281.

[10] M. Sorbiun, E. Shayegan Mehr, A. Ramazani and S. Taghavi Fardood, *Int. J. Environ. Res.*, **2018**, *12*, 29–37.

[11] M. Alagiri and S.B.A. Hamid, *J. Mater. Sci. Mater. Electron.*, **2014**, *25*, 3572-3577.

[12] S.A. Hosseini and P. Moalemzade, *J. Mater. Sci. Mater. Electron.*, **2016**, *27*, 8802-8806.

[13] F. Ahmadi, M. Rahimi-Nasrabadi and M. Behpour, *J. Mater. Sci. Mater. Electron.*, **2017**, *28*, 1531-1536.

[14] S. Taghavi Fardood, A. Ramazani, S. Moradi and P. Azimzadeh Asiabi, *J. Mater. Sci. Mater. Electron.*, **2017**, *28*, 13596–13601.

[15] S. Shabanalizadeh, A. Abedini, A. Alborzi, M. Bahmani, N. Shaghaghi, S. Hajebi and M. Yazdanmehr, *J. Mater. Sci. Mater. Electron.*, **2016**, *27*, 2589-2593.

[16] E. Shayegan Mehr, M. Sorbiun, A. Ramazani and S. Taghavi Fardood, *J. Mater. Sci. Mater. Electron.*, **2018**, *29*, 1333-1340.

[17] N. Zhang, X. Fu and Y.-J. Xu, *J. Mater. Chem.*, **2011**, *21*, 8152-8158.

[18] T.P. Yoon, M.A. Ischay and J. Du, *Nat. Chem.*, **2010**, *2*, 527.

[19] M.Y. Nassar, E.A. El-Moety and M. El-Shahat, *RSC Adv.*, **2017**, *7*, 43798-43811.

[20] S. Farhadi, K. Pourzare and S. Sadeghinejad, *J. Nanostruct. Chem.*, **2013**, *3*, 16.

# Optimization of Parameters for Adsorption of Chromium (III) onto Hydroxyapatite/ Carboxymethyl Cellulose Nanocomposite using Taguchi's Experimental Design Methodology

**Mozhgan Sabzehzari[1*],Zahra Abbasi[2]**

[1]*Department of Chemistry,College of Science, Jundi Shapur University of Technology-Dezfull,Iran,64615-334,*

[2]*Department of Chemistry,College of Science, Shahid Chamran University,Ahwaz,Iran*

*E-mail: *msabzehzari@jsu.ac.ir*

**Abstract**

In the present work nano-hydroxyapatite (n-HAp)/ Carboxymethyl Cellulose (CMC) composite was synthesized by precipitation method and was characterized by Fourier transform infrared (FT-IR) spectroscopy, X-ray diffraction (XRD) crystallography and scanning electron microscopy (SEM). The n-HApCMC composite was tested for the adsorption of Chromium from aqueous solution and compared its removal capacity with nano-hydroxyapatite (n-HAp). Taguchi model indicated optimization conditions for Cr(III) adsorption by using n-HApCMC Nanocomposite were initial metal ion concentration 100 mg/L, pH=4 , temperature 30 ˚C, and contact time 90 min. Equilibrium data were fitted well in the Langmuir and Freundlich isotherm models.

**Keywords**: Adsorption, Heavy metals, Isotherm, Nano-hydroxyapatite/Cellulose, Taguchi.

## Introduction

Heavy metal pollution has become an environmental problem throughout the world because heavy metals can be accumulated into the food chain and cause serious problems, not only for ecosystems but also for human health[1-5]. Hydroxyapatite $Ca_{10}(PO_4)_6(OH)_2$ (HAp) is a main mineral constituent of teeth, bones and phosphate mineral rocks. It belongs to apatite mineral family [6] However, characteristic of HAp existing in the form of white powder therefore isolating the suspended fine solids from aqueous solutions after adsorption of metal ions is not easy [7]. The annual net yield of photosynthesis is 1.8 trillion tonnes of biodegradable substances, about 40% of which is estimated to be cellulose [8]. Hence the general aim of the study is to investigate adsorption capability of cellulose composites made with nano-hydroxyapatite which, biocompatibility, biodegradability, etc than the individual components and hence be utilized at field conditions. Hybrid polymeric composites namely nano-hydroxyapatite (n-HAp)/ Carboxymethyl Cellulose (CMC) were prepared and used for the removal of Cr(III) from drinking water which has not been reported so far. Various parameters namely contact time, pH, coions and temperature were optimized for maximum sorption. The best fit isotherm was identified for the sorption. Suitable mechanism of Cr(III) removal was proposed.

## 1. Experimental

### 1.1. Materials

Carboxymethyl cellulose (CMC) provided by Fluka company whose molecular weight is about $4.2\times10^8$, potassium dichromate, calcium nitrate and ammoniumdihydrogen phosphate ammonia were purchased from Merck (Germany). All other applied chemicals were of analytical grade.

### 1.2. Methods

1.2.1. Synthesis of Nano-Hydroxyapatite (n-HAp)/ Carboxymethyl Cellulose (CMC) Composite:

n-HAp was synthesized by the reaction of calcium nitrate and ammoniumdihydrogen phosphate at a stoichiometric Ca/P ratio of 1.67. The pH value during mixing was maintained at 10–11 by addition of ammonia solution. The resulting precipitate was rinsed with water until the wash water was neutral and then dried at 80 ˚C [9]. The corresponding n-HApCMC composites were prepared by the precipitation method. The aqueous solution of ammoniumdihydrogen phosphate was added to the mixture of aqueous solution of $Ca(NO_3)_2$ with CMC in the ratio 3:2. The precipitate formed was rinsed with water to reach pH 7.The precipitate obtained was dried at 80 ˚C to get n-HApCMC composites.

### 1.2.2. Characterization of Materials

Characterization n-HApCMC and its structural and morphological analysis by SEM, XRD and FTIR techniques.The phases present in the magnetic materials were analyzed using a powder XRD Philips (Holland), model X´ Pert with $CuK_{\alpha1}$ radiation ($\lambda$ = 1.5406 Å), and the X-ray generator was operated at 40 kV and 30 mA. Diffraction patterns were collected from $2\theta$ = 10°–50°.

FT-IR spectra were recorded on a FT-IR spectrometer (Perkin Elmer) with a spectral resolution of 4 $cm^{-1}$ in the wave number range of 500–4000 $cm^{-1}$. The samples and

KBr were fully dried before the FT-IR analyses to exclude the influence of water.

The morphology of the n-HApCMC surface was characterized using a scanning electron microscope SEM model XL30 Philips (Netherlands). SEM micrographs were taken on samples of the adsorbent which were coated with a thin layer of pure silver (100 Å) using high vacuum sputtering.

The pH adjustments were made with a digital pH-meter (Sartorius, Model PP-20) using HCl (0.1 mol $L^{-1}$) and NaOH (0.1 mol $L^{-1}$ ). Mercury content in each experiment were determined with flame atomic absorption spectrophotometer (Perkin Elmer, Analyst 100).

### 1.2.3. Removal and Separation Procedure

Cr(III) adsorption experiments were conducted using batch equilibrium technique in aqueous solutions at pH range 1-4, initial metal ion concentration rang 25-100 mg/l, contact time 15-90 min and temperature at 10–40 ˚C.

The percent removal of Cr(III) by the adsorbent was calculated according where R is the removal efficiency of the Cr(III), $C_0$ and $C_e$ represent the initial and final (after adsorption)heavy metals concentrations in mg/l, respectively.

$$\text{Removal (\%)} = \frac{(C_0 - C_e)}{C_0} * ١٠٠ \qquad (1)$$

### 1.2.4. Designation and Optimization of Adsorption Experiments by Taguchi Method

The Taguchi method was originally seen as an effective statistical method [16]. In the Taguchi method, a small number of tests are done as the main effects of the design factors from a minimum number of experiments to obtain both information and create the optimized conditions [14]. In the design of the experiment using the Taguchi approach, a number of examinations are significantly minimized resulting in decreased experiment time and costs [15]. The Taguchi experiment design entails the use of the standard orthogonal array to study the testing procedures, therefore, examining the optimization of the process and determining the optimum value of the main influence parameters. Therefore, for optimizing was used of the four parameters (pH, contact time, initial metal ion concentration and temperature) at four levels by Minitab software, based on Taguchi experimental design. Signal to noise ratio was used with 'the highest is better' approach for optimization of experimental conditions and the highest Cr(III) removal efficiency. The selected experimental design parameters are as given in Table 1.

The $L_{16}$ orthogonal array, based on afore mentioned operating parameters was also selected for the experiment. Table 2 shows the experimental runs undertaken on combining Table 1 and the L16 orthogonal

**Table 1. Process parameters and four levels**

| *Numbers* | *Variable* | *unit* | *Level1* | *Level2* | *Level3* | *Level4* |
|---|---|---|---|---|---|---|
| *1* | *pH* | *…* | *1* | *2* | *3* | *4* |
| *2* | *contact time* | *min* | *15* | *40* | *65* | *90* |
| *3* | *initial metal ion concentration* | *mg/l* | *25* | *50* | *75* | *100* |
| *4* | *temperature* | *° C* | *10* | *20* | *30* | *40* |

We applied the signal-to-noise (S/N) ratio to evaluate the experimental data. Generally, three kinds of S/N ratio analysis such as the higher the better, lower-better (LB), and the nominal the best may be applicable [16]. As this work aims at understanding maximum adsorption efficiency of the target contaminant, the S/N ratio analysis chosen was the higher the better (Eq. (2)) [15]. Increased rate of S / N Indicates improving conditions.

Signal- to- Noise =

$$-10\log_{10}\left(\frac{1}{n}\sum\left(\frac{1}{Removal_i}\right)^2\right) \qquad (2)$$

According to the Table 2 and Table 3 ( a and b) optimization conditions for Cr(III) adsorption by Hydroxyapatite/ Carboxymethyl Cellulose Nanocomposite were initial metal ion concentration 100 mg $L^{-1}$, pH=4, temperature 30 ˚C, and contact time 90 min.

**Table 2. Experimental layout using an $L_{16}$ orthogonal array and the experimental results**

| | | | | | *n-HApCMC* | | *n-HAp* | |
|---|---|---|---|---|---|---|---|---|
| RUN | pH | contact time | initial metal ion concentration | temperature | Average of MAE (%) | S/N ratio | Average of MAE (%) | S/N ratio |
| 1 | 1 | 15 | 25 | 10 | 43 | 35.67 | 36 | 34.13 |
| 2 | 1 | 40 | 50 | 20 | 61 | 38.71 | 56 | 37.97 |
| 3 | 1 | 65 | 75 | 30 | 74 | 40.39 | 67 | 39.53 |
| 4 | 1 | 90 | 100 | 40 | 82 | 41.28 | 71 | 40.03 |
| 5 | 2 | 65 | 50 | 40 | 78 | 40.85 | 69 | 39.78 |
| 6 | 2 | 90 | 25 | 30 | 89 | 41.99 | 73 | 40.27 |
| 7 | 2 | 15 | 100 | 20 | 65 | 39.26 | 57 | 38.12 |
| 8 | 2 | 40 | 75 | 10 | 73 | 40.27 | 68 | 39.66 |
| 9 | 3 | 90 | 75 | 20 | 85 | 41.59 | 72 | 40.15 |
| 10 | 3 | 65 | 100 | 10 | 76 | 40.62 | 64 | 39.13 |
| 11 | 3 | 40 | 25 | 40 | 68 | 39.66 | 58 | 38.27 |
| 12 | 3 | 15 | 50 | 30 | 59 | 38.42 | 47 | 36.45 |
| 13 | 4 | 40 | 100 | 30 | 94 | 42.47 | 85 | 41.59 |
| 14 | 4 | 15 | 75 | 40 | 72 | 40.15 | 64 | 39.13 |
| 15 | 4 | 90 | 50 | 10 | 89 | 41.99 | 72 | 40.15 |
| 16 | 4 | 65 | 25 | 20 | 93 | 42.37 | 82 | 41.28 |

**Table 3. Estimated individual factor effects on percentage removal of Cr (III) by (a) Hydroxyapatite/ Carboxymethyl Cellulose Nanocomposite and (b) Hydroxyapatite**

**(a)**

| | *Variable* | *unit* | *Level1* | *Level2* | *Level3* | *Level4* |
|---|---|---|---|---|---|---|
| *1* | *pH* | *…* | *65* | *76.25* | *72* | *87** |
| *2* | *contact time* | *min* | *59.75* | *74* | *80.25* | *86.25** |
| *3* | *initial metal ion concentration* | *mg/l* | *73.25* | *71.75* | *76* | *79.25** |
| *4* | *temperature* | *° C* | *70.25* | *76* | *79** | *75* |

*Optimum level

**(b)**

| | *Variable* | *unit* | *Level1* | *Level2* | *Level3* | *Level4* |
|---|---|---|---|---|---|---|
| *1* | *pH* | *…* | *57.5* | *66.75* | *60.25* | *75.75** |
| *2* | *contact time* | *min* | *51* | *66.75* | *70.5* | *72** |
| *3* | *initial metal ion concentration* | *mg/l* | *62.25* | *61* | *67.75* | *69.25** |
| *4* | *temperature* | *° C* | *60* | *66.75* | *68** | *65.5* |

*Optimum level

## 2. Results and Discussion

### 2.1. Characterization of Materials

The FT-IR spectra of n-HApCMC (A), CMC (B) and n-HAp (C) were recorded in the region of 500–4000 $cm^{-1}$ and are shown in Fig. 1. The spectra of n- HAp showed a broad band at 1203 $cm^{-1}$ due to asymmetric stretching of $PO_4^{3-}$ and corresponding symmetric stretching was observed at 875 $cm^{-1}$. The absorption band at 1487 $cm^{-1}$ suggested the presence of $CO_3^{2-}$ [9], which was supposed to have come from atmosphere during the precipitation process. The broad band at 3500 to 3200 $cm^{-1}$ and 1766 $cm^{-1}$ was due to stretching and bending of O–H groups, respectively, present in n-HAp [10]. The FT-IR spectra of n-HApCMC showed a band at 1032 $cm^{-1}$ which was due to stretching vibration of C–O–C group of CMC confirms formation of composite. The peak of $PO_4^{3-}$ group shifted from 1203 to 1132 $cm^{-1}$ due to interaction with CMC. The stretching and bending vibration mode of –OH group of CMC occurred at 3452 and 1627 $cm^{-1}$, respectively which was overlapped with the bands of O–H groups in n-HApCMC composite.

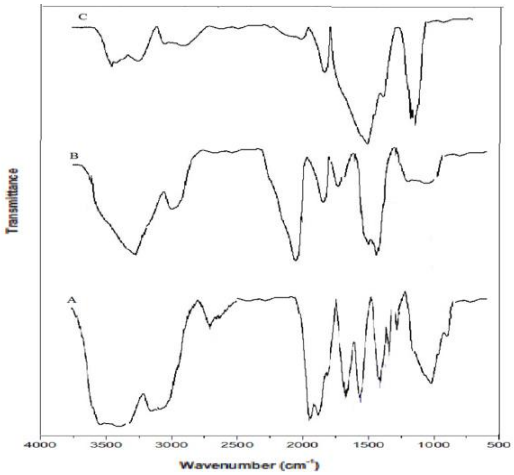


Fig. 1. Infrared spectra of n-HApCMCcomposite (a), CMC (b) and n- HAp (c).

The XRD spectra of CMC, n-HAP and n-HApCMC are shown in Fig. 2. In the XRD pattern of n-HAp, the crystalline peaks at $2\theta$ = 25.9°, 31.9°, 32°, 34.5° and 40° confirm the formation of hydroxyapatite. Crystalline peaks of In Fig. 2B, two main diffraction peaks of CMC at 2 $\theta$ = 32° and 46° can be found.n-HAp at $2\theta$ = 26◦, 32◦, 33.1◦, 34.2◦, 39.9° and 46◦ were found in n-HApCMC. This indicated that there was no marked change in the peak structure after the composite formation and confirms that the crystal structure of n-HAp is retained in n-HApCMC composites.

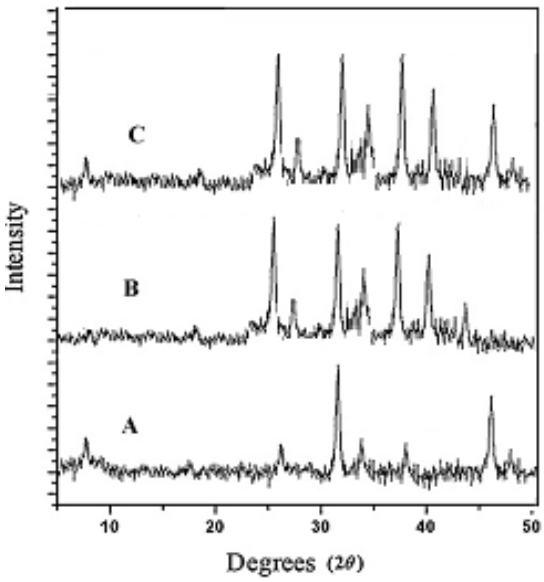


**Fig. 2. XRD spectra of CMC (a), HAp (b) and n-HApCMC (c).**

Fig. 3 shows the morphology of n-HAp (a) and n-HApCMC composite (b). The n-HAp powder exhibited as particles but in case of n-HapCMC composite aggregates appeared and film of CMC over n-HAp, confirmed the formation of n-HApCMC composite.

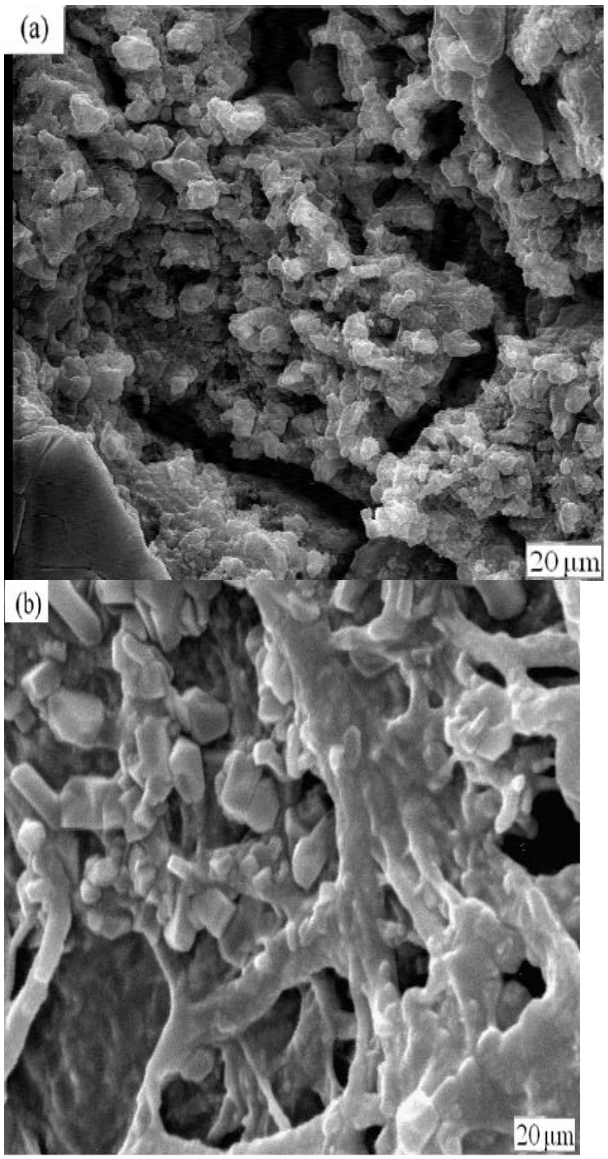


**Fig. 3. SEM micrograph of n-HAp (a) and n-HApCMC composite (b).**

## 2.2. Adsorption Experiments

Analysis of equilibrium data is important for developing an equation that can be used to compare different biomaterials under different operational conditions and to design and optimize an operating procedure [11].

Fig. 4 (a) shows the effects of pH on the adsorption of n-HApCMC composite. pH of the solution is an important operational parameter that governs the adsorption process of organic chemicals or metals in solution. At

the range of pH 1 to 4 the % removal became consistent, ranging between
67 to 87 % for n-HApCMC composite and 57.5 to 75.75 for n-HAp. The low adsorption of metal ions for lower pH was due to high concentration and high mobility of $H^+$ ions, which competed with metal ions for the adsorption sites, hindering the adsorption of metal ions by adsorbent.
The Fig. 4 (b) shows the effect of contact time on sorption of Cr(III) ion by adsorbent. The percentage removal of Cr(III) ion generally increased with increase in the contact time of metal ions.

Fig. 4 (c) shows the recovery obtained at increases when the initial ion concentration increase. Fig. 4 (d) shows the effects of temperature on Cr(III) ion adsorption onto n-HApCMC composite and n-HAp. It could be observed that the percentage removal of Cr(III) from aqueous solution generally increased with increment of the solution temperature.

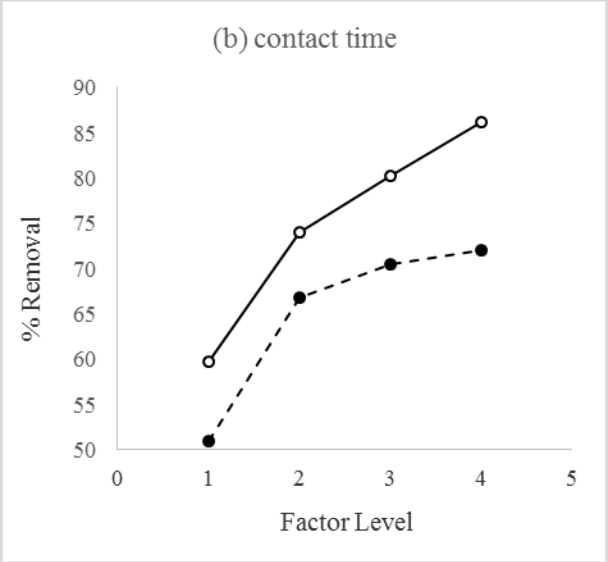


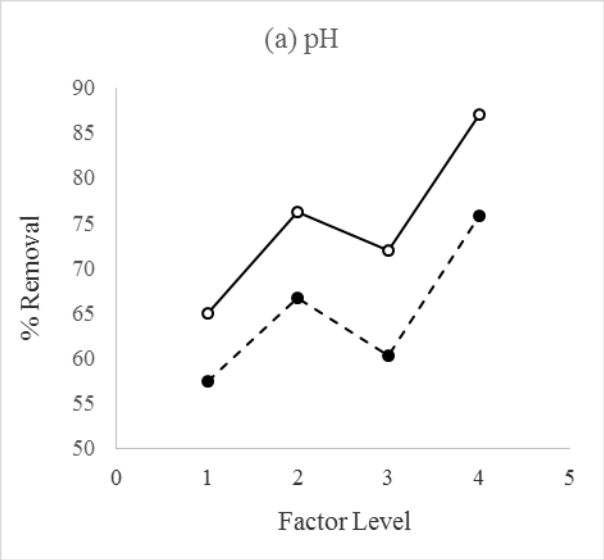


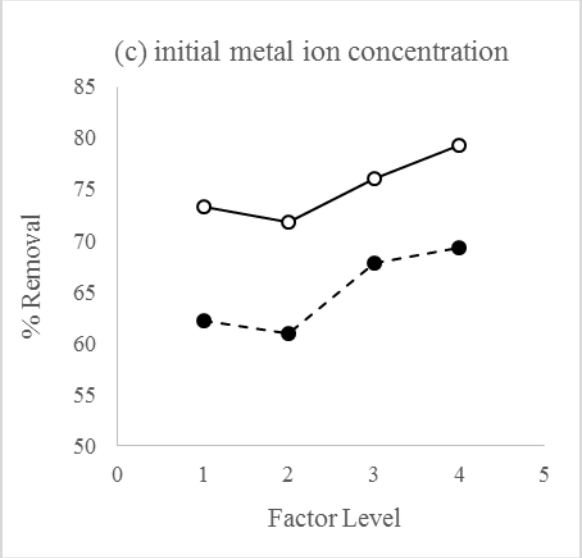


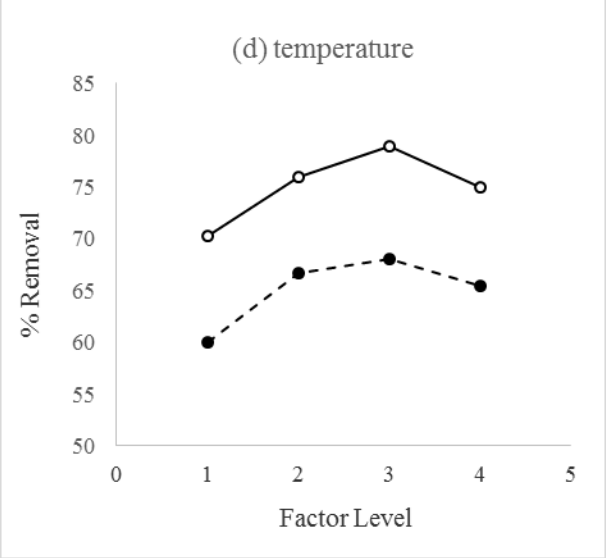

**Fig. 4. Estimated individual factor effects at different factor level on percentage removal of Cr (III) ion adsorption onto nano-hydroxyapatite/ Carboxymethyl Cellulose (n-HApCMC) composite (—o—) and n-Hap (- -●- -). (a) pH (b) contact time (c) initial metal ion concentration (d) temperature**.

## 3. Conclusions

This study showed that the binding of nano-HAp powder with cellulose makes it convenient to use practically and its removal capability was also retained in n-HApCMC which makes n- HApCMC composite as an effective adsorbent for the removal of Cr(III) from aqueous solution. Taguchi statistical method as an efficient, effective, and without the need for a large number of experiments indicated that the the Hydroxyapatite/ Carboxymethyl Cellulose nanocomposite as a new adsorbent, no cost, and without secondary pollutant has a high efficiency for Cr(III) removal from aqueous solution.

## References

[1] Ghanbari Pakdehi Sh. Alipour M., Iran. J. Chem. Chem. Eng. Vol. 32, No. 2,p.49 (2013)

[2] Nekoo S.H., Fatemi Sh., *Iranian Journal of Chemistry and Chmical Engineering (IJCCE):*, **32**(3): 81-89 (2013).

[3] Kumar Jha M., Van Nguyen N., Lee J., Jeong J., Yoo J., *J. Hazard. Mater.*, 164, p. 948 (2009).

[4] Shakeri A., Hazeri N., Valizadeh J., Hashemi E., Kakhky A., *Iranian Journal of Chemistry & Chemical Engineering (IJCCE)*, **31**: 45-50 (2012).

[5] Cavaco S.A., Fernandes S., Augusto C.M., Quina M.J., Gando-Ferreira L.M., *J. Hazard. Mater.*, 169, p. 516 (2009).

[6] Bailliez, S, Nzihou, A, Beche, E and Flamant, G. , *Saf. Environ. Protect.* 82, 175–180 (2004).

[7] Simon, F. G. Birmann, V and Peplinski, B, *Applied Geochem.* 23, 2137–2145 (2008).

[8] Choi S and Jeong Y. , *Fiber Polym.* 9, 267–270 (2008).

[9] Mobasherpour I, Heshajin M.S, Kazemzadeh A and Zakeri M., *J. Alloy Compd.*, 430, 330–333 (2007).

**[**10**]** A. Q. G**.** Leyva, J. Marrero, P. Smichowski and D. Cicerone. *Environ. Sci. Technol.*, 35 (2001): 3669-3675.

[11] E.G. Pacyna, J.M. Pacyna and N. Pirrone, *Atmos. Environ.*, 35 (2001): 2987-2996.

[12] G. McKay, H.S. Blair and J.R. Gardener.. *J Appl Polym Sci.* 27 (1982): 3043-57

[13] Z. Abbasi and M. Alikarami., *Biochemistry and Bioinformatics.* 1 (1) (2012): 001 – 007.

[14] G. Zolfagharia. A. Esmaili-Sari, M. Anbia, H. Younesi, S. Amirmahmoodi, S. and Ghafari Nazari, M. 2011. *J. Hazard. Mater*, 192, 1055.

[15] S. Sadeghi,H Moosavi, V. Karami A. and Behnia. *J. Hydrol.* 180 (2012): 448-449.

[16] G. Taguchi. Introduction to quality engineering. McGraw-Hill New York, USA.1990.